The Addition of Graphene and Novel Fibre Nanotubes to Carbon Fibre Composites: Effects on Mechanical Properties

AYAD AIED MAHUOF

A Thesis Submitted for the Degree of Doctor of Philosophy (PhD) in Mechanical Engineering at Newcastle University, United Kingdom

School of Engineering

January 2019

Abstract

The incorporation of multifunctional carbon nanomaterials, graphene nanoplatelets (GNP) and cup-stacked carbon nanotubes (CSCNT) into the polymer matrix of conventional carbon fibre reinforced composites as fillers, offers the potential for mechanical multifunctional improvements, for instance strength, stiffness and toughness without disrupting the original in plane mechanical properties. In this research, the GNP, the CSCNT and a novel combination of them (hybrid GNP-CSCNT nanofillers) were dispersed within a thermosetting resin matrix via mechanical dispersion techniques, such as ultra-sonication and ball milling/mixing to achieve uniform dispersion and full exfoliation of carbon nanomaterials in the matrix. The principal purpose of the combination of GNP and novel CSCNT into the matrix was to promote the strength and toughness properties of the polymer matrix as well as the conventional CFRP by availing the synergetic influence between these carbon nanomaterials. Three types of polymer nanocomposites (NP) were prepared successfully by the combination of these two dispersion techniques with the following formulations: GNP/epoxy nanocomposites, CSCNT/epoxy nanocomposites and hybrid GNP-CSCNT/epoxy nanocomposites. The greatest improvements of the HNP were achieved in flexural strength and flexural modulus after the combination of 2 wt.% of GNP and 2 wt.% of CSCNT by approximately 40% and 61%, respectively. In addition to significant improvement in fracture toughness by 85% at the same weight content, substantial improvements in the mechanical properties of novel HCFRP (hybrid GNP-CSCNT/CF/epoxy nanocomposites) were also gained after using the same optimum proportional weight content of these combined carbon nanomaterials. The flexural strength and flexural modulus improved by approximately 18% and 28% respectively, while the shear strength improved by 37%. Additionally, the energy propagation of Mode I and Mode II interlaminar fracture toughness increased by approximately 73% and 132% respectively.

Most of the aforementioned properties of HCFRP showed superior improvement when 6 wt.% of CSCNT were individually incorporated, for instance the shear property of CSCNT/CF/epoxy nanocomposites improved by 38%, flexural strength by 25% and interlaminar fracture toughness Mode I and Mode II by 104% and 151% respectively. The GNP produces less improvements at optimum weight concentration 5 wt.% in comparison to CSCNT/CF/epoxy nanocomposites. For instance shear strength of GNP/CF/epoxy nanocomposites improved by 31%, flexural strength 20% and interlaminar fracture toughness Mode I and Mode II by 15% and 84% respectively.

The fracture mechanisms for these enhancements were investigated by extensive fratographyical analysis to show the synergetic associated mechanisms of hybrids composites. Multiple fracture mechanisms systems were generated into the fracture surface of the HCFRP after the addition of combined carbon nanomaterials into the fibre network.

In conclusion, the addition of novel CSCNT is better than GNP in reinforcing the mechanical properties of thermoset resin (i.e. epoxy) and conventional CFRP. Additionally, the inclusion of the combined nanomaterials; GNP and CSCNT is useful in promoting the mechanical properties over the parent hybrid composites. Moreover, it is expected to be harmless to the original mechanical properties of epoxy composites and conventional carbon fibre composites.

Acknowledgements

Firstly, I would like to express my sincere gratitude to my supervisors: Prof Geoff Gibson, Dr George Kotisikos and Dr Roberto Palacin who have provided me with permanent support and guidance throughout my studies. I would also like to express my gratitude to the technicians Adam Richardson and Brian S, for their invaluable assistance.

I wish to thank my sponsors: the Ministry of Higher Education and Scientific Research in Iraq for their financial support.

Finally, I would like to thank my family for their encouragement and continuous prayers, my colleagues and of course Sheila, Maria, Hasan and Peyman.

Contents

List of Figures

List of Tables

List of abbreviations and symbols

AFM	Atomic force microscope
Al_2O_3	Aluminium Oxide
C.V	Coefficient of variation
CCVD	Catalyst chemical vapour deposition
CF	Carbon fibre
CFRP	Carbon fibre reinforced polymer composites
Ch	Chiral vector
CNF	Carbon nanofiber
CNTs	Carbon nanotubes
CSCNT	Cup-stacked carbon nanotubes
DCB	Double cantilever beam
DWCNT	Double walled carbon nanotube
EG	Expanded graphene
ENF	End notched flexure
ESEM	Environmental scanning electron microscope
f-CNTs	Functionalized carbon nanotubes
f-GNP	Functionalised graphene nanoplatelets
FLG	Few-layer graphene
f-MWCNT	Functionalised multi-walled carbon nanotube
FRP	Fibre reinforced polymer composites
FS	Flexural strength
$G.NH_2$	Amino-functionalised graphene nanoplatelets
GCB	Graphene carbon black
GF	Glass fibre
GRP	glass fibre reinforced polymer composites
GNP	Graphene nanoplatelets
GO	Graphene oxide
GONS	Graphene oxide nanosheets
G-Si	Silane modified graphene nanoplatelets
HCFRP	Hybrid carbon fibre reinforced polymer composites
HFRP	Hybrid fibre reinforced polymer composites
HNP	Hybrid polymer nanocomposites
HP-NGPs	Hydrogen passivated nano graphene platelets
HRTEM	High resolution transmission electron microscopy
ILSS	Interlaminar shear strength
Incr.%	Percentage of increase
MBT	Modified beam theory
MWCNT	Multi-walled carbon nanotube
NiO	Nickel oxide
NL	Nonlinear point
NP	Polymer nanocomposites
PA6	Polyamide 6

PE	polyethylene
PEEK	Poly (ether ether ketone)
PMMA	Polymethyl methacrylate
P-MWCNT	Pristine multi-walled carbon nanotube
PP	Polypropylene
PVA	Poly (vinylalcoholl)
PVP	Polyvinylpyrrolidone
rGO	Reduced graphene oxide
RTM	Resin transfer modelling
S.D	Standard deviation
SBS	Short beam shear
SEM	Scanning electron microscopy
SENB	Single-edge-notched bending
SWCNH	Single-walled carbon nanohorns
SWCNT	Single walled carbon nanotube
TEM	Transmission electron microscopy
TRGO	Thermally reduced graphene oxide
TS	Tensile strength
UD CF	Unidirectional carbon fibre
VARTM	Vacuum assistant resin transfer molding
VIS	Optical vision point
0D	Zero dimensional
1D	One dimensional
2D CF	Two dimensional carbon fibre
3pb	Three-point bending test
3D	Three dimensional
3D CNT	Three dimensional carbon nanotubes
3D GNP	Three dimensional graphene nanoplatelets
3ENF	Three end notched flexure
4pb	Four-point bending test

Symbols	Description
a	Crack length (mm)
a_1,a_2	Unit vectors
ASTM	American Section of the International Association for Testing Materials
b	Width of sample (mm)
C	Compliance (mm/N)
C_o	Initial compliance (mm/N)
G_I	Interlaminar fracture toughness energy (Mode I) ($J.m^{-2}$)
G_{II}	Interlaminar fracture toughness energy (Mode II) ($J.m^{-2}$)
h	Thickness of sample (mm)
K_{IC}	Critical intensity factor ($MPa.\ m^{1/2}$)
L	half span of simply supported beam (mm)
P	Force (N)
P_{max}	Maximum force (N)
V_f	Volume fraction of fibre (vol.%)
V_m	Volume fraction of matrix (vol.%)
vol.%	Unit of volume fraction
W	Depth of sample (mm)
$W_{composite}$	Weight of composite (g)
W_f	Weight fraction of fibre (wt.%)
W_{fibre}	Weight of fibre (g)
W_m	Weight fraction of matrix (wt.%)
W_{matrix}	Weight of matrix (g)
wt.%	Unit of weight fraction
x	Ratio of crack length/depth
δ	Deflection (mm)
$\rho_{composite}$	Density of composite (g/cm^3)
ρ_{fibre}	Density of fibre (g/cm^3)
ρ_{matrix}	Density of matrix (g/cm^3)

List of publications and conferences

A.A. Mahuof, Maria Konstantakopoulou, G. Kotsikos, and A.G. Gibson. “Preparation of Novel Nanocomposites Using the Ultra-Sonication Technique”. The International Conference for Students on Applied Engineering 2016, October 20-21, Newcastle, UK.

A.A. Mahuof, G. Kotsikos and A.G. Gibson. “The Effect of Hybrid Nanofillers on Mechanical Properties of Carbon Fibre Epoxy Composites”. Proceedings of Nanotech France 2017 international conference, 28-30 Jun, Paris, France.

A.A. Mahuof, G. Kotsikos and A.G. Gibson. “Preparation of Novel Nanocomposites Modified with Hybrid Nano-Reinforcements”. Proceedings of ANNIC 2017 International conference, October 18-20, Rome, Italy.

A.A. Mahuof, G. Kotsikos, A.G. Gibson and R. Palacin. “Improving the Mechanical Properties of Carbon Fibre Composites Using the Combination of Graphene and Fibre Nanotubes”. Proceedings of IC2NAM 2018 International conference, 4-5 August, Hamburg, Germany.

Chapter 1. Introduction

1.1 Aim of the study

The objective of this experimental study was to produce novel hybrid nanocomposite (HNP) enhanced with multifunctional carbon nanomaterials; graphene nanoplatelets (GNP) and cup-stacked carbon nanotubes (CSCNT) and to use this in the manufacture of hybrid carbon fibre reinforced polymer composites (HCFRP). The HNP was produced by a combination of GNP and CSCNT in a polymer matrix. The reason for the combination of these carbon nanomaterials is to promote the strength and toughness properties of polymer resin, which is the result of their beneficial synergetic properties within the matrix. Additionally, it is to investigate the effect of the optimum strengthened and toughened matrix on the mechanical properties of the carbon fibre reinforced polymer composites (CFRP), such as interlaminar shear strength, interlaminar fracture toughness and flexural strength properties sequentially.

1.2 Introduction

It is acknowledged that carbon fibre composites possess excellent strength and stiffness properties besides being light weight. These beneficial characteristics play a significant role in the structural design of aircraft, spacecraft and automobiles. Furthermore, the reduction of manufacturing costs for such types of fibre composites and an increase in their period of endurance is considered a critical issue in their structural designs when used for advanced engineering applications (Glover, 2004; Pora, 2003).

The structural performance of fibre reinforced polymer composites (FRP) and their engineering applications as a primitive structure is hindered by their sensitivity to damage or defects. Whilst carbon fibre composites have excellent properties in-plane tensile and stiffness performance, they suffer from low resistance to compression loads, interlaminar and other polymer matrix dominated properties (Djabali et al., 2018; Sudarsono & Ogi, 2017; Mall et al., 2009; Liyong et al., 2002; Gamstedt & Sjogren, 1999).

To develop these mechanical resistance properties of conventional FRP, classical approaches have been used to address these issues, such as use of advanced polymer resins through-thickness reinforcement (Kuwata & Hogg, 2011; Wilkinson et al., 1993; Greenhalgh et al., 2006). Nevertheless, the disadvantages of such approaches are costly and have a tendency to reduce the pristine properties of the fibre composites and fatigue performance owing to the sensitivity to synthesising conditions (Liyong et al., 2002). Furthermore, use of a single material, for instance a polymer resin is not sufficient or effective enough to reduce the delamination failure or damage

in the structure of fibre composites, in particular after exposure of the laminated composites to high compressive loads (Kim et al., 1992; Jang et al., 1990).

A further significant and advanced method is the use of nanoreinforcement (i.e. carbon nanomaterials), which has proved successful and is still applied in the promotion of mechanical properties of FRP (Qian et al., 2010). The primary reason for using carbon nanomaterials as additional reinforcement in the matrix is to improve the strength and toughness properties of fibre composites, because these nanomaterials absorb a part of the strain energy before it reaches the pristine fibre networks. Thus, this approach would reduce the degree of damage and, therefore, increase the safety factor in relation to structural composites. In particular, there has been interest in the use of single (SWCNT) and multi-walled carbon nanotubes (MWCNT) to improve the strength and toughness properties of hybrid fibre reinforced polymer composites (HFRP) over the past three decades (Romhany & Szebenyi, 2009; Ashrafi et al., 2011; Wichmann et al., 2006; Fan et al., 2008; Qiu et al., 2007). The known drawbacks of such types of carbon nanomaterials are costly, in particular the SWCNT and dispersion difficulties regarding the polymer resins (Gkika et al., 2017; Ma et al., 2010).

In recent years, GNP and CSCNT have been considered as possible alternatives to these conventional carbon nanomaterials (Roy and Kumar, 2017; Zhang et al., 2013; Wajid et al., 2013; Barrena et al., 2014; Landani, 2015; Yokozeki et al., 2009; Qin et al., 2015; Li et al., 2018). The GNP and CSCNT intrinsically possess extraordinary and excellent mechanical properties, with the strength and elastic modulus of the monolayer nanoplatelets and nanofiber having been measured experimentally as 130 GPa and 1 TPa (Lee et al., 2008) and 3.5 GPa and 172 GPa (Arshad et al., 2011), respectively. Additionally, each one has different morphological properties. For example, fibre nanotube has an excellent geometric structure and length, whilst graphene has a large surface area and high aspect ratio. Consequently, they have the potential to enhance several of the mechanical characteristics, particularly polymer resistance (i.e. strength and toughness). Additionally, the price is low (Kim et al., 2017; Phua et al., 2016; Landani et al., 2015; Gkika et al., 2017). Therefore, use of GNP and CSCNT to reinforce the strength and toughness properties of fibre composites is probably more efficient than conventional carbon nanotubes (Kumar and Roy, 2018; Jia et al., 2015; Kostagiannakopoulou et al., 2015; Du et al., 2017; Zhou et al., 2006; Khan and Kim, 2012; Green et al., 2009; Yokozeki et al., 2009).

Two types of known practical techniques which are used in the manufacturing of HFRP currently are by way of the deposition of nanoparticles onto the surface of fibre networks (Kepple et al., 2008; Kamar et al., 2015; Wang et al., 2011; Qian et al., 2010) or by the dispersion of nanoparticles in the polymer matrix (Ji et al., 2016; Wang et al., 2015; Hadden et al., 2015;

Kostagiannakopoulou et al., 2015; Shen et al., 2013; Ma et al., 2010; Yokozeki et al., 2009), as shown in Figure 1. Both techniques have achieved significant improvements in the strength and toughness properties of HFRP. The possibility of damage in the pristine fibres could be a sensible reason for choosing the dispersion process instead of the deposition process with respect to preparing modified matrix (Mathur et al., 2008). Moreover, it is helpful to implement for scale fabricating and has been commercialised at various nanoparticle loadings, probably due to its simple principles.

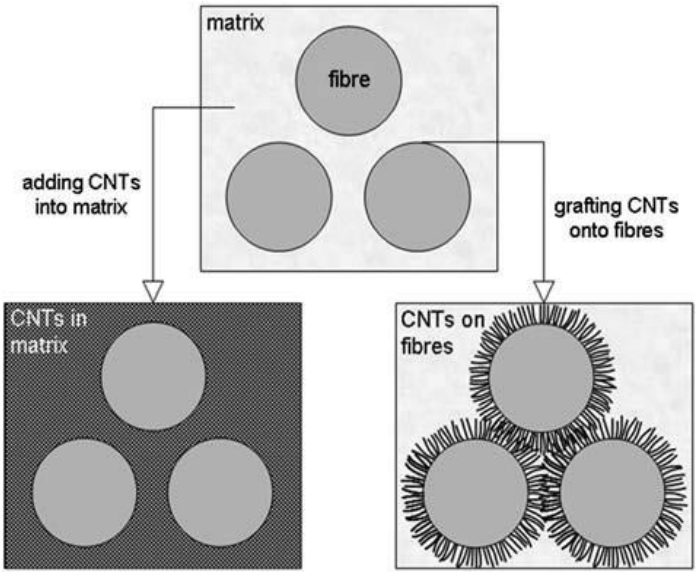

Figure 1 Schematic diagram of conventional fibre composites modified with carbon nanomaterials via two approaches; grafting and dispersing (Qian et al., 2010).

In previous and recent HFRP studies, the focus on dispersed and uniformed distribution of carbon nanomaterials within the matrix (Kumar and Roy, 2018; Du et al., 2017; Jia et al., 2015; Khan and Kim, 2012; Qian et al., 2010); with various synthesising methods and functionalisation have been explored to accomplish homogenous distribution of carbon nanomaterials in the polymer matrix. The purpose of that is to obtain high strength and toughness properties of modified matrix in the nanocomposite. It can then be used to reinforce the mechanical properties of FRP (Wang et al., 2015; Moriche et al., 2016; Zhou et al., 2006). Several fracture mechanism systems to dissipation energy have been suggested as sensible reasons to explain the observed enhancements in strength and toughness properties of the HFRP. For example, nanotubes pull-out (Fenner & Daniel, 2014), crack bridging (Menna et al., 2016; Ye et al., 2007), bi-furcation mechanisms (Kostagiannakopoulou et al., 2017), the fracture of nanofiller (Zaman et al., 2011; Gojny et al., 2005) and matrix distortion (Wetzel et al., 2006).

However, all these mechanisms need a degree of attraction between the reinforcement and the matrix at the interface regions. Therefore, the interface region between these two phases plays a key role in reinforcing the mechanical properties of composites, as it delivers the mechanical

forces between the polymer matrix and filler (Kundalwal and Kumar, 2016; Zhang et al., 2012). Furthermore, due to geometric transformations in size dimensions between the fibre reinforcement and nanomaterial reinforcement, the attraction mechanism remains a mystery with regard to interfacial bonding between these multi-sized reinforcements and the matrix.

A very recent and novel approach is currently applied to promote these mechanical characterisations, which includes use of a combination of multifunctional carbon nanomaterials; GNP and MWCNT. They have been used in developing superior mechanical properties of FRP (Rodriguez-Gonazalez et al., 2017; Kostagiannakopoulou et al., 2017; Liu et al., 2017; Tan et al., 2016; Wang et al., 2015). However, there were moderate enhancements in mechanical properties of hybrid fibre composites modified with a combination of graphene and conventional carbon nanotubes in most of these previous studies, due to their tendency to form agglomerates in the matrix and difficulty in achieving alignment between the fillers and matrix (Ma et al., 2010; Rodriguez-Gonazalez et al., 2017; Punetha et al., 2017). These undesirable behaviours weaken the mechanical interfacial property between the matrix and filler, particularly at the interface regions; therefore, decreasing the improvements in the mechanical properties of HFRP. Therefore, the use of additional dispersants is frequently necessary to improve the dispersion degree of such types of carbon nanomaterials in the matrix and, adhesion between the fillers and the matrix (Cho et al., 2008; Gojny et al., 2005). Thus, the manufacturing cost of hybrid composites is expected to increase.

The high premium characterisation of novel CSCNT are excellent mechanical properties, has a unique geometric structure and the dispersion process of this type of carbon nanomaterials in the polymer resins is easier than conventional carbon nanotubes (Arshad et al., 2011; Yokozeki et al., 2012; Yokozeki et al, 2008; Iwahori et al., 2005). These benefits make it a promising carbon nanomaterial in relation to reinforcing the mechanical properties of HFRP (Landani et al., 2015; Khan and Kim, 2012; Yokozeki et al., 2009). Therefore, the novel combination of GNP and CSCNT instead of conventional carbon nanotubes could be more efficient in reinforcing the mechanical properties of hybrid composites and was adopted in the present work.

To achieve optimum strength and toughness properties of the graphene and fibre nanotubes reinforced nanocomposites, requires high exfoliation and the uniform dispersion of these carbon nanomaterials in the polymer resin. Therefore, challenges lie in the dispersing processes regarding the combination of graphene and fibre nanotubes into the resin and ensuring that their geometric structure is not damaged. A modern approach has been applied successfully by researchers to optimise the dispersion degree of nanoparticles in the polymer resins, which included use of combined dispersive techniques (Guo and Chen, 2014; Tang et al., 2013; Ma et

al., 2010). Therefore, a combination of sonication and the ball milling technique was suggested to disperse these carbon nanomaterials in the polymer matrix mechanically without using the additional dispersants. Moreover, to use their optimum modified matrices in the manufacture of HFRP (Wang et al., 2015).

The hypothesis that underpins the present experimental study suggests that with CFRP containing an optimised mixture of multifunctional carbon nanomaterials; GNP, CSCNT and hybrid GNP-CSCNT nanofillers, the degree of attraction of the fibre/matrix interface region is modulated by their strengthened and toughened matrices. To construct the region with high mechanical interfacial properties between the laminates of HFRP, an optimum modified matrix in each nanocomposite was used to impregnate the surface of the fibre network uniformly. Hence, this created strong support regions composed of multifunctional tough modified matrix around the fibre tows. In contrast, to achieve full and multiple potential strengthening and toughening mechanisms in the composites, the crack path must be restricted or driven to extend into modified matrix. This experimental study explores the fracture mechanism systems besides the mechanical properties of a hybrid composites modified with multifunctional carbon nanomaterials, such as the strength and interlaminar fracture toughness properties, where these mechanical characterisations were promoted by a combination of graphene and novel fibre nanotubes, resulting from engineering integration and synergy property of these carbon nanomaterials within the matrix.

1.3 Research objectives

The specific research objectives of this experimental study are:

a) To perform optimisation for three formulations of polymer nanocomposites (NP), namely: i) GNP/epoxy nanocomposites, ii) CSCNT/epoxy nanocomposites and iii) hybrid GNP-CSCNT/epoxy nanocomposites. This was achieved by changing the weight content of the nanoparticles and the mechanical dispersion processes. The purpose of that is to achieve the optimum strength and toughness properties of the modified matrix in each nanocomposite.

b) To examine the mechanical properties of these NP, which included tensile strength (TS) and flexural strength (FS) to specify the optimal loading of the modified matrix in each nanocomposite.

c) To check the characterisation of fracture toughness properties for the three NP at optimum weight concentrations in order to determine the fracture toughness strength of the modified matrix in each nanocomposite.

d) To produce three types of HCFRP by use of the optimum strength and toughness properties of the modified matrix in each nanocomposite with the following formulations: i) GNP/CF/epoxy nanocomposites, ii) CSCNT/CF/epoxy nanocomposites and iii) hybrid GNP-CSCNT/CF/epoxy nanocomposites.

e) To examine the mechanical properties of the HCFRP, which involved interlaminar shear strength (ILSS), flexural strength (FS) and interlaminar fracture toughness (Mode I) and (Mode II).

f) To characterise the dispersion processing and orientation of nanofillers, besides the fracture surface morphologies of the NP and the HCFRP via Transmission Electron Microscopy (TEM), Scan Electron Microscopy (SEM) and Optical Microscopy.

g) To evaluate the dispersion techniques used in the manufacture of the NP, particularly, the combined dispersive techniques method.

h) To assess the mechanical properties of these three specific types of HCFRP.

1.4 Structure of the thesis

This thesis is classified into seven chapters. This chapter briefly reviews the drawbacks statement and motivation for the present study. Chapter 2 surveys the pertinent literature covering previous studies with similar material, as well as their research findings. The chapter describes the mutual trends that exist in the literature and the suggested important mechanisms. Chapter 3 exhibits the experimental methods which involves the materials used, the production methods of the optimised nanocomposites and the manufacture of hybrid fibre reinforced optimum nanocomposites. Chapter 4 demonstrates the characterisation methods utilised to assess the physical and mechanical properties of NP and HCFRP. Chapters 5 and 6 present the experimental results and discussion relevant to the evaluation of the mechanical properties of the NP and HCFRP respectively besides interpretation of the results. Chapter 7 concludes with the results of the experimental research and suggested future work.

Chapter 2. Literature review

This chapter focuses on state of the art carbon nanomaterials, polymer reinforced with carbon nanomaterials as well as hybrid fibre reinforced polymer composites (HFRP).

Over the last three decades, carbon nanomaterials have sparked significant interest due to the improved strength, stiffness and fracture toughness properties of these novel composites in comparison to those of the parent polymer composites. Challenges in relation to the synthesis preparation of these novel composites are explored and their reported improvements in mechanical properties are evaluated and analysed. Moreover, the behaviour of the fracture mechanisms that had contributed to these reinforced properties are also crucially surveyed in this review.

2.1 Overview

The development of composites has changed rapidly in recent years and they are utilised in numerous advanced engineering designs, particularly in aircraft and automobile structures. The composites can be made via a change to the reinforced materials in the matrix. Two main types of composites are currently being extensively used in these industrial applications. The first one is the conventional fibre composites, composed of a matrix, for instance polymer resins and fibre reinforcements, such as glass and carbon fibres.

The second, novel NP, consist of at least two materials one of which has strong, rigid properties with nanoscale size such as carbon nanomaterial (i.e. CNTs, GNP and CNF). These have a different geometric shape and scale structure besides mechanical properties. The main aim of using such nanomaterials is to promote the mechanical properties of the polymer composites, such as strength, stiffness, toughness and other properties. The other material is the matrix, for example polymers, ceramics and metals. These two materials are connected with each other by the interface region.

Recently, researchers and engineers have developed conventional fibre composites and nanocomposites, created by a combination of them into the polymer matrix to produce novel HFRP. In general, the main difference between these multi-sized reinforcements is transforming the dimensional size from a micro to nanoscale.

The morphological configuration of this conversion is better distinguished by scanning electron micrographs, as depicted in Figure 2 (Thostenson, 2004; Thostenson et al., 2003).

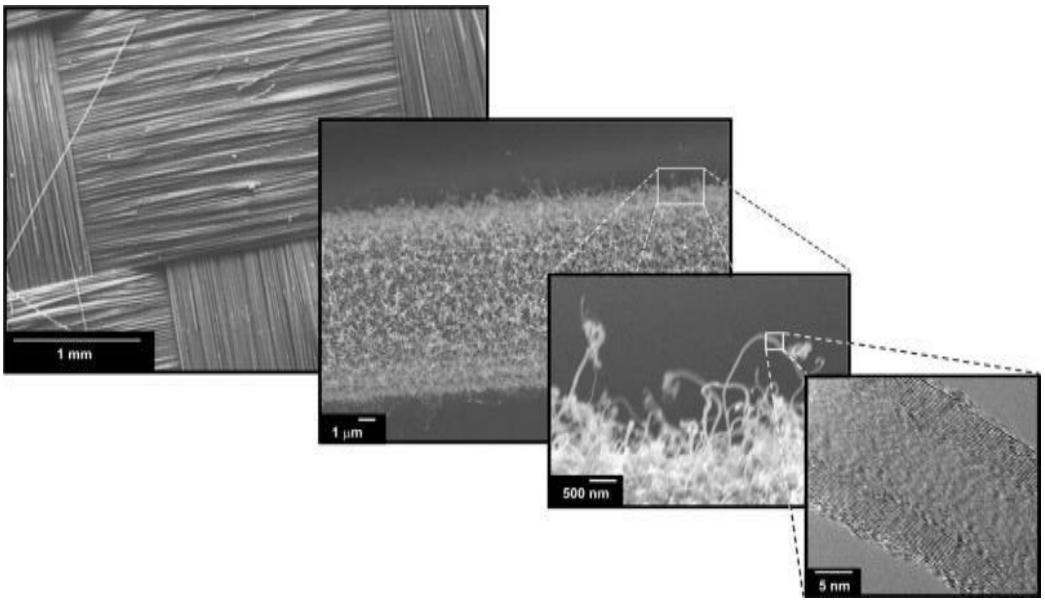

Figure 2 The transformation in scale dimensions of multi-sized reinforcements from millimetres (fibre network) to nanometres (CNTs) (Thostenson, 2004; Thostenson et al., 1998; Thostenson & Chou, 2003).

Thus, the image illustrates the conversion in engineering dimensions and morphological structure for fillers from millimetres and micrometres to the nanometre scale. This is where CNTs with nano-diameters of between 10-20 nm have been coated on the fibre surface his diameter 7 µm. Hence, this can appear as spun packages on it, where the variation in the enhancement scale is apparent. Their geometrical transformation in their size and scale, led to difficulties in discovering the interaction mechanism relevant to interfacial mechanical property between these multi-sized reinforcements and the polymer matrix. Therefore, this engineering problem became a critical case that attracted many researchers to understand the mechanism of fracture, especially after the mixing of more than one type of nanomaterials into the matrix and use of this modified matrix in the manufacture of HFRP.

2.2 Conventional carbon nanotubes (CNTs)

Numerous research efforts have been conducted by engineering researchers over the past three decades to produce different types of CNTs with high purity and quality and excellent morphological structures, such as nano-sized and geometric structure (Thostenson et al., 2001; Collins & Avouris, 2000; Wagner & Vaia, 2004; Curtin & Sheldon, 2004). These studies showed that the mechanical properties of CNTs are largely affected by these engineering issues.

In general, there are three types of CNTs including SWCNT, DWCNT and MWCNT. Each one has a different geometric structure and mechanical properties, which depend on the processes of fabrication and the number of graphene layers in their structures.

The first type consists of a single layer of graphene, whereas the second and third types consist of more than one layer, which have the cylindrical geometric shape of graphene sheets with the bonds between layers held together by van der Waals forces (Bethune et al., 1993; Dresselhaus et al., 1995; Thostenson et al., 2001). Moreover, according to the rolling angle configuration of graphene networks, there are three chiralities that can be classified into three types: armchair, zigzag and chiral, as shown in Figure 3.

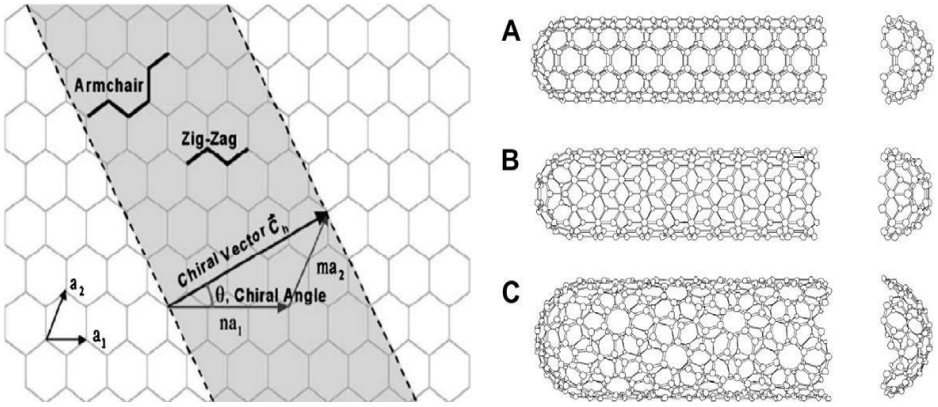

Figure 3 Schematic diagram of hexagonal graphene networks describes three types of chiralities (A: armchair; B: zigzag; C: chiral) (Dreselhaus et al., 1995; Thostenson et al., 2001).

Each chirality is described by the chiral vector $Ch=na_1+ma_2$ where integers (n,m) are represented by the number of steps for both unit vectors (a_1,a_2) of the hexagonal lattice (Dresselhaus et al., 1995; Thostenson et al., 2001). Furthermore, the arrangement of carbon atoms around the circumference of the nanotube is defined by the values of (n, m) if n=m, which is termed an 'armchair', whereas if m=0, it is described as a 'zigzag', otherwise, it is known as a chiral. Every layer of the multi-walled carbon nanotube (MWCNT) has a variety of chiralities. These complications related to the orientation of the nanotube could have a tremendous effect on the physical properties of the CNTs.

Ideal CNTs possess unique and excellent mechanical properties with the elastic modulus of the nanotubes having been estimated as 270-950 GPa and experimentally calculated tensile strength of between 11-63 GPa (Yu et al., 2000). These unique properties have been linking the CNTs to be used in a wide range of mechanical engineering applications (Ma et al., 2019).

However, the mechanical properties of CNTs are sensitive to being affected by the structure of nanotubes and Nano-dimensions, besides the chemical and physical bonding of the graphene network. (Collins and Avouris, 2000; Thostenson et al., 2001; Thostenson and Chuo, 2006).

Here are some examples, Thostenson et al. (2001), reported that the morphological properties of CNTs represent a great degree of variability as an example of the existence of unstable diameters

in nanotubes and multiples of chiralities (i.e. zigzag, armchair) in graphene structure of nanotubes. Therefore, this produces a challenge in understanding the exceptional properties during the stages of preparing or applying CNTs in structural and functional composites. This is because of the lack of information related to control dimensions such as length, diameter and chirality, as well as the geometrical shape or configuration of CNTs. As an example SWCNT are capped at the end and consist of one layer of graphite. The bamboo structure is an extremely good example of the MWCNT. They are composed of graphite assembly tubes, with the basic structural parameters related to the outer and inner diameters, number of layers, generation-induced configuration, in addition to the structural arrangement of graphite layers.

As a result of non-stability in the chemical and physical bonding between the graphene network along the nanotube, such as the rolling angle configuration of graphene (i.e. zigzag, armchair), nanoscale size (i.e. aspect ratio), the mechanical properties of conventional carbon nanotubes (i.e. stiffness) are significantly affected by these geometric imperfections (Li and Chou, 2003) (see Figure 4 for further details).

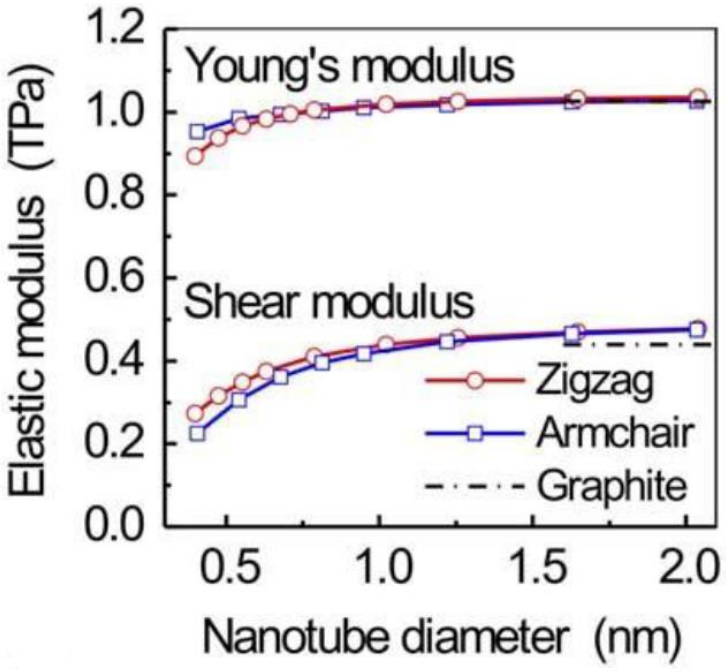

Figure 4 The relationship between diameter sensitivity and shear and elastic modulus of the CNTs estimated by molecular structural mechanics (Li & Chou, 2003).

These engineering issues may affect the efficiency of their use in advanced engineering applications, particularly in the manufacture of NP and HFRP (Wicks et al., 2014; Gojny et al., 2005; Li and Chou, 2003; Hernandez et al., 1998; Lu, 1997; Krishnan et al., 1998).

These facts could be one of the principal reasons for using other nanomaterials and justifying that as much as possible. A further reason is their high cost, particularly in SWCNT (Gkika et al., 2017), which currently led to limiting their use in engineering applications as reinforced material in the manufacture of NP. Therefore, researchers recently started to create new a generation of alternative conventional carbon nanomaterials, such as novel fibre nanotubes supported with the premium and unique structure of graphene layers with excellent mechanical properties and good surface area (Iwahori et al., 2005), that can be applied in the manufacture of advanced composites. Another alternative generation is GNP. The main advantages of this type of carbon nanomaterials are that it is inexpensive, has excellent mechanical properties and a high surface area (Gkika et al., 2017; Li et al., 2018). These two carbon nanomaterials could be more effective in reinforcing the mechanical properties of advanced polymer composites than conventional carbon nanotubes. Therefore, they have been used in the current work.

2.2.1 CNTs/polymer nanocomposites

Extensive studies have been undertaken by researchers to produce various types of polymer nanocomposites (NP) reinforced conventional carbon nanotubes, which can be used in advanced structural applications, with full potential applications. Nevertheless it is well-known that the previous studies had failed (Gkikas et al., 2012; Tang et al., 2011; Ayatollahi et al., 2011; Gojny et al., 2005; Ogasawara et al., 2004; Frogley et al., 2003; Loos et al., 2008; Zhou et al., 2007). The main obstacles that impeded most of these studies were difficulties in achieving the alignment between the nanotubes and polymer resins due to high nanoscale (i.e. high aspect ratio) and complete dispersion of tangled CNTs into the polymer matrix as a result of the influence of surface and van der Waals forces. Furthermore, the drawbacks that exist in nanocomposites may effect the interface property between the matrix and nanotubes. Thus, this decreases the mechanical properties of nanocomposites (Gkikas et al., 2012; Frogley et al., 2003).

Here are a several examples, which address these issues. Gkikas et al. (2012), have used MWCNT to improve the tensile properties of epoxy resin. The results showed an increase in tensile strength and a reduction in elasticity properties at low weigh content (i.e. 0.5 wt.%). The reduction in this property could be relevant to mechanical interfacial property between the matrix and the fillers.

Ogasawara et al. (2004), enhanced phenyl ethyl terminated polyimide by MWCNT that have lengths of less than 100μm and diameters ranging from 20-100nm. Mechanical blending was used to produce NP. The summary of the results explained that there is an improvement in tensile modulus. Meanwhile, there is a decrease in tensile strength. (Frogley et al., 2003), illustrated by the experimental study, which showed in the silicon-based elastomers enhanced with MWCNT,

whilst there is a good increase in the elastic modulus of nanocomposites and a reduction in the ultimate strength. Furthermore, the Raman spectroscopy experiments demonstrated that there is a loss in the load transferred to the CNTs by a strain of approximately 10-20%. This reduction may refer to the weakness of the effective interface between two phases.

Therefore, use of chemicals and dispersant solvents and high advance techniques (i.e. extruder) are probably necessary for such types of carbon nanomaterials to achieve better alignment or dispersion of SWCNT and MWCNT (Tang et al., 2011; Gojny et al., 2005; Sun et al., 2008; Cho and Daniel, 2008; Prashantha et al., 2009). Table 1 reveals various examples of the effect of CNTs on the strength and stiffness properties of NP concerning previous experimental studies. Most of these studies demonstrated moderate improvements in strength and stiffness properties, as the CNTs have a tendency to create clusters in nanocomposites and difficulty in achieving alignment between the nanotubes and matrix (Ma et al., 2010; Gojny et al., 2005; Ayatollahi et al., 2011; Tang et al., 2011). That is why use of alternative carbon nanomaterials such as novel fibre nanotubes (i.e. CSCNT) could be more efficient in reinforcing the mechanical properties of NP. These can be used instead of conventional carbon nanotubes probably due to the lack of difficulties at dispersing them in the matrix and have an excellent resistance structure (Yokozeki et al., 2012; Iwahori et al., 2005).

.

Table 1 Strength and stiffness improvements of CNTs/polymer nanocomposites.

Matrix	Nano filler type	Weight content	Process	Maximum strength (MPa), improvement (%)	Maximum elastic (GPa), improvement (%)	Test method	Ref.
Epoxy (Araldite LY 564 and Aradur 2954)	MWCNT	0.5 wt.%	Sonication	(+25%)	(-4%)	TS	Gkikas et al., 2012
Epoxy (Epon 862)	MWCNT	0 wt.%	Ultrasonic irradiation mixing/high mechanical stirring	93.5	2.46	FS	Zhou et al., 2007
		0.1 wt.%		109(+16%)	2.54(+3%)		
		0.2 wt.%		115(+22%)	2.60(+5%)		
		0.3 wt.%		121(+29%)	2.65(+7%)		
		0.4 wt.%		113(+20%)	2.75(+11%)		
Epoxy (not mentioned)	CNTs	Base(0)		140	3.43	FS	Ma et al., 2010
		-	Ultra-sonication In bath water	144(+2%)	3.41(-1%)		
			Shear mixing	140(0)	3.36(-2%)		
			Probe sonication	143(+2%)	3.47(+1%)		
			Calendering	145(+4%)	3.65(+6%)		
Epoxy (bisphenol-A epoxy)	p-MWCNT	Base(0)		73.4	2.87	TS	Tang et al., 2011
		0.5 wt.%	High speed mixer/three roll milling	72(-2%)	2.89(+1%)		
	p-MWCNT	1 wt.%		66(-10%)	2.96(+3%)		
	f-MWCNT	0.5 wt.%		89(+21%)	2.88(+1%)		
	f-MWCNT	1 wt.%		90(+23%)	2.93(+2%)		
Polypropylene (PP)	MWCNT	Base(0)		28.2	1.28	TS	Prashantha et al., 2009
		1 wt.%	Extruder	33.2(+17%)	1.65(+26%)		
		2 wt.%		35.5(+25%)	1.73(+35%)		
		3 wt.%		36.8(+30%)	1.80(+40%)		

		5 wt.%		35.2(+25%)	2.2(+67%)		
Epoxy (ML-506)	MWCNT	Base(0)		68.4	3.15	TS	Ayatollahi et al., 2011
		0.1 wt.%	High mechanical stirring/sonication	72(+4%)	3.24(+2%)		
		0.5 wt.%		74(+8%)	3.51(+11%)		
		1 wt.%		72(+6%)	3.69(+17%)		
Epoxy (Epon 862)	p-MWCNT	Base(0)		64.1	2.76	TS	Sun et al., 2008
		1 wt.%	Sonication	74(+15%)	3.27(+18%)		
	f-MWCNT	1 wt.%		75(+16%)	3.49(+26%)		
Epoxy (DGEBA-based epoxy resin (L135i))	SWCNT	Base(0)		63.8	2.6	TS	Gojny et al., 2005
		0.05 wt.%	High shear mixing/sonication	66(+3%)	2.7(+3%)		
		0.1 wt.%		66(+3%)	2.7(+3%)		
		0.3 wt.%		67(+5%)	2.8(+8%)		
	DWCNT	0.1 wt.%		62(-2%)	2.8(+8%)		
		0.3 wt%		68(+6%)	2.9(+13%)		
		0.5 wt.%		68(+6%)	2.8(+8%)		
	f-DWCNT	0.1 wt.%		64(-1%)	2.6(0%)		
		0.3 wt.%		67(+5%)	2.9(+13%)		
		0.5 wt.%		69(+8%)	3.0(+14%)		
	MWCNT	0.1 wt.%		63(-1%)	2.8(+8%)		
		0.3 wt.%		63(-1%)	2.7(+6%)		
		0.5 wt.%		62(-4%)	2.6(0%)		
	f-MWCNT	0.1 wt.%		65(+1%)	2.8(+8%)		
		0.3 wt.%		64(-1%)	2.8(+8%)		
		0.5 wt.%		64(+1%)	2.8(+8%)		

2.3 Graphene nanoplatelets (GNP)

Graphene comprises individual nanoparticles, which consist of short stacks of graphene layers that have geometric platelets. Moreover, the fundamental structural geometry of each type of carbon nanomaterials is composed of a graphene network, as shown in Figure 5.

In general, there are different types of GNP depending on the number of graphene layers in their structure; namely, monolayer graphene, bilayer graphene and trilayer graphene. Each one of these types has different mechanical properties depending on the size and chemical bonding of graphene atoms (i.e. chirality), (Zhao et al., 2009; Wang et al., 2012).

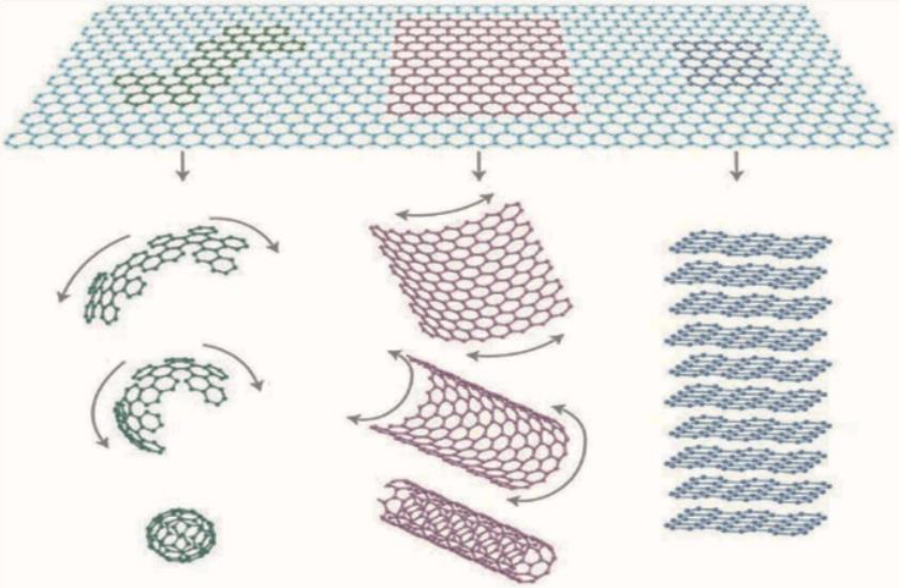

Figure 5 The geometric morphology for graphene nanomaterials in various structure forms and dimensions (0D, 1D, and 3D), (Geim and Novoselov, 2007).

The graphene production methods can be classified into several techniques, for instance, chemical vapour deposition, epitaxial growth, mechanical exfoliation, chemical oxidation-reduction, arc discharge, besides many other techniques. Therefore, the quality of graphene such as mechanical properties could be affected by these production methods (Wang et al., 2017; Qin et al., 2015; Wu, 2010; Zhang et al., 2014).

According to a study conducted by Lee et al. (2008), the mechanical properties of graphene, such as elastic modulus and tensile strength were experimentally estimated at about 1.0 TPa and 130 GPa respectively. These two values have been compared with computer simulation illustrating values of elastic modulus 1.05 TPa and tensile strength 110 GPa (Liu et al., 2007). However, these two properties are more rigid and stronger than other carbon nanomaterials. Table 2 demonstrates the mechanical properties of different types of graphene measured by atomic force microscope (AFM) method.

Table 2 Tensile and elastic modulus of different types of graphene measured experimentally by atomic force microscope (AFM) method.

Graphene type	Mechanical properties		Method measure	References
	Tensile strength (GPa)	Elastic modulus (TPa)		
Monolayer graphene	130±10	1±0.1	AFM	Lee et al., (2008)
Monolayer graphene	130	1.02	AFM	Lee et al., (2009)
Bilayer graphene	126	1.04		
Trilayer graphene	101	0.98		

Due to these excellent mechanical properties as well as high physical properties (i.e. high surface area 750m^2/g) which magnify the characteristics of nanotubes and low cost, it has been used in a wide range of advanced engineering applications (Mittal et al., 2015; Wang et al., 2016; Gkika et al., 2017), (see Figure 6 for further details).

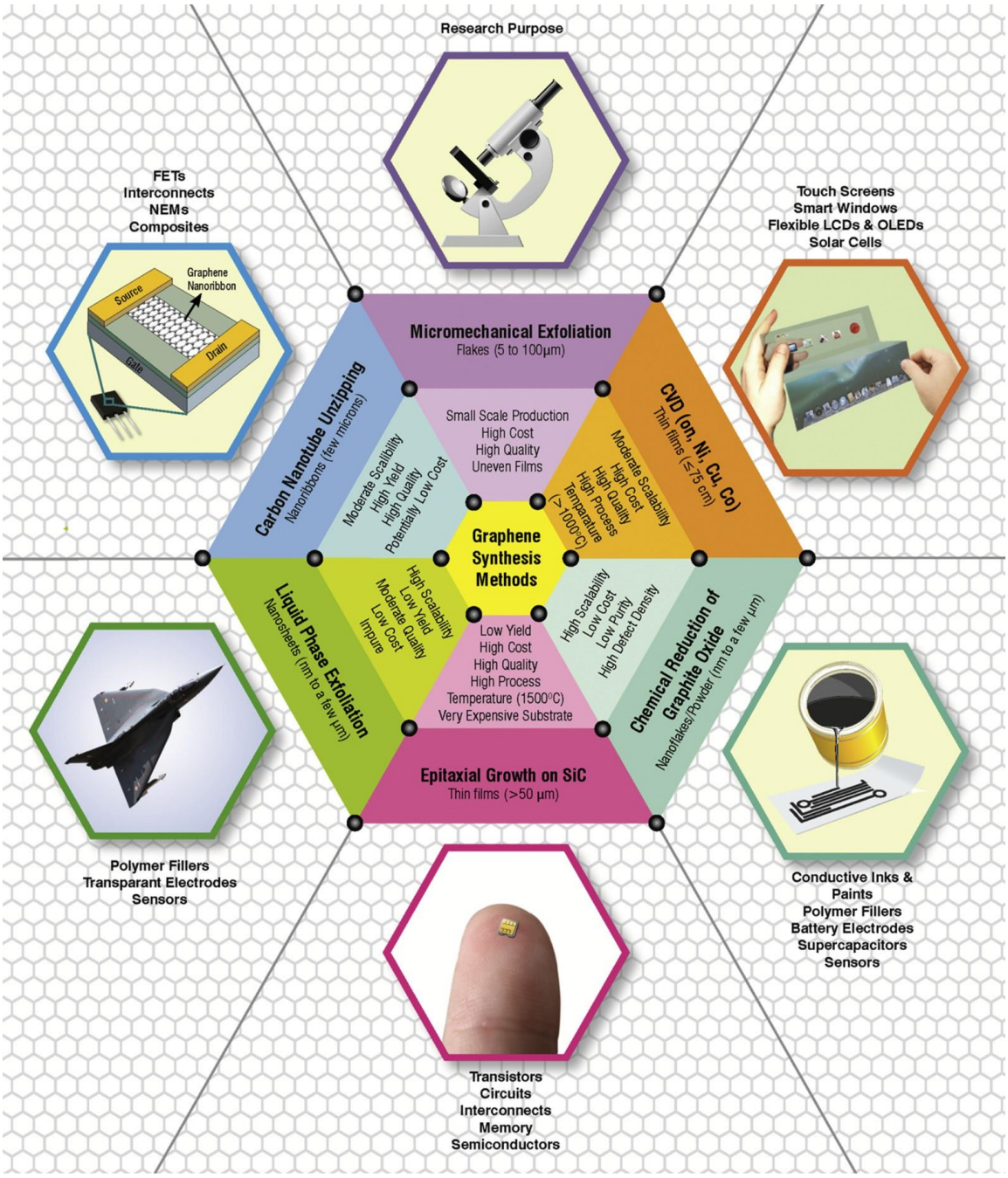

Figure 6 Schematic diagram showing the production methods of graphene nanosheets and their advanced applications in various industrial fields (Mittal et al., 2015).

Therefore, graphene has recently attracted more attention from numerous researchers who wish to use it in advanced composites structures, instead of conventional carbon nanotubes (Li et al., 2018; Bhattachaya et al., 2016). For these reasons, it has been selected to reinforce the mechanical properties of novel polymer composites in the current study.

2.3.1 GNP/polymer nanocomposites

There is a high demand to create advanced composite materials that have optimum physical properties, which could be used in various engineering applications. The extraordinary mechanical properties of graphene have made it one of the most effective nanomaterials that can be used as reinforced nanofiller in polymer matrix for manufacturing novel nanocomposites with an improved performance and superior quality (Chandrasekaran et al., 2013; Du et al., 2017).

However, many studies have been conducted by researchers to improve the mechanical properties of the graphene reinforced nanocomposites. These properties are tensile strength, stiffness, toughness, hardness, wear, buckling resistance and fatigue. They have been prepared by the use of different mechanical dispersion processes with or without chemical solvents as well as at various weight concentrations. These are completed in order to promote these mechanical properties for optimal performance, when used in industrial applications and moreover, to significantly reduce the synthesising cost as much as possible (Li et al., 2017; Hu et al., 2014; Qin et al., 2015; Chandrasekaran et al., 2014; Potts et al., 2011). The reported improvements in strength and stiffness properties of the graphene nanocomposites for previous studies are listed in Table 3. Regardless of the weight content of graphene, type of graphene used, polymer used and manufacturing process, significant improvements in the reported results are related to these two properties. The percentage of strength improvements reached 85%, while the stiffness improvement was 79% (Abdullah and Ansari, 2015). Certain reported results displayed a reduction in these properties, which may indicate the agglomeration of nanoparticles in the matrix (Yasmin et al., 2006; Shen et al., 2013)

Table 3 Strength and stiffness improvements of GNP/polymer nanocomposites.

.Matrix	Nano filler type	Weight content	Process	Maximum strength (MPa), improvement (%)	Maximum elastic (GPa), improvement (%)	Test method	Ref.
Epoxy diglycidyl ether of bisphenol A (DGEBA (GY6010))	EG	1 wt.%	Sonication	(-20%)	(+8%)	TS	Yasmin et al., 2006
			Shear	(-7%)	(+11%)		
			Sonication & shear	(-6%)	(+15%)		
Epoxy (not mentioned)	GNP	Base(0)		7	0.12	TS	Abdullah & Ansari, 2015
		1.5 vol.%	Mechanical mixer	13(+85%)	0.17(+45%)		
		6 vol.%		8(+7%)	0.21(+79%)		
PA6-elastomer	GNP	Base(0)		73	1.62	TS	Thanh et al., 2014
		10 %	Brabender	83(+13%)	1.89(+17%)		
Epoxy diglycidyl ether of bisphenol A DGEBA (GY6010))	Graphite platelets	Base(0)		34	3	TS	Yasmin & Daniel, 2004
		2.5 %	Magnetic stirrer	41(+21%)	3.3(+10%)		
		5 %		37(+9)	3.8(+25%)		
Poly (vinylalcoholl) PVA	Graphene powder	Base(0)		114	0.57	TS	Surudzic et al., 2016
		0.01 %	Solvent & sonication	178(+56%)	0.69(+21%)		
Epoxy (EPO-622)	GNP	Base(0)		54.9	-	TS	Shen et al., 2013
		0.25 wt.%	Solvent, mechanical stirring & sonication	66(+20%)	-		
	GNP	Base(0)		106	2.2	FS	
		0.25 wt.%	Solvent, mechanical stirring & sonication	116(+9%)	2.5(+12%)		
		1.5 wt.%		97(-9%)	2.6(+19%)		

Epoxy (DER 331)	GNP	0.2 vol.%	Stirring & sonication	(+40%)	(+16%)	FS	Phua et al., 2016
Epoxy (Epon44)	f-GNP	Base(0)		49.5	1.5	TS	Zhang et al., 2014
		0.3 wt.%	Sonication and centrifugation	72.4(+46%)	2.0(+31%)		
	GNP	0.5 wt.%		56.9(+14%)	1.7(+14%)		
Epoxy (Araldite LY556)	f-GNP	12 wt.%	Sonication and calendaring technique	(+11%)	(+50%)	FS	Moriche et al., 2016

However, these improvements could be more efficient compared with nanocomposites reinforced with conventional carbon nanotubes (Li et al., 2018; Surudzic et al., 2016; Abdullah and Ansari, 2015; Moriche et al., 2016; Li et al., 2017; Thanh et al., 2014; Shen et al., 2013; Domun et al., 2015; Rafiee et al., 2009; Rafiee et al., 2010; Yavari et al., 2010; Yasmin and Daniel, 2004). For example, Rafiee et al. (2010), illustrated that the addition of 0.125wt.% from graphene into the epoxy resin is sufficient to enhance the mechanical properties of graphene nanocomposites, such as elastic modulus and tensile strength by approximately 50% and 45% respectively. Moreover, these improvements are more efficient compared with nanocomposites reinforced by conventional carbon nanotubes.

In general, several factors could affect the alignment or dispersion process in the manufacture of graphene reinforced nanocomposites, for example type of graphene used, weight content, type and rheological properties of polymer resin (i.e. viscosity) and orientation of nanosheets into polymer. Hence, these can affect the performance of the interference region precisely, and the transmission of mechanical forces between the nanosheets and matrix into this region.

Many studies have addressed these issues raised by researchers to investigate their effect on the mechanical properties of nanocomposites such as strength and stiffness (Costa et al., 2017; Lin et al., 2013; Yasmin and Daniel 2004; Potts et al., 2011; Ma et al., 2010; Thostenson et al., 2005; Phua et al., 2016; Moiche et al., 2016).

Here are several examples: Costa et al. (2017), used multifunctional carbon nanomaterials, few-layer graphene (FLG), graphene nanoplatelets (G-NPL), graphene oxide (GO), reduced graphene oxide (rGO) and single-walled carbon nanohorns (SWCNH) to produce NP. Their results illustrated that the type and weight of content fillers could substantially affect the performance of nanocomposites. Yasmin and Daniel (2004), used two levels of graphite weight content; 2.5 wt. % and 5 wt. % to enhance the mechanical properties of the epoxy resin. Moreover, the tensile strength increased by 21% and 9%, respectively. Liang et al. (2009), illustrated that the improvement in the interfacial adhesion of graphene/PVA nanocomposite leads to an increase in mechanical properties of the nanocomposite. Li et al. (2018), used multifunctional nanofillers to manufacture molecular models of polymer matrix (i.e. polymethyl methacrylate (PMMA)) nanocomposites reinforced with graphene and conventional carbon nanotubes at the same weight content. To conclude, the results indicated that mechanical properties of graphene/PMMA nanocomposites, such as strength and stiffness higher than that of CNT/PMMA nanocomposites. Lee et al. (2012), confirmed that functionalised graphene sheets/epoxy composites can be subjected to composite cry tank in industrial applications. The results of this work showed that there is a significant enhancement in the mechanical properties

of epoxy nanocomposite. Cho et al. (2007), demonstrated the mechanical properties of epoxy nanocomposite are modified with randomly distributed graphite nanoplatelets by using multi-scale analysis, such as the Mori-Tanaka approach in conjunction with molecular mechanics. In conclusion, the results explained that the mechanical properties of nanocomposites, for instance modulus are exceptionally sensitive to variations in the direction of graphene nanosheets or plane into the polymer and nano-size (i.e. aspect ratio).

Lin et al. (2015), used graphene oxide nanosheets (GONS) to improve the mechanical properties of cyanate ester resin, composited by using the solution intercalation method. Their experimental results explained that there are good improvements for both tribological properties such as friction and wear resistance, as well as mechanical properties such as flexural strength and they have an impact on the fracture strength and hardness at different concentration ratios ranging from 0.25 wt.% to 1.25 wt.%. Abdullah and Ansari (2015), illustrated the effect of the graphene oxide on the mechanical properties of epoxy resin. The outcome of their investigation revealed that there is promotion in mechanical properties, such as tensile and modulus at 1.5 vol. %.

Phua et al. (2016), used graphene to prepare epoxy nanocomposites, with their results showing improved flexural strength of about 40% at 0.2 vol. %. Interestingly, Moriche et al. (2016), applied two types of mechanical dispersion processes, such as sonication and the calendaring technique to produce functionalised graphene reinforced epoxy nanocomposite at high weight concentration (i.e. 12wt.%) and moreover, to investigate the effect of modified matrix with graphene on the mechanical properties of fibre composites. To conclude, the nanocomposites were prepared successfully and their results showed, great improvement in flexural modulus and roughly in flexural strength and reduction in flexural strength after the addition of the modified matrix to the glass fibre reinforced polymer composites (GRP). The reason behind this reduction could be related to mechanical interfacial properties between the modified matrix and fillers.

To date, very few researches have focused on optimising the dispersion degree of the GNP in the polymer resins, in order to create high interlocking between graphene and matrix even more, without the need to use additional chemicals or dispersant solvents as much as possible and to investigate the effect of these optimised nanocomposites on the mechanical properties of CFRP.

2.4 Carbon nanofibers (CNF)

Carbon nanofiber is one of the fundamental carbon nanomaterials, which has been newly developed for scientific research and advanced engineering applications. In general, carbon nanofibers have a diameter size ranging from 50-200 nm, whilst their mechanical properties, such as tensile and modulus were estimated experimentally to be 3.5 GPa and 172 GPa

respectively (Arshad et al., 2011; Thostenson et al., 2005). The strength and modulus of microscale fibre nanotubes are not constant, because each one depends on the manufacturing process of fibre nanotubes (i.e. chemical vapour deposition, electrospinning method, etc.) and their morphological properties (i.e. structure, nanoscale), besides mechanical measurement methods (Jeon et al., 2016; Ozkan et al., 2010).

However, there are two types of carbon fibre nanotubes. The first type has an irregular structural build, like the bamboo-like structures, shown in Figure 7a (Merkulov et al., 2000). The second type is the one that possesses a high content of graphite layers and are nested within each other to create regular hollow shells which have a conical shape. As an example, Figures 7b and c show the geometric structures of cup-stacked nanotubes (Endo et al., 2002; Endo et al., 2003).

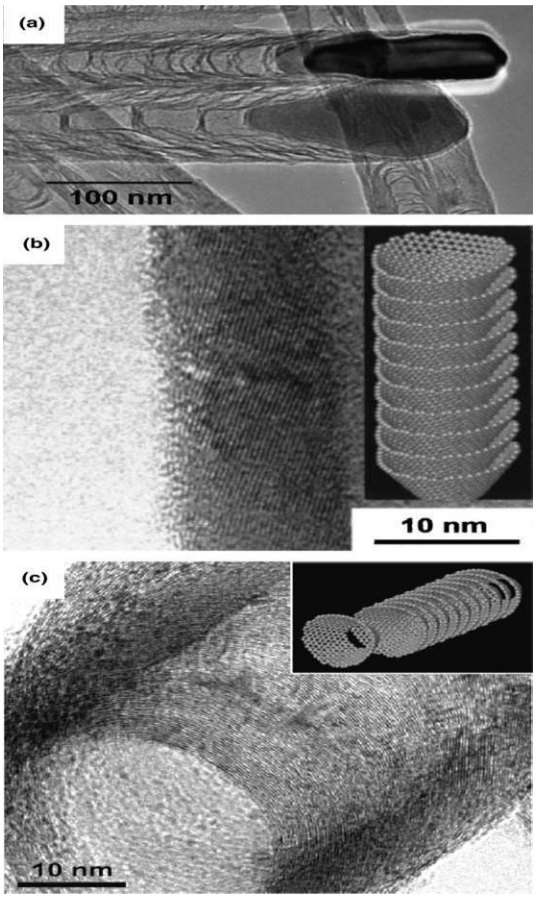

Figure 7 TEM images showing the regular and irregular geometric structure of fibre nanotubes: (a) disordered structures (Mekulov et al., 2000), (b) cup-stacked carbon nanotubes (CSCNT) (Endo et al., 2002) and (c) bundles of stacked layers in CSCNT (Endo et al., 2003).

There are the two principal techniques that are applied to prepare fibre nanotubes: catalytic thermal vapour deposition growth and electrospinning (Jeon et al., 2016; Shi-sheng et al., 2013; Feng et al., 2014; Zhang et al., 2014).

The first technique is predominantly used to produce vapour-grown carbon nanofibers (CNF) which are also known as cup-stacked carbon nanotubes (CSCNT). These nanofibers have excellent mechanical properties and distinctive morphologies that relate to uniform structural build, a conical geometric shape and the contents of graphite layers. These novel characteristics are desirable when such types are used in enhancing the mechanical properties of NP (Landani et al., 2015; Iwahori et al., 2005; Yokozeki et al., 2009; Feng et al., 2014)

The fibre nanotubes synthesised by the electrospinning technique were used as the main reinforcements in the manufacture of electrode materials, such as battery or supercapacitor due to having high quality transport properties and good structural form. Furthermore, in most cases to improve the performance of fibre nanocomposites, additional thermal treatments are probably required (Ji et al., 2011).

It is recognised that the quality of NP is highly dependent on the properties of fibre nanotubes. Many studies have been undertaken to produce fibre nanotubes with optimum morphological (i.e. superior geometric structure, nanoscale) and mechanical properties and moreover, to investigate the effect of these morphologies on the performance quality of fibre nanotubes experimentally and analytically. (Wei & Srivastava 2004; Sandler et al., 2003; Finnegan et al., 2003; Shi-sheng et al., 2013; Lu et al., 2012; Ozkan et al., 2012; Gong et al., 2014).

The following are some examples: Wei & Srivastava (2004), illustrated the effect of a change in morphologies on physical properties, by using numerical simulation software, for example molecular dynamics simulations. In addition, their study showed the change in mechanical properties of CSCNT, particularly the axial modulus of nanofiber depends on the tangential angle of the shell, where the large angle is measured from the axial direction. This demonstrated that there is an increase in this property compared to the one which has a small tangential angle. In addition, the scatter in the experimental results, particularly, the physical properties refers to the complete wide-ranging morphology of the carbon nanofibers, processing mechanism, characterisation, functionalisation and other aspects.

Sandler et al. (2003), produced fibres from semi-crystalline enormous-performance poly (ether ketone) (PEEK) at different contents of weights of up to 10% from the carbon nanofibers. Their experimental results illustrated that evaluating performance depends on understanding both the degree of crystallinity of the matrix and crystal morphology structure of the nanocomposite after the addition of the fibre nanotubes into the matrix. Shi-sheng et al. (2013), demonstrated the processes of a carpet structure composed of long and roughly aligned as well as pure degree CSCNT by the catalyst chemical vapour deposition (CCVD) method.

Gong et al. (2014), demonstrated the effective process CSCNT via catalytic carbonisation of polypropylene (PP) under a combination of halogenated compound and Nickel oxide (NiO) at a temperature of 700^0C. In addition, the effects of this approach on the physical properties, in particular thermal stability, besides morphologies, phase structure and microstructure was reported. The results revealed that low contents of halogenated compound made the surface-smooth CSCNT with graphene nanosheets inclined to the axis of the nanotubes at angles ranging from 21˚ to 25˚. As a consequence of these facts, the mechanical properties of CSCNT are scalable. Furthermore, studies are still continuing to obtain optimum geometric structures with excellent mechanical properties to rival conventional carbon nanomaterials (i.e. CNTs), which can subsequently be used for advanced engineering applications, such as in the manufacture of nanocomposites with superior quality.

2.4.1 CNF/polymer nanocomposites

Carbon nanofiber has been utilised to enhance the mechanical properties of both types of polymer resins. Thermoplastic such as polypropylene, polyvinylpyrrolidone (PVP), poly (ether sulfone), poly (ethylene terephthalate), polymethyl methacrylate (acrylic) and thermosets, such as epoxy resin, melamine formaldehyde and polyester resin.

Many experimental studies have been conducted by researchers to address the mechanical properties of nanocomposites reinforced with fibre nanotubes in terms of compressive, stiffness and strength, as well as the toughness properties and quality of performance (Iwahori et al., 2005; Zhou et al., 2008; Yokozeki et al., 2009; Bal, 2010; Sun et al., 2011; Bal & Saha, 2014; Barrena et al., 2014). Bal & Saha (2014), investigated the effect of multifunctional nanofillers, conventional carbon nanotubes and fibre nanotubes on mechanical properties of epoxy resin, for instance bending stress and hardness. In conclusion, the results indicated a significant enhancement in these properties of epoxy nanocomposites.

Barrena et al. (2014), has used fibre nanotubes modified with chemical solvents to produce CSCNT/epoxy nanocomposites. The result showed high improvements in the tripological properties of nanocomposite, such as the wear resistance. Improvements in the reported results of the strength and stiffness properties of NP that are reinforced by fibre nanotubes in previous studies are listed in Table 4. Regardless of the synthesising process, weight content and type of polymer resin used, high improvements achieved 38% in strength property (Iwahori et al., 2005) and 60% in stiffness property (Bal, 2010). A number of these reported results illustrated a reduction in strength property, which may refer to the agglomerate of nanoparticles in the matrix (Sun et al., 2011).

To date, few studies have focused on the use of CSCNT in improving the strength and stiffness properties of NP. Therefore, further confirmation is required for the purposes of the design when it is used for advanced applications, particularly in the manufacture of HFRP.

Table 4 Strength and stiffness improvements of CNF/polymer nanocomposites.

Matrix	Nano filler type	Weight content	Process	Maximum strength (MPa), improvement (%)	Maximum elastic (GPa), improvement (%)	Test method	Ref.
Epoxy (EP827)	CNF	Base(0)		73	2.48	TS	Iwahori et al., 2005
		10 wt.%	Mechanical stirring	89(+22%)	3.60(+45%)		
		Base(0)		99	2.31	FS	
		10 wt.%		136(+38%)	3.3(+42%)		
Epoxy (SC-15)	CNF	Base(0)		59	2.78	TS	Zhou et al., 2008
		3 wt.%	Sonication and Mechanical stirring	64(+9%)	3.32(+19%)		
		2 wt.%		69(+17%)	3.17(+14%)		
Epoxy (araldite LY-556 based on Bisphenol A)	CNF	Base(0)		-	1.68	FS	Bal, 2010
		0.75 wt.%	Sonication and Mechanical stirring	-	2.69(+60%)		
Epoxy (Epon 862)	CNF	Base(0)		69	1.04	TS	Sun et al., 2011
		1 wt.%	Chemical solvents, Sonication and mechanical stirring	74(+8%)	1.22(+17%)		
		2 wt.%		62(-10%)	1.29(+24%)		

2.5 Comparison of CNTs & CNF

In general, carbon nanotubes (CNTs) and carbon nanofibers (CNF) are hollow structures. They have nanometres dimensions with different morphologies (i.e. geometric shape), physical properties and similar methods of production (Qian et al., 2002; Thostenson et al., 2005). In contrast, there are clear variables that essentially impact on their quality or performance and ability to be synthesised.

Carbon nanofibers are also known as cup-stacked carbon nanotubes (CSCNT). As mentioned previously, they have an individual morphology in which graphite layers are inclined from the axis of the fibre. Moreover, this excellent structure of CSCNT suggests the characteristic in the mechanical loads transfer between fibre nanotubes and matrix because it prevents the graphene layers sliding during loading (Iwahori et al., 2005; Endo et al., 2003; Wei & Srivastava., 2004).

There are several advantages to using CSCNT as enhanced fillers in polymer matrix; specifically, it is easier to disperse compared with other carbon nanomaterials (i.e. SWCNT or MWCNT) (Yokozeki et al., 2012), it is not complex in the processing stages, provides high physical properties, particularly mechanical properties, it is easier to employ in chemical treatments and to functionalise and furthermore, it is not expensive compared with other carbon nanomaterials in particular single-walled carbon nanotubes.

However, CNTs normally feature fibre diameters ranging from 1-30 nm, whereas CSCNT feature fibre diameters of between 50-200 nm (Thostenson et al., 2005). Both of these nanotubes exist in varying lengths and are estimated to be more than a hundred micrometres, basing on the feed stages and production methods. The variations in diameter range and geometric structures between both types of nanotubes appear to be significant. In the CNTs, because the high aspect ratio is very large, van der Waals forces are too strong in the graphene network of the nanotube, which create them in a cluster form until they are dispersed. This is why they frequently require the use of chemical dispersants, such as chemical or physical functionalisation approaches or other technical processes to separate their tangled agglomerate (Sahoo et al., 2010; Ma et al., 2010; Ma et al., 2009). Conversely, in the fibre nanotubes these forces are less influential, compared with CNTs. This specification which makes CSCNT is easier in relation to the dispersion process. Hence, it is inexpensive in regard to the manufacturing process (Yokozeki et al., 2012).

Based on these facts, the CSCNT seem cheaper and easier in comparison with the conventional carbon nanotubes and more favourable structure in the manufacturing of nanocomposites. Therefore, fibre nanotubes were selected to reinforce the mechanical properties of polymer composites instead of conventional carbon nanotubes in the present study.

2.6 Hybrid polymer nanocomposites (HNP)

A hybrid nanocomposite can be defined as a novel composite structure consisting of two or more types of nanoparticles in a common matrix. However, there are two reasons that researchers have been motivated to create such novel nanocomposites.

The first reason is due to the high cost of CNTs particularly SWCNT in contrast with other carbon nanomaterials, such as graphite, graphene sheets, black carbon and fibre nanotubes (Gkika et al., 2017). Consequently, this obstacle has limited their use in industrial applications, over the last decade. The second one is to promote the physical properties of NP (Ma et al., 2010).

HNP modified with two nanoparticles, each with different geometrical structures, nano-dimensions and physical and chemical properties was expected to be a good solution for these economic and engineering issues. Conversely, the combination of multifunctional carbon nanomaterials may induce the promotion of mechanical interfacial property between the polymer matrix and nanomaterials, resulting in their synergy properties within the matrix. Accordingly, this modern approach could increase the mechanical properties (i.e. strength and stiffness) of NP. Therefore, from then until today, the researchers still look for to find a good multifunctionality formula that can be used to develop the performance quality for novel nanocomposites (Liu et al., 2017; Al-Saleh, 2016; Chatterjee et al., 2012; Ma et al., 2009; Li et al., 2008).

The following are some examples: Ma et al. (2009), successfully manufactured a novel nanocomposite modified with two carbon nanomaterials (black carbon and conventional carbon nanotubes) in the polymer resin. The results confirmed that the mechanical properties are stable in novel nanocomposites after the combination of these nanomaterials. In addition, the outcomes explained that the conventional carbon nanotubes to carbon black decreases the percolation threshold. Likewise, this phenomenon may affect the ductility and the toughness of HNP.

Recently, a combination of graphene and conventional carbon nanotubes was used to reinforce the physical properties of polymer resins particularly mechanical properties (Liu et al., 2017; Al-Saleh, 2016; Wang et al., 2015; Li et al., 2013). Table 5 shows the effect of the combination of these two carbon nanomaterials on the strength and stiffness properties of HNP. Additionally, by employing the functionality formula (i.e. graphene and conventional carbon nanotubes) in the manufacture of HNP, there were noticeable improvements in the strength and stiffness properties of most of these previous studies due to difficulty in dispersing them together in the polymer resins (Chatterjee et al., 2012). The reason for this is because they have a tendency to re-agglomerate after they have been dispersed in the matrix. This undesirable phenomenon can affect the synergy property of carbon nanomaterials within the matrix. Furthermore, it affects the efficiency of loads transferred between matrix and hybrid nanoparticles into interface regions.

Accordingly, this behaviour diminishes the mechanical properties of the HNP. Therefore, use of alternative carbon nanomaterials, for example novel fibre nanotubes combined with graphene could be a good functionality formula in relation to reinforcing the strength and stiffness properties of HNP instead of conventional carbon nanotubes. It also can be more efficient at inducing the synergy property of combined nanomaterials within the matrix, which is applied in the present work.

Table 5 Strength and stiffness improvements of HNP.

Matrix	Nano filler type	Weight content	Process	Maximum strength (MPa), improvement (%)	Maximum elastic (GPa), improvement (%)	Test method	Ref.
50/50 PP/PE	Hybrid GNP/CNTs	Base(0)		25	-	TS	Al-Saleh, 2016
		1:4 (ratio)	Batch mixer	(+20%)			
Epoxy (1080S)	Hybrid CNTs/GNP	Base(0)		50	2.2	TS	Li et al., 2013
		0.5 wt.%	Roll milling	68(+36%)	3.1(+40%)		
Epoxy (EPIKOTE 828LVEL)	Hybrid CNTs/GNP	9:1 (ratio)	Solvent, Sonication, high pressure homogeniser, and 3-roll milling	-	(+17%)	FS	Chatterjee et al., 2012
Epoxy (EPO-622)	Hybrid CNTs/GNP	Base(0)		54.9	-	TS	Wang et al., 2015
		5:5 (ratio)	Solvent, homogeniser stirring, sonication, mechanical mixer	73.4(+34%)	-		
		1:9 (ratio)		67.0(+22%)	-		
		Base(0)		106	2.2	FS	
		5:5 (ratio)	Solvent, homogenizer stirring, sonication, mechanical mixer	128(+21%)	2.7(+22%)		
		1:9 (ratio)		134(+26%)	2.8(+24%)		

2.7 Strengthening and toughening matrix

Improvement of the micro-crack resistance and the mechanical properties of fibre polymer composites can be classified into two techniques; specifically, improving the material properties and tailoring the ply in construction (Kuwata & Hogg, 2011; Chan, 1991). The polymer matrix strengthening and toughening technique is the simplest method for enhancing the mechanical properties of polymer composites. However, strengthening and toughening the resin matrix with thermoplastic polymers frequently compromises the pristine in plane mechanical properties, under the static and dynamic loads (Greenhalgh et al., 2009).

Epoxy resins are commonly employed in many advanced industrial applications and have been considered as alternative polymer resins to advanced strengthening polymers because of the low cost and their generally good mechanical properties and environmental resistance. They have been increasingly used as they have high stiffness and strength, good chemical and corrosion resistance, low shrinkage in cure and high adhesion and dimensional stability. In spite of these premium properties, the epoxy resins in single phase suffer a weakness in their toughness and strength properties when using the matrix in the manufacture of advanced fibre composites. In promoting their performance via the addition of a second phase into the matrix, it became necessary to involve a wide range of advanced structural applications. Thus, rubber fillers have been used for this purpose (Greenhalgh et al., 2009; Tang et al., 2011). The drawbacks of such materials are a reduction in the stiffness properties of pristine epoxy resin, which hindered their use in industrial applications, in particular in the manufacture of advanced fibre polymer composites. A modern approach has been applied by engineers to solve such drawbacks, which include the use of rigid nanomaterials. Specifically, there has been interest in using conventional carbon nanotubes (i.e. SWCNT or MWCNT) over the past three decades (Gojny et al., 2005; Karapappas et al., 2009; Wichmann et al., 2006; Qin et al., 2007; Fan et al., 2008).

Recently, graphene and carbon fibre nanotubes were used for this purpose. Both of these carbon nanomaterials have proved their success in developing the strength and toughness properties of epoxy resins. Here are some examples: Zaman et al. (2011), illustrated that the addition of graphene into the epoxy resin led to improvement in the fracture toughness properties of modified matrix in the NP by approximately 104% at 4 wt. %. Chandrasekaran et al. (2014), reviewed the comparison of toughness properties pertaining to previous studies on the epoxy resins modified with various types of nanomaterials, as shown in Figure 21. As a result of this comparison, it appears that graphene is more actively involved in reinforcing the fracture strength property of modified epoxy in nanocomposites than other nanomaterials, in particular conventional carbon nanotubes.

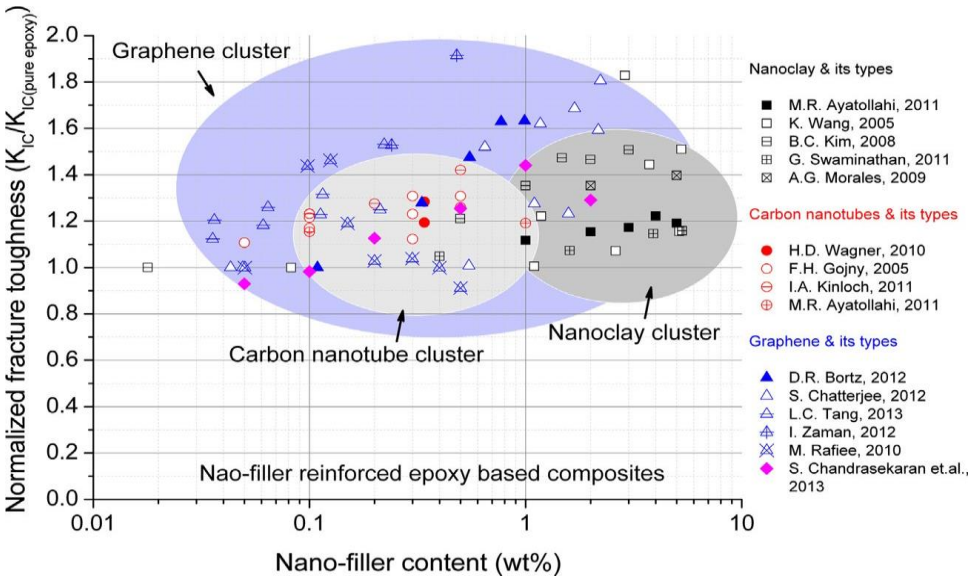

Figure 8 Comparison of fracture toughness property among different types of nanomaterials at various weight content (Chandrasekaran et al., 2014).

In a further study, Chadrasekaran et al. (2014), investigated the effect of the addition of multifunctional carbon nanomaterials (i.e. TRGO, GNP, MWCNT) on mechanical properties of epoxy resin. To conclude, the results revealed that graphene is the best carbon nanomaterial in improving the toughness properties of nanocomposites compared with MWCNT.

Furthermore, the study showed the fracture mechanism systems analytically, particularly in the graphene nanocomposite, such as crack pinning/bi-furcation mechanism of graphene through propagation crack, separation of graphitic sheets and shear failure, which are suggested as reasons for these improvements in the toughness properties of nanocomposites (see Figures 9 and 10).

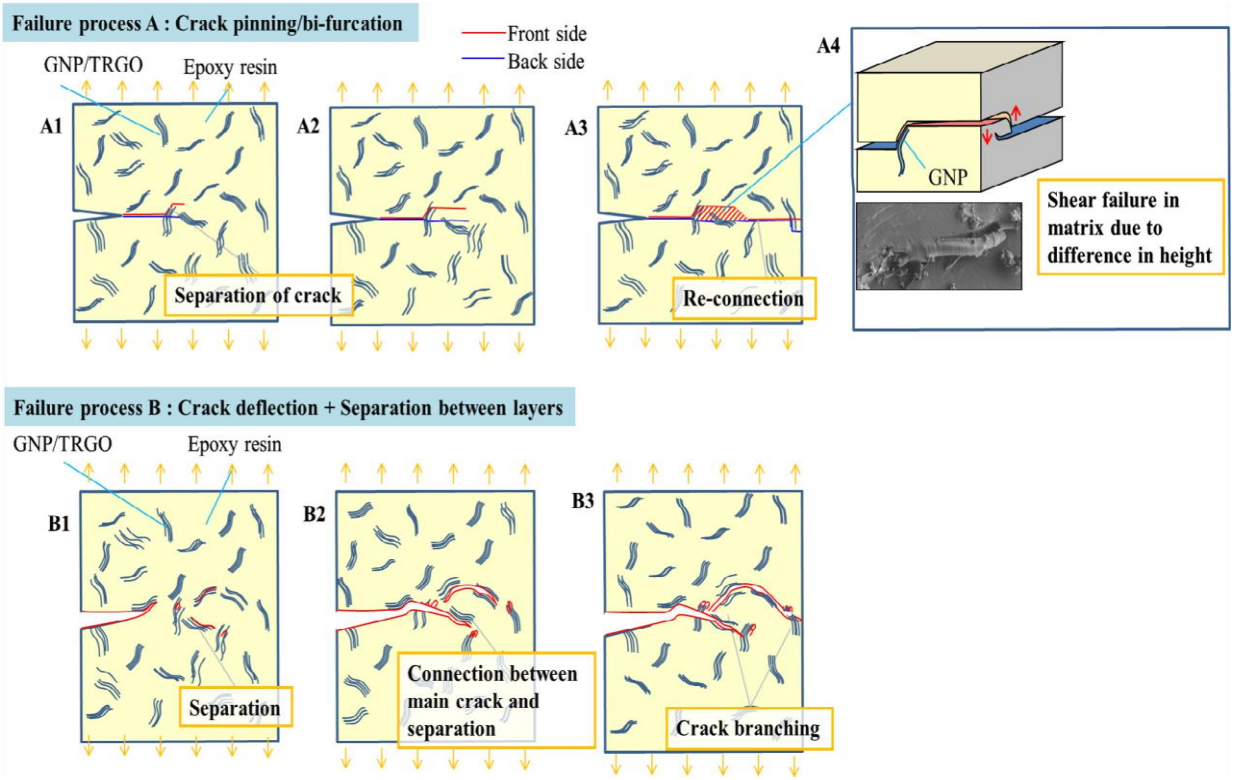

Figure 9 Schematic diagram shows the fracture toughness systems of GNP/TRGO polymer nanocomposite through crack propagation (Chandrasekaran et al., 2014).

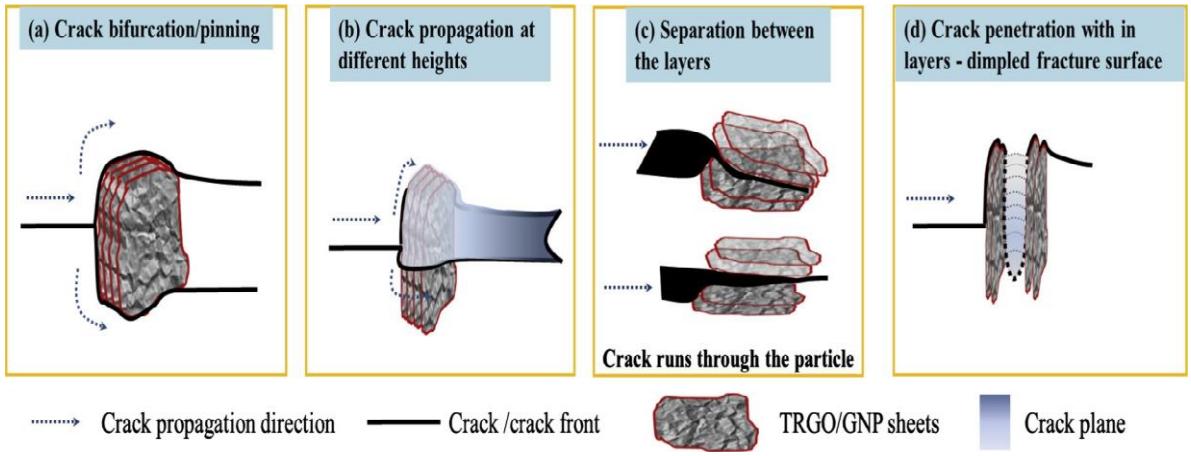

Figure 10 Schematic diagrams shows: the interactions mechanism of the crack tip with GNP/TRGO nanoplatelets (Chandrasekaran et al., 2014).

Further experimental studies included the use of novel fibre nanotubes to modify the strength and toughness properties of polymer resins. For instance, Zhou et al. (2008), investigated the effect of fibre nanotubes on the mechanical properties of epoxy resin sequentially and the use of its modified epoxy matrix to reinforce the mechanical properties for conventional carbon fibre composites. In conclusion, their results illustrated high improvements in toughness and tensile strength at 2 wt. % of nanofibers under static and dynamic loads. More recently, Landani et al.

(2015), investigated whether the addition of novel fibre nanotubes into the epoxy resin improves the fracture toughness property of the epoxy matrix as well as the carbon fibre composites. The results demonstrated significant improvement in the toughness property of the composites modified with nanofibers.

Therefore, the addition of graphene and carbon fibre nanotubes into the epoxy resins could be a practical solution for enhancing the strength and the toughness properties of these resins. It is also more efficient than conventional carbon nanomaterials. Sequentially, using this modified epoxy as reinforced matrix to improve the mechanical properties of conventional carbon fibre composites, where impregnation of the strengthened and toughened matrix into the fibre network would improve the degree of adhesion or the mechanical interfacial property between the fillers and the matrix. Hence, it may lead to an improvement in the mechanical properties of HFRP (Zhou et al., 2006; Yokozeki et al., 2007), (see Figure 11 for further details).

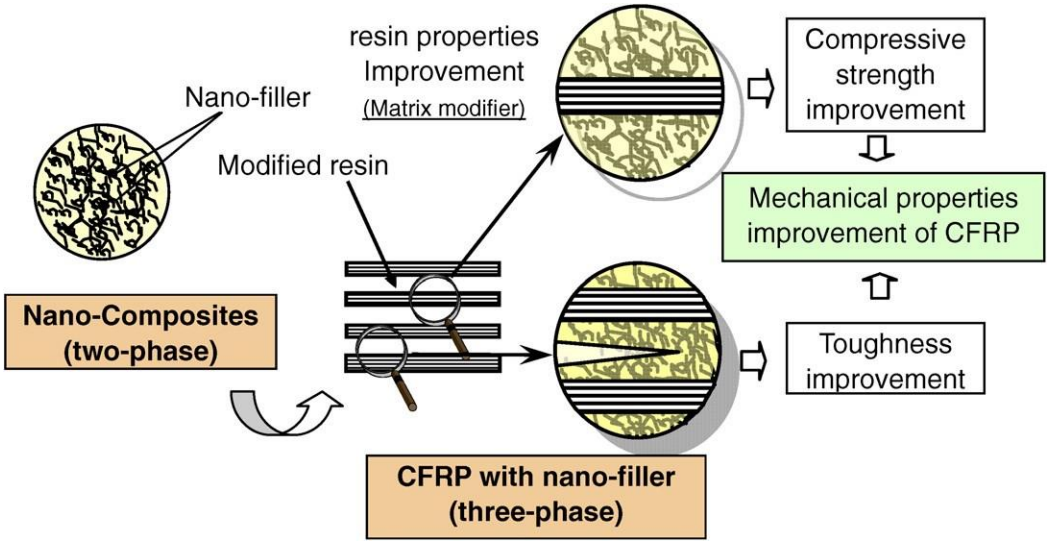

Figure 11 Diagram of the reinforced the mechanical properties of the CFRP via impregnation of the nanocomposite route (Yokozeki et al., 2007).

However, the previous approach has been promoted recently by researchers via a combination of two carbon nanomaterials (i.e. graphene and conventional carbon nanotubes) into the polymer resins. This approach indicated admirable improvements in the strength and toughness properties of epoxy polymers, resulting in the synergy property of two carbon nanomaterials within the matrix. For instance, Chatterjee et al. (2012), used a mixture of multifunctional carbon nanomaterials; GNP and CNTs to improve the strength and toughness properties of epoxy resin. The results illustrated excellent improvements, up to 77% in the toughness property of HNP. Moghadam and Taheri, (2014) investigated whether the combination of graphene and conventional carbon nanotubes into the epoxy resin increased the fracture toughness properties of modified epoxy in nanocomposites up to 75%. Nam et al. (2017), also used a mixture of two

carbon nanomaterials; namely, functionalised graphene oxide and conventional carbon nanotubes to manufacture HNP. The results showed high promotion in the mechanical properties of modified polymer in HNP, such as strength and toughness properties after the combination of 0.9wt % of nanosheets and 0.1wt. % of nanotubes. Interestingly, Wang et al. (2015), used combined carbon nanomaterials (i.e. GNP and CNTs) to modify the strength properties of epoxy resin, sequentially. Moreover, Wang et al. (2015), used the modified epoxy in improving the strength and toughness properties of conventional carbon fibre composites**.** The results showed excellent improvements in strength and toughness properties of HCFRP.

In general, the reasons which led to high improvements in the strength and toughness properties of these composites are possibly relevant to the fracture toughness behaviours of fillers into the matrix. For instance, peeling graphene nanosheet, bridging nanotube or nanosheet, crack distortion and crack pining had also been exhibited in the fracture morphology of graphene nanocomposites, which are basically similar to fracture mechanism systems in conventional carbon nanotubes. Furthermore, the combination of these multiple toughness systems concluded in hybrid polymer composites, such as pinning and pull-out nanofillers, crack pinning and bi-furcation mechanisms (Chadrasekaran et al., 2014; Landani et al., 2015; Yokozeki et al., 2007; Yokozeki et al., 2009; Wang et al., 2015; Menna et al., 2016; Thostenson et al., 2005; Wetzel et al., 2006). These dissipation energy systems have been proposed as having toughening and strengthening effects on novel polymer composites. However, the fracture mechanism systems of hybrid nanocomposite modified with two carbon nanomaterials were not completely translated in the previous studies (Wang et al., 2015; Kostageiannakopoulou et al., 2017). Therefore, this study will offer additional details in relation to the fracture toughness behaviours of the combined nanomaterials into composites.

To the best of my knowledge, the novel structure of fibre nanotubes was not combined with graphene to improve the strength and toughness properties of epoxy resin, which is expected to be more active than conventional carbon nanotubes. Thereafter, use of this novel matrix to promote the mechanical properties of CFRP in the present study.

2.8 Critical cases in manufacturing of NP

2.8.1 Dispersion

The dispersion of nanomaterials plays a key factor in influencing significant performance and the quality of NP. This critical issue was also considered as an immense challenge in the manufacture of NP. It is well-known that van der Waals forces are responsible for joining the graphite networks with each other, in nanotube or nanosheet layers. Therefore, such forces in the

atomic structure of nanoparticles require high quality techniques (i.e. extruder) to separate their tangled agglomerate into the matrix and in order to obtain optimum exfoliation and homogenous dispersion of the nanoparticles. In addition, chemical dispersants (i.e. BYK additives) may regularly be used for this purpose via the dispersion process of nanoparticles, particularly with MWCNT (Cho and Daniel, 2008; Sahoo et al., 2010; Hu et al., 2014). Further details about the dispersion of carbon nanomaterials will be discussed in this review.

2.8.2 Alignment

There are difficulties in controlling the distribution and orientation of nanoreinforcements into the polymer matrix, as a result of their nano-sized dimensions. Thus, this may affect the degree of their adhesion to the matrix. Furthermore, the mechanical interfacial properties are improved by modulating the properties of the interface regions, between matrix and fillers. Therefore, any weakness in this property could affect the performance of nanocomposites and their engineering applications. As a result, alignment of carbon nanomaterials (i.e. CNTs, CNF and GNP) with polymer matrix is too complex compared with micro-reinforcements, such as glass or carbon fibre (Thostenson et al., 2005). For these reasons, additional uses of chemical solvents are probably necessary to achieve the alignment between the reinforcements and the matrix (Punetha et al., 2017; Ma et al., 2010).

2.8.3 Rate of production vs cost

The rapid transformation in the manufacturing of structural composites from conventional fibre composites to advanced novel nanocomposites, is a clear demonstration of the evolution in science nanotechnology in terms of the conversion of size reinforcements from micro to nanoscale. This evolution is still continuous over time and indispensable. Therefore, the competition between companies has produced highly distinctive specifications of nanomaterials with the least cost possible (see Figure 12), which provides superior efficiency in advanced industrial applications (Gkika et al., 2017). While, the prices of raw nanomaterials are linked to their type and quality, and demand size and rate production increase, it is evident that the cost of nanomaterials may be expected to reduce dramatically with increased size applications.

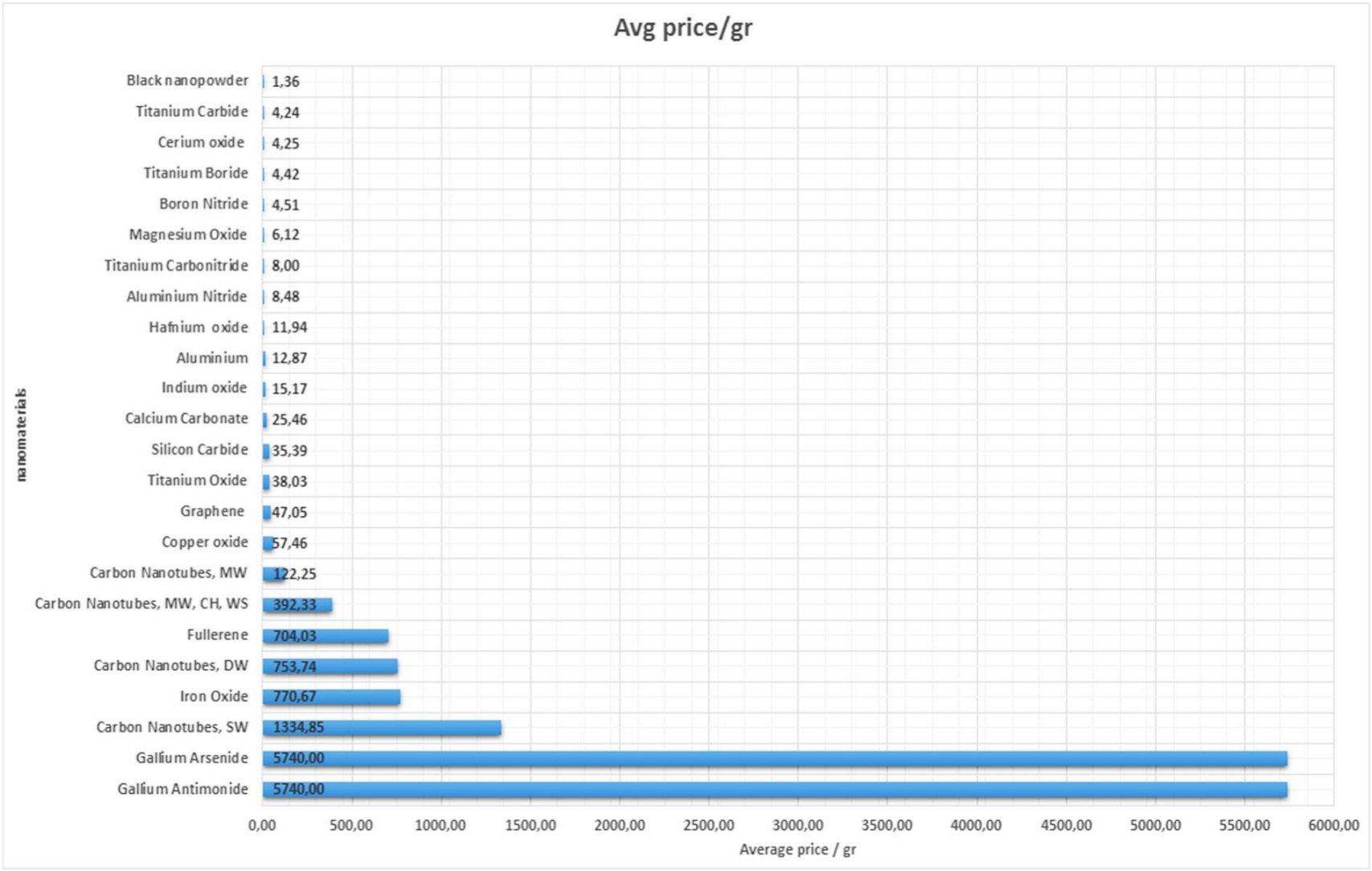

Figure 12 Average price (in euro) per gram for various types of nanomaterials (Gkika et al., 2017).

2.9 Mechanical interfacial properties of NP

Advanced polymer composites which transact with the behaviour of nanoparticles dispersion, thin sheets, fibres and other reinforcements are strongly affected by the properties of their interface. Furthermore, this region is sensitive to the morphological properties of these reinforcements, for instance sized dimensions and geometric design. Figure 13 reveals different designs and volumes in some reinforcement materials (Thostenson et al., 2005; Park and Seo, 2011).

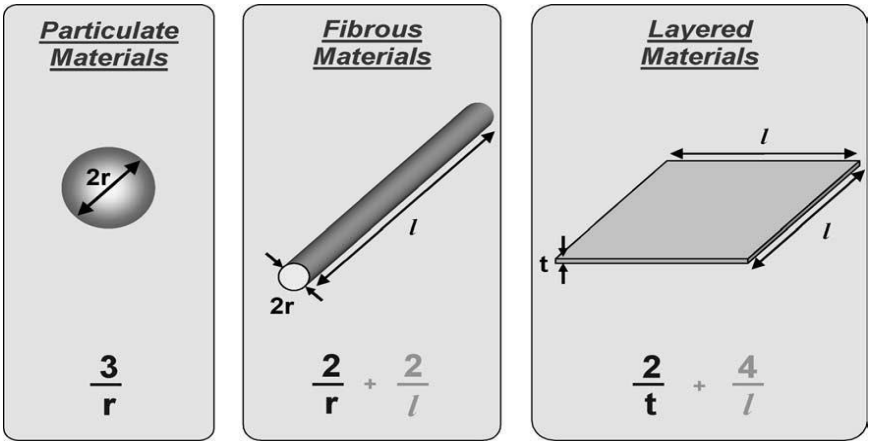

Figure 13 Geometric shape and (surface area/volume) relationship to vary the structure of the reinforcement nanomaterial (Thostenson et al., 2005).

In general, the performance quality in advanced polymer composites, such as NP s is relevant to the interfacial attraction between nanoparticles and polymer matrix. To achieve a high contact area or adhesion between matrix and nanoparticles, they need to disperse and separate their bundles uniformly in the matrix (see Figure 14).

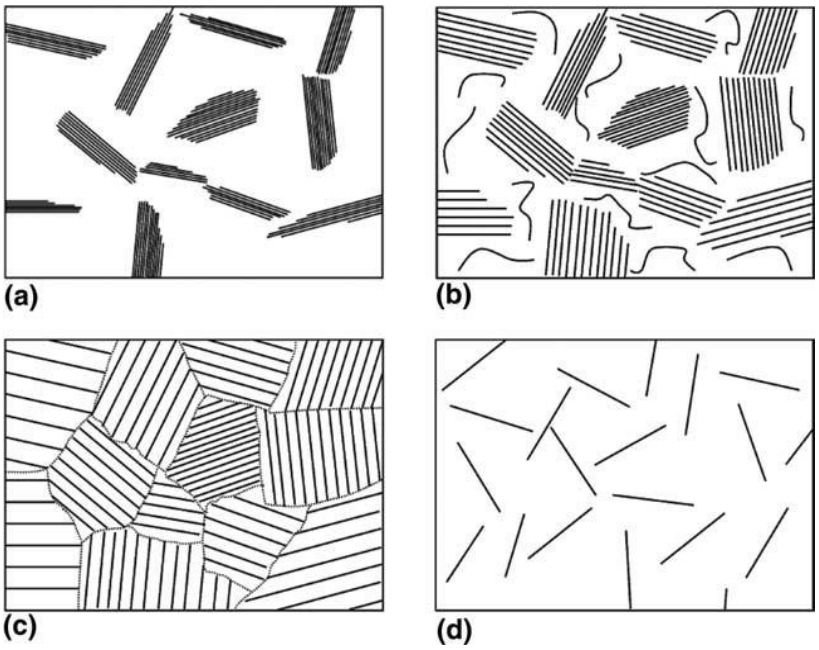

Figure 14 Nanocomposite model showing the dispersion process of clay/nanocomposite completely; a) tangled layers (undispersed), b) partly dispersed and intercalated, c) complete dispersed and intercalated, d) completely exfoliated and dispersed (Luo and Daniel, 2003).

Furthermore, additional processes, such as chemical modifications are regularly used as a precondition to achieve better dispersion or alignment between the side-walls of the nanoparticles and the polymer matrix. However, the modifications on the side wall or the structure of the nanoparticles can be classified into two main effective functionalisation approaches; chemical functionalisation and physical functionalisation.

Numerous studies have been conducted by researchers to address these issues concerning different carbon nanomaterials, such as conventional carbon nanotubes (Gojny et al., 2005; Sahoo et al., 2010; Ma et al., 2010), graphene (Moriche et al., 2016; Moriche et al., 2015; Hu et al., 2014; Bhattacharya, 2016; Tkaya et al., 2012) and novel fibre nanotubes (Barrena et al., 2014; Ji et al., 2011). Mechanical dispersion techniques, for instance the sonication technique was used for most of these chemical treatments. The addition of the chemical modifications may improve the surface area of the nanoparticles. Additionally, the generation of covalent chemical bonds between the nanoparticles and matrix reinforce their interactions to present optimum interfacial shear strength, which is more than that of van der Waals bonds. Hence, this technique can increase the properties of NP (Mittal et al., 2015; Criado et al., 2015; Barrena et al., 2014; Layek & Nandi, 2013; Chua and Pumera, 2013; Thostenson et al., 2001; Wagner & Vaia, 2004).

In spite of the additional chemical modifications, such as covalent or non-covalent, functionalisation is useful in maintaining the stability of nanoparticles (Sinnott, 2002; Fang et al., 2010). In contrast, the quantity of functionalisation, atomic structure and molecular weight

of the chemical function groups are sensitive variables that may have influenced the mechanical properties of the nanoparticles negatively. For example, Zheng et al. (2010), illustrated that the increase in the weight concentration of functional groups could significantly affect the elastic modulus of the graphene. Conversely, this property is not sensitive to their molecular weight. As a consequence, this method is not without flaws or complications because of the possibility of the re-agglomeration of nanoparticles as well as damage to the nanoparticles structure, which in most cases generates a weak interaction instead of a strong one between the matrix and nanoparticles (Esumi et al., 1996; Avila-Orta et al., 2009; Ma et al., 2010).

The physical functionalisation method based on the functionalisation of nanoparticles using the covalent or non-covalent method may provide beneficial chemical groups on the side wall or the surface area of the nanoparticle. Nevertheless, this technique can also produce damage to and defects on the geometric structure of the nanoparticles (Geng et al., 2008; Hirsch, 2002; Ma et al., 2010; Mittal et al., 2015). That is why the use of other processes, for example advanced mechanical dispersion techniques particularly combined dispersive techniques are probably better than chemical processes to achieve optimum dispersion of the nanoparticles and high interlocking between the nanoparticles and the matrix. Therefore, the dispersion processes of graphene and novel fibre nanotubes were performed as much as possible without the use of additional chemical solvents, in the present study.

2.10 Dispersion of carbon nanomaterials

One of the great challenges which hinders the manufacture of NP and can have an influence on their engineering performance is the dispersion process of carbon nanomaterials in the polymer resins. Furthermore, the dispersion process for each type of carbon nanomaterials into the resin is not equivalent because the specifications for each one are different. As examples: nanoscale, geometric structure, atomic structure, besides physical and chemical properties (Punetha et al., 2017; Yokozeki et al., 2012). Therefore, there is difficulty in controlling their distributions or orientations into the matrix and in separating their agglomerates completely, as well as the homogeneous dispersion of very small size particles with high aspect ratio (i.e. CNTs) and without damage, remain challenging due to the issues relating to surface effects, electro-static interaction and van der Waals forces. Therefore, the dispersion drawbacks of carbon nanomaterials, such as SWCNT and MWCNT as well as GNP are more complex compared with other carbon nanomaterials such as fibre nanotubes. This is because of their tendency to create agglomeration in the nanocomposite as mentioned previously which negatively effects the

physical and mechanical properties of NP (Yokozeki et al., 2012; Thostenson et al., 2005; Coleman et al., 2006; Jin et al., 2007; Potts et al., 2011; Prolongo et al., 2014).

The following are several clarifications: Hernandez et al. (2008), demonstrated only slight modifications in the elastic modulus and tensile strength of epoxy nanocomposites modified with two types of MWCNT, with a variety of aspect ratios. In this work, the results illustrated that there is a significant improvement for both the fracture toughness and impact resistance in specimens that have a high aspect ratio. However, the increase in the tensile strength and elastic modulus were limited to approximately 5% because of the weak bonds between the nanomaterials and polymer matrix in addition to the agglomeration phenomenon.

Lin et al. (2015), used the graphene as the filler in the silicone resin to manufacture NP. Their study demonstrated a good dispersion of graphene sheets in the silicone matrix composite. Furthermore, rheological properties of polymers, for example degree of viscosity and temperature were suggested as further reasons that can affect the dispersion processes. Thus, this factor may promote the performance of NP. Interestingly, Yokozeki et al., (2012) used multifunctional carbon nanomaterials in order to prepare MWCNT/epoxy and CNF/epoxy suspension by using the shear mixing technique. The main aim of their study was to investigate the influence of steady-state viscosity on these two nanomaterials, under different shear rates ranging of 0.1-100 S^{-1} and at different thermal conditions (see Figure 15). To summarise, results reported that the viscosity of the polymer resin and the temperature of the mixture at a high shear rate, could possibly be a key factor in obtaining the optimal dispersion of nanoparticles into the polymer matrix. In addition, the dispersion degree of the novel fibre nanotube into the matrix is better than the CNTs.

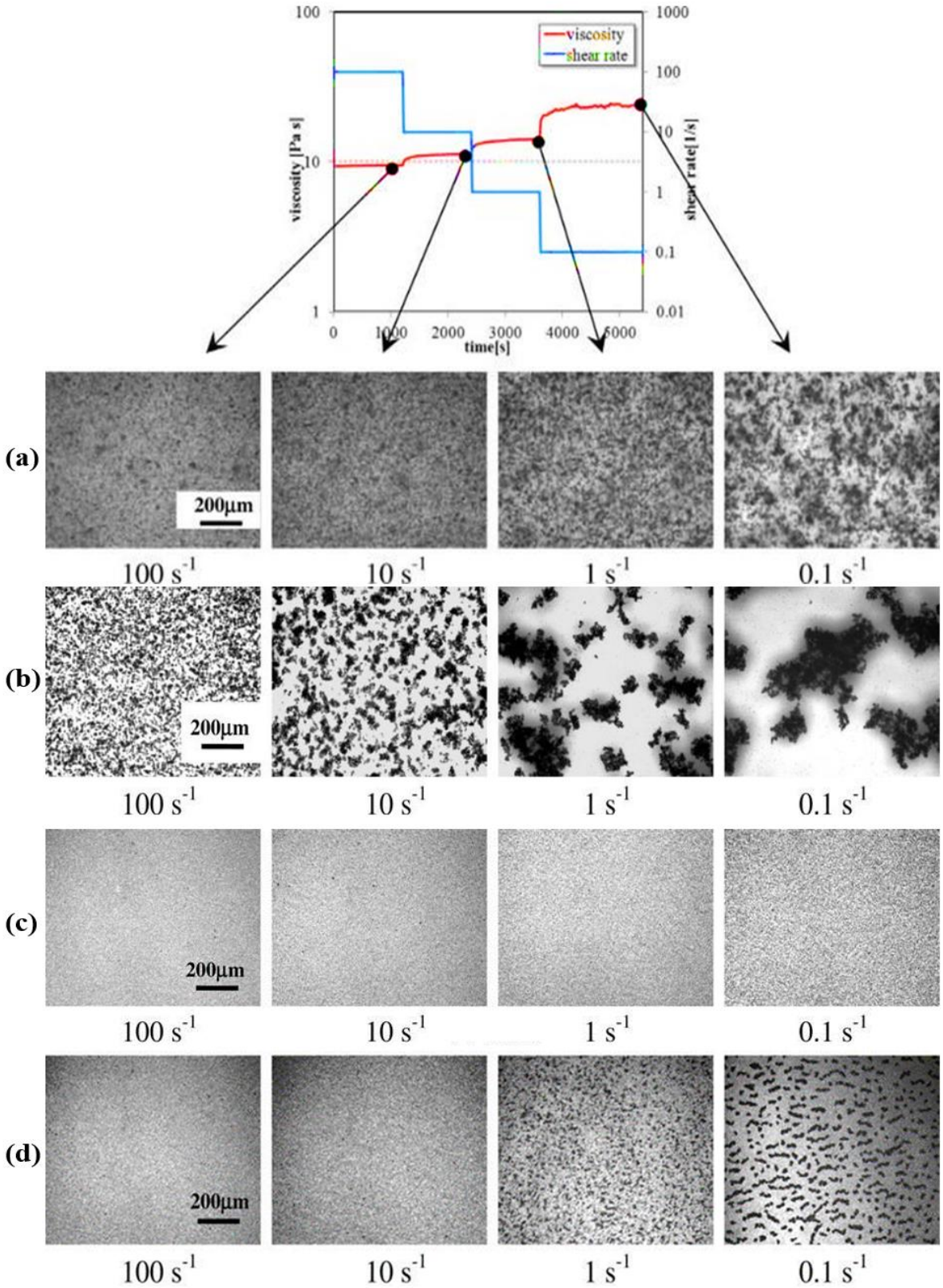

Figure 15 Diagram with SEM images shows the dispersion of MWCNT and CNF in epoxy matrix at different shear rates and temperatures: a) 0.1 wt. % MWCNT 25 ºC, b) 0.1wt.% MWCNT at a temperature of 60 ºC, c) 0.5wt.% CNF at temperature 25 ºC, d) 0.5wt.% CNF at 60ºC (Yokozeki et al., 2012).

Mechanical dispersion techniques were considered as a good practical approach to disperse the nanoparticles homogeneously in the matrix. In particular, there has been interest in the use of ultra-sonication, roll mill mixing, ball mill mixing and magnetic stirring (Tess et al., 1996; Breuer & Sundararaj, 2004; Xie et al., 2005; Ma et al., 2010; Lin et al., 2015; Bal & Saha, 2014; Iwahori et al., 2005; Yasmin et al., 2006). These techniques showed good dispersion of nanoparticles in the polymer resins. However, the challenges are continuous regarding these mechanical dispersion techniques because insufficient information has been provided about the use of such mechanical techniques. Moreover, there are principles or required procedures which should be followed by researchers when using these techniques, in order to achieve full dispersion of the nanoparticles. Therefore, further details are required to understand these issues.

In general, the work mechanisms applied for most of these dispersion techniques is by means of generating three mechanical forces, such as shear, compressive and extension. Figure 16 depicts the behaviour of nanoparticles under the effect of these forces.

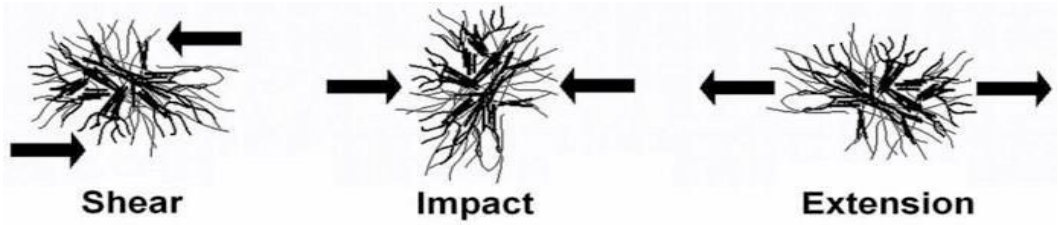

Figure 16 The main mechanical forces applied on the nanoparticles.

The improving dispersion quality of the nanoparticles into the matrix could significantly increase the mechanical properties of the NP. The modern approach of combined dispersive techniques is currently applied by researchers to obtain high level de-agglomeration and homogenous distribution of the nanoparticles in the polymer matrix. This approach has demonstrated success in the dispersion of various types of carbon nanomaterials (Tang et al., 2013; Lee et al., 2012; Chandrrasekaran et al., 2013; Morechi et al., 2015; Wang et al., 2015).

Tang et al. (2013), used combined dispersive techniques, sonication and ball milling/mixing to disperse graphene nanomaterials in the epoxy resin. To conclude, the results illustrated that the combined techniques could highly improve the dispersion degree of graphene in nanocomposites, as shown in Figure 17.

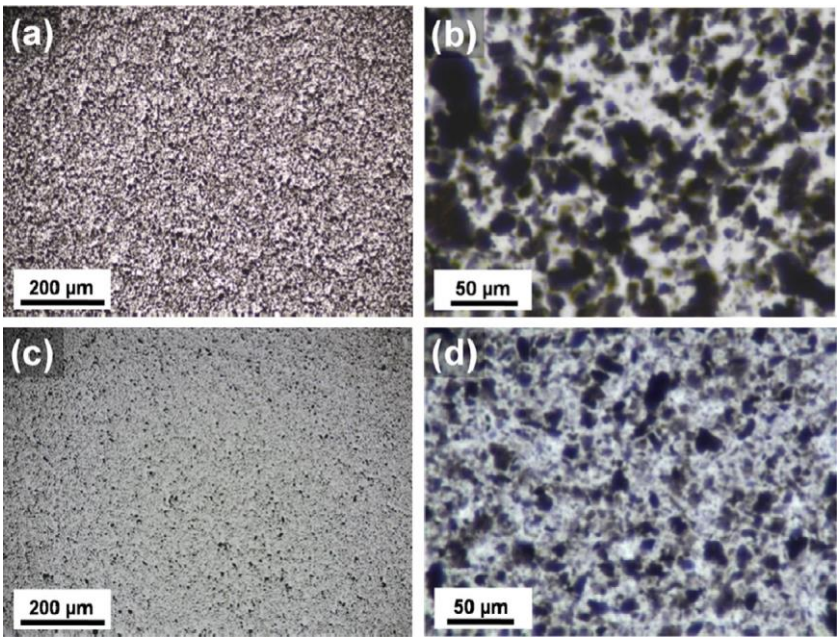

Figure 17 The TOM images shows the dispersion process of graphene/epoxy nanocomposites at 0.2wt.%: a) and b) sonication and c), d) combined techniques (sonication and ball milling) (Tang et al., 2013).

Lee et al. (2012), manufactured graphene/epoxy nanocomposites by combining two mechanical techniques; specifically, shearing mixer and ultra-sonication. In conclusion, their results observed that the modification of the dispersion degree of graphene into the epoxy matrix raises the mechanical properties of NP. Interestingly, Moriche et al. (2015), investigated the influence of dispersion processes on the morphological properties of GNP, particularly the structure. Mechanical combined techniques were used for this purpose. Their results showed that the dispersion processes can significantly affect the geometric structure of graphene. Moreover, the performance quality of graphene nanocomposite improved after combining sonication and a few cycles of the calendaring technique (see Figure 18).

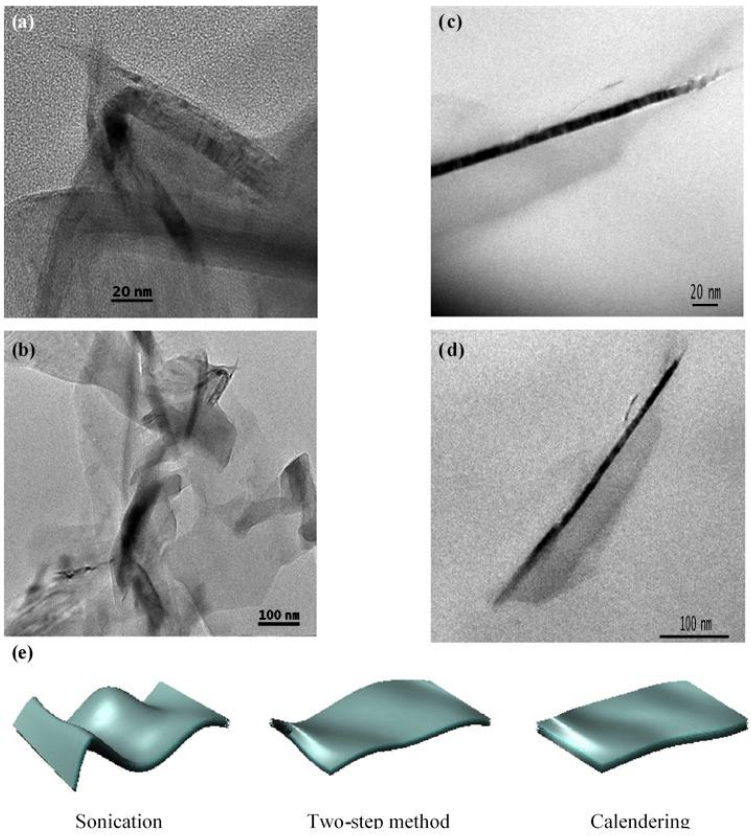

Figure 18 TEM images show the effect of dispersion processes on the morphological properties of GNP (a) and (b) GNP dispersed by sonication technique, (c) and (d) GNP dispersed by calendaring, (e) GNP disposition diagram scheme(Moriche et al., 2015)

Consequently, the combined dispersive techniques have high effectiveness in dispersing the carbon nanomaterials uniformly in polymer resins. To achieve high exfoliation of carbon nanomaterials and uniform dispersion, the combination of sonication and ball milling technique was suggested to disperse GNP, CSCNT and a combination of them in the polymer resin for the present study.

2.10.1 Mechanical dispersion

The most common and practical mechanical dispersion techniques used currently in the preparation of NP are ultra-sonication, ball mill mixing and shear mixing (Breuer & Sundararaj, 2004; Xie et al., 2005; Yasmin et al., 2006; Sun et al., 2011; Yokozeki et al., 2012). The two effective techniques used in this present study can be described as follows.

2.10.1.1 Ultra-sonication technique

Ultra-sonication is an active method used to disperse nanoparticles into the polymers. Its work mechanism depends on ultrasound energy to vibrate the particles in a solution or resin. The vibration energy generates pressure waves in the resin and the energy waves convert to mechanical forces on the agglomerated particles. Hence, contribute to separating nanoparticle agglomerates homogeneously in order to create a large contact area between the nanoparticles and the matrix.

Furthermore, this technique is a highly effective method used to disperse the nanoparticles in liquids that have a low viscosity or volatile solvents, such as acetone, water and other liquids (Lee et al., 2012; Ma et al., 2010).

Two sonication techniques are used for dispersing the nanoparticles in a matrix: ultrasonic bath and an ultrasonic probe/horn (see Figure 19).

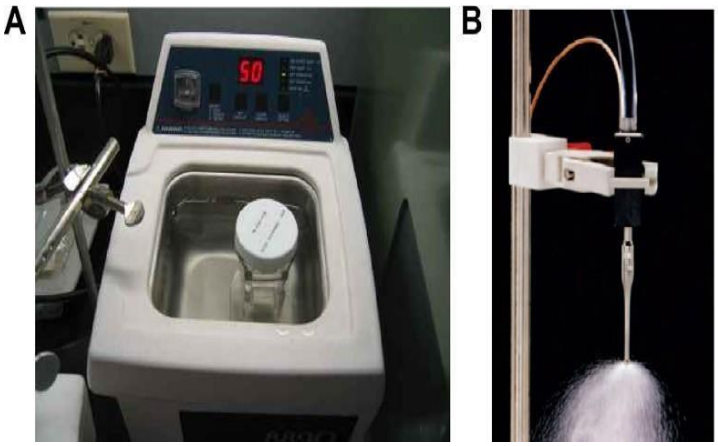

Figure 19 Two types of ultra-sonication techniques (A: a water bath sonicator; B: probe/horn sonicator) (Lu et al., 1996; Ma et al., 2010).

In accordance with Standard laboratory syndicators, the ultrasonic bath technique can be run at vibration cycles ranging from 20 to 23 KHz and energy less than 100W in a water bath. In addition, the other sonicator is the ultrasonic probe that has changeable amplitudes with a range of 20% to 70% and energy of 100-1500W, (Moniruzzaman & Winey, 2006; Ma et al., 2010).

The geometric structures of most probes are tapered. The diameter at the bottom tip range ranges between 1.6 to 12.7mm. The wide diameter probe is attached with a rule unit. Therefore, the

ultrasound energy is typically focused on the tip of the probe with high intensity energy. The consequence of this design is that a substantial amount of heat can be generated rapidly. Hence, in case the nanoparticles are dispersed in volatile solvents such as acetone, it may well be better to keep these solvents at a cold temperature (e.g. using pieces of ice as a bath).

Further, using the sonication technique over a long period could cause damage in the nanoparticles. Therefore, this period must be brief to avoid this drawback. Such consequences has been confirmed by Raman spectroscopy, which reveals that the dispersion of conventional carbon nanotubes over a long time creates a significant rise in the intensity of the D band (appearing troubled sp^3 carbon into carbon nanotube, as shown in Figure 20, (Lu et al., 1996). Moreover, in many cases, the graphene layers which forms the structure of the CNTs are crushed consequently, transformed to structure less or amorphous fibre nanotubes (Mukhopadhyay et al., 2002). This results in the deterioration of the physical properties of the NP, such as electrical and mechanical properties.

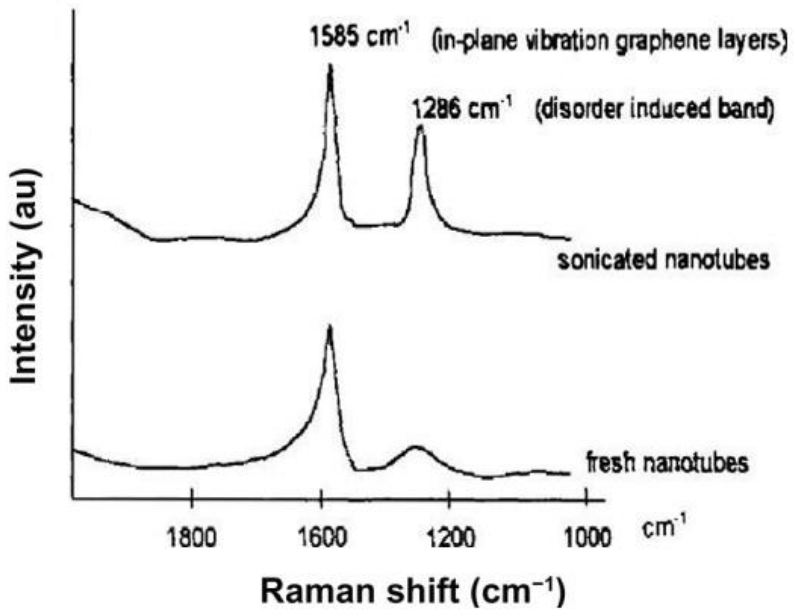

Figure 20 The influence of sonicated dispersion on the morphological construction of CNT before and after dispersion processing measured by Raman spectra (Lu et al., 1996).

Therefore, a reasonable period of time is recommended for the dispersion process of carbon nanomaterials by means of the sonication technique, particularly at high amplitude, in order to avoid any damage to the structure of the nanomaterials. These recommendations have been applied in the current study.

2.10.1.2 Ball milling/mixing technique

Ball milling/mixing technique is a practical and successful technique in dispersing nanoparticles in a matrix. A high level of dispersion for different types of nanoparticles has been achieved by applying this type of advanced technique (Guo & Chen 2014; Zhang et al., 2013; Inkyo et al., 2008). Furthermore, high weight concentration of particles can be dispersed uniformly by this method. The ball milling/mixing techniques can be designed within two planes of rotational speed; specifically, horizontal or vertical design (see Figure 21).

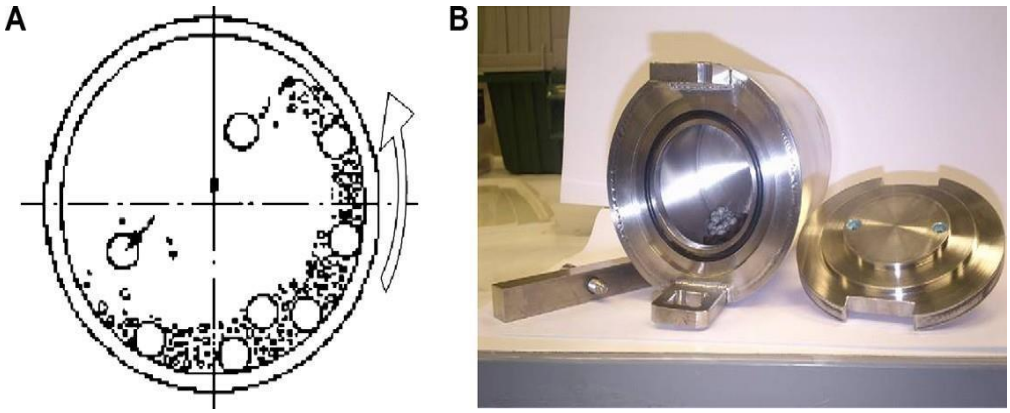

Figure 21 Schematic diagram of ball milling technique (horizontal design) b) container (Ma et al., 2010).

Due to possible abrasion on the smooth surface of the milling balls during the mixing period, hard materials, such as ceramic and stainless steel have been used for manufacturing the milling balls to obtain high efficiency for the milling or mixing process and high quality with regard to the final mixture.

The type and size of balls used for mixing or milling and their hardness could affect the quality of the dispersion process as well. Furthermore, the adjustment of the main parameters, for instance mixing or milling time, rotation speed and the diameter of the milling balls is necessary for optimal dispersion of the particles into the matrix (Ma et al., 2010). Therefore, processing optimisation of these controlling parameters for each type of particles is required, to avoid the possibility of them being crushed through the dispersion process.

In both cases, this technique can be employed for dry milling and the wet mixing of particles into the polymer resins (Inkyo et al., 2008). The wet mixing method was considered the most common method used to disperse different types of nanomaterials, such as CNTs, CNF and GNP. The reasons for this is that they deliver better interlocking of nanoparticles and matrix and to maintain stabilisation of the particles in the polymer resins. Two mechanical forces are generated during the rotation of the mixture in the container: shear and compressive. The level of these forces

depend on the collision between the rigid balls and particles inside the rotational closed container, which signifies that a high pressure will be internally generated in the container, which may change the morphological structure in addition to reducing the size of the nanomaterials. Additionally, it subsequently increases their surface area (Yokozeki et al., 2008; Shin et al., 2009; Ma et al., 2009; Ma et al., 2008; Guo & Chen, 2014).

The probability of a particle crash is expected during the high speed milling/mixing process with heavy or large balls, over an extended period. Therefore, lower collision energy with small balls or a short period of dispersion are recommended at high collision energy.

The dispersion degree of carbon nanomaterials into the matrix can be affected by the chemical or physical cases of the polymer resins, which are represented as thermoplastic or thermoset materials, the morphological properties of the nanoparticles, for example geometric structure and the weight content of the nanomaterials. Numerous studies have been conducted by researchers to address these issues by using the ball milling technique.

The following are some explanations: Yokozeki et al. (2008), confirmed the main conceptions to disperse CSCNT using the ball milling process to control the length of nanotubes required to obtain optimal dispersion without damage to the structure of the fibre nanotubes. Tang et al. (2013), illustrated the influence of graphene dispersion degree on the physical and mechanical properties (i.e. strength and toughness) of epoxy resin. The sonication technique was used for this purpose at the initial stage. Subsequently, the dispersion degree of the mixture has been improved by re-dispersing the graphene by using the ball milling technique. In this work, the results demonstrated uniform dispersion and good exfoliation of nanosheets in the matrix. Additionally, there were significant improvements in the level of mechanical properties of the NP. Guo & Chen (2014), prepared epoxy nanocomposite modified with a high level content of graphene, using the ball mill technique. Their results identified good quality dispersion of graphene sheets into the epoxy resin and improvement in physical properties (i.e. thermal conductivity) with high loading of graphene weight fractions ranging from 5wt. % to 25wt %. Zhang et al. (2014), used this technique to control the graphitization degree of carbon black nanomaterials at different milling periods. As a result, the milling time can have a significant effect on the structure of carbon black, nano-dimensions and the size of the defects, as depicted in Figure 22.

As a consequence of this evidence, it appears that ball milling is an essential technique in relation to obtaining good dispersion of nanoparticles at various level loading of the nanoparticles. Therefore, it is used to disperse the graphene and novel fibre nanotubes in the polymer resin in current studies.

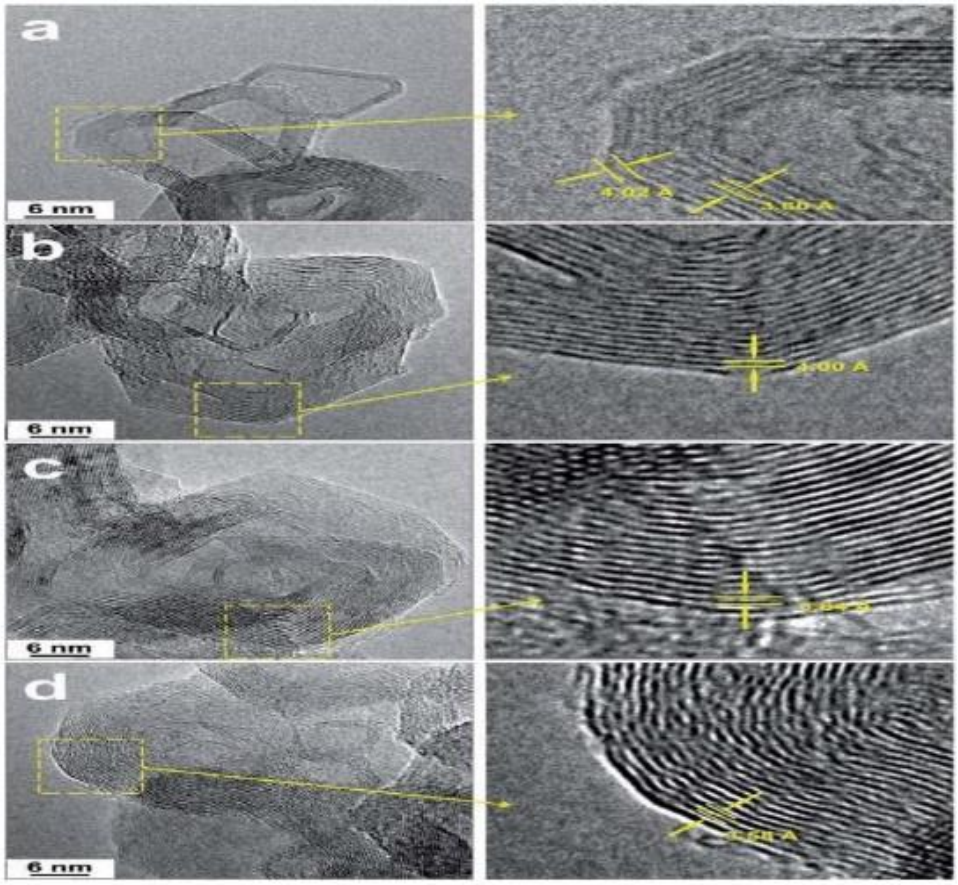

Figure 22 HRTEM images showing the structure of graphene carbon black (GCB) at various milling time a) The cross-section for milled GCB b) 0.1 hr, c) 9 hr and d) 24hrs (Zhang et al., 2013).

2.11 Main concepts and evaluation of NP

The key issues that assist with understanding the manufacture of NP and which contributes dramatically to their development in nanotechnology science can be described as fabrication methods, mechanism processing, usage of materials, functionalisation, characterisation, quality of devices and the control system on the dimension of nanoparticles. Each one of these concepts could significantly affect the quality performance of nanocomposites (Ji et al., 2016; Sahoo et al., 2010; Hu et al., 2015; Thostenson et al., 2005).

Furthermore, several factors, such as dispersion processes, alignment and the weight concentration of the nanoparticles, aspect ratio and viscosity of the polymer resins appear essential concepts and keys in the manufacture of the NP. However, the concept of dispersion or alignment is not only related to creating a huge surface area and the best contact between the polymer and nanoparticles, it is also to prevent the aggregation phenomenon, which effects the mechanical interfacial property between the filler and matrix. Moreover, the improvements in the mechanical properties of the NP are dependent on this property which is controlled by the critical interface region.

Other issues relevant to the mechanical dispersion techniques used for this application still lack sufficient information. For instance, operational control keys to accomplish complete exfoliation and optimum dispersion of particles in the matrix and moreover, avoid re-agglomeration or crushing of the nanoparticles through the preparation stages for the nanocomposites (Ma et al., 2010; Thostenson et al., 2005).

There are other significant issues. Transforming the engineering dimensions and geometric designs of the reinforcements from micro to nanometres presents important methods and opportunities and innovative approaches in the processing mechanism and preparation of novel advanced composites, functionalisation, characterisation, as well as the simulation analysis of modern generation of composite materials. (Punetha et al., 2017; Ji et al., 2016; Koo, 2006). In addition, the most appropriate geometric shape and size of the particles, plus the multi-functionality formula of the nanomaterials can be used to obtain the highest physical and mechanical novel composites (Wang et al., 2016; Zheng et al., 2012; Chatterjee et al., 2012). Thus, researchers and engineers continue to work with nano and micro-reinforcements to create novel composites with excellent engineering performance and less cost.

2.12 Composites

There are several drawbacks, in using glass or carbon fibre reinforced polymer composites. For engineering applications and advanced structural designs, there are poor resistance for compression loads, interlaminar shear and interlaminar toughness resistance. These mechanical characterisations are dominated by the polymer matrix and interface properties that are frequently degrees of proportion inferior to the fibre composites dominated properties. In other words, the grade of attraction between the matrix and filler at the interface region is dependent on the mechanical interfacial property. Moreover, it controls the amount of stress and strain energy transferred between them as mentioned previously (Kundalwal and Kumar, 2016).

As a consequence, this makes fibre reinforced polymer composites vulnerable to unanticipated design failures, when stressed under compressive forces conditions or exposed to delamination damage in the engineering structure (Djabali et al., 2018). Using fibre composite materials in critical stress bearing structural designs therefore requires validation via extensive confirmation and mechanical engineering testing (Greenhalgh et al., 2006).

Countless studies have been conducted to address these difficulties, in order to promote the performance of fibre reinforced polymer composites for optimal use in engineering and industrial applications. Conventional approaches used for this purpose over past decades via through-thickness reinforcements, such as transverse stitching (Shu & Mai 1993; Chen et al., 2001),

tufting (Mourtiz et al., 2011) and pinning (Bianchi et al., 2012; Lenzi et al., 2007; Liu & Mai 2003) have been comprehensively studied (Greenhalgh and Hiley, 2003) and demonstrated to significantly improve interlaminar shear strength, interlaminar fracture toughness and impact resistance (Greenhalgh et al., 2006; Mourtiz, 2007). However, these through-thickness reinforcements predominantly damage the parent fibre materials and, as a consequence, reduce the pristine in-plane mechanical properties of the composites.

A further approach to enhancing the mechanical properties of HFRP includes the use of toughened and strengthened polymer matrix. In particular, there has been interest in the use of elastomer or thermoplastic particles to dope the matrix (Scott and Phillips, 1975; Zulkifli et al., 2002). A modern and alternative method to promote this conventional approach is by doping the fibre reinforced polymer composites with one rigid nanoreinforcement (i.e. CNTs, GNP, CNF) which possess extraordinary strength and stiffness properties (Godara et al., 2009; Kumar and Roy, 2018; Kostagiannakopoulou et al., 2015; Yokozeki et al., 2009). This modern practical technique has been shown to enhance delamination failure and damage tolerance in the structural design of composites, without any reduction in the pristine in-plane mechanical properties and will be debated further in this review.

However, the previous modern approach has also been further developed by researchers recently by combining two rigid nanoreinforcements into the polymer resin and applying this in the manufacture of novel HFRP (i.e. combination of conventional carbon nanotubes and graphene), (Kostagiannakopoulou et al., 2017; Rodriguez-Gonazalez et al., 2017; Wang et al., 2015). Although, the combination of graphene and conventional carbon nanotubes have achieved success in improving the mechanical properties of HFRP, only moderate improvements have been sensed in these properties (Rodrizguez-Gonazalez et al., 2017; Kostagiannakopoulou et al., 2017). The main obstacle that impeded this approach is the difficulty in dispersing them uniformly and achieving high exfoliation of these two carbon nanomaterials in the polymer resins (Ma et al., 2010; Yu et al., 2000). Therefore, additions of chemical dispersants are often necessary to achieve uniform dispersions and alignment between the matrix and hybrid carbon nanomaterials (Wang et al., 2015; Ma et al., 2010).

Alternative novel carbon nanomaterials called CSCNT are suggested as a good solution for this obstacle because they have excellent mechanical properties supported with unique geometric structure, as well as ease of dispersion (Iwahori et al., 2005; Yokozeki et al., 2009; Yokozeki et al., 2012). Therefore, the combination of GNP and CSCNT is expected to be more satisfactory than conventional carbon nanotubes, in improving the mechanical properties of conventional carbon fibre composites, which are adopted in the present work.

2.13 Hybrid fibre reinforced polymer composites (HFRP)

The modified matrix dominated properties in traditional fibre composites can potentially benefit from the inclusion of multifunctional carbon nanomaterials: graphene, novel fibre nanotubes, conventional carbon nanotubes, and moreover, combined carbon nanomaterials (i.e. a combination of GNP and CNTs). These novel composites are currently known as hybrid composites. In spite of the constituents, the hybrid composites have been formed from fairly weak materials although they possess high mechanical properties (Mayer, 2005).

2.13.1 Synthesis methods for HFRP

The combination of multi-sized reinforcements; carbon nanomaterials (i.e. GNP, CNF and CNTs), fibre materials (i.e. carbon fibre, glass fibre) into the polymer resins to manufacture HFRP can be described via two main practical techniques:

i) Growing the carbon nanomaterials onto the surfaces of fibre networks as the primary stage.

ii) Dispersion of the carbon nanomaterials into the polymer matrix (Qian et al., 2010; Ma et al., 2010).

Both techniques have exhibited high improvements with the addition of such carbon nanomaterials. As there is the possibility of damage occurring in the fibre network, it is more appropriate for the dispersion technique to be used instead of grafting nanoparticles onto the fibre network, whilst it is also a simple principle (Qian et al., 2008; Zhang et al., 2009). Therefore, for the current study, the dispersion of the carbon nanomaterials into the polymer matrix was chosen to manufacture the carbon fibre composites to avert such an obstacle. Furthermore, many experimental studies have been reported and are still continuing with novel nanoreinforcements and innovative modifications in all three main methods; specifically, the chemical treatment of carbon nanomaterials, surface treatment of carbon fibre network and chemical modulation of the polymer resins and physical optimisation of synthesising proceedings.

Principally, NP can be prepared by different practical techniques as mentioned previously. However, the simplest technique would be by mixing and dispersing the nanoparticles in the polymer resins directly via mechanical dispersion (Feng et al., 2014; Chen et al., 2015; Qian et al., 2010). The manufacturing of NP by this method is considered a challenge, due to the tendency of the nanoparticles to aggregate into the matrix as a result of van der Waals forces or surface influence. Furthermore, excessive mechanical dispersion over a long time could damage the structure of the particles (Ma et al., 2010).

Further techniques by means of chemical treatments: The main purpose of this procedure is to improve the surface properties of the nanoparticles to create high adhesion between the particles

and the matrix, despite the significant mechanical improvements that have been reported in relation to the nanocomposites modified with chemical treatment in comparison to the parent nanocomposites (Moghadam and Taheri, 2015; Davis and Whelan 2011; Barrena et al., 2014). This method also has challenge related to the chemical treatment of carbon nanomaterials without damage or defect in the structure of the nanomaterials, especially their side walls (Zheng et al., 2010; Avila-Orta et al., 2009; Esumi et al., 1996).

Modern methods known as combined dispersive techniques were used to achieve high levels of dispersion mechanically (Tang et al., 2013; Liang et al., 2009). This mechanical dispersion method has the ability to disperse various weight contents of carbon nanomaterials with high exfoliation and uniform dispersion. Therefore, the combination of ball milling and ultra-sonication are suggested to disperse the nanomaterials into the polymer resin in the present study, without the need to use additional dispersants as possible.

Once the dispersion of nanoparticles in the polymer resin is accomplished, the resulting modified matrix was composited with carbon fibre composites via the impregnation of the matrix onto the carbon fibre network. Various classical techniques are available for this purpose including resin transfer moulding or infusion modelling (RTM), compression moulding or autoclave moulding, spray-up technique, etc (Kawasetu et al., 2004). Whilst, the conventional hand lay-up process is considered to be a good method in the industrial field, due to its an open moulding technique, which is appropriate for fabricating a large amount of fibre composite products ranging from small to large, it is useful for manufacturing substantial production quantities utilising various moulds. Hand lay-up is also a modest composites moulding technique, displaying low price tooling, a simple manufacturing processing and an enormous range of piece sizes. Moreover, design variations are easily made.

However, the viscosity of polymer resin plays a significant role in manufacturing processes and resin flowing into the fibre network. In particular, after the addition of nanoparticles into the resin, choosing one of these techniques is not straightforward with regard to producing the HFRP, as the increase in the degree of viscosity is probable in the present work. Hence, this will significantly affect the resin flow used in the manufacturing of HFRP, in particular with high weight content of nanoparticles. Thus, the use of the RTM or spray-up technique undoubtedly will be challenging for manufacturing HFRP (Qian et al., 2010; Yokozeki et al., 2012; Gojny et al., 2005), as the high viscosity will hinder the flow of modified resin through the tubes used in these techniques, besides making its diffusion onto the ply surface and penetration into fibre networks more challenging (Fan et al., 2008; Wickmann et al., 2006). This is whilst the principle work of the hand lay-up technique is based on the impregnation of modified polymer resin directly onto the surface of the fibre network, even though the viscosity has showed relative

changes after the addition of the nanoparticles into the polymer resin. Additionally, this technique has been exhibited successfully in many engineering applications relevant to the creation of HFRP, in spite of the existence of several voids in the produced composites (Wicks et al., 2014). Furthermore, the modification of this simple technique was performed by vacuum bagging in the present work. The purpose of that was to reduce the volume fraction of voids and improve the quality of produced HFRP as much as possible.

With regard to these valuable benefits and some modifications on the practical principles of the hand lay-up technique, this technique was used to construct the design structure for the HCFRP in the present work.

2.13.2 Mechanical properties of HFRP

Most of the experimental studies have reported that carbon and glass fibre composites dominated properties, such as tensile and flexural strength properties remain comparatively uninfluenced (Hadden et al., 2015; Zhang et al., 2009). The basic attention of HFRP were on the nanofilled matrix dominated properties. For example, interlaminar shear strength and interlaminar fracture toughness and in-plane compression. Enhancements in these mechanical properties were expected after the impregnation of the modified epoxy resins, with graphene, conventional carbon nanotubes, fibre nanotubes and combined carbon nanomaterials into the fibre composites, which are explained in detail in the subsequent sections (Kumar and Roy, 2018; Fan et al., 2008; Kostagiannakopoulou et al., 2017; Wang et al., 2015; Landani et al., 2015; Li et al., 2014).

2.13.2.1 Interlaminar shear strength (ILSS)

Interlaminar shear strength is one mechanical characterisation that had demonstrated significant enhancements after the inclusion of the multifunctional carbon nanomaterials with the fibre polymer composites at low and high weight content, even with the type variation of a fibre (Jia et al., 2015; Green et al., 2009; Tang et al., 2011; Li et al 2014; Yao et al., 2015; Li et al., 2013; Green et al., 2009; Qin et al., 2015; Wang et al., 2015). This mechanical characterisation is predominantly controlled by the interface performance between the polymer matrix and fibre network (Park and Seo, 2011; Greenhalgh, 2009). Consequently, any enhancement in the degree of adhesion or mechanical interfacial property between these two phases at this region would produce a gain in ILSS.

The short beam shear (SBS) test is one of the most common methods based on classical beam theory (Bernoulli Euler), to estimate the value of interlaminar shear strength for laminated composites. Generally, the delamination failure shear occurs between the layers of enhancing fibres, particularly the mid-thickness of the laminated composite via tensile and compressive bending force subjected to the top and bottom fibre planes.

A strengthened and toughened interphase between the fibre network and the nanomaterials was suggested as a possible enhancement mechanism; thus, providing the increased shear strength (Gojny et al., 2005; Zhang et al., 2012). The direct improvement of the strength and stiffness properties of the polymer matrix by the inclusion of the carbon nanomaterials had increased the capacity of the strain and stress energy transfer between the nanofilled matrix and the fibre network.

In spite of the utilisation of multiple conventional carbon nanotubes modified or unmodified by chemical solvents, even with various types of fibre composites, moderate enhancements were achieved in the interlaminar shear strength of the HFRP, as shown in Table 6. The level of shear property improvements in the reported results related to conventional carbon nanotubes dispersed into the polymer resin was (3-20%). The low proportion of increases may indicate that the grades of adhesion are relatively poor between the laminates of HFRP, particularly at interface regions. Furthermore, the efficiency of conventional carbon nanotubes in absorbing the stress energy probably was low, due to weak alignment between the matrix and the nanotubes and therefore have an effect on the level of mechanical properties improvements.

Table 6 The improvements in shear strength properties of HFRP (modified with conventional carbon nanotubes).

Matrix	Fibre (Type)	Nano-filler type	Weight content	Maximum strength (MPa), improvement (%)	Technique, (Lay-up)	Test method	Ref
Epoxy (JC-02A)	CF (Not mentioned)	CNTs	Base(0)	66	RTM (UD)	SBS	Yao et al., 2015
			5 wt.%	75(+13%)			
Epoxy (L135i)	GF (Non-crimp fabrics)	DWCNT	Base(0)	33.4	RTM (Quasi-isotropic)	SBS	Wichmann et al., 2006
			0.3 wt.%	38.7(+16%)			
Epoxy (EPON 862)	GF (Prepreg)	f-MWCNT	1 wt.%	(+8%)	VA RTM (UD)	SBS	Qiu et al., 2007
Epoxy (SC-15)	GF (Woven fibre mats)	MWCNT	Base(0)	32.5	VA RTM (UD)	SBS	Fan et al., 2008
			0.5 wt.%	33.5(+3%)			
			1 wt.%	38.4(+18%)			
Epoxy (L135i)	GF (Non-crimp fabric)	f-DWCNT	Base(0)	31.8	RTM (Quasi-isotropic)	SBS	Gojny et al.,2005
			0.1 wt.%	36.8(+16%)			
			0.3 wt.%	38.1(+20%)			
Epoxy (EPON 862)	CF (Fabric)	Grafted/MWCNT	0.25 wt.%	(+27%)	VARTM (Not mentioned)	SBS	Bekyarova et al., 2007

The reported enhancement in the interlaminar shear strength of the fibre polymer and composites modified with graphene and novel fibre nanotubes at low and high weigh content is listed in Table 7. Although, most of these studies have not mentioned the weight content of the nanomaterials and complete details of the fibre composite used, significant improvements were reported in interlaminar shear strength after the addition of graphene and novel fibre nanotubes, which seems relatively more efficient than conventional carbon nanotubes (Jia et al., 2015; Khan and Kim, 2012). The range of improvements in the reported results related to graphene and novel fibre nanotubes dispersed into the polymer resins, regardless of the type of fibre composite used were (11-36%) and (8-31%) respectively.

Table 7 The improvements in shear strength properties of HFRP (modified with graphene and novel carbon fibre nanotubes).

Matrix	Fibre (Type)	Nano-filler type	Weight content	Maximum strength (MPa), improvement (%)	Technique, (Lay-up)	Test method	Ref
Epoxy (E54)	CF (Prepreg)	GO	Base(0)	105.8	Hand lay-up and hot press (UD)	SBS	Li et al., 2016
			0.1 wt.%	117.5(+11%)			
Epoxy (E54)	CF (Prepreg)	GO	Base(0)	45.5	Wet lay-up (UD)	SBS	Zhang et al., 2012
			5 wt.%	51.3(+13%)			
Epoxy (Araldite F)	GF (Prepreg)	3D GNP	Base(0)	46.1	Hot press molding (UD)	SBS	Jia et al., 2015
			-	62.5(+36%)			
Epoxy (Epon 828)	CF (Prepreg)	Grafted/ GNP	3 wt.%	(+19%)	Hand lay-up and autoclave (UD)	SBS	Qin et al., 2015
Epoxy (EPON 815C)	GF (Plain weave)	CNF	Base(0)	35.5	VARTM (Not mentioned)	SBS	Green et al., 2009
			0.1 wt.%	43.9(+23%)			
			1 wt.%	38.5(+8%)			
Epoxy (LY 1564)	CF (Prepreg)	CNF	Base(0)	52	Hand lay-up (UD)	SBS	Khan and Kim, 2012
			10 wt.%	68(+31%)			

However, exceptionally few studies involved a combination of multifunctional nanomaterials to promote the interlaminar shear strength properties of fibre composites. The level of improvements in the reported results are listed in Table 8. One of reported studies does not involve using graphene instead of aluminium oxide (Al_2O_3) powder combined with conventional carbon nanotubes (Li et al., 2014). Thus, the direct connection between the combined nanomaterials used and property improvement would not be deduced. Conversely, an additional study conducted by Wang et al., (2015), included using a mixture of graphene and conventional carbon nanotubes to improve the interlaminar shear strength property of carbon fibre (plain weave) by approximately 40%. Hence, the direct connection between property improvement and hybrid carbon nanomaterials probably would be deduced. Furthermore, the addition of these multifunctional carbon nanomaterials into the polymer resin had promoted the adhesion property between the filler and the resin and consequently, influenced the synergy property of the carbon nanomaterials within the matrix (Wang et al., 2015; Liu et al., 2017). Therefore, the combined

nanomaterials could be more effective than single nanomaterial in improving the shear property of conventional fibre composites.

Table 8 The improvements in the shear strength properties of HFRP (modified with combined carbon nanomaterials).

Matrix	Fibre (Type)	Nano-filler type	Weight content	Maximum strength (MPa), improvement (%)	Technique, (Lay-up)	Test method	Ref
Epoxy (EPO-622)	CF (Fibre cloth)	Hybrid CNTs/GNP	Base(0)	54.6	Hand lay-up and Hot press molding (Not mentioned)	SBS	Wang et al., 2015
			1:9 (ratio)	76.5(+40%)			
Epoxy (1080S)	GF (Plain woven fabric)	Hybrids CNTs-Al_2O_3	Base(0)	26.3	Hand lay-up (Not mentioned)	SBS	Li et al., 2014
			0.5 wt.%	29.1(+11%)			

Generally, the characterisation of the interlaminar adhesion must be treated carefully, as most of the reported outcomes were dependent on the low and high loading of the nanomaterials. With high loading of nanomaterials content, agglomeration phenomenon could negatively affect the shear property given. This phenomenon prevents adhesion between the fibre and nanophase matrix, thus revising the trend, in shear strength property. Zhang et al. (2012), demonstrated that this phenomenon undoubtedly causes a reduction in the strength properties of the carbon fibre composite, in case the weight concentration of graphene oxide exceeds 5 wt. %. Therefore, high exfoliation of carbon nanomaterials in the resin is possibly required prior to the addition of modified matrix into the carbon fibre composites, to avoid such problem.

Few experimental studies have been conducted using CSCNT and GNP dispersed uniformly into the matrix to enhance the shear property of the fibre composites. In addition to the effect of the combination of two carbon nanomaterials (i.e. GNP and CSCNT) on the interlaminar shear strength of carbon fibre composites (i.e. woven carbon fibre), to the best of my knowledge, this novel formula has not been applied until now.

2.13.2.2 Flexural properties

It is recognised that conventional fibre composites under static flexural load can exhibit three modes of failure; tensile, compression and delamination failure in mid-plane (i.e. interlaminar shear failure and interlaminar fracture toughness failure). Furthermore, the compressive failure and mid-plane delamination failure are influenced by the strength and toughness properties of the polymer matrix. In the meantime, the inclusion of carbon nanomaterials, such as graphene,

novel fibre nanotubes and conventional carbon nanotubes are expected to modify the flexural strength and stiffness properties of the fibre composite where such failure modes were illustrated in the HFRP.

The reported flexural properties results of HFRP are modified with dispersed conventional carbon nanotubes in the polymer resins which are listed in Table 9**.** Although, different types of fibre composites were used (i.e. woven carbon fibre), the flexural modulus were not expected to be greatly affected by the inclusions of conventional carbon nanotubes for most of these previous studies (Zhou et al., 2008; Kepple et al., 2008). Moreover, modifications to the fibre network via depositing or nanoparticles growth, could damage the parent fibre. This could result in an inferior fibre composite compared to the original composite (Mathur et al., 2008).

Table 9 The improvements in flexural properties of HFRP (modified with conventional carbon nanotubes).

Matrix	Fibre (Type)	Nano-filler type	Weight content	Maximum stiffness (GPa), improvement (%)	Maximum strength (MPa), improvement (%)	Technique, (lay-up)	Test method	Ref
Phenolic	CF (UD fibre)	Grafted/ CNTs	Base(0)	43.7	471	Hand lay-up (Not mentioned)	3 pb	Mathur et al., 2008
			9.1 wt.%	56(+28%)	580(+20%)			
	CF (2D Plain weave)		8.3 wt.%	(+54%)	(+75%)			
	CF (3D felt)		18.42 wt.%	(+46%)	(+66%)			
Epoxy (SC-15)	CF (Satin weave fabric)	MWCNT	Base(0)	63	608	VARTM (Not mentioned)	3 pb	Zhou et al., 2008
			0.3 wt.%	66.1(+5%)	626(+3%)			
Epoxy (MGS L285)	CF (Plain weave fabric)	Grafted/ f.CNTs	-	(+5%)	-	Hand lay up (Not mentioned)	3 pb	Kepple et al., 2008
Epoxy (JC-02A)	CF (Not mentioned)	CNTs	Base(0)	-	800	RTM (UD)	3 pb	Yao et al., 2015
			5 wt.%	-	927(+20%)			

The effect of the addition of graphene and novel fibre nanotubes on flexural properties of HFRP for previous studies are listed in Table 10. Reported improvements in the flexural modulus of carbon fibre composites (i.e. woven carbon fibre) modified with graphene or novel fibre nanotubes were slight (Iwahori et al., 2005; Zhou et al., 2006). Furthermore and regardless of the

type of fibre that is used, the use of polymer resin modified with functionalised graphene, in improving the strength and stiffness property demonstrated no improvement (Moriche et al., 2016). This case probably refers to the weak attraction between the fibre and modified matrix particularly at the interface regions. However, the improvements in strength property were more significant in most of the previous studies, after the addition of these carbon nanomaterials into the fibre composites, in particular woven carbon fibre. For example, the level of the improvement in strength property of woven carbon fibre composites was (14-22%) after the addition of novel fibre nanotubes to carbon fibre network (Iwahori et al., 2005; Zhou et al., 2006).

Table 10 The improvements in flexural properties of HFRP (modified with graphene and novel carbon fibre nanotubes).

Matrix	Fibre (Type)	Nano-filler type	Weight content	Maximum Stiffness (GPa), improvement (%)	Maximum strength (MPa), improvement (%)	Technique, (Lay-up)	Test method	Ref
Epoxy (SC-15)	GF (Plain weave)	Grafted/ GNP	Base(0)	-	325	RTM (Not mentioned)	4 pb	Kamar et al., 2015
			0.25 wt.%	-	419(+29%)			
Epoxy (Epon 828)	CF (Prepreg)	Grafted/ GNP	3 wt.%	-	(+52%)	Hand lay-up and autoclave (UD)	3 pb	Qin et al., 2015
Epoxy (Epon 828)	GF (Plain weave)	GNP-C750	5 wt.%	(+12%)	-	Hand lay-up and autoclave (Not mentioned)	3 pb	Wang et al., 2016
		GNP-5	5 wt.%	(+26%)	-			
			3 wt.%	-	(+16%)			
Epoxy (Araldite LY556)	GF (UD fabric)	f-GNP	12 wt.%	None	None	Hand lay-up (UD)	3 pb	Moriche et al., 2016
Epoxy (EP827)	CF (Plain woven fabric)	CNF	Base(0)	51.4	667	Not mentioned	3 pb	Iwahori et al., 2005
			5 wt.%	54.7(+6%)	760(+14%)			
			10 wt.%	53.5(+4%)	790(+18%)			
Epoxy (EP827)	CF (Prepreg)	CNF	Base(0)	53	875	Autoclave (UD)	3 pb	Yokozeki et al., 2007
			5 wt.%	55.1(+4%)	912(+4%)			
			10 wt.%	55.8(+5%)	888(+2%)			
Epoxy (SC-15)	CF (Plain weave fabric)	CNF	Base(0)	48.9	488	VARTM (Not mentioned)	3 pb	Zhou et al., 2006
			2 wt.%	49.4(+2%)	597(+22%)			
Epoxy (EPON 815C)	GF (Plain weave)	CNF	Base(0)	17	337	VARTM (Not mentioned)	3 pb	Green et al., 2009
			0.1 wt.%	21(+23%)	393(+17%)			
			1 wt.%	22(+26%)	404(+20%)			
			5 wt.%	-	927(+20%)			

In general, the level of improvements in the strength and stiffness properties of the fibre composites seems relatively compatible among these three carbon nanomaterials; conventional carbon nanotubes, graphene and novel fibre nanotubes.

In addition, the results illustrated that the surface grown carbon nanomaterials approach had provided the greatest flexural strength improvements, whereas the carbon nanomaterials dispersed in the matrix approach exhibited only modest improvements.

Despite previous studies relating to the use of the combined nanomaterials to improve the flexural properties being limited, the few reported results in Table 11 revealed that the addition of the combination of both reinforcements could significantly contribute to improving the flexural strength and modulus properties of the fibre composite. This is regardless of the type of reinforcements used (Wang et al., 2015; Li et al., 2014). Interestingly, the improvements in flexural strength and stiffness properties of the carbon fibre composites, (i.e. carbon fabric cloth) modified with a combination of GNP and CNTs were significantly exciting, after the impregnation of hybrid nanophase matrix onto the surface of the fibre networks. Hence, this improvement is possibly the result of the high attraction between the hybrid matrix and the fibre tows, which has been gained from the synergistic effect of these multifunctional carbon nanomaterials within the matrix.

Table 11 The improvements in flexural properties of HFRP (modified with combined carbon nanomaterials).

Matrix	Fibre (Type)	Nano-filler type	Weight content	Maximum stiffness (GPa), improvement (%)	Maximum strength (MPa), improvement (%)	Technique, (lay-up)	Test method	Ref
Epoxy (EPO-622)	CF (Fabric cloth)	Hybrid CNTs/GNP	Base(0)	31.3	580	Hand lay-up and Hot press molding (Not mentioned)	-	Wang et al., 2015
			1:9 (ratio)	34.4(+10%)	682(+18%)			
Epoxy (1080S)	GF (Plain woven fabric)	Hybrids CNTs-Al_2O_3	Base(0)	21.7	-	Hand lay-up (Not mentioned)	3 pb	Li et al., 2014
			0.5 wt.%	25.7(+19%)	(+12%)			

However, the enhancement of mechanical properties in the carbon fibre composite by means of the impregnation route is subject to whether the uniform nanoparticles dispersion were completely achieved in the polymer resin, before using it as a reinforced matrix to impregnate the surface of the fibre networks. Therefore, any modification in the flexural properties of carbon fibre composite modified with carbon nanomaterials dispersed into the polymer resins, could be

obstructed by the agglomeration of the nanoparticles into the matrix and nonhomogeneous distribution of modified matrix onto surface of the fibre network. This is because these engineering problems which are related to the manufacturing processes, weaken the mechanical interfacial property between the modified matrix and fillers (Moriche et al., 2016; Iwahori et al., 2005). Hence, this case may affect the flexural properties of the HFRP.

In general, any modifications in the mechanical properties of HFRP are highly dependent on the strength and toughness properties of the modified polymer matrix (Veedu et al., 2006). Therefore, use of the optimum strength and toughness properties of the modified polymer with carbon nanomaterials would contribute to improving the flexural properties of the HFRP (Wang et al., 2015; Zhou et al., 2006). Moreover, the enhancement in this property is attributed to other mechanisms involved in the filler bridging and the mechanical interfacial properties between the matrix and fillers (Zhou et al., 2008; Ye et al., 2007; Park and Seo, 2011; Qin et al., 2015). Therefore, the addition of strengthened and toughened matrix modified by the combination of graphene and novel fibre nanotubes to the carbon fibre composites probably reinforce the strength and toughness properties around the fibre network, which contributes to improving the flexural properties of the HFRP.

2.13.2.3 Delamination fracture toughness

A further indispensable mechanical characterisation that has illustrated significant enhancement with nanomaterials inclusion was the failure delamination resistance and the crack head arrest. Reported improvements in the fracture toughness properties Mode I and Mode II of the hybrid fibre composites modified with conventional carbon nanotubes are listed in Table 12.

Table 12 Interlaminar fracture toughness improvements (propagation values only) of HFRP (modified with conventional carbon nanotubes).

Matrix	Fibre (Type)	Nano filler type	Weight content	Maximum fracture toughness ($KJ.m^{-2}$), improvement (%)	Technique, (Lay-up)	Test method	Ref.
Epoxy (Aradur-5021)	CF (Prepreg)	DWCNT	0.5 wt.%	(+55%)	Drum-winder (UD)	DCB	Godara et al., 2009
		MWCNT	0.5 wt.%	(+83%)			
Epoxy (Araldite LY564)	CF (UD fabric)	MWCNT	1 wt.%	(+60%)	Autoclave (UD)	DCB	Karapappas, 2009
				(+75%)		ENF	
Epoxy (Bisphenol A)	GF (Multi-axial Woven)	MWCNT	0.5 wt.%	(+15%)	Vacuum bagging (Quasi-isotropic)	DCB	Silva et al., 2014
				(+40%)		ENF	
Epoxy (FM-20)	CF (UD fabric)	MWCNT	0.1 wt.%	(+4%)	Hand lay-up (UD)	DCB	Romhany & Szebenyi, 2009
			0.3 wt.%	(+13%)			
			0.5 wt.%	(+9%)			
			1 wt.%	(+5%)			
Epoxy (Bisphenol A)	CF (Prepreg)	SWCNT	Base(0)	0.343	Autoclave (UD)	DCB	Ashrafi et al., 2011
			0.1 wt.%	0.387(+13%)			
			Base(0)	1.79		ENF	
			0.1 wt.%	2.01(+28%)			
Epoxy (L135i)	GF (Non-crimp fabrics)	DWCNT	0.30 wt.%	(None)	RTM (Quasi-isotropic)	DCB/ENF	Wichmann et al., 2006
Epoxy (EPON 862)	CF (weave fabric)	f-CNTs	Base(0)	0.191	Heated VARTM (UD)	ENF	Davis & Whelan, 2011
			0.5 wt.%	0.242(+27%)			
Epoxy (L-930HT)	CF (Prepreg)	MWCNT	1.32 g/m^2	(+32%)	Spray (UD)	DCB	Joshi & Dikshit, 2012
Epoxy (MGS L285)	CF (Plain weave fabric)	Grafted/ f.CNTs	-	(+50%)	Hand lay-up (Not mentioned)	DCB	Kepple et al., 2008

Epoxy (BPA)	Alumina Fabric (Alumina cloth)	Grafted/ CNTs	Base(0)	1.19	Hand lay-up (Not mentioned)	DCB	Wicks et al., 2014
			-	2.38(+100%)			
Epoxy (Araldite F)	CF (Plain woven fabric)	Grafted/ CNTs	Base(0)	0.48	Hand lay-up (Not mentioned)	DCB	Du et al., 2014
			-	0.8(+67%)			
			Base(0)	1.4		ENF	
			-	2.22(+60%)			

Although, the addition of multiple types of carbon nanotubes dispersed into the matrix to improve the toughness properties of fibre composites regardless of the type of fibre composites used, there were modest improvements in this property in comparison with the graphene and novel fibre nanotubes. The maximum range of this improvement was 83%, while the level of improvements in the carbon fibre composites (i.e. plain woven fabric) modified with functionalised carbon nanotubes dispersed into the polymer resins was 27% (Davis and Whelan, 2011).

The improvement results after the addition of dispersed graphene and novel fibre nanotubes into the polymer resins to various types of fibre composites for previous studies are listed in Table 13. Generally, this improvement appears more efficient than conventional carbon nanotubes. The percentage of improvements in the fracture toughness properties of multiple types of carbon or the glass fibre composites modified with dispersed novel fibre nanotubes, specifically Mode II was moderately better than graphene. The range of this improvement related to the novel fibre nanotubes is between 30%-209% approximately (Yokozeki et al., 2007; Yokozeki et al., 2009). However, the multiple types of graphene do not exceed 206% (Jia et al., 2015). Interestingly, one of these reported results included high improvement, after adding the dispersed graphene into epoxy resin to the woven carbon fibre composites, which was roughly 145% (Du et al., 2017).

Table 13 Interlaminar fracture toughness improvements (propagation values only) of HFRP (modified with graphene and novel carbon fibre nanotubes).

Matrix	Fibre (Type)	Nano filler type	Weight content	Maximum fracture toughness ($KJ.m^{-2}$), improvement (%)	Technique, (Lay-up)	Test method	Ref.
Epoxy (SC-15)	GF (Plain weave)	Grafted/ GNP	0.25 wt.%	(+25%)	VARTM (Not mentioned)	DCB	Kamar et al., 2015
Epoxy (Araldite F)	GF (Prepreg)	3D GNP	Base(0)	0.95	Hot press molding (UD)	DCB	Jia et al., 2015
			-	1.62(+70%)			
			Base(0)	0.83		ENF	
			-	2.54(+206)			
Epoxy (JER806)	CF (Prepreg)	GO	Base(0)	0.161	Hand lay-up (UD)	DCB	Ning et al., 2015
			2 g/m^2	0.436(+171%)			
Epoxy (Araldite F)	CF (Plain woven fabric)	GO	Base(0)	0.53	Hand lay-up (Not mentioned)	DCB	Du et al., 2017
			1 wt.%	1.3(+145%)			
Epoxy (EPON 862)	CF (fibre mats)	HP-NGPs	Base(0)	0.458	Hand lay-up and compression molding machine (UD)	DCB	Kumar and Roy, 2018
			0.5 wt.%	0.917(+100%)			
Epoxy (LY1564)	GF (fabric cloth)	GO	0.5 wt.%	(+4%)	VARTM (UD)	DCB	Moghadam and Taheri, 2015
		$G.NH_2$		(+39%)			
		G.Si		(+33%)			
		GO		(None)		ENF	
		$G.NH_2$		(+12%)			
		G.Si		(+11%)			
Epoxy (Araldite LY 556)	CF (Non-crimp fabric)	GO	Base(0)	0.49	Hand lay-up and Autoclave (UD)	DCB	Kostagiannakopoulou et al., 2015
			0.5 wt.%	0.75(+53%)			
		GNP	0.5 wt.%	0.79(+61%)			
Epoxy (EP827)	CF (Prepreg)	CNF	Base(0)	0.086	Autoclave (UD)	DCB	Yokozeki et al., 2009
			5 wt.%	0.227(+164 %)			
			Base(0)	0.57		ENF	
			5 wt.%	1.75(+209%)			
Epoxy (EP827)	CF (Prepreg)	CNF	Base(0)	0.086	Autoclave (UD)	DCB	Yokozeki et al., 2007
			5 wt.%	0.17(+98%)			
			Base(0)	0.605		ENF	
			5 wt.%	0.786(+30%)			

Epoxy (LY 1564)	CF (Prepreg)	CNF	10 wt.%	(+104%)	Hand lay-up (UD)	ENF	Khan and Kim 2012
Polyester	GF (fibre mat)	CNF	1 wt.%	(+100%)	VARTM (Not mentioned)	DCB	Sadeghian et al., 2006

In general, improvements in the fracture toughness properties of hybrid fibre composites fabricated by graphene and fibre nanotubes or the conventional carbon nanotubes grown/grafted technique exhibits modest improvements (Kamar et al., 2015; Kepple et al., 2008). Whilst the hybrid fibre composites fabricated by carbon nanomaterials (particularly graphene and fibre nanotubes) dispersed into the polymer matrix have illustrated excellent improvements in toughness properties, except for some results relevant to conventional carbon nanotubes**,** which offered slight improvements that may refer to the agglomeration phenomenon of carbon nanomaterials into the matrix (Wichmann et al., 2006).

Improvement in results related to the addition of dispersed combined carbon nanomaterials into the polymer resins to carbon fibre composites for previous studies are listed in Table 14. There were modest improvements after the addition of graphene and conventional carbon nanotubes dispersed into the matrix onto the surface of unidirectional carbon fabric composites (Kostagiannakopoulou et al., 2017).

Interestingly, one of the results in Table 14 demonstrated significant improvements in this property, after impregnation of the hybrid carbon nanomaterials (i.e. graphene and conventional carbon nanotubes) dispersed into the epoxy matrix onto the surface of fibre cloth composites by 100% (Wang et al., 2015).

Table 14 Interlaminar fracture toughness improvements (initial or propagation values) of HFRP (modified with combined carbon nanomaterials).

Matrix	Fibre (Type)	Nano filler type	Weight content	Maximum fracture toughness ($KJ.m^{-2}$), improvement (%)	Technique, (lay-up)	Test method	Ref.
Epoxy (Araldite LY556)	CF (UD fabric)	Hybrid1 GNP-MWCNT	Base(0)	0.55 (Propagation)	Hand lay-up and Autoclave (UD)	DCB	Kostagiannakopoulou et al., 2017
			Ratio (0.5wt.%/0.5 wt.%)	0.76(+38%) (Propagation)			
		Hybrid2 GNP-MWCNT	Ratio (0.5wt.%/1 wt.%)	0.8(+45%) (Propagation)			
		Hybrid1 GNP-MWCNT	Base(0)	1.57 (Propagation)		ENF	
			Ratio (0.5wt.%/0.5 wt.%)	1.88(+20%) (Propagation)			
		Hybrid2 GNP-MWCNT	Ratio (0.5wt.%/1 wt.%)	1.97(+25%) (Propagation)			
Epoxy (not mentioned)	CF (Prepreg	Hybrid MWCNT/GO	Base(0)	0.552 (Propagation)	Spray, Vacuum bag and autoclave (UD)	DCB	Rodriguez-Gonazalez et al., 2017
			0.25 wt.%	0.644(+17%) (Propagation)			
			Base(0)	1.76 (Propagation)		ENF	
			0.25 wt.%	2.01(+14%) (Propagation)			
Epoxy (EPO-622)	CF (Fibre cloth)	Hybrid CNTs/GNP	Base(0)	469 (Initial)	Hand lay-up and Hot press molding (Not mentioned)	DCB	Wang et al., 2015
			1:9 (ratio)	938(+100%) (Initial)			

However, the improvements in these fracture toughness properties for hybrid fibre composites modified by strengthened and toughened matrix must be handled carefully. For example, the modified matrix must be distributed uniformly onto the surface of the fibre network as well as fill all the gaps with this modified matrix because the inhomogeneous distribution of the modified matrix onto the surface ply and the existence of gaps in the produced composites could affect the micro crack resistance and toughness properties of the HFRP negatively. Hence, this may affect the fracture toughness results (Gouda et al., 2014; An et al., 2012).

Multiple fracture mechanism systems were suggested to address the dissipation systems of fracture energy, which caused the increase in the fracture toughness properties of conventional fibre composites (modified and unmodified) with nanofillers. Therefore, it is better to separate these two composites to understand the fracture systems in each one of them individually. The schematic diagrams as depicted in Figure 23 show the stages of the fracture into the matrix and fillers for the fibre composite unmodified in detail. It is evident in this model that when the laminated composites are damaged due to out-of-plane forces**,** the mode failure which is basically interlaminar delamination and resistant compression in-plane of these laminates decreases significantly. Consequently, the toughness mechanism systems to dissipate the strain energy will be generated through crack propagation stages in the fibre composites.

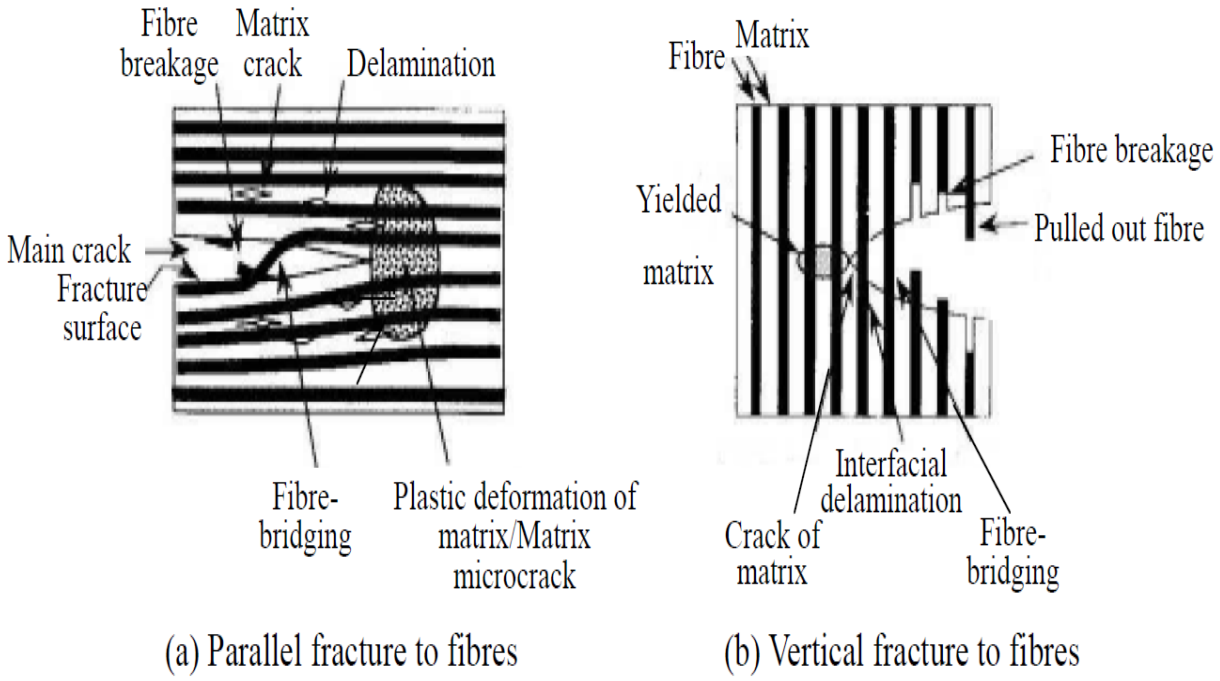

Figure 23 Schematic diagram of toughening mechanisms in conventional fibre composite unmodified (Miki et al., 1997).

The addition of rubber particles or liquid rubber was considered as one of toughening materials approaches, which could improve the resin toughness property and hence, would reinforce the delamination resistance of the fibre polymer composites (Ashrafi et al., 2011; Kim & Mai, 1998). Furthermore, strengthened and toughened fibre networks via impregnation of the modified polymer matrix into the fibre composite also restrict the plastic deformation regions and arrest the crack extension into the matrix. This is because of the existence of rigid nanomaterials contributing to the absorption of a part of the strain energy, before the possibility of its transfer to the basic fibre network. Hence, this improves the fracture toughness energy.

The fracture mechanism system of the modified polymer matrix and into nanocomposite is shown in Figure 24. These dissipation energy systems are also rather similar to counterparts in novel HFRP. Therefore, such fracture mechanism systems have been suggested to discuss the causes of improvement in the fracture toughness energy for HFRP.

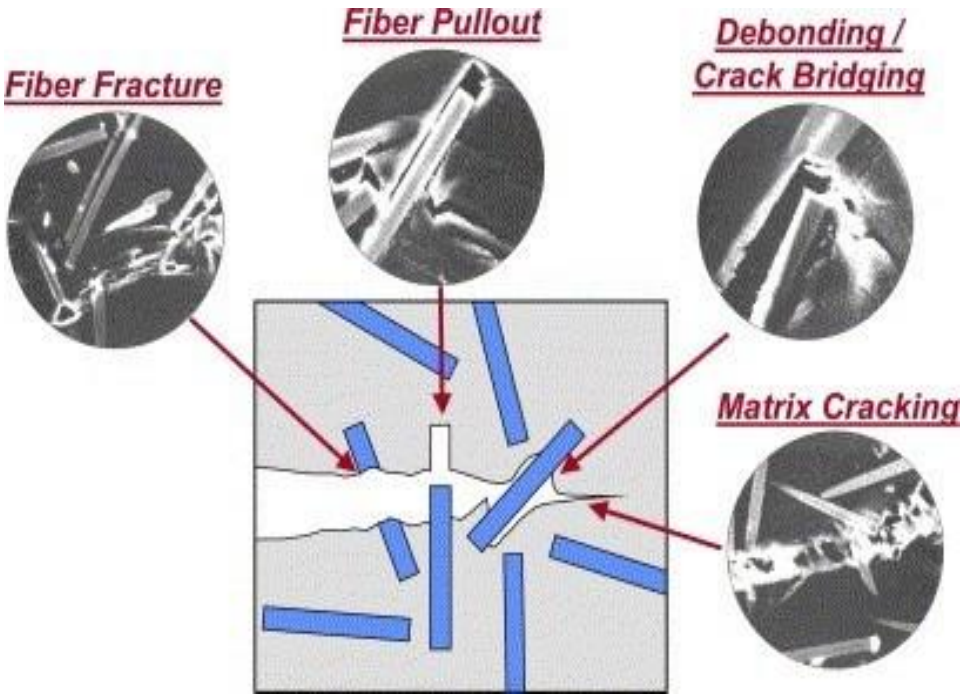

Figure 24 Keys for dissipation energy by means of fracture mechanisms in NP (modified) (Thostenson et al., 2005).

Yokozeki et al. (2009) and Godara et al. (2009), suggested that the principal reason of improvements in HFRP were as a result of rougher fracture surfaces. This indicates that more energy had been required to foreword the crack head. Further studies have demonstrated that the geometric structure, size of the nanoparticle and weight content of nanoparticles into the matrix have a significant influence on the transfer load between the polymer matrix and the fibre network. The high capacity of transferred loads through the modified matrix means more energy absorption was gained in the HFRP. This mechanical behaviour would contribute to increasing the fracture toughness properties and moreover, pinning and pull-out nanofillers were suggested as toughening systems to dissipate the stress energy into the fracture surface of HFRP (Wicks et al., 2014; Romhany and Szebenyi, 2009). Furthermore, crack bridging by the nanotubes, crack pinning/bi-furcation could blunt the crack pathway during the propagation stage (Landani et al., 2015; Chadrasekaran et al., 2014). The inclusion of carbon nanomaterials, for instance conventional carbon nanotubes was utilised to steer or deviate the crack pathway by adjusting

the reinforcement distribution or orientation generating zigzag path (Wicks et al., 2014; Ashrafi et al., 2011).

Interestingly, Kostagiannakopoulou et al. (2017), used the combination of graphene and conventional carbon nanotubes to improve the mechanical properties of carbon fibre composites. The results showed that the existence of two carbon nanomaterials in the matrix causes the formation of multiple fracture mechanisms into HFRP, such as the pinning of crack head and bi-furcation mechanisms of crack. These mechanical behaviours contributed to the additional improvement of the toughness properties for such novel HFRP in comparison with conventional HFRP (modified with one type of nanoparticles).

However, the interactions between the multiple fracture mechanism systems are still obscure in novel HFRP, due to the existence of multi sized reinforcements particularly after the impregnation of the modified matrix with two carbon nanomaterials into fibre composites. Therefore, further clarifications are required regarding an interpretation of the interaction fracture mechanism systems in novel hybrid fibre composites modified with the combination of multifunctional carbon nanomaterials (Kostagiannakopoulou et al., 2017; Wang et al., 2015).

2.14 Fibre/matrix adhesion

The design structure of the FRP can predominantly fail in the interface region of the fibre/polymer matrix at the primary or early stage (Lee, 1992). The interface region in fibre laminated composites can be described as the three dimensional boundary between the fibre plies and polymer matrix.

The interface region is critical to governing FRP properties, because of the interaction between the two materials occurred at this region. However, the interaction mechanisms can occur via three approaches: mechanical alignment or mechanical interlocking to fill the gap between micro-reinforcement, physical or chemical coupling which involves van der Waals forces or electrostatic attractions and covalent bonding between the fibre network and the polymer matrix (for further details see Figure 25), (Park and Seo, 2011; Bekyarova et al., 2007; Davis and Whelan, 2011; Li et al., 2013).

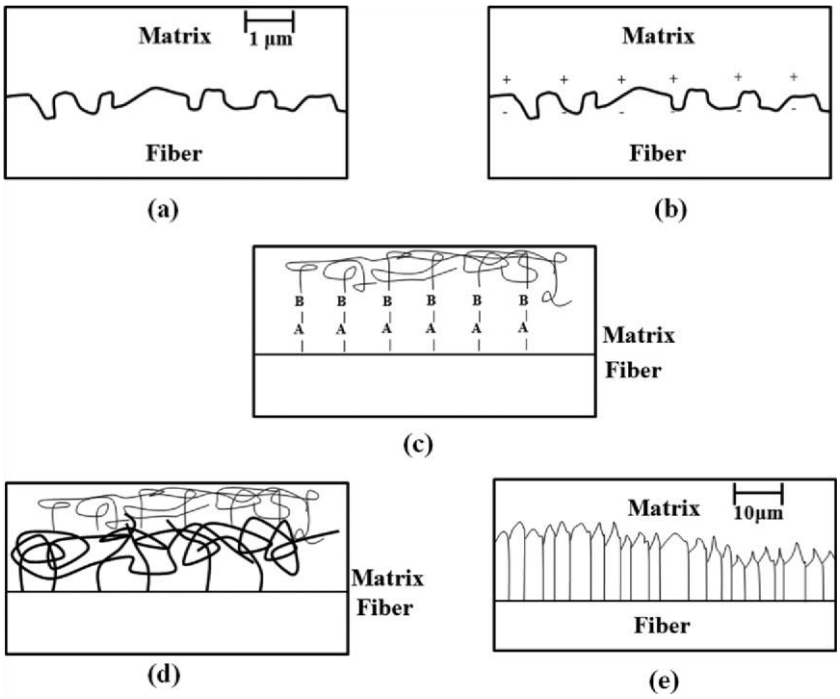

Figure 25 Schematic diagrams showing the various interaction mechanisms at the fibre/matrix interface regions: a) micromechanical interlocking, b) permanent interactions, c) chemical bonding, d) chain tangle, and e) trans-crystallinity (Park, and Seo, 2011).

In general, the fibre/matrix interfaces are weaker than the polymer matrix. In addition, the fracture toughness properties of the fibre composites are extremely affected by the interfacial region of the matrix and fibres, as well as the strength and toughness properties of the polymer matrix surrounding fibre networks. Therefore, the weakness in interfacial bonding of the fibre/matrix or toughness properties produces a deterioration in the mechanical properties of structural composites. For this reason, the modification of the interfacial region for the composites is necessary to create the strong bond between the fibre network and polymer matrix. It is well known that the addition of nanoreinforcements into the polymer matrix could improve the interfacial bonding region in the fibre/polymer matrix (Qian et al., 2010; Gojny et al., 2005). In particular, there has been an interest recently in using the combined carbon nanomaterials to induce the mechanical interfacial properties of polymer composites (Liu et al., 2017). Additional uses can also be carried out on fibre networks or nanomaterials, such as chemical treatments which are regularly used the fibre surface to modify the interface regions (Wang et al, 2015;Qian et al, 2010; Du et al., 2017; Zhang et al., 2014).

The bridging and pull-out of filler, bi-furcation mechanisms, pinning of the crack head besides the combination of these fracture mechanisms (i.e. pinning of crack head and bi-furcation mechanisms), often occur in novel hybrid fibre composites modified with two carbon nanomaterials (Kostagiannakopoulou et al., 2017). These mechanisms are quite significant energy dissipation systems, regarding the interlaminar shear strength and interlaminar fracture toughness of the novel composites. Furthermore, the mechanical fracture mechanisms of these

cases occur when fibres or fillers are pulled-out of the delamination plane at the region of failure. Therefore, any modification of the fracture systems would improve the mechanical properties of HFRP.

2.15 Fibre orientation in laminated composites

The mechanical properties of the carbon fibre composites can be affected by the geometric structure of the composites and the orientation (Chou, 1998). It has been acknowledged that the shear strength and fracture toughness properties of the carbon fibre composites are highly dependent on the direction of the stacking sequence. As an example, unidirectional or quasi-isotropic and other distributions are one of them (Pereira & Morais, 2004; Shekar et al., 2014). Therefore, distribution and orientation are significant factors in relation to laminate composite designing.

The modes of failure in the structure design of fibre composites are also significantly based on the stacking sequence and orientation of the fibre network (Herakovich, 1989). In general, there are three modes of load-deformation curves relating to fracture toughness testing of the fibre composites; zigzag or jagged mode, bow mode and triangle mode, as shown in Figure 26.

Further cases may affect the behaviour of failure mode, such as the geometric design of fibre material and dimensions of testing samples, conditions of tests and fracture mechanism systems (Kuwata & Hogg, 2011; Hwang et al., 2001; Morais and Pereira, 2007; Landani et al., 2015; Fenner and Daniel, 2014; Gill et al., 2009).

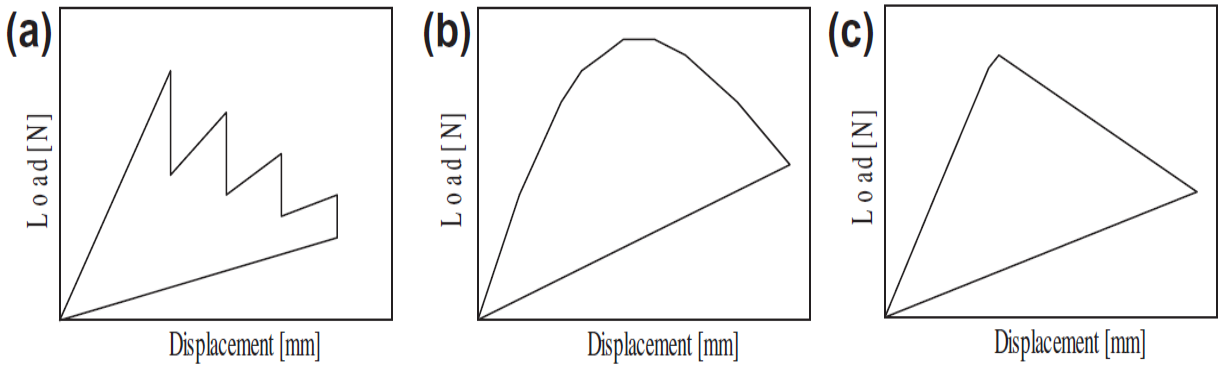

Figure 26 Typical load-displacement curves for DCB and 4ENF tests divided into three modes of deformations: a) zigzag, b) bow, and c) triangle (Kuwata and Hogg, 2011).

Here are some explanations: the symmetric stack between the woven plies could minimise the jumping crack during the propagation stage (Hunston, 1983). Moreover, the crack propagation could be effected by the presence of 90 and 0 plies at the mid plane orientation or in the interlaminar region (Robinson & Song, 1992; Yokozeki et al., 2009). Numerous experimental

and analytical studies for altering the fibre distribution and orientation have been conducted by researchers (Robinson and Song, 1992; Chou, 1998). Morais et al. (2002), reported the fracture toughness properties of two types of asymmetric stacking sequences: $[0/90]_{12}$ samples and $[0/0]_{24}$ samples. They exhibited a zigzag crack behaviour mechanism between two neighbouring plies [0/90] at their interface regions for plain weave fibre composite, as shown in Figure 27.

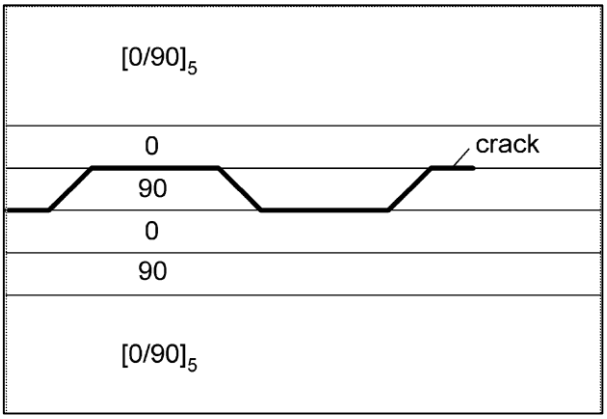

Figure 27 Schematic diagram shows the behaviour mechanism of crack propagation in [0/90]12 (Morais et al., 2002).

As a consequence, modes of load-deformation curves of conventional carbon fibre composites (i.e. woven carbon fabric) probably are affected by the orientation of fibres, fracture mechanisms and other factors. Therefore, symmetric stacking sequences were applied to construct the structure of laminated composites with the aim of avoiding these problems as much as possible in the present study.

Chapter 3. Experimental work

The goal of this chapter was to undertake optimisation of three nanocomposites; specifically, GNP/epoxy nanocomposite, CSCNT/epoxy nanocomposite, hybrid GNP-CSCNT/epoxy nanocomposite. The reason for that is to obtain the optimum strength and toughness properties of the modified matrix in each one of the novel nanocomposites and thereafter, to use this in the manufacture of HCFRP. Therefore, this chapter characterises the experimental procedures employed for optimisation of these nanocomposites, as well as the mechanical dispersion techniques used for this purpose. In addition, it describes the manufacture of hybrid composites modified with optimum modified matrix during the course of this experimental research. The selection of ingredients are justified and their mechanical properties are listed.

3.1 Materials

3.1.1 The thermoset resin

The resin used in this study was (RS-L135 epoxy and RS-H137 hardener), supplied by a PRF composite material company in the UK. It was chosen because of its low viscosity and the ability to achieve a room temperature cure. The mixing ratio for the resin and hardener is 100:35 and density 1.18 g/cm^3, whilst the gelling time is 12 hours at 25^{0}C with a mixed viscosity of 1000 mPa s at 25^{0}C. Glass transition temperature as given by the resin supplier is between 60 to 65°C.

3.1.2 Graphene nanoplatelets (GNP)

Nano-graphene xGnP®-Grade C was supplied by XG Sciences, Inc. (Lansing, USA). The average diameter was 1-50 µm, the thickness amounted to 20 nm, whereas the surface area was 500m^2/g. Figure 28 presents the configuration of the nano-graphene xGnP®-Grade C structure.

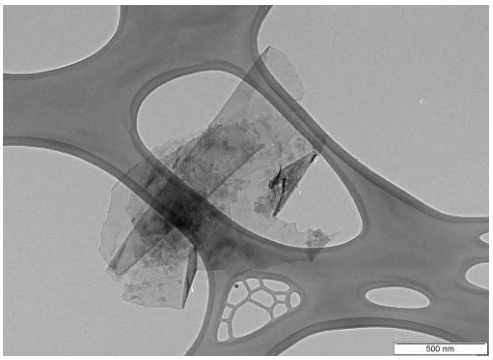

Figure 28 The geometric structure in nanoscale for graphene grade C taken by TEM.

Graphene was considered as an alternative carbon nanomaterial recently in modifying functional and structured polymer composites and conventional fibre composites instead of conventional

carbon nanotubes (i.e. SWCNT or MWCNT), due to its low cost. Furthermore, it has a platelet shape (i.e. single sheets with high specific area) and excellent mechanical properties, such as stiffness and strength properties (Gkika et al., 2017; Mittal et al., 2015; Bhattachaya et al., 2016; Li et al., 2018).

3.1.3 Cup-stacked carbon nanotubes (CSCNT)

Cup-stacked carbon nanotubes (CSCNT) were purchased from CARBERE® (GSI Croes Corporation) in Japan. Figure 29 exhibits the novel geometric structure of this type of fibre nanotube. Table 15 provides the physical properties of the CSCNT as supplied by the manufacturer. CSCNT have an individual morphology in which graphite layers are inclined from the axis of the fibre. As a result of this novel structure, graphene layers emanate from edge planes on both the interior and exterior surfaces of the fibre. These characteristics conduct nanofiber length adjustment and high dispersion into the polymer resin that provides better performance in many types of industrial applications.

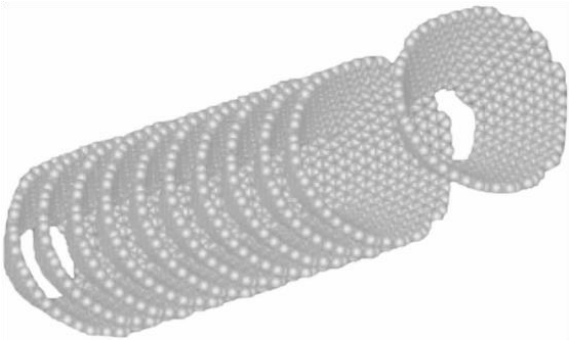

Figure 29 The geometric structure of a CSCNT.

Table 15 Physical properties and nanometre size of CSCNT.

Properties	Unit	Value
Diameter	nm	70˜80
Length	μm	5
Specific Surface Area	m^2/g	50

3.1.4 Carbon fibre (CF)

Carbon fibres used for this experimental study were Pyrofill TR30S 3L (Figure 30) supplied by the Easy Composite Company in the UK. This carbon fibre comprised woven fabric in a 3k plain weave, which was balanced, bi-directional with orientation [0̊,90̊], continuous and had a fibre weight of 200 gsm with a thickness of 0.3mm, besides high strength and stiffness properties, as

listed in Table 16. The selection of the fibre was based on the hypothesis; 'which sized carbon fibre would create excellent bonding with the epoxy resin and better handling characteristics. Therefore, it is appropriate for application in wet-lay, vacuum bagging and resin impregnation manufacture. Furthermore, due to the high flexibility of carbon woven fabric for the layup of convoluted shapes in comparison with unidirectional carbon fibre, it is applied in most fabric constructions engineering (i.e. aerospace structures). Additionally, it has strength and stiffness in two directions in each ply, whereas the unidirectional carbon fibre has these properties in one direction only. As a consequence, it was selected in the manufacture of HCFRP in the present work.

Figure 30 Pyrofill TR30S 3L carbon fibre composite.

Table 16 Properties of Pyrofil TR30S 3L.

Property	Unit	Value
Tensile Strength	MPa	4120
Tensile Modulus	GPa	234
Ultimate Elongation at Failure	%	1.8
Filament Diameter	µm	7
Density	g/cm^3	1.79

3.2 Preparation of optimised NP

3.2.1 Weight content in NP formulations

The weight concentration of GNP, CSCNT, and hybrid GNP-CSCNT nanofillers were prepared as shown in Table 17. Pure epoxy samples (base tests) were also manufactured, in order to assess any property enhancement compared with the three types of NP developed in this work (i.e.

GNP/epoxy nanocomposites, CSCNT/epoxy nanocomposites and hybrid GNP-CSCNT/epoxy nanocomposites).

Table 17 Formulations of prepared nanocomposites

Sample	GNP Concentration wt. %	CSCNT Concentration wt.%
Pure Epoxy	0	0
GNP/epoxy nanocomposite	2.5	0
	4	0
	5	0
	6	0
	7	0
CSCNT/epoxy nanocomposite	0	2.5
	0	4
	0	5
	0	6
	0	7
Hybrid GNP-CSCNT/ epoxy nanocomposite	1.25	1.25
	2	2
	2.5	2.5
	3	3
	3.5	3.5

3.2.2 Sonication mixing

Three types of NP were manufactured at different weight concentrations ranging from 0 wt.% to 7 wt.%; specifically, GNP/epoxy nanocomposites, CSCNT/epoxy nanocomposites as well as hybrid GNP-CSCNT/epoxy nanocomposites. As the sonication technique is effective in dispersing various types of nanoparticles, it has been employed to disperse graphene and fibre nanotubes in resin (Guo and Chen, 2014). The preparation stages of these NP are shown in Figure 31. The initial processing stages included dispersing the nanofillers in acetone (13% weight of epoxy resin), (Guo and Chen, 2014) and applying ultrasonic vibration to the mixture for 15 min by means of the ultra-sonication technique. A UP200S sonicator (Figure 32a) supplied by Medical Products Ltd was used. Then, the mixture was added to the epoxy resin and further ultrasonic dispersion was performed for 15, 30 and 45 min as the secondary stage. The purpose of these intervals is to optimise the nanofilled matrix and moreover, to investigate the effect of sonication mixing time on the strength and stiffness properties of the nanocomposites at critical weight

concentration. After that, the mixture was heated to a temperature of 65^{0}C in a vacuum oven to dry the mixture of acetone completely. Subsequently, hardener was added to the mixture, which was blended together using mechanical stirring (Klarstein) for 10 min at 2000 rpm, (Figure 32b). The final stages involved further evacuation to remove all the bubbles from the mixture, which was then poured into moulds. The samples were thermally cured by utilising the following curing processes: 48 hrs at 26^{0}C for the initial curing, followed by 15 hrs at 50^{0}C for the post curing. Next, the cured samples were removed from the mould for mechanical strength testing.

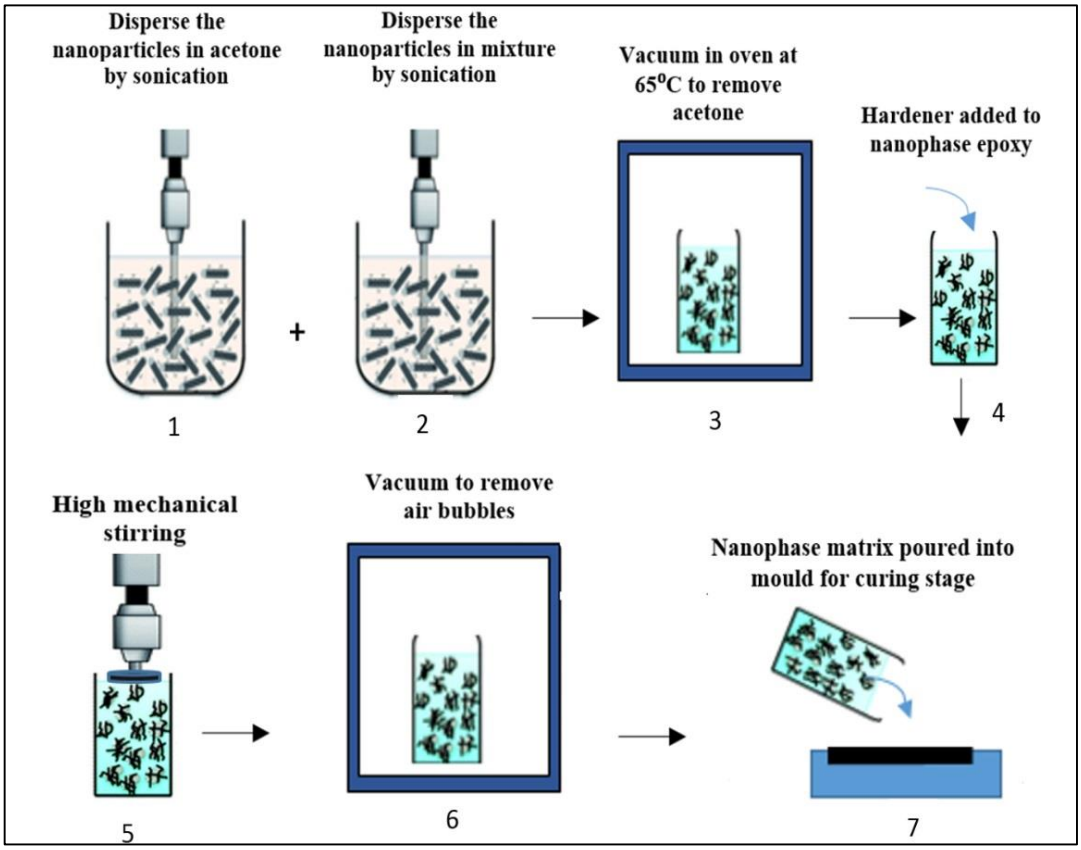

Figure 31 Nanofiller dispersion process in the epoxy resin by means of the sonication technique.

(a) (b)

Figure 32 a) UP200S sonication technique, b) High mechanical stirring.

3.2.3 Ball mill mixing

Owing to the superior efficiency of the milling technique in dispersing various quantities of nanoparticles in the resin, it has been used to achieve high exfoliation of graphene and fibre nanotubes in the matrix (Guo and Chen, 2014). Hence, this contributes to improving the mechanical interfacial properties between the nanoparticles and the matrix and consequently, improves the strength and toughness properties of the nanocomposites. However, in the preparation sequence, Figure 33, GNP, CSCNT and hybrid GNP-CSCNT nanofillers, as well as RS-L135 epoxy resin, were weighed and mixed together before being placed in the ball mill (FRITSCH, Germany, see Figure 34) containing 350 balls 5 mm in diameter. The rotation speed of the closed container was 400 rpm and the milling periods were 15, 30, 45 and 60 min. The purpose of these periods of ball mill mixing time is to optimise the nanofilled mixture and moreover, to investigate the effect of milling time on the strength and stiffness properties of the nanocomposites at critical weight concentration. Subsequently, the RS-H137 hardener was added and blended by mechanical stirring for 2 min at 2,000 rpm. The resin was then vacuum de-gassed and poured into moulds. The specimens were cured for 48 hrs at 26^0C, followed by 15 hrs at 50^0C. The cured specimens were removed from the mould for mechanical strength testing.

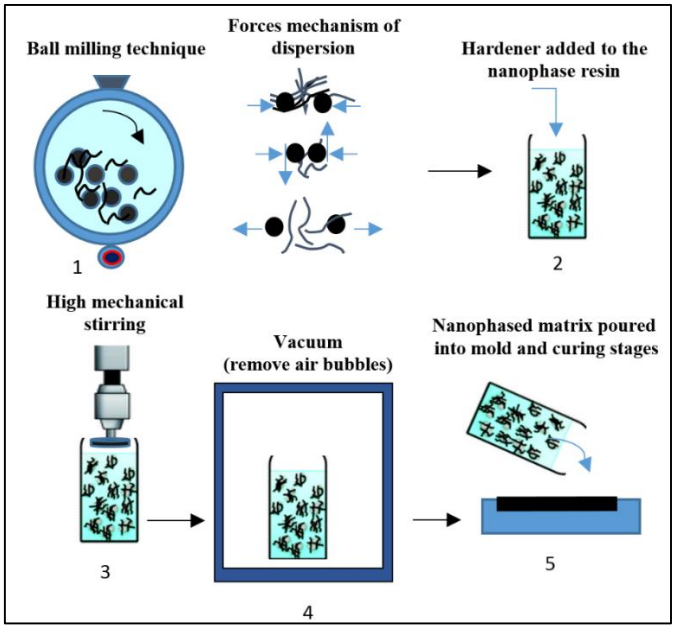

Figure 33 Nanofiller dispersion process in the epoxy resin by means of the ball milling technique.

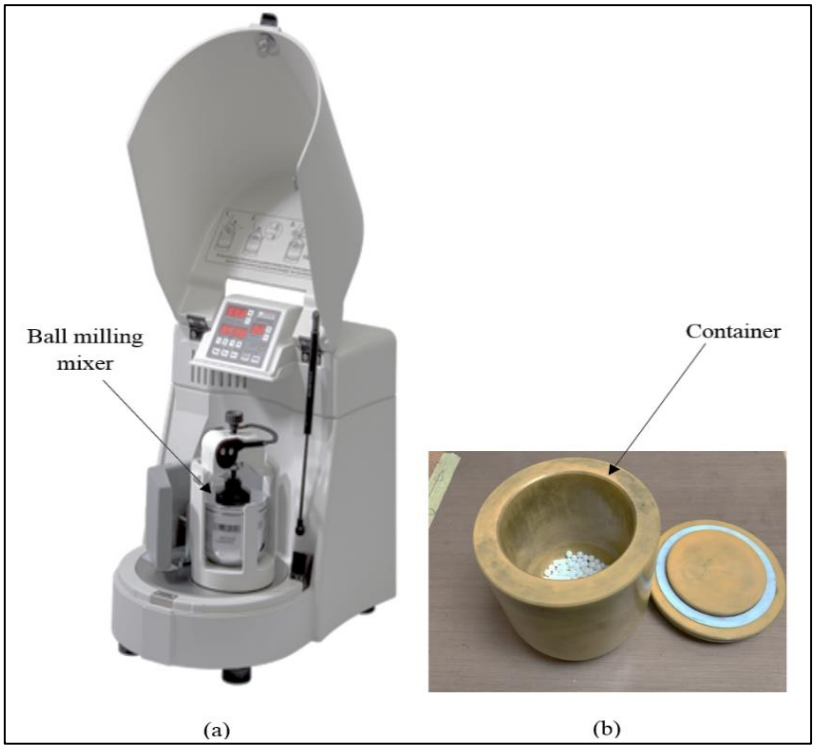

Figure 34 a) FRITSCH ball milling technique b) the container for mixing and milling balls.

3.2.4 Combined techniques mixing

Combined sonication and ball milling techniques were used to improve the degree of nanoparticles dispersion in the epoxy resin and moreover, to obtain high exfoliation of nanoparticles into the matrix. Hence, this increases the grade of attractions between the nanoparticles and the matrix which contributes to the promotion of strength and toughness

properties of the nanocomposites (Tang et al., 2013). The novel procedure for these combined techniques which has been applied in the present work is dispersion of graphene and fibre nanotubes into the epoxy resin over a reasonable period of time without the need to use chemical dispersants. To achieve that, a high shear force, compressive force, and extension force were applied to the nanoparticles to break up all the clusters into the resin via two main dispersion processes.

The preparation sequence is described in Figure 35. The initial stage included dispensing the nanoparticles into epoxy resin by means of the ball milling technique (FRITSCH, Germany) for 45 min at high speed of 400 rpm. The mixing container consisted of 350 balls each with a diameter of 5 mm. Subsequently, the suspension was transferred to the ultra-sonication technique (Ultrasound Technology, UP200S) to re-disperse it for 8 min at high amplitude (100%) as the secondary stage. Hardener was added to the resin which was mixed together using high mechanical stirring for 2 min at 2000 rpm to ensure that the mixture blended well. The final process involved robust vacuuming to remove the bubbles from the blend. Afterwards, the resin blend was poured into moulds. Subsequently, two stages of thermal curing were performed on the nanocomposite specimens: initial curing for 48 hrs at 26^0C, followed by the post curing stage for 15 hrs at 50^0C. The specimens were then released from the mould for further mechanical strength and toughness tests.

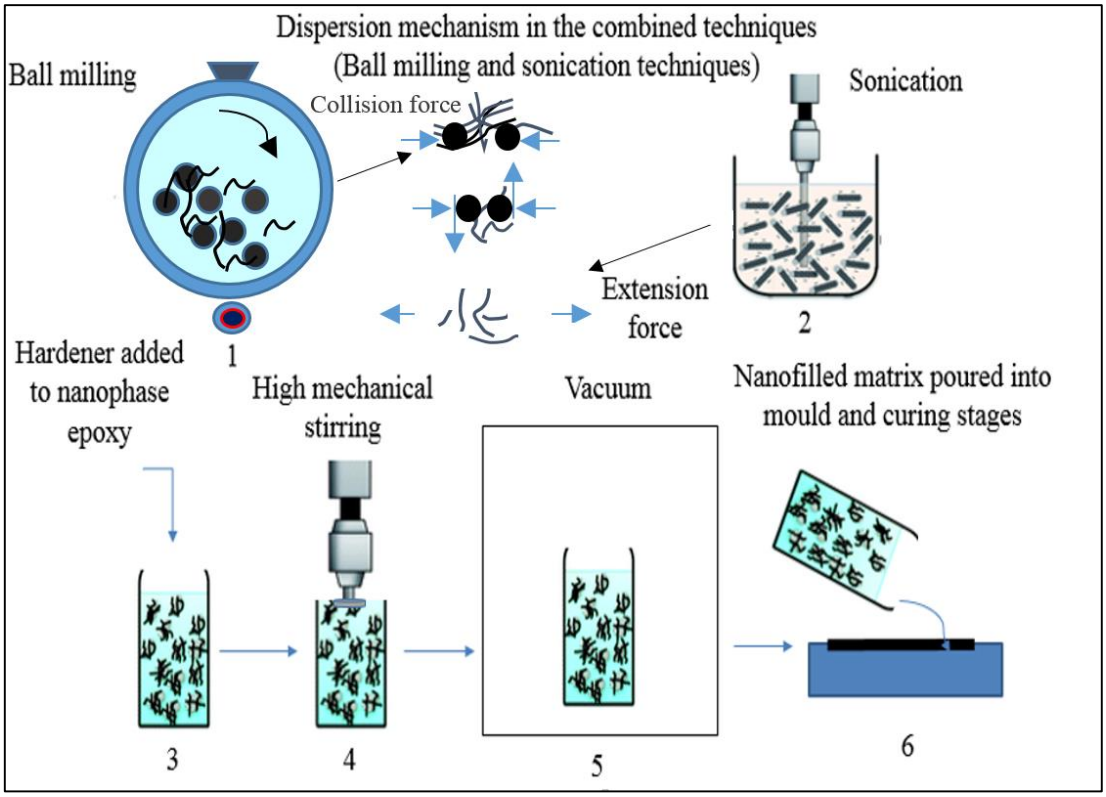

Figure 35 Nanofiller dispersion process in the epoxy resin by means of combined techniques.

3.3 Manufacturing of HCFRP

The optimum modified matrix in each one of the novel NP that is processed by combined techniques mixing was chosen to fabricate the design of the HCFRP as it showed the highest improvement in strength and toughness properties (Wang et al., 2015; Zhou et al., 2006). Hybrid laminated composites were fabricated by using woven fabric carbon fibre, 5wt.% GNP, 6 wt.% CSCNT and 4 wt.% GNP-CSCNT (hybrid nanofillers). The hand lay-up technique was used to fabricate four types of laminated composites modified and unmodified by nanofillers, (i.e. GNP/CF/epoxy nanocomposite, CSCNT/CF/epoxy nanocomposite, hybrid GNP-CSCNT/CF/epoxy nanocomposite and CF/epoxy composite unmodified, as guidance to check for any enhancement in mechanical properties after adding the nanoparticles to the carbon fibre composites. Schematic diagrams of this fabricating process are illustrated in Figure 36.

The modified epoxy matrix was sufficiently impregnated into the woven fabric carbon. A laminate of peel ply was laid down on the flat glass mould to avoid adhesion of the laminated composites and to remove it easily after the curing stage. The layer of woven fabric was laid down on the peel ply. Next, the nanophase matrix was infused on both sides of each laminate uniformly by using suitable tools, such as a brush and roller. Subsequently, another sheet of peel ply was used to cover the upper surface of laminated composites. Two strips of steel plates were inserted as spacers to maintain the stability of pressure on the laminated composites and a homogeneous laminate thickness. The stacked laminates were then compressed using a steel plate inside the vacuum bagging, (Wicks et al., 2014). A nylon layer was used as an insulator to surround the steel plates. Then, a coat of breather cloth was laid down to absorb excessive resin and to secure a sufficient path for the vacuum pressure process. The vacuum bag film was laid down and plaster surrounds the laminated composites to insulate the composite from the effect of environmental conditions. A valve connected to a vacuum bag was attached to the plastered part. The primary purpose of this vacuum pressure is to generate an internal pressure force to improve the adhesion between the laminated composites and to remove the air completely from the vacuum bag.

Two stages of thermal curing were performed for the panels of the hybrid composite as follows: the initial stage lasted for 48 hrs at 26^0C under vacuum bagging pressure conditions, the laminated composites were then released from the vacuum bagging and followed by post curing for 15 hrs at 50^0C as the secondary stage. The curing stages and vacuum pressure are shown in Figure 37. The cured panel composites were machined and cut into suitable specimens with standard required dimensions to undertake the mechanical tests. The neat weight concentration of the nanofilled matrix was estimated to be between 37-39 wt.% in each laminated composite.

The orientation of the produced hybrid composites balanced the symmetric stacking sequences of the woven carbon plies with direction [0̊,90̊]. The nominal composites thickness for the samples was approximately 2 mm for shear and flexural tests and 4 mm for fracture toughness tests, as shown in Table 18.

Table 18 Experimental set up of the four formulation composites produced.

Sample	Weight nanofillers (wt.%)	Stacking sequence	Thickness (mm)
CF/epoxy composite unmodified	0	Symmetric $[(90̊,0̊)_4/(0̊,90̊)_4]$	2.00±0.10
		Symmetric $[(90̊,0̊)_8/(0̊,90̊)_8]$	3.98±0.15
GNP/CF/epoxy nanocomposite	5	Symmetric $[(90̊,0̊)_4/(0̊,90̊)_4]$	1.97±0.13
		Symmetric $[(90̊,0̊)_8/(0̊,90̊)_8]$	3.90±0.10
CSCNT/CF/epoxy nanocomposite	6	Symmetric $[(90̊,0̊)_4/(0̊,90̊)_4]$	2.00±0.10
		Symmetric $[(90̊,0̊)_8/(0̊,90̊)_8]$	4.00±0.08
Hybrid GNP-CSCNT/CF/epoxy nanocomposite	4	Symmetric $[(90̊,0̊)_4/(0̊,90̊)_4]$	1.98±0.11
		Symmetric $[(90̊,0̊)_8/(0̊,90̊)_8]$	3.98±0.12

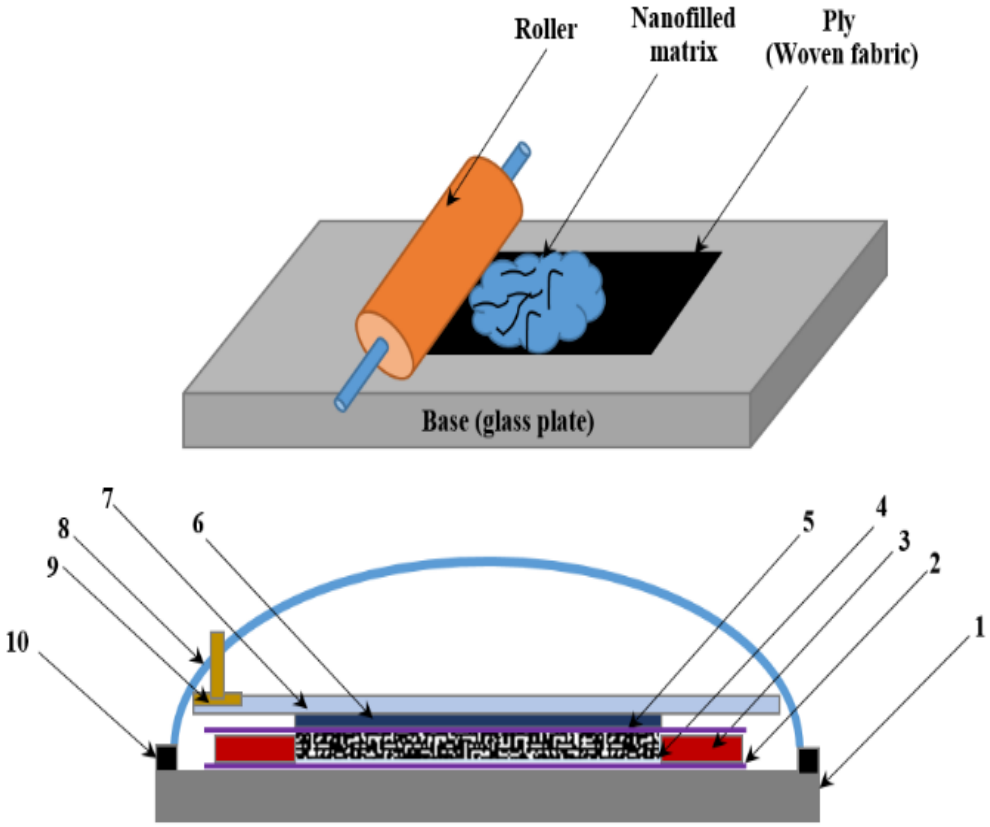

Figure 36 Manufacturing HCFRP and the experimental setup for vacuum curing: 1, glass plate (base); 2, peel ply; 3, spacers; 4, carbon fibre fabric; 5, peel ply; 6, steel plate; 7, breather materials; 8, vacuum bag film; 9, valve; 10 sealant tape.

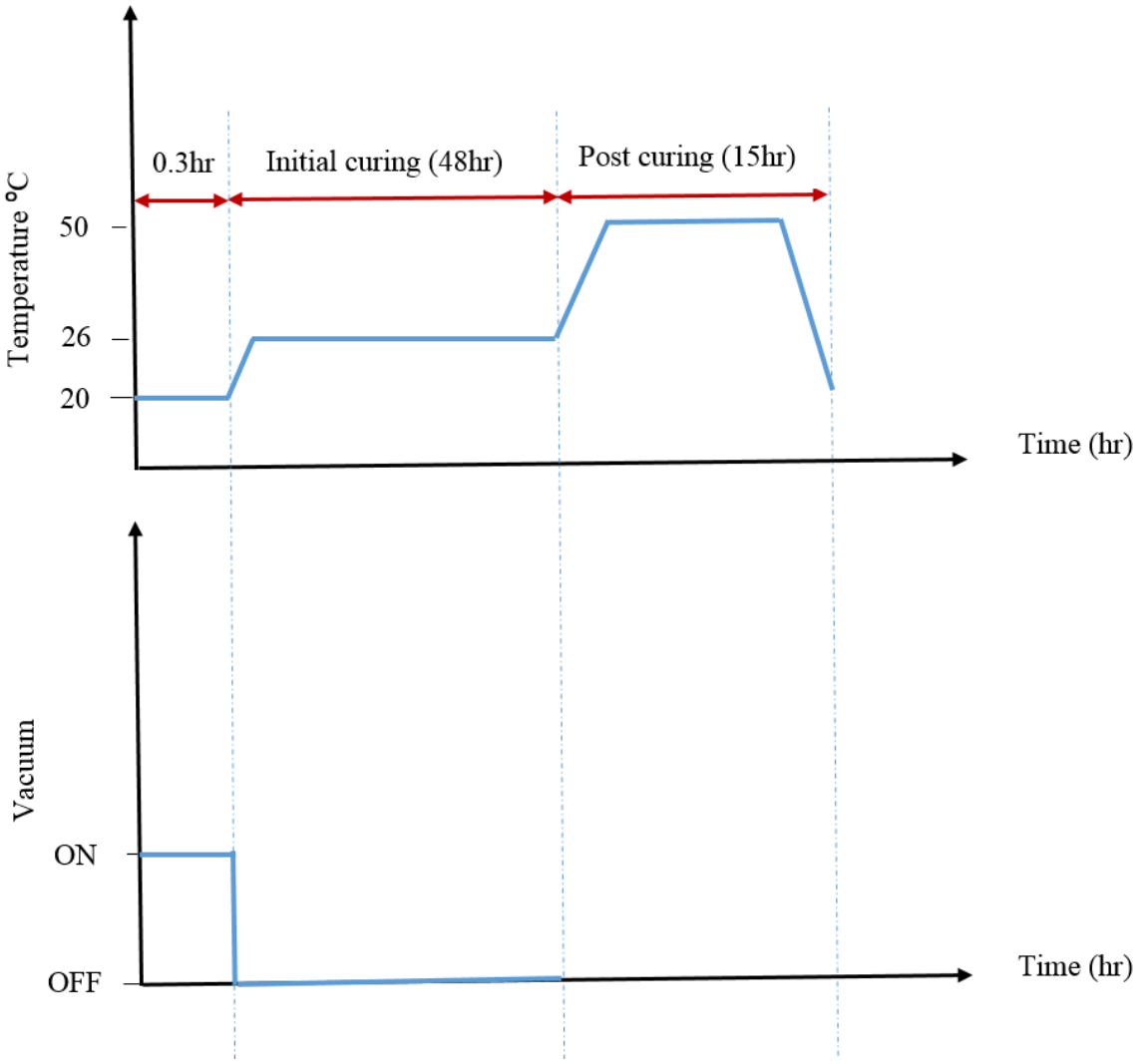

Figure 37 Curing stages for the HCFRP with temperature and vacuum shown.

Chapter 4. Characterisation

This chapter describes the characterisation methods used to assess the mechanical properties of the NP besides the HCFRP. The quality of the dispersion process of the carbon nanomaterials into the matrix was evaluated to ensure that the optimum dispersion was achieved in the nanocomposites. The tensile strength and flexural strength at different weight concentrations as well as fracture strength at critical weight concentration were measured to check for any improvement in the mechanical properties of the modified matrix in the nanocomposites. Short beam shear strength, flexural strength properties as well as Mode I and Mode II interlaminar fracture toughness were also measured to quantify the improvement in mechanical properties of the carbon fibre composites modified with optimum modified matrix.

4.1 Mechanical characterisation of NP

4.1.1 Tensile properties

Tensile loading was applied on the three types of NP by means of a Shimadzu Universal Test Machine with load capacity of 100 KN at a cross head speed of 5mm/min maximum tensile strength, while the modulus and maximum strain were estimated according to the ASTM D638 standard. The test specimens were “dogbone” shape with a gauge length of 25 mm, a width of 6 mm and thickness of 4 mm. All specimens’ tests were performed at room temperature and the average value of samples was recorded.

4.1.2 Flexural properties

Three-point bend tests were conducted using a Shimadzu Universal Test Machine with a load capacity of 100 KN. The geometric dimensions of the specimens tested had a length of 88 mm, width of 20 mm and a thickness of 5 mm. The maximum flexural strength, flexural modulus and maximum strain were calculated according to ASTM D790 standard. All tests were performed at a constant cross head speed of 2 mm/min and room temperature. The average stress properties of the samples were recorded.

4.1.3 Quasi-static fracture toughness properties

Single-edge-notched bending specimens were prepared according to the ASTM D5045 standard. Figure 38 illustrates the configuration of the SENB specimen test with standard dimensions. First a notch was created using a sawing cutter machine of approximately 4 mm depth (d), the initial crack tip was created by a sharp razor blade throughout the notch root. The pre-crack length in

the specimens was measured by using an optical microscope with a 5x objective lens to determine the actual crack length (α). It was found to range from 4.6 mm to 4.9 mm.

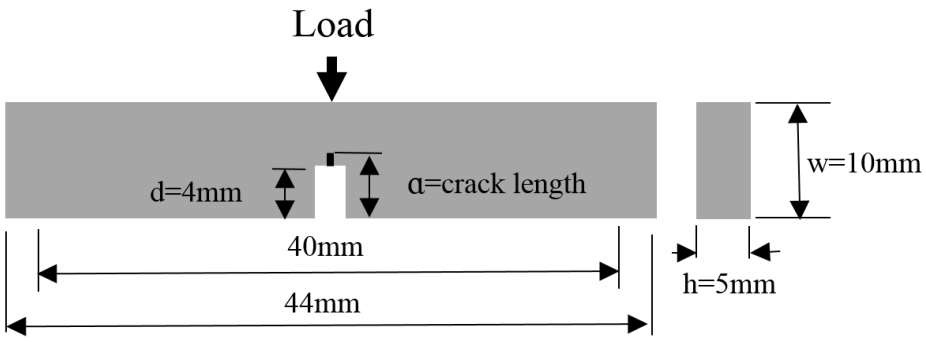

Figure 38 Configuration of SENB specimen.

A three point bend method was applied to all test specimens by using a Shimadzu Universal Test Machine equipped with a 100 KN load capacity. The bending load was applied with a rate of 1 mm/min test speed. The value of critical stress-intensity factor, K_{IC} (plane strain fracture toughness) was calculated by applying Equation 1 and the average value of samples was recorded.

$$K_{IC} = \frac{P_{max}}{h\, W^{1/2}}\, f(x) \qquad Equation\ 1$$

$$f(x) = 6x^{1/2}\frac{[1.99 - x(1-x)(2.15 - 3.93x + 2.7x^2)]}{(1+2x)(1-x)^{3/2}} \qquad Equation\ 2$$

Where P_{max} is the maximum load, W is the depth of specimen, h is the thickness of specimen, α is the actual crack length and x is the ratio (α/W) which can be calculated by Equation 2.

4.2 Weight and volume fraction measurement of laminated composites

While the weight fraction of the fibre and the matrix content in the HCFRP was easily estimated by simply weighing, the volume fraction is relatively difficult to estimate. However, determination of the fibre weight fraction and volume fraction were measured in accordance with ASTM D 3171. The analytical approach was applied in the present work to calculate the following two physical parameters: the fibre weight content in the laminated composite is based on its actual weight measured. Moreover, the weight of laminated composite is known and measured during the manufacturing process. The real weight of the nanofilled matrix (W_{matrix})

in the composite involves the weights of the epoxy resin and the nanoparticles. Additionally, the amount of this nanofilled matrix is the difference between the weight content of the laminated composite ($W_{composite}$) and the actual weight of the fibre content (W_{fibre}) used in the manufactured composite, as shown in Equation 3.

$$W_{matrix} = W_{composite} - W_{fibre} \qquad Equation\ 3$$

The neat weight of the matrix content (W_m)was calculated in accordance with Equation 4

$$W_m = \frac{W_{matrix}}{W_{composite}} \times 100 \qquad Equation\ 4$$

The weight of the fibre content (W_f)was calculated in accordance with Equation 5

$$W_f = \frac{W_{fibre}}{W_{composite}} \times 100 \qquad Equation\ 5$$

To calculate the volume fraction of the matrix and the fibre content in each composite requires calculating the actual density of the composites after addition of the nanoparticles to the resin. It is assumed that the density of the nanocomposites is not affected too much after the addition of the nanoparticles to the pure epoxy resin, (Yasmin and Daniel, 2004). Thus, the value of the density in each nanocomposite for the present work was assumed constant and equalised to the density of the pure epoxy composite.

The volume fraction of the matrix (V_m) in hybrid composites was estimated by applying the following Equation 6

$$V_m = \left(\frac{W_{matrix}}{W_{composite}}\right) \times 100 \times \left(\frac{\rho_{composite}}{\rho_{matrix}}\right) \qquad Equation\ 6$$

The volume fraction of the fibre content (V_f)in hybrid composites was calculated by applying the following Equation 7.

$$V_f = \left(\frac{W_{fibre}}{W_{composite}}\right) \times 100 \times \left(\frac{\rho_{composite}}{\rho_{fibre}}\right) \qquad Equation\ 7$$

In accordance with this standard method, the volume fraction of the voids was assumed equal to zero.

4.3 Mechanical properties of HCFRP

4.3.1 Interlaminar shear strength (ILSS)

Short beam specimens were prepared in standard dimensions with lengths of 20 mm, widths of 10 mm and thicknesses of 2 mm, as shown in Figure 39, (British Standard). The tests were performed using the three point bend flexure test using a Shimadzu Universal Test Machine; AG-X Plus with a load capacity of 100 KN at a cross head speed of 1mm/min. The maximum load was recorded and the interlaminar shear strength (ILSS) was calculated by applying Equation 8 as follows. The specimens were tested at room temperature and the average value was recorded.

$$\tau_{ILSS} = \frac{3\,P_{max}}{4\,bh} \qquad Equation\ 8$$

Where, P_{max} is the maximum force, b is the width of the specimen and h is a thickness

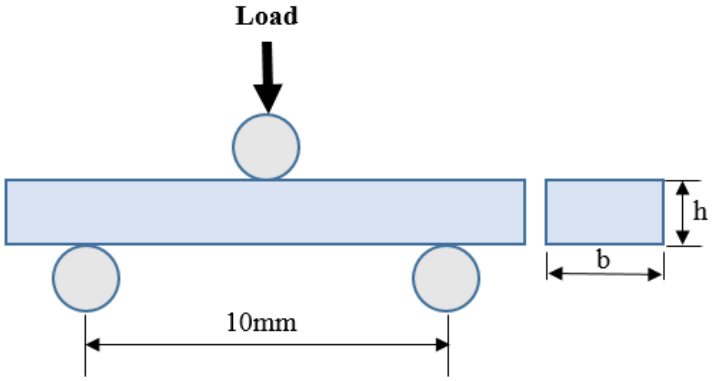

Figure 39 Schematic diagram shows the short beam shear (SBS) testing.

4.3.2 Flexural strength testing of laminate composites

Flexural tests were performed on the standard samples to determine the strength of the HCFRP using the three-point bend flexure test (Shimadzu Universal Test Machine with load capacity of 100 KN) at a cross head speed of 1 mm/min at room temperature. The standard dimensions of the samples are 56 mm long, 25 mm wide with a thickness of 2 mm. The flexural strength, flexural modulus and elongation at failure were calculated according to ASTM D790 standard.

4.3.3 Interlaminar fracture toughness testing (Mode I) of laminate composites

A double cantilever beam test was applied to measure the values of fracture toughness energy in Mode I. The mould design of the DCB samples is revealed in Figure 40. The DCB of the samples were rectangular in geometric shape, prepared into standard dimensions with lengths of 143 mm, widths of 25 mm and a thickness of 4 mm (ASTM D5528). A 12 µm thick aluminium film was inserted at one end of the sample to generate a crack length of 63 mm in the mid-plane for each sample. Both sides of the DCB samples were marked from the end edge of the film insert vertically every 1 mm up to 60 mm.

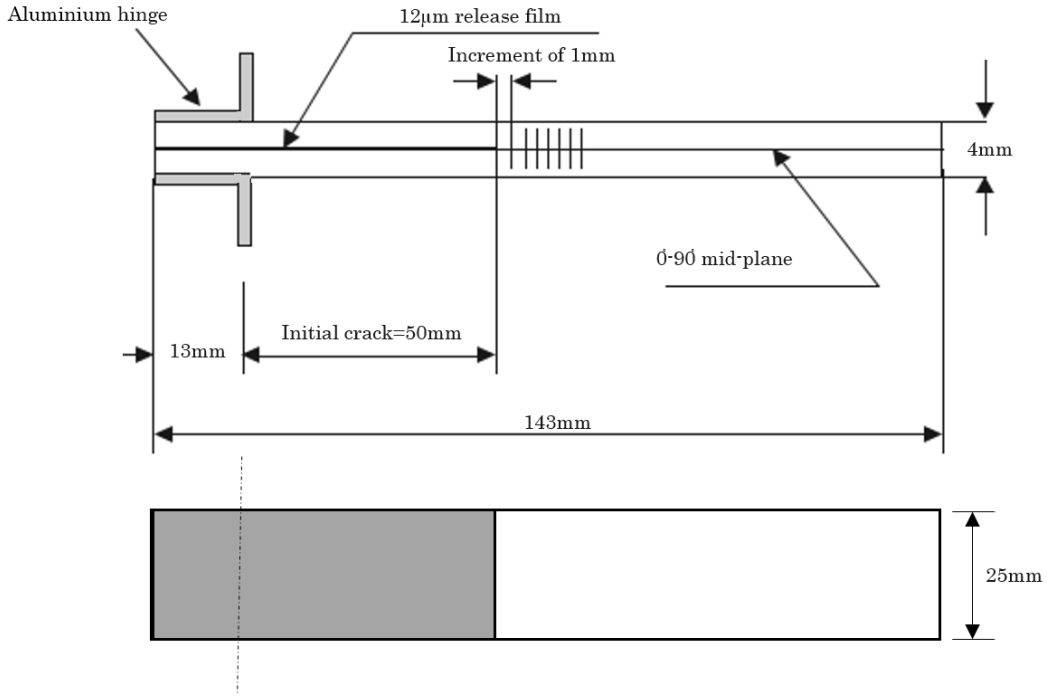

Figure 40 The geometric structure and dimensions of the DCB sample.

The DCB tests were performed by using a Shimadzu Universal Test Machine with load capacity of 10 KN. Travelling optical microscope with a 10x objective lens was used to monitor and record any extension in crack length during period of loading, as shown in Figure 41. The DCB samples were loaded in tension to create an initial crack in Mode I at a rate of 1mm/min test speed. After pre-cracking, the DCB samples were unloaded into the initial location at a rate of 10 mm/min. Thereafter, the testing was restarted at a cross head speed of 1 mm/min until the 50 mm crack length had been extended.

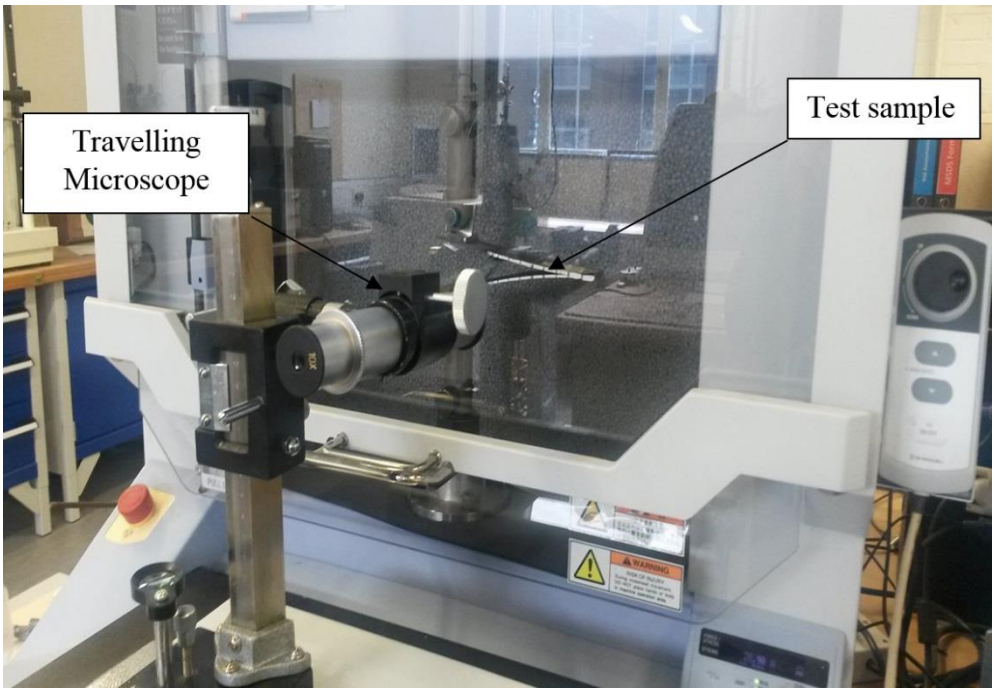

Figure 41 The DCB sample test under load conditions.

The modified beam theory (MBT) was applied to estimate the values of the interlaminar fracture toughness energy (G_I) as shown in Equation 9.

$$G_I = \frac{3P\delta}{2b(a + |\Delta|)} \qquad Equation\ 9$$

Where P is the tensile force, δ is the deflection, b is the width of the sample, α is the crack length and Δ is estimated experimentally by creating a least square plot of the cube root of compliance, $C^{1/3}$, as a function of the crack length, as shown in Figure 42. The value of compliance (C) can be calculated from Equation 10.

$$C = \frac{\delta}{P} \qquad Equation\ 10$$

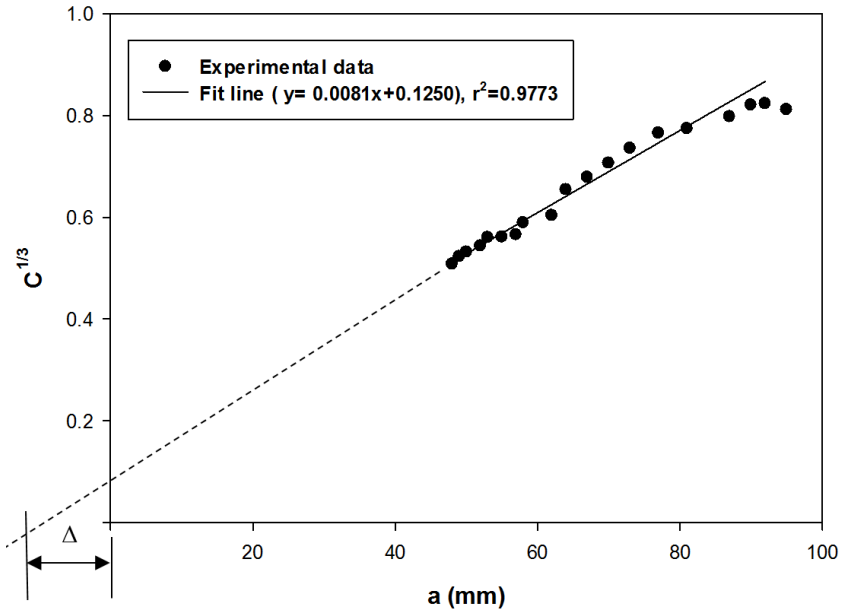

Figure 42 Typical linear fit curve used to measure Δ (mm) via experimental data related to the compliance calibration.

The initial values were estimated by means of three different techniques; specifically, optical vision at the onset crack (VIS) and the nonlinear point (NL) which could be recognised on the deflection curve (deviation of linearity), whereas, the 5%/MAX offset of this value was calculated by determining the intersection point of the line compliance (C_o + 5%) with the load-deflection curve. In case this value exceeded the maximum load, this maximum load should be taken to calculate it. The propagation toughness energy is the average of the total values excluding the initial values, as revealed in Figure 43.

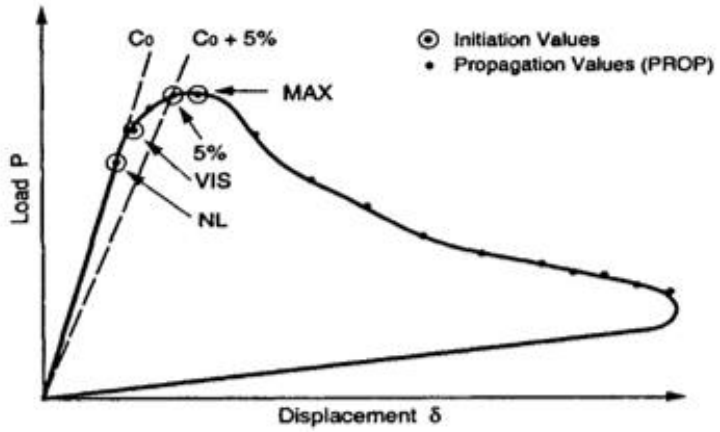

Figure 43 The analytical criteria to determine the values of initial and propagation fracture toughness energy (David et al., 2001).

4.3.4 Interlaminar fracture toughness testing (Mode II) of laminate composites

The most common method used to measure the value of G_{II} fracture toughness energy Mode II is the three end notched flexure test (3ENF). This type of test is applied less in the design structure than the opening tensile system Mode I. The geometric design of the 3ENF samples is similar to the DCB samples. The interlaminar fracture toughness test (Mode II) remains debatable because of friction influences, as well as the instability of the crack during the propagation stage.

The ratio (a/L>0.7) for actual crack length could be the solution for the instability of the crack through load conditions, which has been suggested by many researchers (Davies et al., 1998). Therefore, the ratio (a/L) of 3ENF samples for the present study was designed to be roughly 0.74. The 3ENF test samples were rectangular in geometric shape, 178 mm (in length), 25 mm (in width) and 4 mm (in thickness), as shown in Figure 44 (Toland et al., 2010). A 12 µm thick aluminium film was inserted at one end of the sample to create a crack length of 76 mm in the mid plane for each sample. Both sides of the 3ENF samples were painted using white paint and marked form the end of the film insert every 1 mm up to 100 mm. The span between the two support rollers is 100 mm.

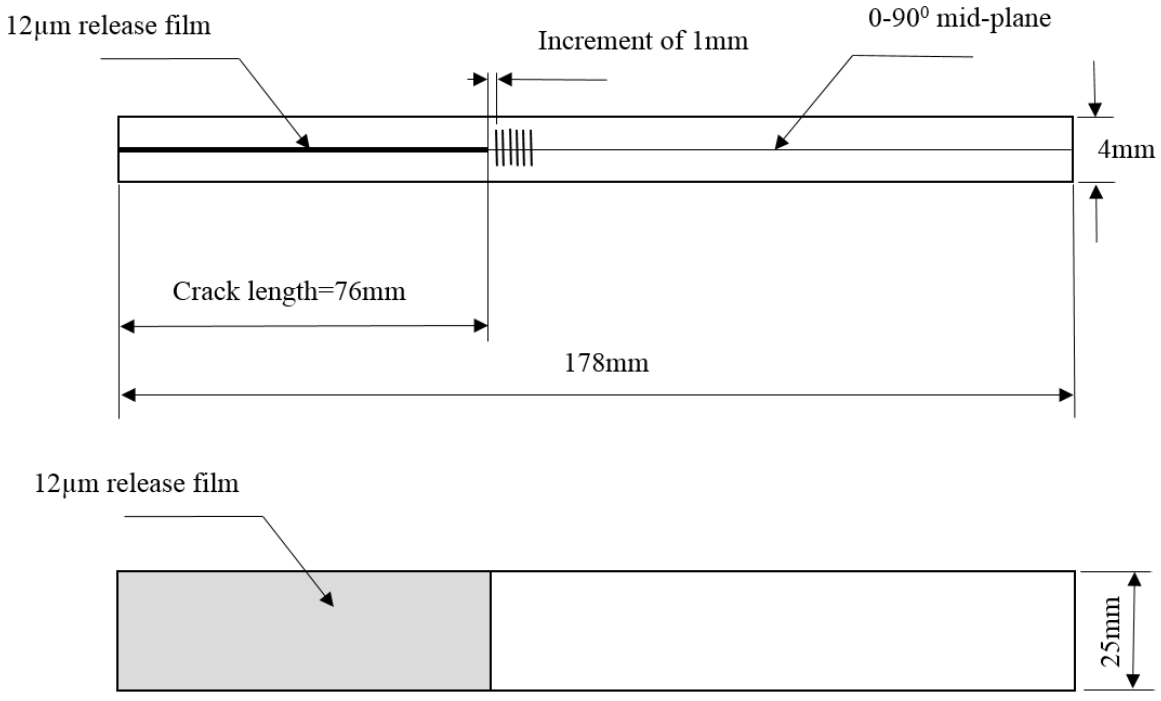

Figure 44 The geometric structure and dimensions of the 3ENF sample.

Figure 45 illustrates the configuration of the 3ENF test. The 3ENF samples were loaded in A Shimadzu Universal Test Machine with a 100 KN load capacity, as shown in Figure 46. An Initial

crack in Mode II was created at a constant cross head speed of 1mm/min. After generating the initial crack at the insert film, the samples were then unloaded at a rate of speed of 10mm/min. Thereafter, the load was restarted on the specimen at the same cross head speed of 1mm/min. The force and deflection were recorded for every 1 mm during the extension of the crack if possible. The extension in crack length was recorded until samples failure. If the bending failure started in the sample, the extension of crack would not be developed and the 3ENF test was stopped.

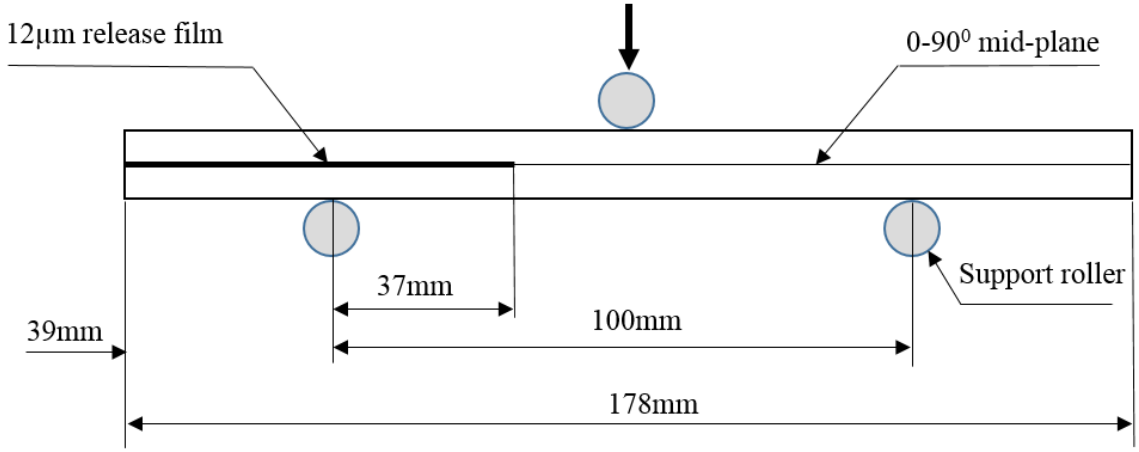

Figure 45 Schematic of the 3ENF test.

Figure 46 Jig setup for Mode II 3ENF testing.

The following experimental analysis was applied to determine the fracture toughness energy: The values of initial and propagation fracture energy in Mode II were calculated in accordance with direct beam theory (DBT) using Equation 11 (Silva et al., 2014; Khan and Kim, 2012).

$$G_{II} = \frac{9Pa^2\delta}{2b(2L^3 + 3a^3)} \qquad Equation\ 11$$

Where P is the bending force, a is the crack length, δ is the deflection, b is the width of sample, and L is the half span of simply supported sample.

4.4 Fractography

4.4.1 Optical Microscopy

The microstructural details of HCFRP samples were described using bright field imaging on a Brunel Optical Microscope LTD, the UK. The objective magnification of 5x, 10x, 20x and 40x using reflective illumination. The test samples were cut from the end edges of the un-fractured region of the HCFRP samples. A diamond saw was used for this purpose. After that the samples were mounted onto the epoxy matrix and subsequently, left to cure. After the curing stage, the samples were polished with a Buehler EcoMet 300 Pro grinder-polisher, as illustrated in Figure 47. The polishing sequence for the samples is described in Table 19 followed at 40N pressure force per specimen at a head rotational speed of 150 rpm. In addition, the samples were washed in bath water by using VWR Ultrasonic cleaner machine between each stage of the polishing processes. The purpose of using the optical microscopy was to check the quality of samples, for instance the distribution of nanofilled matrix among the plies, the mechanical bonding between the nanofilled matrix and the fibre networks, and the defects such as voids.

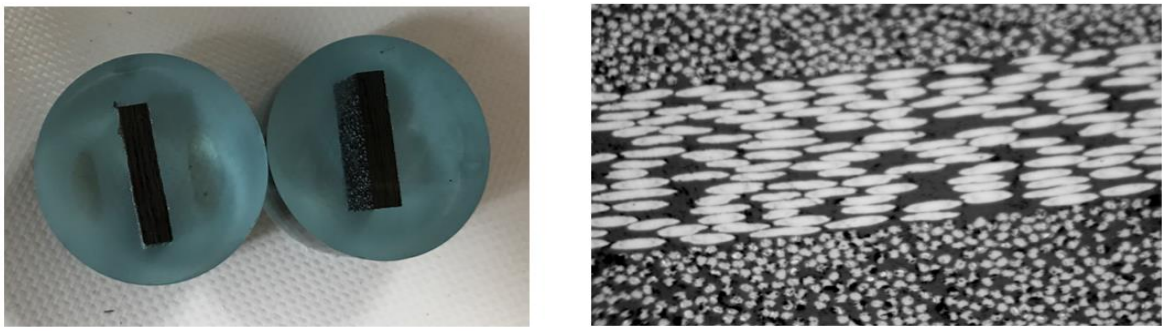

(a) (b)

Figure 47 a) Fibre composite in epoxy matrix; and b) Optical micrograph illustrating cross-sectional homogenous distribution of carbon fibres network in the epoxy matrix.

Table 19 Polishing process sequentially for the HCFRP.

Grit/Cloth	Medium	Time	Cycles
120 Grit SiC	Water	3 minutes	1
240 Grit SiC	Water	3 minutes	1
240 Grit SiC	Water	3 minutes	1
Buehler MicroFloc	9µm diamond suspensions	3 minutes	2
Buehler MicroFloc	3µm diamond suspensions	3 minutes	2
Buehler MicroFloc	1µm diamond suspensions	3 minutes	2

4.4.2 Scanning Electron Microscopy (SEM)

An environmental scanning electron microscope (ESEM), (XL Series, PHLIPS) was used to provide high resolution images and a range of analytical techniques to investigate the network of nanofillers and their fracture morphology in composites, on the nanoscale. The surface of fractured NP and HCFRP samples were scanned with additional conductive coating, such as gold, so as to improve the conductivity and to create a charge contrast imaging between the GNP or CSCNT and the electrically insulating epoxy matrix. Additionally, 20KV was used for ultra-high resolution on the surface of the samples. A secondary electron detector was utilised to obtain images of the network of nanofillers in the matrix.

Fracture morphology for each type of the NP and the HCFRP at critical weight concentration were tested to check the fracture toughness systems and mechanical bonding between the modified matrix and fibre networks.

4.4.3 Transmission Electron Microscopy (TEM)

A transmission electron microscope (Philips CM100 Compustage FEI) was used to investigate the dispersion extent, such as the exfoliation of nanoparticles, their orientation and distribution into the epoxy resin at critical weight concentrations and defects in the structure of nanoparticles. Micro-sections of 0.5µm are cut from the top surface of the nanocomposites samples by using a diamond knife. The micro-sections are then stretched on copper grids for inspection. The digital images are collected by using an AMT CCD camera (Deben).

Chapter 5. Evaluation of mechanical properties of NP: Results and discussion

This chapter presents the experimental results with discussion on the characterisation methods of the NP, as described in chapter 4. The evaluation of mechanical properties characterised involve the tensile strength, flexural strength and fracture toughness of the NP. The degree of nanoparticles dispersion was assessed by transmission electrons microscopy TEM for the NP at critical weight concentrations. Furthermore, evaluation of mechanical dispersion processes was assessed based on the quality of nanoparticles dispersion in the matrix. Analysed fractography details using scanning electron microscopy SEM spotlighted distinguished surface fracture morphologies which were employed to interpret the illustrated mechanical interfacial behaviour and fracture mechanism systems.

5.1 Mechanical characterisation of optimised NP

5.1.1 Microstructural details of NP processed by sonication mixing

The TEM and SEM images of the GNP /epoxy nanocomposite illustrate the dispersion degree of nanoparticles in the epoxy resin and the fracture morphology of nanocomposite at critical weight concentration (5 wt.%), as shown in Figure 48. The TEM image of the GNP/epoxy nanocomposites demonstrate a relatively inhomogeneous distribution of the nanoplatelets and poor dispersion with lesser exfoliation in the matrix. This is probably as a result of strong van der Waals forces in the network of graphene (see Figure 48a). In addition, it can be seen in Figure 48b that the surface of the GNP is rough and it is challenging to recognise the individual layers in the matrix due to the existence of agglomeration phenomenon between the graphene layers. Figure 48b also shows the folded or wrinkled structure of the graphene layers in the matrix and clusters. These undesirable behaviours may lead to poor interlocking between the areas of layered graphene and the matrix. Furthermore, the existence of such defects in the nanocomposites may also generate high residual stresses after curing the samples of nanocomposites (Moriche et al., 2015). Thus, any defect in the structure of nanosheets could be a negative factor affecting the performance of the nanocomposite and its mechanical properties.

As a consequence, using the sonication technique to disperse the GNP undoubtedly is not enough to obtain optimum dispersion and high exfoliation of the graphene in the epoxy resin.

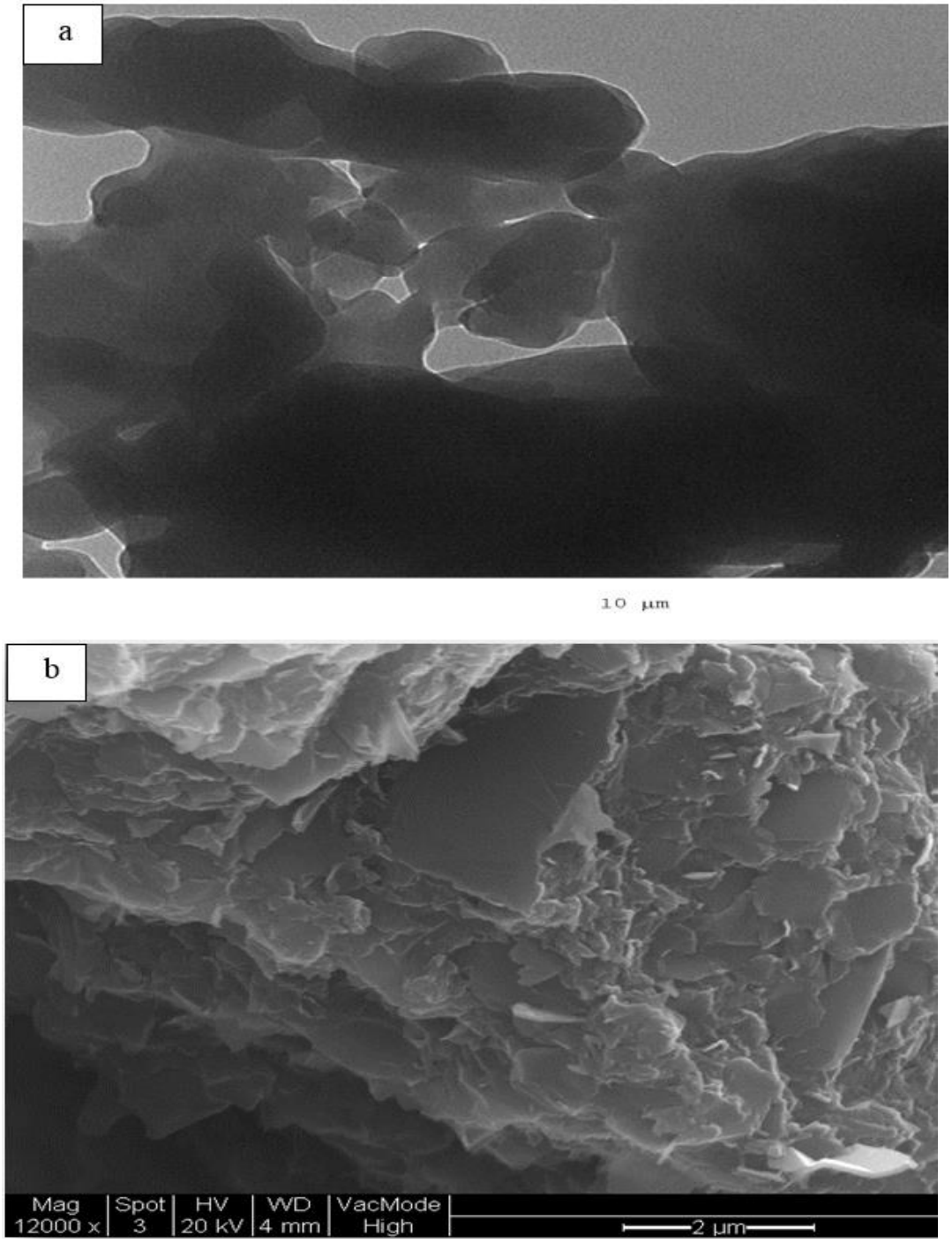

Figure 48 a) TEM image shows the dispersion degree of GNP in the matrix prepared by the sonication technique. b) SEM image shows the fracture surface morphology of GNP/epoxy nanocomposite at critical weight concentration (5 wt. %).

The TEM image of the CSCNT/epoxy nanocomposite demonstrates a good dispersion of the fibre nanotubes in the epoxy resin at the critical weight concentration (6 wt.%). It can be observed that there is uniform dispersion and good exfoliation of the fibre nanotubes with a uniform gap between the nanotubes, as shown in Figure 49a. In addition, it is apparent from the SEM image that the CSCNT morphology is tubular without damage in geometric structure. Moreover, it can recognise the individual fibre nanotubes in the matrix (see Figure 49b). Hence, the interlocking

of the fibre nanotubes and the matrix appears to be good. Based on the fractographic analysis, this technique appears suitable for dispersing the CSCNT into the epoxy resin.

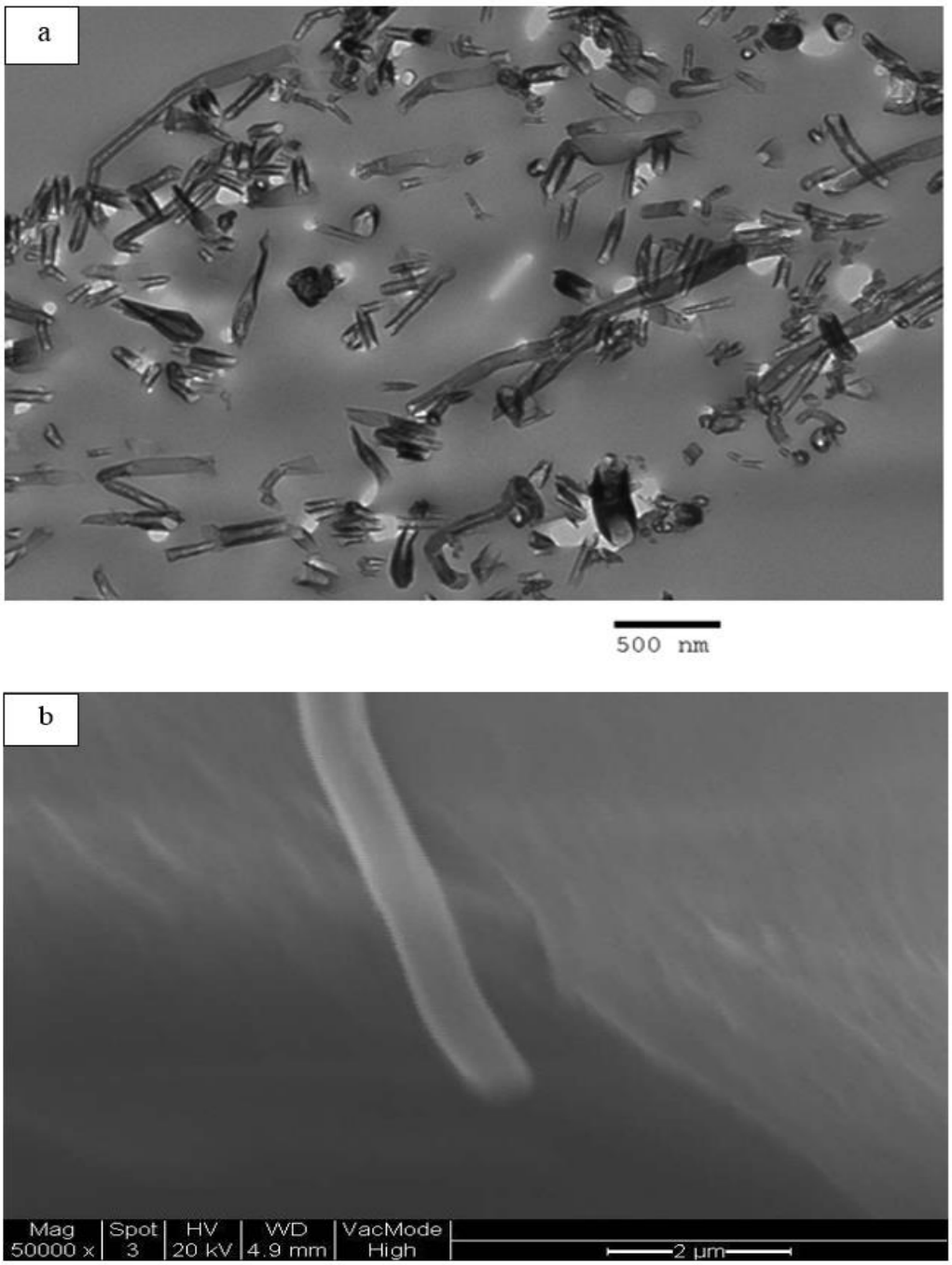

Figure 49 a) TEM image shows the dispersion degree of fibre nanotubes in the matrix prepared by the sonication technique. b) SEM image shows the fracture surface morphology of CSCNT/epoxy nanocomposite at critical weight concentration (6 wt. %).

Within the TEM image of the hybrid GNP-CSCNT/epoxy nanocomposite, at critical weight concentration (4 wt.%), were some vast agglomerated areas found in the matrix after combining the GNP and CSCNT. Additionally, clusters were found in several cross sectional areas of the hybrid nanocomposite, in particular the graphene as well as the agglomeration phenomenon and

heterogeneous distribution of the combined nanofillers within the epoxy resin, as shown in Figure 50a. Furthermore, Figure 50b shows there are pull-out mechanisms for some fibre nanotubes and the sharp, rough surface of the nanofilled matrix, suggesting a toughening influence.

The result of the fractography analysis suggest that for graphene as well as the combination of nanofillers, other dispersion methods such as ball milling, or a combination of techniques may be necessary to improve the dispersion degree of nanoparticles in the epoxy resin. Furthermore, such a procedure may contribute to the increase in synergy property of the hybrid nanoparticles into the matrix which improves the mechanical properties of the nanocomposites and their performance (Tang et al., 2013; Yue et al., 2014).

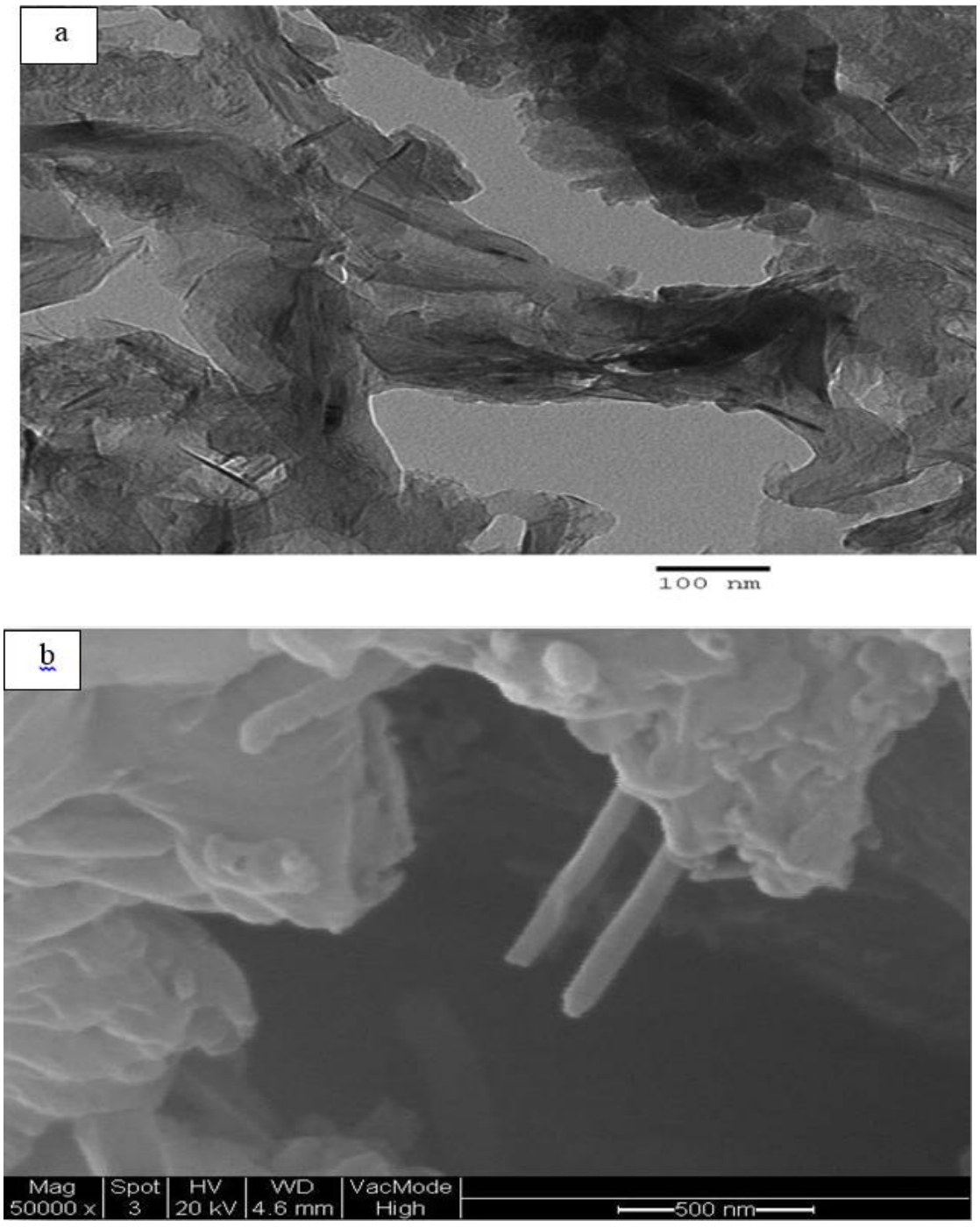

Figure 50 a) TEM image shows the dispersion degree of hybrid nanofillers in the matrix prepared by sonication technique. b) SEM image shows the fracture surface morphology of hybrid GNP-CSCNT/epoxy nanocomposite at critical weight concentration (4 wt. %).

5.1.2 Tensile properties of NP processed by sonication mixing

The typical tensile stress-strain curves of three NP (i.e. GNP/epoxy nanocomposite, CSCNT/epoxy nanocomposite and hybrid GNP-CSCNT/ nanocomposite) at various weight contents is shown in Figure 51. Table 20 reveals the data calculated from the tensile curves for the three classes of NP, in addition to pure epoxy composite as the reference.

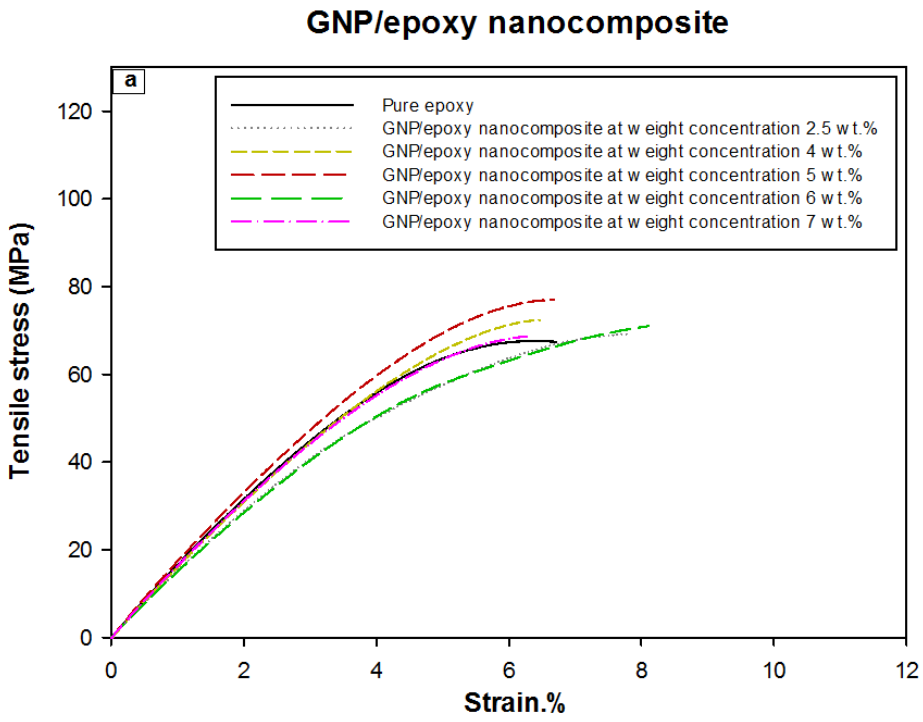
GNP/epoxy nanocomposite
a
Pure epoxy
GNP/epoxy nanocomposite at w eight concentration 2.5 w t.%
GNP/epoxy nanocomposite at w eight concentration 4 w t.%
GNP/epoxy nanocomposite at w eight concentration 5 w t.%
GNP/epoxy nanocomposite at w eight concentration 6 w t.%
GNP/epoxy nanocomposite at w eight concentration 7 w t.%
Tensile stress (MPa)
Strain.%
0
20
40
60
80
100
120
0
2
4
6
8
10
12

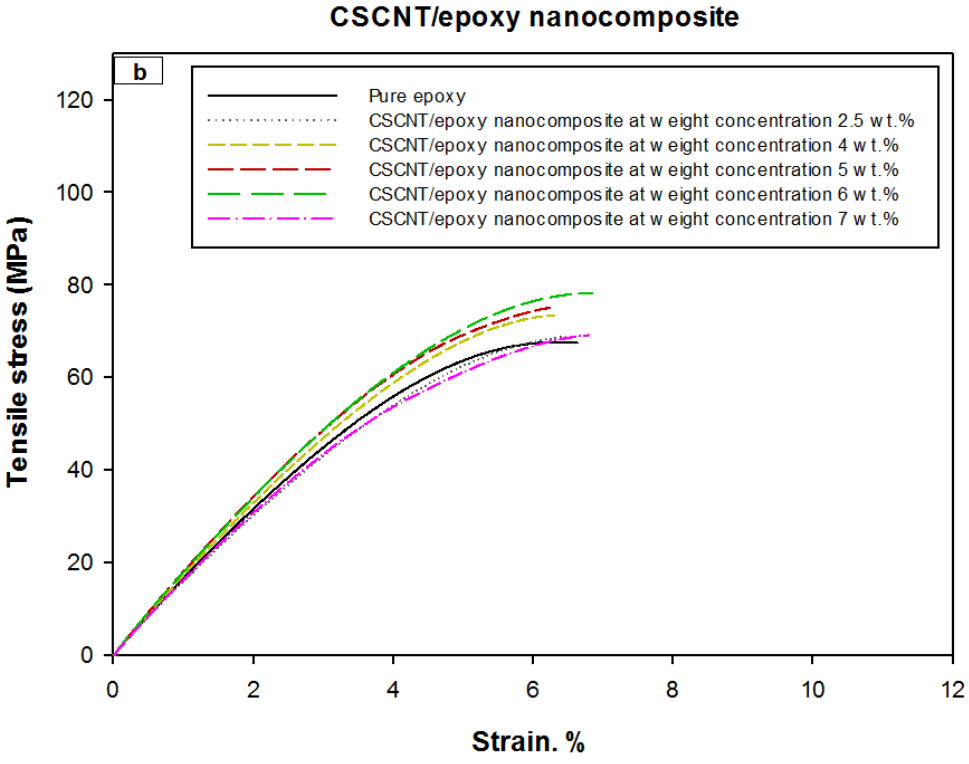
CSCNT/epoxy nanocomposite
b
Pure epoxy
CSCNT/epoxy nanocomposite at w eight concentration 2.5 w t.%
CSCNT/epoxy nanocomposite at w eight concentration 4 w t.%
CSCNT/epoxy nanocomposite at w eight concentration 5 w t.%
CSCNT/epoxy nanocomposite at w eight concentration 6 w t.%
CSCNT/epoxy nanocomposite at w eight concentration 7 w t.%
Tensile stress (MPa)
Strain. %
0
20
40
60
80
100
120
0
2
4
6
8
10
12

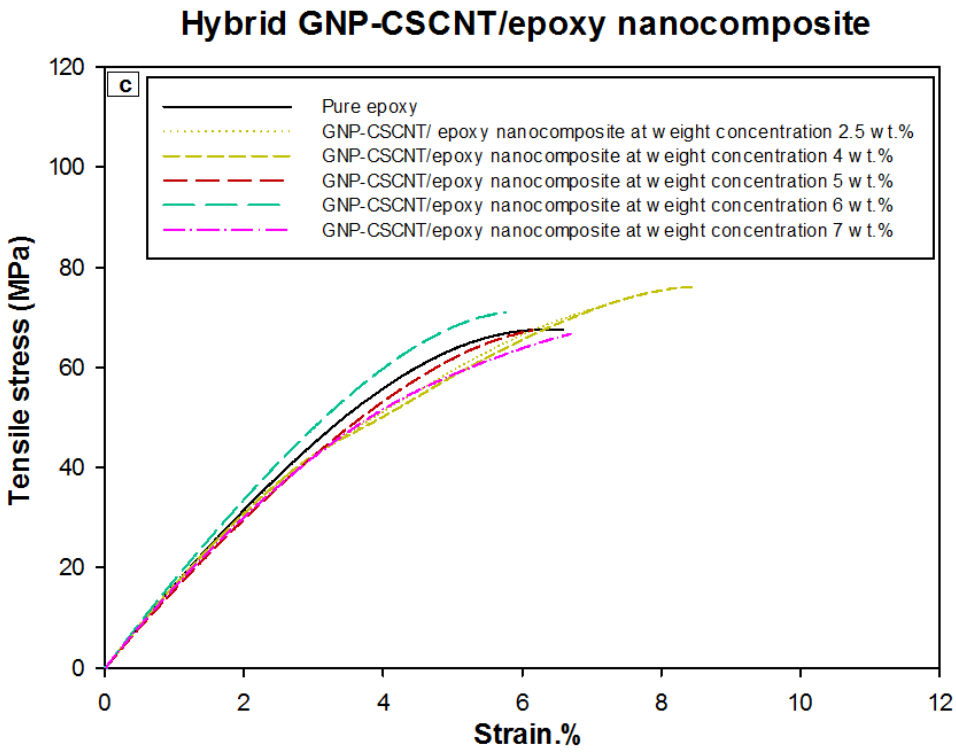

Figure 51 Typical tensile stress-strain curves at different weight concentrations; a) GNP/epoxy nanocomposite, b) CSCNT/epoxy nanocomposite, c) hybrid GNP-CSCNT/ epoxy nanocomposite, processed by the sonication technique.

Table 20 Maximum tensile strength and tensile modulus of the NP processed by the sonication technique during 55 min of dispersing and mixing time as a function of nanofiller content.

Sample	Number of samples	Weight content (wt.%)	Tensile strength (MPa)	Improvement (%)	Tensile modulus (GPa)	Improvement (%)
Pure epoxy	4	0.0	67.64±0.92	00.0	1.34±0.03	00.0
GNP/epoxy nanocomposite	4	2.5	69.26±3.11	+2.4	1.21±0.04	-9.7
	4	4	72.40±2.60	+7.0	1.32±0.02	-1.5
	4	5	77.10±2.30	+13.9	1.48±0.03	+10.8
	4	6	72.30±1.24	+6.8	1.22±0.05	-8.9
	4	7	69.20±0.50	+2.3	1.29±0.02	-3.7
CSCNT/epoxy nanocomposite	4	2.5	68.90±1.65	+1.8	1.30±0.03	-2.9
	3	4	73.50±1.65	+8.6	1.49±0.02	+11.2
	4	5	75.91±1.73	+12.2	1.52±0.02	+13.4
	4	6	78.21±1.33	+15.6	1.53±0.01	+14.2
	4	7	69.40±1.76	+2.6	1.30±0.02	-2.9
Hybrid GNP-CSCNT/epoxy nanocomposite	4	2.5	74.70±1.85	+10.4	1.31±0.02	-2.2
	4	4	76.14±1.18	+12.6	1.29±0.03	-3.7
	3	5	68.50±2.26	+1.3	1.32±0.02	-1.5
	3	6	71.30±1.27	+5.4	1.54±0.04	+14.9
	3	7	68.70±1.58	+1.5	1.33±0.02	-0.7

A comparison of the tensile properties of three types of NP is shown in Figure 52. It can be concluded that the tensile strength increases after adding the graphene to the epoxy resin, as shown in Figure 52a. This improvements was compatible with previous reported studies (Thanh et al., 2014; Shen et al., 2013; Moriche et al., 2016).

The present results show that there is an optimum weight content resulting in a maximum increase in tensile properties of GNP/epoxy nanocomposites regardless of dispersion degree, for the tensile strength and elastic modulus which increased by approximately 14% and 11% respectively at a 5 wt. % weight content. Incremental improvements with regard to these mechanical properties may be a result of the large surface area as well as the good orientation of nanofillers in the matrix (Zhao et al., 2010). In spite of the existence of defects such as folded nanosheets and agglomerated nanosheets and poor dispersion of graphene, there is a relatively good interfacial interaction between GNP and the epoxy matrix, as shown in Figure 53. In contrast, there is a decrease in the elastic modulus of roughly 10% and 9% at low GNP loading (i.e. 2.5 wt. %) and high GNP loading (i.e. 6 wt.%), respectively as shown in Figure 52 (b). Thus, the proportional weight of nanoparticles have significant influence on the mechanical properties of nanocomposites (Zaman et al., 2011).

The influence of novel fibre nanotubes loading on the tensile strength and modulus of the epoxy composite is portrayed in Figure 52. The tensile strength increases after adding the fibre nanotubes to the epoxy resin (Choi et al., 2005; Iwahori et al., 2005; Sun et al., 2011).

The highest increase in tensile strength and modulus of CSCNT/epoxy nanocomposites was found at approximately 16% and 14% at a critical weight concentration of 6 wt.%. Furthermore, when the amount of fibre nanotubes reaches this critical content (6 wt. %), the distance between the two nanotubes refers to good exfoliation and dispersion of the fibre nanotubes into the matrix. Pull-out of fibre nanotubes in the fracture surface was also observed by fractographic analysis, as shown in Figure 54. Therefore, the uniform distribution may be suitable for attaining good quality adhesion of nanotubes into the epoxy matrix, owing to the superior dispersion of nanotubes and moreover, the alignment (Ma et al., 2010). Conversely, the 2.5wt % of CSCNT loading indicates that the enhanced influence is limited because the amount of nanofiller may not be satisfactory. For example, there is a small increase in tensile strength and decrease in elastic modulus of approximately 2% and 3 %, respectively. Although, there is a slight increase in tensile strength by 3% at a high concentration (7 wt. %), the tensile modulus also starts decreasing at the same content, which may refer to the agglomeration phenomenon in the nanocomposite.

The objective of incorporating both nanofillers; graphene and novel fibre nanotubes into the epoxy matrix was to create a hybrid GNP-CSCNT/epoxy nanocomposite with high mechanical properties. The effect of the combination of these carbon nanomaterials on the mechanical tensile

properties is also shown in Figure 52. It appears that there is a moderate increase in the tensile properties of the HNP in comparison with other NP.

To explain, any increase in the level of improvements for strength and stiffness properties of the HNP are largely linked to the degree of exfoliation of combined carbon nanomaterials in the matrix, orientation of each one of nanomaterials and homogenous distribution (Zhao et al., 2010). These mechanical factors could influence the mechanical interfacial properties of HNP. In addition, these mechanical properties depend on the synergy property of combined nanomaterials within the matrix. Moreover, the degree of this property is relevant to the uniform dispersion and exfoliation of nanofillers in the matrix (Yue et al., 2014). Therefore, any improvements in these mechanical properties of the HNP probably are the result of the synergetic effect of combined nanomaterials within the matrix. This desirable behaviour induces the adhesion between the fillers and the matrix. In contrast, the inhomogeneous dispersion and poor exfoliation of the nanofillers in the matrix possibly indicates that the weakness of the synergy property and the adhesion between the nanofillers and the matrix is simple. Furthermore, existence of various defects for combined nanomaterials in the matrix (i.e. wrinkled nanosheets) could affect the level of improvements in mechanical properties of the HNP (Moriche et al., 2015). The fractographic analysis indicated that there is poor dispersion and simple exfoliation of the combined nanofillers, especially GNP into the epoxy matrix. Moreover, it shows the rough surface with inhomogeneous conglomerates of nanoparticles and agglomeration of nanosheets, as shown in Figure 55. Hence, these issues could weaken the synergy properties and mechanical interfacial properties of the combined nanofillers within the matrix.

However, the optimum improvements of hybrid GNP-CSCNT/epoxy nanocomposites in tensile strength is found to be by approximately 10% and 13% at weight concentrations 2.5 wt. % and 4 wt. %, respectively. These improvements probably result from the existence of some synergetic properties of the combined nanofillers into the matrix. Moreover, the addition of both nanofillers into the epoxy resin increases relatively, the size of the contact area between the matrix and the nanofillers particularly the graphene which has a high surface area. In contrast, there is a slight decrement in tensile modulus at these weight concentrations, whilst there is a good increase in the elastic modulus of approximately 15% and a small improvement in tensile strength of 5% at a weight concentration of 6 wt. %. In contrast, at high loading (i.e. 7 wt. %), both the tensile and elastic values are unaffected. This may be due to the existence of particles agglomerates and inhomogeneous distribution in the matrix.

As a consequence, the combination of the graphene and fibre nanotube could improve the tensile strength. Furthermore, the combination of the nanofillers could decrease somewhat the weight content (i.e. 2.5wt.% and 4wt.%) in comparison to GNP and CSCNT incorporated in the matrix

individually. In addition, the combination of such nanoparticles contributes to inducing their synergy property into the matrix, which has a significant influence on the level of improvements in the mechanical properties of HNP (Al-Salaeh et al., 2016; Wang et al., 2015; Li et al., 2013; Chatterjee et al., 2012).

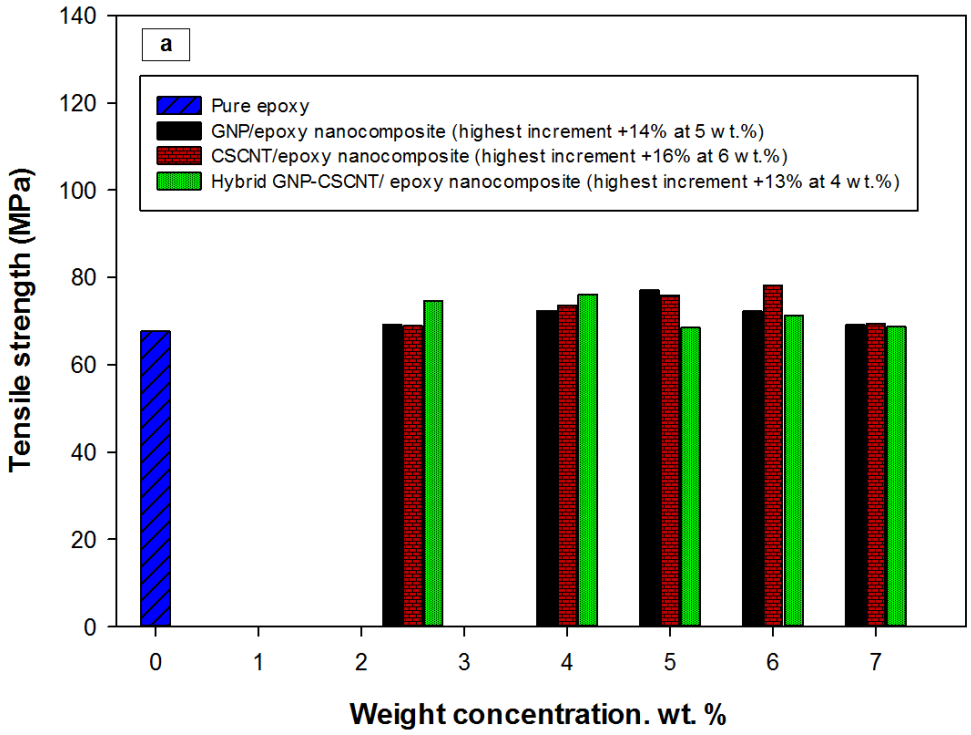

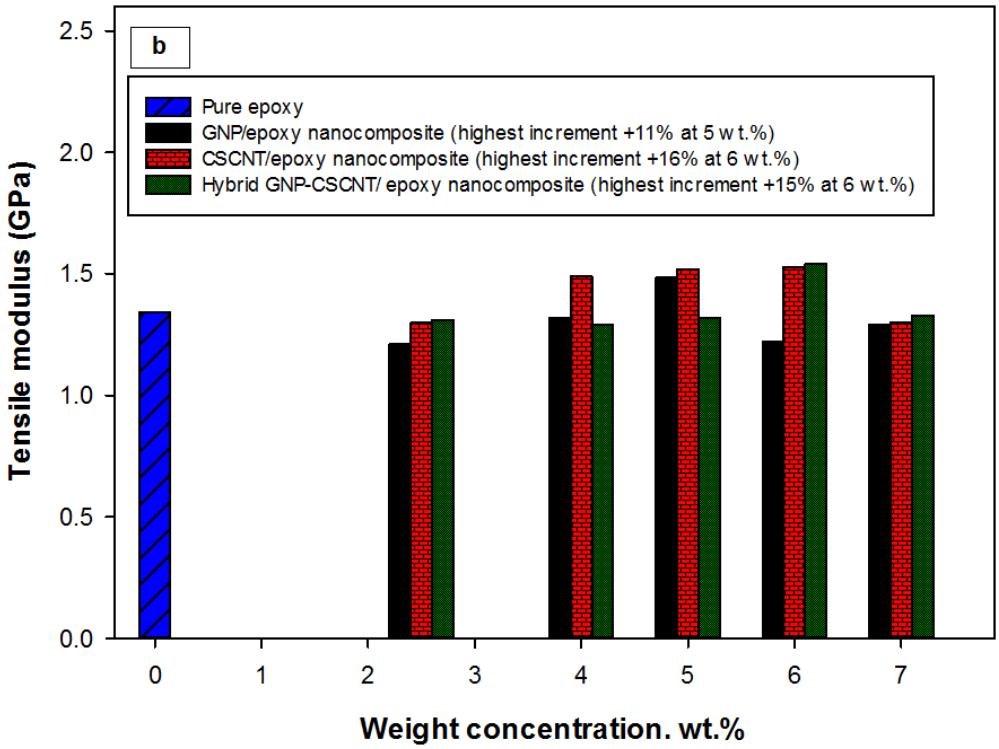

Figure 52 Comparison and evaluation of the optimised matrix in the NP processed by the sonication technique at different weight concentrations a) Maximum tensile strength, b) Tensile modulus.

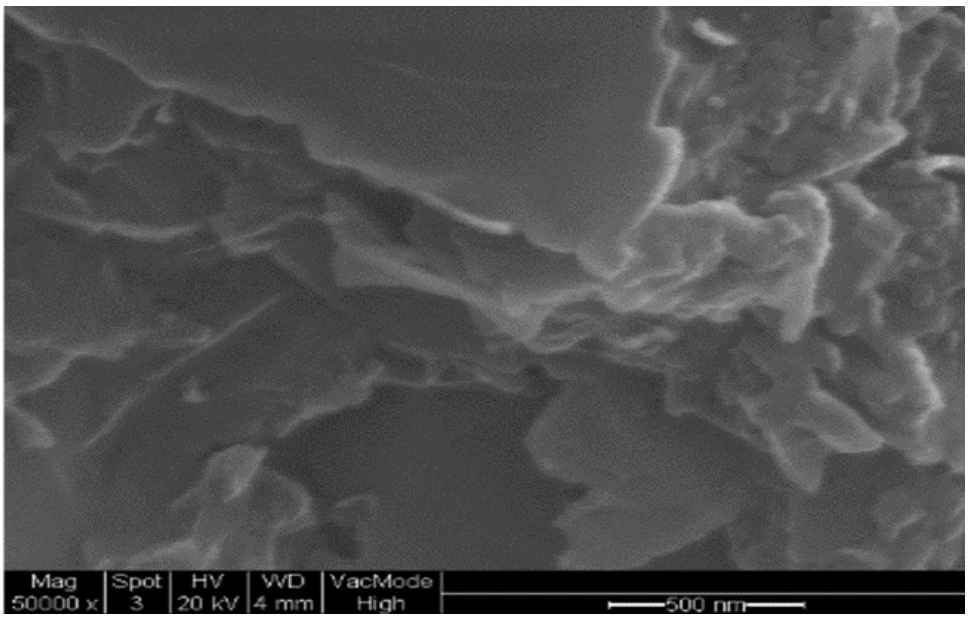

Figure 53 The SEM image shows the defects, such as folds in the network of graphene layers at critical weight concentration 5 wt. % by means of the sonication technique.

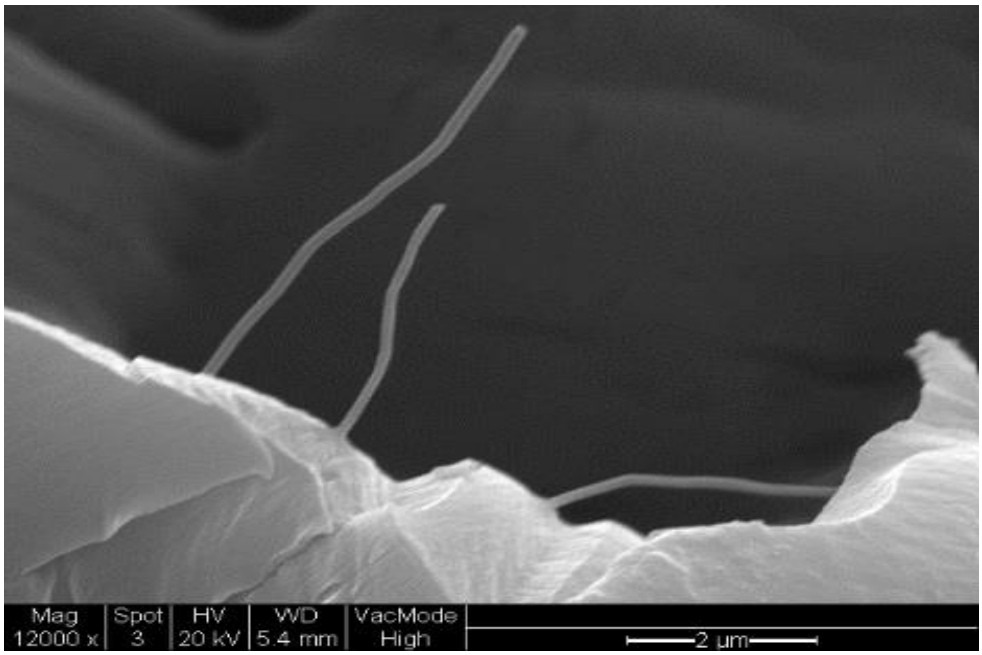

Figure 54 The SEM clearly shows the exfoliated fibre nanotubes with a good gap at the fractured area in CSCNT/epoxy nanocomposite processed by the sonication technique.

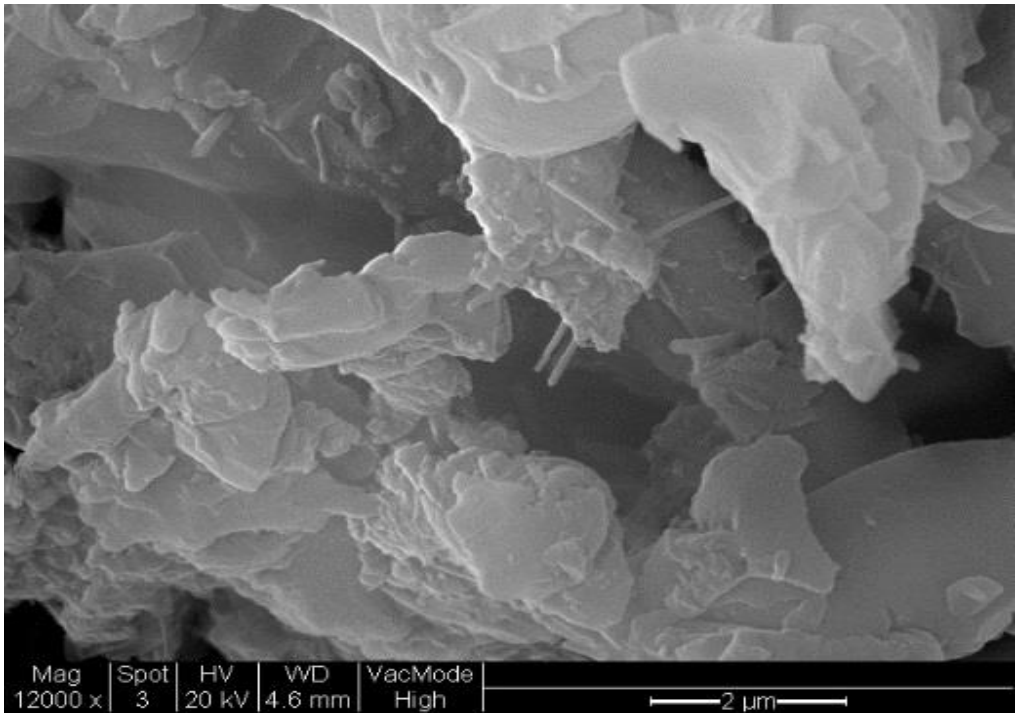

Figure 55 The SEM image illustrates fracture surface morphology of hybrid GNP-CSCNT/epoxy nanocomposite processed by the sonication technique at critical weight concentration (4 wt. %).

5.1.3 Flexural properties of NP processed by sonication mixing

Figure 56 shows the flexural stress-strain curves for the three types of NP at different nanoparticle loadings. Table 21 illustrates the experimental data of flexural properties which were derived from theses curves.

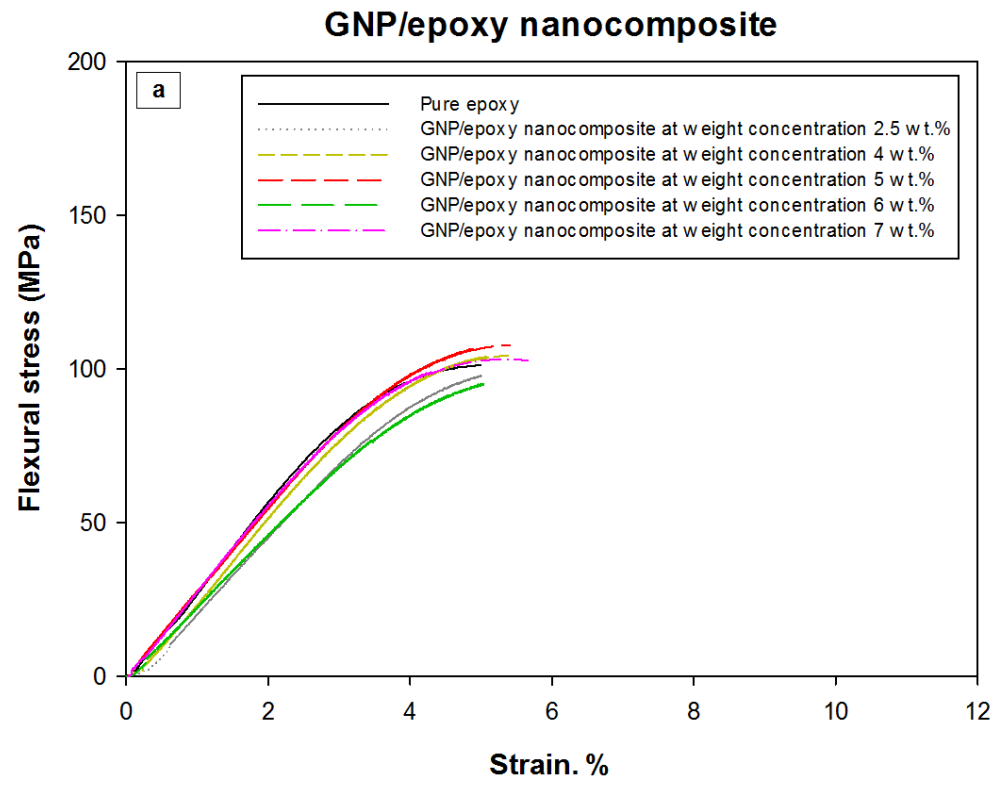
GNP/epoxy nanocomposite
a
Pure epoxy
GNP/epoxy nanocomposite at weight concentration 2.5 wt.%
GNP/epoxy nanocomposite at weight concentration 4 wt.%
GNP/epoxy nanocomposite at weight concentration 5 wt.%
GNP/epoxy nanocomposite at weight concentration 6 wt.%
GNP/epoxy nanocomposite at weight concentration 7 wt.%
Flexural stress (MPa)
Strain. %
0
50
100
150
200
0
2
4
6
8
10
12

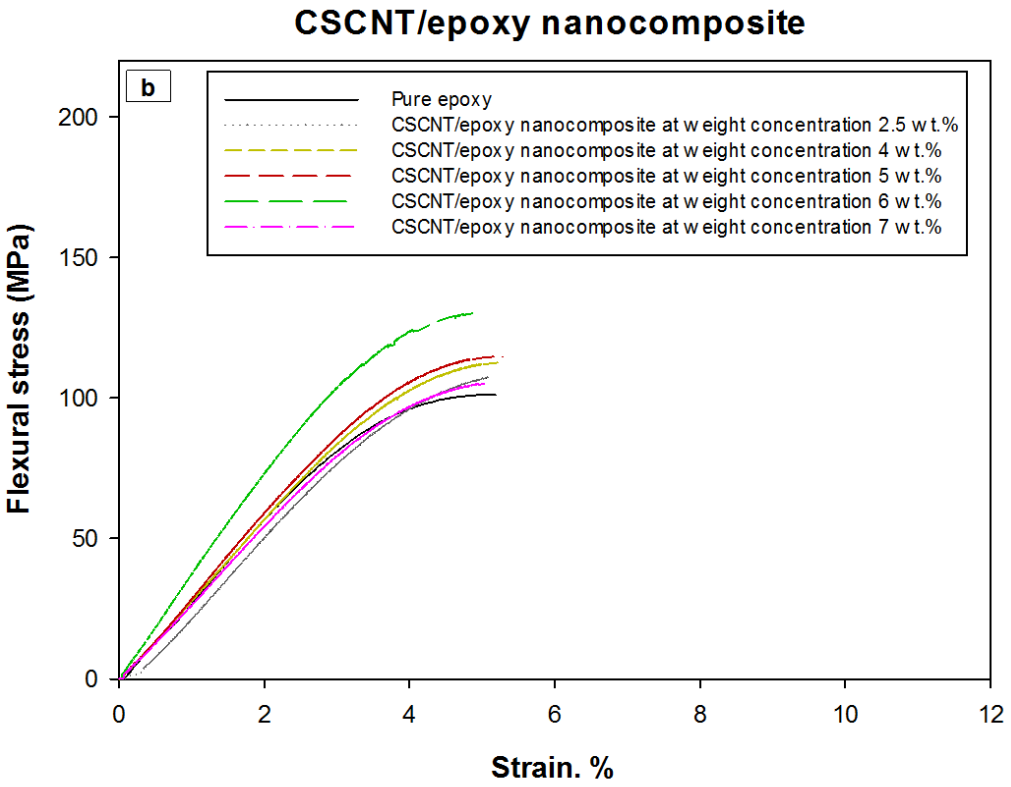
CSCNT/epoxy nanocomposite
b
Pure epoxy
CSCNT/epoxy nanocomposite at weight concentration 2.5 wt.%
CSCNT/epoxy nanocomposite at weight concentration 4 wt.%
CSCNT/epoxy nanocomposite at weight concentration 5 wt.%
CSCNT/epoxy nanocomposite at weight concentration 6 wt.%
CSCNT/epoxy nanocomposite at weight concentration 7 wt.%
Flexural stress (MPa)
Strain. %
0
50
100
150
200
0
2
4
6
8
10
12

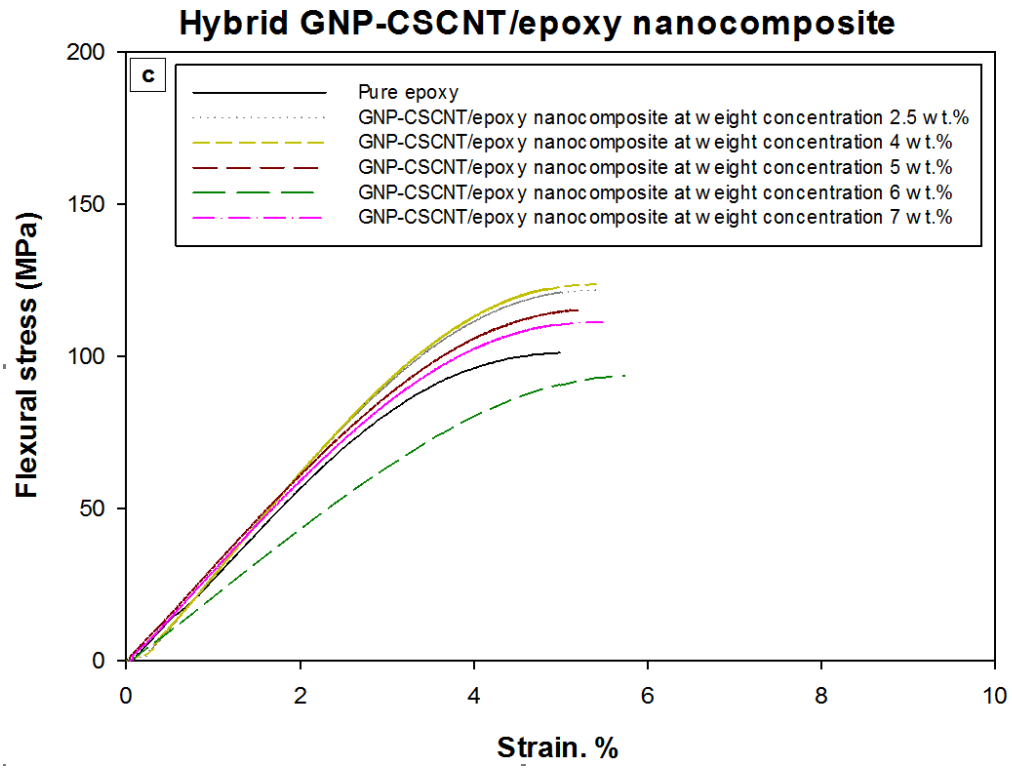

Figure 56 Typical flexural stress-strain curves of three NP at different weight concentrations; a) GNP/epoxy nanocomposite, b) CSCNT/epoxy nanocomposite, c) hybrid GNP-CSCNT/epoxy nanocomposite, processed by the sonication technique.

Table 21 Maximum flexural strength and flexural modulus of the NP processed by the sonication technique during 55 min of dispersing and mixing time as a function of nanofiller content.

Sample	Number of samples	Weight content (wt.%)	Flexural strength (MPa)	Improvement (%)	Flexural modulus (GPa)	Improvement (%)
Pure epoxy	4	0	101.21±1.52	00.0	2.80±0.13	00.0
GNP/epoxy nanocomposite	4	2.5	100.03±1.78	-1.2	2.20±0.18	-21.4
	4	4	104.43±2.57	+3.2	2.50±0.05	-10.7
	4	5	107.75±3.34	+6.5	2.60±0.08	-7.1
	4	6	097.86±1.79	-3.3	2.10±0.09	-25.0
	3	7	103.12±1.70	+1.9	2.65±0.02	-5.3
CSCNT/epoxy nanocomposite	4	2.5	108.87±3.37	+7.5	2.49±0.09	-11.1
	3	4	112.84±0.17	+11.5	2.85±0.02	+1.7
	4	5	114.70±2.86	+13.3	2.87±0.04	+2.5
	3	6	130.10±1.90	+28.5	3.50±0.11	+25.0
	4	7	105.96±4.00	+4.7	2.68±0.12	-4.2
Hybrid GNP-CSCNT/epoxy nanocomposite	4	2.5	121.60±2.64	+20.1	3.10±0.12	+10.7
	3	4	123.00±1.27	+21.5	3.15±0.03	+12.5
	4	5	115.26±3.60	+13.8	3.00±0.10	+7.1
	3	6	093.94±1.03	-7.2	2.07±0.03	-26.0
	3	7	111.13±2.14	+9.8	2.87±0.09	+2.6

The comparison of flexural properties of the three NP are illustrated in Figure 57. The flexural strength and flexural modulus of GNP/epoxy nanocomposites with different graphene concentrations show there is a small improvement in flexural strength by approximately 6% at 5 wt. % weight concentration (see Figure 57a), while there is no improvement in flexural modulus at the same weight content (see Figure 57b). In contrast, a marked decrease in the flexural modulus was observed with an increase in GNP loading, particularly at a 6 wt. %. This decrease is in the region of 25%, in addition to the small decrease in flexural strength of approximately 3% at the same graphene loading.

The maximum flexural strength and flexural modulus of the CSCNT/epoxy nanocomposite with various fibre nanotubes contents are also explained in Figures 57a and 57b. It is well known that the uniformity of the NP, level of dispersion, orientation of the enhancements and the strong adhesion between nanofillers and the epoxy matrix should have a significant effect on the mechanical properties. Undoubtedly, an increase in fibre nanotubes loading produces significant improvement in the flexural strength and modulus. Such improvements in flexural properties were also confirmed by previous reported studies (Iwahori et al., 2005; Bal, 2010). The highest values for these properties at maximum strain failure are observed to be approximately 29% and 25% respectively at a 6 wt. % CSCNT loading ratio. Conversely, a higher CSCNT content (i.e. 7 wt. %) produces an evident decrease in elastic modulus, in addition to a small increase in flexural strength of approximately 5 %.

The effect of adding a mixture of the graphene and fibre nanotubes dispersed together in the matrix on the flexural mechanical properties of the epoxy resin, such as flexural strength and flexural modulus is shown in Figures 57a and 57b. The highest improvement pertaining to these two properties is observed to be approximately 22% and 13% at weight content 4 wt. %, respectively. Subsequently, there is a decrease in the flexural properties, principally the elastic modulus of approximately 26% at 6 wt. % weight concentration. In addition, there is a small improvement in flexural strength and modulus of approximately 10% and 3%, respectively at high loadings of hybrid nanofillers (i.e. 7 wt. %).

As a consequence of these results, the combination of such carbon nanomaterials is promising in enhancing the flexural properties of the epoxy composite (Wang et al., 2015; Chatterjee et al., 2012) and for a relatively low percentage of weight content loading in the nanocomposites. Furthermore, mixing the fibre nanotubes with the graphene promotes the performance of nanocomposites in comparison to graphene incorporated in the matrix individually (i.e. GNP/epoxy nanocomposites).

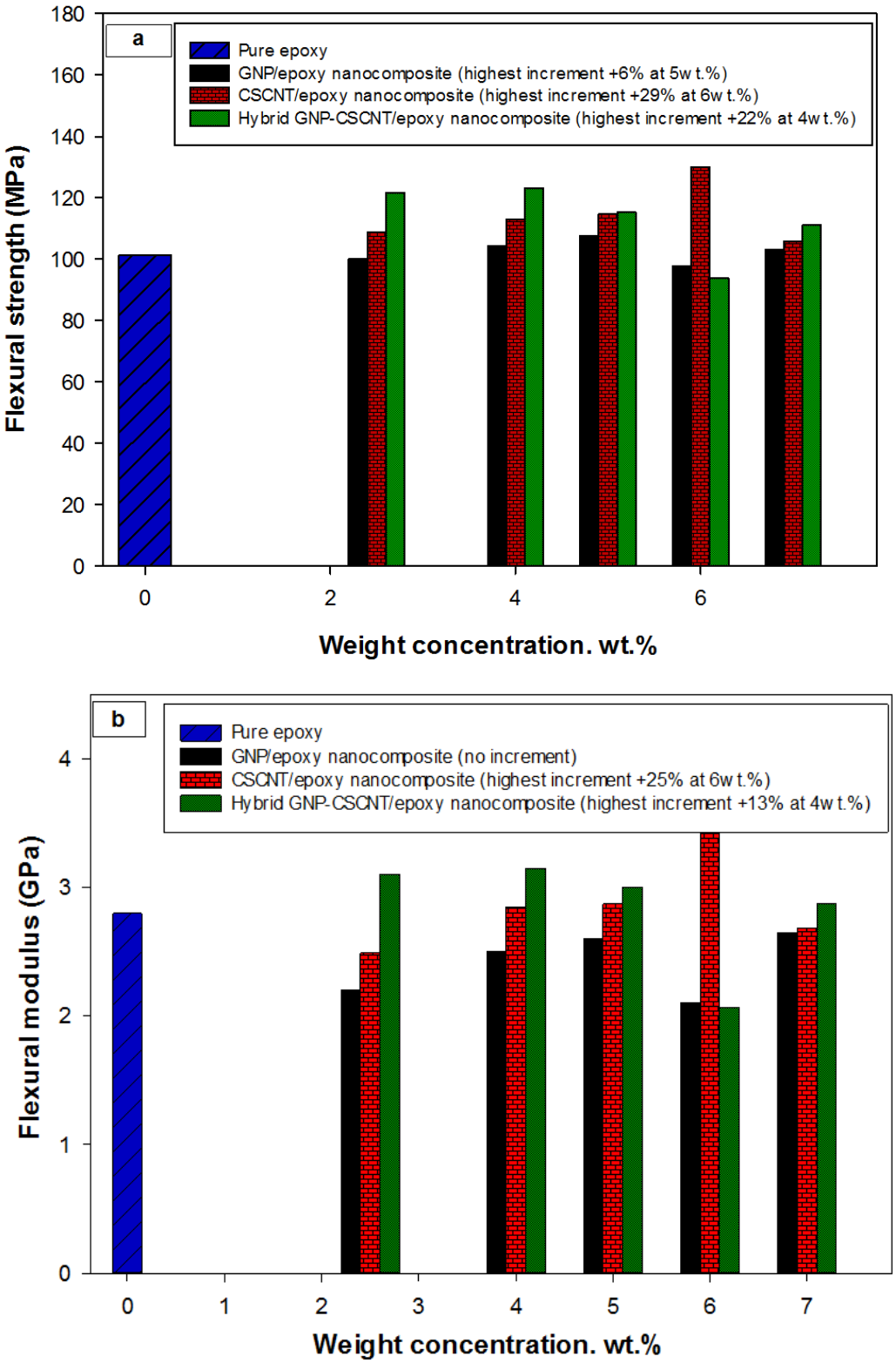

Figure 57 Comparison and evaluation of the optimised matrix in the NP processed by the sonication technique at different weight concentrations a) Maximum flexural strength, b) Flexural modulus.

5.1.4 Microstructural details of NP processed by ball milling/mixing

The TEM and SEM images of the cross-sections of GNP/epoxy nanocomposite at 5wt.% are shown in Figure 58. The images show moderately good dispersion and exfoliation of the GNP as

well as homogenous distribution. This could be clear evidence of an improvement in the mechanical dispersion of the NP by using the ball milling technique.

However, several defects can also be seen in the cross-section of nanocomposites. For example, some graphene agglomeration can be seen in Figure 58a and there is evidence of incomplete graphene exfoliation. Pull-out of nanosheets and bi-furcation mechanisms could be seen in the micro-section view of the fracture surface (see Figure 58b) (Chandrasekaran et al., 2014). These toughness mechanisms could contribute to reinforcing the mechanical properties of the GNP/epoxy nanocomposites.

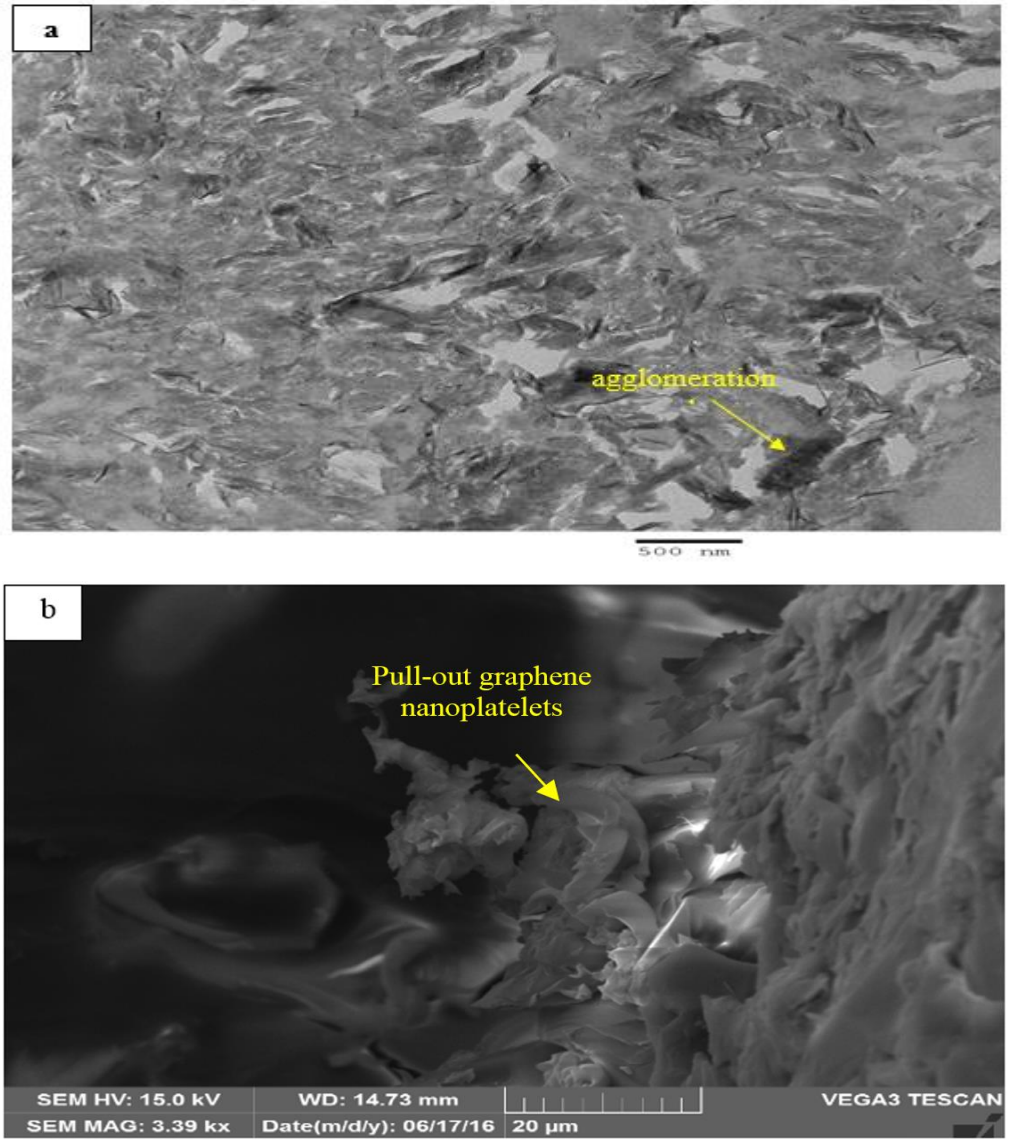

Figure 58 a) TEM image shows the dispersion degree of nanoplatelets in the matrix processed by the ball milling technique, b) SEM image shows the fracture surface morphology of GNP/epoxy nanocomposite at critical weight concentration (5 wt.%).

The TEM image of the CSCNT/epoxy nanocomposites at critical weight concentration shows good exfoliation and uniform dispersion of the fibre nanotubes in the epoxy resin (see Figure 59a). The SEM image shows a rough surface of nanocomposite at the fracture surface area and good interlocking of the fibre nanotubes and the epoxy resin as shown in Figure 59b.

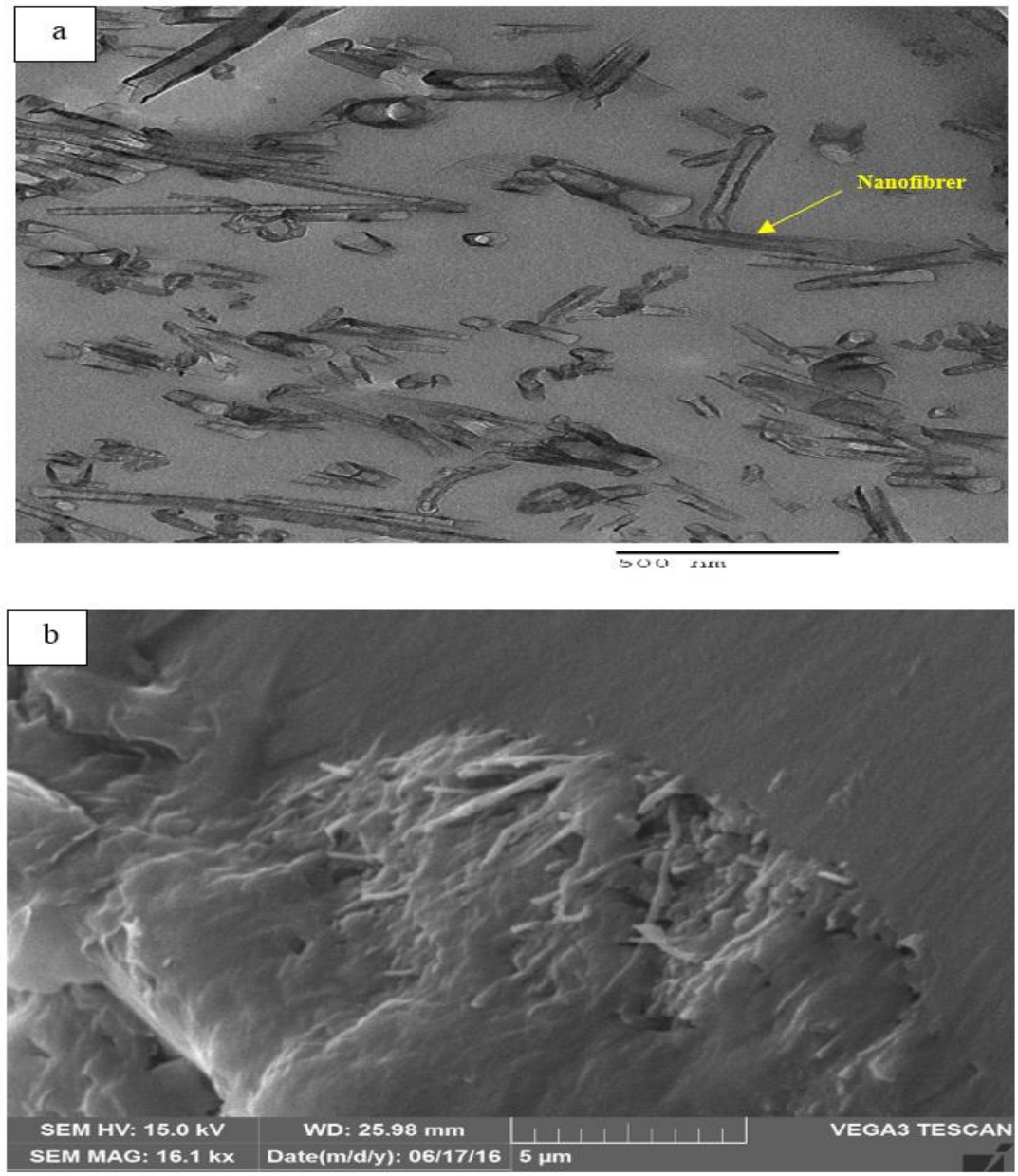

Figure 59 a) TEM image shows the dispersion degree of fibre nanotubes in the matrix processed by the ball milling technique, b) SEM image shows the roughness of fracture surface morphology in the CSCNT/epoxy nanocomposite at critical weight concentration (6 wt. %).

The TEM image of the hybrid GNP-CSCNT/epoxy nanocomposite shows undispersed agglomerations of graphene, whilst wrinkled nanosheets can also be seen in the hybrid matrix as shown in Figure 60a. In addition, the graphene agglomerates cause flaws in the hybrid matrix which may affect the performance of the nanocomposites. The difficulty with regards to

dispersing GNP with CSCNT together into the epoxy resin is due to the reason that van der Waals forces in the graphene network are probably stronger than that of the fibre nanotube network. The TEM image also reveals breakages in several nanotubes from the milling process (see Figure 60b). This was also reported by Konya et al., 2004. Figure 60c illustrates the fractographic analysis of the fracture surfaces of the hybrid nanocomposite sample after testing. Agglomeration in graphene nanosheets can be seen in the fractured area. Moreover, the SEM image shows some pull-out of the nanofillers and bi-furcation mechanisms, suggesting a toughening effect.

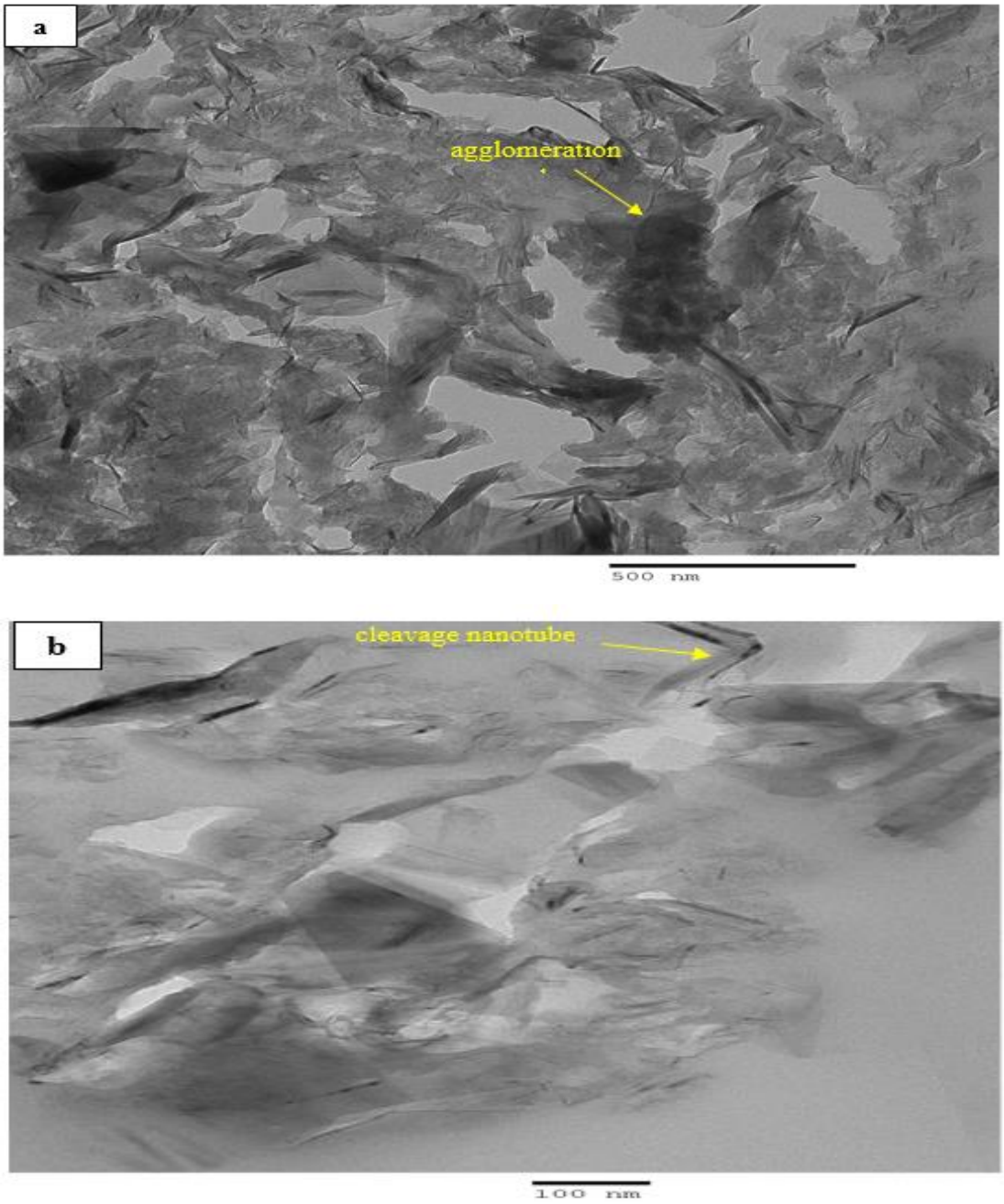

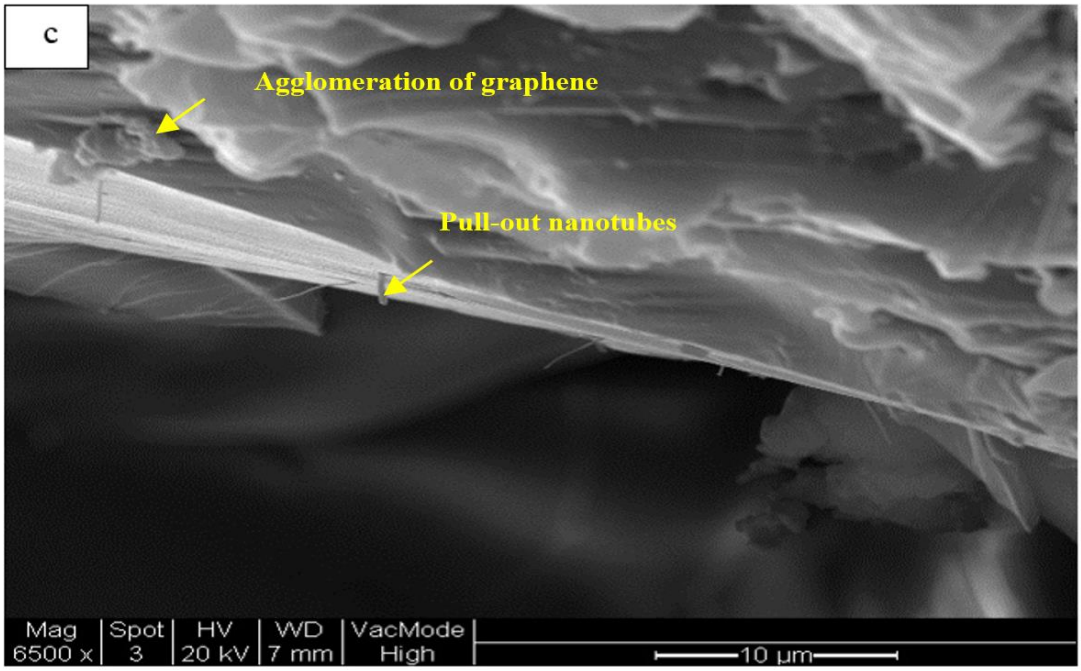

Figure 60 a) TEM images show the dispersion degree of hybrid nanofillers in the matrix processed by the ball milling technique, and b) the nanotube breakage, c) SEM image shows the fracture surface morphology of hybrid GNP-CSCNT/epoxy nanocomposite at critical weight concentration (4 wt.%)

As a result of the fractographic analysis, other mechanical dispersion techniques and new methods, such as the combination of dispersion techniques may be required to achieve a greater dispersion of the nanofillers uniformly with less defect on the structure of nanoparticles (Moriche et al., 2015; Tang et al., 2013; Liang et al., 2009). Therefore, the combination of sonication and ball milling techniques may be preferred to improve the quality of dispersion and to achieve high exfoliation of the hybrid nanofillers in the epoxy resin (Guo & Chen, 2014; Tang et al., 2013). Furthermore, excellent dispersion induces the synergy property between the graphene and fibre nanotubes, which is responsible for the improvements in the mechanical properties of the HNP (Yue et al., 2014).

5.1.5 Tensile properties of NP processed by ball milling/mixing

The typical stress-strain curves for GNP/epoxy nanocomposite, CSCNT/epoxy nanocomposite and hybrid GNP-CSCNT/epoxy nanocomposite is shown in Figure 61. Table 22 shows the summary of tensile properties for the three NP.

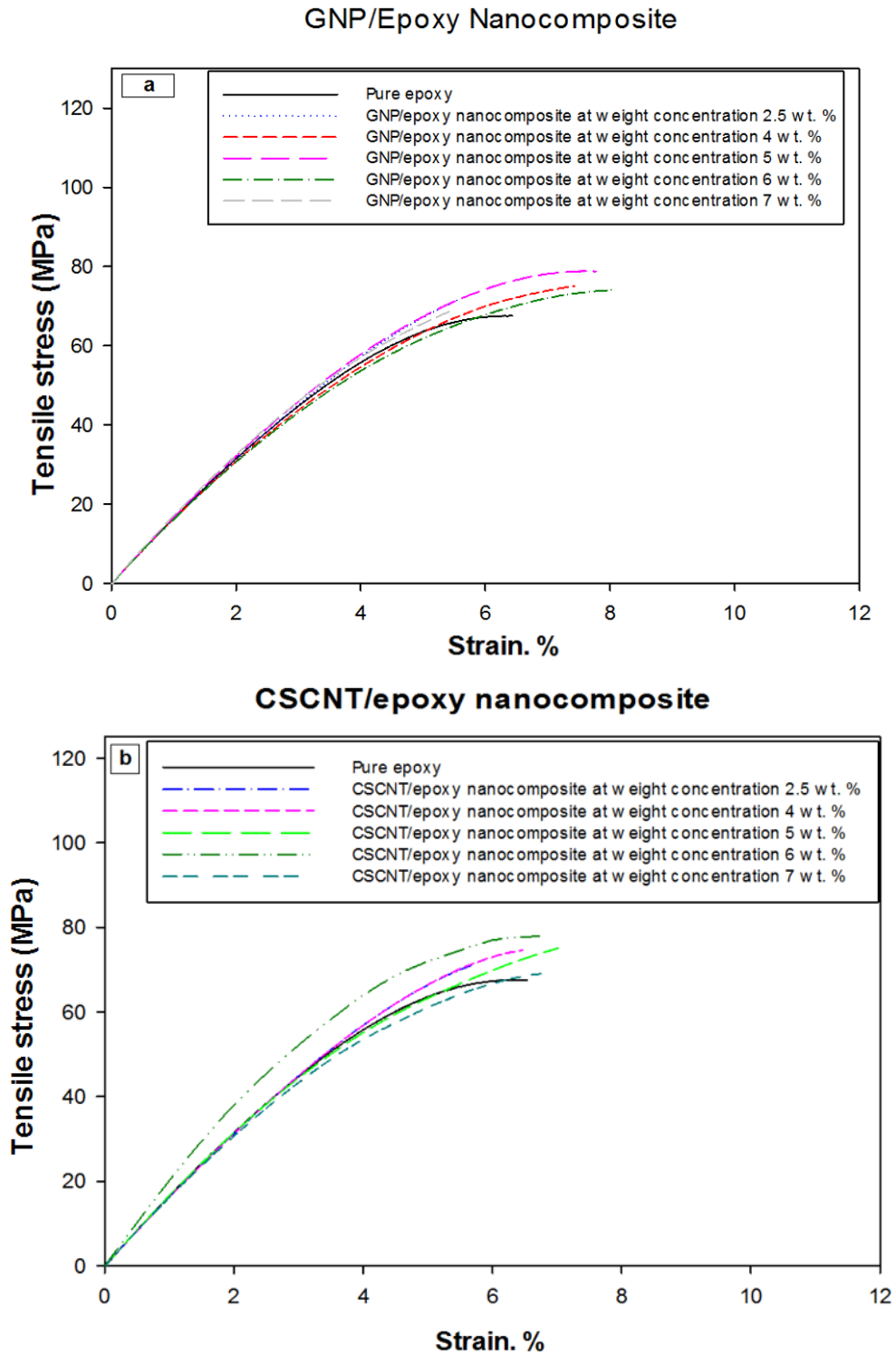

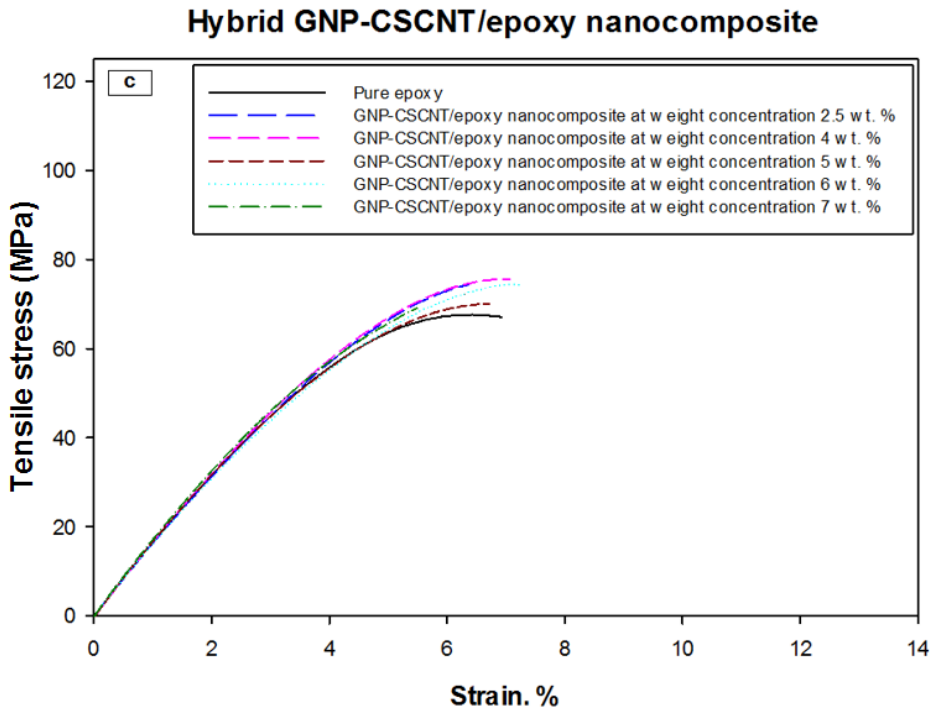

Figure 61 Typical tensile stress-strain curves at different weight concentrations a) GNP/epoxy nanocomposite, b) CSCNT/epoxy nanocomposite, c) Hybrid GNP-CSCNT/ epoxy nanocomposite, processed by the ball milling technique.

Table 22 Maximum tensile strength and tensile modulus of the NP processed by the ball milling technique during 47 min of mixing time as a function of nanofiller content.

Sample	Number of samples	Weight content (wt.%)	Tensile strength (MPa)	Improvement (%)	Tensile modulus (GPa)	Improvement (%)
Pure epoxy	4	0	67.64±0.92	00.0	1.34±0.03	00.0
GNP/epoxy nanocomposite	3	2.5	75.00±3.76	+10.8	1.37±0.01	+2.2
	3	4	75.50±0.45	+11.6	1.42±0.06	+8.2
	4	5	78.90±0.49	+16.6	1.50±0.06	+11.9
	3	6	74.00±1.14	+9.4	1.31±0.01	-2.2
	3	7	73.30±0.36	+8.3	1.40±0.03	+4.4
CSCNT/epoxy nanocomposite	3	2.5	74.10±4.25	+9.5	1.40±0.08	+4.4
	3	4	76.10±2.20	+12.5	1.49±0.05	+11.1
	3	5	77.98±2.80	+15.2	1.50±0.03	+11.9
	3	6	80.20 ±1.34	+18.5	1.58±0.01	+17.9
	3	7	70.10±1.15	+3.6	1.29±0.02	-3.7
Hybrid GNP-CSCNT/epoxy nanocomposite	3	2.5	74.40±0.65	+9.9	1.40±0.02	+4.4
	3	4	74.60±3.97	+10.2	1.41±0.04	+5.2
	3	5	71.10±1.86	+5.1	1.35±0.04	+0.7
	3	6	74.30±0.65	+9.8	1.53±0.02	+14.1
	3	7	73.03±0.83	+7.9	1.42±0.07	+5.9

The tensile strength of the three classes of NP increases with the increase in graphene, fibre nanotubes and hybrid nanofillers weight content, as shown in Figure 62a. A maximum improvement of approximately 17% in tensile strength was illustrated with the addition of 5wt.% of graphene, roughly 19% with the addition 6 w.% of fibre nanotubes and 10% after the hybridisation of 4 wt.% of GNP and CSCNT into the epoxy resin.

The improvement in elastic modulus for the graphene reinforced nanocomposites fluctuated with load level content. In contrast, the best improvement in elastic modulus was showed with about 12% after adding 5wt. % of graphene. The tensile modulus of the modified epoxy gradually increases the fibre nanotube content, except for high load content (i.e. 7wt. %).

The highest increase was recorded of approximately 18% at 6wt. % in fibre nanotubes reinforced nanocomposite. In addition, continuously increasing the tensile modulus of the hybrid GNP-CSCNT/epoxy nanocomposites by increasing the load level content. This behaviour illustrates that the hybridisation of the nanoparticles, such as graphene and fibre nanotube can have a significant effect on the tensile properties of the epoxy resin with level loads contents. Moreover, the highest modulus of hybrid nanofillers was observed by approximately 14% at 6wt. %. In addition, there was a slight improvement in this value at 4 wt. % by approximately 5% (see Figure 62b).

The reasons for the enhancements in mechanical properties in relation to the three epoxy nanocomposites particularly HNP were perhaps due to the improvements in dispersion degree of the nanofillers in the epoxy resin (Yasmin et al., 2006; Tang et al., 2013).

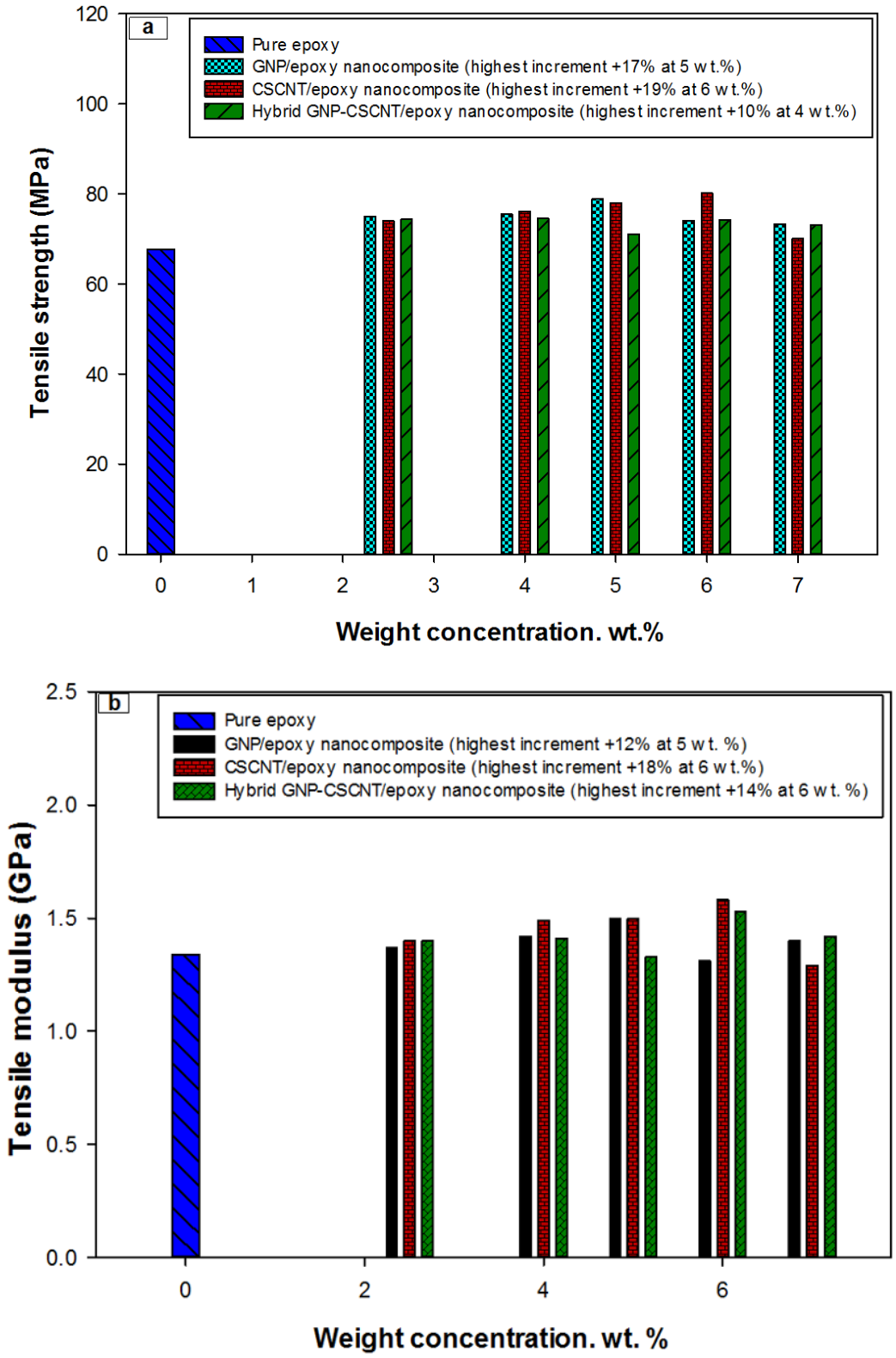

Figure 62 Comparison and evaluation of the optimised matrix in the NP processed by the ball milling technique at different weight concentrations a) Maximum tensile strength, b) Tensile modulus.

5.1.6 Flexural properties of NP processed by ball milling/mixing

Figure 63 shows typical flexural stress-strains curves of the three NP at various weight content. Table 23 reveals the summary of the flexural properties results for the NP.

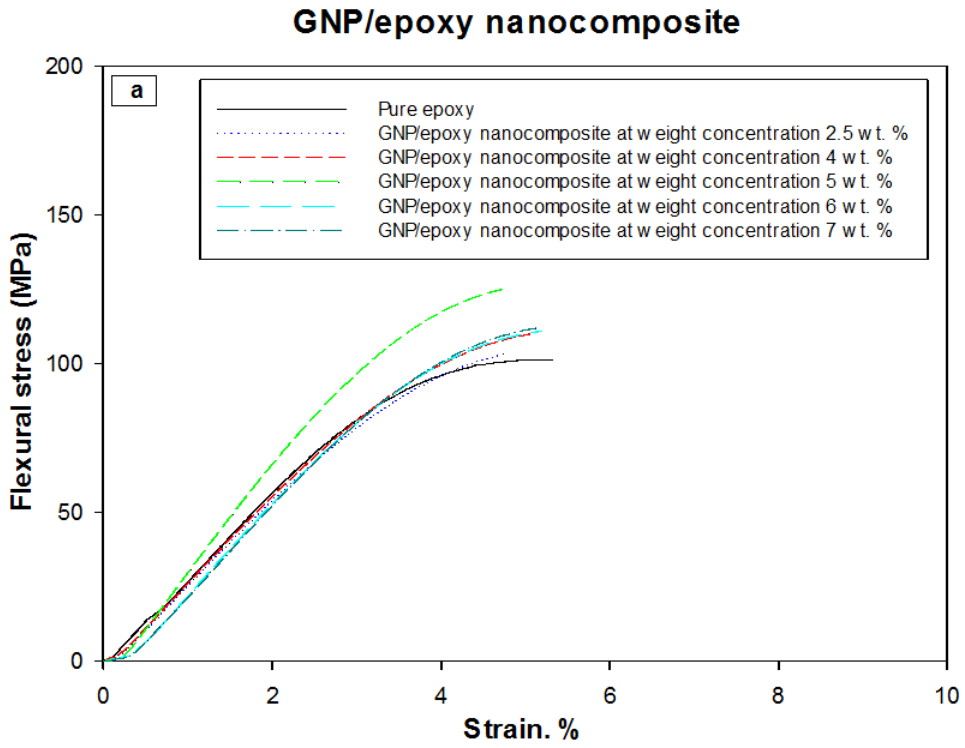
GNP/epoxy nanocomposite
a
Pure epoxy
GNP/epoxy nanocomposite at w eight concentration 2.5 w t. %
GNP/epoxy nanocomposite at w eight concentration 4 w t. %
GNP/epoxy nanocomposite at w eight concentration 5 w t. %
GNP/epoxy nanocomposite at w eight concentration 6 w t. %
GNP/epoxy nanocomposite at w eight concentration 7 w t. %
Flexural stress (MPa)
Strain. %
0
50
100
150
200
0
2
4
6
8
10

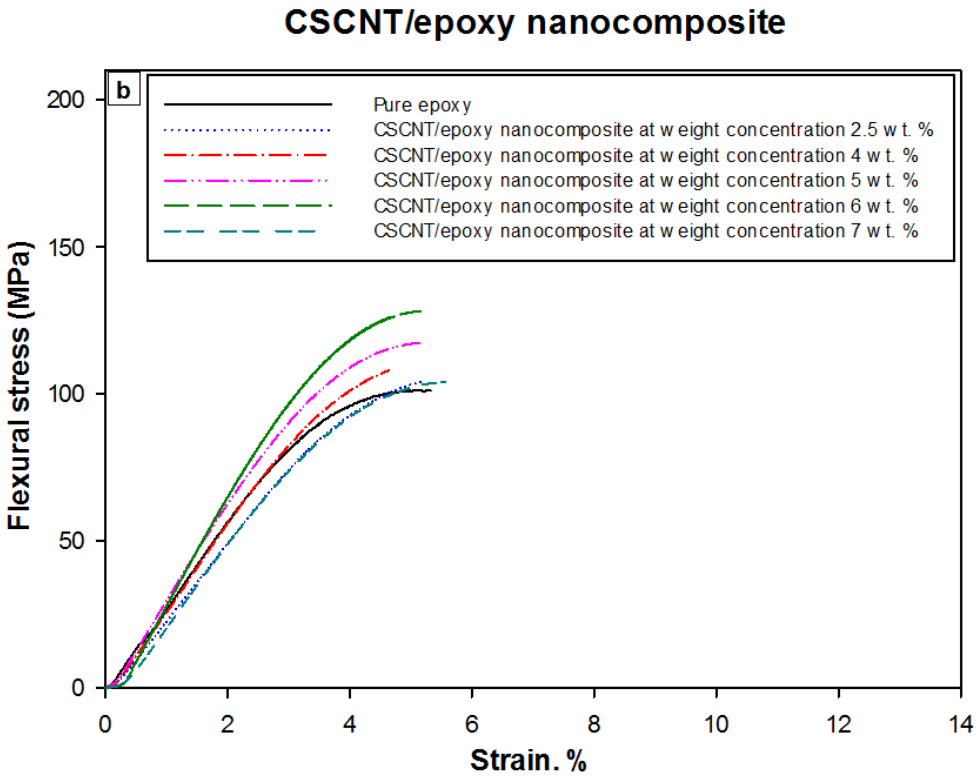
CSCNT/epoxy nanocomposite
b
Pure epoxy
CSCNT/epoxy nanocomposite at w eight concentration 2.5 w t. %
CSCNT/epoxy nanocomposite at w eight concentration 4 w t. %
CSCNT/epoxy nanocomposite at w eight concentration 5 w t. %
CSCNT/epoxy nanocomposite at w eight concentration 6 w t. %
CSCNT/epoxy nanocomposite at w eight concentration 7 w t. %
Flexural stress (MPa)
Strain. %
0
50
100
150
200
0
2
4
6
8
10
12
14

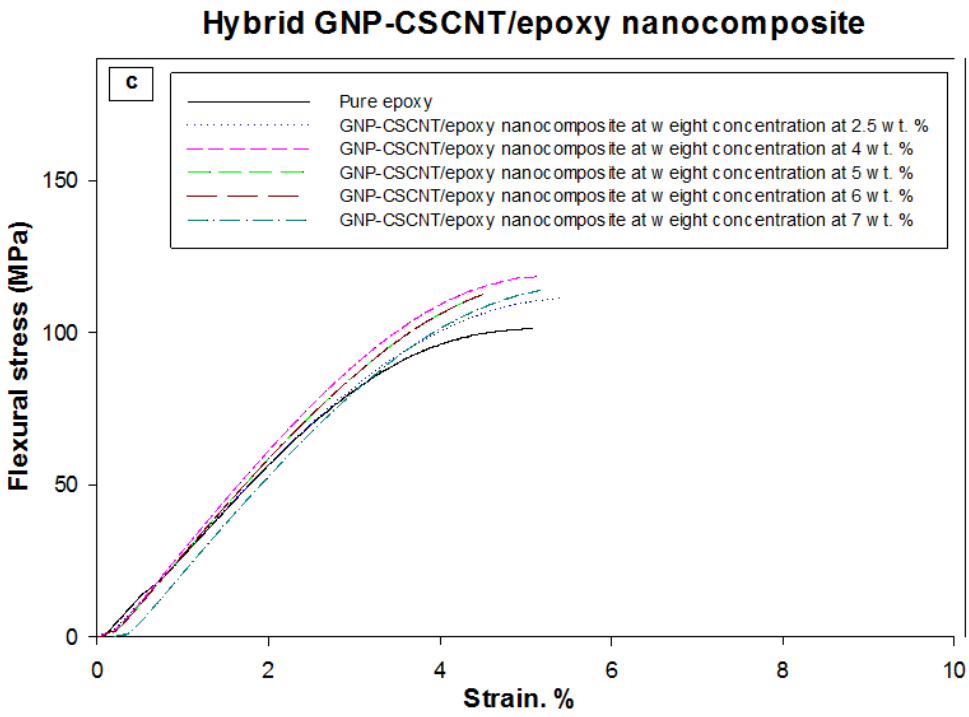

Figure 63 Typical flexural stress-strain curves at different weight concentrations, a) GNP/epoxy nanocomposite, b) CSCNT/epoxy nanocomposite, c) Hybrid GNP-CSCNT/epoxy nanocomposite processed by the ball milling technique.

Table 23 Maximum flexural strength and flexural modulus of the NP processed by the ball milling technique during 47 min of mixing time as a function of nanofiller content.

Sample	Number of samples	Weight content (wt.%)	Flexural strength (MPa)	Improvement (%)	Flexural modulus (GPa)	Improvement (%)
Pure epoxy	4	0	101.21±1.52	00.0	2.80±0.13	00.0
GNP/epoxy nanocomposite	3	2.5	108.30±5.10	+7.0	2.78±0.02	-0.7
	3	4	111.10±1.19	+9.7	2.83±0.06	+1.1
	3	5	123.30±3.34	+21.8	3.20±0.20	+14.3
	4	6	111.30±0.81	+9.9	2.76±0.06	-1.4
	3	7	112.00±1.50	+10.6	2.81±0.05	+0.3
CSCNT/epoxy nanocomposite	3	2.5	105.00±1.71	+3.7	2.65±0.13	-5.3
	3	4	110.90±5.64	+9.5	2.90±0.17	+3.5
	3	5	118..00±3.14	+16.6	3.40±0.14	+21.4
	3	6	128.20±0.85	+26.6	3.80±0.14	+35.7
	3	7	104.00±2.15	+2.7	2.74±0.02	-2.1
Hybrid GNP-CSCNT/epoxy nanocomposite	3	2.5	115.15±0.78	+13.8	2.90±0.12	+3.6
	3	4	118.30±1.38	+16.9	3.20±0.10	+14.3
	3	5	110.00±3.81	+8.7	3.00±0.26	+7.1
	3	6	117.10±3.40	+15.7	3.00±0.10	+7.1
	3	7	115.20±1.51	+13.8	2.82±0.02	+0.7

The flexural properties of the three NP exhibit a continuous increase in flexural strength after adding GNP, CSCNT and hybrid nanofillers to the epoxy resin after improving their dispersion extent in the matrix, as revealed in Figure 64a. The highest improvement, 27% was recorded in the CSCNT/epoxy nanocomposite with the addition of 6wt. % of the fibre nanotubes, 22% in the GNP/epoxy nanocomposite at 5wt. % and 17% after hybridisation with 4wt.% from graphene and novel fibre nanotube into the epoxy resin.

In contrast, the flexural modulus fluctuated in the three types of NP, as shown in Figure 64b. The highest increase showed approximately 14% after adding 5wt. % of the GNP, roughly 36% in the CSCNT/epoxy nanocomposite at 6wt. % and 14% after the addition of 4wt. % hybrid nanofillers. Generally, the highest increase in modulus pointed to a good dispersion and orientation of the nanofillers (Yasmin et al., 2006) and good adhesion between the surface area of the nanofiller and matrix (Zhao et al., 2010). Although there was an increase in flexural strength regarding the hybrid GNP-CSCNT/epoxy nanocomposites, poor dispersion was evident in certain regions of the matrix. Conversely, the improvements in flexural strength properties of the hybrid nanocomposite were possibly due to the existence of some synergy between the graphene and fibre nanotube (Chatterjee et al., 2012; Moghadam and Taheri, 2014).

The reasonable causes of the minor differences in level of flexural strength improvements for the hybrid GNP-CSCNT nanocomposites and CSCNT/epoxy nanocomposites compared with those prepared by sonication mixing may be due to the existence of various defects and damages in geometric structure of some nanoparticles resulting from the dispersion process (i.e. tortuosity or cleavage in fibre nanotubes, wrinkled and agglomeration in graphene layers) during the dispersion process (Li et al., 2013). It is well known that maintaining the geometric structure of the nanoparticles without damage is highly necessary to reinforce the mechanical properties and the performance of nanocomposites (Yokozeki et al., 2008; Moriche et al., 2015).

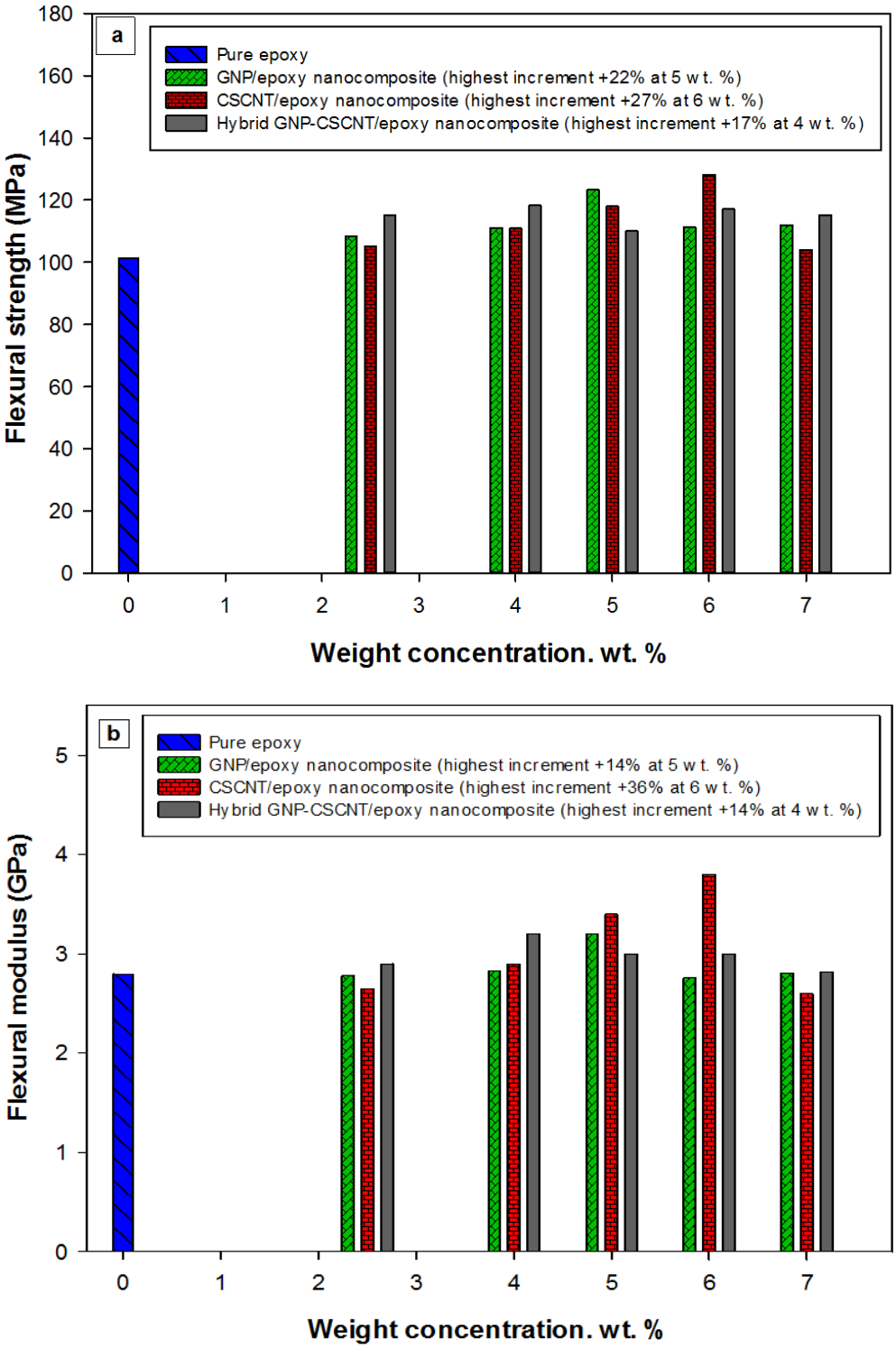

Figure 64 Comparison and evaluation of the optimised matrix in the NP processed by the ball milling technique at different weight concentrations, a) Maximum flexural strength, b) Flexural modulus.

5.1.7 Microstructural details of NP processed by combined techniques mixing

In spite of the TEM image of the GNP/epoxy nanocomposites at critical weight concentration shows optimum uniform dispersion and high exfoliation of the GNP in the epoxy resin, some defects such as wrinkled nanosheets are still present in the matrix, as shown in Figure 65a. The SEM image illustrates a rough surface in the GNP/epoxy nanocomposites as well as bi-furcation

mechanisms (see Figure 65b) and smooth fractures on the surface area of the epoxy composite unmodified (see Figure 65c).

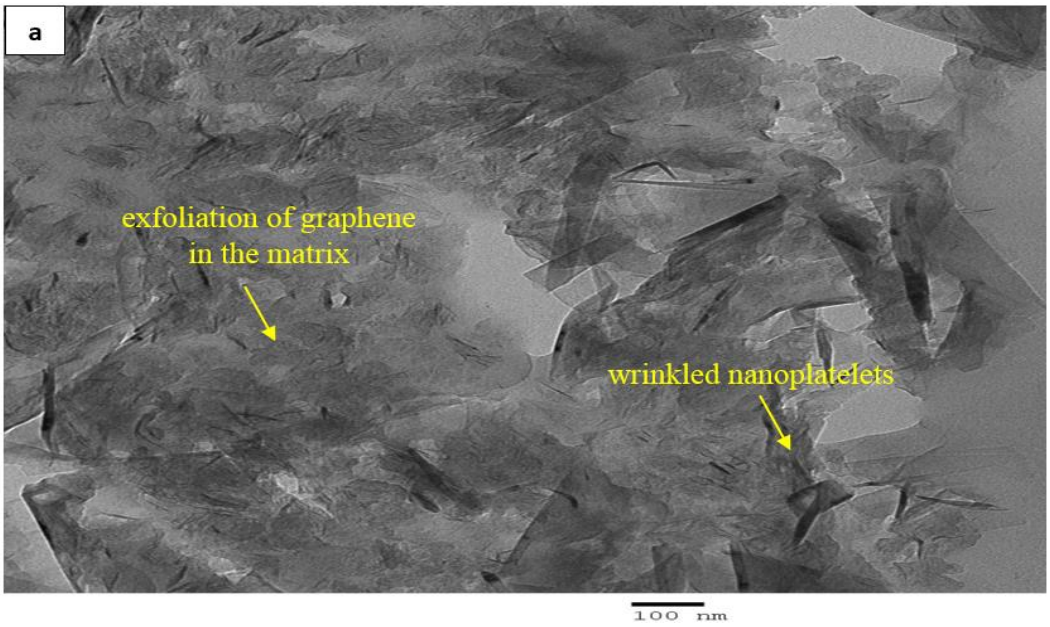

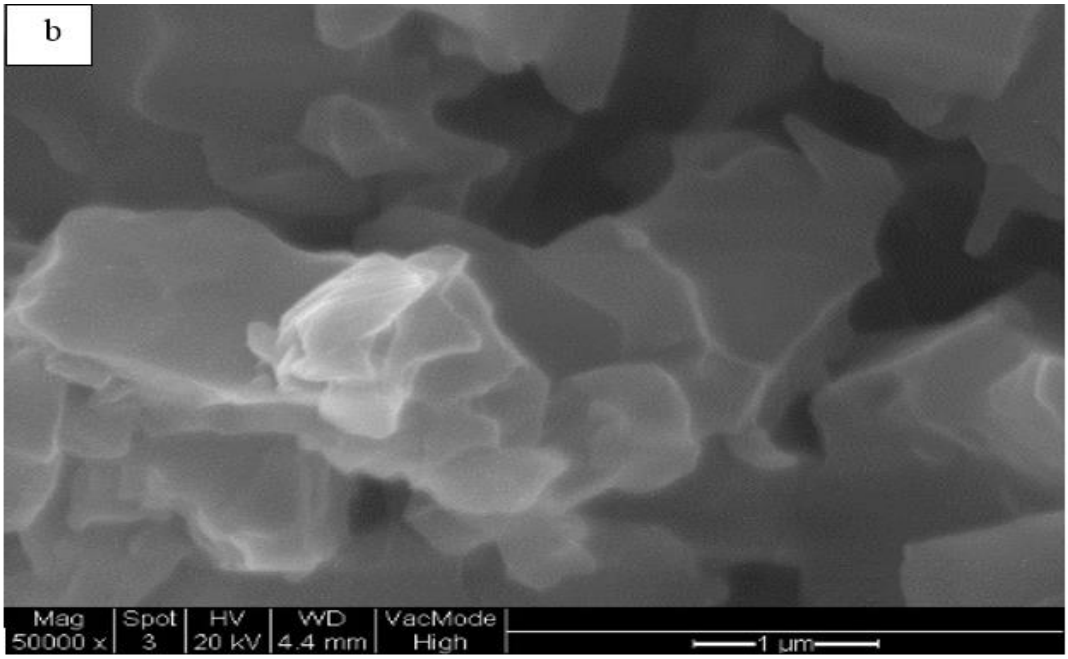

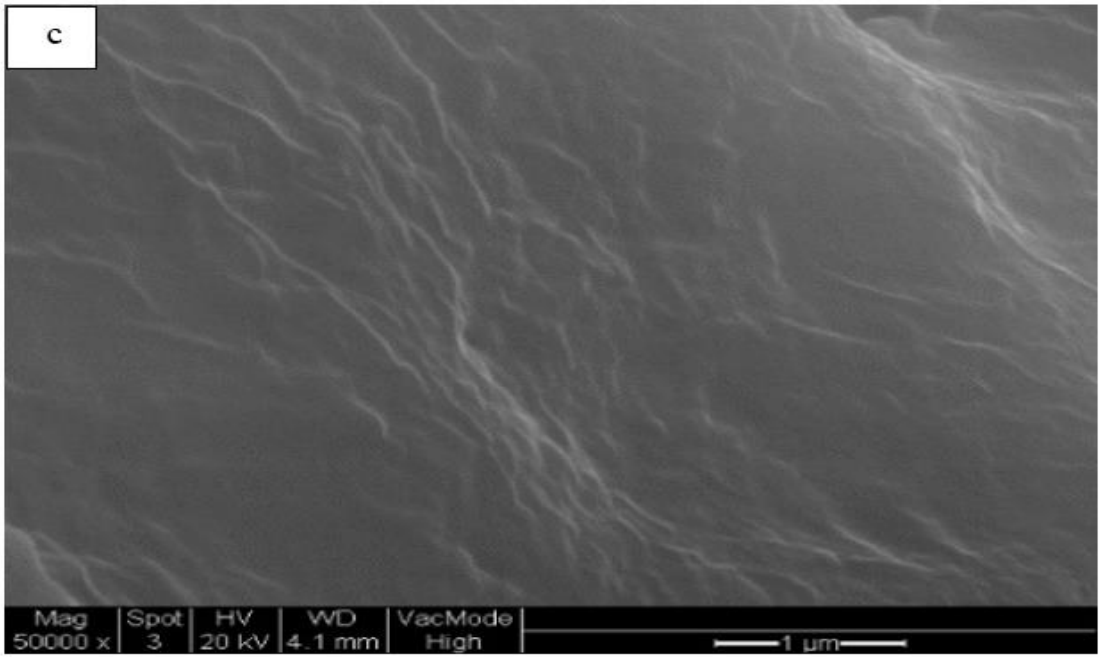

Figure 65 a) TEM image shows the optimum dispersion of nanoplatelets in the matrix processed by combined techniques. b) SEM image shows the rough fracture surface morphology of GNP/epoxy nanocomposite at critical weight concentration (5 wt. %), c) smooth fracture surface of unmodified epoxy.

The TEMs image of CSCNT/epoxy nanocomposite shows high exfoliation of the fibre nanotubes and uniform distribution in the epoxy resin, as shown in Figure 66a. The SEM image demonstrates that many pull-out fibre nanotubes were seen at the fractured area, as shown in Figure 66b.

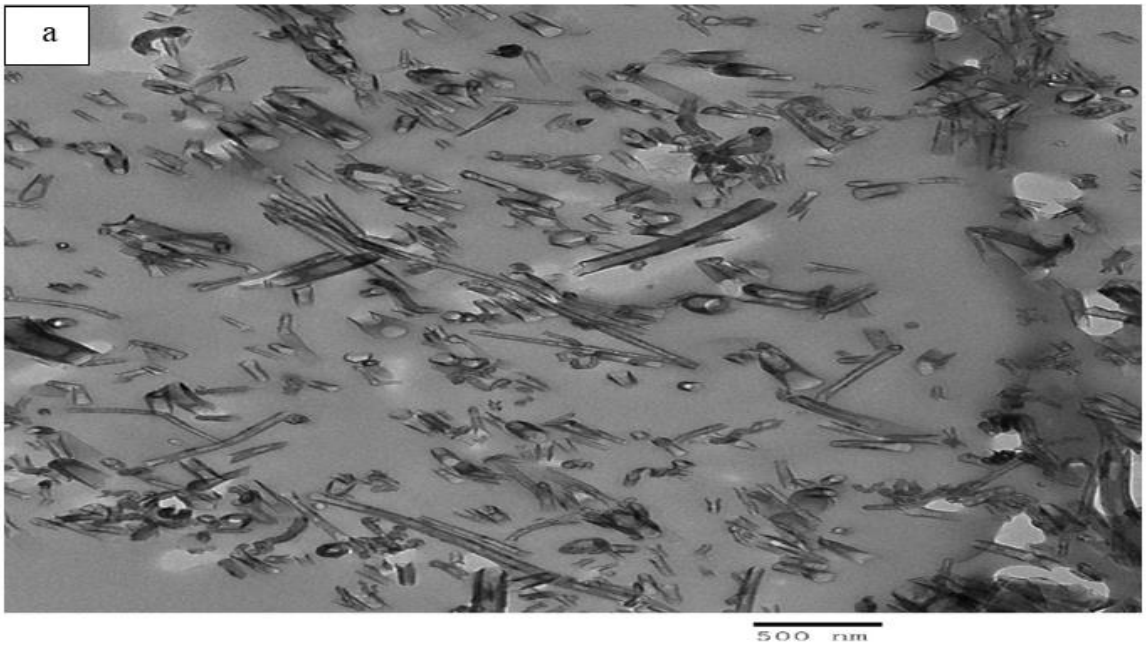

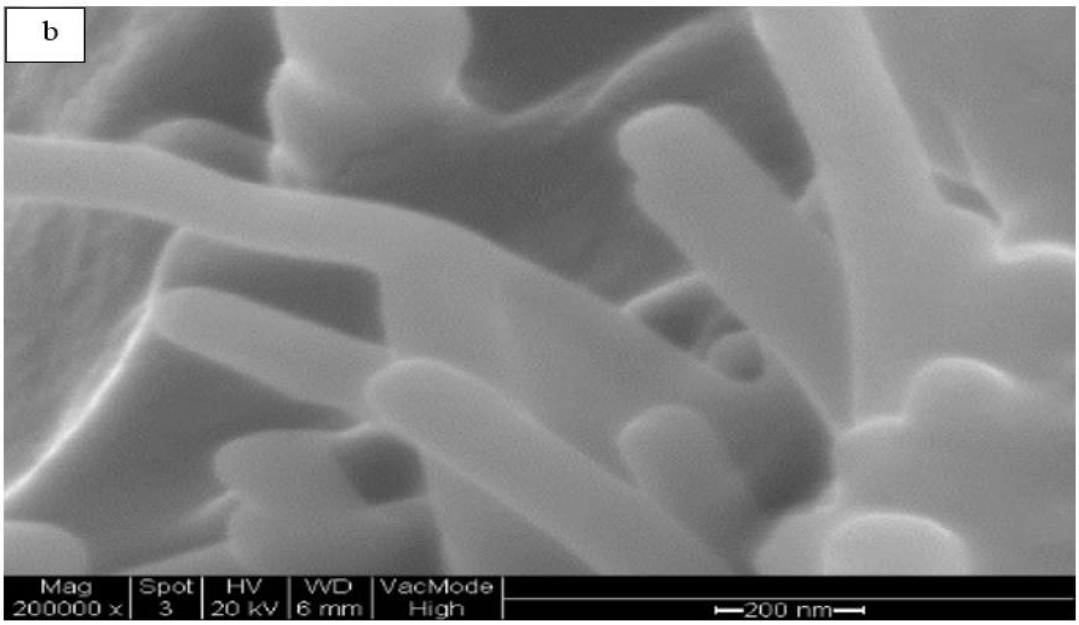

Figure 66 a) TEM image shows high exfoliation of the fibre nanotubes in the matrix processed by combined techniques, b) SEM image shows the fibre nanotubes pull-out of the fracture surface in the CSCNT/epoxy nanocomposite at critical weight concentration (6 wt.%)

The TEM image shows optimum dispersion of the hybrid nanofillers (GNP-CSCNT), high exfoliation and homogenous distribution in the epoxy resin, as revealed in Figure 67a. In contrast, there were still some wrinkled nanosheets in the matrix. Meanwhile, the SEM image shows the pull-out of fibre nanotubes at the fractured area of the hybrid nanocomposite besides the difficulty in recognising the fracture mechanism of nanoplatelets in the nanofilled matrix, as shown in Figure 67b.

Based on this fractographic evidence, using the combined techniques could improve the dispersion degree of the nanofillers and obtain high exfoliation of the nanofillers, particularly the combined nanofillers in the matrix, which appears better in comparison to individual mechanical dispersion processes (i.e. sonication or ball milling).

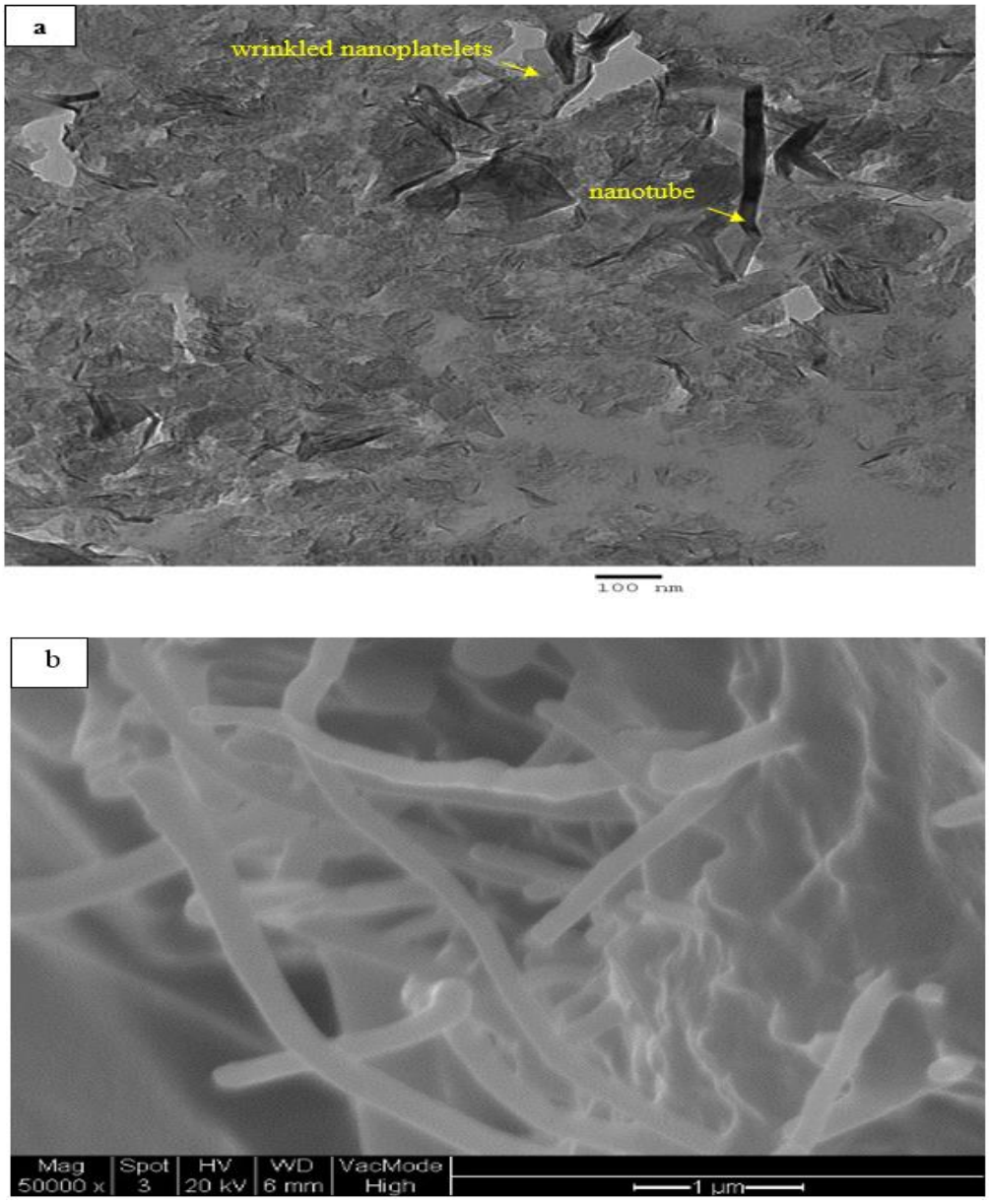

Figure 67 a) TEM image shows the optimum exfoliation and dispersion of the hybrid GNP-CSCNT nanofillers in the matrix processed by combined techniques. b) SEM image shows many fibre nanotubes pull-out at the fracture surface in the hybrid GNP-CSCNT/epoxy nanocomposite at critical weight concentration (4 wt.%)

5.1.8 Tensile properties of NP processed by combined techniques mixing

The typical tensile stress-strain curves mechanism of the three NP at different weight concentrations is illustrated in Figure 68. In addition, Table 24 shows the total statements with regard to the mechanical tensile behaviour of the three types of NP (i.e. GNP/epoxy nanocomposite, CSCNT/epoxy nanocomposite and hybrid GNP-CSCNT/epoxy nanocomposite.

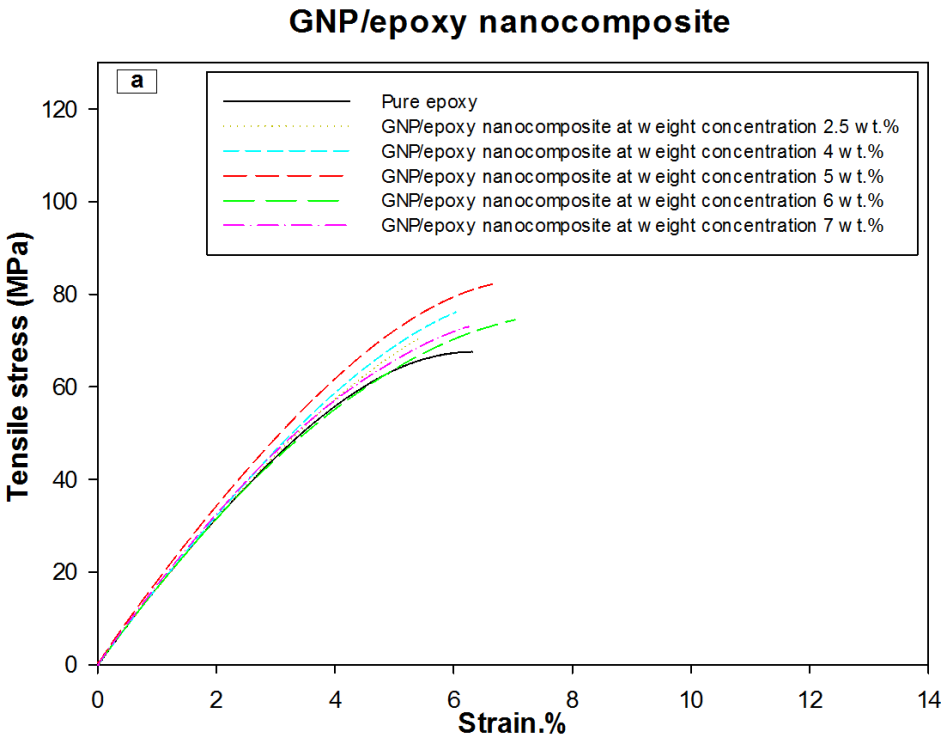
GNP/epoxy nanocomposite
a
Pure epoxy
GNP/epoxy nanocomposite at weight concentration 2.5 wt.%
GNP/epoxy nanocomposite at weight concentration 4 wt.%
GNP/epoxy nanocomposite at weight concentration 5 wt.%
GNP/epoxy nanocomposite at weight concentration 6 wt.%
GNP/epoxy nanocomposite at weight concentration 7 wt.%
Tensile stress (MPa)
Strain.%
0
20
40
60
80
100
120
0
2
4
6
8
10
12
14

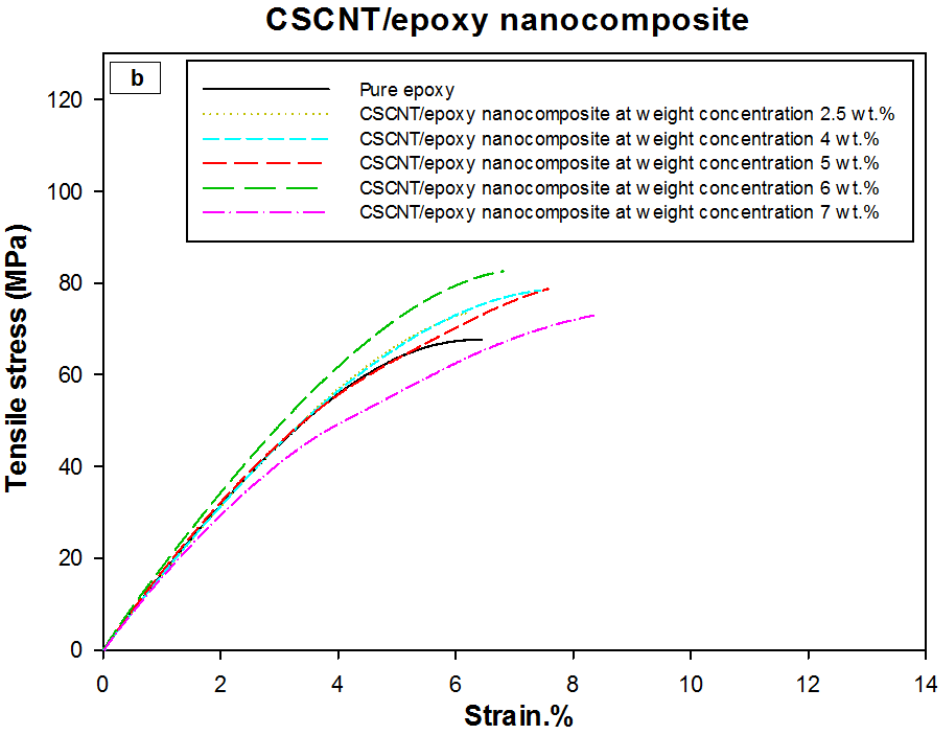
CSCNT/epoxy nanocomposite
b
Pure epoxy
CSCNT/epoxy nanocomposite at weight concentration 2.5 wt.%
CSCNT/epoxy nanocomposite at weight concentration 4 wt.%
CSCNT/epoxy nanocomposite at weight concentration 5 wt.%
CSCNT/epoxy nanocomposite at weight concentration 6 wt.%
CSCNT/epoxy nanocomposite at weight concentration 7 wt.%
Tensile stress (MPa)
Strain.%
0
20
40
60
80
100
120
0
2
4
6
8
10
12
14

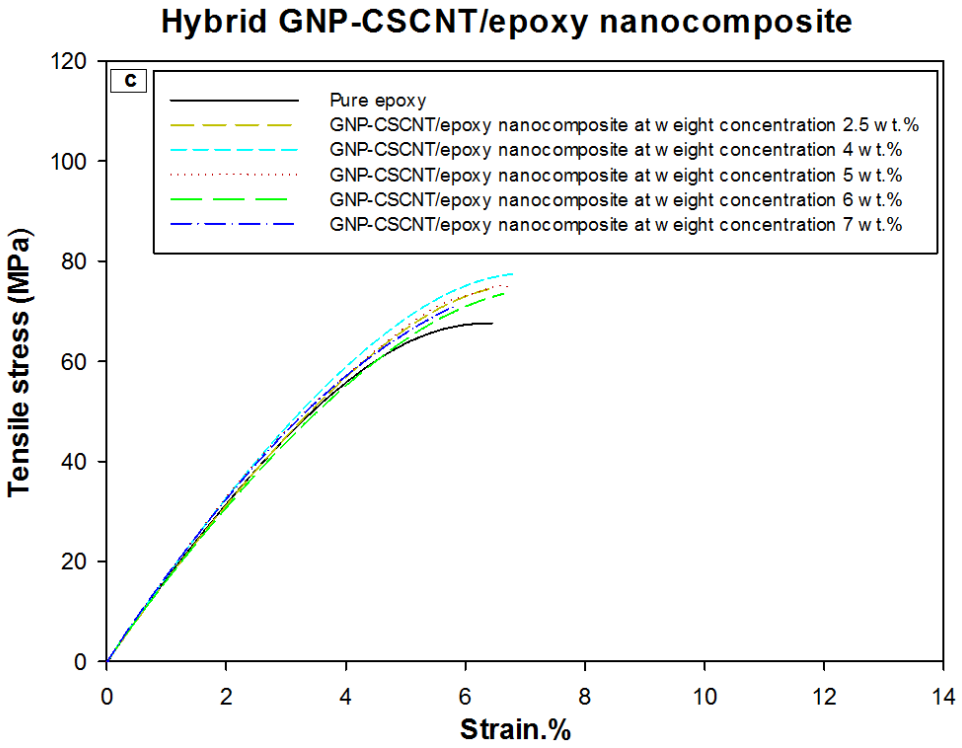

Figure 68 Typical tensile stress-strain curves at different weight concentrations: a) GNP/epoxy nanocomposite, b) CSCNT/epoxy nanocomposite, c) Hybrid GNP-CSCNT/epoxy nanocomposite processed by combined techniques.

Table 24 Maximum tensile strength and tensile modulus of the NP processed by combined techniques during 55 min of mixing and dispersing time as a function of nanofiller content.

Sample	Number of samples	Weight content (wt.%)	Tensile strength (MPa)	Improvement (%)	Tensile modulus (GPa)	Improvement (%)
Pure epoxy	4	0	67.64±0.92	00.0	1.34±0.03	00.0
GNP/epoxy nanocomposite	4	2.5	70.80±1.29	+4.7	1.53±0.03	+14.2
	4	4	76.13±2.23	+12.5	1.53±0.02	+14.2
	4	5	79.38±1.84	+17.3	1.56±0.03	+16.4
	4	6	74.09±2.02	+9.5	1.52±0.01	+13.4
	3	7	73.40±0.62	+8.5	1.55±0.14	+15.7
CSCNT/epoxy nanocomposite	4	2.5	74.93±1.80	+10.8	1.38±0.03	+2.9
	4	4	78.65±0.43	+16.3	1.42±0.05	+5.9
	3	5	80.72±2.62	+19.3	1.40±0.10	+4.4
	3	6	82.03±3.02	+21.3	1.70±0.19	+26.8
	3	7	74.04±0.99	+9.4	1.46±0.04	+8.9
Hybrid GNP-CSCNT/epoxy nanocomposite	4	2.5	74.83±0.33	+10.6	1.45±0.02	+8.2
	4	4	77.60±0.81	+14.7	1.63±0.08	+21.6
	4	5	74.14±0.91	+9.6	1.40±0.02	+4.5
	3	6	73.50±0.40	+8.6	1.50±0.01	+11.9
	3	7	72.57±1.30	+7.3	1.50±0.03	+11.9

The effect of the addition of nanofillers on tensile properties of the epoxy resin is shown in Figure 69. The maximum tensile strength and elastic modulus increase with the increase in the weight content of graphene from 2.5 wt. % to 7 wt. % (see Figures 69a and 69b). The critical increase in relation to the tensile strength and elastic modulus was 17% and 16%, respectively at a weight concentration of 5 wt. %.

The tensile strength and modulus increase dramatically with the increase in the loading levels with regard to the CSCNT (see Figures 69a and 69b). The maximum improvement in tensile strength and elastic modulus was approximately 21% and 27% respectively at a weight concentration of 6 wt. %.

The novel type of nanocomposites produced is the hybrid GNP-CSCNT/epoxy nanocomposite. In relation to the two combined nanomaterials, each one has different morphological properties, whilst there is a significant improvement in tensile properties of hybrid nanocomposites. For example, Figures 69a and 69b illustrate that there is a significant improvement in tensile strength and modulus with loads level concentrations from 2.5 wt.% to 7 wt.%. The highest increase in the tensile strength and elastic modulus of approximately 15% and 22% respectively at weight concentration (i.e. 4 wt. %). Thus, this behaviour explains that the tensile properties could

essentially increase after combining two nanoparticles, as each one has substantial strength properties and geometric structures and improves the dispersion degree of the hybrid nanofillers in the matrix. However, the optimum tensile strength and elastic properties of the three NP were calculated to be 17%, and 16% of 5wt.% GNP, 21%, and 27% of 6 wt.% CSCNT and 15%, and 22% of 4 wt.% hybrid nanofillers (GNP-CSCNT) respectively. These improvements are better than those prepared by sonication mixing and ball milling/mixing.

The difference in these improvements for each one of NP depends on the type of nanofiller, given that each nanoparticle has different morphological and mechanical properties, such as geometric shape, nano-size and strength and stiffness properties (Li et al., 2018; Domun et al., 2015; Bal and Saha, 2014). In addition, the quality of dispersion could affect the level of increase in the mechanical properties of the NP, (Tang et al., 2013). This is because the extent of dispersion in each type of nanofiller may relate to van der Waals forces as mentioned previously. For instance, these forces in the graphene network are probably stronger than that of the fibre nanotube network (Chen et al., 2015; Li et al., 2013). Furthermore, the high exfoliation of nanofillers contributes to increasing their contact area with the matrix, which promotes the mechanical interfacial properties. Hence, this was expected to improve the performance of the nanocomposite (Yue et al., 2014; Liu et al., 2017).

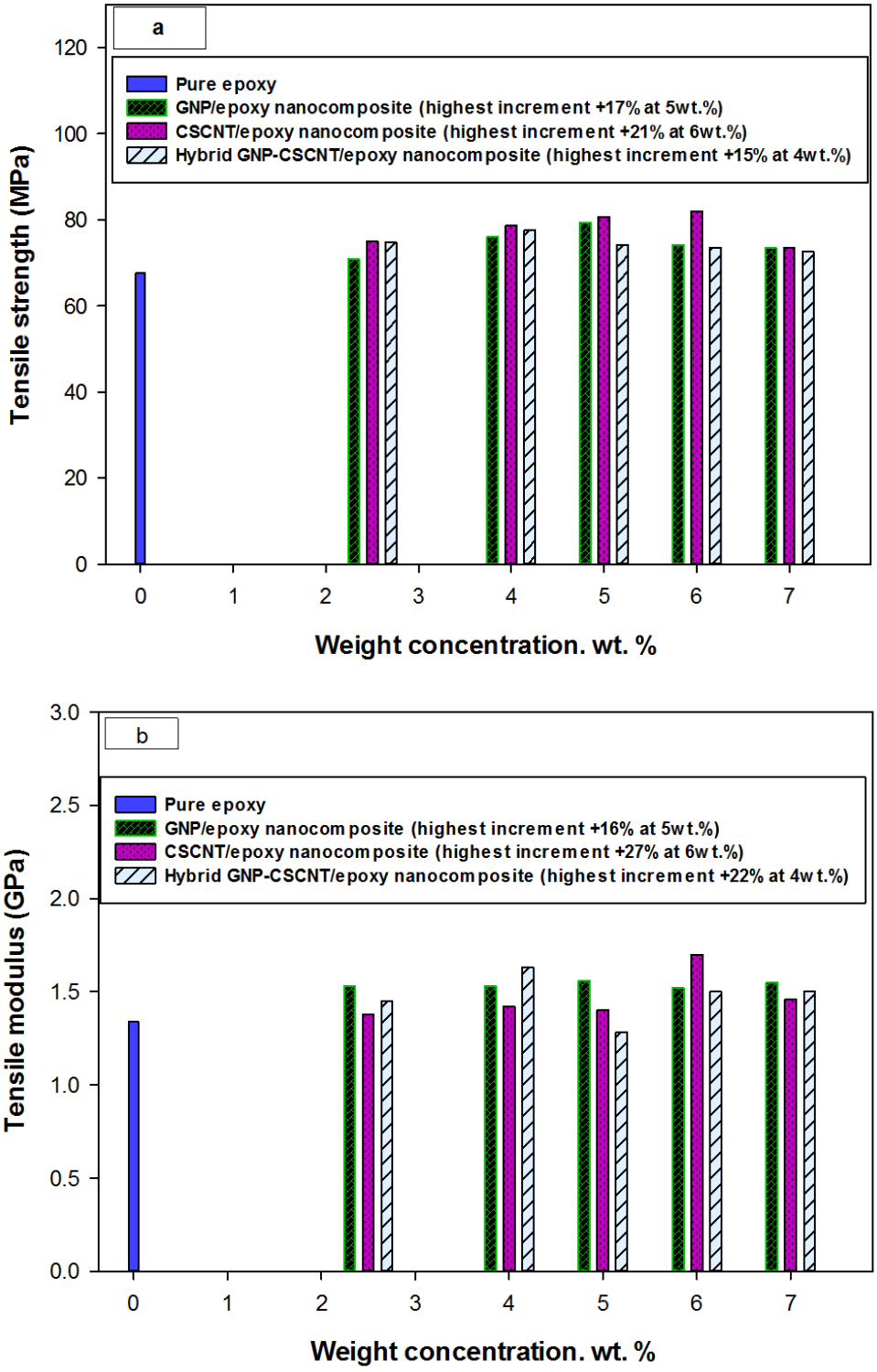

Figure 69 Comparison and evaluation of the optimised matrix in the NP processed by combined techniques at different weight concentrations: a) Maximum tensile strength, b) Tensile modulus.

5.1.9 Flexural properties of NP processed by combined techniques mixing

Typical stress-strain curves in Figure 70 demonstrate the behaviour of flexural properties tests for three classes of the three NP, under static conditions. Table 25 explains the data derived from these curves.

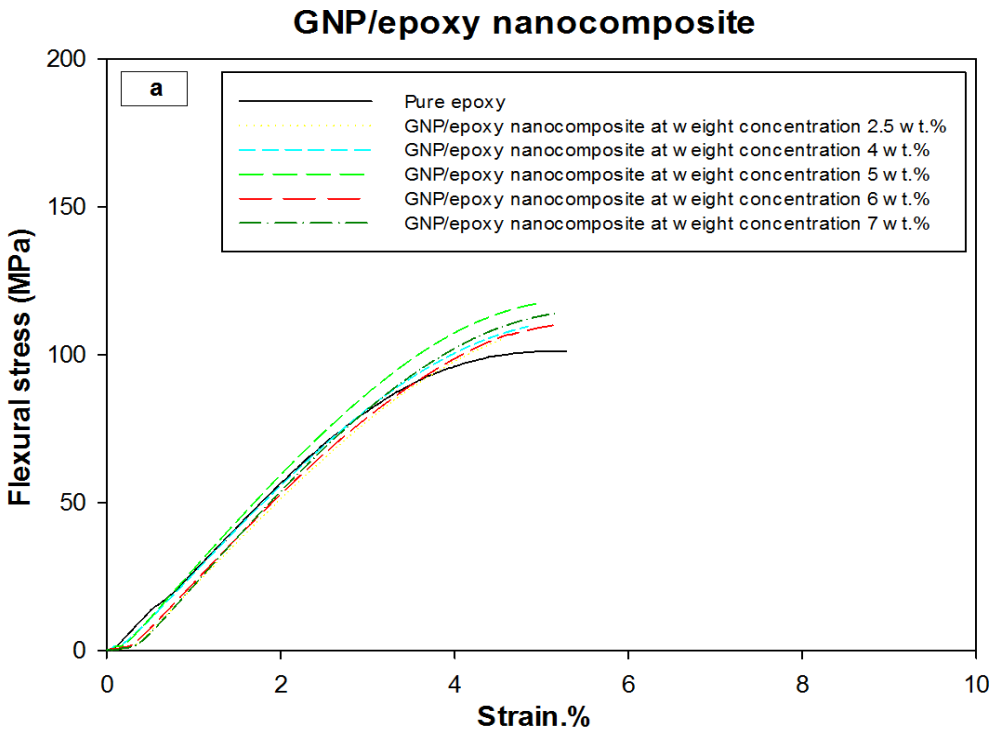

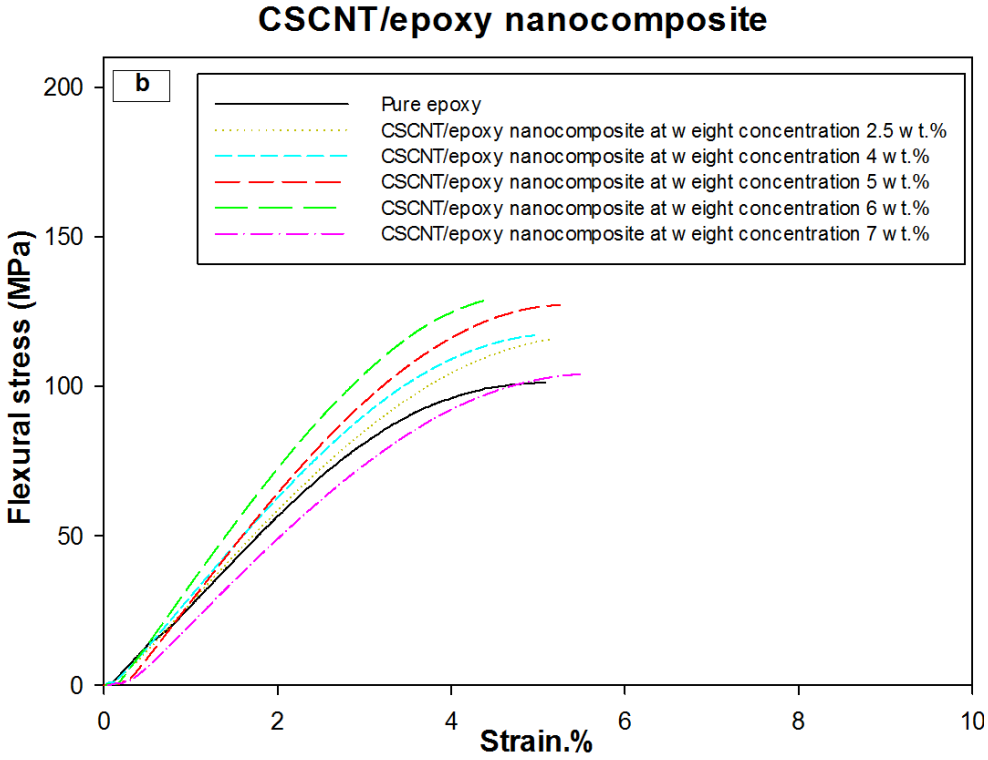

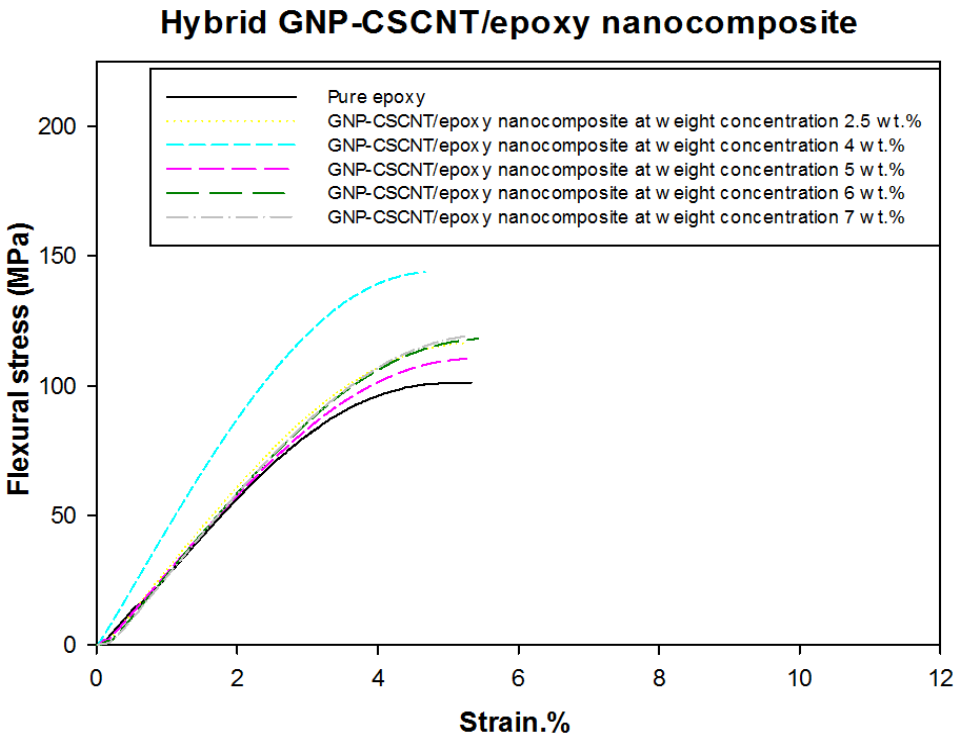

Figure 70 Comparison and evaluation of the optimised matrix in the NP processed by combined techniques at different weight concentrations: a) Maximum tensile strength, b) Tensile modulus.

Table 25 Maximum flexural strength and flexural modulus of the NP processed by combined techniques during 55 min of mixing and dispersing time as a function of nanofiller content.

Sample	Number of samples	Weight content (wt.%)	Flexural strength (MPa)	Improvement (%)	Flexural modulus (GPa)	Improvement (%)
Pure epoxy	4	0	101.21±1.52	00.0	2.80±0.13	00.0
GNP/epoxy nanocomposite	4	2.5	108.40±2.45	+7.1	2.85±0.08	+1.8
	4	4	109.49±3.69	+8.2	2.88±0.11	+2.8
	3	5	118.60±3.06	+17.2	3.10±0.20	+10.7
	3	6	110.98±0.30	+9.6	2.90±0.04	+3.6
	4	7	115.24±2.68	+13.8	2.82±0.02	+0.7
CSCNT/epoxy nanocomposite	4	2.5	116.73±2.56	+15.3	2.95±0.11	+5.3
	3	4	117.49±0.48	+16.1	3.20±0.20	+14.3
	3	5	127.20±1.01	+25.6	3.35±0.08	+19.6
	4	6	130.70±4.49	+29.1	3.70±0.29	+32.1
	4	7	104.00±2.05	+2.7	2.83±0.05	+1.1
Hybrid GNP-CSCNT/epoxy nanocomposite	4	2.5	116.56±1.89	+15.1	3.23±0.19	+15.3
	4	4	141.50±6.87	+39.8	4.50±0.18	+60.7
	3	5	110.46±0.85	+9.1	3.00±0.08	+7.1
	3	6	118.25±2.10	+16.8	3.21±0.12	+14.6
	3	7	117.10±2.05	+15.7	2.90±0.05	+3.6

Figure 71a distinguishes the comparison in flexural strength regarding the GNP/epoxy nanocomposite with various weight contents after improving the dispersion level by using combined techniques. Furthermore, it is illustrated that there is a rough improvement in flexural strength, and moreover, that the critical increase was approximately 17% at a weight concentration of 5 wt.%. In contrast, Figure 71b reveals that there is a rough increase in flexural modulus at the same loading levels by approximately 11%.

The maximum flexural strength and modulus increase dramatically when the contents loading is less than 7 wt. % in CSCNT/epoxy nanocomposites, as shown in Figures 71a and 71b. Subsequently, the flexural properties start to drop significantly in relation to percentage increase, which is expected due to the increase in loading levels. The best improvements in maximum strength and elastic were approximately 29% and 32% respectively at 6 wt. %.

The novel hybrid GNP-CSCNT/epoxy nanocomposite displays a significant increase in flexural properties. It can be observed that the combined nanoparticles in the epoxy composite produce an important rise in flexural properties at low loading levels, as shown in Figures 71a and 71b. The critical increase in both flexural strength and modulus was approximately 40% and 61% respectively at a 4 wt.% weight concentration in relation to the combined nanoparticles. Afterwards, these properties gradually decrease, although their reduction remains positive at high weight contents (i.e. 7 wt.%). This increase in flexural strength properties after the combination of the nanoparticles shows that high uniform dispersion increases the synergy property of the graphene and fibre nanotube in the epoxy resin, which significantly increases the mechanical properties of the HNP (Yue et al., 2014).

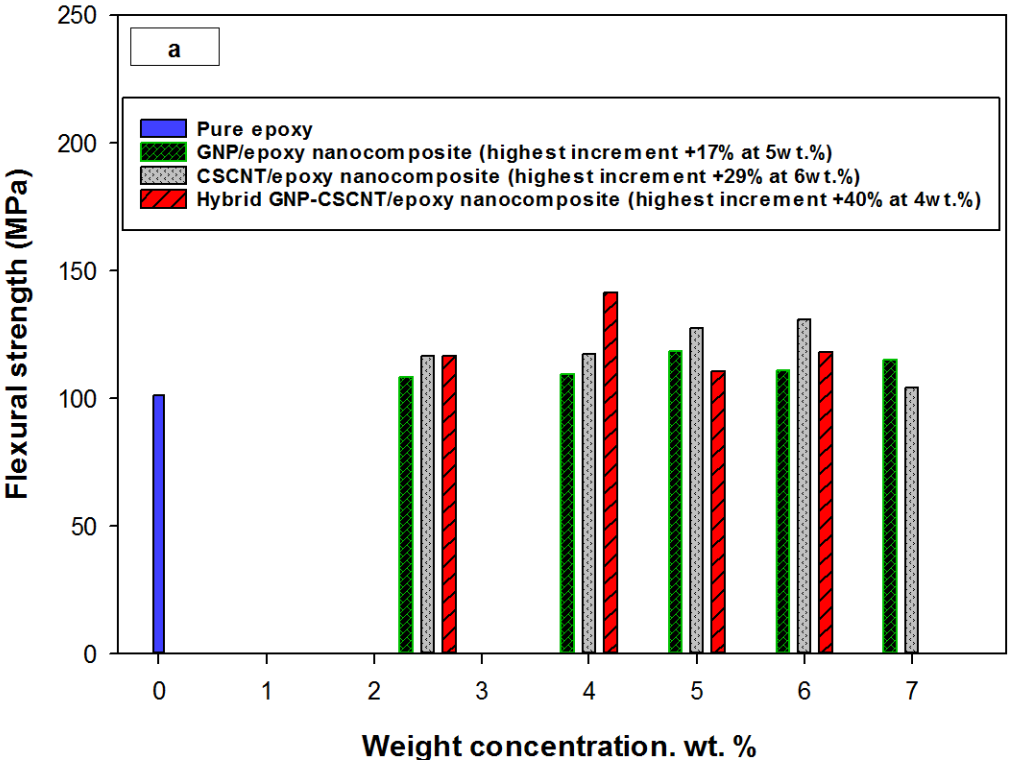

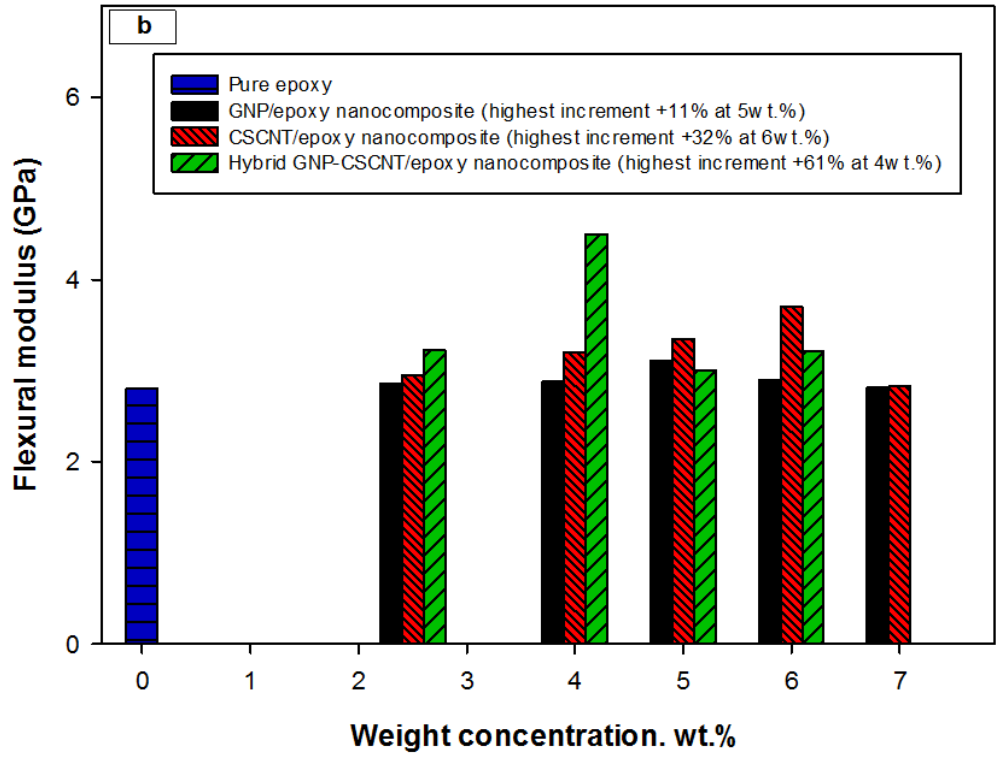

Figure 71 Comparison and evaluation of the optimised matrix in the NP processed by combined techniques at different weight concentrations: a) Maximum flexural strength, b) Flexural modulus.

5.2 The effect of sonication mixing time on strength and modulus properties of the NP

It is well known that there are numerous challenges during the dispersion process of nanoparticles using the ultra-sonication technique. These include amplitude and period of dispersion that have an effect on the dispersion degree of the nanoparticle in the nanocomposite. Hence, this may affect their mechanical properties and the performance of NP (Gkikas et al., 2012). Furthermore, the high exfoliation of the nanofillers increases the level of mechanical properties of the nanocomposites. However, Table 26 shows the values of tensile strength and flexural strength for various periods of dispersion; 15 min, 30 min, 45 min and 60 min, for three formulations of the NP; GNP/epoxy nanocomposite, CSCNT/epoxy nanocomposite and hybrid GNP-CSCNT/epoxy nanocomposite. All the dispersion processes for these NP were accomplished at an amplitude of 75%.

Table 26 Tensile and flexural properties of the NP at critical weight concentrations and at various periods of nanoparticles dispersion processed by sonication technique.

Sample	Time (min)	Sonication mixing			
		Tensile strength (MPa)	Tensile modulus (GPa)	Flexural strength (MPa)	Flexural modulus (GPa)
Pure epoxy	-	67.64±0.92	1.34±0.03	101.21±1.52	2.80±0.13
GNP/epoxy nanocomposite at 5 wt.%	15	60.00±1.50	1.20±0.10	076.00±2.90	2.20±0.10
	30	71.80±2.90	1.37±0.09	093.94±3.10	2.40±0.08
	45	77.10±2.30	1.49±0.03	107.75±3.34	2.60±0.08
	60	73.30±1.90	1.52±0.08	106.40±2.70	2.90±0.12
CSCNT/epoxy nanocomposite at 6 wt.%	15	63.00±3.70	1.30±0.08	086.00±2.60	2.67±0.09
	30	71.50±1.50	1.40±0.11	105.10±2.40	2.87±0.06
	45	78.21±1.33	1.53±0.01	130.10±1.90	3.50±0.11
	60	75.10±2.70	1.55±0.07	119.50±2.80	3.63±0.07
Hybrid GNP-CSCNT/epoxy nanocomposite at 4 wt.%	15	55.00±1.60	1.13±0.06	072.00±2.30	2.78±0.06
	30	69.00±3.20	1.20±0.07	114.26±1.70	2.89±0.02
	45	76.14±1.18	1.29±0.03	123.00±1.27	3.15±0.03
	60	75.71±1.65	1.36±0.05	120.10±2.10	3.10±0.05

Figure 72 illustrates the influence of the sonication mixing time on the strength and modulus properties of the modified matrix in each nanocomposite.

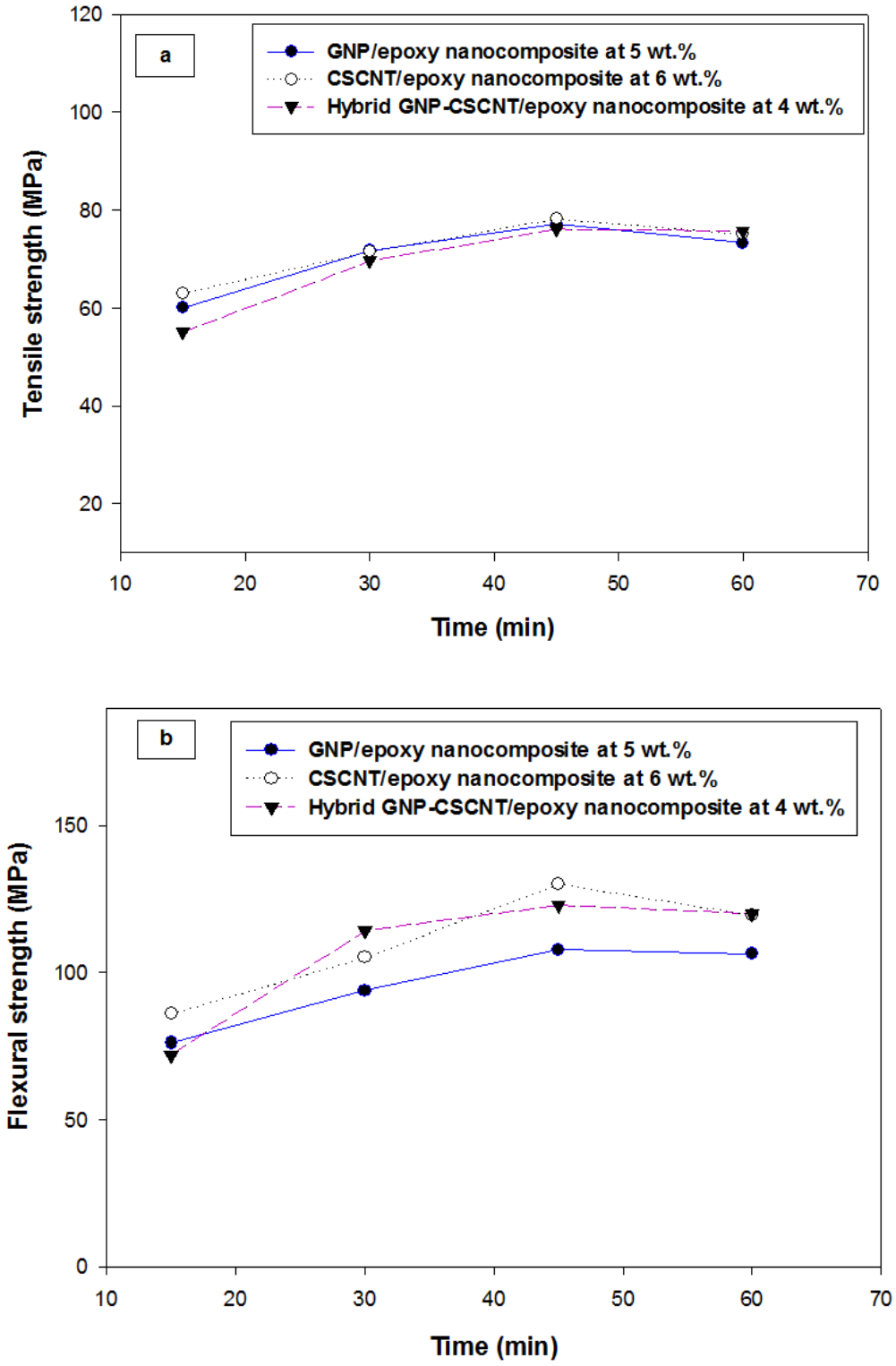

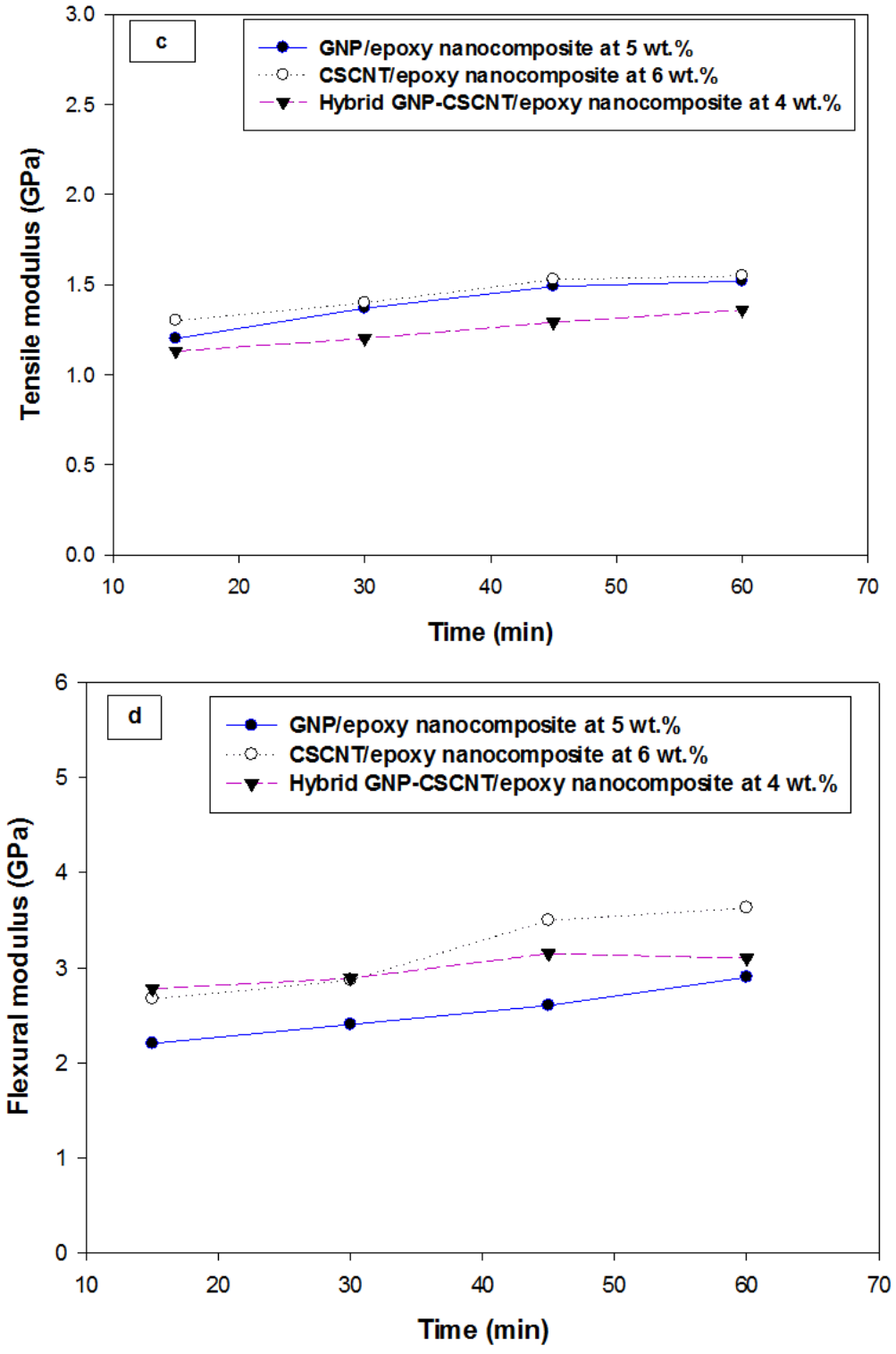

Figure 72 The influence of sonication mixing time on strength and modulus properties of the three NP at critical weight concentration; a) Tensile strength, b) Flexural strength, c) Tensile modulus, d) Flexural modulus.

Figures 73a and 73b also show that there is significant difference of tensile and flexural strength between 15 and 60 min. In general, the existence of the nanoparticle clusters in the nanocomposite lead to cracks being formed in the sample. This analysis could prove the main reason for the reduction in the mechanical properties of the three NP with poorly dispersed nanofillers in the matrix at 15 min (Zaman et al., 2012). The TEM images show the poor dispersion of the nanoparticles and existence of the clusters phenomenon besides the percolation phenomenon in the micro-cross sectional of NP particularly the novel HNP (Chandrasekaran et al., 2013), as shown in Figure 73c.

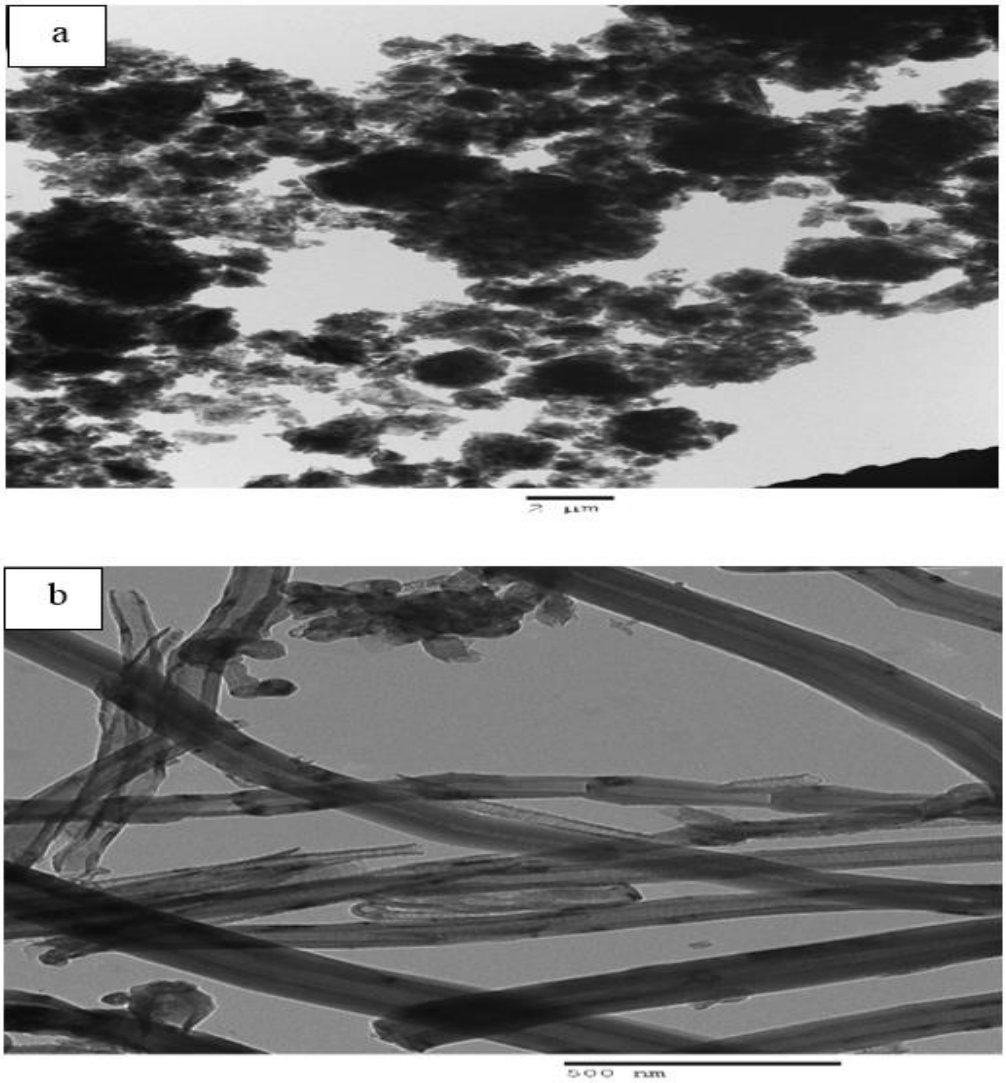

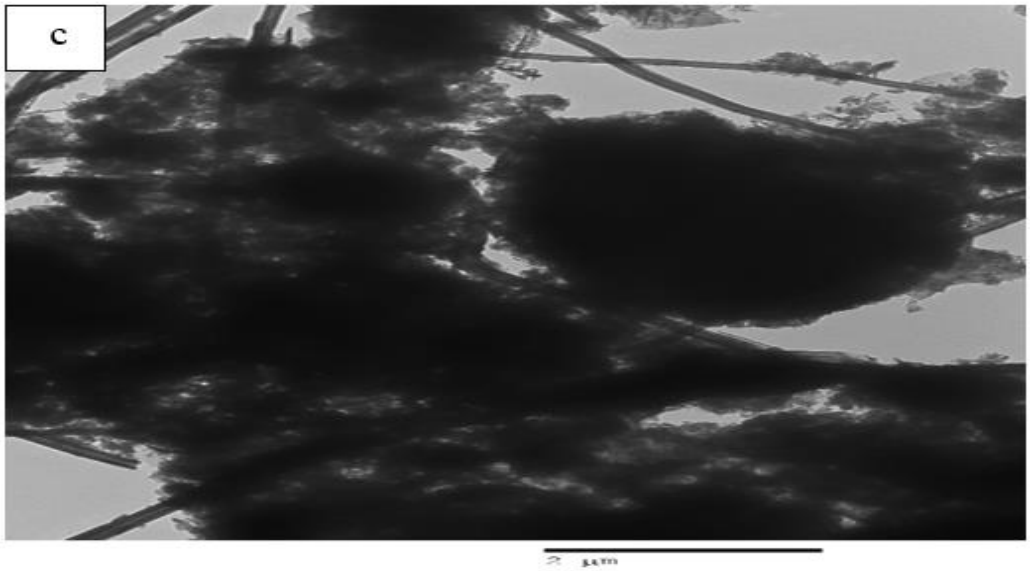

Figure 73 The TEM images show the poor dispersion of the nanofillers in each nanocomposite prepared by the sonication technique; a) GNP/epoxy nanocomposite, b) CSCNT/epoxy nanocomposite c) Hybrid GNP-CSCNT/epoxy nanocomposite.

The optimum period to reinforce the strength properties in NP was at 45 min. After this optimum period, the strength properties showed little effect on the tensile and flexural strength of the three NP, whereas there is a continuous and slight increase in elastic modulus for each sample after increasing the interval time of dispersion to 60 min for the mixture by using sonication mixing, as shown in Figures 72c and 72d, (Yasmin et al., 2006; Wang et al., 2012; Zaman et al., 2012; Tang et al., 2013). Comparatively, the good dispersion degree for the nanofillers in resin contributes to increasing the mechanical properties of the NP due to the high efficiency in transferring the mechanical forces between the nanoparticles and the matrix in the nanocomposite (Rafiee et al., 2010). In contrast, the dispersion process and type of nanofiller used could significantly affect the mechanical properties of the NP. Yasmin et al. (2006), reported that use of sonication mixing for a long period may degrade the strength and stiffness properties of the NP.

5.3 The effect of ball milling time on strength and modulus properties of the NP

Table 27 shows the level of increase in the strength and stiffness properties of the three NP at various periods of the dispersion process. The three NP were dispersed at the critical weight concentration for each sample by using the ball milling technique for the mixing periods; 15 min, 30 min, 45 min and 60 min and a mixing speed of 400rpm.

Table 27 Tensile and flexural properties of the NP at critical weight concentrations and at various period of nanoparticles dispersion processed by the ball milling technique.

Sample	Time (min)	Ball milling/mixing			
		Tensile strength (MPa)	Tensile modulus (GPa)	Flexural strength (MPa)	Flexural modulus (GPa)
Pure epoxy	-	67.64±0.92	1.34±0.03	101.21±1.52	2.80±0.13
GNP/epoxy nanocomposite at 5 wt.%	15	64.10±3.20	1.12±0.10	096.10±5.10	2.20±0.13
	30	70.10±1.70	1.35±0.03	104.40±2.70	2.80±0.09
	45	78.90±0.49	1.50±0.06	123.30±3.34	3.20±0.20
	60	76.30±2.30	1.58±0.09	118.10±2.14	3.40±0.17
CSCNT/epoxy nanocomposite at 6 wt.%	15	70.10±4.10	1.30±0.15	097.10±3.54	2.50±0.18
	30	75.10±1.75	1.45±0.07	107.10±1.76	2.90±0.01
	45	80.20±1.34	1.58±0.01	128.20±0.85	3.80±0.13
	60	78.10±2.23	1.62±0.08	118.90±2.80	3.86±0.07
Hybrid GNP-CSCNT/epoxy nanocomposite at 4 wt.%	15	54.10±2.62	1.10±0.13	070.30±1.98	2.03±0.17
	30	69.60±1.63	1.30±0.07	114.20±2.90	2.79±0.18
	45	74.60±3.97	1.41±0.04	118.30±1.38	3.20±0.10
	60	74.10±2.12	1.43±0.09	118.10±2.33	3.80±0.20

Figure 74 shows the effect of mixing time on the strength and modulus properties of GNP/epoxy nanocomposite, CSCNT/epoxy nanocomposite and hybrid GNP-CSCNT/epoxy nanocomposite.

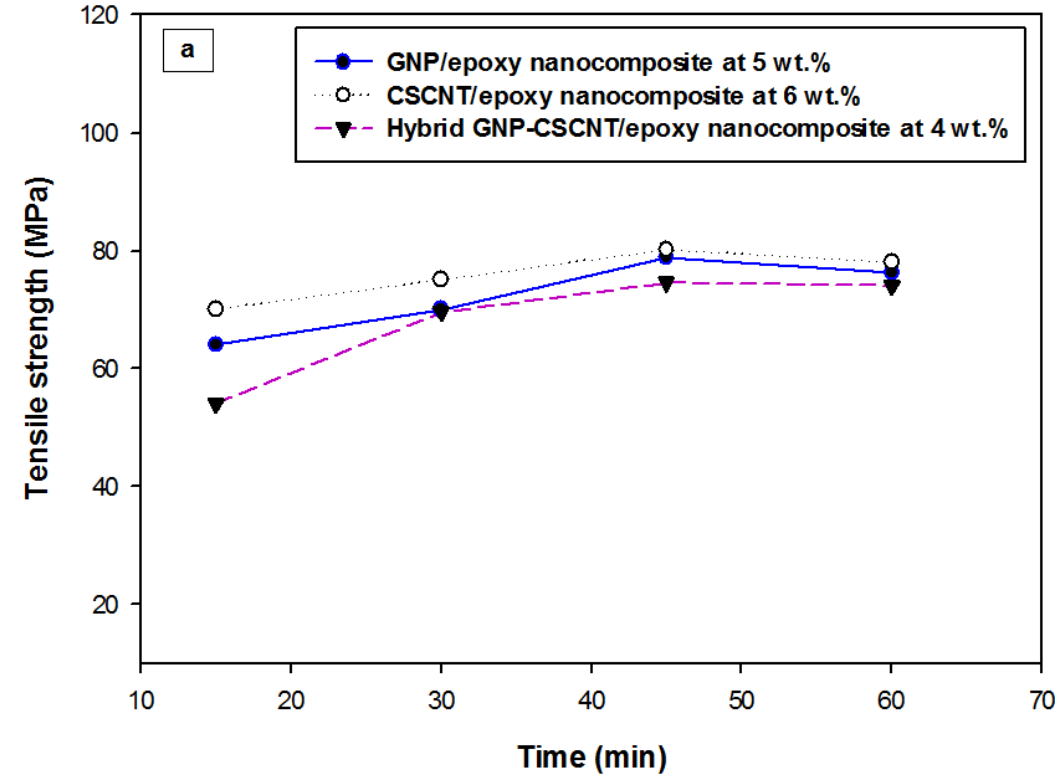

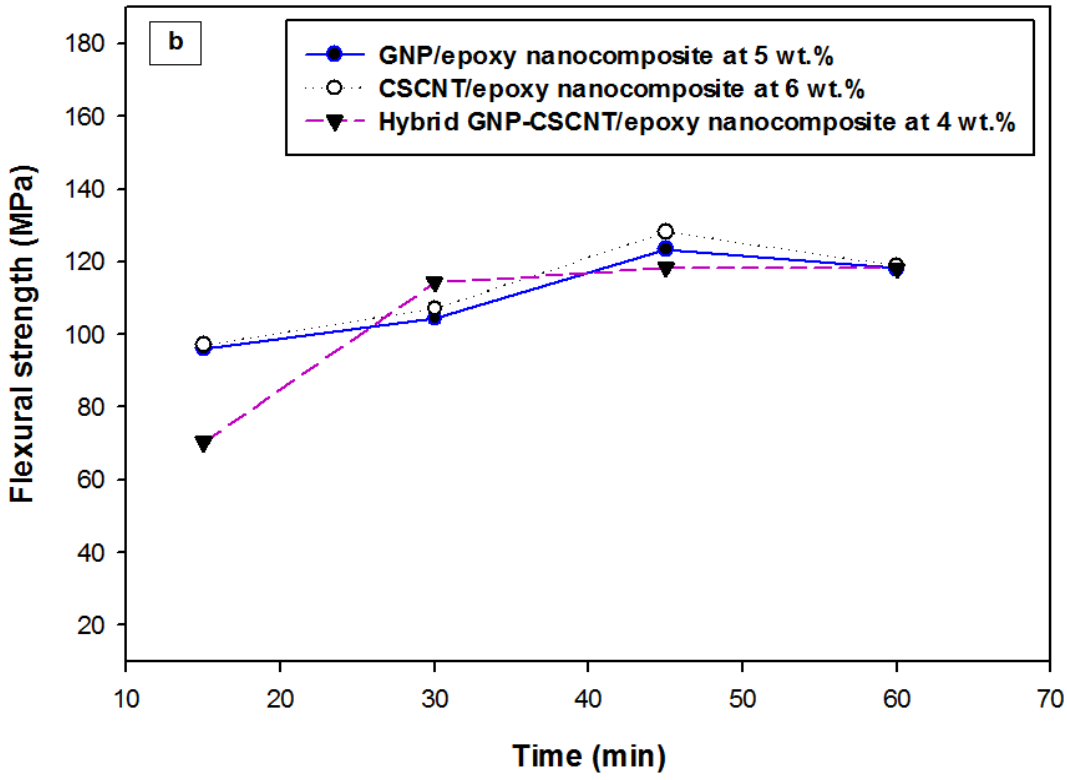

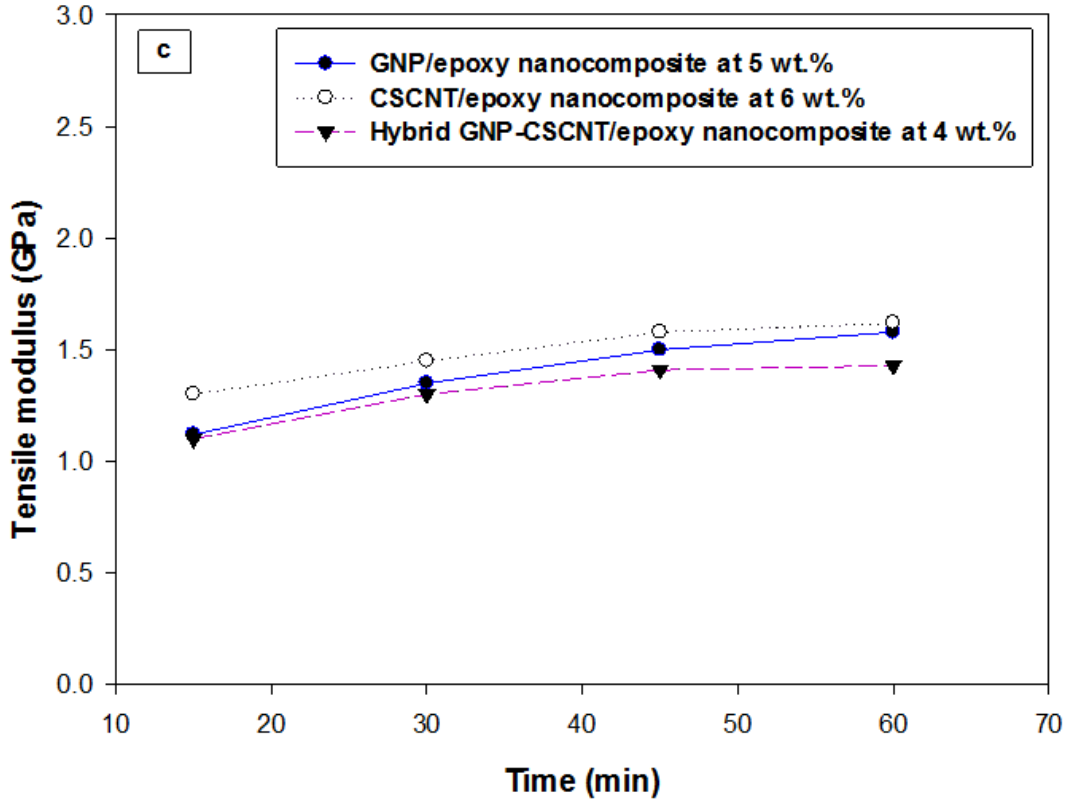

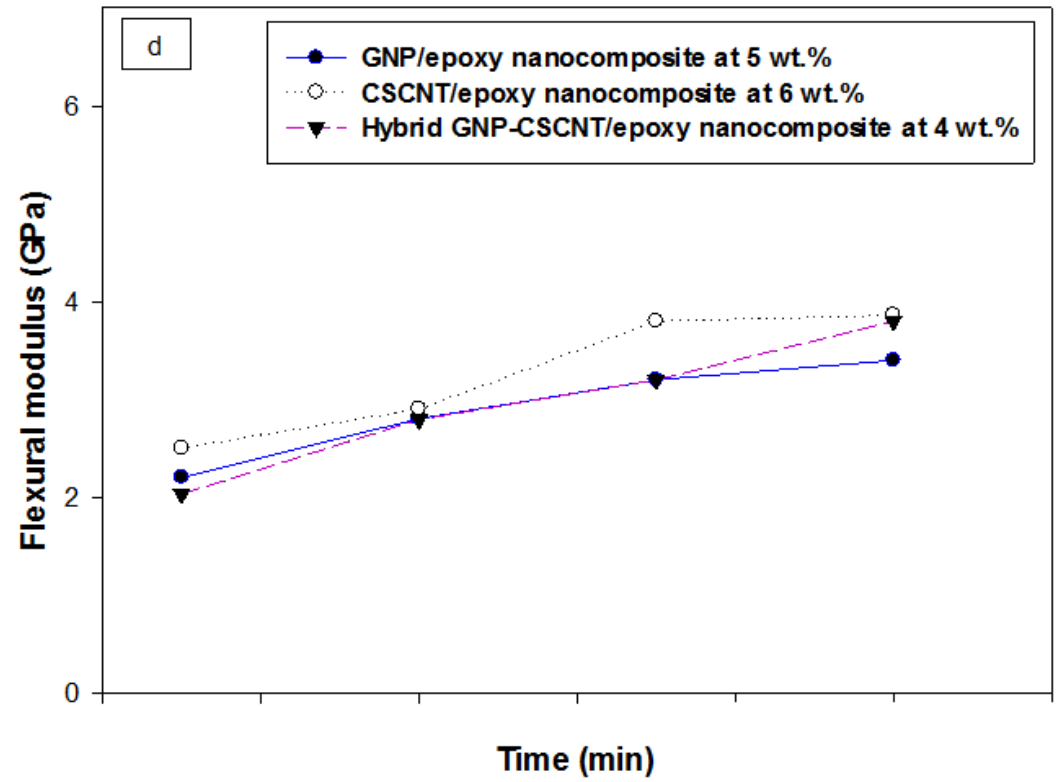

Figure 74 The influence of milling/mixing time on strength and modulus properties of the three NP at critical weight concentration; a) Tensile strength, b) Flexural strength, c) Tensile modulus, d) Flexural modulus.

Strength and modulus properties were affected significantly by the dispersion time of nanoparticles in the three NP by using the ball milling technique between the periods of 15 min to 60 min. The short period of dispersion was not sufficient to obtain a reasonable dispersion to improve the mechanical properties of the NP by using the ball milling technique particularly at 15 min. A massive of agglomeration of particles were seen in the micro-section areas of the NP, as shown in fractographic images (see Figures 75a and 75c).

After this short period, the strength properties showed a significant difference between 30 min and 60 min. The optimum period was at 45 min. After this period (60 min), the improvement in strength showed a somewhat low difference compared with the optimum period. This may be due to some damage occurring in the geometric structure and a reduction in size dimensions of the nanoparticles, particularly the length of the fibre nanotubes, as a result of increasing the period of milling and mixing time (see Figure 75b), besides the high shear and compressive forces generated in the closed container (Yokozeki et al., 2008; Konya et al., 2004). Additionally, the elastic modulus values showed a slight increase with the increasing time period, as shown in Figures 74c and 74d.

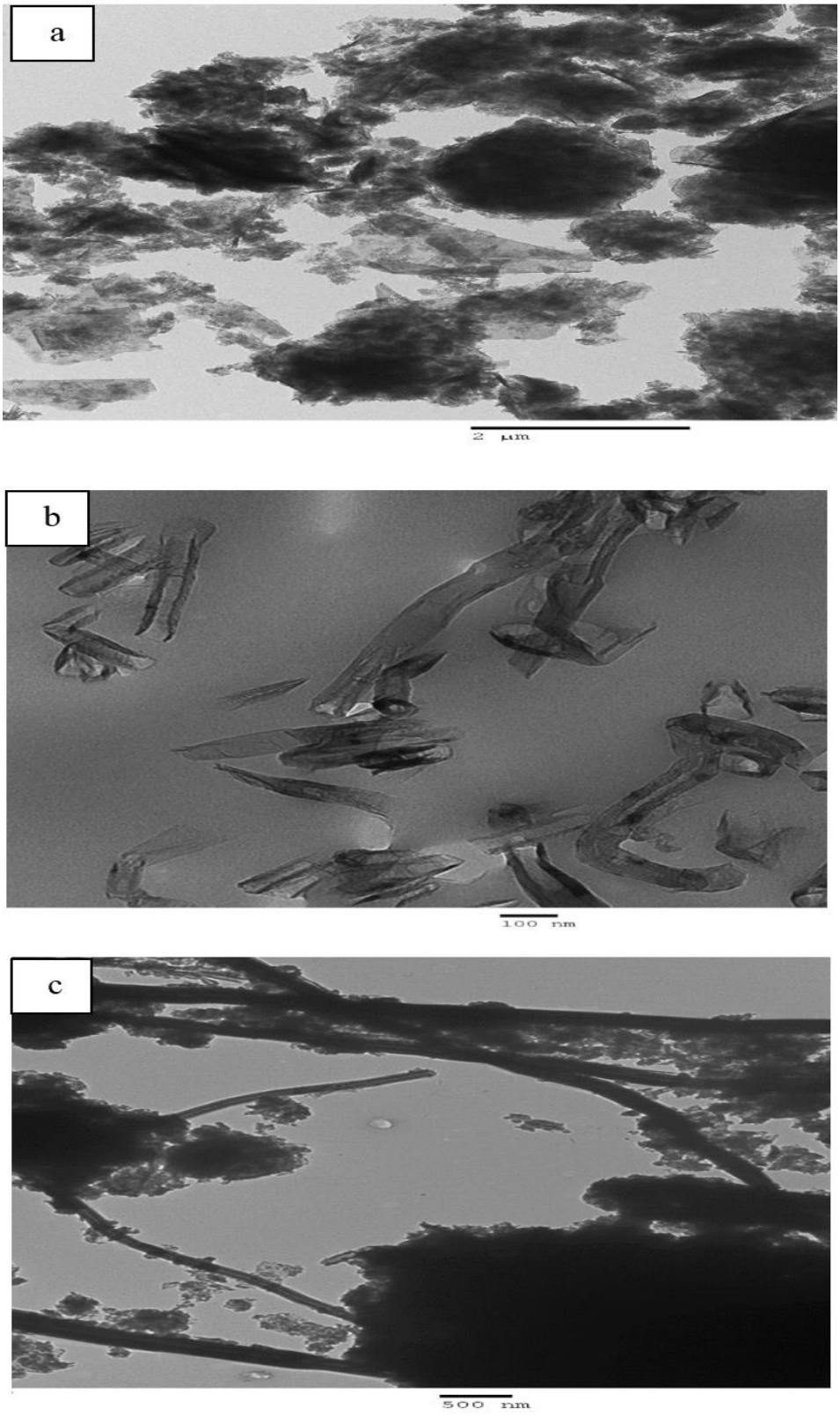

Figure 75 The TEM images show the poor dispersion and defect of the nanoparticles for each nanocomposite processed by the ball milling technique; a) GNP/epoxy nanocomposite, b) CSCNT/epoxy nanocomposite, c) Hybrid GNP-CSCNT/epoxy nanocomposite.

5.4 Assessment of mechanical properties of the NP

The evaluation of mechanical properties for the three NP processed by the sonication technique, ball milling technique and combined techniques based on the level of increase in the strength and modulus properties at critical weight concentration (see Tables 28 and 29).

Figure 76 shows the critical increase and the variation in strength and modulus properties of the three NP processed by three practical mechanical dispersion techniques. The variation of improvement in strength and elastic modulus of the three NP could be related to dispersion processes in each stage. Furthermore, using the ball milling technique contributed to increasing the mechanical properties of the NP. This improvement was relatively better than the sonication mixing results, particularly the values of elastic modules. The reason for this could be attributed to additional mechanical forces (i.e. shear and compressive forces) created in the ball milling container, which may promote the dispersion degree of the nanoparticles and the orientation in the matrix (Tang et al., 2013; Zao et al., 2010).

Furthermore, the increased level of these properties for the novel NP processed by using combined techniques was better than those prepared by the sonication and ball milling technique specially HNP. Thus, this practical method was valuable to disperse and exfoliate the nanofillers into the epoxy resin, particularly hybrid nanofillers. The reason for this high increase difference could also be related to the additional mechanical dispersion forces generated after the combination of ball milling and sonication mixing, shear, compressive and extension. These dispersion forces may primarily induce high exfoliation of nanoparticles in the matrix. Moreover, they improve the performance of NP via additional shear forces which may reduce the strains and residual stresses on the structure of the nanofillers (Moriche et al., 2015). Hence, this may significantly contribute the promotion of mechanical properties for the NP. Based on these facts, the combination of the sonication and ball milling technique is valuable in promoting the mechanical properties of NP.

Table 28 Level of increase in the strength of the three NP processed by sonication, ball milling and combined techniques at critical weight concentrations.

Sample	Dispersion processes											
	Sonication method				Ball milling method				Combined method			
	Tensile strength (MPa)	Incr. (%)	Flexural strength (MPa)	Incr. (%)	Tensile strength (MPa)	Incr. (%)	Flexural strength (MPa)	Incr. (%)	Tensile strength (MPa)	Incr. (%)	Flexural strength MPa	Incr. (%)
GNP/epoxy nanocomposites at 5 wt.%	77.10±2.30	+13.9	107.75±3.34	+6.4	78.9±0.49	+16.6	123.3±3.34	+21.8	79.38±1.84	+17.3	118.6±3.06	+17.2
CSCNT/epoxy nanocomposite at 6 wt.%	78.21±1.33	+15.6	130.10±1.90	+28.5	80.2±1.34	+18.5	128.2±0.85	+26.6	82.03±3.02	+21.3	130.7±4.49	+29.1
Hybrid GNP-CSCNT/epoxy nanocomposite at 4 wt.%	76.14±1.18	+12.5	123.00±1.27	+21.5	74.6±3.97	+10.2	118.3±1.38	+16.9	77.60±0.81	+14.7	141.5±6.87	+39.8

Table 29 Level of increase in stiffness of the three NP processed by sonication, ball milling and combined techniques at critical weight concentrations.

Sample	Dispersion processes											
	Sonication method				Ball milling method				Combined method			
	Tensile modulus GPa	Incr. (%)	Flexural modulus (GPa)	Incr. (%)	Tensile modulus (GPa)	Incr. (%)	Flexural modulus (GPa)	Incr. (%)	Tensile modulus (GPa)	Incr. (%)	Flexural modulus (GPa)	Incr. (%)
GNP/epoxy nanocomposites at 5 wt.%	1.48±0.03	+10.8	2.60±0.08	-7.1	1.50±0.06	+11.9	3.20±0.20	+14.3	1.56±0.04	+16.4	3.10±0.20	+10.7
CSCNT/epoxy nanocomposite at 6 wt.%	1.53±0.01	+14.2	3.50±0.11	+25.0	1.58±0.01	+17.9	3.80±0.14	+35.7	1.70±0.19	+26.8	3.70±0.29	+32.1
Hybrid GNP-CSCNT/epoxy nanocomposite at 4 wt.%	1.29±0.03	-3.7	3.15±0.03	+12.5	1.41±0.04	+5.2	3.20±0.10	+14.3	1.63±0.08	+21.6	4.50±0.17	+60.7

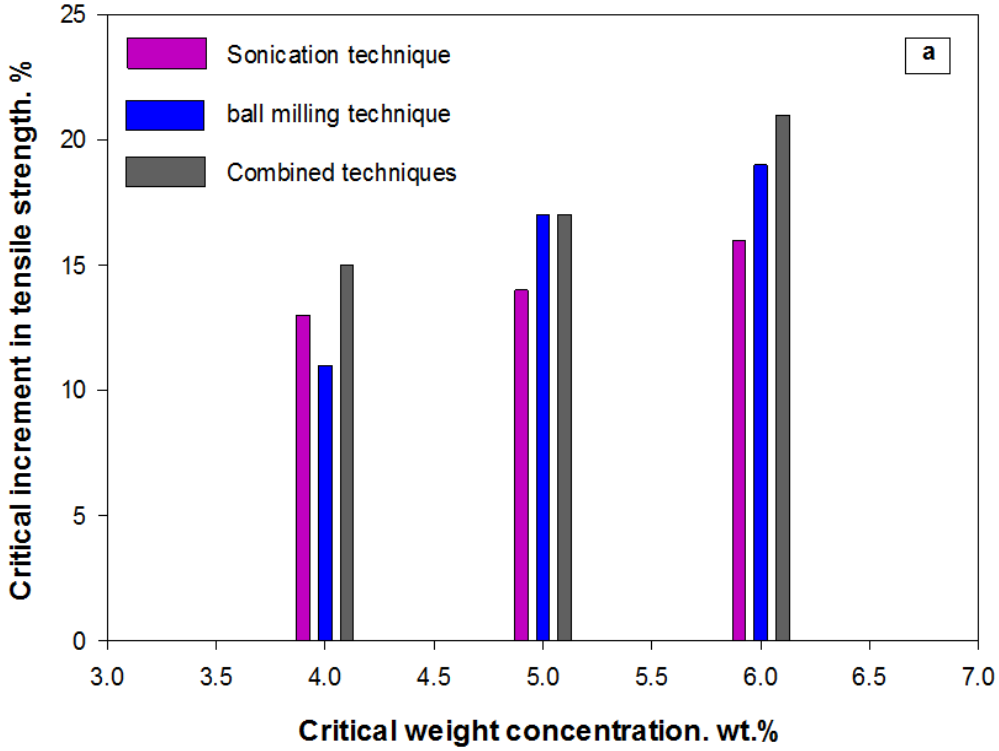
Sonication technique
ball milling technique
Combined techniques
a
Critical increment in tensile strength. %
Critical weight concentration. wt.%
0
5
10
15
20
25
3.0
3.5
4.0
4.5
5.0
5.5
6.0
6.5
7.0

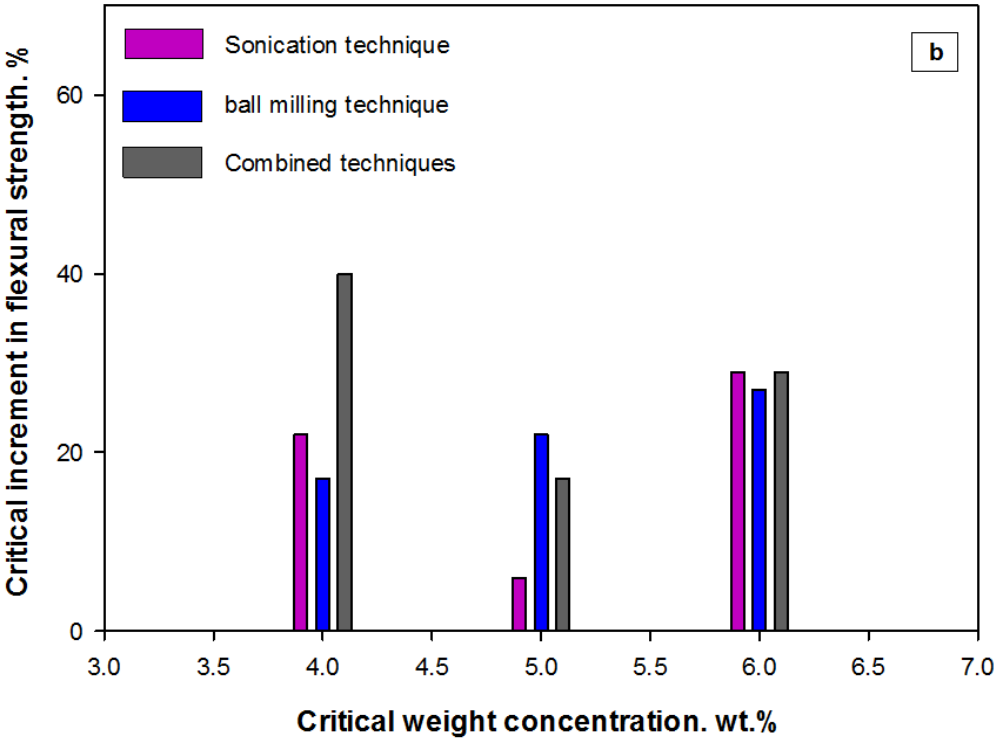
Sonication technique
ball milling technique
Combined techniques
b
Critical increment in flexural strength. %
Critical weight concentration. wt.%
0
20
40
60
3.0
3.5
4.0
4.5
5.0
5.5
6.0
6.5
7.0

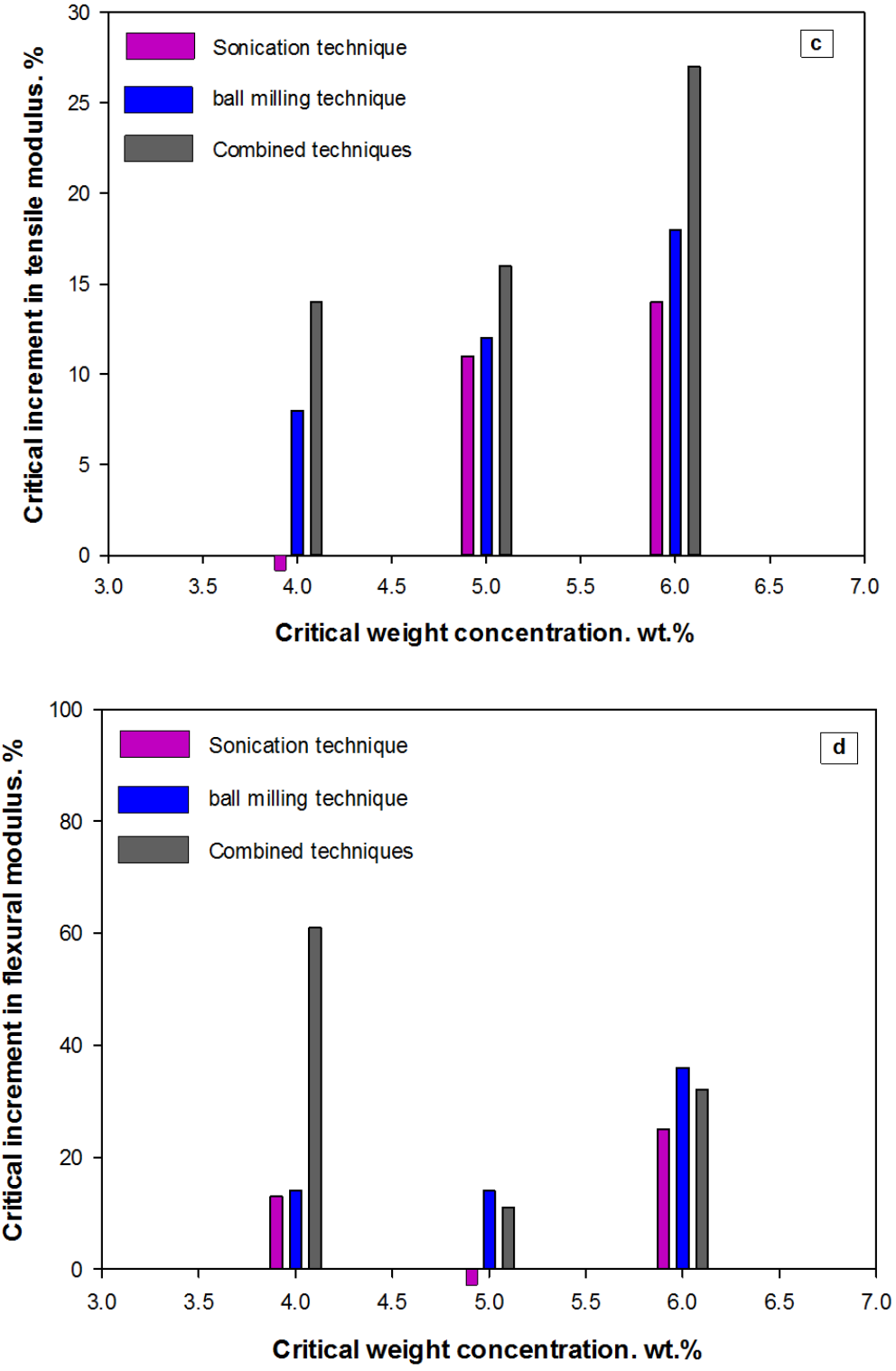

Figure 76 The increased levels of mechanical properties in the NP processed by three methods at critical weight concentration; 4wt.% of hybrid GNP-CSCNT, 5wt. % of GNP, 6wt.% of CSCNT a) Tensile strength, b) Flexural strength, c) Tensile modulus, d) Flexural modulus.

5.5 Fracture toughness properties of the NP processed by combined techniques

5.5.1 Fracture surface morphology

The surface morphologies of pure epoxy composite and three NP are presented in Figure 77. It can be seen that the surface morphology at the fracture area of the pure epoxy composite is smooth (see Figure 77a). This could be evidence of weak resistance to the crack extension. Conversely, rough surface was seen in the three NP (see Figures 77b, 77c and 77d). In addition, several other fracture mechanism techniques were seen on the fracture surface morphologies of the NP, such as tortuous, hackles, riverlines and ribbons. These fracture mechanism systems increase the energy dissipation in the nanocomposite which reflects the causes of the increase in fracture energy of the three NP (Tang et al., 2013). Furthermore, the pinning and pull-out of nanoparticles were seen in the fractured area of the nanocomposites which are considered the keys for energy absorption systems in nanocomposites (Chadrasekaran et al., 2014). In addition, the SEM images also show the bi-furcation mechanism of the crack when it encounters the carbon nanomaterials after the combination of graphene and fibre nanotubes. Moreover, the existence of such GNP that have large specific areas contributes to the deviation in the cracks in the nanocomposite. This may also improve the fracture energy in the nanocomposites.

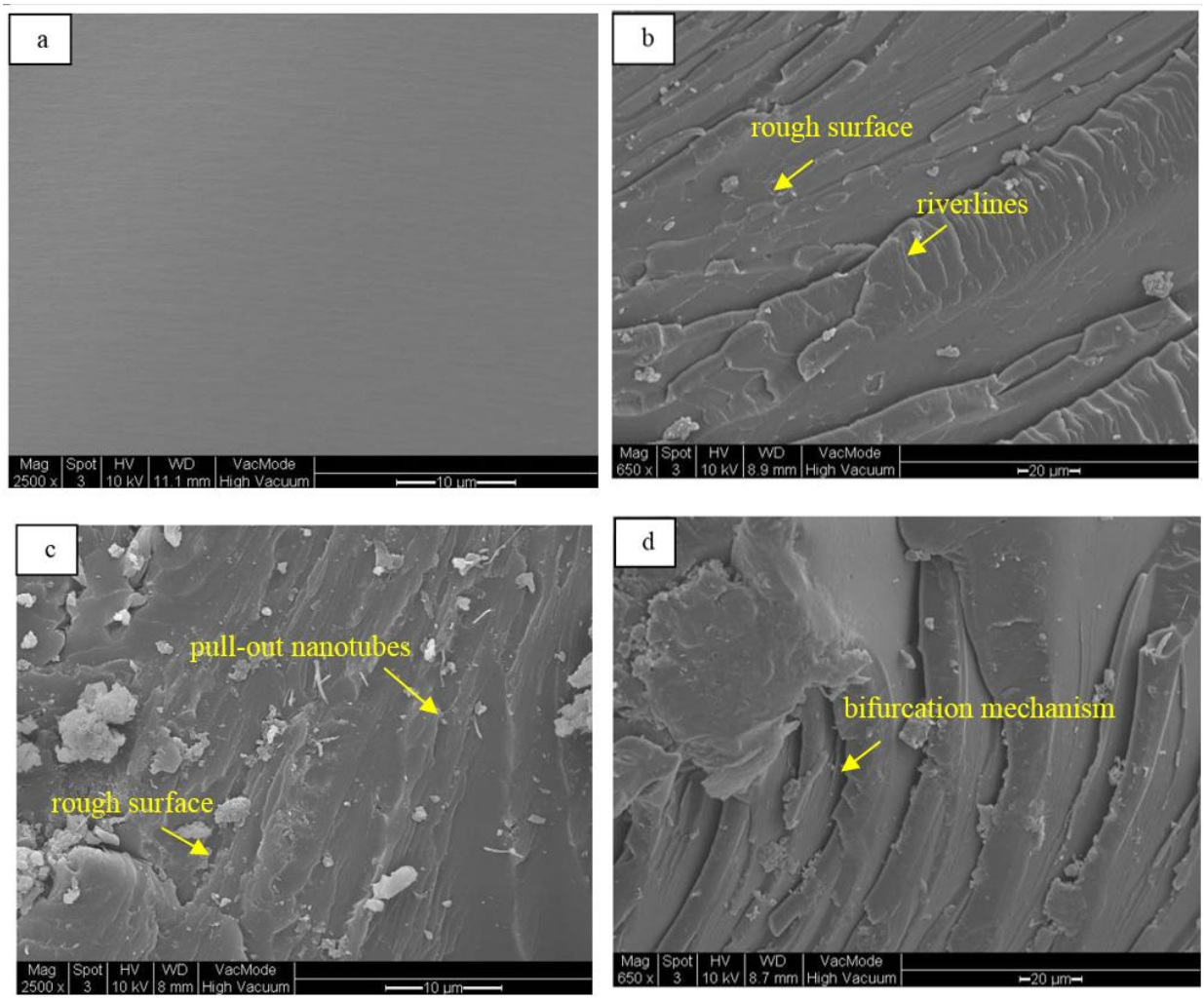

Figure 77 SEM images show the fracture surface morphology for each nanocomposites at critical weight concentration compared with pure epoxy composite; a) Pure epoxy, b) GNP/epoxy nanocomposite, c) CSCNT/epoxy nanocomposite, d) hybrid GNP-CSCNT/epoxy nanocomposite

5.5.2 Fracture strength properties

The purpose of this fracture toughness measurements is to check the fracture strength of the modified matrix in each nanocomposite processed by the combined techniques at optimum weight concentration.

The mechanical fracture toughness criterion for fractured material based on the work of Griffith and Irwin (Griffith, 1920; Irwin, 1964) is that the fracture mechanism occurs when there is sufficient work energy for the crack extension at the instant of loading. The stresses concentration criteria at the crack tip relevant to the subjected stress is determined by the critical stress intensity factor (K_{IC}) and is periodically called the fracture strength.

Figure 78 shows the typical force-deflection curves for SENB testing for each sample at optimum weight concentration. Table 30 shows the statement which is derived from these curves.

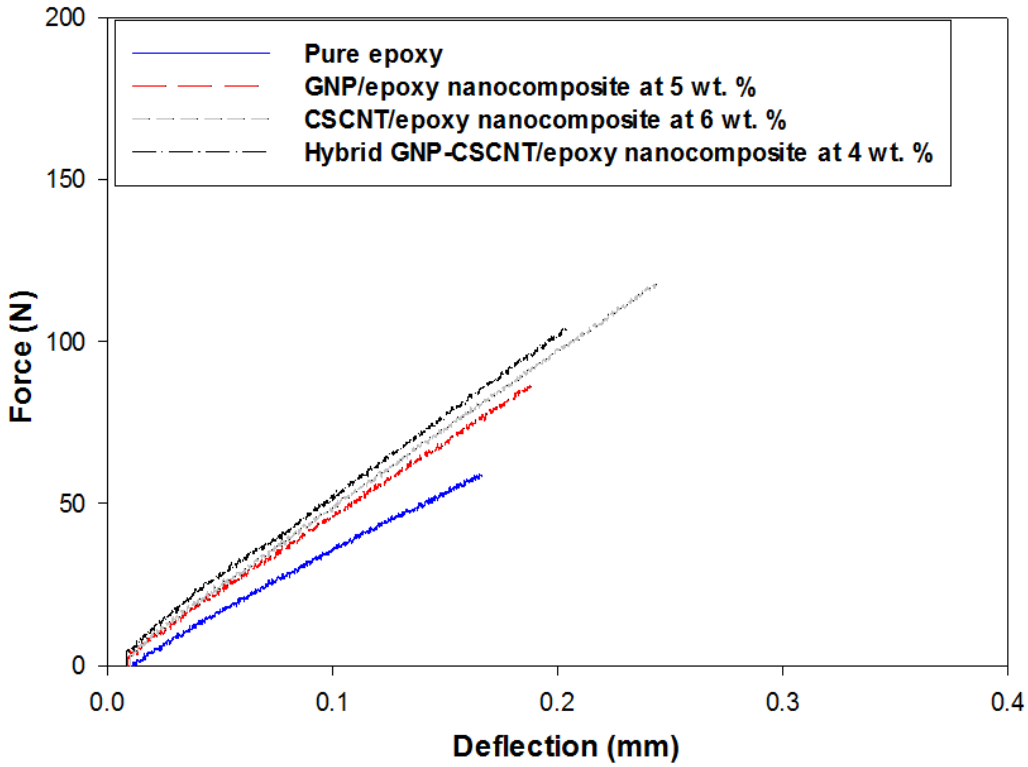

Figure 78 Typical force-deflection curves as a function of optimum nanofillers content.

Table 30 The fracture toughness (K_{IC}) as a function of optimum nanofiller content.

Sample	Number of samples	Optimum weight (wt.%)	Maximum force (N)	Critical stress intensity factor, K_{IC} (MPa.m$^{1/2}$)	Toughness improvement (%)
Pure epoxy	5	0	50.50±8.90	0.96±0.17	00.0
GNP/epoxy nanocomposite	5	5	77.65±6.52	1.46±0.12	+52.0
CSCNT/epoxy nanocomposite	5	6	110.60±5.70	2.08±0.12	+116.7
Hybrid GNP-CSCNT/epoxy nanocomposite	5	4	94.60±6.20	1.78±0.10	+85.4

The critical stress intensity factor K_{IC} was calculated by using the maximum force. The comparison of K_{IC} values among the three nanocomposites are plotted in Figure 79.

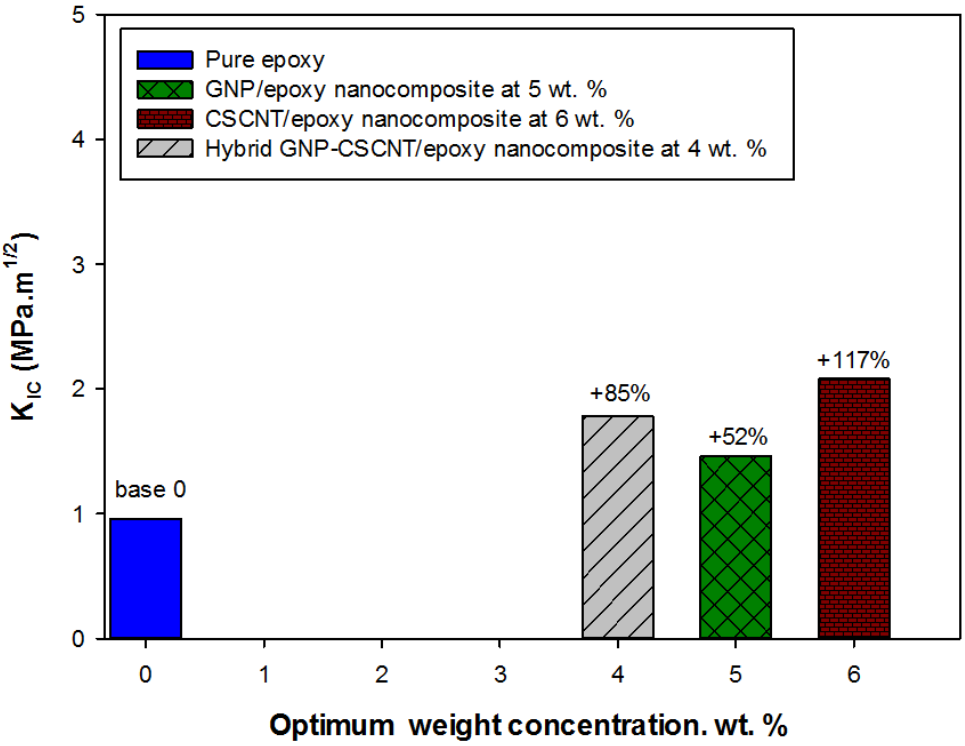

Figure 79 The fracture toughness of epoxy composite as a function of GNP, CSCNT and hybrid GNP-CSCNT content.

It illustrates that K_{IC}, is increasingly significant with the addition of GNP, CSCNT and hybrid GNP-CSCNT at critical weight concentration. These improvements were compatible with previous reported studies (Nam et al., 2017; Chadrasekaran et al., 2014; Zaman et al., 2011; Zhou et al., 2007; Moghadam and Taheri, 2014; Chatterjee et al., 2012). Due to the difference in nanoscale size for GNP and CSCNT, each one has a different aspect ratio. Hence, this property could affect the path of the crack head and amount of energy absorption in each nanocomposite. When extending, the crack encounters rigid nanosheets or nanotubes, particularly with optimum strengthened and toughened matrix. The larger crack propagation should tilt or deviate in larger angles in order to cross the nanosheets or nanotubes. In addition, crack deflection results in greater fracture surface regions than those generated by undeflected regions. The amount of released energy is a function of the fracture regions in the composite. Therefore, surface roughness is one of the characteristics which can be considered as an assessment of the plastic regions of the fractured areas in each nanocomposite. Therefore, the addition of nanoparticles to the polymer could increase the surface roughness, hence, this improves the weak zones in the composite (Moghadam and Taheri, 2014; Tang et al., 2013).

The SEM images of the fracture surface of the three NP nanocomposites reported previously at optimum weight concentration, within a cross-sectional area close to the crack head (see Figure 77). The fractographic analysis reveals evidence of several nanosheets and nanotubes that have been pulled-out of the side of the fractured area, proposing toughening and strengthening effects. Furthermore, the mechanical forces (i.e. pull-out forces) in the fibre nanotubes reinforced nanocomposite possibly have greater efficiency to resist the extension of the crack and absorb the fracture energy in the nanocomposites than that of the nanosheets. This is probably due to the characteristics of the geometric structure of fibre nanotubes compared with GNP which have a weak structure. Therefore, this analytical explanation may show one of the reasons that led to the high difference in the values of the fracture energy in fibre nanotubes reinforced epoxy nanocomposites in comparison with graphene reinforced nanocomposite.

Extra fracture mechanisms such as bi-furcation and pinning of the crack head in nanocomposites could be the other important reason for the improvement in the fracture strength in HNP. In addition, existence of graphene with fibre nanotubes together in the matrix contributes to increasing their contact areas in the HNP, interfacial friction energy and corrugation mechanism which may promote the fracture toughness property (Kostagiannakopoulou et al., 2017; Wang et al., 2015).

Moreover, the orientation of the nanofillers could be additional evidence which may have an effect on the level of the increase in the fracture energy of the NP (Menna et al., 2016). Furthermore, the different grades of graphene and fibre nanotubes in terms of morphological properties (i.e. nanoscale, geometric structure), mechanical properties (i.e. strength, stiffness) and their manufacturing processes could have an influence on the level of interfacial shear forces increase. Hence, this changes the amount of released energy and resistance in each nanocomposite (Ozkan et al., 2012; Zaman et al., 2011; Chatterjee et al., 2012).

Furthermore, the combination of graphene and fibre nanotubes could increase the pull-out forces resulting from synergetic influence between the nanosheets and nanotubes (Liu et al., 2017). This behaviour may demonstrate the reason for the optimal increase in fracture energy in HNP in comparison with NP (i.e. graphene reinforced nanocomposites).

Chapter 6. Evaluation of mechanical properties of HCFRP: Results and discussion

This chapter offers the experimental results with discussion of the characterisation methods on the HCFRP as described in chapter 4. The evaluation of mechanical properties characterised involve interlaminar shear strength, flexural strength and Mode I and Mode II interlaminar fracture toughness for the HCFRP at optimum weight concentrations. Analysed fractography details using optical microscopy and scanning electron microscopy SEM spotlighted notable surface fracture morphologies, which were utilised to translate the depicted mechanical interfacial behaviour and fracture mechanism systems for hybrid composites.

6.1 The constituent weight and volume fractions of HCFRP produced

As shown in Table 31, the fibre weight and matrix weight fractions of the HCFRP samples were calculated to be between 60-62% and 38-39% respectively, whilst the fibre volume and matrix volume fractions were estimated to be between 47 to 49% and 46 to 48% respectively. The possibility of inaccuracy is expected in these results because the actual density of the composite was not applied to determine the actual volume fractions of the samples in the present work (see section 4.2) besides the volume fraction of the voids in each sample has been neglected in accordance with ASTM D 3171. Therefore, the values of weight and volume fractions could be affected by these engineering issues and assumptions in each sample.

Table 31 Weight fraction and volume fraction for HCFRP.

Sample	Thickness of laminate (mm)	Weight fraction		Volume fraction	
		Fibre weight (%)	Matrix weight (%)	Fibre volume (%)	Matrix volume (%)
CF/epoxy composite unmodified at 0 wt.%	2.00±0.11	61.44±0.55	38.55±0.37	49.41±0.41	47.96±0.31
	3.98±0.14	61.74±0.70	38.25±0.41	49.53±0.46	46.48±0.44
GNP/CF/epoxy nanocomposite at 5 wt.%	1.97±0.13	61.47±0.37	38.41±0.44	49.57±0.30	46.44±0.62
	3.91±0.11	61.00±1.10	38.96±0.71	49.38±0.72	47.96±0.42
CSCNT/CF/epoxy nanocomposite at 6 wt. %	2.00±0.01	61.30±0.91	38.58±0.46	49.43±0.21	48.13±0.32
	4.00±0.09	61.00±1.32	38.98±0.82	47.39±0.57	48.58±0.74
Hybrid GNP-CSCNT/CF/epoxy nanocomposite at 4 wt. %	1.99±0.12	60.49±0.50	39.19±0.27	49.36±0.33	47.43±0.33
	3.98±0.12	62.00±0.93	37.96±0.83	49.41±0.67	46.21±0.41

6.2 Shear testing of short beam sample

6.2.1 Modes of failure

The modes of failure in hybrid composites were checked by an optical microscope, as shown in Figure 80. Several modes of failure were seen in the samples, such as single or multiple shear, which were considered as acceptable failure in accordance with standard measurements, whilst the samples that had shown mixed modes of failure, such as shear and tension or compressive bending failure were neglected from the test results (see Figure 80a1).

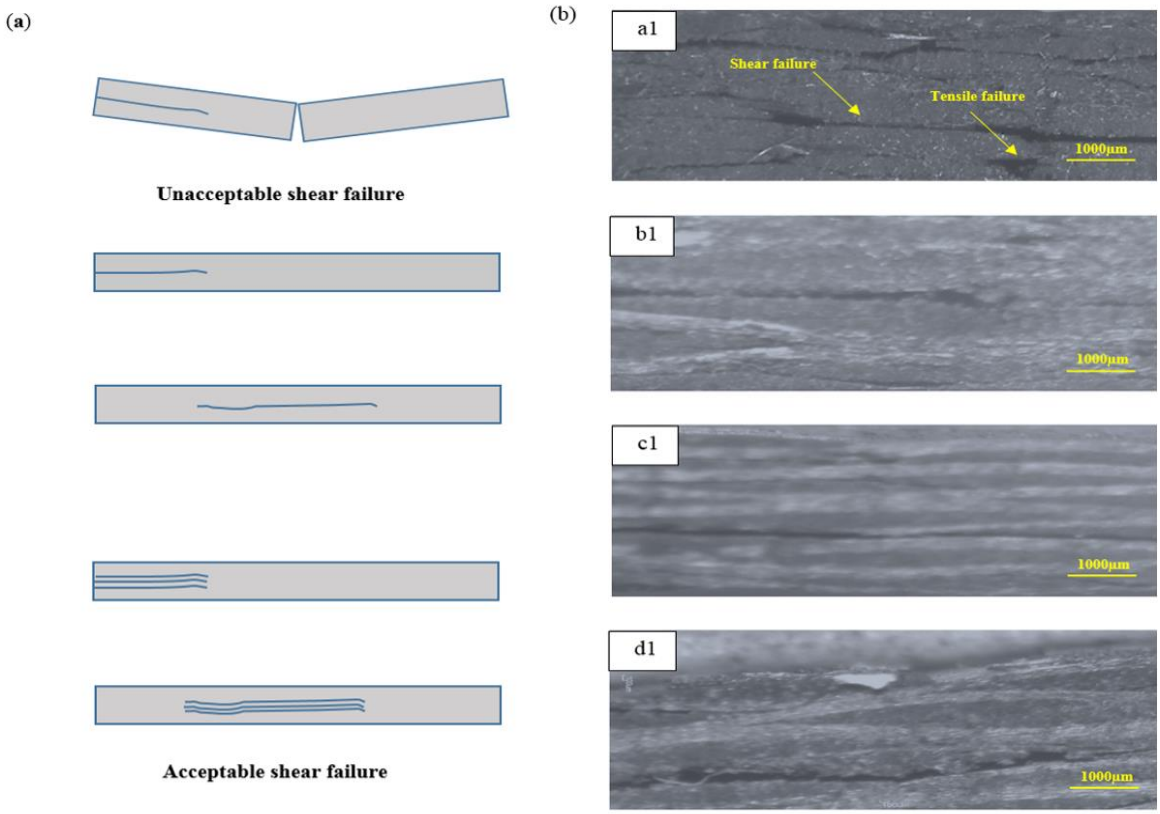

Figure 80 a) Schematic diagrams shows the acceptable and unacceptable shear failure in short beam testing samples; b) Optical micrograph showing cross-sectional shear failure in the samples (5x); a1) CF/epoxy composite unmodified , b1) GNP/CF/epoxy nanocomposite, c1) CSCNT/CF/epoxy nanocomposite, d1) Hybrid GNP-CSCNT/epoxy nanocomposite.

6.2.2 Microstructural details of shear failure

To explain the morphologies and bonding quality of the synthesised hybrid laminated composites (i.e. HCFRP), particularly the interfacial bonding and fracture mechanism systems, a cross-section of the fractured area views was assessed using SEM, as shown in Figure 81. The images reveal that massive cracks were evident in the matrix film at the regions of failure after applying the bending load on the specimens of CF/epoxy composite unmodified.

The reason for these microstructural cracks is the low resistance of the CF/epoxy composite unmodified, smooth surface and the weak adhesion between the carbon fibre filaments and the epoxy matrix. Conversely, the lack of these cracks in the modified matrix of hybrid composites indicates the high strength and toughness of the modified matrix and surface roughness of the nanofilled matrix, which reinforces the adhesion between the nanofilled matrix and carbon fibre network (Zhang et al., 2009; Yokozeki et al., 2007; Li et al., 2014).

The optimum extent of dispersion of nanomaterials improves the adhesion between the matrix and fibre networks. Furthermore, the improvement in mechanical interfacial properties is probably attributed to the high interlocking of fillers, enhancing the loads transfer between the fibre and matrix (Zhang et al., 2009).

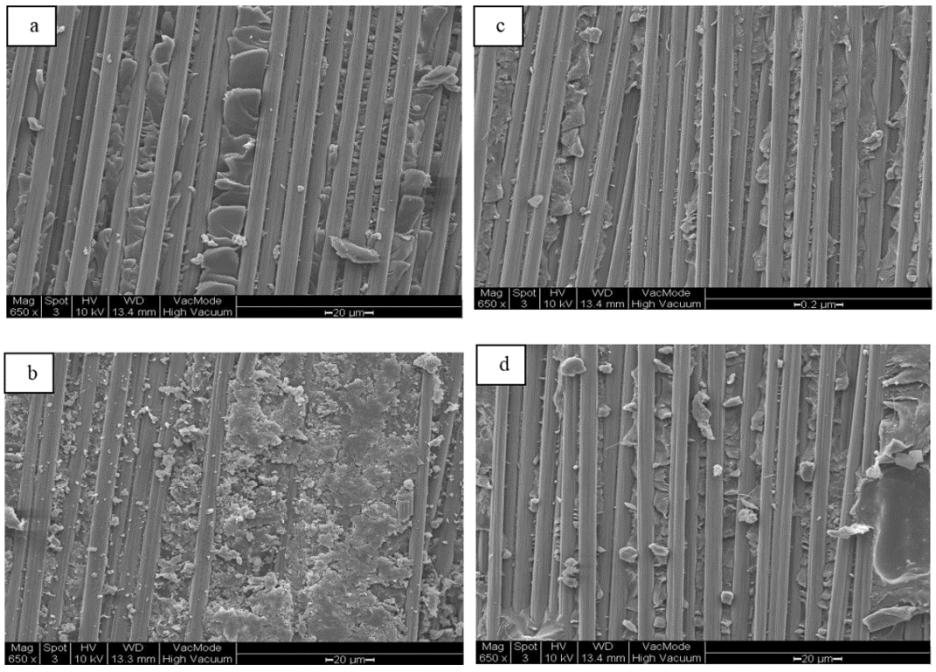

Figure 81 The SEM images show the fracture surface morphology of composites at the failure regions for shear beam samples: (a) CF/epoxy composite unmodified (b) GNP/CF/epoxy nanocomposite, (c) CSCNT/CF/epoxy nanocomposite, (d) Hybrid GNP-CSCNT/CF/epoxy nanocomposite.

6.2.3 Interlaminar shear strength properties

The influence of the addition of GNP, CSCNT and the combination of them on the interlaminar shear force of the carbon fibre reinforced epoxy composites is shown in Figure 82. Table 32 shows the summary of the SBS test results.

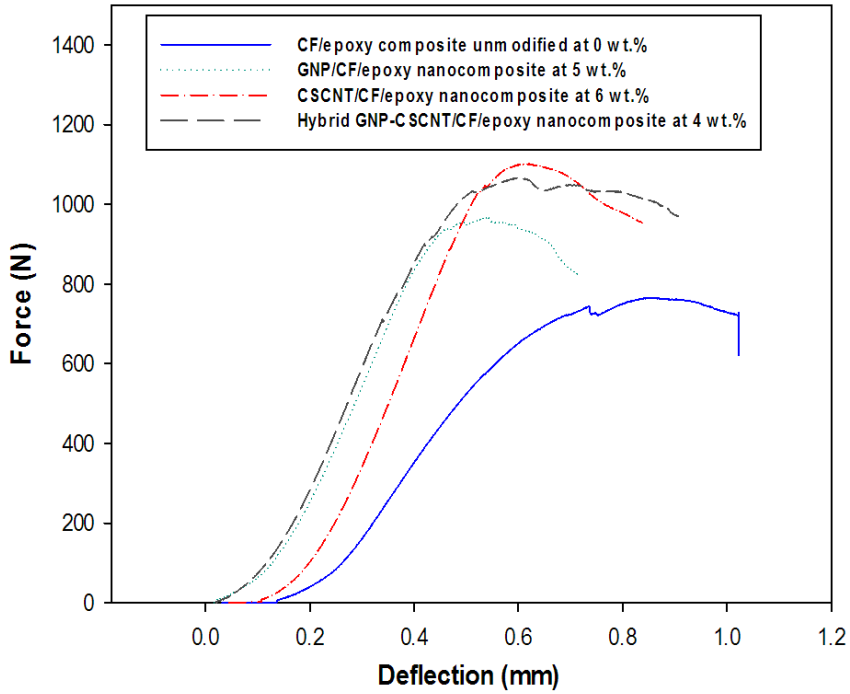

Figure 82 Typical force-deflection curves for short beam samples of the HCFRP at optimum weight concentration.

Table 32 The interlaminar shear strength (ILSS) of HCFRP measured by short beam shear (SBS).

Sample	Number of samples	Weight content (wt.%)	ILSS (MPa)	Incr. (%)
CF/epoxy composite unmodified	8	0	28.50±2.31	00.0
GNP/CF/epoxy nanocomposite	6	5	37.45±0.88	+31.4
CSCNT/CF/epoxy nanocomposite	6	6	39.24±0.64	+37.7
Hybrid GNP-CSCNT/CF/epoxy nanocomposite	6	4	39.04±1.72	+36.9

A comparison of the interlaminar shear strength (ILSS) of three types of HCFRP is revealed in Figure 83.

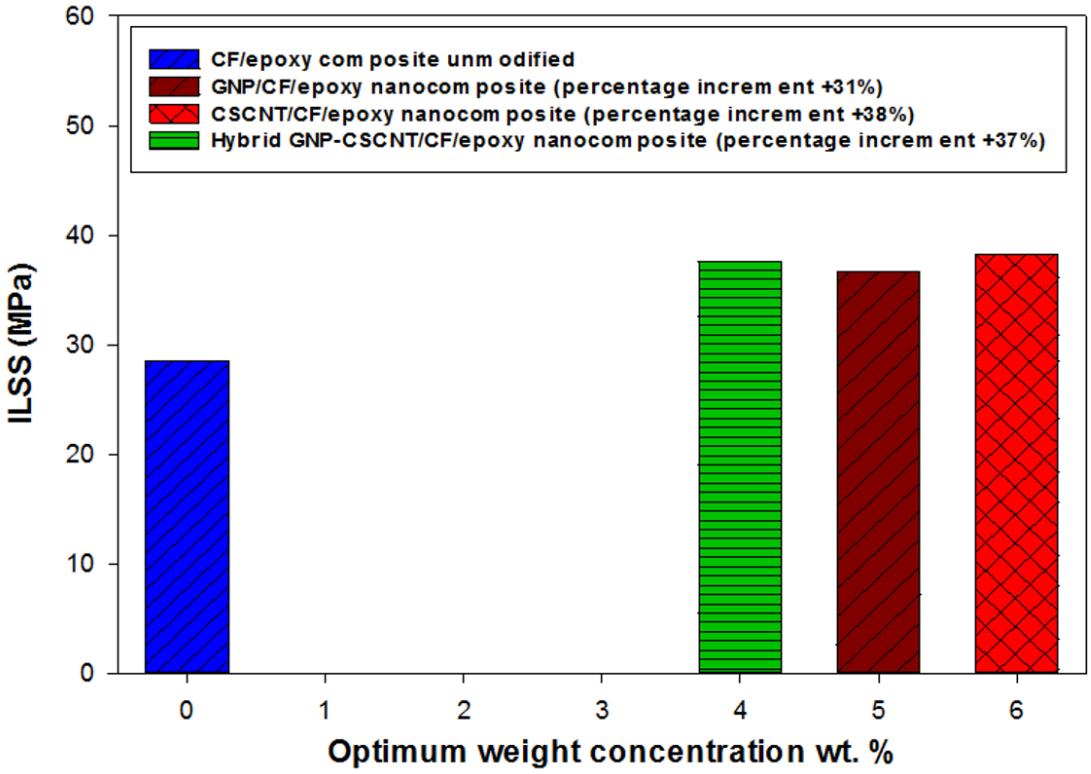

Figure 83 Comparison among three types of HCFRP at optimum weight concentrations.

The experimental results demonstrate that there is an optimum weight content resulting in a maximum increase in shear strength of approximately 31% in GNP/CF/epoxy nanocomposite, 38% in CSCNT/CF/epoxy nanocomposite and 37% after impregnation of the hybrid nanofillers (GNP and CSCNT) onto the surface of the carbon fibre network. Therefore, the addition of such nanofillers had improved the mechanical interfacial properties between the fibre network and the matrix. These enhancements agree with previously reported experimental studies that the addition of carbon nanomaterials could significantly increase the interlaminar shear strength properties of the fibre composites (Jia et al., 2015; Khan and Kim, 2012; Qin et al., 2015; Green et al., 2009; Li et al., 2014).

The reasons for the increase in the interlaminar shear strength are probably due to the good strength and toughness properties of the modified matrix, which induce the adhesion between the fibre networks and the nanophase matrix. In addition, the hybridisation of GNP and CSCNT enhances their synergy in the epoxy matrix which may increase the strength properties and toughness of the interface areas surrounding the fibre networks, (Nam et al., 2017; Liu et al., 2017; Kandare et al., 2015; Li et al., 2014; Zhang 2012). Furthermore, the SEM image in Figure 84 reveals the fracture mechanism of the carbon fibre modified with combined nanofillers such as

pull-out, pinning/bi-furcation and fracture nanofillers at interlaminar regions, which reflect the percentage of increase in the shear strength property (Chandrasekaran et al., 2014; Kostagiannakopoulou et al., 2017; Fenner and Daniel, 2014).

Figure 84 SEM image shows the fracture mechanisms systems into the hybrid GNP-CSCNT nanofilled matrix.

Furthermore, the hybrid nanofillers exhibit a significant increase in shear strength properties of carbon fibre composite at the lowest load level content (i.e. 4wt. %) compared with GNP/CF/epoxy nanocomposite at 5wt.% and CSCNT/CF/epoxy nanocomposite at 6wt.%. This indicates that the hybrid nanofillers have a positive effect on the mechanical properties of the carbon fibre composites.

6.3 Flexural properties of HCFRP

6.3.1 Fractography analysis

In general, several types of fracture mechanism systems, such as debonding mechanism of filler, bi-furcation mechanisms, bridging the micro-crack and pull-out fillers as well as deformation matrix were suggested to dissipate the stress and strain energy in the composites modified with nanofiller and unmodified, as shown in Figure 85.

The sample of CF/epoxy composite illustrates weak bonding between the unmodified matrix and the fillers, deboning failure was seen in the fracture surface of the sample as shown in Figure 85a. The sample of GNP/CF/epoxy nanocomposite demonstrates good bonding between the fibre and the modified matrix. Moreover, deformation matrix, bi-furcation mechanisms, pull-out nanosheets toughening mechanisms were seen in the nanofilled matrix at the fracture surface morphology of the sample, as revealed in the SEM image (Figure 85b). The sample of CSCNT/epoxy nanocomposites illustrates strong adhesion between the fillers and the modified matrix, plus pull-out nanotubes, bridging crack fracture toughening and strengthening mechanisms were observed on the fracture area of the sample, as shown in Figure 85c.

The sample of hybrid GNP-CSCNT/epoxy nanocomposite shows great bonding between the fibre network and the hybrid matrix. Moreover, pull-out nanotubes, bi-furcation mechanisms were seen into the hybrid nanofilled matrix at the fracture area of the sample, as shown in Figure 85d. Furthermore, the hybrid nanofillers can also generate an anchoring influence against cracking in the matrix structure. This behaviour may improve the strength and stiffness properties around the fibre networks of hybrid composites (Li et al., 2014).

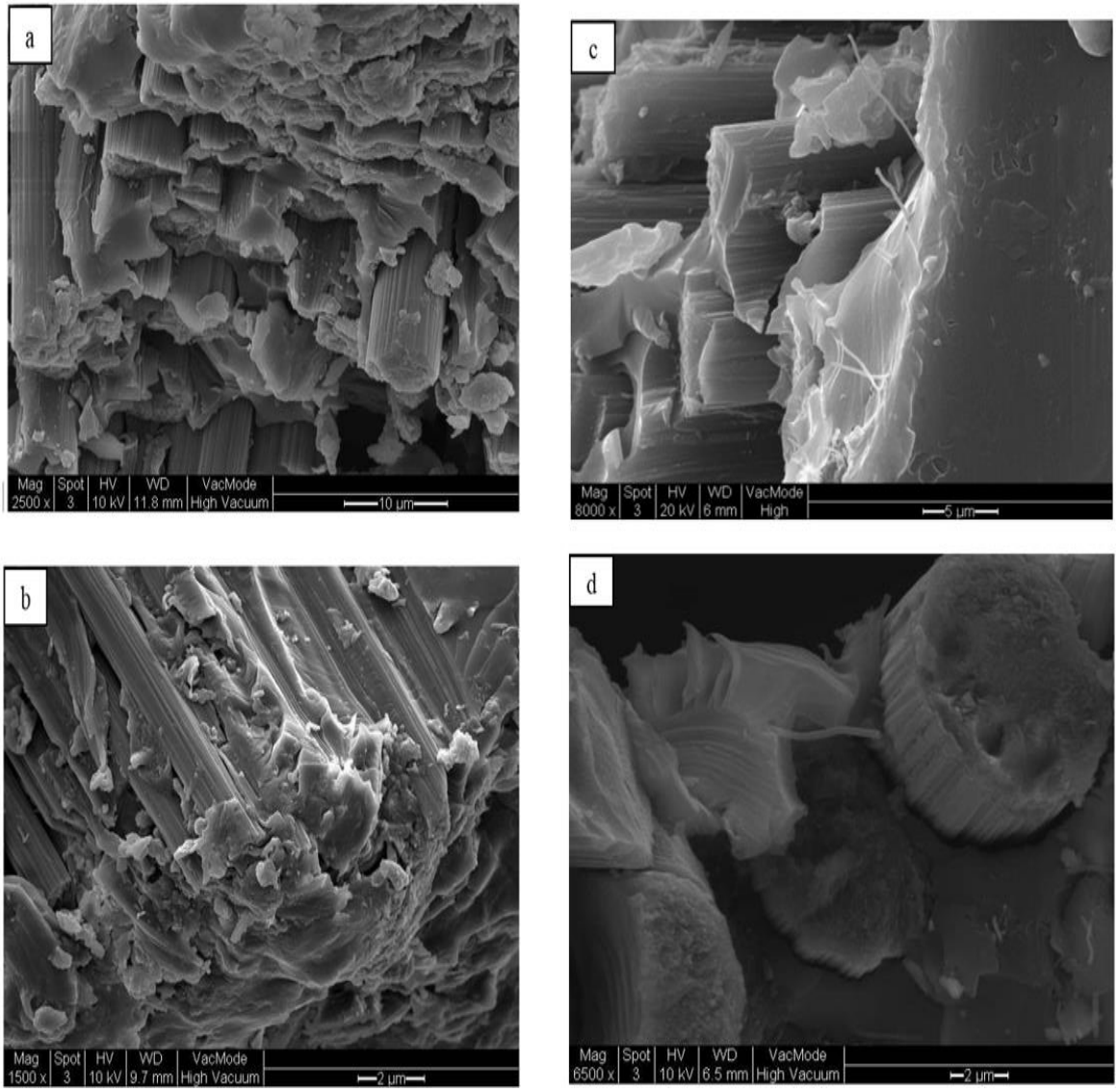

Figure 85 The SEM images show the fracture behaviour of carbon fibre composites. a) CF/epoxy composite unmodified, b) GNP/CF/epoxy nanocomposite, c) CSCNT/CF/epoxy nanocomposite, d) Hybrid GNP-CSCNT/CF/epoxy nanocomposite.

6.3.2 Flexural strength and stiffness properties

The flexural properties of the HCFRP provide clarification and concepts regarding that force energy applied, in order to rupture the sample. However, the effect of the impregnation of the optimum modified matrix into the carbon fibre network on the flexural stress-strain curves for three types of hybrid fibre composites; GNP/CF/epoxy nanocomposite, CSCNT/CF/epoxy nanocomposite and hybrid GNP-CSCNT/CF/epoxy nanocomposite in addition to CF/epoxy composite unmodified is shown in Figure 86. Table 33 shows the summary of the flexural properties results. The results have been estimated from these flexural stress-strain curves for each sample. The stress-strain curves for some samples relating to modified and unmodified with nanofiller explain the linear deformation and the regularities in the curves were attributed to uniform filament breakage during the period of loading. These samples failed rapidly after reaching the peak load, while the curves of the other samples detect nonlinear deformation before the failure of the samples. This behaviour may refer to random filament breakage during interval loading and some defects (i.e. voids), (Zhou et al., 2006). In addition, some noise was observed when the single filament failed or the inter-ply delaminated.

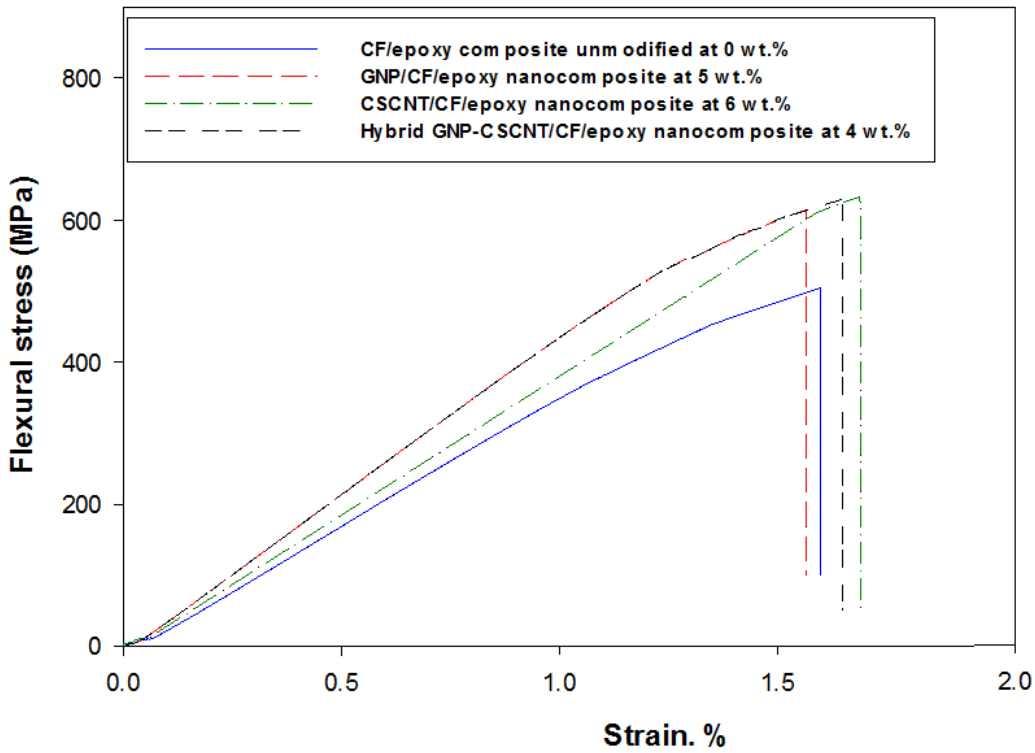

Figure 86 Typical stress-strain curves of three types of HCFRP and CF/epoxy composite unmodified.

Table 33 The maximum flexural strength and flexural modulus as a function of optimum weight content.

Sample	Number of samples	Weight content (wt. %)	Flexural strength (MPa)	Improvement in flexural strength (%)	Flexural modulus (GPa)	Improvement in flexural modulus (%)	Elongation at failure (%)	Improvements in elongation (%)
CF/epoxy composite	5	0	508.30±49.30	00.0	33.50±0.80	00.0	1.51±0.14	0.00
GNP/CF/epoxy nanocomposite	5	5	612.00±15.12	+20.4	42.50±1. 58	+26.8	1.51±0.12	0.00
CSCNT/CF/epoxy nanocomposite	5	6	635.50±20.49	+25.0	41.30±1.19	+23.3	1.62±0.10	+7.3
Hybrid GNP-CSCNT/CF/epoxy nanocomposite	4	4	597.90±53.28	+17.6	42.90±0.84	+28.1	1.54±0.14	+1.9

However, the evaluation of flexural properties for the three types of hybrid fibre composites are presented in Figure 87. The figure shows significant improvements in flexural strength and flexural modulus after impregnation of the optimum modified matrix into the carbon fibre composite. Generally, the homogeneity of the composites, orientation of the reinforcements and the excellent adhesion between the ply and matrix should have a clear effect on the flexural properties of the HCFRP.

The improvements concluded in three HCFRP indicate that the optimum strengthened and toughened matrix induces the adhesion between the fibre network and the matrix. Hence, it increases the strength and stiffness properties of the fibre composite. Interestingly, the combination of multifunctional carbon nanomaterials; graphene and novel fibre nanotube in the matrix improves the strength and toughness of the interfacial areas surrounding the fibre network, moreover, it creates an anchoring effect against the extension of cracks into the matrix (Li et al., 2014). This behaviour may justify the reason for significant improvements in the strength and stiffness properties of the hybrid fibre composites modified with combined nanomaterials (Wang et al., 2015).

However, the present improvements for the three types of hybrid composites were compatible to previous reported experimental studies (Wang et al., 2015; Zhuo et al., 2008; Iwahori et al., 2005; Qin et al., 2015; Wang et al., 2016; Li et al., 2014). The relatively small difference in the value of the increase for each type of the HCFRP could be attributed to the type of nanomaterial used in the matrix (Rodriguez-Gonzalez et al., 2017) and their manufacturing processes (Wang et al., 2016; Jia et al., 2016; Feng et al., 2014).

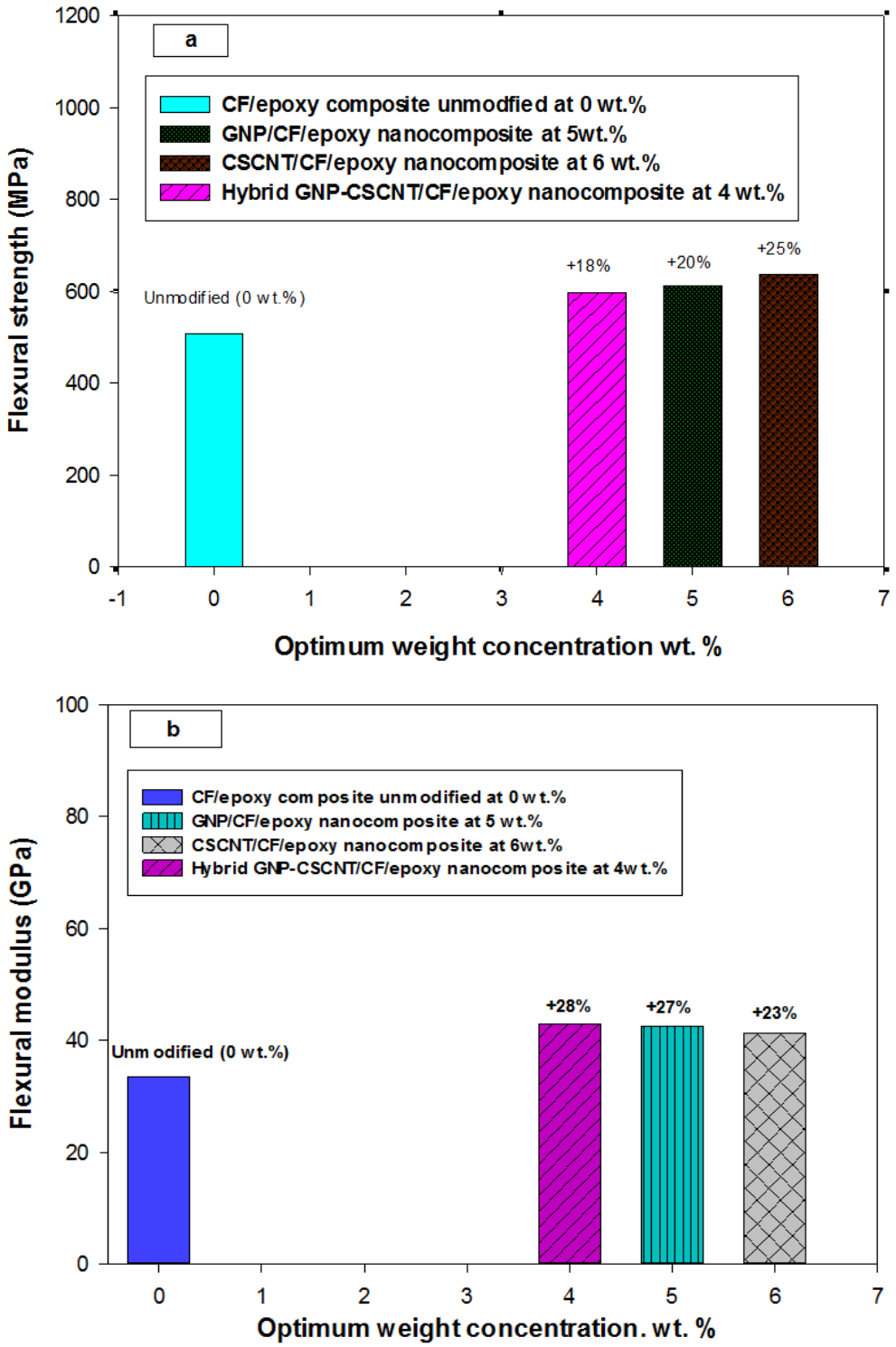

Figure 87 Comparison and evaluation of flexural properties among three productions of HCFRP: a) Flexural strength, b) Flexural modulus.

6.4 Fracture toughness tests results

6.4.1 Micrographs of DCB and ENF samples

To check the interface regions, defects (i.e. voids) and ply waviness of the tested samples, an optical microscope was used for this purpose. Photographic image analysis of the polished DCB

samples in Figure 88 and ENF samples in Figure 89 illustrates the distribution of the resin in each type of HCFRP besides the reference (CF/epoxy composite unmodified). As seen from the fractographic view there was inhomogeneous distribution of the resin for some samples (i.e. rich and poor regions with nanofilled matrix at the mid plane).

The adjacent fibre layers for DCB samples and 3ENF samples were noted to have nested with each other, with an average lay-up of [+2º,-2º] and [+3º,-3º] respectively at the mid-plane of the samples. The micrograph of the samples demonstrated clear voids away from the critical mid-plane interface regions except for a few samples that showed some voids that were relatively close to the mid plane region, which may affect the performance of the fibre composites.

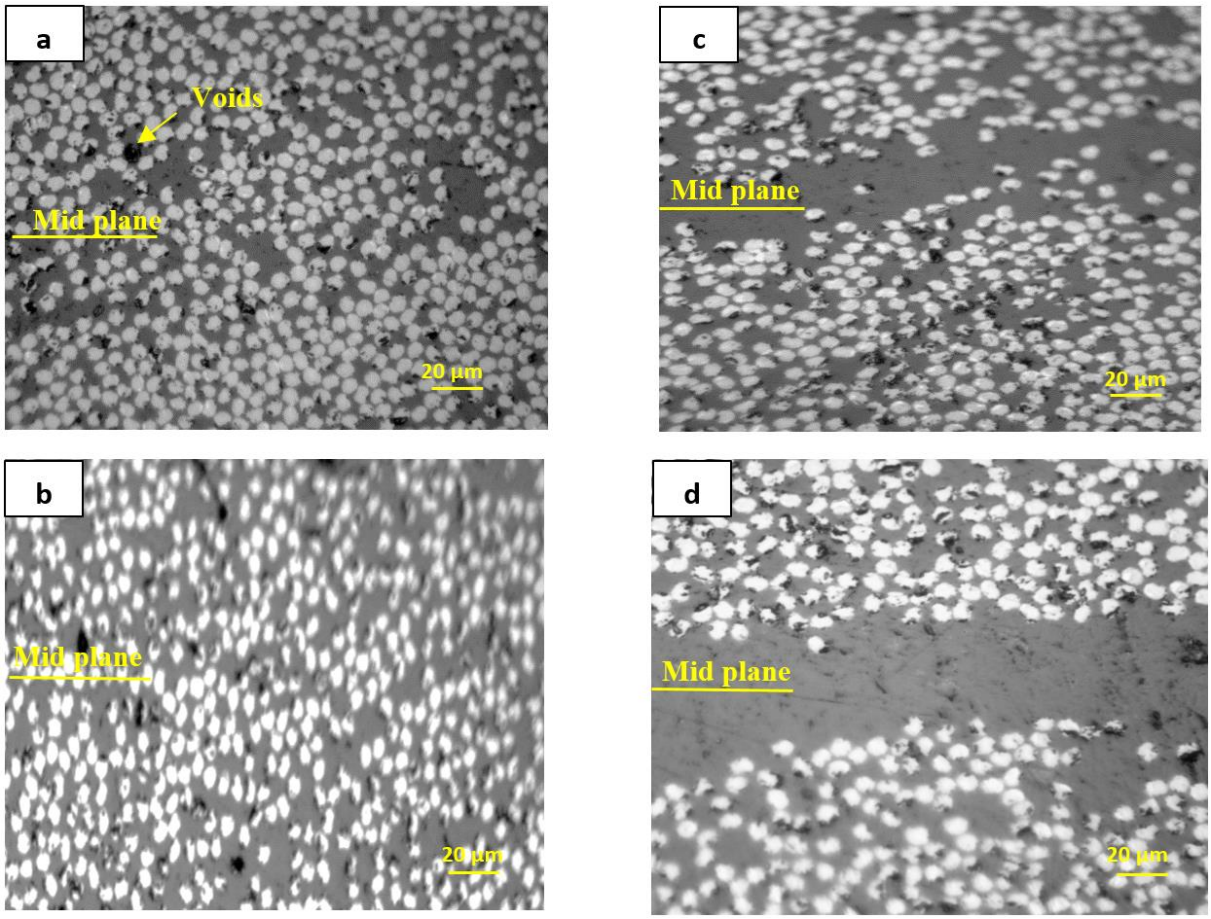

Figure 88 The micrograph images illustrate the distribution of the matrix into the polymer composites: a) CF/epoxy composite unmodified, b) GNP/CF/epoxy nanocomposite, c) CSCNT/CF/epoxy nanocomposite, d) Hybrid GNP-CSCNT/CF/epoxy nanocomposite [20x].

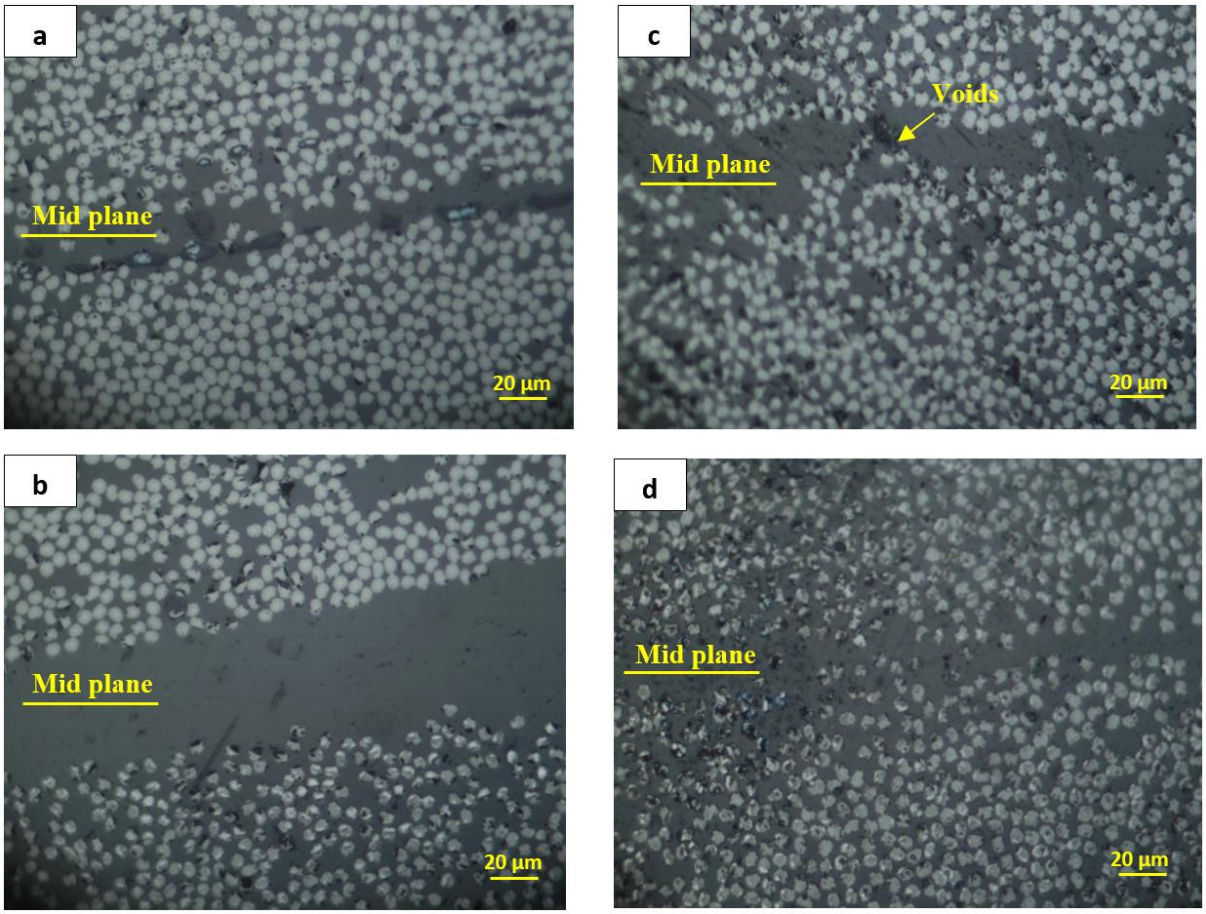

Figure 89 The micrograph images show the distribution of the matrix into the polymer composites: a) CF/epoxy composite unmodified, b) GNP/CF/epoxy nanocomposite, c) CSCNT/CF/epoxy nanocomposite, d) Hybrid GNP-CSCNT/CF/epoxy nanocomposite [20x].

6.4.2 Micrograph of optimal nanofilled matrix in DCB samples

Scanning electron microscope was used to examine the fracture surface morphology of optimum nanofilled matrix in the fibre surface of the hybrid composites. It also shows the distribution of carbon nanomaterials in the matrix and the types of fracture mechanisms (see Figure 90). The fractographic analysis showed that the cracks clearly penetrated and extended into the nanofilled matrix. This confirms that the nanofillers absorbed an amount of fracture energy before reaching the pristine fibres network (see Figure 90c).

However, several of the dissipation energy systems were seen in the fracture area of nanofilled matrix for each type of HCFRP, such as pinning and pull-out of nanofillers, bi-furcation mechanisms and pinning of cracks, debonding fillers, in addition to shear failure of the nanofilled matrix, suggesting toughening mechanisms.

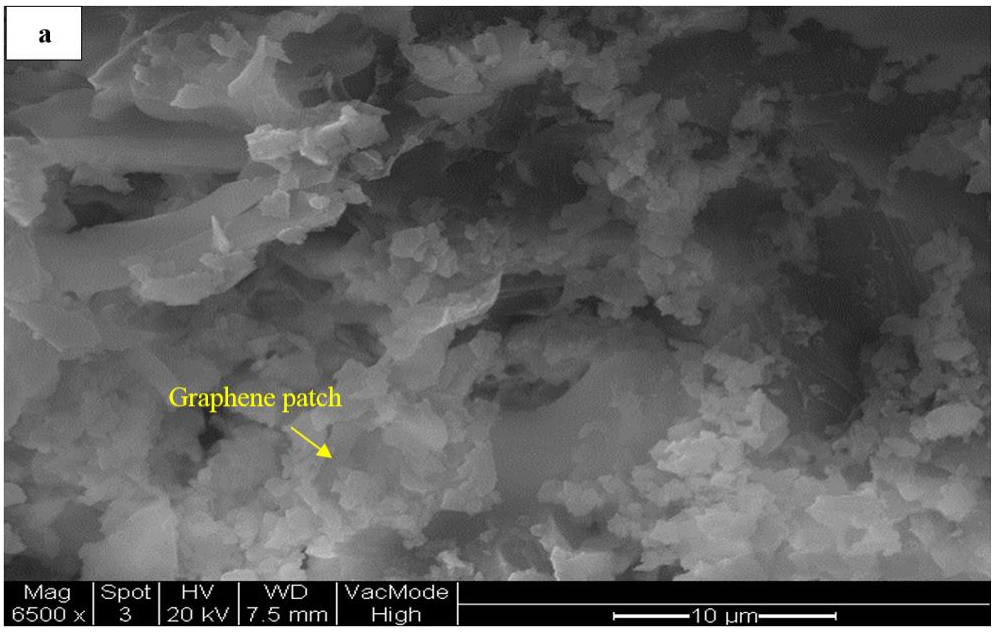
a
Graphene patch
Mag
6500 x
Spot
3
HV
20 kV
WD
7.5 mm
VacMode
High
10 µm

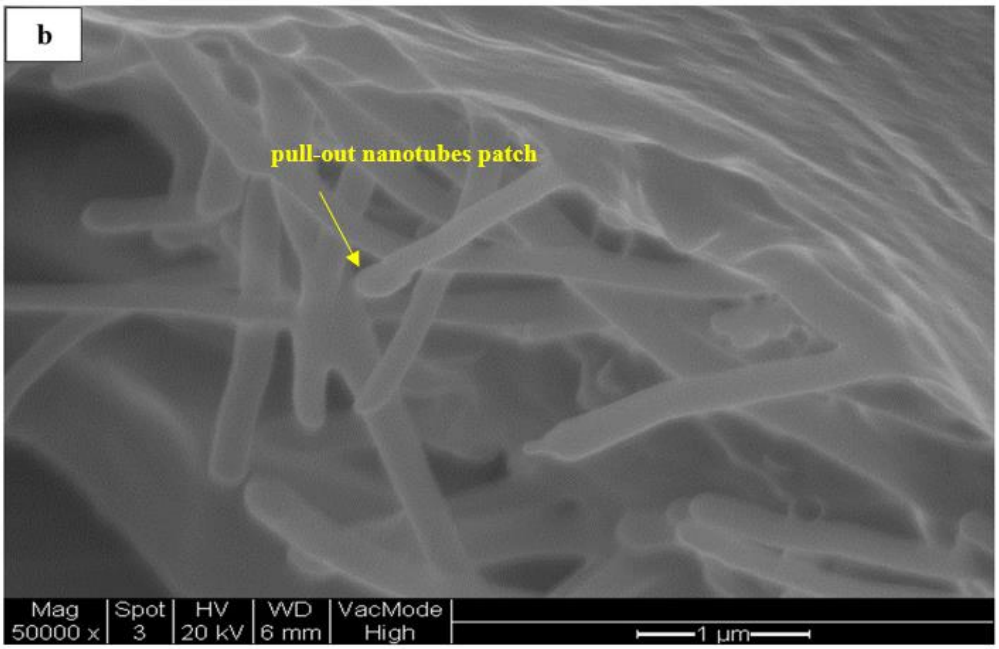
b
pull-out nanotubes patch
Mag
50000 x
Spot
3
HV
20 kV
WD
6 mm
VacMode
High
1 µm

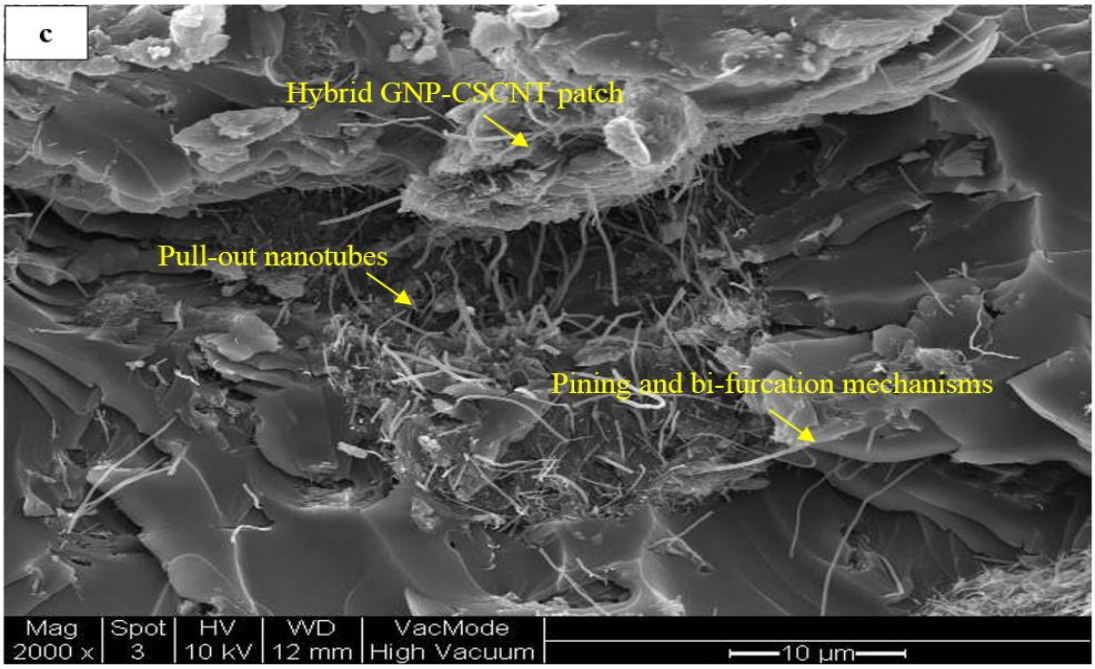

Figure 90 The SEM images exhibit the fracture behaviour systems of the optimal nanofilled matrix penetrated onto the surface of HCFRP, in addition to the quality of particles dispersion: a) GNP/CF/epoxy nanocomposite, b) CSCNT/CF/epoxy nanocomposite, c) Hybrid GNP-CSCNT/CF/epoxy nanocomposite.

The quality of nanoparticles dispersion, the mechanical bonding between the matrix and fibre networks, the fracture mechanisms systems were also predicted by SEMs, as shown in Figure 91. The micrograph of the CF/epoxy composite unmodified that had completely impregnated the fibre network is shown in Figure 91a. Furthermore, as seen from this image, no interfacial voids are visible.

The existence of riverline mechanisms with several clean fibre surfaces (Figures 91a and 91c) after the crack extension illustrates that the crack had started at the interface regions (fibre/matrix) and subsequently, extended into the matrix. However, in most regions the fracture surface of hybrid fibre composites illustrated a tortuous path of cracks and rougher surface than the CF/epoxy composite unmodified.

Further checking of the interfacial bonding at the interface regions, as highlighted by Figure 92, suggests that the interface strength was relatively good. However, Figure 93 illustrates that the crack head was driven into the nanofilled matrix from the interface region at the end of the crack extension during the propagation stage. In addition, there were clear broken fibres in the interface region which were reflected in the nesting of the fibre network at the mid plane of the DCB sample. Furthermore, the peeling and pull-out of nanofillers, bridging nanofillers, pinning of the crack tip and bi-furcation mechanisms crack driven into the nanofilled matrix and shear failure, suggest failure mechanisms of HCFRP.

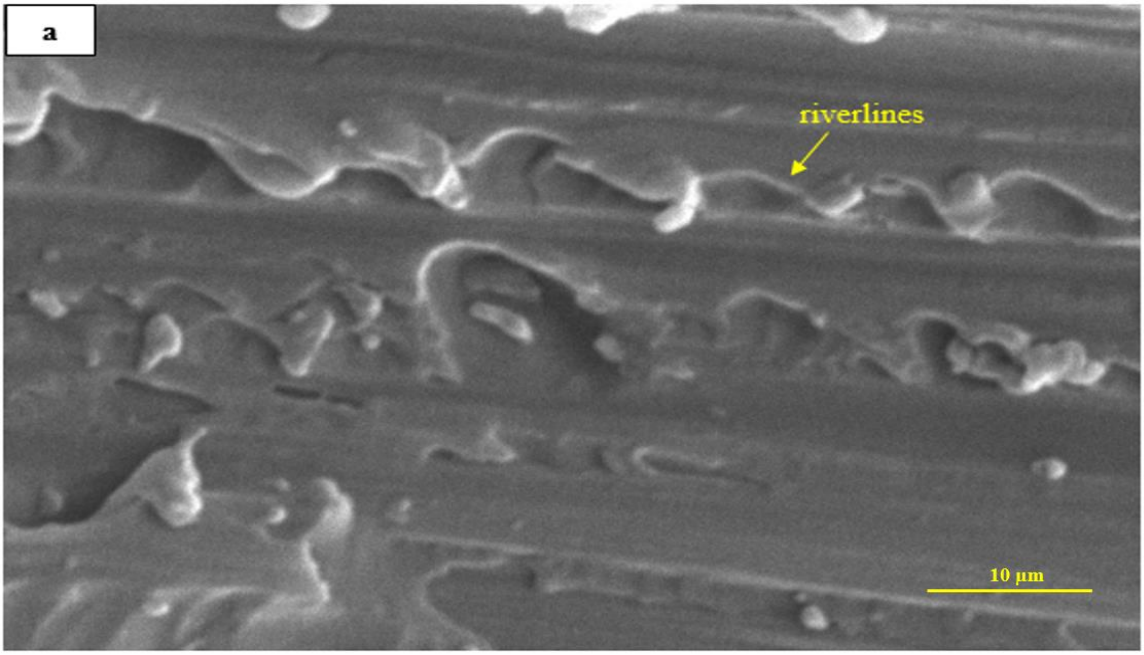
a
riverlines
10 µm

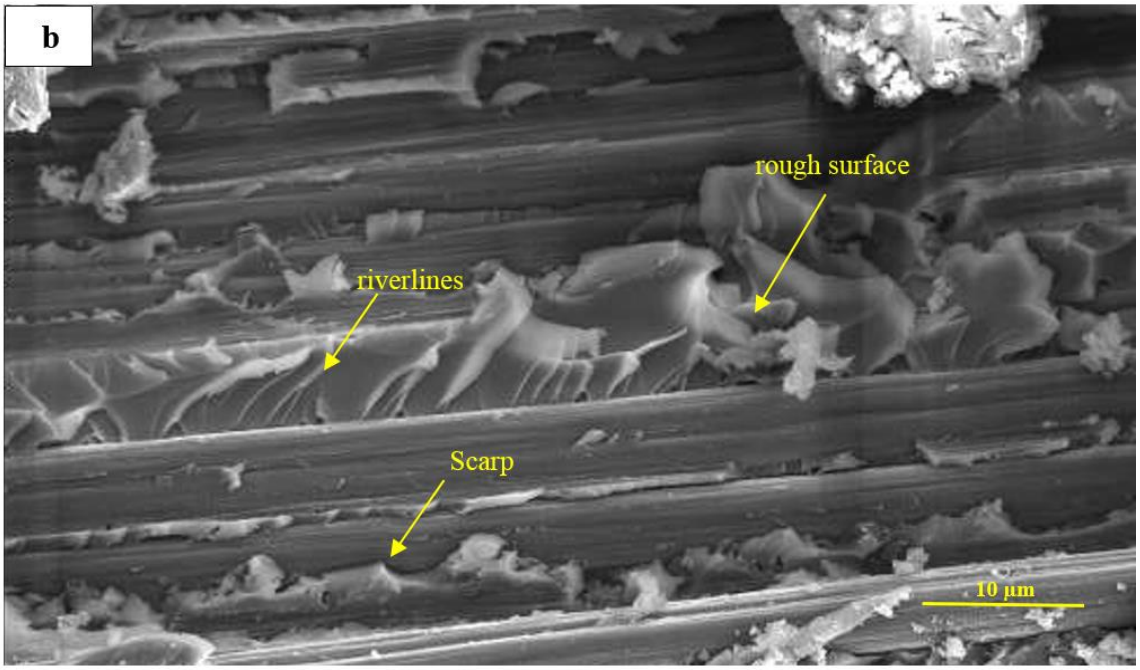
b
rough surface
riverlines
Scarp
10 µm

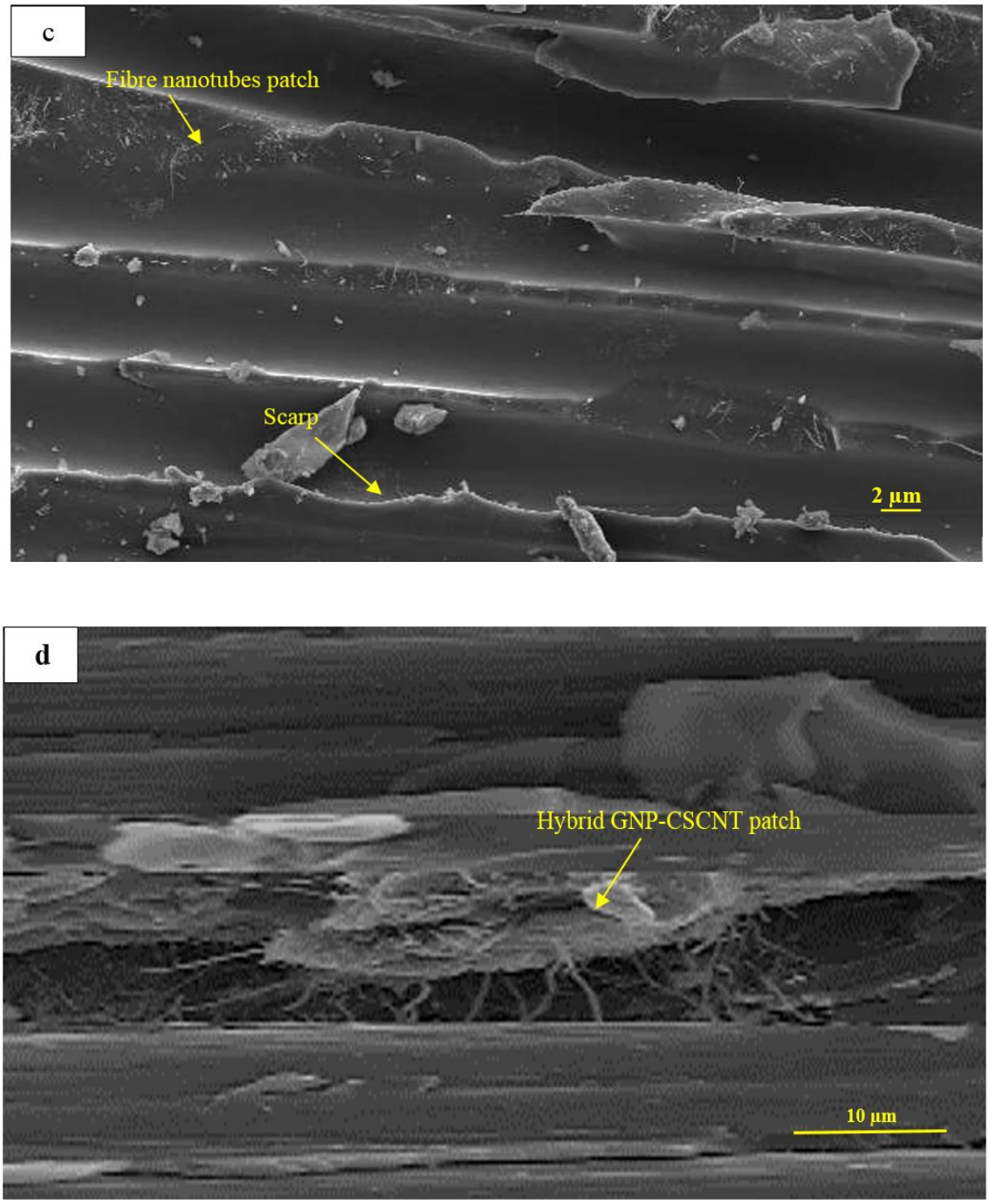

Figure 91 The SEM images illustrate the fracture behaviour systems of the composites and the quality of particles dispersions in HCFRP: a) CF/epoxy composite unmodified, b) GNP/CF/epoxy nanocomposite, c) CSCNT/CF/epoxy nanocomposite, d) Hybrid GNP-CSCNT/CF/epoxy nanocomposite. The crack extension was from left to right [1000x].

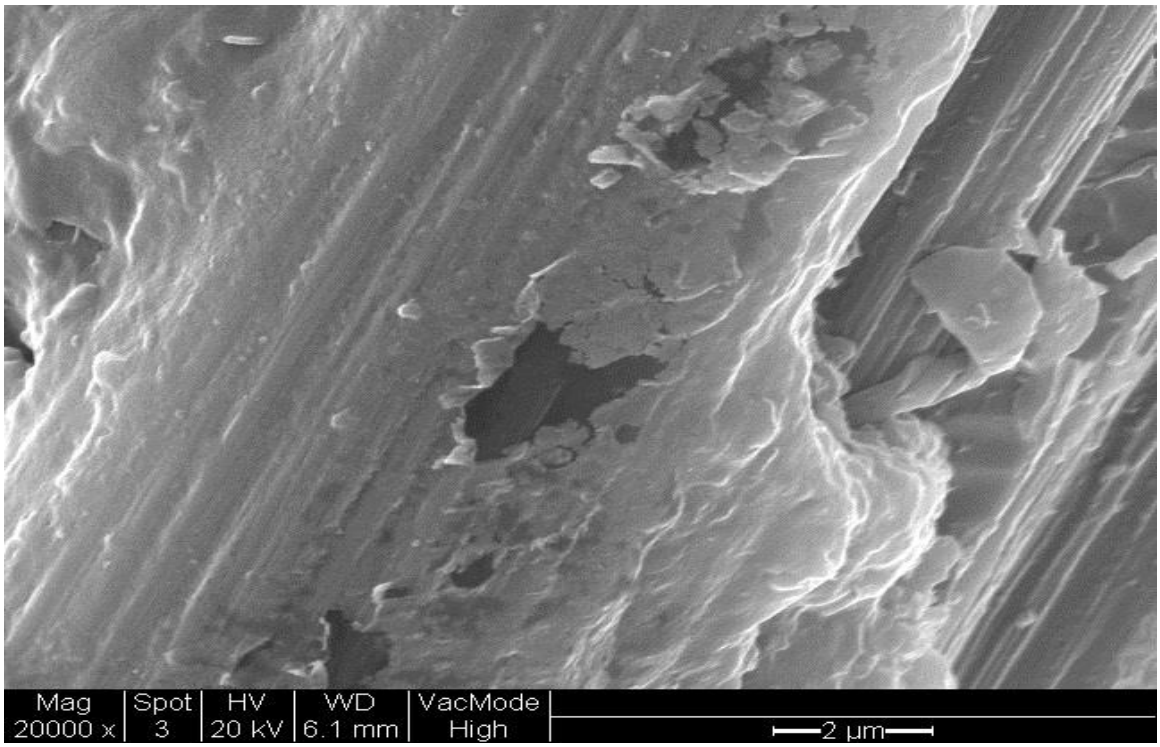

Figure 92 The SEM image illustrates the bonding of hybrid GNP-CSCNT nanofilled matrix with fibre.

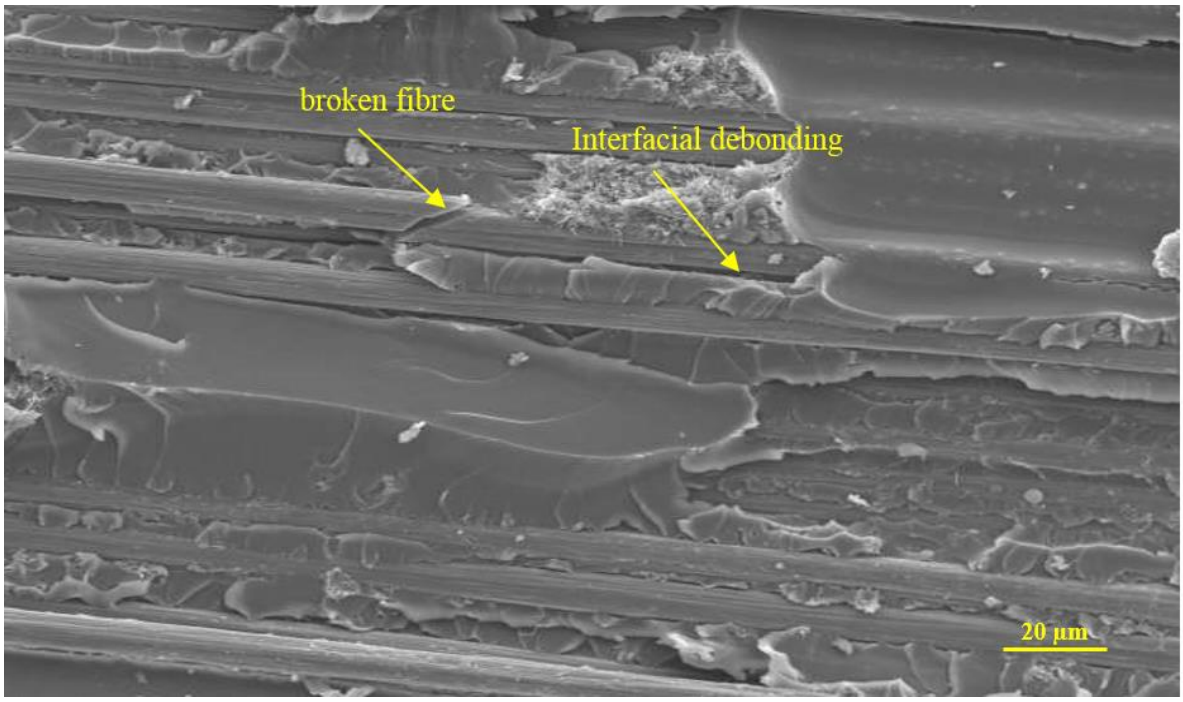

Figure 93 The SEM image illustrates the broken fibres at the interface regions of hybrid GNP-CSCNT/CF/epoxy nanocomposite. The crack extended from left to right [1000x].

6.4.3 Micrograph of optimal nanofilled matrix in 3ENF samples

The quality of nanofillers dispersion, distribution of the nanofilled matrix onto the fibre networks, bonding mechanism between the nanofilled matrix and fibre network and the keys for the dissipation fracture energy systems in the fractured area were discovered via SEM, as shown in Figure 94. The images illustrated good bonding between the nanofilled and fibres. Moreover, there were no interfacial voids noticed, although riverlines behaviour with some smooth surface fibre was seen on the surface of the fracture area in hybrid fibre composites after crack expansion shows that the crack had begun at the interface zones and subsequently, propagated into the nanophase matrix.

However, the fracture surface morphology for HCFRP samples were rougher than the CF/epoxy composite unmodified and exhibited interfacial debonding, as shown in Figure 95. Additionally, the crack tip had clearly propagated into the nanofilled matrix from the interface zones at the end of the crack expansion, as revealed in Figure 96. This behaviour contributes to generating multiple fracture mechanisms into the nanofilled matrix, which absorb the stress energy before it reaches the fibre network.

Several fracture dissipation energy systems were seen in the micro-section area of the 3ENF samples. The fracture mechanisms systems (i.e. pullout nanotubes, bi-furcation mechanisms, etc) in the ENF sample are similar to the DCB sample.

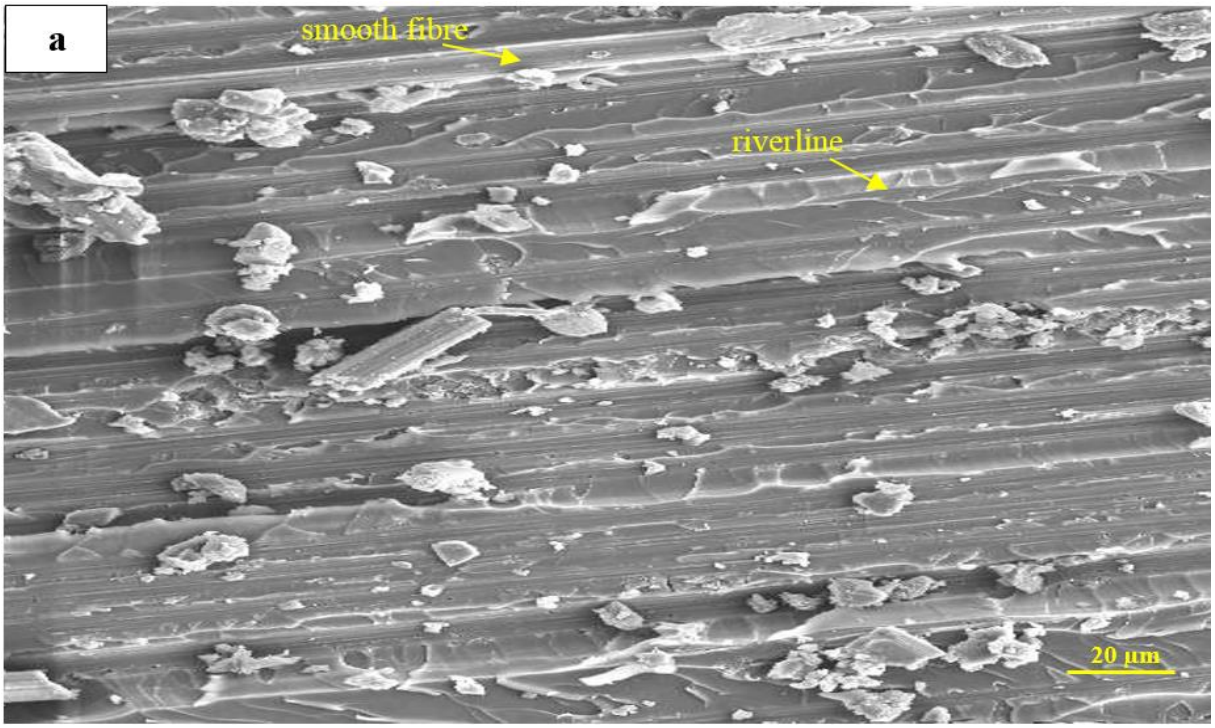

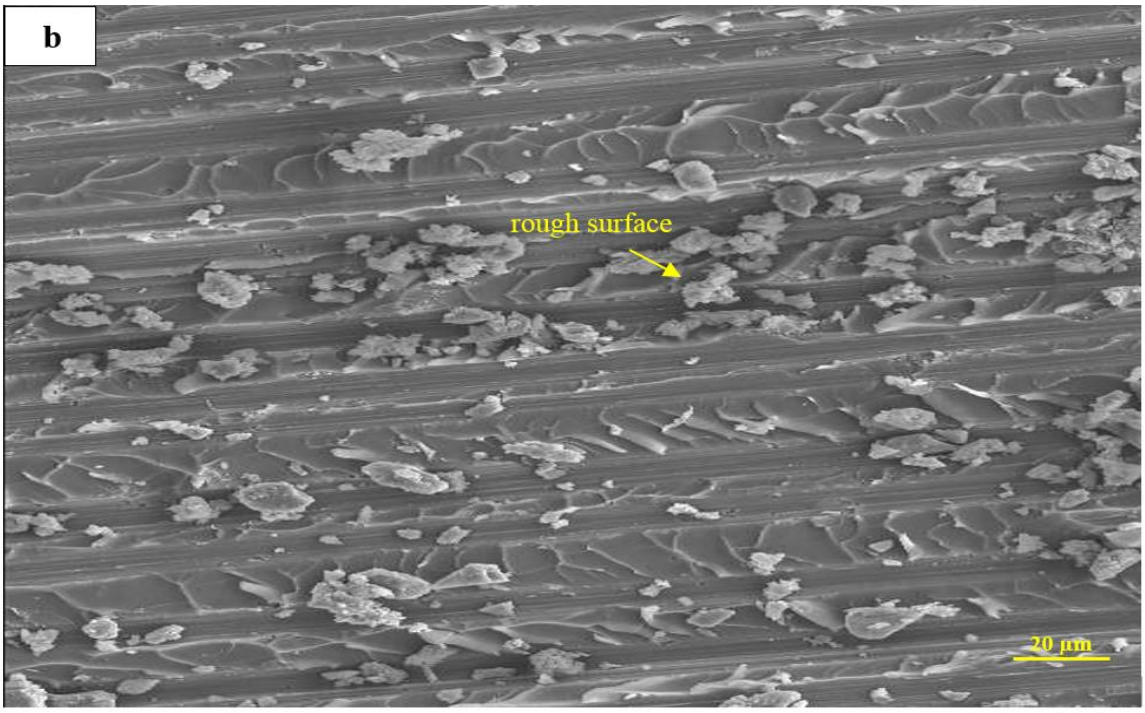
b
rough surface
20 µm

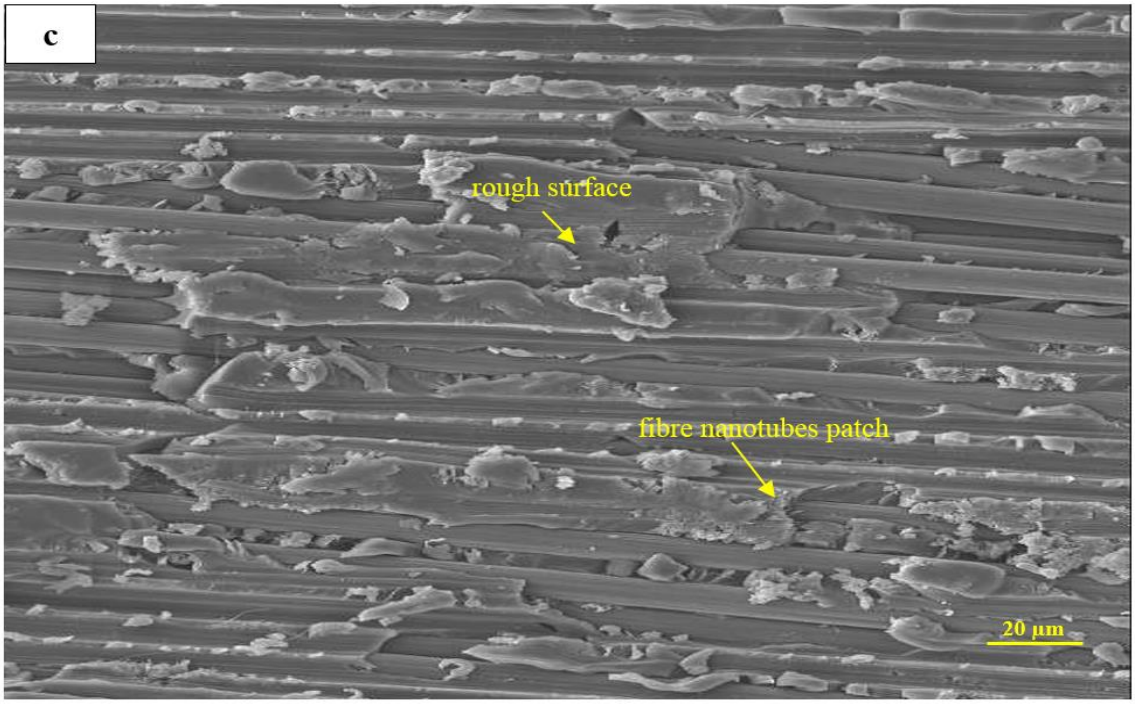
c
rough surface
fibre nanotubes patch
20 µm

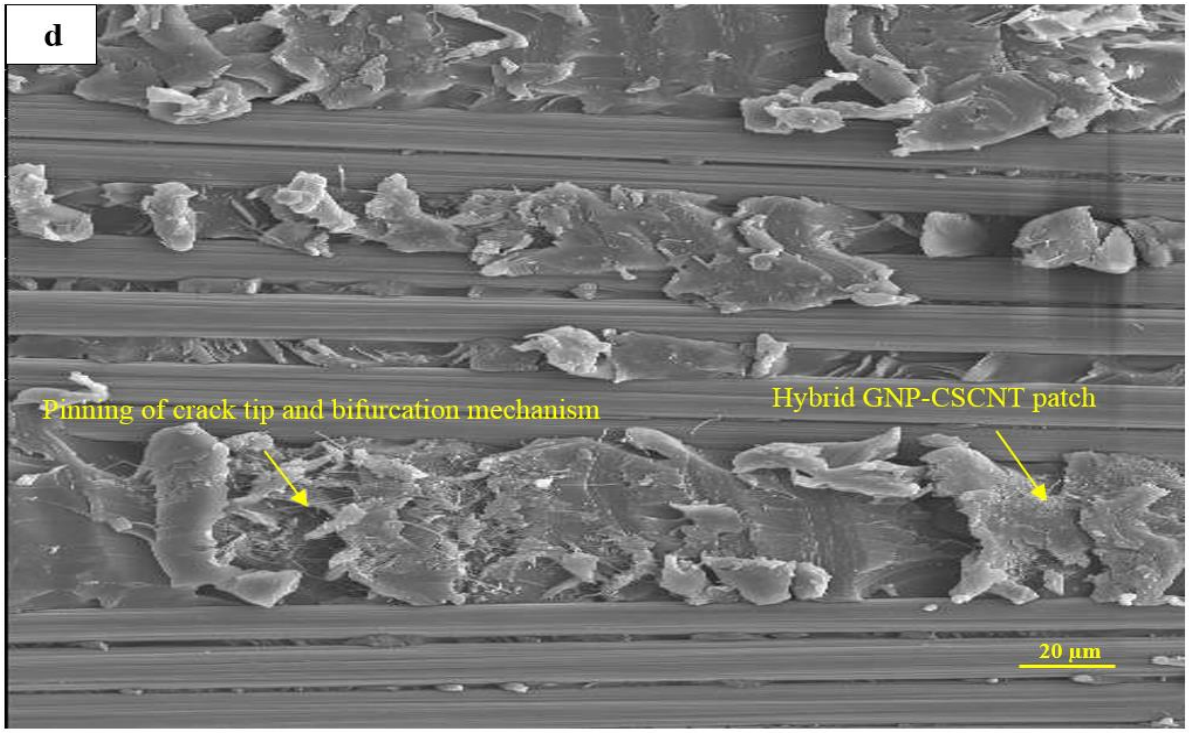

Figure 94 The SEM images illustrate the fracture behaviour systems of the composites and the quality of particles dispersions in HCFRP: a) CF/epoxy composite unmodified, b) GNP/CF/epoxy nanocomposite, c) CSCNT/CF/epoxy nanocomposite, d) Hybrid GNP-CSCNT/CF/epoxy nanocomposite. The crack extension was from left to right [1000x].

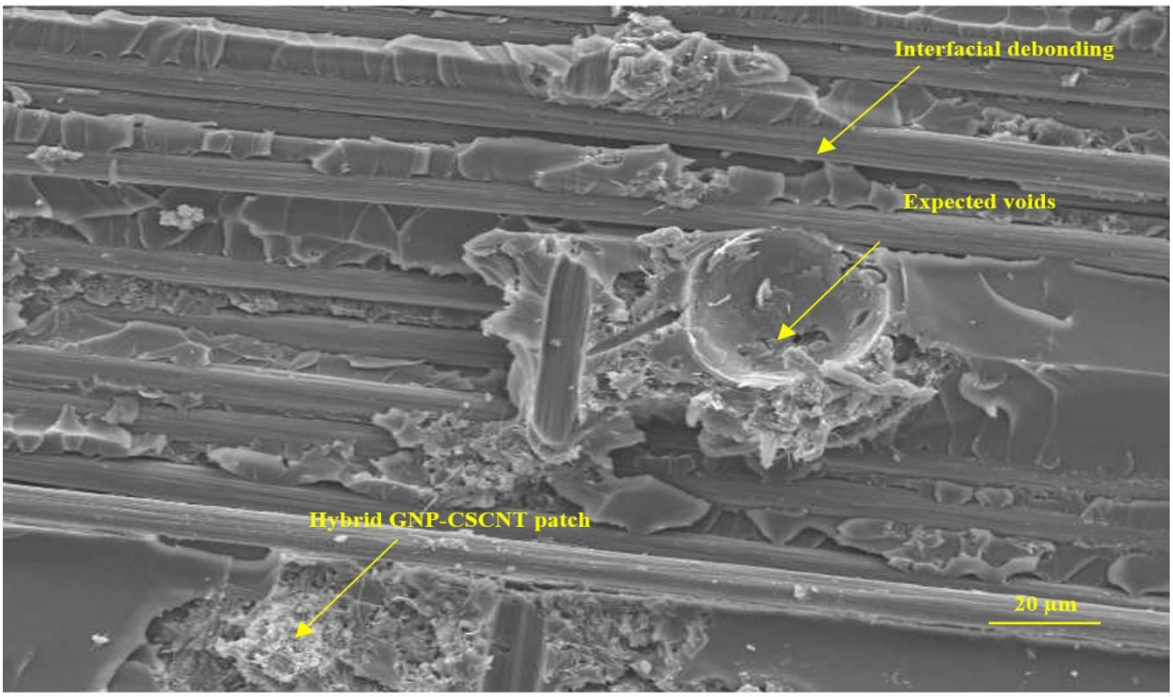

Figure 95 The SEM image illustrates the interfacial debonding between the hybrid GNP-CSCNT nanofilled matrix and fibre network. The crack extension from left to right [1000x].

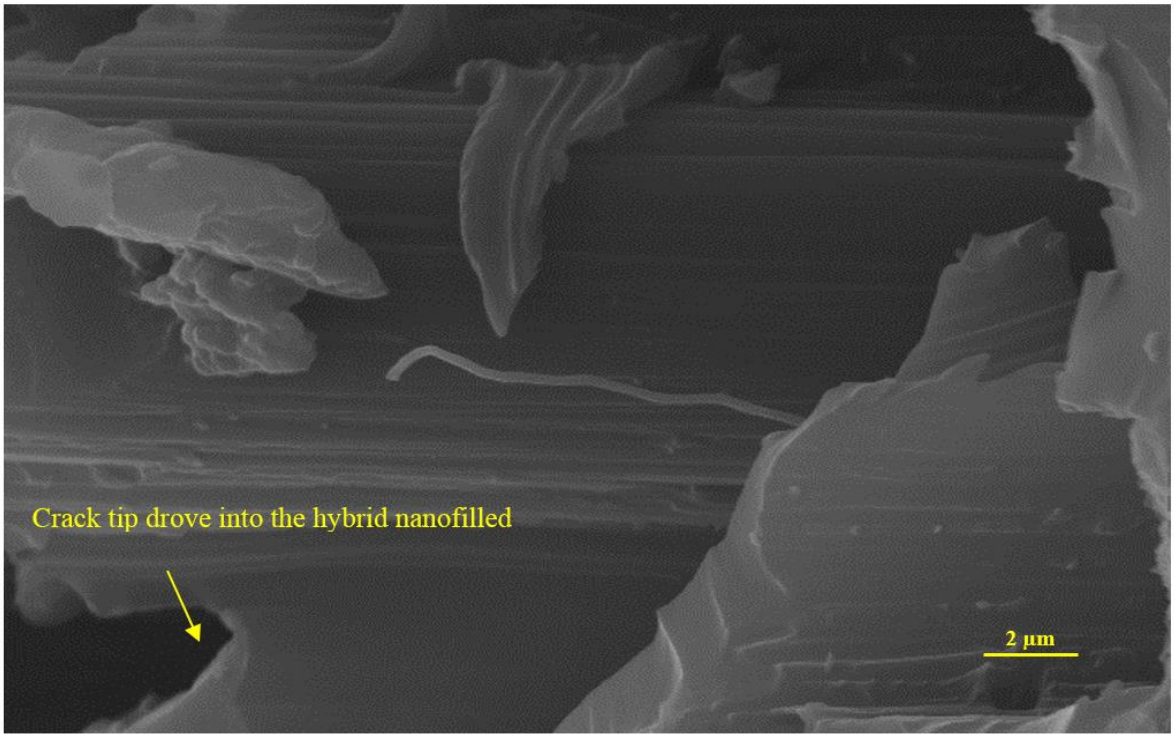

Figure 96 The SEM image illustrates the driven and extended crack into the hybrid GNP-CSCNT nanofilled matrix over the interface region [15000x].

6.4.4 Interlaminar fracture toughness properties Mode I and Mode II

The fracture toughness of the three HCFRP was characterised by double cantilever beam (DCB) tests and three end notched flexural (3ENF) tests. The experimental results for both tests were analysed by graphing the load-deflection curves and the toughness resistance curves (R-curves). The graphs characterise the fracture toughness behaviour of the hybrid fibre composites, particularly the stability of the crack.

6.4.4.1 Load versus deflection curves for toughness testing (Mode I)

Representative load-deflection curves for the three types of HCFRP under DCB testing in which the crack tip has extended by approximately 50 mm from the pre-crack is illustrated in Figure 97.

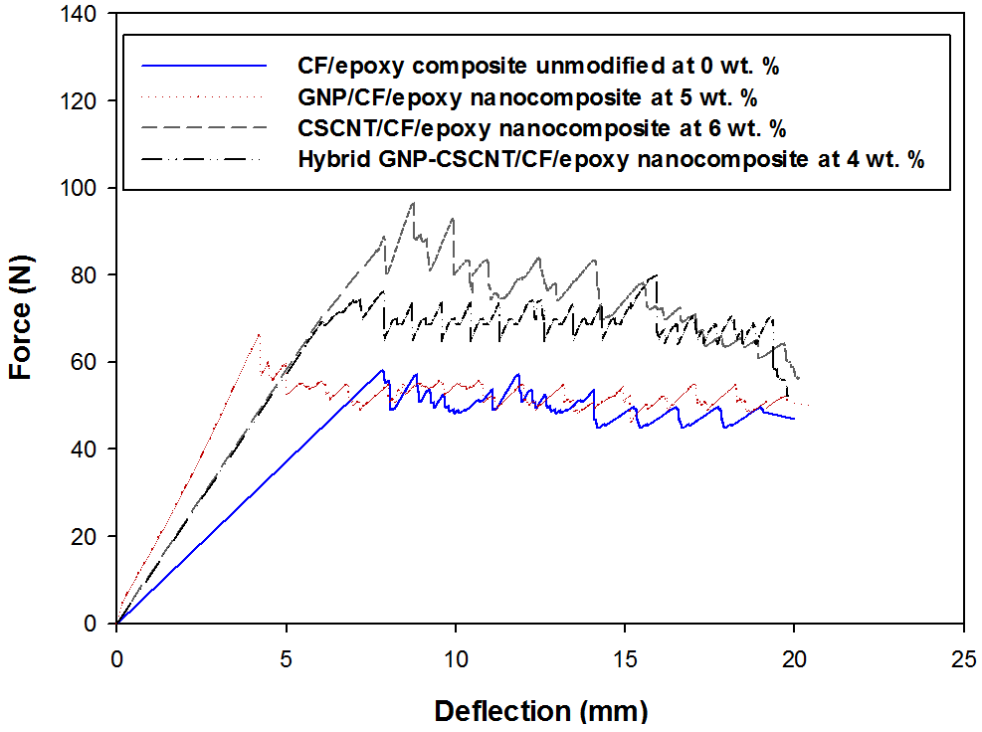

Figure 97 Typical load-deflection curves for the three types of HCFRP as well as CF/epoxy composite unmodified.

The GNP/CF/epoxy nanocomposite had exhibited relatively shorter deflection and less load to extend the same crack length in comparison to the CSCNT/CF/epoxy nanocomposite and hybrid GNP-CSCNT/CF/epoxy nanocomposite, in addition to CF/epoxy nanocomposite unmodified. Conversely, the load-deflection curves for each sample could also be affected by the stiffer delaminated arm, besides several differences in the actual geometric dimensions of the tested samples, such as thickness and initial crack length. These engineering issues could be one of the reasonable reasons to justify this mechanical behaviour in the GNP/CF/epoxy nanocomposite.

However, the crack head also started earlier in the CF/epoxy composite unmodified in comparison to the three HCFRP. In addition, the crack head at initial points for some samples of hybrid fibre composites (i.e. hybrid GNP-CSCNT/CF/epoxy nanocomposites) also appeared earlier in comparison to the other composites. This behaviour could be relevant to insert film at this elastic and sensitive area (i.e. the actual length of the crack or the real distance from edge of insert film to the crack tip after an initial delamination pre-crack growth) as well as some defects relating to the manufacturing process, for instance the plane waviness of the fibre networks, which may negatively affect the modulus mismatch and the efficiency of mechanical forces transferred between the nanofilled matrix and the fibre networks. Hence, this could reflect the percentage of data errors resulting from tests of the samples.

In contrast, the visual crack point was crossed with the nonlinear point in some samples of the fibre composites (David et al., 2001). Zig zag mode of deflection was illustrated for all fibre composites. Therefore, the transition of the force after the initial stage is fluctuated with extension of crack in the samples tested. Several of the samples showed sharp downs in the force during the extension of the crack, which is a characteristic of slip-stick growth, as observed in Figure 97. Most of the force-deflection curves in the samples had exhibited slight differences in the compliance of the elastic zone. These differences were probably attributed to various stiffness properties among the three HCFRP, the inequivalent and inhomogeneous distribution of the modified matrix onto the fibre network as well as the fibre network waviness, resulting from the manufacturing process of the laminated fibre composites (Zhu et al., 2015; Morais and Pereira, 2007).

6.4.4.2 Mode I initial and propagation fracture toughness energy

It should be reported that the displacements of the micro-insert film in the samples during the manufacturing process by means of the hand lay-up method created a slight difference in the inert lengths among the samples. A value of 66 mm was calculated as the guidance point, seeing as this value was commonly participated between the samples of the fibre composites and the crack head had sufficiently extended through the ply to have arrived at a steady stage.

It is well known that Mode I fracture toughness is linked to the process region forward of the crack head propagating into the fibre plies adjacent to the interface area (Bradley and Cohen, 1985; Crews et al., 1988). Therefore, the poorer the fibre/matrix interface, the larger the sensibility to fibre bridging in open system testing (DCB).

The typical fracture toughness energy vs crack length for all samples are shown in Figure 98. These graphs mostly demonstrated stable crack growth except in some cases which have localised short slip stick behaviour. The main reasons for this mechanism behaviour may be reflected in the severe fibre bridging within some specimens, besides the formation of minor delamination planes. At those points of jumping, the planes of crack converged after collapsing the bridging fibre networks and therefore, released the load energy. Another reason could be relevant to the defects (i.e. voids) in the specimens in particular at the mid plane regions. Existence of such defects means that the nanofilled matrix is absent from the restriction of the crack extension. Hence, occurrence of crack jumping is rapidly expected.

Principally, the stability of the crack extension was calculated by the slope of the resistance curves from the initial crack stage until the crack had extended. Most of the resistance curves are virtually unstable regarding the level of fracture toughness vs crack extension, however, the resistance curves for the hybrid GNP-CSCNT/CF/epoxy nanocomposites and CF/epoxy composite unmodified continuously increased over the delamination crack.

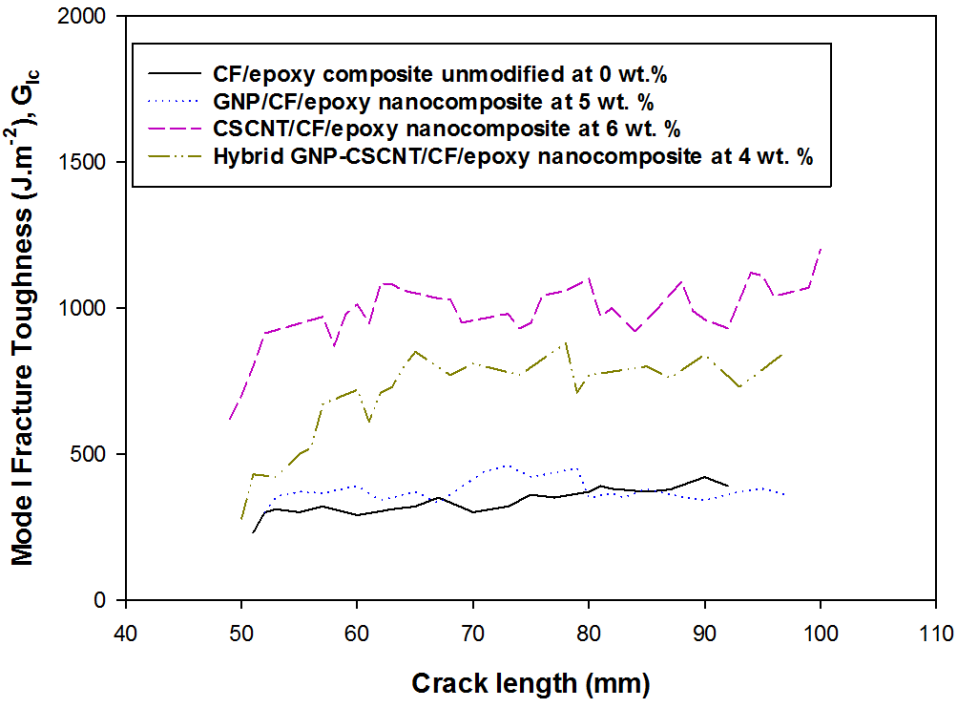

Figure 98 Typical Resistance curves of the three types of HCFRP as well as CF/epoxy composite unmodified.

The results of the initial fracture toughness energy and propagation toughness energy for the fibre composites were tabulated in Table 34, which also demonstrates the evaluation of the fracture toughness of the three types of HCFRP.

Table 34 The evaluation of fracture toughness energy (Mode I).

Sample	Number of samples	Weight content (wt.%)	Initial propagation toughness ($J.m^{-2}$)						Propagation toughness ($J.m^{-2}$)	Inc. (%)
			Visual onset (VIS)	Inc. (%)	Non-linear (NL)	Inc. (%)	Offset/ MAX5%	Inc. (%)		
CF/epoxy composite	4	0	301.30±9.0	00.0	314.20±9.0	00.0	321.20±8.0	00.0	405.00±5.0	00.0
GNP/CF/epoxy nanocomposite	4	5	399.60±9.0	+32.6	324.50±4.0	+3.2	337.60±7.0	+5.1	465.50±8.0	+14.9
CSCNT/CF/epoxy nanocomposite	5	6	567.7±16.0	+88.4	579.90±17.0	+84.5	591.10±16.0	+84.0	826.20±18.0	+103.9
Hybrid GNP-CSCNT/CF/epoxy nanocomposite	4	4	285.10±2.0	-5.3	314.10±6.0	-0.1	358.30±10.0	+11.5	700.00±13.0	+72.8

Figure 99 demonstrates the significant improvements in interlaminar fracture toughness Mode I. These improvements were compatible with previous experimental studies relating to fibre composited reinforced by carbon nanomaterials (Moghadam and Taheri, 2015; Kostagiannakopoulou et al., 2015; Yokozeki et al., 2009; Kostagiannakopoulou et al., 2017).

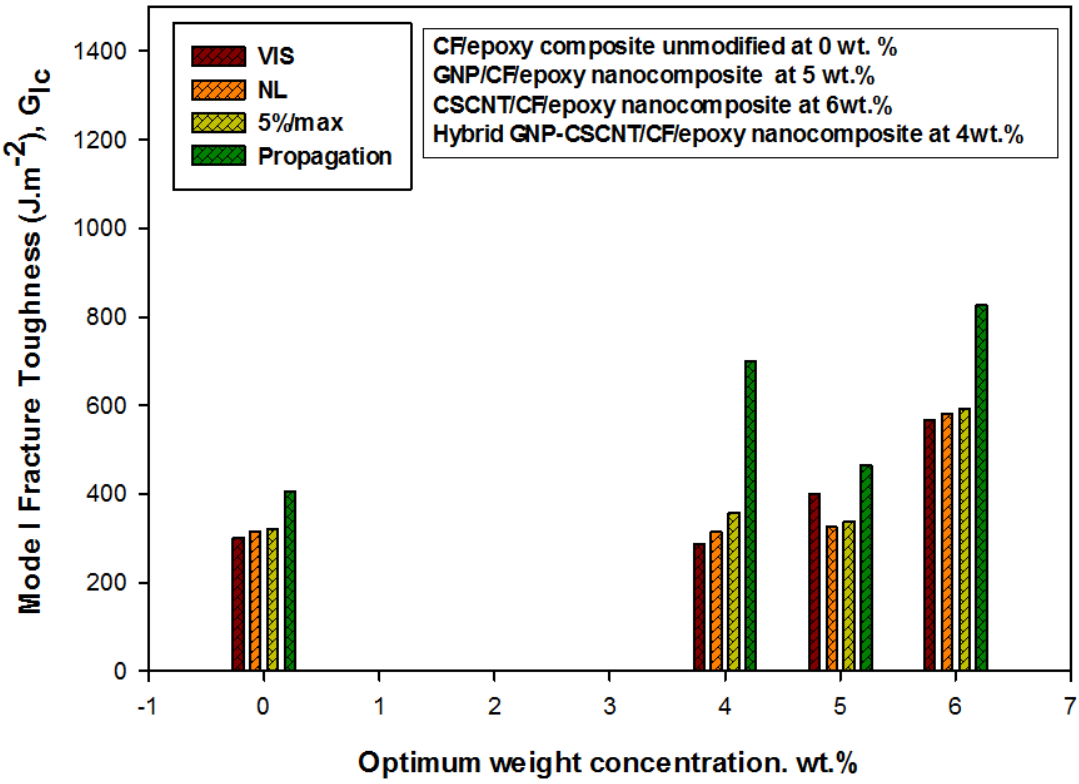

Figure 99 The evaluation of initial and propagation fracture toughness energy among three types of HCFRP in comparison with CF/epoxy composite unmodified.

The highest improvement regarding initial fracture energy (i.e. 5%/MAX) and propagation fracture energy was achieved after addition of fibre nanotubes to the fibre composite by approximately 84% and 104% respectively. This may explain the improved effectiveness of the morphological properties of fibre nanotubes, particularly the premium geometric structure compared with other carbon nanomaterials. This has a significant effect on reinforcing the strength and toughness properties around the fibre network and hence, this may improve the adhesion between the fibre network and the matrix (Landani, 2015).

The combination of GNP and CSCNT improves the toughness energy, particularly the propagation toughness energy by approximately 73%. In addition, there was a gradual increase in the initial toughness energy (i.e. 5%/MAX) approximately 12%. The lowest improvement in the propagation energy was achieved in the GNP/CF/epoxy nanocomposite. This may explain that the morphological properties of graphene, predominantly the weak geometric structure are

less effective than that of the fibre nanotube, which may also have an effect on the mechanical interfacial properties (i.e. bonding strength) between the particles and the matrix. Moreover, the structure morphology of graphene is affected by the dispersion process which may refer to the existence of several defects in the graphene structure (i.e. wrinkled nanosheets) before its impregnation process onto the surface of the fibre networks (Li et al., 2016; Moriche et al., 2015; Domun et al., 2015). In contrast, there was a slight improvement in the initial fracture energy (i.e. 5%/MAX) and propagation fracture energy after the addition of the GNP optimum nanofiller into the carbon fibre composite by approximately 5% and 15% respectively.

In general, the variance in these increases between the initial and propagation fracture energy could be conducted with the type of nanofiller, the quality of nanoparticles dispersion into the matrix and the behaviour of the fracture mechanisms in the composite in dissipating the mechanical fracture energy during the expansion stage of the cracks (Silva et al., 2014; Thostenson et al., 2005).

These three cases have been illustrated by further fractographic analysis via SEM, as shown in Figure 100. The images showed a uniform dispersion of the nanoparticles, principally the hybrid nanofillers (GNP-CSCNT), which may have contributed to increasing the synergetic strength between the graphene and fibre nanotube into the matrix; hence, promoting composite resistance against the cracks during the propagation stage. The SEM images also reveal the rough surface of the nanofilled matrix and good bond with carbon fibre network in the three types of HCFRP (see Figure 100).

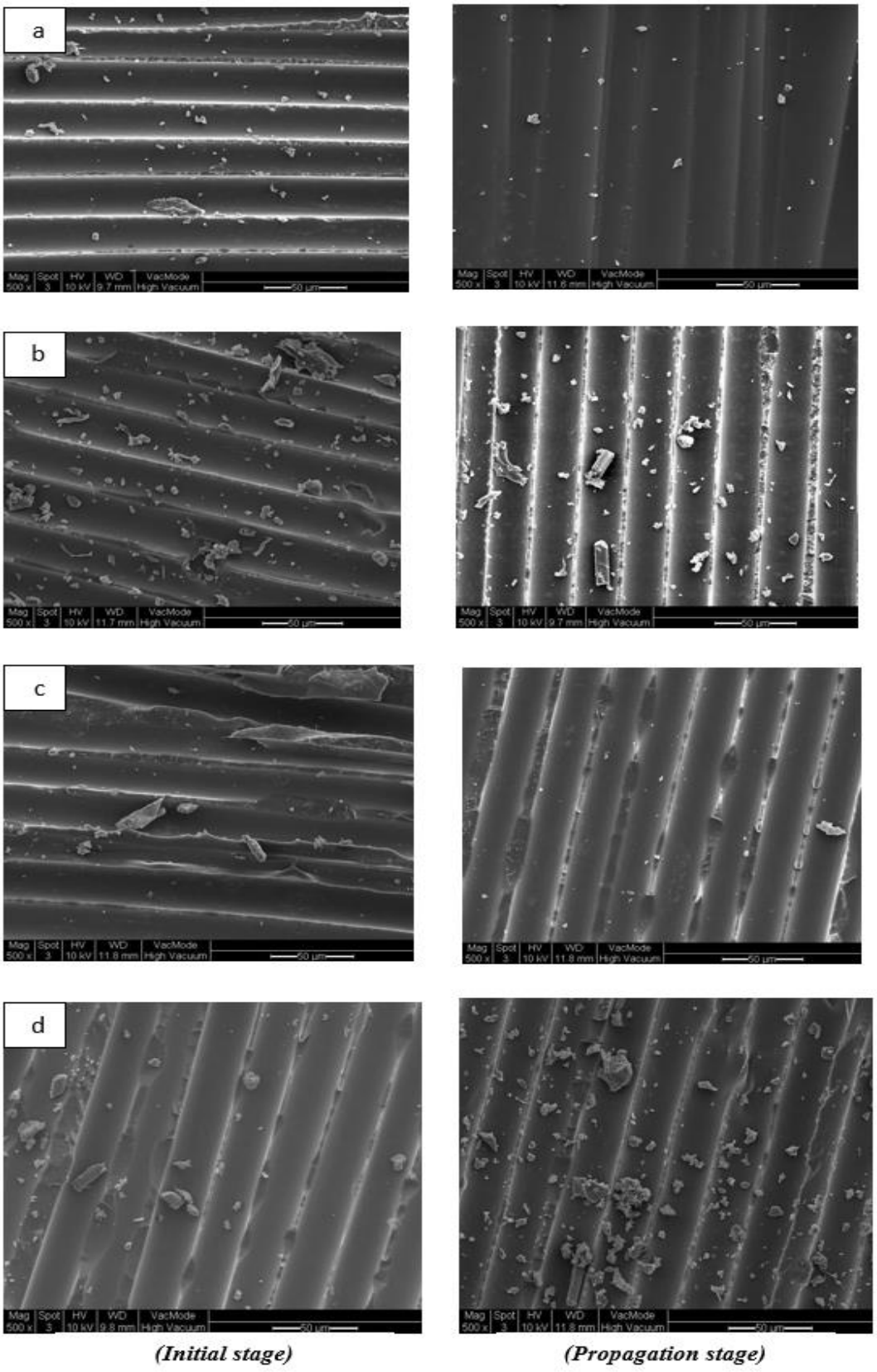

Figure 100 The SEM images illustrate the fracture behaviour systems at the initial and propagation stage for fractured areas, in addition to the quality of dispersions in HCFRP; a) CF/epoxy composite unmodified, b) GNP/CF/epoxy nanocomposite, c) CSCNT/CF/epoxy nanocomposite, d) Hybrid GNP-CSCNT/CF/epoxy nanocomposite, (images on left (initial stage), on the right (propagation stage).

Additionally, Table 34 shows that the initial fracture toughness values of the interlaminar fracture toughness (Mode I) were lower than the values of propagation toughness energy in the CSCNT/CF/epoxy nanocomposite and hybrid GNP-CSCNT/CF/epoxy nanocomposite. The reason for this variance probably depends on the fracture mechanism systems for the fillers in the matrix at the interlaminar area. For instance, in the initial propagation stage, the increasing delamination starts from the edge of the film insert (initial crack), where the fracture mechanism system in this fractured area is suggested. Only one mechanism, bridging or peeling of the filler is indicated, after the extension of the crack into the CSCNT or hybrid GNP-CSCNT nanofilled matrix (Seyan et al., 2008).

Conversely, in the propagation stage of the crack, two or more fracture mechanism systems were proposed to increase the propagation fracture energy. For instance, the images reveal that the carbon fibre nanotubes in the carbon fibre network indicate micro-scale alterations on the fracture surface. The fracture surfaces are dominated by rough nanofilled regions with a micro-fibre network. The fracture surface of the long fibre network show rougher fracture regions compared with the unmodified fracture surface. The fracture behaviour of the rough matrix is the fibre nanotubes that were a combination of bridging and pull-out of nanofibers from the matrix during the extension crack. These fracture mechanisms were clearly illustrated by SEM, as shown in Figure 101.

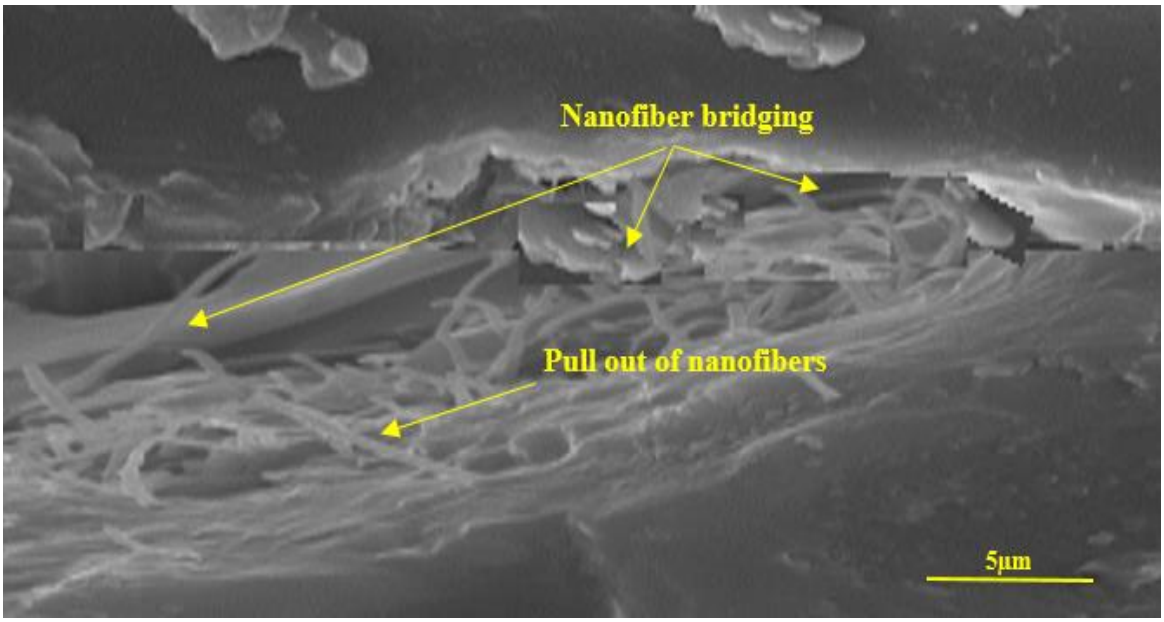

Figure 101 The SEM image shows nanofiber bridging and pull out of nanotubes into the nanofilled matrix at the mid plane for HCFRP. The crack extension was from left to right [10000x].

Moreover, there is a unique fracture mechanism, such as bridging which could be the cause of the significant increase in fracture toughness energy, suggesting fibre nanotube bridging, or a combination of bridging and pull-out as a mechanism for toughening energy in the nanofilled matrix, as shown in Figures 102a and 102b. In addition, a combination of peeling sheets and pull-out of nanotubes, plus bi-furcation and pinning of the crack tip were suggested to increase propagation fracture energy in the hybrid composite after crack extension into the matrix, as shown in Figure 102c. In contrast, peeling or pull-out of the sheet or a combination of them, plus bi-furcation mechanism were suggested to increase the initial fracture energy and the propagation fracture energy in the carbon fibre composite modified with graphene nanofiller, as described in Figure 102.d.

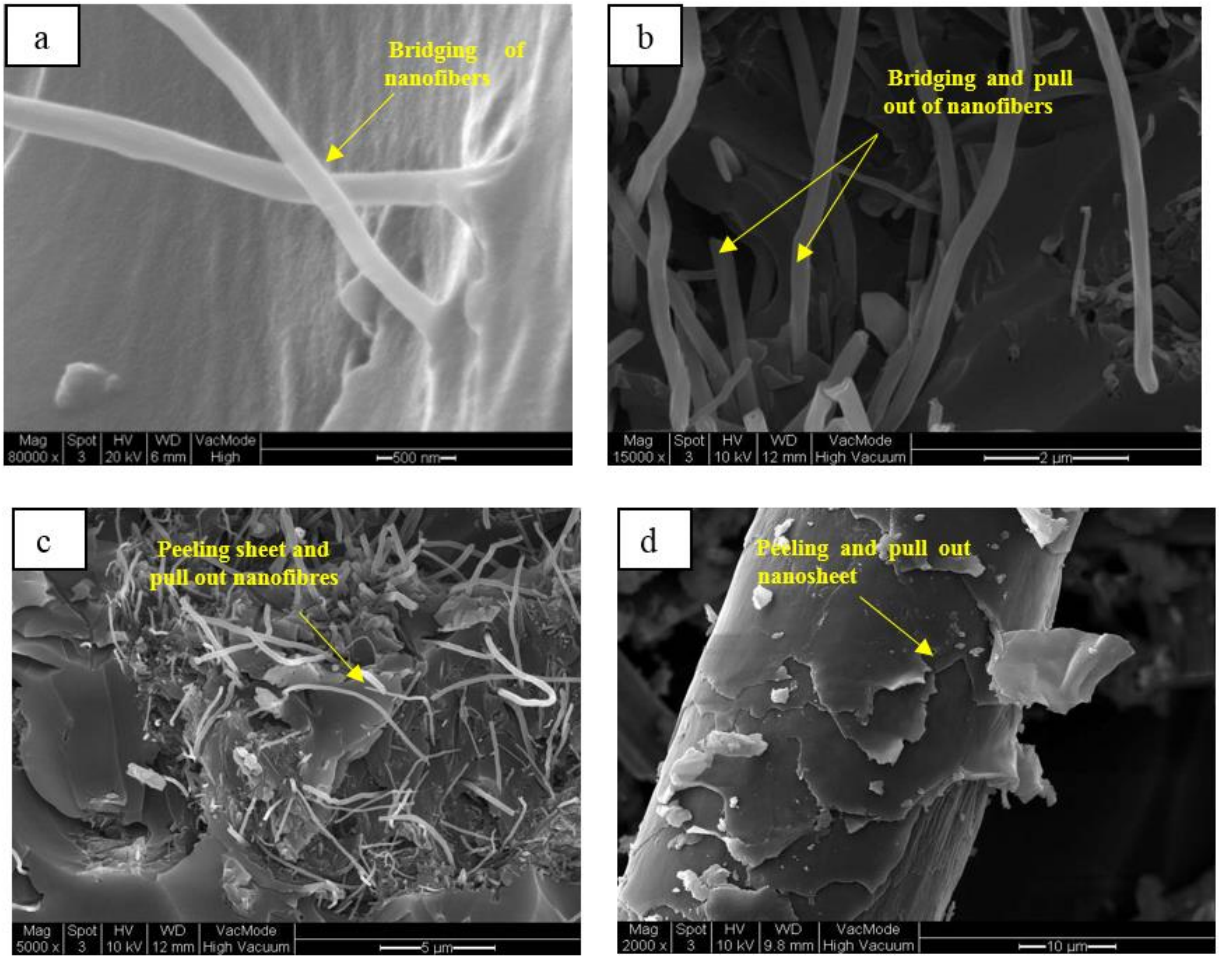

Figure 102 The SEM images illustrate the fracture behaviour systems in hybrid fibre composites at the initial and propagation stage in relation to the fractured areas: a) and b) CSCNT/CF/epoxy nanocomposite, c) Hybrid GNP-CSCNT/CF/epoxy nanocomposite, d) GNP/CF/epoxy nanocomposite.

More expected possibilities could affect the initial and propagation fracture energy; the orientation of the fillers into the matrix may affect the deviation and direction of the cracks into

the matrix, which could influence the dissipation of fracture energy in the composite (Hwang et al., 2001; Menna et al., 2016). This case has also been clearly confirmed by the TEM image, as illustrated in Figure 103. In addition, the quantity of the nanoparticles diffused into the matrix in the interlaminar regions could affect the expansion of cracks in the composite as illustrated in Figure 104, the mechanism of adhesion at rich regions of nanofilled matrix are probably stronger and more adhesive than that of poor to resist extension cracks in the matrix (Gouda et al., 2014; Ashrafi et al., 2011).

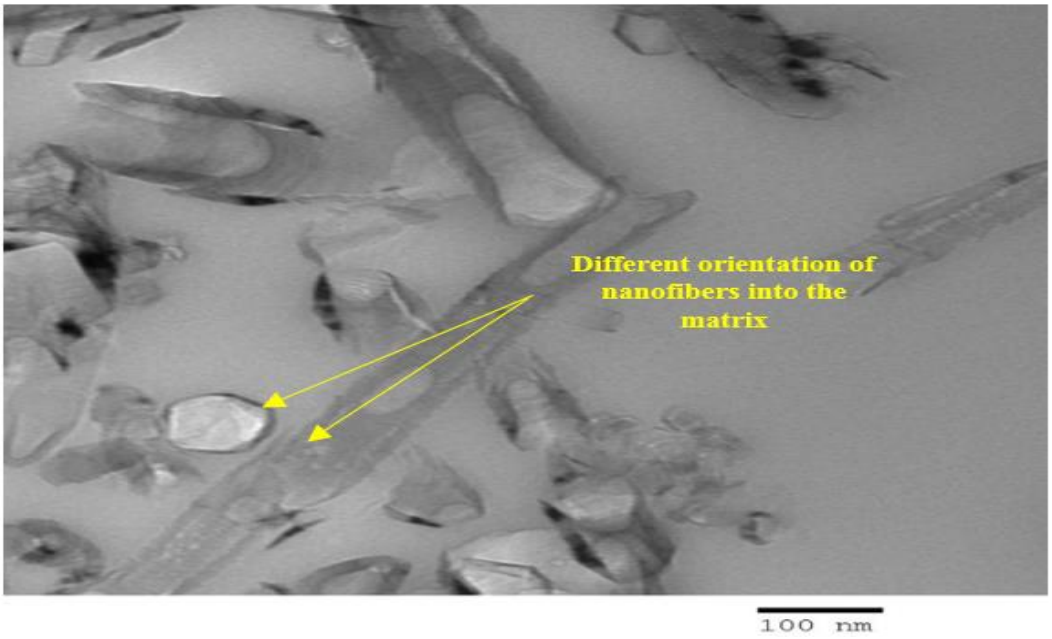

Figure 103 TEM image shows the orientation of fibre nanotubes in the matrix.

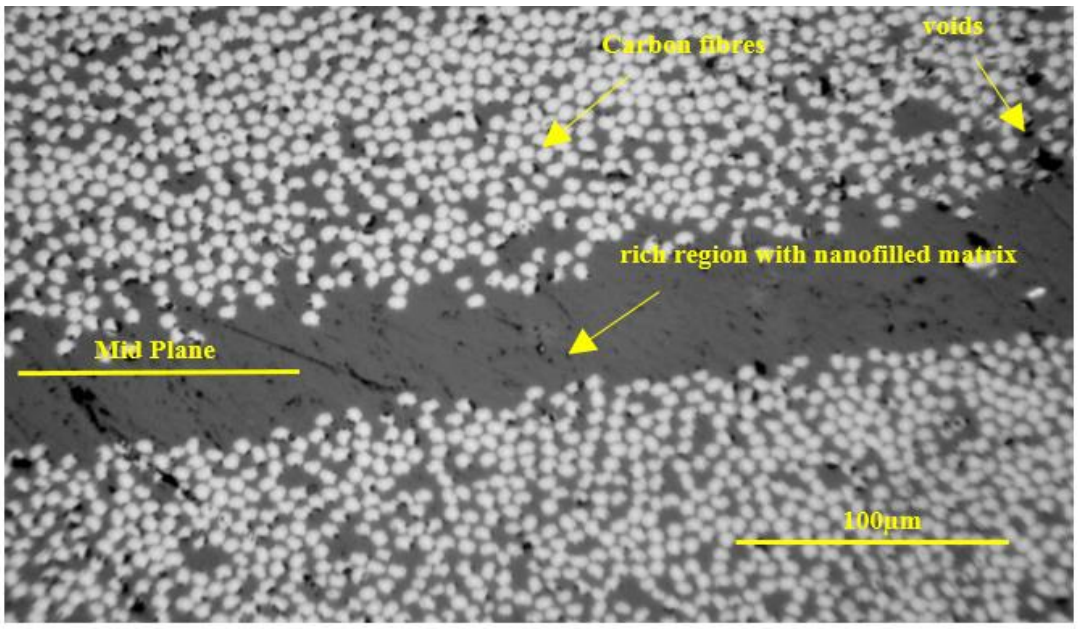

Figure 104 A microscope image shows the distribution of nanofilled matrix at mid plane [20x].

6.4.4.3 Load versus deflection curves for toughness testing (Mode II)

Representative load-deflection curves for the three HCFRP under 3ENF testing, in which the crack front has propagated approximately 16 mm from the pre-crack is shown in Figure 105.

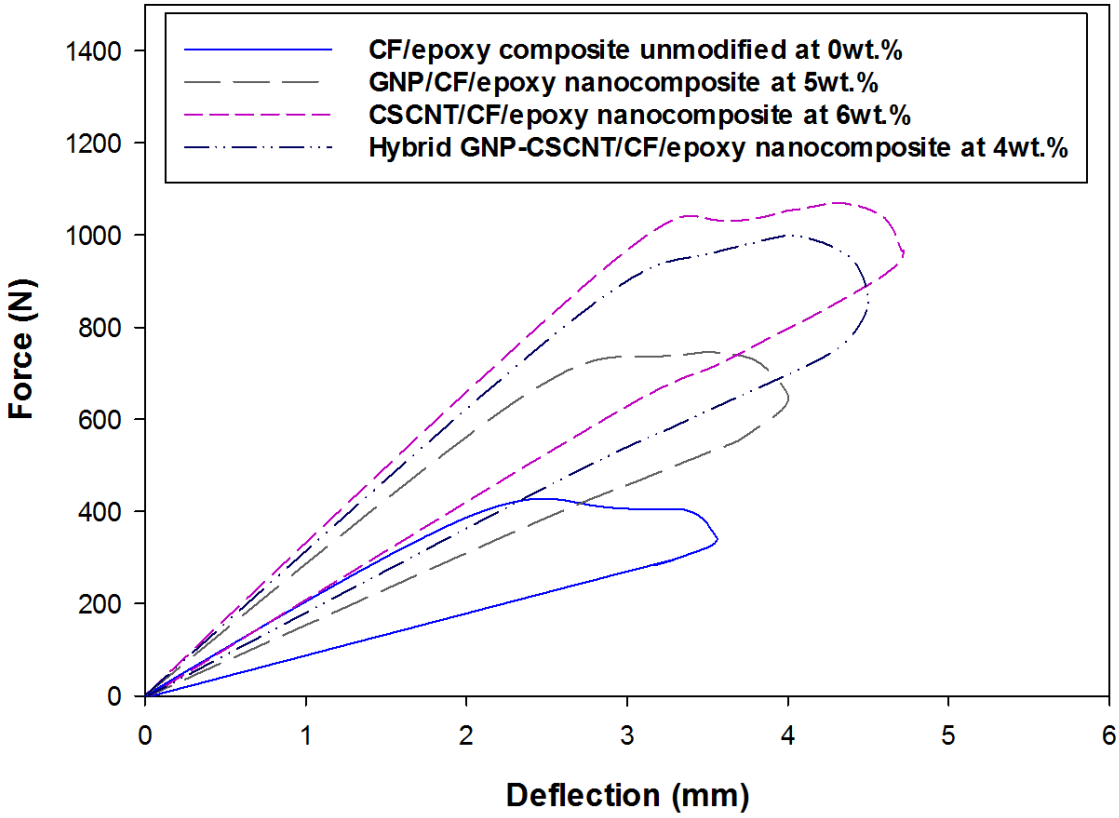

Figure 105 Typical load-deflection curves for the three types of HCFRP as well as CF/epoxy composite unmodified.

The CSCNT/CF/epoxy nanocomposite had exhibited a longer deflection and higher resistance load to extend the same crack length compared with the CF/epoxy composite unmodified and HCFRP. Its crack head also started later in comparison to these composites. In contrast, the load-deflection curves for each sample could also be affected by the actual engineering dimensions of the tested samples, for instance the initial crack length and thickness. However, the initial critical load for hybrid GNP-CSCNT/CF/epoxy nanocomposite was higher than that of the CF/epoxy composite unmodified and GNP/CF/epoxy nanocomposite. Bow mode of deformation was illustrated for all fibre composites without sharp drops in the force during the crack extension. Moreover, the force-deflection curves showed stable propagation during crack expansion in the composites.

6.4.4.4 Mode II initial and propagation fracture toughness energy

The influence of the addition of optimum modified matrix on Mode II interlaminar fracture toughness is shown in typical resistance curves (R-curves), as observed in Figure 106. These curves demonstrated stable crack growth and the experimental results are tabulated in Table 29.

Most of the resistance curves are nearly level, however, the resistance curves for the CF/epoxy composite unmodified and hybrid GNP-CSCNT/CF/epoxy nanocomposite continuously increased over the delamination crack.

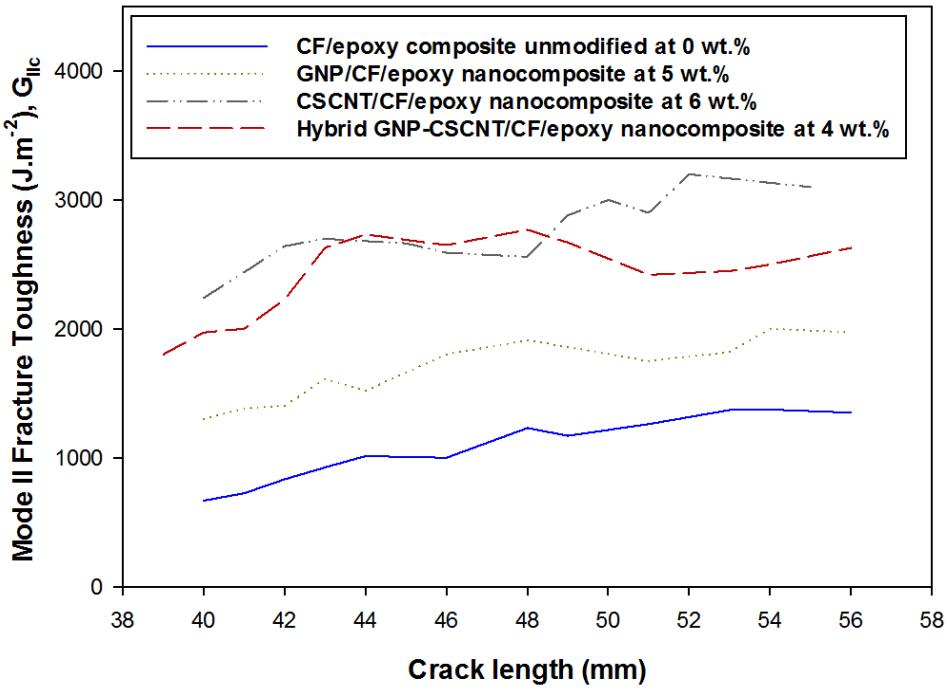

Figure 106 Typical Resistance curves for the three types of HCFRP as well as CF/epoxy composite unmodified.

The initial fracture toughness energy and the average propagation toughness energy were measured from the 3ENF tests as shown in Table 35.

Table 35 also demonstrates the comparison and assessments of three values of the initial fracture toughness which were measured by applying three techniques (i.e. VIS, NL, 5%/MAX) similar to DCB tests as previously described, and the average fracture toughness energy for the three HCFRP and CF/epoxy composite unmodified. The three types show a significant increase in Mode II interlaminar fracture toughness energy. This increase is compatible with previous research (Jia et al., 2015; Yokozeki et al., 2009; Rodriguez-Gonzalez et al., 2017; Kostagiannakopoulou et al., 2017).

Figure 107 shows the evaluation of initial and propagation fracture energy for the three HCFRP in comparison with CF/epoxy composite unmodified. The highest increase regarding initial (i.e. VIS) and propagation toughness energy was accomplished after impregnation of the modified matrix with fibre nanotubes onto fibre networks by approximately (179%), (151%) respectively. This showed an excellent increase in both properties after the combination of graphene and novel fibre nanotubes by approximately (155%), (132%).

Addition of the modified matrix with graphene into the fibre reinforced composite shows less enhancement compared with the two other types; CSCNT/CF/epoxy nanocomposites and Hybrid GNP-CSCNT/CF/epoxy nanocomposite. These improvements were by approximately 33% in initial fracture energy (i.e. VIS) and 84% in propagation fracture energy.

Table 35 The experimental results of Mode II interlaminar fracture toughness energy.

Sample	Number of samples	Weight content (wt.%)	Initial propagation toughness ($J.m^{-2}$)						Propagation toughness ($J.m^{-2}$)	Inc. (%)
			Visual onset (VIS)	Inc. (%)	Non-linear (NL)	Inc. (%)	Offset /MAX5%	Inc. (%)		
CF/epoxy composite	5	0	659.70±5.0	00.0	742.80±7.0	00.0	776.60±6.0	00.0	1143.10±12.0	00.0
GNP/CF/epoxy nanocomposite	4	5	878.20±7.0	+33.1	1469.70±9.0	+97.8	1523.20 ±11.0	+96.1	2098.00±29.0	+83.5
CSCNT/CF/epoxy nanocomposite	5	6	1843.20±25.0	+179.4	2148.60±43.0	+189.2	2227.00±46.0	+186.7	2866.60±24.0	+150.7
Hybrid GNP-CSCNT/CF/epoxy nanocomposite	5	4	1683.90±26.0	+155.2	2016.20±21.0	+171.4	2086.60±24.0	+168.7	2655.20±29.0	+132.3

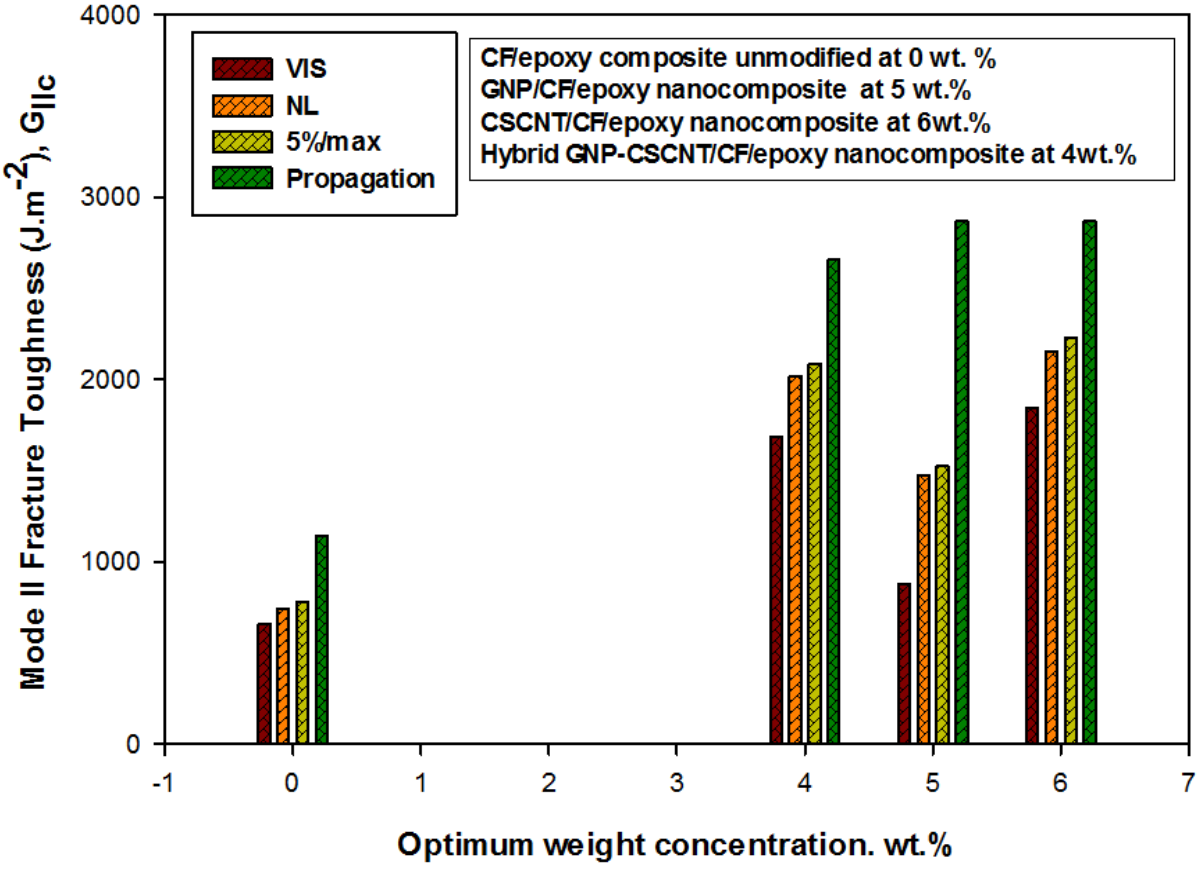

Figure 107 The evaluation of initial and propagation fracture toughness energy among three types of HCFRP in comparison with CF/epoxy composite unmodified.

The addition of fibre nanotubes to the epoxy matrix enhances the performance of fibre composites, which confirms its superiority in comparison to other carbon nanomaterials. Furthermore, there was high increase in the toughness property after the combination of fibre nanotubes and graphene which was greater than that of the carbon fibre reinforced by graphene only. This shows that mixing the fibre nanotubes with graphene shows good functionality to promote the mechanical properties of fibre composites through their positive synergetic property in the matrix.

However, the SEM in Figure 107 demonstrate the hybrid failure mechanism in the fracture area of hybrid GNP-CSCNT/CF/epoxy nanocomposites. The images revealed the same dissipation energy systems that were seen in Mode I hybrid failure mechanisms. Extra toughening mechanisms of the hybrid nanofillers that are responsible for the significant increase in fracture toughness energy involve pinning of the crack and bi-furcation, bridging and pull-out of fillers, in addition to debonding shear. The images prove the existence of both carbon nanomaterials within the polymer matrix. Multiple types of fracture mechanisms are detected on the surface morphology which prove the synergetic influence of graphene and novel fibre nanotubes. More

precisely, the bi-furcation mechanism was seen in the fractured area. Furthermore, the existence of fibre nanotubes in the resin resist the extension of the crack, whilst the GNP prevent the creation of huge cracks as much as possible. Hence, under their combination, the fracture toughness energy of hybrid composites is improved.

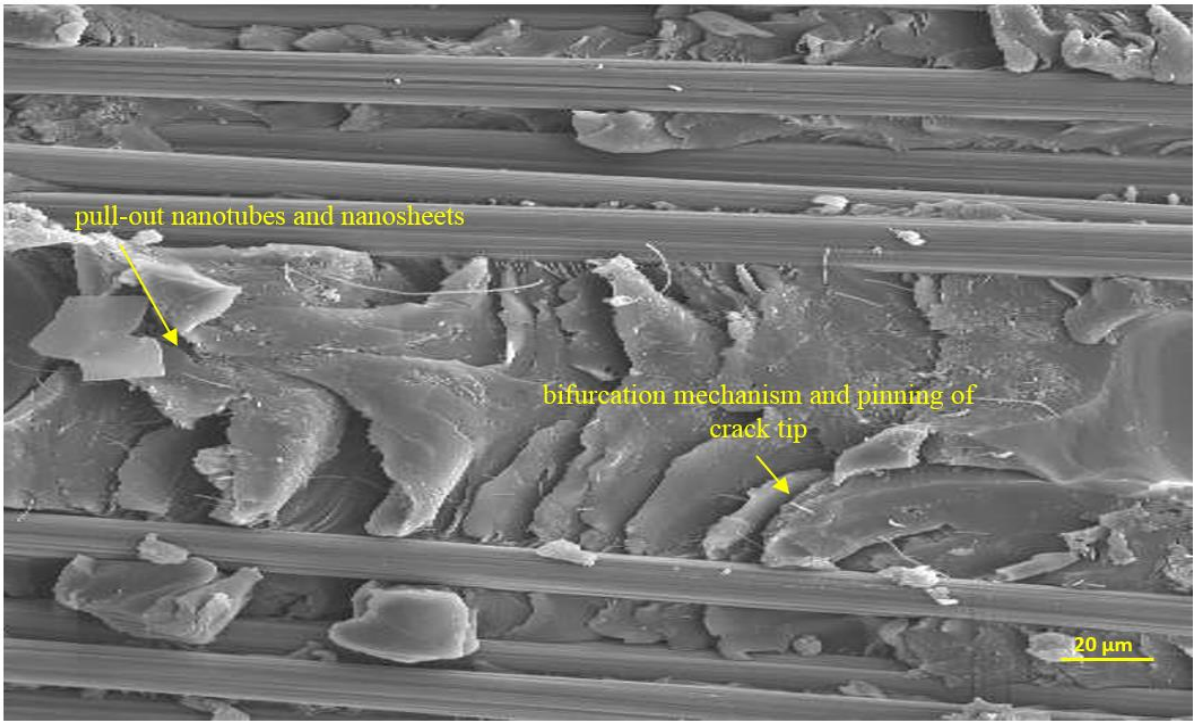

Figure 108 The SEM image showing the hybrid failure mechanisms [1000x].

Chapter 7. Conclusion and outlook

This chapter reveals the summary of the experimental results and discussion from chapter 5. The common trends presented by the NP and the HCFRP in the strength, stiffness and toughness are highlighted. Suggestions for potential future work are shown in line with the reported results.

7.1 Concluding remarks

Three types of NP with the following formulations; GNP/epoxy nanocomposites, CSCNT/epoxy nanocomposites and hybrid GNP-CSCNT/epoxy nanocomposites were successfully prepared and optimised by using the mechanical dispersion techniques (i.e. combination of sonication and ball milling technique). Moreover, these NP containing GNP and CSCNT in a thermosetting resin system have been promoted by the novel combination of these multifunctional carbon nanomaterials into the matrix in this study.

Multiple mechanical properties were investigated with regard to the influence of these multifunctional carbon nanomaterials on the strength, stiffness and toughness properties of the epoxy resin. The optimum mechanical properties of the novel HNP was achieved after using the combined dispersive techniques, where the hybrid GNP-CSCNT/epoxy nanocomposites showed the highest improvement in flexural strength and flexural modulus by approximately 40% and 61% respectively at 4 wt.%. In addition to a significant improvement in toughness property by 85% at the same weight concentration. This significant influence shows the significant synergetic behaviour resulting from the combination of graphene and novel fibre nanotubes within the matrix. The CSCNT/epoxy nanocomposites showed improvements in the flexural strength, flexural modulus and toughness properties by approximately 29%, 32% and 117% respectively at 6 wt.%, whilst the GNP/epoxy nanocomposites observed only 17%, 11% and 52% respectively at 5 wt.%. As a consequence, the CSCNT are more efficient for the reinforcement of the strength, stiffness and toughness properties of the epoxy resin in comparison with the GNP. This is perhaps attributable to the premium geometric structure of the CSCNT in comparison with the GNP which have weak structures. In addition, the dispersion process of the CSCNT in the resin was easier than that of GNP.

Subsequently, the effect of the optimum strength and toughness properties of the modified matrix in each one of these novel NP on the mechanical properties of CFRP were also investigated in this study. This included investigating the interlaminar shear strength properties, flexural strength properties, and Mode I and Mode II fracture toughness properties.

The optimum strengthened and toughened matrices for these NP improved these mechanical properties for three types of HCFRP produced; specifically, GNP/CF/epoxy nanocomposites, CSCNT/CF/epoxy nanocomposites and hybrid GNP-CSCNT/CF/epoxy nanocomposites. The addition of the CSCNT and GNP to the fibre composites improved the shear property by 38% and 31% respectively, flexural strength by 25% and 20% respectively, and the flexural modulus by 23% and 27% respectively. In addition to significant improvements in interlaminar fracture toughness (Mode I) by 104% and 15% respectively and (Mode II) by 151% and 84% respectively. Consequently, the novel fibre nanotubes were also more superior in improving most of these mechanical properties, whereas the graphene displayed less improvement in Mode I and Mode II interlaminar fracture toughness.

The novel combination of GNP and CSCNT in the matrix contributes to improving the mechanical interfacial properties of carbon fibre composites. Hence, this led to an improvement in flexural strength and flexural modulus by 18% and 28% respectively, interlaminar shear strength by 37% and Mode I and Mode II fracture toughness properties by 73% and 132% respectively. These improvements were better in comparison to individual graphene reinforced carbon fibre polymer composites (GNP/CF/epoxy nanocomposites). The synergetic influence of these multifunctional carbon nanomaterials within the matrix led to the introduction of further strengthening/toughening mechanisms, such as the combination of the fracture mechanism systems, the pull-out and bridging of the nanofillers, bi-furcation mechanisms and the pinning of the crack head. Hence, this is probably responsible for the enhanced mechanical properties of the HCFRP.

In conclusion, this study illustrates that the inclusion of novel CSCNT is better than GNP in improving the mechanical properties of polymer composites. In addition, the inclusion of the combined multifunctional carbon nanomaterials; GNP and novel CSCNT is beneficial in enhancing the strength, stiffness and fracture toughness over the parent HNP and HCFRP. Furthermore, in comparison to the inclusion of the carbon nanomaterials, the mechanical properties improvements from the inclusion of the combination of GNP and novel CSCNT is expected to be non-deleterious to the pristine mechanical properties of epoxy resin and in plane properties of the fibre composites. Moreover, this multifunctionality formula is expected to be more efficient in reinforcing the mechanical properties of the polymer composites than conventional carbon nanotubes. Additionally, the optimum modified matrix with combined carbon nanomaterials in the fibre composites was illustrated to be a viable route in developing the fracture surface morphology to accomplish better fracture mechanisms in comparison to that of the modified matrix with individual carbon nanomaterial.

7.2 Recommendation for future work

7.2.1 Manufacturing process

The quality of the manufacturing methods of hybrid fibre laminate composites can be developed via the use of advanced methods to reduce the defects and voids. Thus, any reduction in these problems should significantly increase the carbon fibre dominated properties, such as tensile, stiffness and flexural strength (Kalantari et al., 2017; Sutcliffe et al., 2012).

7.2.2 Optimisation of HNP

A further experimental study changing the proportional weight content or the ratio of hybrid nanofillers (graphene and fibre nanotubes) could shed more light on the influence of hybrid content ratio on the strength, stiffness and toughness properties of the composites.

7.2.3 Mechanical characterisations

Further characterisation could be employed to discover the influence of hybrid nanofillers, graphene and fibre nanotubes on the wear resistance of nanocomposites, where this property was expected to improve after adding these carbon nanomaterials to the polymer matrix (Barrena et al., 2014; Shen et al., 2014).

Additional important characteristics can be measured to explore the influence of the carbon nanomaterials inclusion on the in plane compression property of the fibre composites, where this property was expected to benefit from the inclusion of graphene, fibre nanotubes and a combination of them (Kamar et al., 2015; Yokozeki et al., 2007).

Beyond static loading, other properties such as fatigue resistance could also disclose the dynamic loading. It is well known that traditional fibre reinforced composites primarily possess good fatigue properties (Liao et al., 1998). However, the inclusion of carbon nanomaterials is often expected to modify the dynamic performance level of fibre composites and nanocomposites (Fenner and Daniel, 2014; Shen et al., 2013). Although, the inclusion of carbon nanomaterials could actually promote the topical stress concentration that could cause failures. Damage resistance (after damage has started) under dynamic loading is frequently weak, consequently the carbon nanomaterials (i.e. graphene, novel fibre nanotubes and conventional carbon nanotubes) and a combination of them could be engineered to address this mechanical performance.

7.2.4 Physical characterisations

Thermal and electrical conductivity would be anticipated to improve after the addition of graphene, fibre nanotubes and hybrid GNP-CSCNT nanofillers to the polymer with successful dispersion. Excellent impregnation and homogenous distribution of the nanofilled matrix onto the fibre surface (Moosa et al., 2016; Al-Saleh, 2016; Bal, 2010; Bose, 2017).

Further influence on the physical properties includes chemical resistance and moisture absorption which can be studied to confirm the inclusion of graphene, fibre nanotubes and a combination of them and it could be beneficial to compare them with the parent composites.

7.2.5 Finite element modelling and analytical simulation

The experimental results can be predicted through finite element modelling. The finite element modelling could be applied to predict the inhomogeneous distribution of the nanofilled matrix onto the fibre networks (i.e. rich and poor regions with nanofilled matrix) and the orientation of fillers and defects (i.e. voids) (Hadden et al., 2015; Dong, 2016).

To understand the synergetic effect of hybrid nanofillers (graphene and fibre nanotubes) in enhancing the interfacial mechanical properties of the epoxy polymer composites, molecular dynamics simulation can be used (Liu et al., 2017).

References

Abdullah, S.I. and Ansari. (2015) “Mechanical properties of graphene oxide (GO)/epoxy composites”, HBRC Journal 11, pp.151-156.

Ajayan, P.M, Schadler, L.S, and Braun, P.V. (2003) “Nanocomposite science and technology”. Weinheim, Wiley-VCH, pp.77–80.

Al-Saleh, M.H. (2016) “Electrical, EMI shielding and tensile properties of PP/PE blends filled with GNP: CNT hybrid nanofiller”, Synthetic Metal, 217, pp.322-330.

An, Q., Rider, A.N., and Thostenson, E.T. (2012). “Electrophoretic deposition of carbon nanotubes onto carbon-fiber fabric for production of carbon/epoxy composites with improved mechanical properties”, Carbon, 50 (11), pp.4130-4143.

Arshad, S.N, Naraghi, M., and Chasiotis, .I. (2011) “Strong carbon nanofibers from electrospun polyacrylonitrile”, Carbon, 49, pp.1710-1719.

Ashrafi, B., et al., (2011) “Enhancement of mechanical performance of epoxy/carbon fiber laminate composites using single-walled carbon nanotubes”, Composites Science and Technology, 71(13), pp.1569-1578.

Ávila-Orta, C.A., Cruz-Delgado, V.J., Neira-Velázquez, M.G., et al. (2009) “Surface modification of carbon nanotubes with ethylene glycol plasma”, Carbon, 47, pp.1916–1921.

Ayatollahi, M.R., Shadlou, S., Shokrieh, M.M., and Chitsazzadeh, M. (2011) “Effect of multi-walled carbon nanotube aspect ratio on mechanical and electrical properties of epoxy-based nanocomposites”, Polymer testing, 30, pp.548-556.

Bal, S. (2010) “Experimental study of mechanical and electrical properties of carbon nanofiber/epoxy composites”, Materials and Design, 31, pp.2406-2413.

Bal, S., and Saha, S. (2014) “Assesment of electrical and mechanical properties of carbon nanomaterial doped polymer composites”, 978-1-4799-2206-2l14/$31.00©2014 IEEE.

Barrena, M.I., Salazar, J.M., Soria, A., and Canas, R. (2014) “Improved of the wear resistance of carbon nanofiber/epoxy nanocomposite by a surface functionalization of the reinforcement, Applied surface science, 289, pp.124-128.

Bekyarova, E., et al. (2007) “Multiscale carbon nanotube-carbon fiber reinforcement for advanced epoxy composites”, Langmuir, 23(7), pp.3970-3974.

Bethune, D.S., Klang, C.H., De Vries, M.S., et al. (1993) “Cobalt-catalysed growth of carbon nanotubes with single-atomic-layer walls”, Nature, 363, pp.605–607.

Bhattacharya, M. (2016) “Review: Polymer Nanocomposites-A comparison between carbon nanotubes, graphene, and clay as nanofillers”, Materials, 9, 262, doi:10.3390/ma9040262.

Bianchi, F., Koh, T.M., Zhang, X, et al. (2012) “Fininte element modelling of z-pinned composite T-joints“, Composites Science and Technology, 73, pp.48-56.

Bose, S., Basu, S., Das, A., Rahman, M. and Drzal, L. T. (2017) “Fabrication of a sulfonated aramid-graphene nanoplatelet composite paper and its performance as a supercapacitor electrode” J. Appl. Polym. Sci, 134, 45099. doi: 10.1002/app.45099.

Bradley, W.L., and Cohen, R.N. (1985) “Matrix deformation and fracture in graphite reinforced epoxies”, American Society for Testing and Materials.

Breuer, O., and Sundararaj, U. (2004) “Big returns from small fibers: a review of polymer/carbon nanotube composites”, Polym Compos, 25, pp.630–645.

Chan, W.S. (1991) “Design approaches for edge delamination resistance in laminated composites”, Journal of Composites Technology & Research, 14(2), pp. 91-96.

Chandrasekaran, S., Sato, N., Tolle, F. et al. (2014) “Fracture toughness and failure mechanism of graphene based epoxy composites”. Composites Science and Technology, 97, pp.90-99.

Chandrasekaran, S., Seidel, C., and Schulte, K. (2013) “Preparation and characterization of graphite nano-platelet (GNP)/epoxy nano-composite: Mechanical, electrical and thermal properties” European Polymer Journal, 49, pp.3878-3888.

Chatterjee, S., Nafezarefi, F., Tai, N.H., Schlagenhauf, L., Naesch, F.A., and Chu, B.T.T. (2012) “Sized and synergy effects on nanofiller hybrids including graphene nanoplatelets and carbon nanotubes in mechanical properties of epoxy composites” Carbon, 50, pp.5380-5386.

Chen, B., Li, S., Imai, H., Jia, L., Umeda, J., Takahashi, M., and Kondoh, K. (2015) “An approach for homogenous carbon nanotube dispersion in Al matrix composite”, Materials and Design, 72, pp.1-8.

Chen, L., Ifju, P.G, and Sankar, B.V. (2001) “A novel double cantilever beam test for stiched composite laminates”. J Compos Mater, 35(13), pp.1137-1149.

Chen, R.J., Zhan, Y.G., Wang, D.W, and Dai, H.J. (2001) “Noncovalent sidewall functionalization of singlewalled carbon nanotubes for protein immobilization”, J Am Chem Soc, 123(16), pp.3838–3849.

Cho, J., and Daniel, I.M. (2008) “Reinforcement of carbon/epoxy composites with multi-wall carbon nanotubes and dispersion enhancing block copolymers”. Scripta Materialia, 58, pp.533-536.

Cho, J., Luo, J.J., and Dan, I.M. (2007), “Mechanical characterization of graphite/epoxy nanocomposites by multi-scale analysis”, Composite science and technology, 67, pp.2399-2407.

Choi, Y.K., Gotoh, Y., Sugimoto, K., Song, S.M., Yanagisawa, T., and Endo, M. (2005). "Processing and characterization of epoxy nanocomposites reinforced by cup-stacked carbon nanotubes".,Polymer 46, pp.11489-11498.

Chou, I. (1998) "Effect of fiber orientation and moisture absorption on the interlaminar fracture toughness of CFRP laminates", Advanced Composite Materials, 7(4), pp.377-394.

Chua, C.K., and Pumera, M. (2013) "Covalent chemistry on graphene", Chem Soc Rev, 42, pp.3222–3233.

Coleman, J.N., Khan, U., and Gunko, Y.K. (2006) "Mechanical reinforcement of polymers using carbon nanotubes", Adv Mater, 18: pp.689–706.

Collins, P.G., and Avouris, P. (2000) "Nanotubes for electronics", Scient Am, 283(6), pp.62-69.

Costa, P., Pereira-Nunes, J., Oliverira, J., et al. (2017) "High-performance graphene-based carbon nanofiller/polymer composites for piezoresistive sensor applications", Composites Science and Technology, 153, pp.241-252.

Crews, J., Shivakumar, K., and Raju, I. (1988) "Factors influencing elastic stresses in double cantilever beam specimens", American Society for Testing and Materials.

Criado, A., Melchionna, M., Marchesan, S., and Prato, M. (2015) "The Covalent Functionalization of Graphene on Substrates", Angew Chem Int Ed, 54, pp.10734-10750.

Curtin, W.A., and Sheldon, B.W. (2004) "CNT-reinforced ceramics and metals", Mater Today, 7(11), pp.44-49.

David, M., Pavan, A., and Williams, J.G., (2001) "Fracture mechanics testing methods for polymers, adhesives, and composites", ESIS Publication 28, pages 375.

Davies, P., Blackman, B.R.K., and Brunner, A.J. (1998) "Standard test methods for delamination resistance of composite materials: Current status", Applied Composite Materials, 5, pp.345-364.

Davis, D.C., and Whelan, B.D. (2011) "An experimental study of interlaminar shear fracture toughness of a nanotube reinforced composite", Composites, Part B 42, pp.105-116.

Djabali, A., Toubal, L., Zitoune., R., and Rechak, S. (2018) "An experimental investigation of mechanical behaviour and damage of thick laminated carbon/epoxy composite", Composite structures, 184, pp.178-190.

Domun, N., Hadavinia, H., Zhang, T., Sainbury, T., Liaghat, G.H, and Vahid, S. (2015) "Improving the fracture toughness and the strength of epoxy using nanomaterials-a review of the current status", Royal Society of Chemistry, Nanoscale, 7, pp.10294-10329

Dong, C. (2016) "Effects of Process-Induced Voids on the Properties of Fibre Reinforced Composites", Journal of Materials Science & Technology 32, pp.597-604.

Dresselhaus, MS., Dresselhaus, G., and Saito, R. (1995) “Physics of carbon nanotubes”, Carbon, 33, pp.883-891.

Du, X., et al. (2014) “Flame synthesis of carbon nanotubes onto carbon fiber woven fabric and improvement of interlaminar toughness of composite laminates”, Composites Science and Technology, 101(0), pp.159-166.

Du, X., Zhuo, H., Sun, W., et al. (2017) “Graphene/epoxy interleaves for delamination toughening and monitoring of crack damage in carbon fibre/epoxy composite laminates”, Composites Science and Technology, 140, pp.123-133.

Endo M, Kim YA, Ezaka M, Osada K, Yanagisawa T, Hayashi T, et al. (2003) “Selective and efficient impregnation of metal nanoparticles on cup-stacked-type carbon nanofibers”, Nano Letters, 3(6):723-726.

Endo, M., Kim, Y.A., Hayashi, T., Fuka,i Y., Oshida, K., Terrones, M., et al. (2002) “Structural characterization of cup-stacked-type nanofibers with an entirely hollow core”, Appl Phys Lett, 80(7), pp.1267–1269.

Esumi, K., Ishigami, M., Nakajima, A., et al. (1996) “Chemical treatment of carbon nanotubes”, Carbon, 34, pp.279-281.

Fan, Z.H., Santare, M.H. and Advani, S.G. (2008) “Interlaminar shear strength of glass fiber reinforced epoxy composites enhanced with multi-walled carbon nanotubes”, Composites Part A, Applied Science and Manufacturing, 39(3), pp.540-554.

Fang, M., Wang, K., Lu, H., et al. (2010) “Single-layer graphene nanosheets with controlled grafting of polymer chains”, J Mater Chem, 20, pp.1982-1992.

Feng L, Xie N, Zhong J. (2014) “Carbon nanofibers and their composites: A review of synthesizing, properties and applications”, Materials, 7, pp.3919-3945.

Fenner, J.S., and Daniel, I.M. (2014) “Hybrid nanoreinforced carbon/epoxy composites for enhanced damage tolerance and fatigue life”, Composites: Part A 65, pp.47-56.

Finegan, I.C., Tibbetts, G.G., and Gibson, R.F. (2003) “Modeling and characterization of damping in carbon nanofiber/polypropylene composites”, Compos Sci Technol, 63(11), pp.1629-1635.

Frogley, M.D., Ravich, D., and Wagner, H.D. (2003) “Mechanical properties of carbon nanoparticle-reinforced elastomers”, Compos Sci Technol, 63(11), pp.1647-1654.

Gamstedt, E.K., and Sjogren, B.A. (1999) “Micromechanisms in tension-compression fatique of composite laminates containing transverse plies”, Comps Sci Technol,59(2), pp.167-178.

Geim, A.K., and Novoselov, K. S. (2007) “The rise of graphene”, Nat Mater, 6, pp.183-191.

Geng, Y., Liu, M.Y, Li, J., Shi, X.M., and Kim, J.K. (2008) “Effects of surfactant treatment on mechanical and electrical properties of CNT/epoxy nanocomposites”, Composites Part A, 39, pp.1876-1883.

Gill, A.F., Robinson, P., and Pinho, S. (2009) “Effect of variation in fibre volume fraction on modes I and II delamination behaviour of 5HS woven-composites manufactured by RTM”, Composites science and technology, 69, pp.2368-2375.

Gkika, D.A, Vordos, N., Nolan, J.W et al. (2017) “Price tag in nanomaterials?”, J Nanopart Res,19, pp.177.

Gkikas, G., Barkoula, N.M., and Paipetis, A.S. (2012) “Effect of dispersion conditions on the thermos-mechanical and toughness properties of multi-walled carbon nanotubes-reinforced epoxy”, Composites, Part B, 43, pp.2697-2705.

Glover, B.M. (2004) “History of development of commercial aircraft and 7E7 dreamliner”, Aviat Eng, 592, pp.16-21.

Godara, A., Mezzo, L., Luizi, F. et al. (2009) “Influence of carbon nanotube reinforcement on the processing and the mechanical behaviour of carbon fiber/epoxy composites”, Carbon, 47, pp.2914-2923.

Gojny, F.H., et al. (2005) “Influence of nano-modification on the mechanical and electrical properties of conventional fibre-reinforced composites”, Composites Part A, Applied Science and Manufacturing, 36(11), pp.1525-1535.

Gojny, F.H.,Wichmann, M.H.G., Fiedler, B., and Schulte, K. (2005) “Influence of different carbon nanotubes on the mechanical properties of epoxy matrix composites – A comparative study”, Composites Science and Technology, Vol. 65(15), pp.2300-2313.

Gong, J., Feng, J., Liu, J., Jiang, Z., Chen, X., Mijowska, E., Wen, X., and Tang, T. (2014) “Catalytic carbonization of polypropylene into cup-stacked carbon nanotubes with high performances in adsorption of heavy metallic ions andorganic dyes”, Chemical engineering journal, 248, pp.27-40.

Greef, N.D, Gorbatikh, L., Godara, A., Mezzo, L., Lomov, S.V, and Verpoest, I. (2011) “The effect of carbon nanotubes on the damage development in carbon fibre/epoxy composites”, Carbon, 49(14), pp.4650-4664.

Green, K. J., Dean, D.R., Vaidya, U.K., and Nyairo, E. (2009) “Multiscale fiber reinforced composites based on a carbon nanofiber/epoxy nanophased polymer matrix: Synthesis, mechanical, and thermomechanical behaviour”, Composites Part A: Applied Science and Manufacturing, 40(9), pp.1470-1475.

Greenhalgh, E. (2009) “Failure analysis and fractography of polymer composites”, 1st ed., Cambridge: Woodhead Publishing Ltd.

Greenhalgh, E., and Hiley, M. (2003) “The assessment of novel materials and processes for the impact tolerant design of stiffened composite aerospace structures”, Composites Part A: Applied Science and Manufacturing, 34(2), pp.151-161.

Greenhalgh, E., Lewis, A., Bowen, R., and Grassi, M. (2006) “Evaluation of toughening concepts at structural features in CFRP - Part I: Stiffener pull-off”, Composites Part A: Applied Science and Manufacturing, 37(10), pp.1521-1535.

Griffith A. A., (1920) “The phenomena of rupture and flow in solids”. Proceeding of Royal Sociaty London, A221, pp.163-198.

Guo, W. and Chen, G. (2014) “Fabrication of Graphene/Epoxy Resin Composites with Much Enhanced Thermal Conductivity via Ball Milling Technique”, J. APPL POLYM. SCI. DOI: 10.1002/APP. 40565.

Hadden, C.M., Mc Donald, K.D.R., and Pineda, E.J. (2015) “Mechanical properties of graphene nanoplatelet/carbon fibre/epoxy hybrid composites: multiscale modelling and experiments”, 20th international conference on composite Materials, Denmark, NASA/TM-2015-218731.

Herakovich, C.T. (1989) “Failure modes and damage accumulation in laminated composites with free edge”, Composites Science and Technology, 36, pp.105-119.

Hernández-Pérez, A., Avilés, F., May-Pat, A., Valadez-González, A., Herrera-Franco, P.J., Bartolo-Pérez, P. (2008) “Effective properties of multiwalled carbon nanotube/ epoxy composites using two different tubes”, Compos Sci Technol, 68, pp.1422–14231.

Hirsch A. (2002) “Functionalization of single-walled carbon nanotubes”, Angew Chem Int Ed, 41, pp.1853-1859.

Hu, K., Kulkarni, D.D., Choi, I., and Tsukruk, V.V. (2014) “Graphene-polymer nanocomposites for structural functional applications”, Prog. Polym.Sci, 39, 1934-1972.

Hua, Y., Li, F., Liu, Y., Huang, G.W., Xiao, H.M., Li, Y.Q., Hu, N., and Fu, S.Y. (2017) “Positive synergetic effect of graphene oxide/carbon nanotube hybrid coating on glass fiber/epoxy interfacial normal bond strength”, Composites Science and Technology 149, pp.294-304.

Hunston, D.L., and Bascom, W.D. (1983) “Effects of lay-up, temperature, and loading rate in double cantilever beam tests of interlaminar crack growth”, Composites Technology Review, 5 (Winter), pp.118-119.

Hwang, J.H., Lee, C.S., and Hwang, W. (2001) “Effect of crack propagation directions on the interlaminar fracture toughness of carbon/epoxy composite materials”, Applied Composite Materials 8, pp.411-433

Inkyo M, Tokunaga Y, Tahara T et al., (2008) “Beads mill-assisted synthesis of poly Methyl Methacrylate (PMMA)-TiO2 nanoparticle composites”. Ind,Eng.Chem. 47, pp.2597-2604.

Irwin G.R. (1964) “Crack-toughness testing of strain-rate sensitive materials. Journal of engineering for power”, Transaction of the ASME Series A, No.86, pp.444.

Iwahori, Y., Ishiwata, S., Sumizawa, T., and Ishikawa, T. (2005) “Mechanical property improvements in two-phase and three-phase composites using carbon nano-fiber dispersed resin”, Composites: Part A 36, pp.1430-1439.

Jang, B.Z., Liau, J.Y., Hawng, L.R., Shih, W.K., (1990), “Particulate and whisker modifications of matrix resin for improved toughness of fibrous composites”, Journal of Reinforced Plastic and Composites, 9(July), pp.314-334.

Jeon, S.K., Jang, H.S., Kwon, O.H., and Nahm, S.H. (2016) “Mechanical test method and properties of a carbon nanomaterial with a high aspect ratio”, Springer, Nano Convergence, Vol.3(1), pp.29.

Ji, L., Rao, M., Aloni S., Wang, L., Cairns, E., and Zhang, Y.J.L., (2011) “Porous carbon nanofiber-sulfur composite electrodes for lithium/sulphur cells”, Energy and Environmental Science, Vol.4(12), pp. 5053-5059.

Ji, X., Xu, Y., Zhang, W., Cui, L., and Liu, J. (2016) “Review of functionalization, structure and properties of graphene/polymer composite fibers”, Composites Part A, Vol.87, pp.29-45.

Ji, X., Xu, Y., Zhang, W., Cui, L., and Liu, J. (2L016) “Review of functionalization, structure and properties of graphene/ polymer composite fibres”, Composites: Part A 87, pp.29-45.

Jia, J., Du, X., Chen, C., Sun, X., Mai, Y.W., and Kim, J.K. (2015) “3D network graphene interlayer for excellent toughness and strength in fiber reinforced composites”, Carbon 95, pp.978-986.

Joshi, S.C., and Dikshit, V. (2012) “Enhancing interlaminar fracture characteristics of woven CFRP prepreg composites through CNT dispersion”, Journal of Composite Materials, 46(6), pp.665-675.

Kalantari, M., Dong, C., and Davies I.J. (2017) “Effect of matrix voids, fibre misalignment and thickness variation on multi-objective robust optimization of carbon/glass fibre-reinforced hybrid composites under flexural loading”, Composites Part B 123, pp.136-147.

Kamar, N.T., Hossain, M.M., Khomenko A, Haq, M., Drzal, L.T., and Loos, A. (2015) “Interlaminar reinforcement of glass fibre/epoxy composites with graphene nanoplatelets”, Composites: Part A 70, pp.82-92.

Kandare, E., Khatibi, A.A., Yoo, S., Wang, R., Ma, J., Olivier, P., Gleizes, N., and Wang, C.H. (2015) “Improving the through-thickness thermal and electrical conductivity of carbon

fibre/epoxy laminates by exploiting synergy between graphene and silver nano-inclusions", Composites Part A, Vol.69, pp.72-82.

Karapappas, P.,Vavouliotis, A., Tsotra, P., Kostopoulos, V., and Paipetis, A. (2009) "Enhanced fracture properties of carbon reinforced composites by the addition of multi-wall carbon nanotubes", Journal of Composite Materials, Vol.43(9), pp.977-985.

Kawasetsu, N., Shindo, K., Takita, K., and Kato, E., "Behaviour of resin flow during VaRTM process for FRP structure", Procedure of 12th The Japan Society of Mechanical Engineering Materials and Processing, (2004), pp.137-138.

Kepple, K.L., Sanborn, G.P., Lacasse, P.A., Gruenberg, K.M., and Ready, W.J. (2008) "Improved fracture toughness of carbon fiber composite functionalized with multi walled carbon nanotubes", Carbon, 46(15), pp. 2026-2033.

Khan, S.U., and Kim J.K. (2012) "Improved interlaminar shear properties of multiscale carbon fiber composites with bucky paper interleaves made from carbon nanofibers", Carbon 50, pp.5265-6277.

Kim, H., Jalili, R., Spinks, G.M., and Wallace G.G. (2017) "High-strength graphene and polyacrylonitrile composite fiber enhanced by surface coating with polydopamine", Composites science and technology,149, pp.280-285.

Kim, J., Baillie, C., Poh, J., Mai, Y.W., (1992), "Fracture toughness of CFRP with modified epoxy resin matrices", Composites Science and Technology, 43, pp.283-297.

Kim, J.K., and Mai, Y.W. (1998) "Engineered interfaces in fiber reinforced composites". Oxford: Elsevier, pp.1-100.

Kim, YA., Hayashi, T., Fukai, Y., Endo, M., Yanagisawa, T., and Dresselhaus, M.S. (2002) "Effect of ball milling on morphology of cup- stacked carbon nanotubes", Chem Phys Lett,355, pp.279-284.

Konya, Z., Zhu, J., Niesz, K., Mehn D, and Kiricsi, I. (2004) "End morphology of ball milled carbon nanotubes", Carbon 42, pp. 2001-2008.

Koo, J.H., (2006) "Polymer nanocomposites: processing, characterization, and applications", Science, pages 272.

Kostagiannakopoulou, C., Loutas, T.H., Sotriadis, G., Markou, A., and Kostopoulos, V. (2015) "On the interlaminar fracture toughness of carbon fiber composites enhanced with graphene nano-species", Composites Science andTechnology 118, pp.217-225.

Kostagiannakopoulou, C., Tsilimigkra, X., Sotiriadis, G., and Kostopoulos, V. (2017) "Synergy effect of carbon nano-fillers on the fracture toughness of structural composites" Composites Part B 129, pp.18-25.

Krishnan, A., Dujardin, E., Ebbesen, T.W., Yianilos, P.N., and Treacy, M.M.J. (1998) "Young's modulus of single-walled nanotubes", Phys Rev B,58(20), pp.14013-14019.

Kumar, A., and Roy, S. (2018) "Characterization of mixed mode fracture properties of nanographene reinforced epoxy and Mode I delamination of its carbon fiber", Composites Part B 134, pp.98-105.

Kundalwal, S.I., and Kumar, S. (2016) "Multiscale modelling of stress transfer in continuous microscale fiber reinforced composites with nano-engineered interphase", Mechanics of Materials, 102, pp.117–131.

Kuwata, M., and Hogg, P.J. (2011) "Interlaminar toughness of interleaved CFRP using non-woven veils: Part 2. Mode-II testing", Composites: Part A 42, pp.1560-1570.

Kuwata, M., and Hogg, P.J. (2011) "Interlaminar toughness of interleaved CFRP using non-woven veils: Part 1. Mode-I testing", Composites Part A: Applied Science and Manufacturing, Vol. 42, No.10, pp.1551-1559.

Landani, R.B., Wu, S., Kinloch, J.A., Ghorbani, K., Zhang, J., Mouitz, A.P., and Wang C.H. (2015) "Improving the toughness and electrical conductivity of epoxy nanocomposites by using aligned carbon nanofibers", Composites Science and Technology 117, pp.146-158.

Layek, and Nandi, A.K. (2013) "A review on synthesis and properties of polymer functionalized graphene" Polymer 54, pp.5087-5103.

Lee, C., Wei, X., Li, Q., Carpick, R., Kysar, J.W., and Hone, J. (2009) "Elastic and frictional properties of graphene", Phys. Status Solidi B 246, No. 11–12, pp.2562-2567.

Lee, C., Wei, X.D., Kysar, J.W., and Hone J., (2008) "Measurement of the Elastic Properties and Intrinsic strength of Monolayer Graphene", Science 321, pp.3385-3888.

Lee, J.K., Song, S., and Kim, B. (2012) "Functionalized graphene sheets-epoxy based nanocomposite for cryotank composite application", Polymer composites, Vol.33 (8), pp.1263-1273.

Lee, S.M. (1992) "Influence of fiber/matrix interfacial adhesion on composite fracture behavior", Composites Science and Technology, 43, pp.317-327.

Lenzi, F., Riccio, A., Clarke, A., and Creemers, R. (2007) "Coupon tests on z-pinned and unpinned composite samples for damage resistant application", Macromol Sympos Times Polym Compos, 27(1), pp.230-237.

Li Y, Zhang H, Huang Z,2 Bilotti E., and Peijs, T.B.S. (2017) "Graphite Nanoplatelet Modified Epoxy Resin for Carbon Fibre Reinforced Plastics with Enhanced Properties", Journal of Nanomaterials Volume, Vol 2017, pp.10.

Li, C.Y., and Chou, T.W. (2003) “A structural mechanics approach for the analysis of carbon nanotubes”. Int J Solids Struct, 40, pp.2487–2499.

Li, C.Y., and Chou, T.W. (2003) “Elastic moduli of multi-walled carbon nanotubes and the effect of van der Waals forces”, Compos Sci Technol, 63, pp.1517.

Li, J., Ma, P.C., Chow, W.S., To, C.K., Tang, B.Z., and Kim, J.K. (2007) “Correlations between percolation threshold, dispersion state and aspect ratio of carbon nanotube”, Adv Funct Mater,17, pp.3207-3215.

Li, J., Wong, P.S., and Kim, J.K. (2008) “Hybrid nanocomposites containing carbon nanotubes and graphite nanoplatelets, Mater Sci Eng A, 483–484, pp.660-663.

Li, M., Gue, Y., Li, Y., Zhang, Z. (2013) “Interfacial improvement of carbon fibre/epoxy composites using a simple process for depositing commercially functionlized carbon nanotubes on the fibres, Carbon, 52, pp.109-121.

Li, W., Dichiara, A., and Bai, J. (2013) “Carbon nanotube-graphene nanoplatelet hybrid as high-performance multifunctional reinforcements in epoxy composites”, Composites Science and Technology, 74, pp.221-227.

Li, W.,Dichiara, A., Zha, J., Su, Z., and Bai, J. (2014) “On improvement of mechanical and thermo-mechanical properties of glass fabric/epoxy composites by incorporating CNT–Al_2O_3 hybrids”, Composites Science and Technology, 103(0), pp.36-43.

Li, Y., Wang, S., Wang, Q., and Xing, M. (2018) “A comparison study on mechanical properties of polymer composites reinforced by carbon nanotubes and graphene sheet”, Composites Part B 133, pp.35-41.

Li, Y., Zhao, Y., Sun, J., Hao, Y., Zhang, J., and Han, X. (2016) “Mechanical and Electromagnetic Interference Shielding Properties of Carbon Fiber/Graphene Nanosheets/Epoxy composite”, Polymer Composites, Vol. 37(8), pp.2494-2502

Liang, Y., Ozawa, M., and Krueger, M. (2009) “A general procedure to functionalize agglomerating nanoparticles demonstrated on nanodiamond”, ACSNANO 3 (8) , pp.2288-2296.

Liao, K., et al., (1998) “Long-term durability of fiber-reinforced polymer-matrix composite materials for infrastructure applications: A review”, Journal of Advanced Materials, 30(4): pp. 30-40.

Lin, J., Zhang, H., Tang, M., Tu, W., and Zhang, X. (2015) “Improved thermal property of a multi-layered graphite nanoplatelets filled silicone resin composite”, JMEPEG 24, pp.920-929.

Lin, Q., Qu, L., Lu, Q., and Fang, C. (2013) “Preparation and properties of graphene oxide nanosheets/ cyanate ester resin composites”. Polymer Testing 32, pp.330-337.

Liu F, Hu N, Ning H., Atobe, S., Yan, C., Liu, Y., Wu, L., Liu, X., Fu, S., Xu, C., Li, Y., Zhang, J., Wang, Y., and Li, W. (2017) "Investigation on the interfacial mechanical properties of hybrid graphene-carbon nanotube/polymer nanocomposites", Carbon 115, pp.694-700.

Liu, F., Ming, P., and Li, J. (2007) "Ab initio calculation of ideal strength and phonon instability of graphene under tension", Physical Review B, 8/2007, Vol.76(6), 064120.

Liu, H.Y., and Mai, Y.W. (2003) "Delamination fracture mechanics of composite laminates with through thickness pining", Strength fract Complex,1(3),pp.139-146.

Liyong Â Tong., Adrian, P.M., and Michael, K.B. (2002) "Introduction 3D fibre reinforced polymer composites", Ch1, pp.1-12.

Loos, M.R., Ferreira, C.L.A., Pezzin, S.H., and Amico, S.C. (2008) "Effect of carbon nanotubes addition on the mechanical and thermal properties of epoxy matrices". Mater Res, 11(3), pp.347-352.

Lu, JP. (1997) "Elastic properties of carbon nanotubes and nanoropes", Phys Rev Lett 79(7), pp.1297-1300.

Lu, K.L., Lago, R.M., Chen, Y.K., Green, M.L.H., Harris, P.J.F., and Tsang, S.C. (1996) "Mechanical damage of carbon nanotubes by ultrasound". Carbon, 34, pp.814-816.

Lu, W., Zu, M., Byun, J.H., Kim, B.S., and Chou, T.W. (2012) State of the art of carbon nanotube fibres: Opportuinities and challenges, Adv Mater, pp.1805-1833.

Luo J.J., and Daniel I.M. (2003) "Characterization and modeling of mechanical behavior of polymer/clay nanocomposites", Compos Sci Technol,63(11), pp.1607-1616.

Ma, H.M., Zeng, J.J., Realff, M.L., Kumar, S., and Schiraldi, D.A. (2003) "Processing, structure, and properties of fibers from polyester/ carbon nanofiber composites", Compos Sci Technol,63(11), pp.1617-1628.

Ma, P.C, Siddiqui, N.A., Marom, G., and Kim J.K. (2010) "Dispersion and functionalization of carbon nanotubes for polymer-based nanocomposites: A review", Composites: Part A 41, pp.1345-1367.

Ma, P.C., Liu, M.Y., Kim, J.K., Tang, B.Z., et al. (2009) "Development of electrically conducting nanocomposites by employing hybrid fillers of carbon nanotubes and carbon black", ACS Appl Mater Interfaces,1,pp.1090-1096.

Ma, P.C., Tang, B.Z., and Kim, J.K. (2008) "Converting semiconducting behavior of carbon nanotubes using ball milling", Chem Phys Lett,458, pp.166–169.

Ma, P.C., Wang, S.Q., Tang, B.Z., and Kim, J.K. (2009) "In-situ amino functionalization of carbon nanotubes using ball milling", J Nanosci Nanotechnol, 9, pp.749–753.

Mall, S., Katwyk, D.W., Bolick, R.L., Kelkar, A.D., and Davis, D.C. (2009) “Tension-Compression fatique behaviour of a H-VARTM manufactured unnotched and notched carbon/epoxy composite”, Compos Struct,90, pp.201-207.

Mathur, R.B., S. Chatterjee, and Singh, B.P. (2008) “Growth of carbon nanotubes on carbon fibre substrates to produce hybrid/phenolic composites with improved mechanical properties”, Composites Science and Technology, 68(7-8), pp.1608-1615.

Mayer, G., (2005) “Rigid Biological Systems as Models for Synthetic Composites”, Science, 310(5751), pp.1144-1147.

Menna, C., Bakis, C.E., and Porta, A., (2016) “Effect of nanofiller length and orientation distributions on Mode I fracture toughness of unidirectional fibre composites”, Journal of Composite Materials, Vol.50(10), pp.1331-1352.

Merkulov, V.I., Lowndes, D.H., Wei, Y.Y., Eres, G., and Voelkl E. (2000) “Patterned growth of individual and multiple vertically aligned carbon nanofibers”, Appl Phys Lett, 76(24), pp.3555–3557.

Miki M., Fukuda T., Motoki S., Hojo M. (1997) “Composite Materials”, Kyouritsu Publication, Chapter 6, pp.159-185.

Mittal, G., Dhand, V., Rhee, K.Y., Park, S.J., and Lee, W.R. (2015) “A review on carbon nanotubes and graphene as fillers in reinforced polymer nanocomposites”, Journal of industrial and engineering chemistry 21, pp.11-15.

Moghadam-Ahmadi, B., and Taheri, F. (2014) “Fracture and toughening mechanisms of GNP-based nanocomposites in mode I and II fracture”, Engineering Fracture Mechanics, 131, pp.329-339.

Moghadam-Ahmadi, B., and Taheri, F. (2015) “Influence of graphene nanoplatelets on modes I, II and III interlaminar fracture toughness of fibre-reinforced polymer composites”, Engineering Fracture Mechanics, 143, pp.97-107.

Moniruzzaman, M., and Winey, K.I. (2006) “Polymer nanocomposites containing carbon nanotubes”, Macromolecules, 39, pp.5194-5205.

Moosa, A.A., Ramazani A.S.A., and Ibrahim, M.N. (2016) “Mechanical and electrical properties of graphene properties and carbon nanotubes hybrid epoxy nanocomposites. American Journal of Materials Science, 6(6), pp.157-165.

Morais, A.B, and Pereira, A.B. (2007) “Application of the effective crack method to mode I and mode II interlaminar fracture of carbon/epoxy unidirectional laminates”, Composites: Part A 38, pp.785-794.

Morais, A.B., Moura, M.F., Marques, A.T., de Castro, P.T. (2002) “Mode-I interlaminar fracture of carbon/epoxy cross-ply composites”, Composites Science and Technology, 62, pp.679-686.

Moriche, R., Prolongo, S.G., Sanchez, M et al., (2015) “Morphological changes on graphene nanoplatlets induced during dispersion into an epoxy resin by different methods”, Composites: Part B 72, pp.199-205.

Moriche, R., Sanchez, M., Prolongo, S.G et al. (2016) “Reversible phenomena and failure localization in self-monitoring GNP/epoxy nanocomposites”, Composite Structures 136, pp.101-105.

Moriche, R., Sanchez, M., Suarez, A.J., Prolongo S.G et al., (2016) “Strain monitoring mechanisms of sensors based on the addition of graphene nanoplatelets into an epoxy matrix”, Composites science and technology 123, pp.65-70.

Moriche, R., Sanchez, M., Suarez-Jimenez, A. et al., (2016) “Electrical conductive functionalized-GNP/epoxy based composites: From nanocomposite to multiscale glass fibre composite material”, Composites Part B 98, pp.49-55.

Mouritz, A.P. (2007) “Review of z-pinned composite laminates”, Composites Part A: Applied Science and Manufacturing, 38(12), pp.2383-2397.

Mouritz, A.P., Chang, P., and Isa, M.D. (2011) “Z-pin composites: Aerospace structural design considerations”, Journal of Aerospace Engineering, 24(4), pp.425-432.

Mukhopadhyay, K., Dwivedi, C.D., and Mathur, G.N. (2002) “Conversion of carbon nanotubes to carbon nanofibers by sonication”, Carbon,40, pp.1373–1376.

Nam, K.H., Yu J., You, N.H., Han, H., and Ku, B.C. (2017) “Synergetic toughening of polymer nanocomposites by hydrogen-bond assisted three-dimensional network of functionalized graphene oxide and carbon nanotubes”, Composites Science and technology, 149, pp. 228-234.

Ning, H., Li, J., Hu, N., Yan, C., Liu, Y., Wu, L., Liu, F., and Zhang, J. (2015) “Interlaminar mechanical properties of carbon fiber reinforced plastic laminates modified with graphene oxide interleaf”, Carbon, 91, pp.224-233.

Ogasawara, T., Ishida, Y., Ishikawa, T., and Yokota, R. (2004) “Characterization of multi-walled carbon nanotube/phenylethynyl terminated polyimide composites”, Composites Part A,35(1), pp.67–74.

Ozkan, T., Chen, Q., and Chasiotis, I. (2012) “Interfacial strength and fracture energy of individual carbon nanofibers in epoxy matrix as a function of surface conditions”, Composites science and Technology, 72, pp.965-975.

Ozkan, T., Chen, Q., Naraghi, M., and Chasiotis, I. (2010) “Mechanical properties of vapour grown carbon nanofibers”, Carbon, 84, pp. 239-244.

Park, S. J., and Seo, M.K. (2011) “Types of Composites”, Interface Science and Technology, Volume 18, Ch7, pp.501-629.

Park, S.J., and Seo, M.K. (2011) “Interface Applications in Nanomaterials”, Interface Science and Technology, Volume 18, Ch5, pp. 333-429.

Pereira, A.B., and Morais, A.B. (2004) “Mode I interlaminar fracture of carbon/epoxy multidirectional laminates”, Composites science and technology 64, pp. 2261-2270.

Phua, J.L., The, P.L., Ghani, S.A., and Yeoh, C.K. (2016) “Effect of heat Assisted bath sonication on the mechanical and thermal deformation behaviours of graphene nanoplatelets filled epoxy polymer composites”, Hindawi Publishing corporation International Journal of polymer science, volume 2016, Article ID 9767183, pp.8.

Pora, J. (2003) “Advanced materials and technologies for A380 structure”, Flight Airworthiness support technology, Airbus Customer Services, 32, pp.3-8.

Potts, J.R., Dreyer, D.R., and Bielawski, C.W. (2011) “Graphene-based polymer nanocomposites”, Polymer, 52, pp.5-25.

Prashantha K, Soulestin J, Lacrampe M.F et al., (2009) “Masterbatch-based multi-walled carbon nanotube filled polypropylene nanocomposites: Assessment of rheological and mechanical properties”, Composites science and technology 69, pp.1756-1763.

Prolongo, S.G., Suarez-Jimenez, A., Moriche, R., and Urena, A. (2014) “Graphene nanoplatelets thickness and lateral size influence on the morphology and behavior of epoxy composites”, European Polymer Journal, 53, pp.292-301.

Punetha V.D., Rana, S., Yoo, H.J., Chaurasia, A., Mcleskey, J.T., Ramasamy, M.S., Sahoo, N.G., and Cho, J.W. (2017) “Functionalization of carbon nanomaterials for advanced polymer nanocomposites: A comparison study between CNT and graphene”, Progress in Polymer Science 67, pp.1-47.

Qian, D., Wagner, G.J., Liu, W.K., Yu, M.F., and Ruoff, R.S. (2002) “Mechanics of carbon nanotubes”, Appl Mech Rev, 55, pp.495-532.

Qian, H., Bismarck, A., Greenhalgh, E.S., Kalinka, G., and Shaffer, M.S.P. (2008) “Hierarchical Composites Reinforced with Carbon Nanotube Grafted Fibers: The Potential Assessed at the Single Fiber Level”, Chem. Mater, 20, pp.1862-1869.

Qian, H., et al., (2010) “Carbon nanotube-based hierarchical composites: A review”, Journal of materials chemistry, 20(23), pp.4751-4762.

Qin, W., Vautard, F., Drzal, L.T., et al. (2015) “Mechanical and electrical properties of carbon fiber composites with incorporation of graphene nanopatelets at the fiber-matrix interface”, Composites: Part B 69, pp.335-341.

Qiu, J., Zhang, C., Wang, B., and Liang, R. (2007) “Carbon nanotube integrated multifunctional multiscale composites”, Nanotechnology, Volume 18, Number 27, pp.275708.

Rafiee, M.A., Rafiee, J., Srivastava, I., Wang, Z., Song, H., Yu, Z.Z., and Koratkar, N. (2010) “Fracture and fatigue in graphene nanocomposites”, Small 6, pp. 179-183

Rafiee, M.A., Rafiee, J., Yu, Z.Z., and Koratkar, N. (2009) “Buckling resistant graphene nanocomposites”, Appl. Phys. Lett. 95, pp.223103.

Robinson, P., and Song, D.Q. (1992) “A modified DCB specimen for Mode I testing of multidirectional laminates”, Journal of Composite Materials, 26(11), pp.1554-1577.

Rodríguez-González, J.A., Rubio-González, C., Jiménez-Mora, M., Ramos-Galicia, L., Velasco-Santos, C. (2017) “Influence of the hybrid combination of multi-walled carbon nanotubes and graphene oxide on interlaminar mechanical properties of carbon fiber/epoxy laminates”, Appl Compos Mater, pp.1-17.

Romhany, G., and Szebenyi, G. (2009) “Interlaminar crack propagation in MWCNT/fiber reinforced hybrid composites”, Express Polymer Letters, 3(3), pp.145-151.

Roy, S., and Kumar, A. (2017) “Effect of particle size on mixed-mode fracture of nanographene reinforced epoxy and ModeI delamination of its carbon fiber composite”, Composite Structures, 181, pp.1-8.

Sadeghian, R., Gangireddy, S., Minaie, B., and Hsiao, K.T. (2006) “Manufacturing carbon nanofibers toughened polyester/glass fiber composites using vacuum assisted resin transfer molding for enhancing the mode-I delamination resistance”, Composites Part A, Vol.37(10), pp.1787-1795.

Sahoo, N.G., Rana, S., Cho, J.W. et al. (2010) “Polmer nanocomposites based on functionalized carbon nanotubes”, Progress in polymer science, 35, pp.837-867.

Sandler, J., Windle, A.H., Werner, P., Altstadt, V., Es, M.V., and Shaffer, M.S.P. (2003) “Carbon-nanofibre reinforced poly (ether ether ketone) fibres”, J Mater Sci, 38(10), pp.2135-2141.

Scharfenberg, S., Rocklin, D.Z., Chialvo, C., Weaver, R.L., Goldbart, P.M., and Mason, N. (2012) “Observation of a snap-through instability in graphene”. Applied Physics Letters, Vol.100 (2).

Scott, J.M., and Phillips, D.C. (1975) “Carbon fibre composites with rubber toughened matrices”, Journal of Materials Science, 10, pp.551-562.

Seyan, T.A., Tanoglu, M., and Schulte, K. (2008) “Mode I and mode II fracture toughness of E-glass non-crimp fabric/carbon nanotube (CNT) modified polymer based composites”, Eng Fract Mech, 75 (18), pp.5151-5162.

Shekar, K.C., Prasad, B.A., and Prasad, N.E. (2014) “Interlaminar Shear Strength of Multi-walled Carbon Nanotube and Carbon Fiber Reinforced, Epoxy – Matrix Hybrid Composite”, Procedia Materials Science, Vol.6, pp.1336-1343.

Shen, M.Y., Chang, T.Y., Hsieh, T.H., Li, Y.L. et al. (2013) “Mechanical properties and tensile fatigue of graphene nanoplatelets reinforced polymer nanocomposites”, Journal of Nanomaterials, 2013, Vol.2013, 9 pages.

Shen, X.J., Pei, X.Q., Liu, Y., and Fu, S.Y. (2014) “Tribological performance of carbon nanotube-graphene oxide hybrid/epoxy composites”, Composites Part B: Engineering, volume 57, pp.120-125.

Shin, J., Kim, C., and Geckeler, K.E. (2009) “Single-walled carbon nanotube-polystyrene nanocomposites: dispersing nanotubes in organic media”, Polym. Int. 58, pp.579-583.

Shin, M.K., Lee, B., Kim, S.H., et al., (2012) “Synergistic toughnening of composite fibres by self-alignment of reduced graphene oxide and carbon nanotubes”, Nature Communications, Vol.3, pp.650.

Shi-sheng, L., Peng-xiang, H., and Chang, L. (2013) “Growth of a cup-stacked carbon nanotube carpet with a superhydrophobic surface”, Carbon, Vol.64, pp.558-558.

Shu, D., and Mai, Y.W. (1993) “Effect of sitching on interlaminar delamination extension in composites laminates”, Compos Sci Technol, 49, pp.165-171.

Silva, H., Ferreira, J.A.M., Capela, C., and Richardson, M.O.W. (2014) “Mixed mode interlayer fracture of glass fibre/nano-enhanced epoxy composites”, Composites: Part A 64, pp.211-222.

Sinnott, S.B. (2002) “Chemical functionalization of carbon nanotubes”, J Nano sci Nanotechnol, 2(2), pp.113-123.

Song, Y., and Lan, X. (2017) “Permeability, thermal and wetting properties of aligned composite nanofiber membranes containing carbon nanotubes”, International Journal of hydrogen energy, Volume 42, pp.19961-19966.

Srivastava, D., Wei, C., and Cho, K. (2003) “Nanomechanics of carbon nanotubes and composites”, Appl Mech Rev, 56(2), pp.215-230.

Sudarsono, and Ogi, K. (2017) “Fatigue behavior of open-holed CFRP laminates with initially cut fibers”, Open Journal of Composite Materials,7, pp.49-62.

Sun, L., Warren, G.L., O.Reilly, J.Y, et al. (2008) “Mechanical properties of surface-fuctionalized SWCNT/epoxy composites”, Carbon, 46, pp.320-328.

Sun, L.H., Ounaies, Z., Gao, X.L., et al. (2011) “Preparation, Characterization, and modelling of carbon nanofiber/epoxy nanocomposites”, Journal of Nanomaterials, Vol.2011, 8 pages.

Surudzic, R., Jankovic, A., Mitric, M., Matic, I., Juranic, Z.D., et al., (2016) "The effect of graphene loading on mechanical, thermal and biological properties of poly(vinyl alcohol)/graphene nanocomposites", Journal of Industrial and engineering chemistry 34, pp.250-257.

Sutcliffe, M.P.F., Lemanski, S.L., and Scott, A.E. (2012) "Measurement of fibre waviness in industrial composite components", Composites Science Technology, 72, pp.2016-2023.

Tan, Q.C., Shank, A.R., Hui, D., and Kong, I. (2016) "Functionalised graphene-multi-walled carbon nanotube hybrid poly (styrene-b-butadiene-b-styrene) nanocomposites", Composites, Part 90, pp.315-325.

Tang, L.C., Wan,Y.J., Yan, D., Pei, Y.B., Zhao, L., Li, Y.B., Wu, L.B., Jiang, J.X., and Lai, G.Q. (2013) "The effect of graphene dispersion on the mechanical properties of graphene/epoxy composites", Cabron, 60, pp.16-17.

Tang, L.C., Zhang, H., Han, J.H., et al. (2011) "Fracture mechanisms of epoxy filled ozone fuctionalized multi-walled carbon nanotubes", Composites science and technology, 72, pp.7-13.

Tang, Y.H. et al., (2011) "Characterization of transverse tensile, interlaminar shear and interlaminate fracture in CF/EP laminates with 10 wt% and 20 wt% silica nanoparticles in matrix resins", Composites Part A: Applied Science and Manufacturing, 42(12), pp.1943-1950.

Thanh, T.D., Kapralkova, L., Hromadkova, J., and Kelnar, I. (2014) "Effect of graphite nanoplatelets on the structure and properties of PA6-elastomer nanocomposites", European polymer journal, 50, pp.39-45.

Thess, A., Lee, R., Nikolaev, P. et al. (1996) "Crystalline ropes of metallic carbon nanotubes", Science, 273, pp.483-488.

Thostenson, E.T. (2004) "Carbon nanotube-reinforced composites: processing, characterization and modelling", Ph.D. Dissertation, University of Delaware.

Thostenson, E.T., and Chou, T.W. (2003) "On the elastic properties of carbon nanotube-based composites: modeling and characterization", J Phys D,36(5), pp.573-582.

Thostenson, E.T., Li, C., Chou, T.W. (2005) "Nanocomposites in context; Review", Composites Science and Technology 65, pp.491-516.

Thostenson, E.T., Li, W.Z., Wang, D.Z., Ren, Z.F., and Chou, T.W. (1998) "Carbon nanotube/carbon fiber hybrid multiscale composites", J Appl Phys, 91(9), pp.6034-6037.

Thostenson, E.T., Ren, Z.F., and Chou, T.W. (2001) "Advances in the science and technology of carbon nanotubes and their composites: a review", Composites Science and Technology, Vol.61(13), pp.1899-1912

Tkalya, E.E., Ghislandi, M. et al. (2012) “The use of surfactants for dispersing carbon nanotubes and graphene to make conductive nanocomposites”, Curr. Opin. Colloid Interface Sci. 17, pp.225-232.

Toland, G.J., Johnston, W.M., O'Brien, T. K. (2010) “Mode II Interlaminar Fracture Toughness and Fatigue Characterization of a Graphite Epoxy Composite Material”, NASA Langley Research Center 2010, NASA/TM-2010-216838, pp.28.

Veedu, V.P., et al., (2006) “Multifunctional composites using reinforced laminae with carbon-nanotube forests”, Nature materials, 5(6): pp.457-462.

Wagner, H.D., and Vaia, R.A. (2004) “Nanocomposites: issues at the interface”, Mater Today 7(11), pp.38-42.

Wang, B., Wolfe, D.E., Terrones, M., Haque, M.A. et al. (2017) “Electro-graphitization and exfoliation of graphene on carbon nanofibers”, Carbon 117, pp.201-207.

Wang, F., Drzal, T.L., Qin, Y., and Huang, Z. (2016) “Size effect of graphene nanoplatelets on the morphology and mechanical behaviour of glass fiber/epoxy composites”, J Mater Sci, 51, pp.3337-3348.

Wang, M.C., Yan, C., Ma, L., Hu, N., and Chen, M.W. (2012) “Effect of defects on fracture strength of graphene sheets”, Computational Materials Science, 54, pp.236–239.

Wang, P.N., Hsieh, T.H., Chiang, C.L., Shen, M.Y., and Myoung, W. (2015) “Synergetic Effects of Mechanical Properties on Graphene Nanoplatelet and Multiwalled Carbon Nanotube Hybrids Reinforced Epoxy/Carbon Fiber Composites”, Journal of Nanomaterials, Vol.2015, pp.9.

Wang, Y.K., Xu, Z., Chen, L., Jiao, Y., and Wu, X. (2011) Multi-scale hybrid composites-based carbon nanotubes”, Polymer Composites, 32(2), pp.159-167.

Wei, C.Y., and Srivastava, D. (2004) “Nanomechanics of carbon nanofibers: structural and elastic properties”, Appl Phys Lett, 85(12), pp.2208-2210.

Wetzel, B., et al. (2006) “Epoxy nanocomposites–fracture and toughening mechanisms”, Engineering Fracture Mechanics, 73(16), pp.2375-2398.

Wichmann, M.H.G., et al. (2006) “Glass-fibre-reinforced composites with enhanced mechanical and electrical properties - Benefits and limitations of a nanoparticle modified matrix”, Engineering Fracture Mechanics, 73(16), pp.2346-2359.

Wicks, S.S., Wang, W., Williams, M.R., and Wardle, B.L. (2014) “Multi-Scale interlaminar fracture mechanisms in woven composite laminates reinforced with aligned carbon nanotubes”, Composites Science and Technology, 100, pp.128-135.

Wilkinson, S.P., Ward, T.C., McGrath, J.E., (1993), “Effect of thermoplastic modifier variables on toughening a bismaleimide matrix resin for high-performance composite materials”, Polymer, 34(4), pp.870-884.

Wu, Y., Wang, B., Ma, Y. et al. (2010) “Efficient and large-scale synthesis of few-layered graphene using an arc-discharge method and conductivity studies of the resulting films”, Nano Res, 3(9), pp.661-669.

Xie, X.L., Mai, Y.W., and Zhou, X.P. (2005) “Dispersion and alignment of carbon nanotubes in polymer matrix: a review”, Mater Sci Eng R,49, pp.89-112.

Yao, H., Sui, X., Zhoa, Z. et al. (2015) “Optimization of interfacial microstructure and mechanical properties of carbon fiber/epoxy composites via carbon nanotube sizing”, Applied surface science 347, pp.583-590.

Yasmin, A., and Daniel, I.M. (2004) “Mechanical and thermal properties of graphite platelet/epoxy composites”, Polymer 45, pp.8211-8219.

Yasmin, A., Luo, J.J., and Daniel, I.M. (2006) “Processing of expanded graphite reinforced polymer nanocomposites”, Composites Science and Technology 66, pp.1179-1186.

Yavari, F., Rafiee, M.A., Rafiee, J., Yu, Z.Z., and Koratkar, N. (2010) “Dramatic increase in fatigue life in hierarchical graphene composites”, ACS Appl. Mater. Inter. 2(10), pp.2738-2743.

Ye, Y. et al. (2007) “High impact strength epoxy nanocomposites with natural nanotubes”, Polymer, 48(21), pp.6426-6433.

Yokozeki, T. et al. (2007) “Mechanical properties of CFRP laminates manufactured from unidirectional prepregs using CSCNT-dispersed epoxy” Composites Part A: Applied Science and Manufacturing, 38(10), pp.2121-2130.

Yokozeki, T., Aoki, T., Arai, A., Ishilbashi, M., Ynagaisawa, T., Imai, K., Takahashi, T. (2008) “Effect of CNT length distribution on mechanical properties of nanocomposites: measurement and estimation”, Priceeding of 13th US-Japan Conference on Composite material, CD-ROM.

Yokozeki, T., Iwahori, Y., Ishibashi, M., Yanagisawa, T, Imai, K. et al. (2009) “Fracture toughness improvement of CFRP laminates by dispersion of cup-stacked carbon nanotubes”, Composites Science and Technology, 69, pp.2268-2273.

Yokozeki, T., Schulz, S., Buchhorn, S., Schulte, K. (2012) “Investigation of shear thinning behaviour and microstructures of MWCNT/epoxy and CNF/epoxy suspensions under steady shear conditions”, European Polymer Journal, 48, pp.1042-1049.

Yu, Lourie, Dyer, Moloni, Kelly, Ruoff (2000) “Strength and breaking mechanism of multi-walled carbon nanotubes under tensile load”, Science, 287(5453), pp. 637-40.

Yu, M.F., Files, B.S., Arepalli, S., Ruoff, R.S. (2000) “Tensile loading of ropes of single wall carbon nanotubes and their mechanical properties”, Phys Rev Lett, 84(24), pp.5552-5555.

Yue, L., Pircheraghi, G., Monemain, S.A., and Zloczower, I.M., (2014) “Epoxy composites with carbon nanotubes and graphene nanoplatelets-Dispersion and synergy effects”, Carbon 78, 268-278.

Zaman, I., Phan, T.T., Kuan, H.C. et al. (2011) “Epoxy/graphene platelets nanocomposites with two levels of interface strength, Polymers 52, pp.1603-1611.

Zhang, F., Wang, R., He, X., and Wang, C. (2009) “Interfacial shearing strength and reinforcing mechanisms of an epoxy composite reinforced using a carbon nanotube/ carbon fiber hybrid”. J Mater Sci, 44, pp.3574-3577.

Zhang, L., Aboagye, A., Kelkar, A. et al. (2014) “A review: Carbon nanofibers from electrospun polyacrylonitrile and their applications”, J. Mater. Sci,,49, pp.463-480.

Zhang, Q.H., Liu, J.W., Sager, R., Dai, L.M., and Baur, J. (2009) “Hierarchical composites of carbon nanotubes on carbon fiber: Influence of growth condition on fiber tensile properties”, Compos. Sci, Technol., 69, pp.594-601.

Zhang, S., Cui, Y., Wu, B., Song, R., Song, H., Zhou, J., Chen, X., Liu, J., Cao, L. (2013) “Control of graphitization degree and defects of carbon blacks through ball-milling”, RSC Advances, Vol.4(1), pp.505-509.

Zhang, X., Fan, X., Yan, C., Li, H., Zhu, Y., Li, X., Yu, L. (2012) “Interfacial microstructure and properties of carbon fiber composites modified with graphene oxide”, ACS Appl. Mater. Interfaces, 4, pp.1543-1552.

Zhang, X., Rajaraman, B. R. S., Liu, H., and Ramakrishna, S. (2014) “Graphene’s potential in materials science and engineering”, RSC Adv., vol. 4, no. 55, pp. 28987.

Zhang, Y., Wang, Y., Yu, J. et al. (2014) “Tuning the interface of graphene platlets/epoxy composites by the covalent grafting of polybenzimidazole”, Polymers 55, pp.4990-5000.

Zhao, H., Min, K., and Aluru, N.R. (2009) “Size and Chirality Dependent Elastic Properties of Graphene Nanoribbons under Uniaxial Tension”, Nano Letters Vol (9),No.88, pp. 3012-3015.

Zhao, X., Zhang, Q., Chen, D., Lu, P. (2010) “Enhanced mechanical properties of graphene-based poly (vinyl alcohol) composites”, Macromolecules, 43, pp.2357-2363.

Zheng Y, Xu L, Fan Z et al. (2012) “A molecular dynamics investigation of the mechanical properties of graphene nanochains”, Journal of Materials Chemistry, Vol.22(19), pp.9798.

Zheng, Q., Geng, Y., Wang, S., Li, Z., Kim, J. (2010) “Effects of functional groups on the mechanical and wrinkling properties of graphene sheets”, Carbon, 48, pp.4315-4322.

Zhou, Y., Pervin, F., Jeelani, S., Mallick, P.K. (2008) “Improvement in mechanical properties of carbon fabric-epoxy composite using carbon nanofibers”, Journal of Materials Processing Technology 198, pp.445-453.

Zhou, Y., Pervin, F., Lewis, L., and Jeelani, S. (2008) “Fabrication and characterization of carbon/epoxy composites mixed with multi-walled carbon nanotubes”, Materials science & engineering. A, Structural materials, 475(1-2), pp.157-165.

Zhou, Y., Pervin, F., Lewis, L., Jeelani, S. (2007) “Experimental study on the thermal and mechanical properties of multi-walled carbon nanotube-reinforced epoxy”, Materials science and engineering A 452-453, pp.657-664.

Zhou, Y., Pervin, F., Rangari, V., and Jeelani, S. (2006) “Fabrication and evaluation of carbon nano fiber filled carbon/epoxy composite”, Materials Science and Engineering A 426, pp.221-228.

Zhu, J., Wang, J., Zu, L. (2015) “Influence of out-of-plane ply waviness on elastic properties of composite laminates under uniaxial loading”, Composite structures 132, pp.440-450.

Zulkifli, R., Fatt, L.K., Azhari, C.H., and Sahari, J. (2002) “Interlaminar fracture properties of fibre reinforced natural rubber/polypropylene composites”, Journal of Materials Processing Technology, 128, pp.33-37.

Appendix A. Tensile Properties

Appendix A.1. Typical tensile stress-strain curves for the pure epoxy composite (base (0)) as well as three epoxy nanocomposites modified with carbon nanomaterials at various weight concentrations processed by sonication technique.

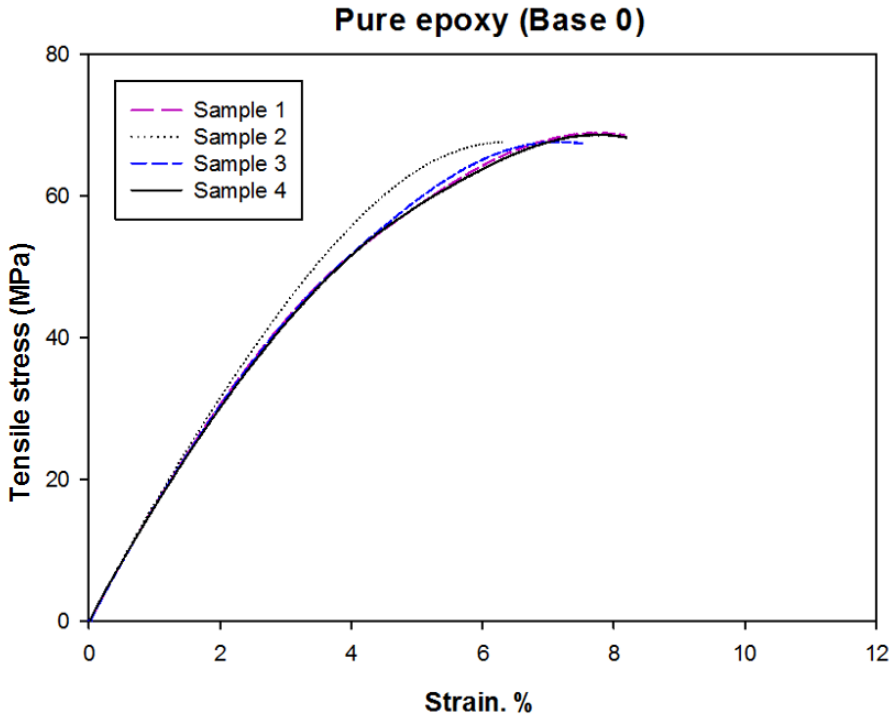

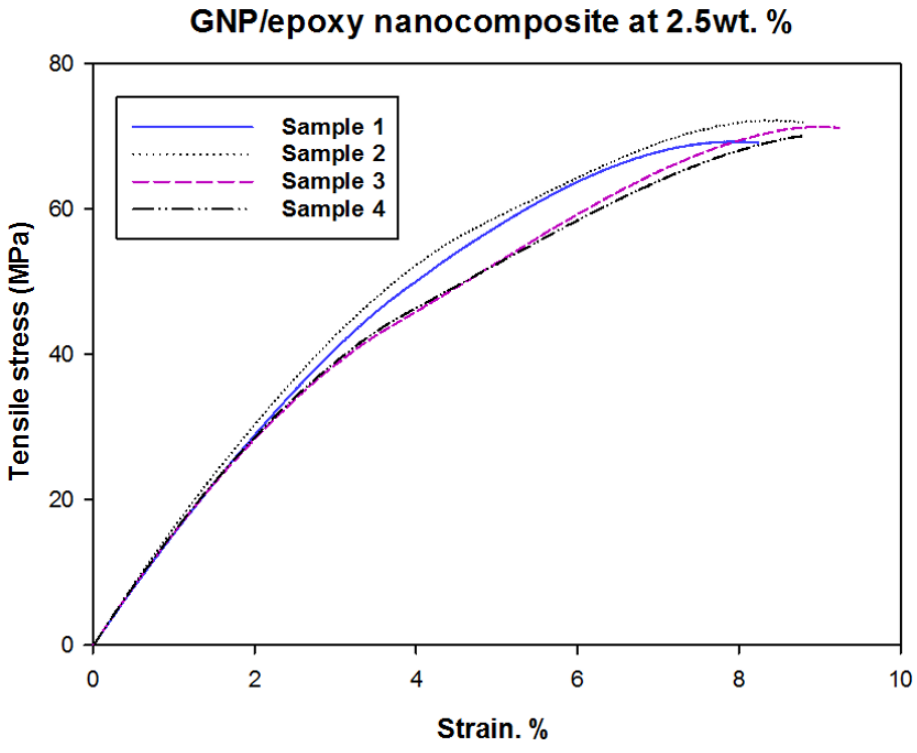

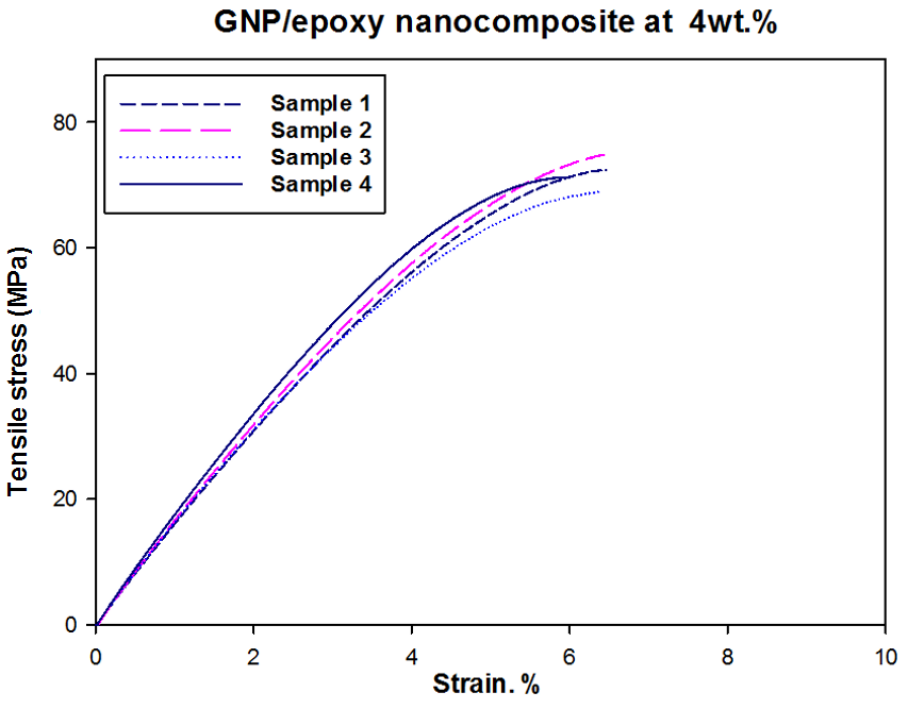
GNP/epoxy nanocomposite at 4wt.%
Sample 1
Sample 2
Sample 3
Sample 4
Tensile stress (MPa)
0
20
40
60
80
0
2
4
6
8
10
Strain. %

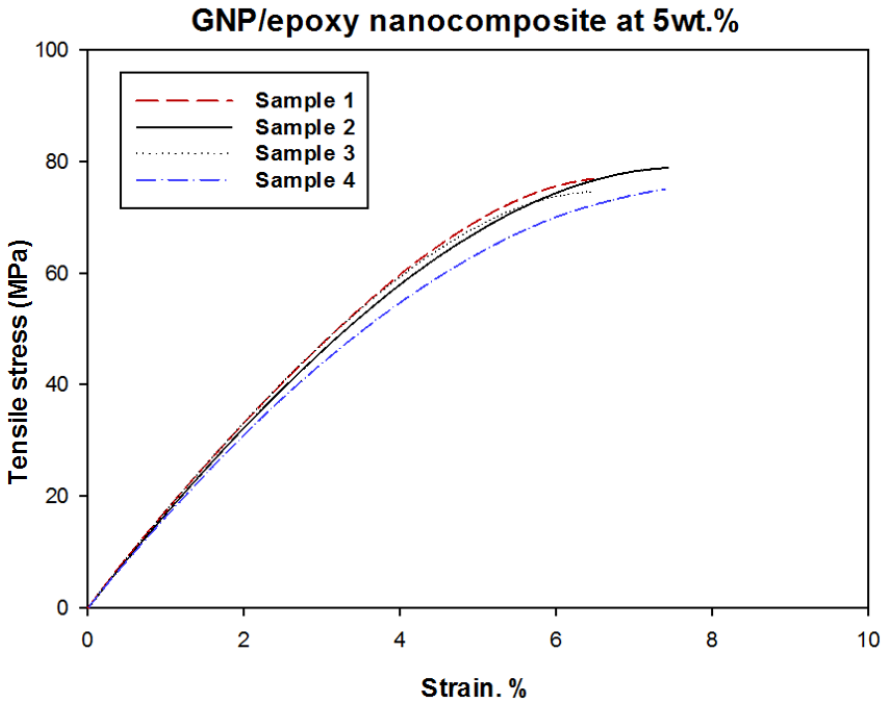
GNP/epoxy nanocomposite at 5wt.%
Sample 1
Sample 2
Sample 3
Sample 4
Tensile stress (MPa)
0
20
40
60
80
100
0
2
4
6
8
10
Strain. %

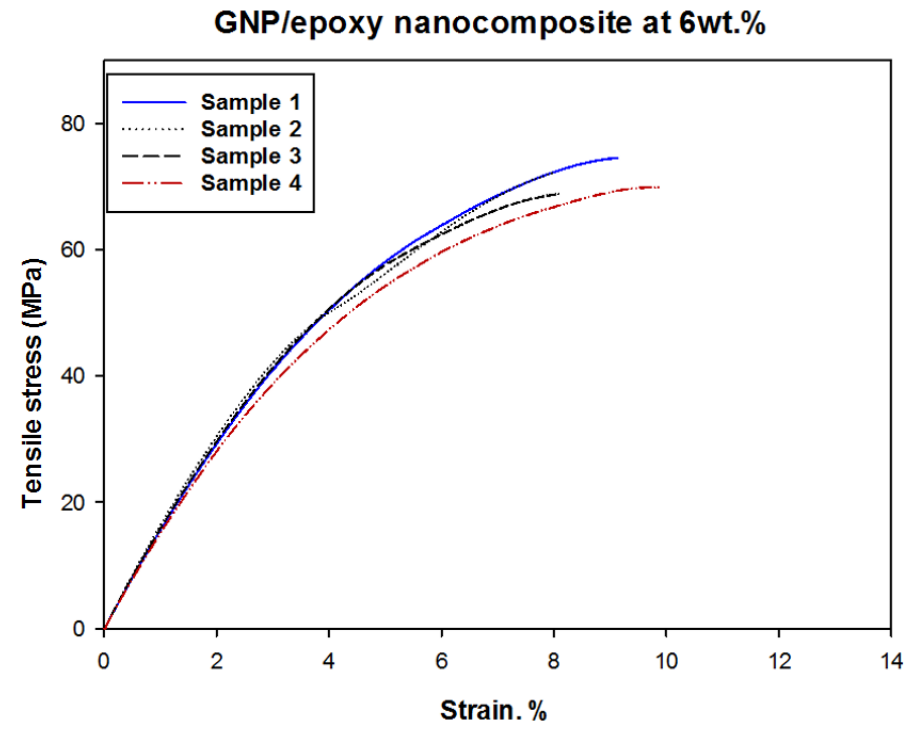

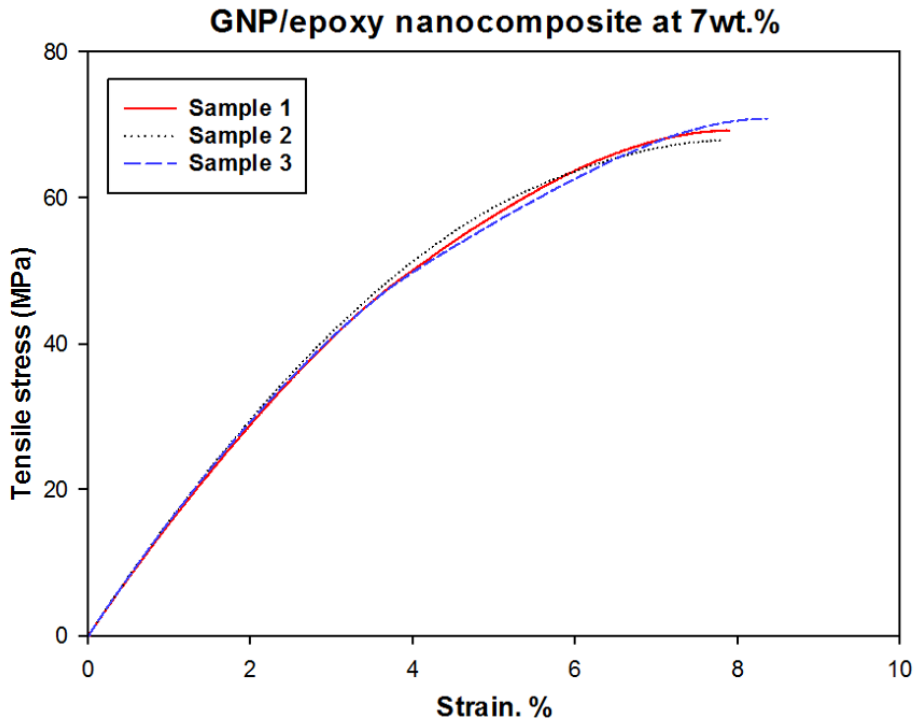

Figure A.1.1. The typical tensile stress-strain curves for the GNP/epoxy nanocomposites at various weight concentrations.

Table A.1.1. Summary of tensile tests results for the GNP/epoxy nanocomposites specimens at various weight concentrations.

GNP/epoxy nanocomposites processed by sonication method																		
Specimen Number	Maximum Tensile Strength (MPa)						Tensile Modulus (GPa)						Maximum Strain (%)					
	0 wt. %	***2.5 wt.%***	***4 wt.%***	***5 wt.%***	***6 wt.%***	***7 wt.%***	***0 wt. %***	***2.5 wt.%***	***4 wt.%***	***5 wt.%***	***6 wt.%***	***7 wt.%***	***0 wt. %***	***2.5 wt.%***	***4 wt.%***	***5 wt.%***	***6 wt.%***	***7 wt.%***
1	67.63	69.20	72.39	77.07	74.01	69.20	1.33	1.18	1.30	1.54	1.22	1.27	8.16	7.85	6.47	6.48	9.13	7.90
2	66.53	72.10	75.60	79.50	72.29	68.70	1.38	1.16	1.31	1.50	1.29	1.31	6.34	8.34	6.43	7.44	8.01	7.82
3	67.60	70.80	69.20	74.00	71.10	69.70	1.30	1.20	1.35	1.46	1.20	1.29	8.16	8.45	6.38	6.47	8.08	8.38
4	68.80	64.95	72.41	77.84	71.80	-	1.35	1.30	1.32	1.44	1.17	-	8.18	9.20	5.95	7.39	9.91	-
Average	67.64	69.26	72.40	77.10	72.30	69.20	1.34	1.21	1.32	1.48	1.22	1.29	7.71	8.46	6.30	6.94	8.78	8.02
S.D C.V	±0.92 1.37%	±3.11 4.49%	±2.60 3.60%	±2.30 2.98%	±1.24 1.72%	±0.50 0.72%	±0.03 2.51%	±0.04 3.69%	±0.02 1.63%	±0.03 2.46%	±0.05 4.17%	±0.02 1.55%	±0.91 11.80%	±0.55 6.50%	±0.24 3.83%	±0.54 7.82%	±0.90 10.3%	±0.30 3.78%
Incr.%	base (0)	+2.4	+7.0	+13.9	+6.8	+2.3	base (0)	-9.7	-1.5	+10.8	-8.9	-3.7	base (0)	+9.7	-18.3	-9.9	+13.8	+4.0

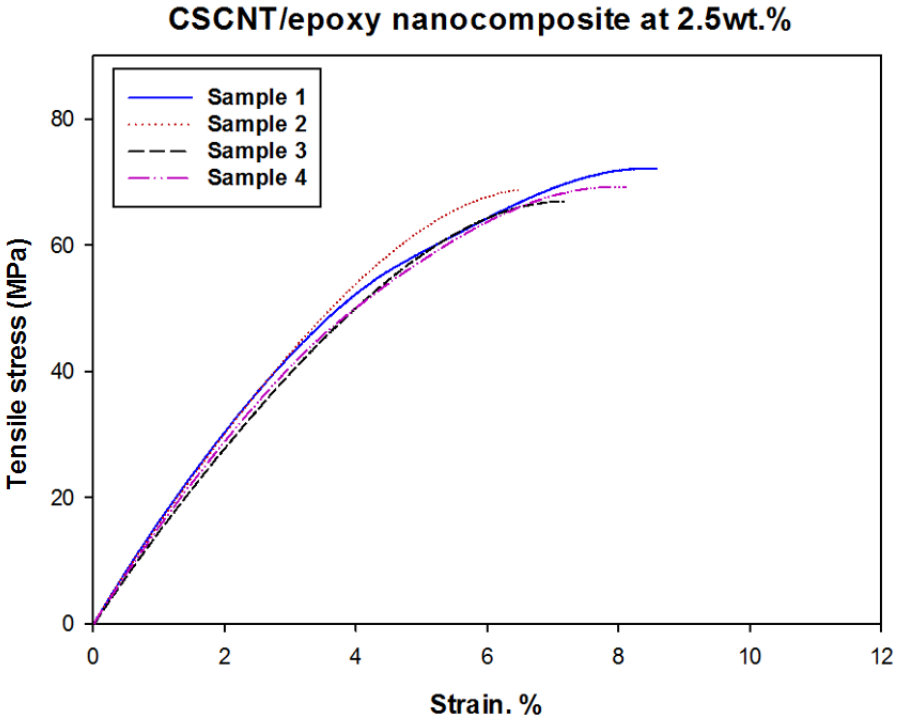
CSCNT/epoxy nanocomposite at 2.5wt.%
Sample 1
Sample 2
Sample 3
Sample 4
Tensile stress (MPa)
Strain. %
0
20
40
60
80
0
2
4
6
8
10
12

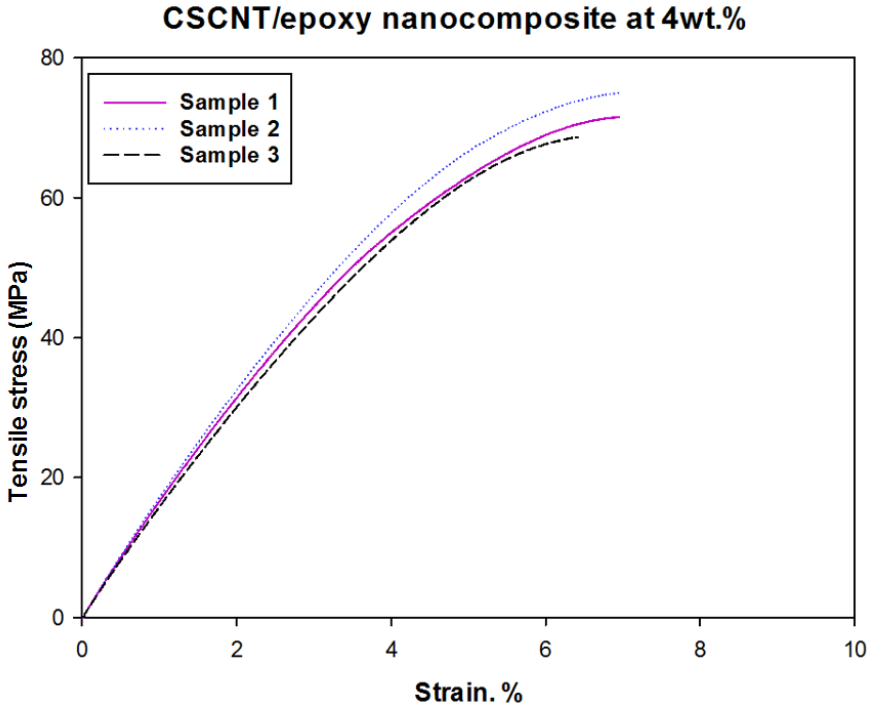
CSCNT/epoxy nanocomposite at 4wt.%
Sample 1
Sample 2
Sample 3
Tensile stress (MPa)
Strain. %
0
20
40
60
80
0
2
4
6
8
10

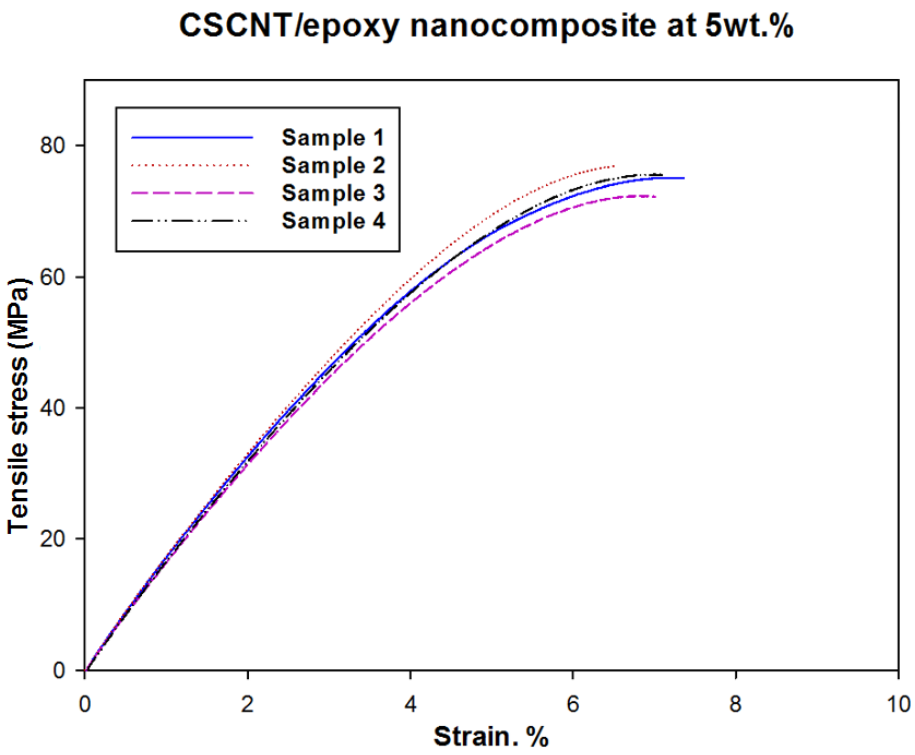
CSCNT/epoxy nanocomposite at 5wt.%
Sample 1
Sample 2
Sample 3
Sample 4
Tensile stress (MPa)
Strain. %
0
20
40
60
80
0
2
4
6
8
10

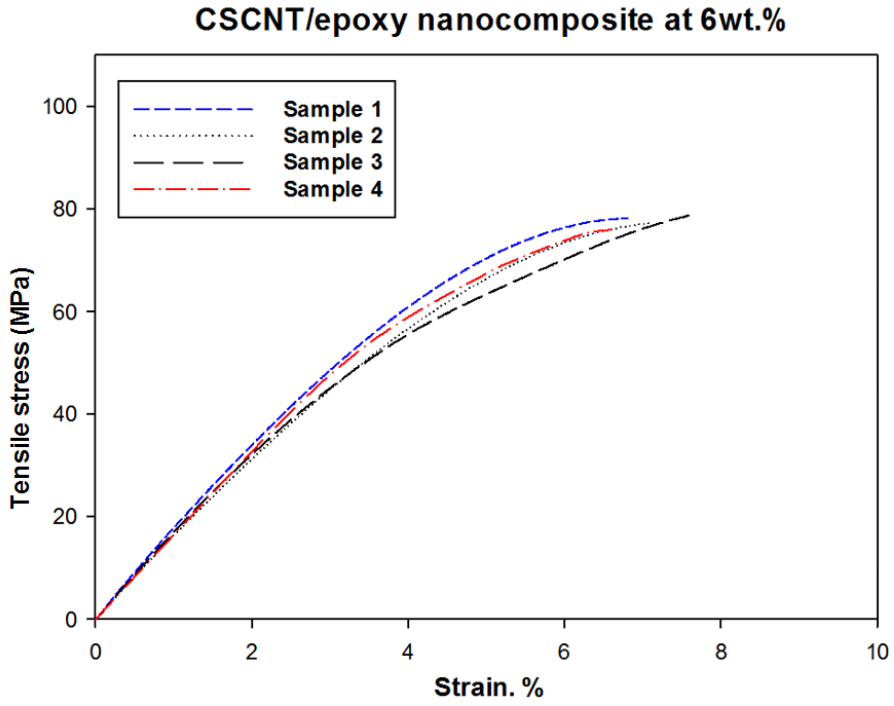
CSCNT/epoxy nanocomposite at 6wt.%
Sample 1
Sample 2
Sample 3
Sample 4
Tensile stress (MPa)
Strain. %
0
20
40
60
80
100
0
2
4
6
8
10

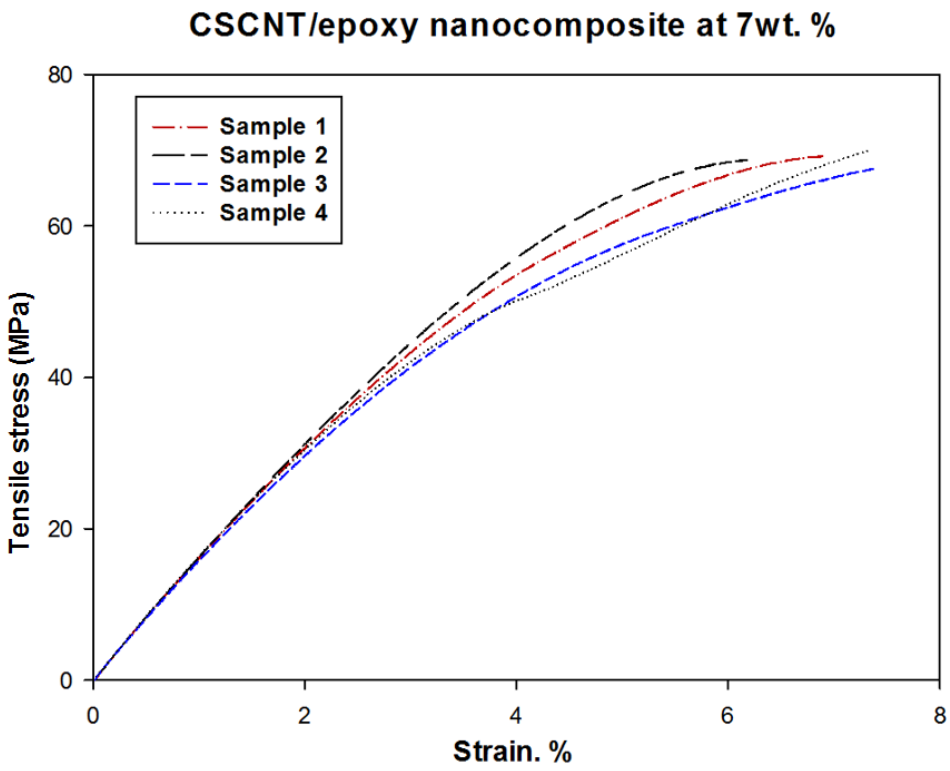

Figure A.1.2. The typical tensile stress-strain curves for the CSCNT/epoxy nanocomposites at various weight concentrations.

Table A.1.2. Summary of tensile tests results for the CSCNT/epoxy nanocomposites specimens at various weight concentrations in comparison with pure epoxy composites (base (0)).

CSCNT/epoxy nanocomposites processed by sonication method																		
Specimen Number	Maximum Tensile Strength (MPa)						Tensile Modulus (GPa)						Maximum Strain (%)					
	0 wt. %	***2.5wt.%***	***4wt.%***	***5 wt.%***	***6wt.%***	***7 wt.%***	***0 wt. %***	***2.5wt.%***	***4wt.%***	***5 wt.%***	***6 wt.%***	***7 wt.%***	***0 wt.%***	***2.5 wt.%***	***4wt.%***	***5 wt.%***	***6wt.%***	***7 wt.%***
1	67.63	68.80	73.40	75.90	78.20	69.10	1.33	1.33	1.51	1.55	1.53	1.33	8.16	8.58	6.96	7.38	6.80	6.90
2	66.53	66.95	75.20	75.10	77.17	70.10	1.38	1.32	1.48	1.54	1.54	1.27	6.34	6.50	6.98	6.50	7.09	6.20
3	67.60	68.85	71.90	74.60	77.40	68.80	1.30	1.25	1.47	1.50	1.53	1.29	8.16	7.16	6.42	7.01	7.67	7.38
4	68.80	71.00	-	78.05	80.10	72.30	1.35	1.30	-	1.54	1.52	1.31	8.18	8.12	-	7.10	6.60	7.34
Average	67.64	68.90	73.50	75.91	78.21	69.40	1.34	1.30	1.49	1.52	1.53	1.30	7.71	7.59	6.78	7.00	7.04	6.95
S.D C.V	±0.92 1.37%	±1.65 2.40%	±1.65 2.24%	±1.73 2.28%	±1.33 1.70%	±1.76 2.54%	±0.03 2.51%	±0.03 2.73%	±0.02 1.16%	±0.02 1.74%	±0.01 0.55%	±0.02 1.98%	±0.91 11.80%	±0.93 12.30%	±0.32 4.80%	±0.36 5.20%	±0.21 3%	±0.54 7.80%
Incr.%	base(0)	+1.8	+8.6	+12.2	+15.6	+2.6	base(0)	-2.9	+11.2	+13.4	+14.2	-2.9	base(0	-1.5	-12.0	-9.2	-8.7	-9.8

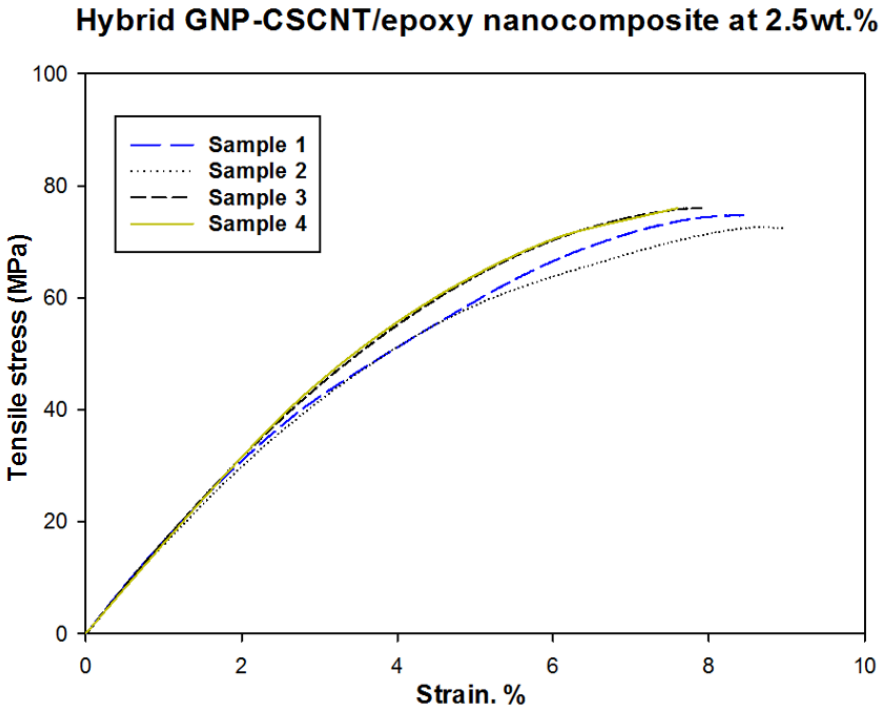
Hybrid GNP-CSCNT/epoxy nanocomposite at 2.5wt.%
Sample 1
Sample 2
Sample 3
Sample 4
Tensile stress (MPa)
Strain. %
0
20
40
60
80
100
0
2
4
6
8
10

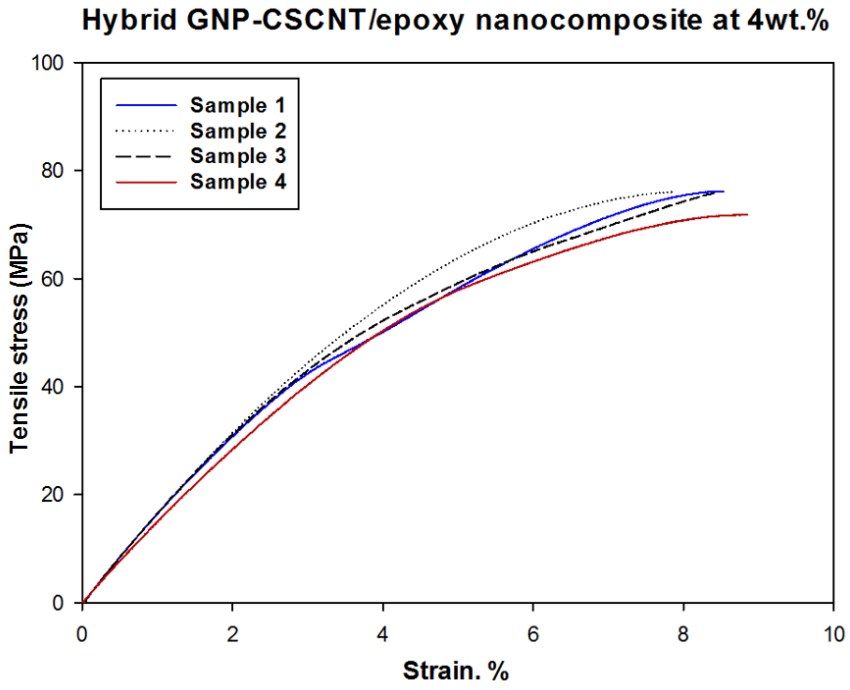
Hybrid GNP-CSCNT/epoxy nanocomposite at 4wt.%
Sample 1
Sample 2
Sample 3
Sample 4
Tensile stress (MPa)
Strain. %
0
20
40
60
80
100
0
2
4
6
8
10

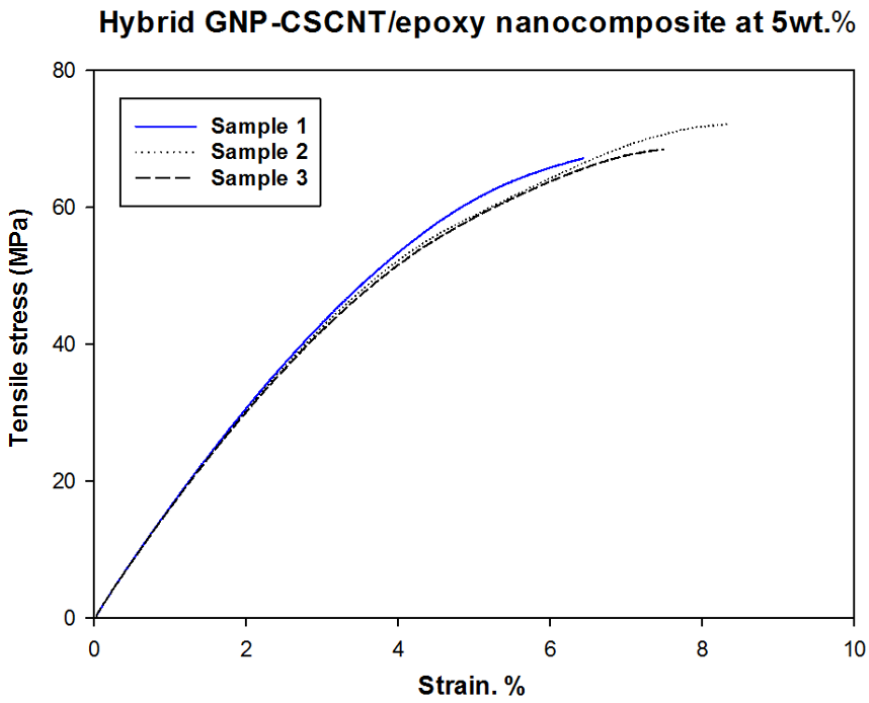
Hybrid GNP-CSCNT/epoxy nanocomposite at 5wt.%
Sample 1
Sample 2
Sample 3
Tensile stress (MPa)
Strain. %
0
20
40
60
80
0
2
4
6
8
10

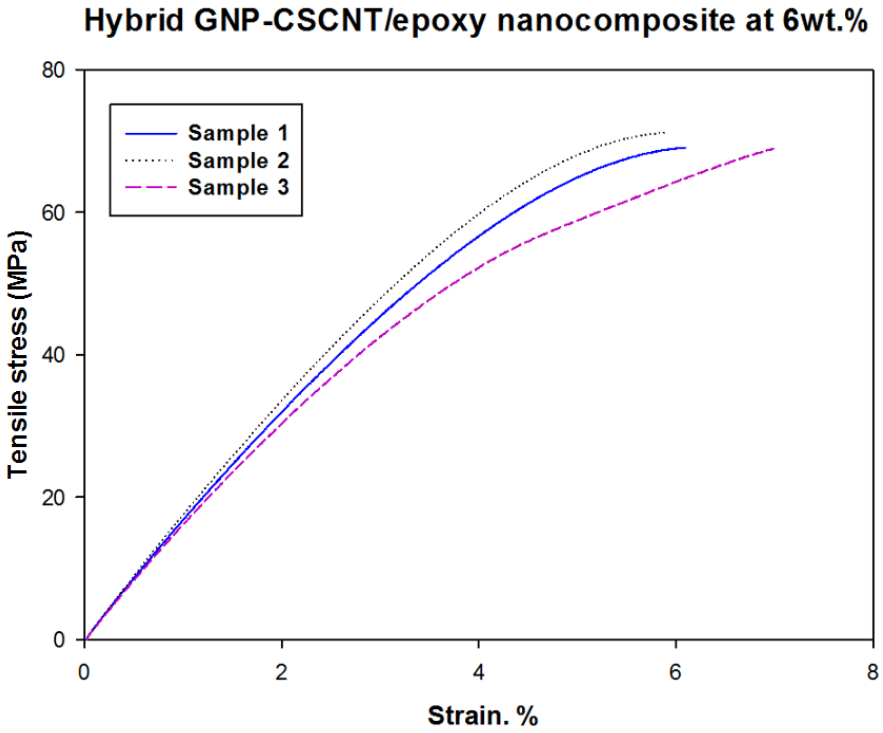
Hybrid GNP-CSCNT/epoxy nanocomposite at 6wt.%
Sample 1
Sample 2
Sample 3
Tensile stress (MPa)
Strain. %
0
20
40
60
80
0
2
4
6
8

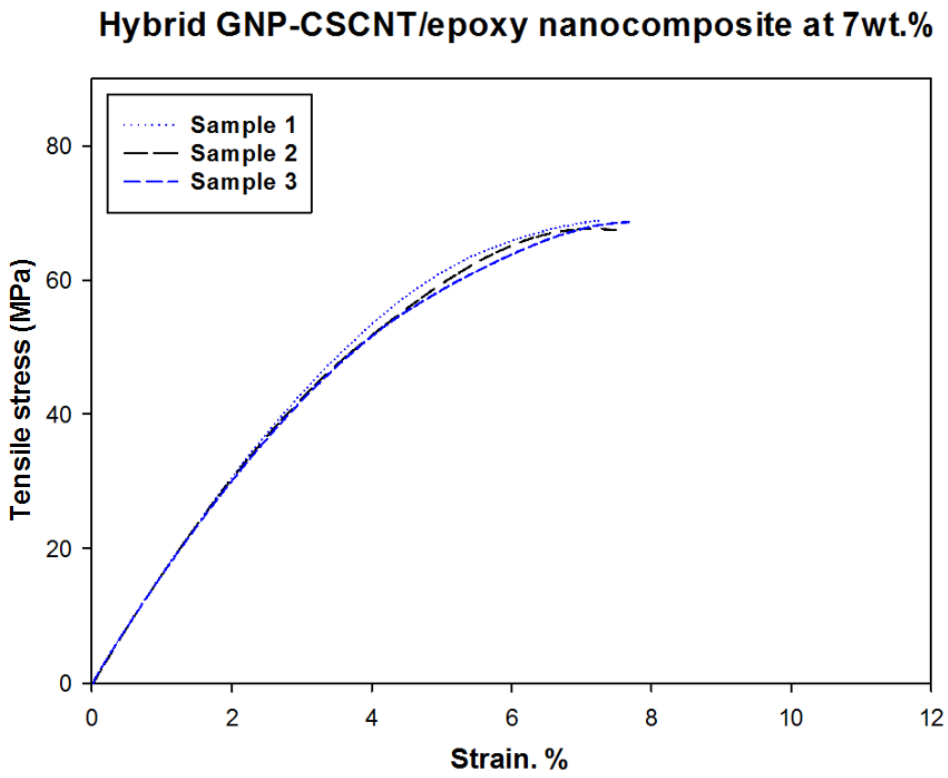

Figure A.1.3. The typical tensile stress-strain curves for the hybrid GNP-CSCNT/epoxy nanocomposites at various weight concentrations.

Table A.1.3. Summary of tensile tests results for the hybrid GNP-CSCNT/epoxy nanocomposites specimens at various weight concentrations in comparison with pure epoxy composites (base (0)).

Hybrid GNP-CSCNT/ epoxy nanocomposites processed by sonication method																		
Specimen Number	Maximum Tensile Strength (MPa)						Tensile Modulus (GPa)						Maximum Strain (%)					
	0 wt. %	***2.5wt.%***	***4wt.%***	***5 wt.%***	***6wt.%***	***7 wt.%***	***0 wt. %***	***2.5wt.%***	***4wt.%***	***5 wt.%***	***6 wt.%***	***7 wt.%***	***0 wt. %***	***2.5wt.%***	***4wt.%***	***5 wt.%***	***6wt.%***	***7 wt.%***
1	67.63	74.40	76.11	67.40	70.18	69.70	1.33	1.28	1.33	1.34	1.53	1.35	8.16	8.46	8.54	6.45	6.12	7.38
2	66.53	72.19	74.74	71.10	71.10	69.71	1.38	1.30	1.28	1.31	1.51	1.33	6.34	8.98	7.89	8.40	5.88	7.50
3	67.60	76.00	77.64	67.00	72.70	66.70	1.30	1.34	1.28	1.30	1.58	1.31	8.16	7.96	8.84	7.50	7.00	7.68
4	68.8	76.20	76.09	-	-	-	1.35	1.32	1.27	-	-	-	8.18	7.60	8.85	-	-	-
Average	67.64	74.70	76.14	68.50	71.30	68.70	1.34	1.31	1.29	1.32	1.54	1.33	7.71	8.25	8.53	7.45	6.30	7.52
S.D	±0.92	±1.85	±1.18	±2.26	±1.27	±1.58	±0.03	±0.02	±0.03	±0.02	±0.04	±0.02	±0.91	±0.47	±0.45	±0.97	±0.59	±0.15
C.V	1.37%	2.48%	1.55%	3.30%	1.79%	2.30%	2.51%	1.97%	2.10%	1.59%	2.40%	1.50%	11.80%	5.70%	5.20%	13.00%	9.30%	2.00%
Incr.%	base(0)	+10.4	+12.6	+1.3	+5.4	+1.5	base(0)	-2.2	-3.7	-1.5	+14.9	-0.7	base 0)	+7.0	+10.6	-3.3	-18.2	-2.4

Appendix A.2. Typical tensile stress-strain curves for the pure epoxy composite (base (0)) as well as three epoxy nanocomposites modified with carbon nanomaterials at various weight concentrations processed by ball milling technique.

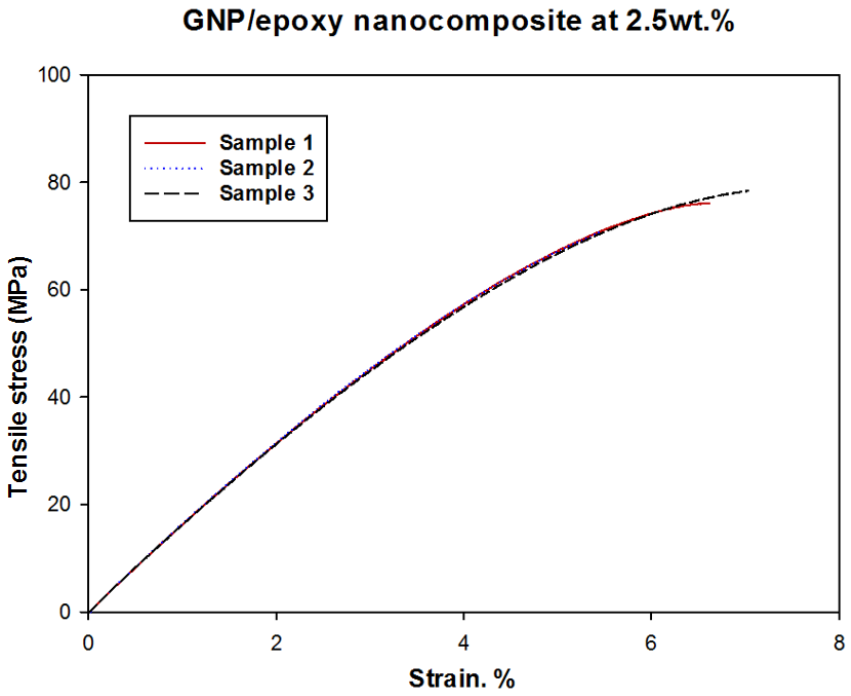

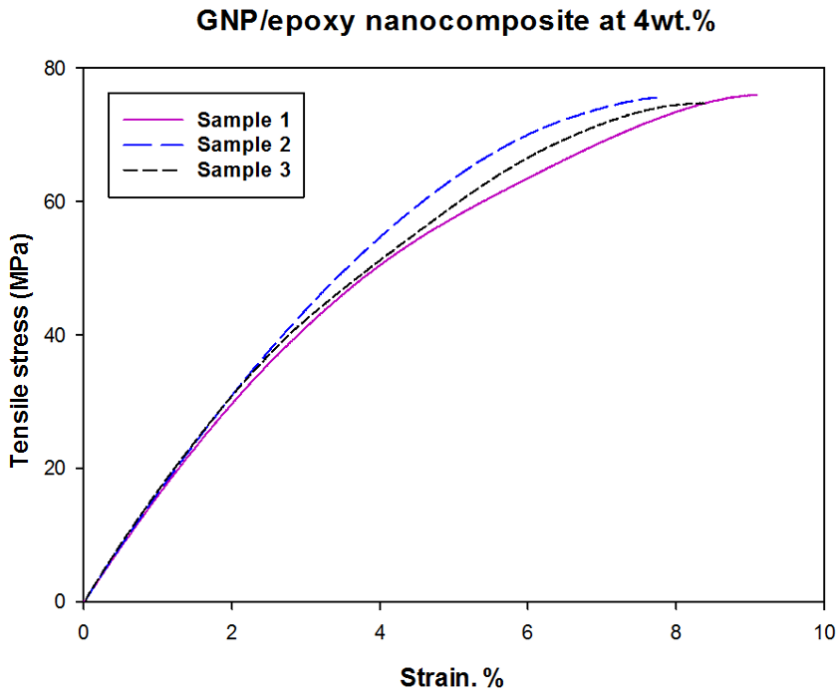

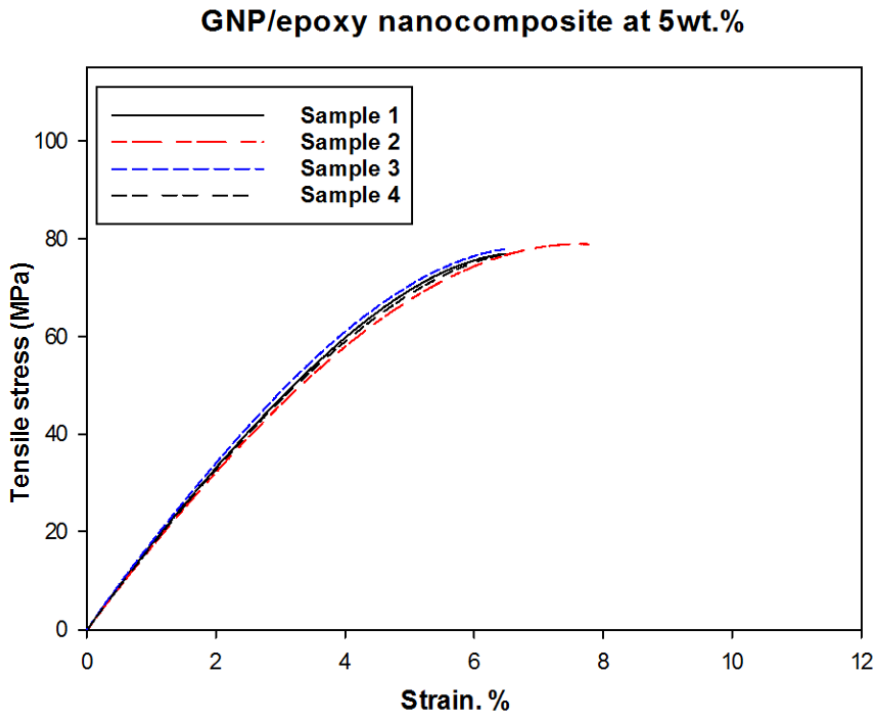
GNP/epoxy nanocomposite at 5wt.%
Sample 1
Sample 2
Sample 3
Sample 4
Tensile stress (MPa)
Strain. %
0
20
40
60
80
100
0
2
4
6
8
10
12

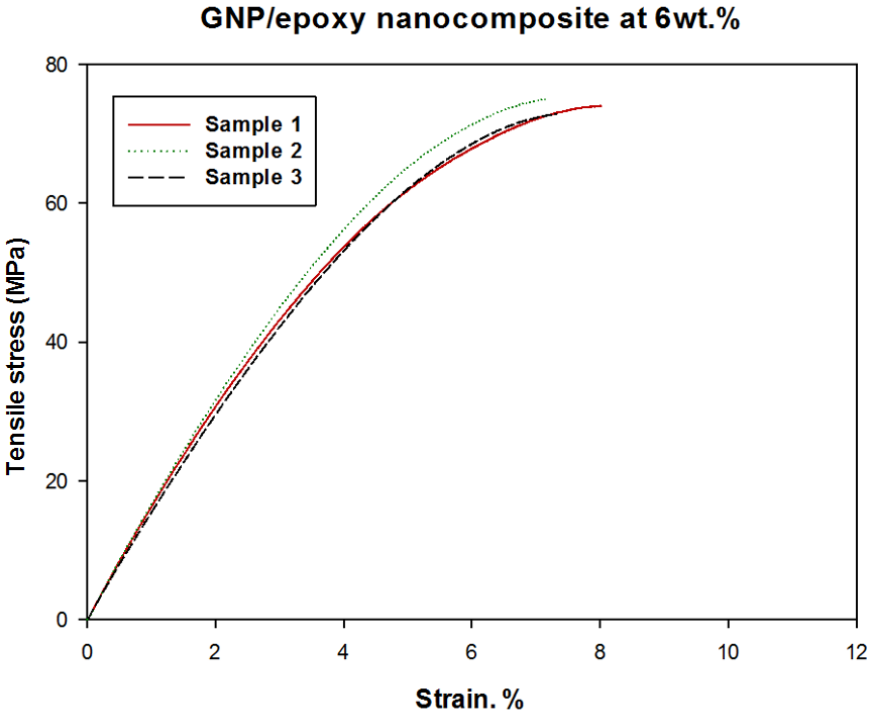
GNP/epoxy nanocomposite at 6wt.%
Sample 1
Sample 2
Sample 3
Tensile stress (MPa)
Strain. %
0
20
40
60
80
0
2
4
6
8
10
12

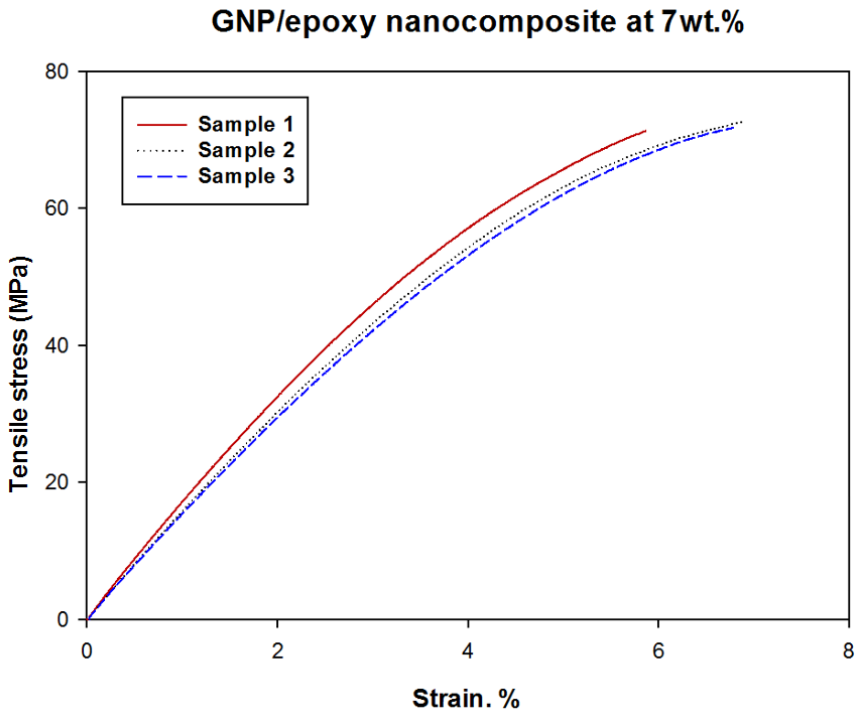

Figure A.2.1. The typical tensile stress-strain curves for the GNP/epoxy nanocomposites at various weight concentrations.

Table A.2.1. Summary of tensile tests results for the GNP/epoxy nanocomposites specimens at various weight concentrations in comparison to the pure epoxy composites (base (0)).

GNP/epoxy nanocomposites processed by ball milling method																		
Specimen Number	Maximum Tensile Strength (MPa)						Tensile Modulus (GPa)						Maximum Strain (%)					
	0 wt. %	***2.5wt.%***	***4wt.%***	***5 wt.%***	***6wt.%***	***7 wt.%***	***0 wt. %***	***2.5wt.%***	***4wt.%***	***5 wt.%***	***6 wt.%***	***7 wt.%***	***0 wt. %***	***2.5wt.%***	***4wt.%***	***5 wt.%***	***6wt.%***	***7 wt.%***
1	67.63	76.10	75.90	79.19	74.09	73.40	1.33	1.38	1.37	1.52	1.30	1.40	8.16	6.60	9.08	6.50	8.05	5.88
2	66.53	70.81	75.50	79.30	75.10	73.60	1.38	1.37	1.45	1.41	1.32	1.43	6.34	5.40	7.80	7.80	7.20	6.90
3	67.60	78.09	75.10	78.91	72.81	72.90	1.30	1.36	1.44	1.56	1.31	1.37	8.16	7.02	8.40	6.48	7.30	6.80
4	68.80	-	-	78.20	-	-	1.35	-	-	1.51	-	-	8.18	-	-	6.46	-	-
Average	67.64	75.00	75.50	78.90	74.00	73.30	1.34	1.37	1.42	1.50	1.31	1.40	7.71	6.34	8.42	6.81	7.51	6.52
S.D	±0.92	±3.76	±0.45	±0.49	±1.14	±0.36	±0.03	±0.01	±0.06	±0.06	±0.01	±0.03	±0.91	±0.84	±0.64	±0.65	±0.46	±0.56
C.V	1.37%	5.00%	0.59%	0.62%	1.55%	0.49%	2.51%	0.73%	3.93%	4.25%	0.76%	2.1%	11.80%	13.20%	7.60%	9.60%	6.18%	8.62%
Incr.%	base(0)	+10.8	+11.6	+16.6	+9.4	+8.3	base(0)	+2.2	+8.2	+11.9	-2.2	+4.4	base(0)	-17.7	+9.2	-11.6	-2.6	-15.4

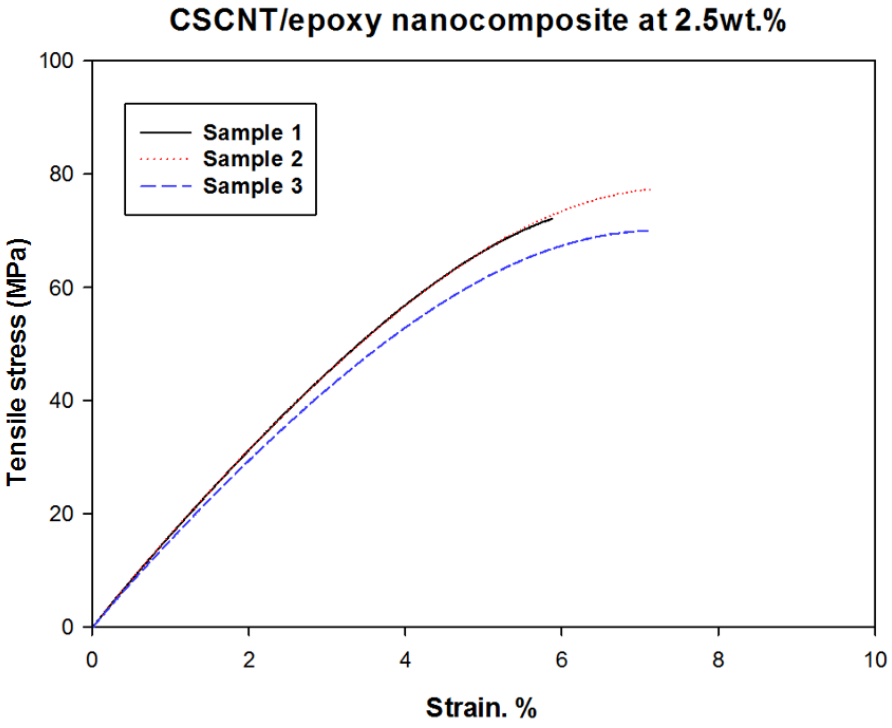
CSCNT/epoxy nanocomposite at 2.5wt.%
Sample 1
Sample 2
Sample 3
Tensile stress (MPa)
Strain. %
0
20
40
60
80
100
0
2
4
6
8
10

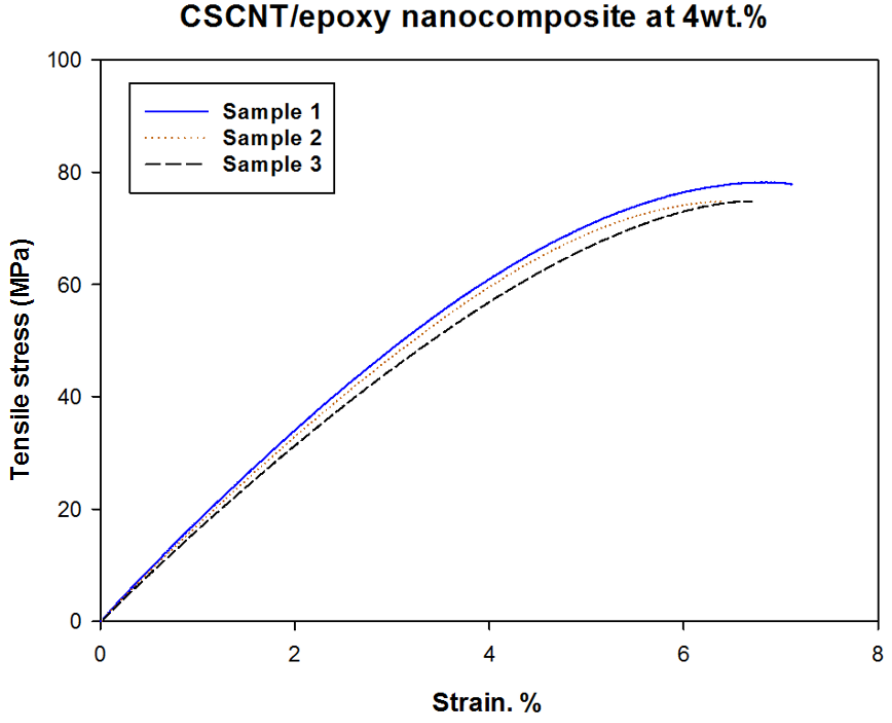
CSCNT/epoxy nanocomposite at 4wt.%
Sample 1
Sample 2
Sample 3
Tensile stress (MPa)
Strain. %
0
20
40
60
80
100
0
2
4
6
8

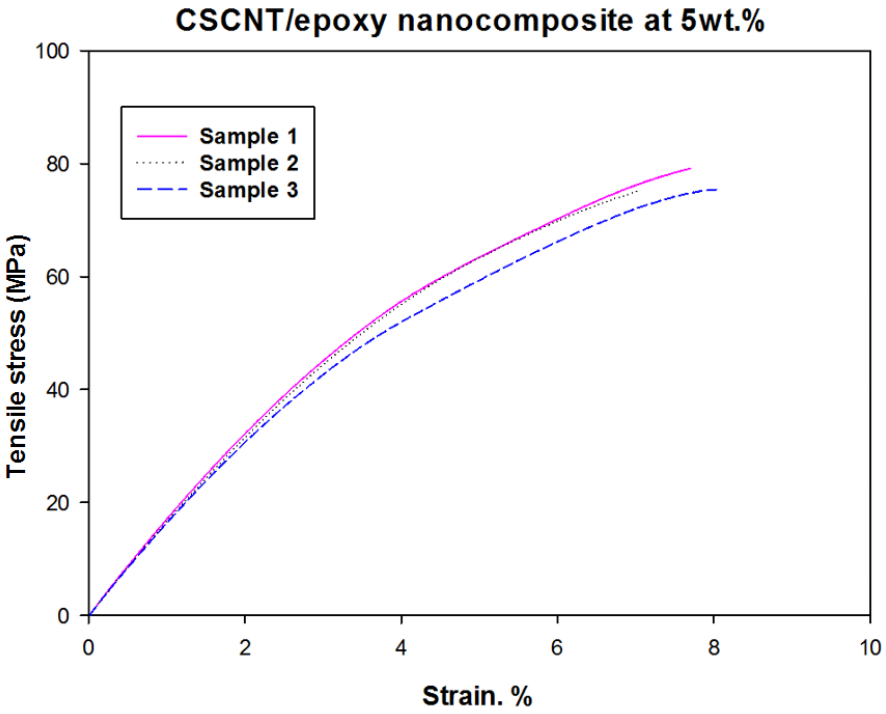
CSCNT/epoxy nanocomposite at 5wt.%
Sample 1
Sample 2
Sample 3
Tensile stress (MPa)
Strain. %
0
20
40
60
80
100
0
2
4
6
8
10

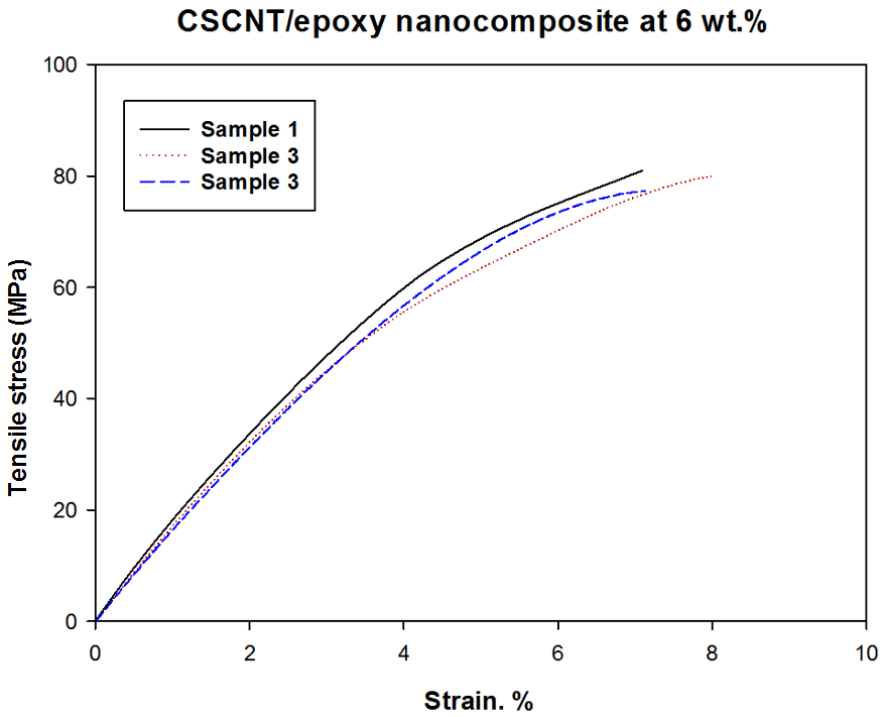
CSCNT/epoxy nanocomposite at 6 wt.%
Sample 1
Sample 3
Sample 3
Tensile stress (MPa)
Strain. %
0
20
40
60
80
100
0
2
4
6
8
10

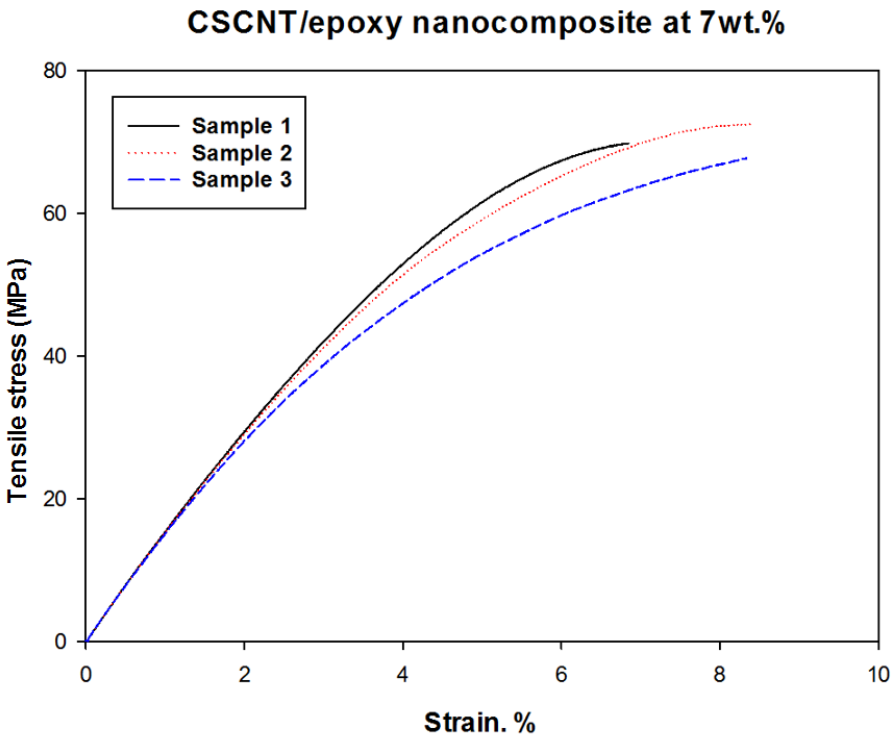

Figure A.2.2. The typical tensile stress-strain curves for the CSCNT/epoxy nanocomposites at various weight concentrations.

Table A.2.2. Summary of tensile tests results for the CSCNT/epoxy nanocomposites specimens at various weight concentrations in comparison with pure epoxy composites (base (0)).

CSCNT/epoxy nanocomposites processed by ball milling method																		
Specimen Number	Maximum Tensile Strength (MPa)						Tensile Modulus (GPa)						Maximum Strain (%)					
	0 wt. %	***2.5wt.%***	***4wt.%***	***5 wt.%***	***6wt.%***	***7 wt.%***	***0 wt. %***	***2.5wt.%***	***4wt.%***	***5 wt.%***	***6 wt.%***	***7 wt.%***	***0 wt. %***	***2.5wt.%***	***4wt.%***	***5 wt.%***	***6wt.%***	***7 wt.%***
1	67.63	74.90	78.65	80.72	81.22	70.50	1.33	1.45	1.54	1.53	1.59	1.31	8.16	5.89	7.12	7.70	7.10	6.86
2	66.53	77.90	74.90	75.11	80.70	71.00	1.38	1.45	1.5	1.51	1.58	1.30	6.34	7.18	6.40	7.01	8.60	8.40
3	67.60	69.50	74.75	78.11	78.68	68.80	1.30	1.30	1.43	1.46	1.57	1.26	8.16	7.12	6.74	8.03	7.18	8.38
4	68.80	-	-	-	-	-	1.35	-	-	-	-	-	8.18	-	-	-	-	-
Average	67.64	74.10	76.10	77.98	80.20	70.10	1.34	1.40	1.49	1.5	1.58	1.29	7.71	6.73	6.75	7.58	7.62	7.88
S.D	±0.92	±4.25	±2.20	±2.80	±1.34	±1.15	±0.03	±0.08	±0.05	±0.036	±0.01	±0.02	±0.91	±0.72	±0.36	±0.51	±0.84	±0.88
C.V	1.37%	5.74%	2.90%	3.59%	1.67%	1.64%	2.51%	6.18%	3.73%	2.40%	0.63%	2.05%	11.80%	10.80%	5.30%	6.70%	11.07%	11.2%
Incr.%	base(0)	+9.5	+12.5	+15.2	+18.5	+3.6	base(0)	+4.4	+11.1	+11.9	+17.9	-3.7	base(0)	-12.7	-12.4	-1.7	-1.1	+2.2

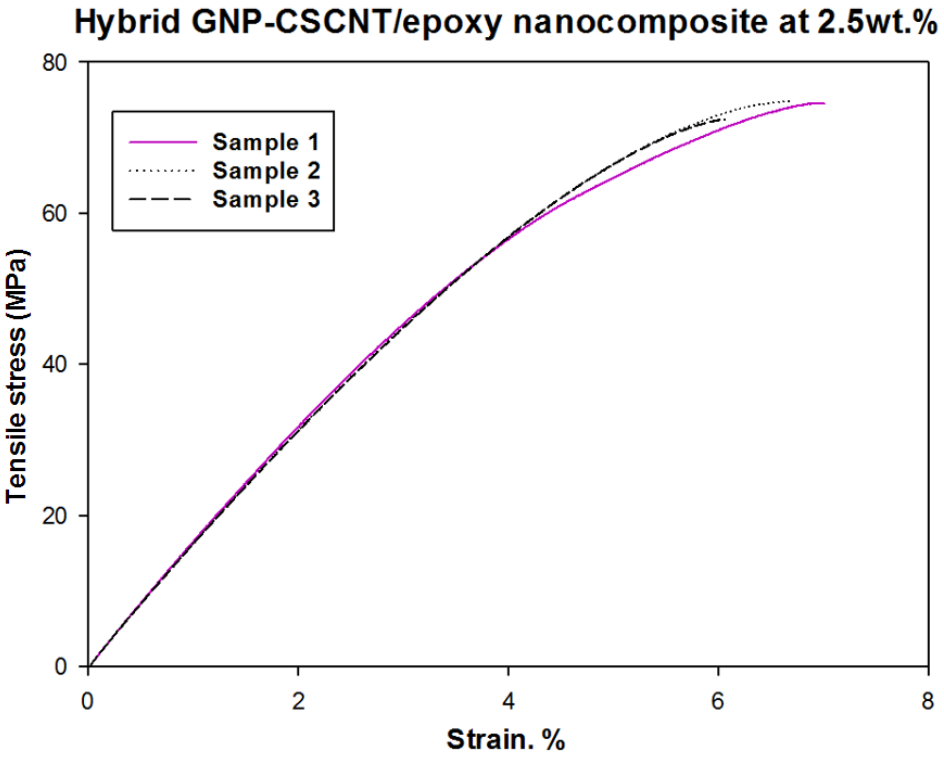
Hybrid GNP-CSCNT/epoxy nanocomposite at 2.5wt.%
Sample 1
Sample 2
Sample 3
Tensile stress (MPa)
Strain. %
0
20
40
60
80
0
2
4
6
8

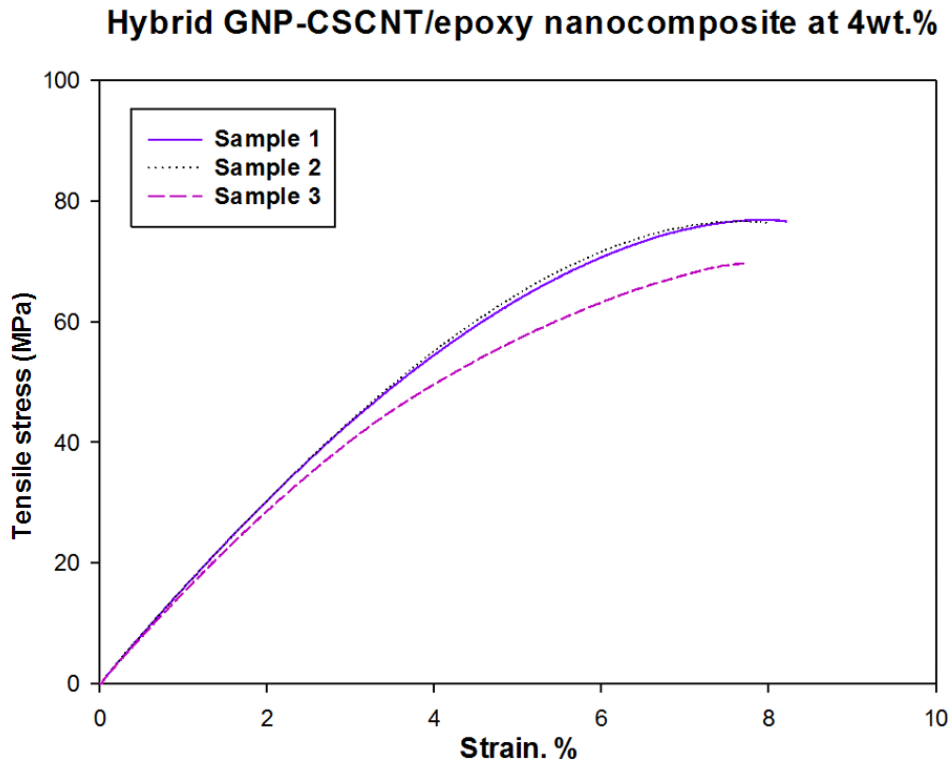
Hybrid GNP-CSCNT/epoxy nanocomposite at 4wt.%
Sample 1
Sample 2
Sample 3
Tensile stress (MPa)
Strain. %
0
20
40
60
80
100
0
2
4
6
8
10

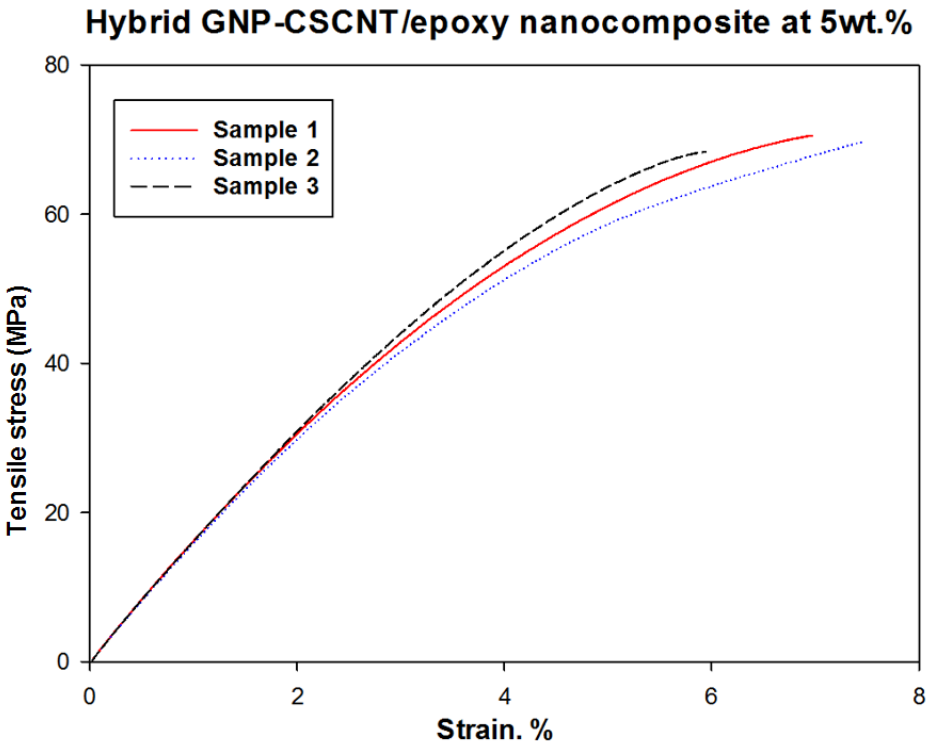
Hybrid GNP-CSCNT/epoxy nanocomposite at 5wt.%
Sample 1
Sample 2
Sample 3
Tensile stress (MPa)
Strain. %
0
20
40
60
80
0
2
4
6
8

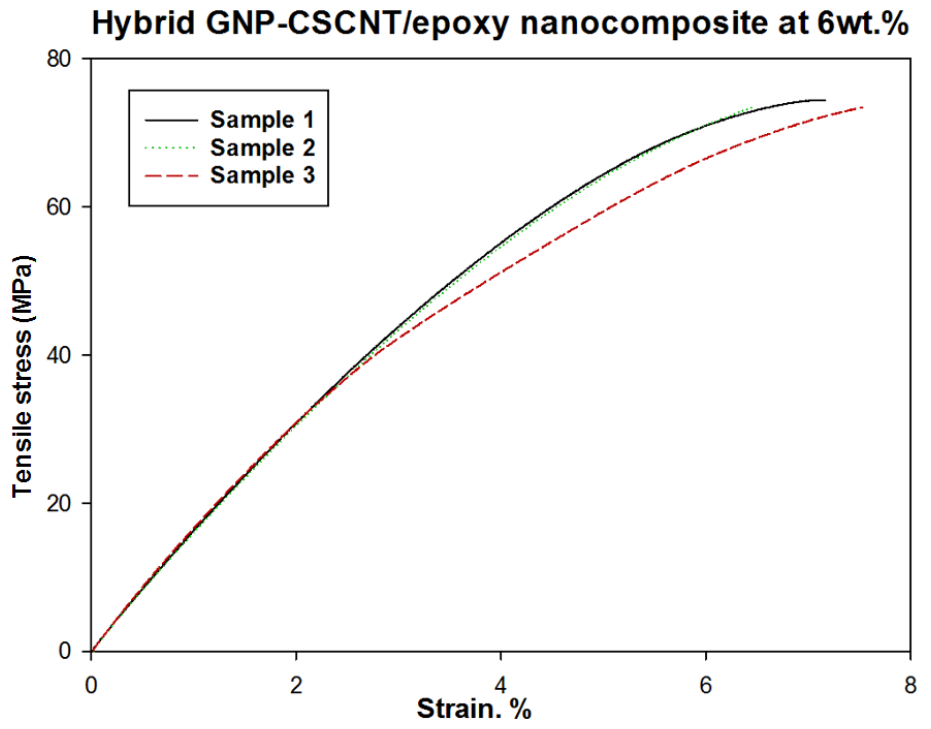
Hybrid GNP-CSCNT/epoxy nanocomposite at 6wt.%
Sample 1
Sample 2
Sample 3
Tensile stress (MPa)
Strain. %
0
20
40
60
80
0
2
4
6
8

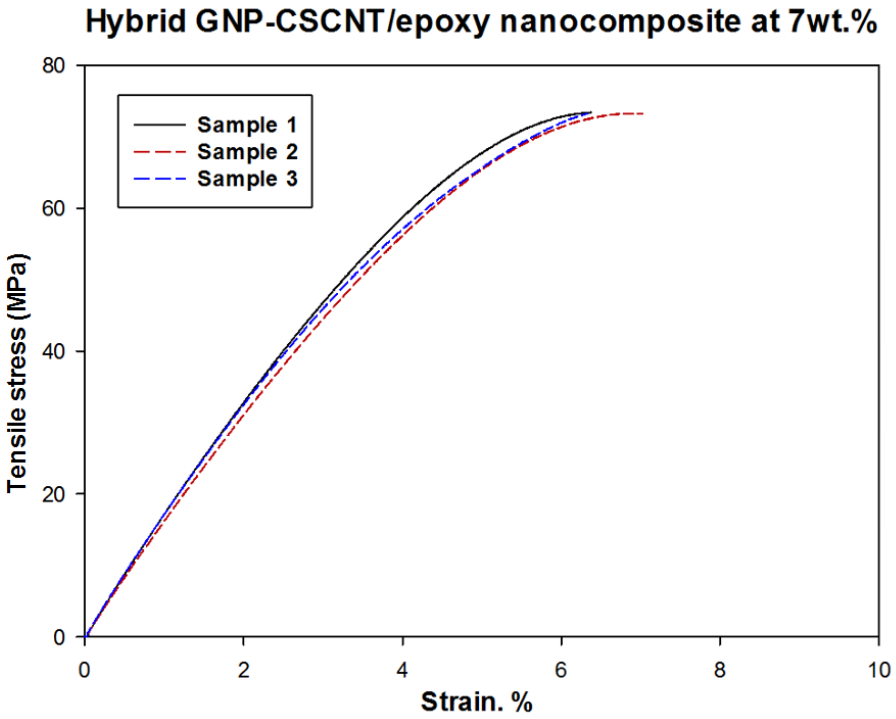

Figure A.2.3. The typical tensile stress-strain curves for the hybrid GNP-CSCNT/epoxy nanocomposites at various weight concentrations.

Table A.2.3. Summary of tensile tests results for the hybrid GNP-CSCNT/epoxy nanocomposites specimens at various weight concentrations in comparison with the pure epoxy composites (base (0)).

Hybrid GNP-CSCNT/epoxy nanocomposites processed by ball milling method																		
Specimen Number	Maximum Tensile Strength (MPa)						Tensile Modulus (GPa)						Maximum Strain (%)					
	0 wt. %	***2.5wt.%***	***4wt.%***	***5 wt.%***	***6wt.%***	***7 wt.%***	***0 wt. %***	***2.5wt.%***	***4wt.%***	***5 wt.%***	***6 wt.%***	***7 wt.%***	***0 wt. %***	***2.5wt.%***	***4wt.%***	***5 wt.%***	***6wt.%***	***7 wt.%***
1	67.63	74.50	77.60	71.40	74.90	72.50	1.33	1.43	1.43	1.30	1.52	1.50	8.16	7.06	8.30	7.02	7.20	6.40
2	66.53	75.00	76.10	72.80	73.60	72.60	1.38	1.39	1.44	1.39	1.51	1.40	6.34	6.70	8.01	7.55	6.44	7.10
3	67.60	73.70	70.10	69.10	74.20	73.99	1.30	1.38	1.36	1.36	1.56	1.36	8.16	6.01	7.74	5.98	7.54	6.34
4	68.80	-		-	-	-	1.35	-	-	-	-	-	8.18	-	-	-	-	-
Average	67.64	74.40	74.60	71.10	74.30	73.03	1.34	1.40	1.41	1.35	1.53	1.42	7.71	6.59	8.01	6.85	7.06	6.61
S.D	±0.92	±0.65	±3.97	±1.86	±0.65	±0.83	±0.03	±0.026	±0.04	±0.04	±0.02	±0.07	±0.91	±0.53	±0.28	±0.79	±0.56	±0.42
C.V	1.37%	0.88%	5.31%	2.62%	0.88%	1.14%	2.51%	1.88%	3.09%	3.39%	1.73%	5.00%	11.80%	8.00%	3.50%	11.60%	7.97%	6.40%
Incr.%	base(0)	+9.9	+10.2	+5.1	+9.8	+7.9	base(0)	+4.4	+5.2	+0.7	+14.1	+5.9	base(0)	-14.5	+3.9	-11.1	-8.4	-14.2

Appendix A.3. Typical tensile stress-strain curves for the pure epoxy composite (base (0)) as well as three epoxy nanocomposites modified with carbon nanomaterials at various weight concentrations processed by combined techniques.

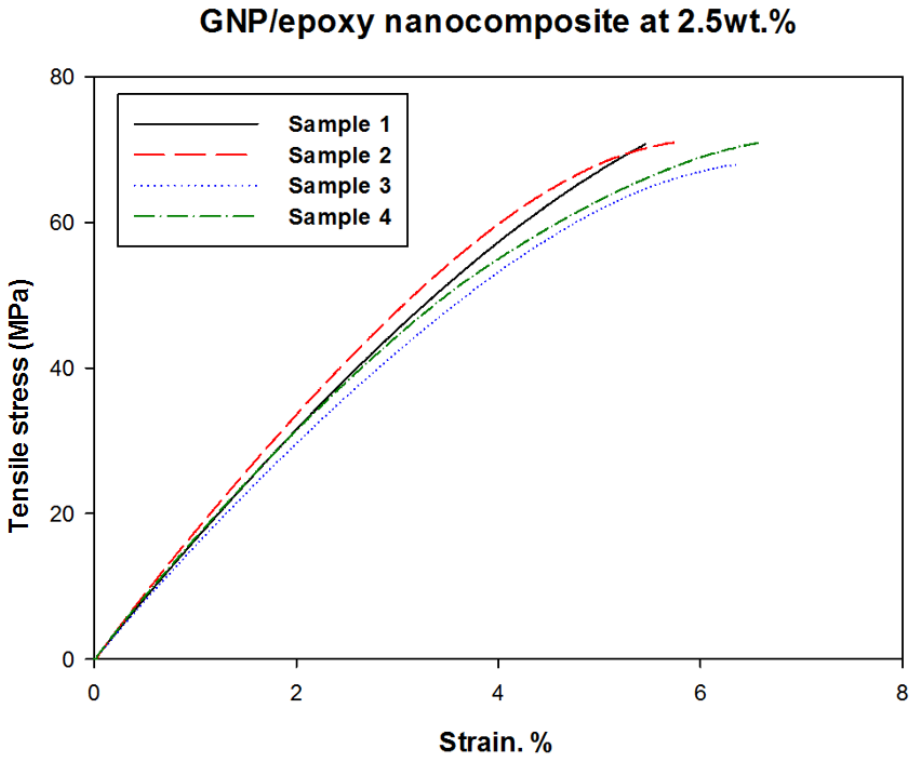

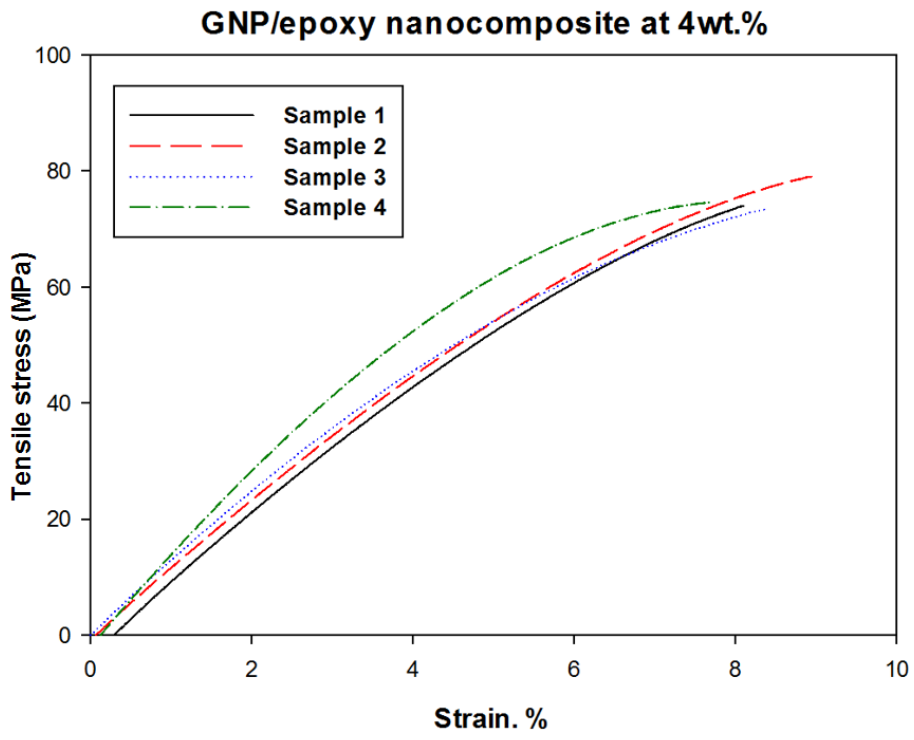

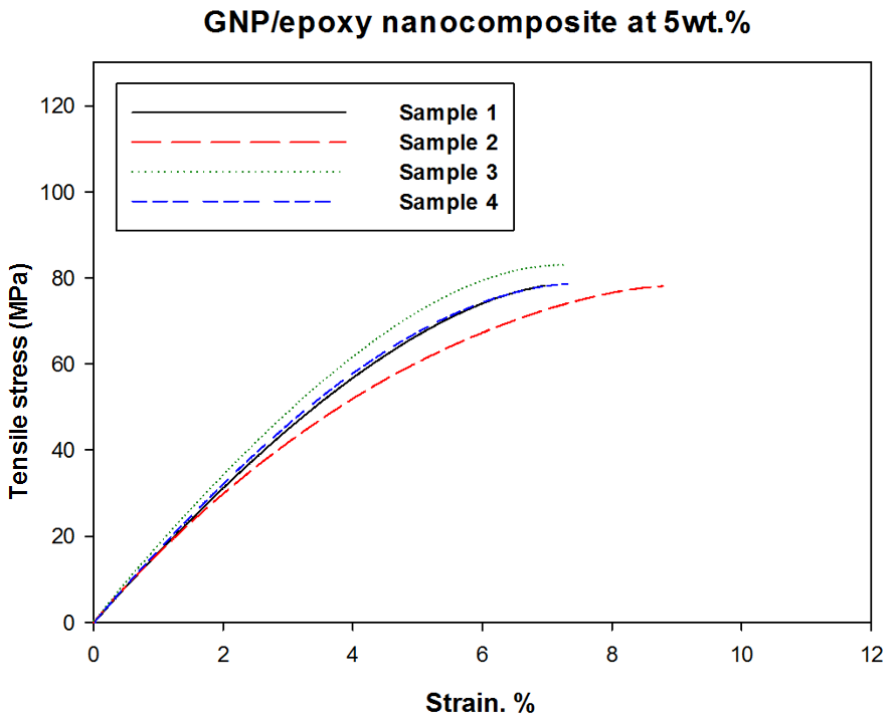
GNP/epoxy nanocomposite at 5wt.%
Sample 1
Sample 2
Sample 3
Sample 4
Tensile stress (MPa)
Strain. %
0
20
40
60
80
100
120
0
2
4
6
8
10
12

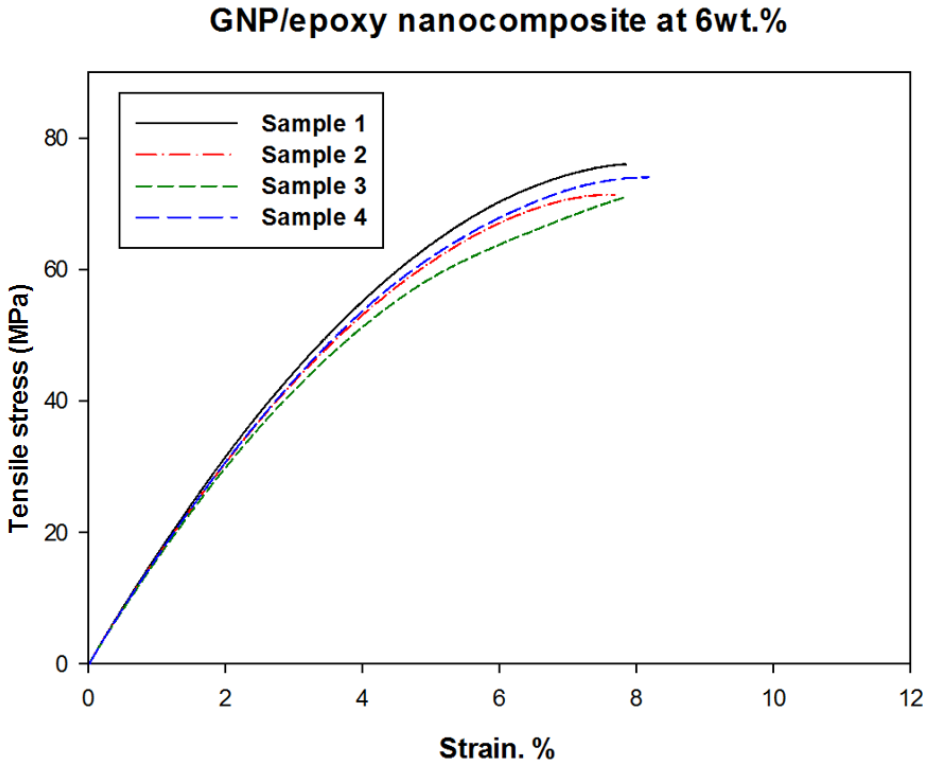
GNP/epoxy nanocomposite at 6wt.%
Sample 1
Sample 2
Sample 3
Sample 4
Tensile stress (MPa)
Strain. %
0
20
40
60
80
0
2
4
6
8
10
12

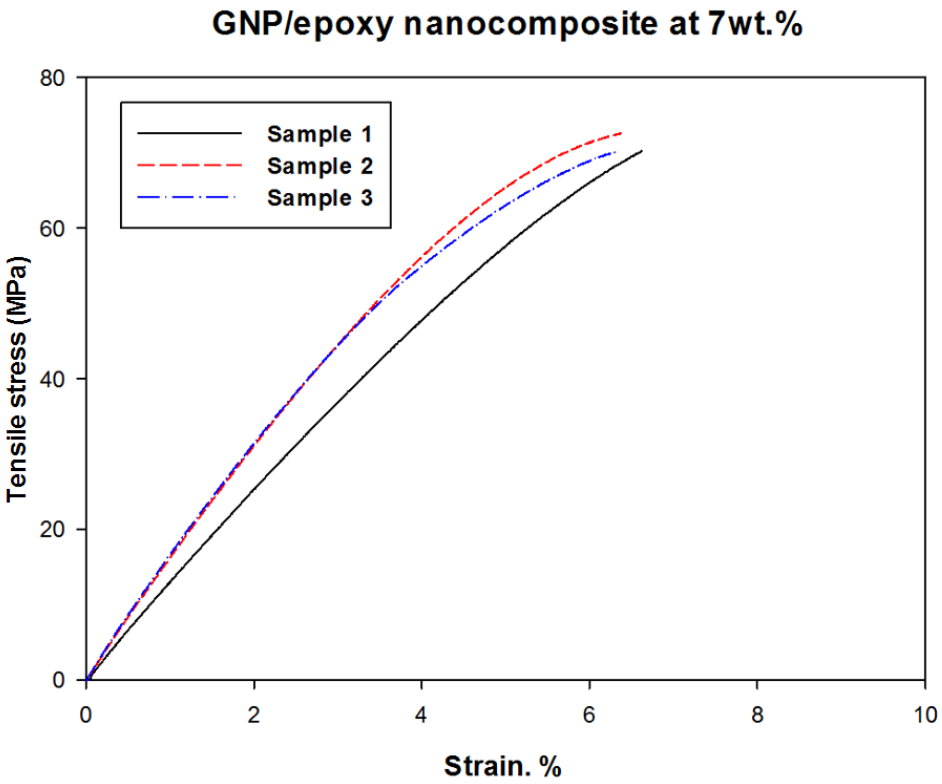

Figure A.3.1. The typical tensile stress-strain curves for the GNP/epoxy nanocomposites at various weight concentrations.

Table A.3.1. Summary of tensile tests results for the GNP/epoxy nanocomposites specimens at various weight concentrations in comparison with the pure epoxy composites (base (0)).

GNP/epoxy nanocomposites processed by combined techniques method																		
Specimen Number	Maximum Tensile Strength (MPa)						Tensile Modulus (GPa)						Maximum Strain (%)					
	0 wt. %	***2.5wt.%***	***4wt.%***	***5 wt.%***	***6wt.%***	***7 wt.%***	***0 wt. %***	***2.5wt.%***	***4wt.%***	***5 wt.%***	***6 wt.%***	***7 wt.%***	***0 wt. %***	***2.5wt.%***	***4wt.%***	***5 wt.%***	***6wt.%***	***7 wt.%***
1	67.63	71.90	75.10	78.76	76.80	73.10	1.33	1.52	1.50	1.50	1.53	1.35	8.16	5.40	8.10	6.84	7.89	6.50
2	66.53	70.50	79.20	77.96	72.60	74.12	1.38	1.57	1.52	1.56	1.53	1.64	6.34	5.60	8.90	8.80	7.78	6.20
3	67.60	69.10	74.04	82.10	72.49	72.98	1.30	1.50	1.56	1.61	1.52	1.66	8.16	6.20	8.40	7.02	7.80	6.10
4	68.80	71.10	76.18	78.70	74.47	-	1.35	1.53	1.54	1.57	1.50	-	8.18	6.40	7.88	7.10	8.10	-
Average	67.64	70.80	76.13	79.38	74.09	73.40	1.34	1.53	1.53	1.56	1.52	1.55	7.71	5.90	8.32	7.44	7.89	6.26
S.D	±0.92	±1.29	±2.22	±1.84	±2.02	±0.62	±0.03	±0.03	±0.02	±0.04	±0.01	±0.14	±0.91	±0.47	±0.44	±0.91	±0.14	±0.21
C.V	1.37%	1.82%	2.92%	2.32%	2.72%	0.85%	2.51%	1.92%	1.46%	2.91%	0.75%	9.10%	11.80%	8.00%	5.30%	12.24%	1.85%	3.32%
Incr.%	base(0)	+4.7	+12.5	+17.3	+9.5	+8.5	base(0)	+14.2	+14.2	+16.4	+13.4	+15.7	base(0)	-23.4	+7.9	-3.5	-2.3	-18.8

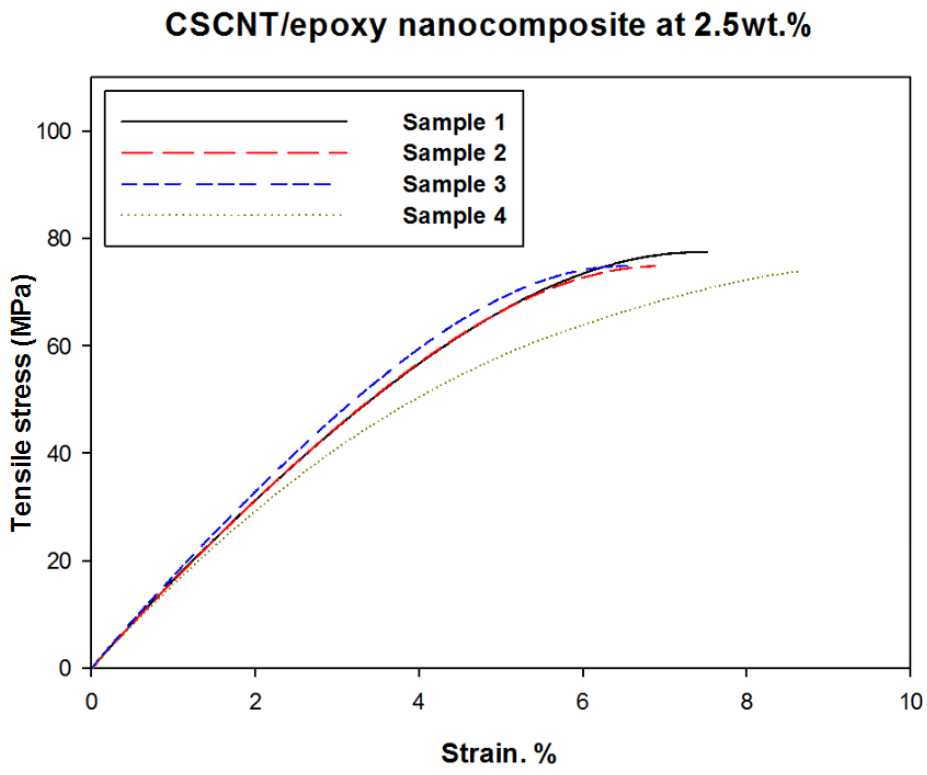
CSCNT/epoxy nanocomposite at 2.5wt.%
Sample 1
Sample 2
Sample 3
Sample 4
Tensile stress (MPa)
0
20
40
60
80
100
0
2
4
6
8
10
Strain. %

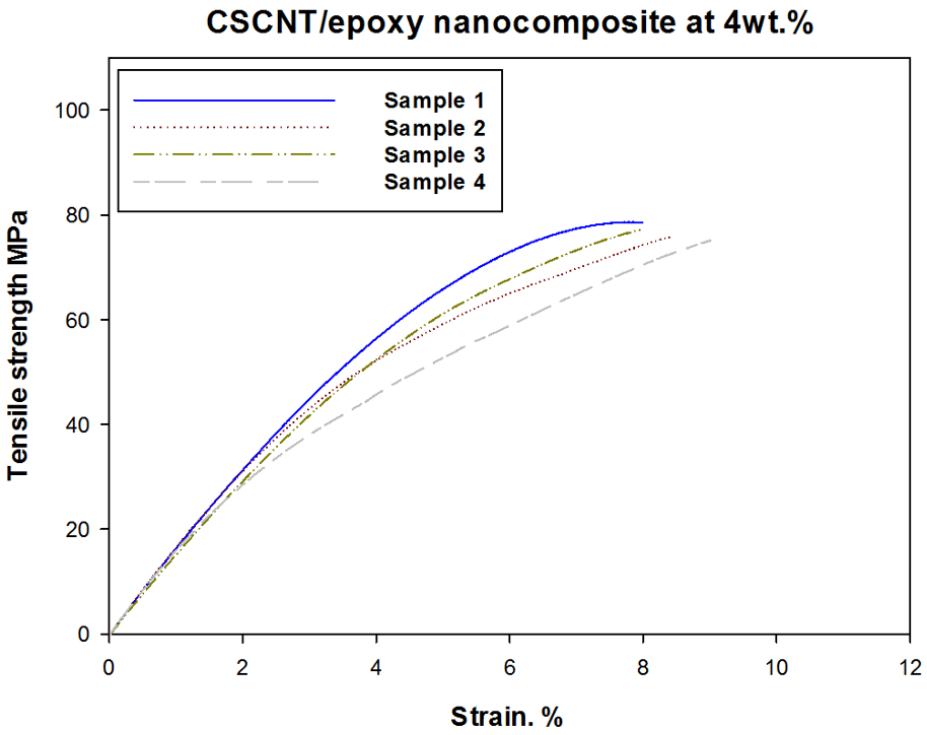
CSCNT/epoxy nanocomposite at 4wt.%
Sample 1
Sample 2
Sample 3
Sample 4
Tensile strength MPa
0
20
40
60
80
100
0
2
4
6
8
10
12
Strain. %

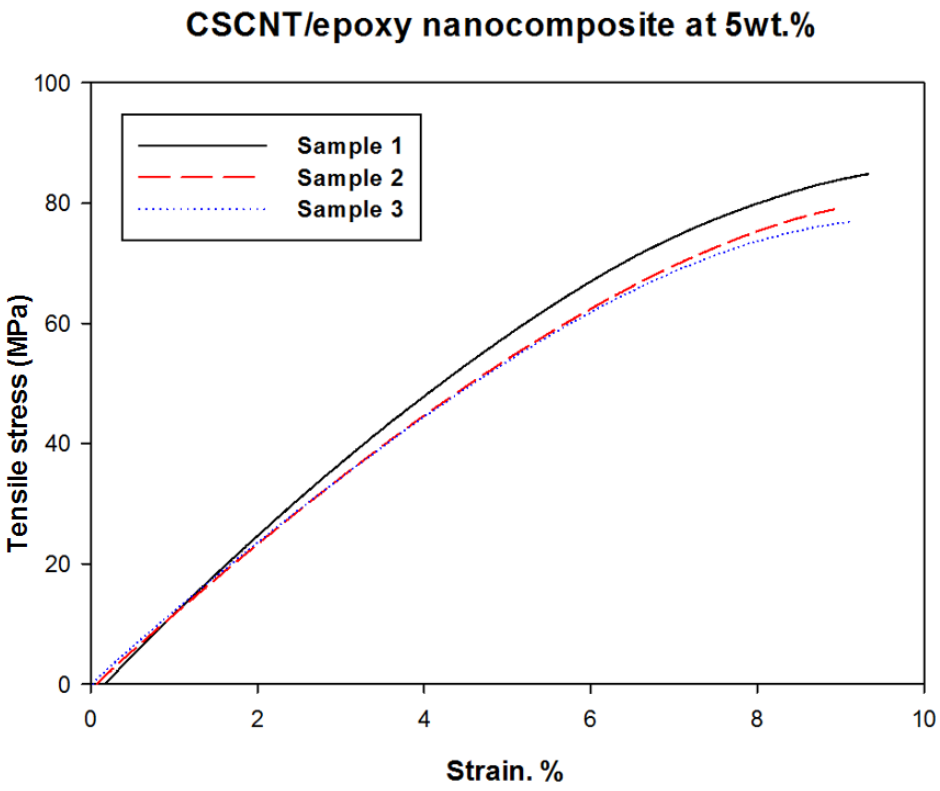
CSCNT/epoxy nanocomposite at 5wt.%
Sample 1
Sample 2
Sample 3
Tensile stress (MPa)
Strain. %
0
20
40
60
80
100
0
2
4
6
8
10

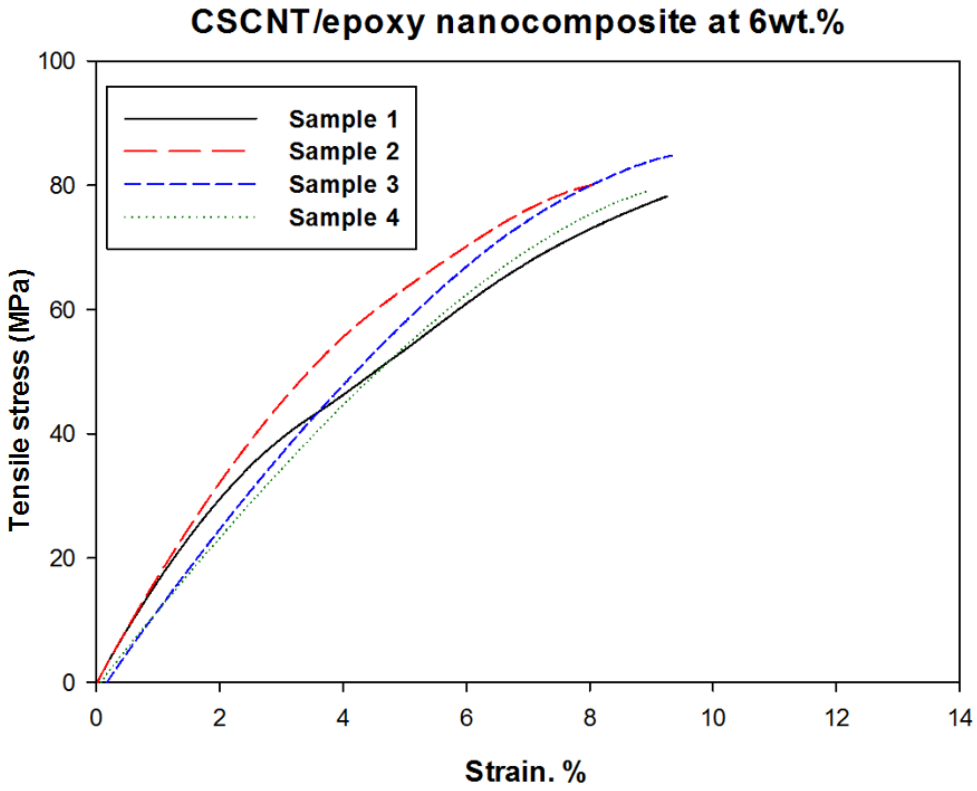
CSCNT/epoxy nanocomposite at 6wt.%
Sample 1
Sample 2
Sample 3
Sample 4
Tensile stress (MPa)
Strain. %
0
20
40
60
80
100
0
2
4
6
8
10
12
14

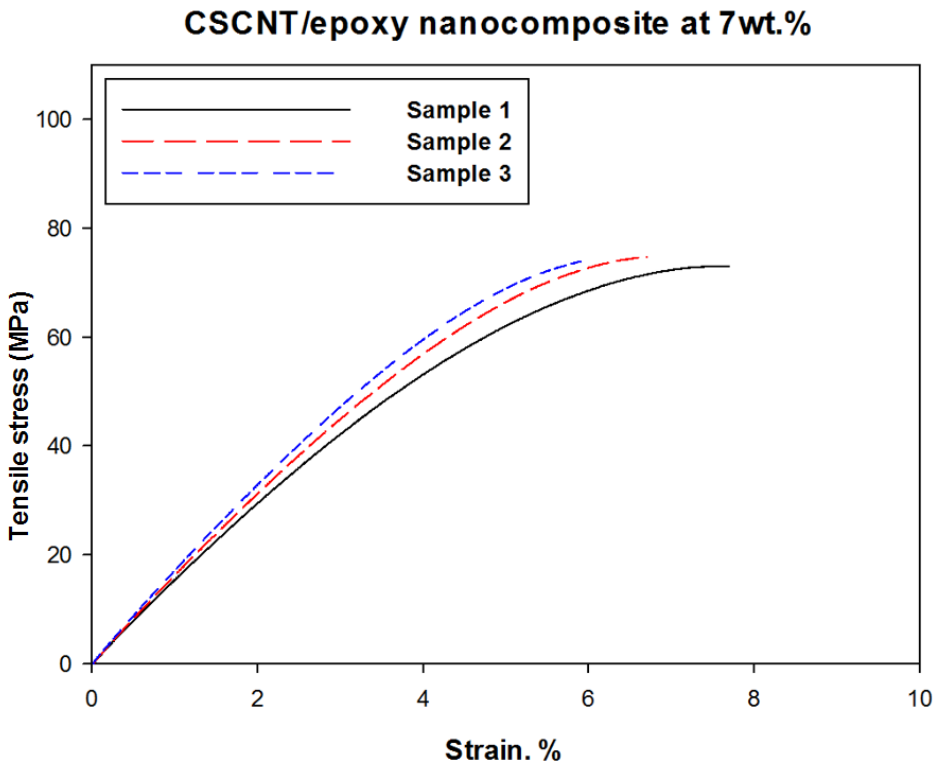

Figure A.3.2. The typical tensile stress-strain curves for the CSCNT/epoxy nanocomposites at various weight concentrations.

Table A.3.2. Summary of tensile tests results for the CSCNT/epoxy nanocomposites specimens at various weight concentrations in comparison with the pure epoxy composites (base (0)).

CSCNT/epoxy nanocomposites by combined techniques method																		
Specimen Number	Maximum Tensile Strength (MPa)						Tensile Modulus (GPa)						Maximum Strain (%)					
	0 wt. %	***2.5wt.%***	***4wt.%***	***5 wt.%***	***6wt.%***	***7 wt.%***	***0 wt. %***	***2.5wt.%***	***4wt.%***	***5 wt.%***	***6 wt.%***	***7 wt.%***	***0 wt. %***	***2.5wt.%***	***4wt.%***	***5 wt.%***	***6wt.%***	***7 wt.%***
1	67.63	77.50	79.00	83.70	79.40	72.90	1.33	1.38	1.49	1.29	1.78	1.42	8.16	7.52	8.04	9.20	9.36	7.80
2	66.53	74.00	78.30	79.70	82.50	74.70	1.38	1.38	1.44	1.41	1.80	1.46	6.34	6.90	8.36	8.90	7.80	7.60
3	67.60	73.42	78.70	78.76	86.10	74.53	1.30	1.42	1.40	1.50	1.81	1.50	8.16	6.40	8.01	9.02	9.40	6.10
4	68.80	74.80	78.60	-	-	-	1.35	1.34	1.36	-	1.41	-	8.18	8.50	9.02	-	8.80	-
Average	67.64	74.93	78.65	80.72	82.03	74.04	1.34	1.38	1.42	1.40	1.70	1.46	7.71	7.33	8.35	9.04	8.84	7.16
S.D	±0.92	±1.80	±0.43	±2.62	±3.02	±0.99	±0.03	±0.03	±0.05	±0.10	±0.19	±0.04	±0.913	±0.90	±0.47	±0.24	±0.74	±0.92
C.V	1.37%	2.40%	0.54%	3.24%	3.68%	1.34%	2.51%	3.14%	3.92%	7.50%	11.40%	2.70%	11.80%	12.3%	5.61%	2.70%	8.4%	12.9%
Incr.%	base(0)	+10.8	+16.3	+19.3	+21.3	+9.4	base(0)	+2.9	+5.9	+4.4	+26.8	+8.9	base(0)	-4.9	-8.3	+17.2	+14.6	-7.1

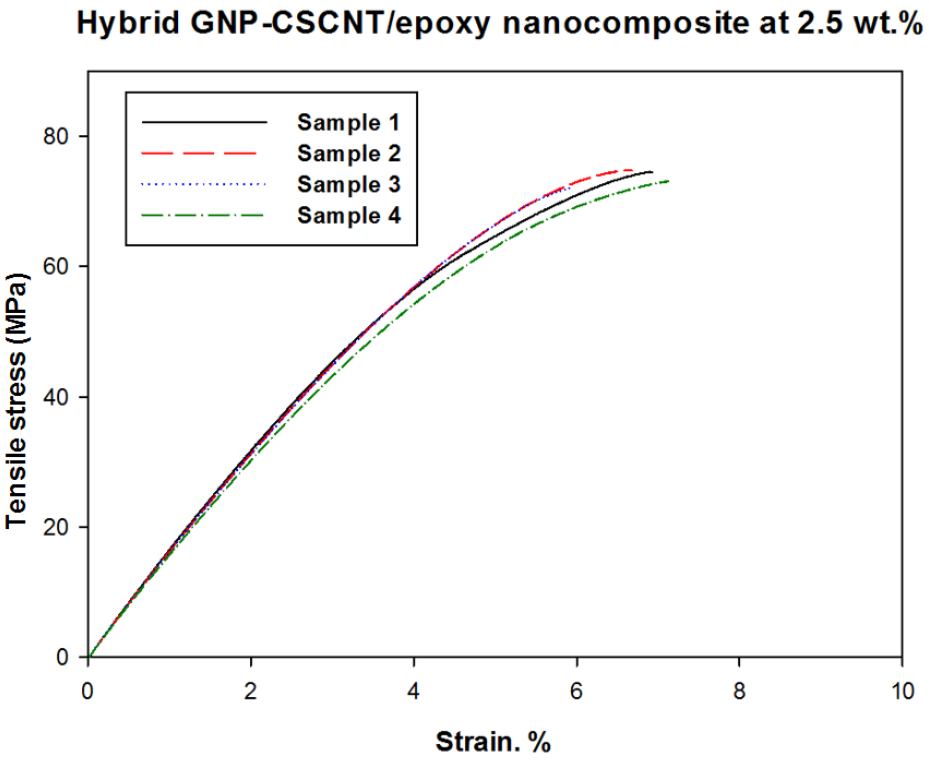
Hybrid GNP-CSCNT/epoxy nanocomposite at 2.5 wt.%
Sample 1
Sample 2
Sample 3
Sample 4
Tensile stress (MPa)
Strain. %
0
20
40
60
80
0
2
4
6
8
10

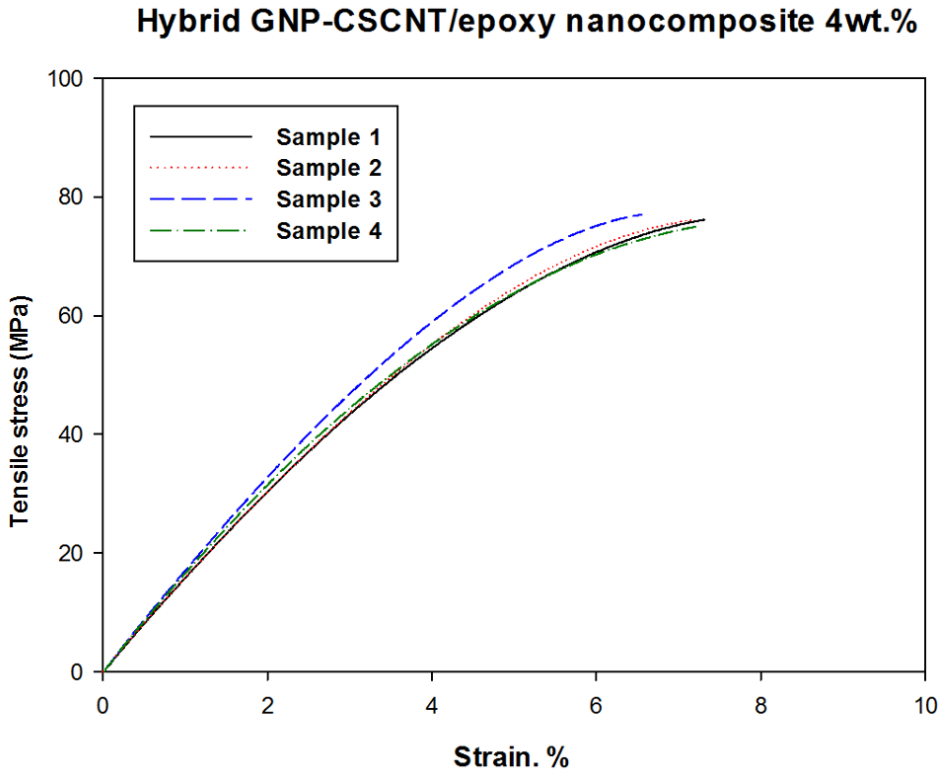
Hybrid GNP-CSCNT/epoxy nanocomposite 4wt.%
Sample 1
Sample 2
Sample 3
Sample 4
Tensile stress (MPa)
Strain. %
0
20
40
60
80
100
0
2
4
6
8
10

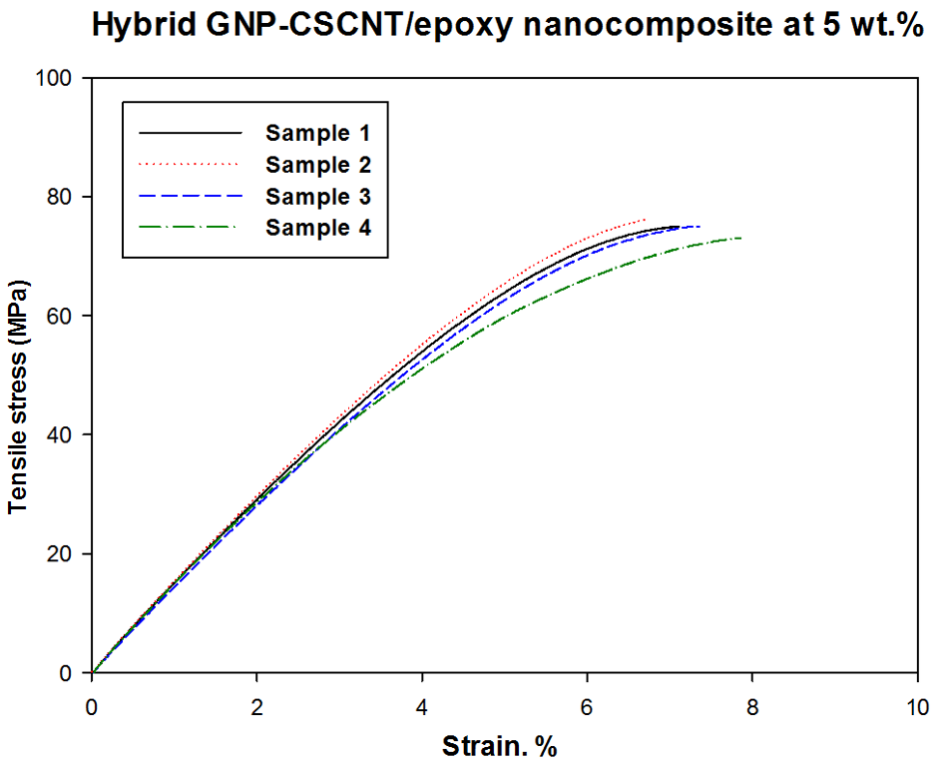
Hybrid GNP-CSCNT/epoxy nanocomposite at 5 wt.%
Sample 1
Sample 2
Sample 3
Sample 4
Tensile stress (MPa)
Strain. %
0
20
40
60
80
100
0
2
4
6
8
10

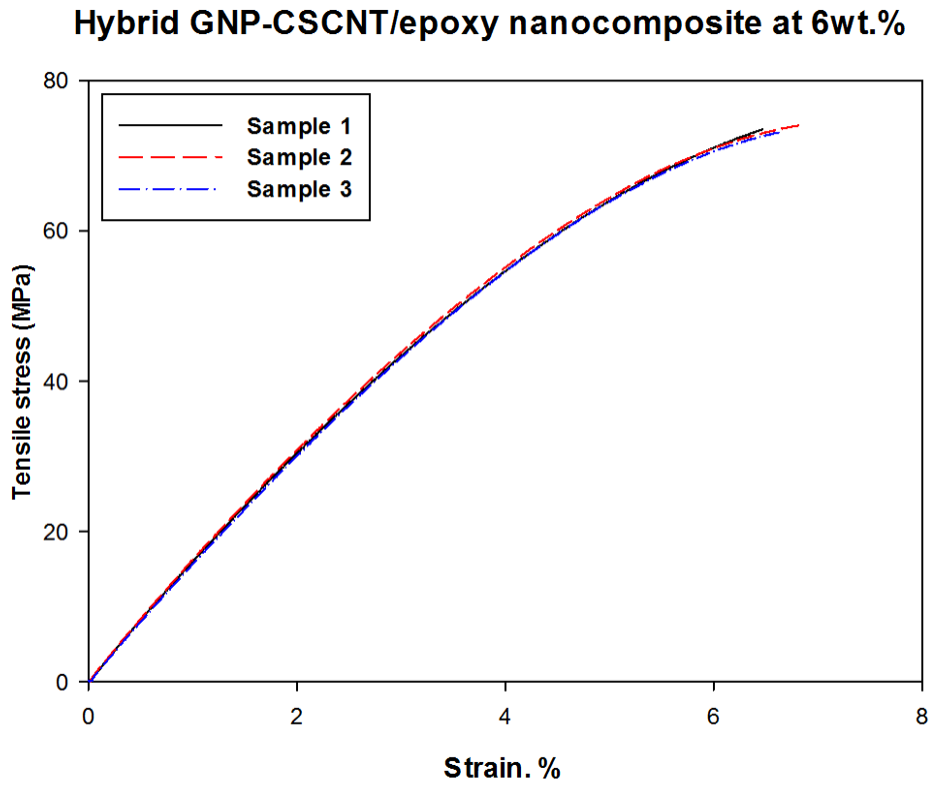
Hybrid GNP-CSCNT/epoxy nanocomposite at 6wt.%
Sample 1
Sample 2
Sample 3
Tensile stress (MPa)
Strain. %
0
20
40
60
80
0
2
4
6
8

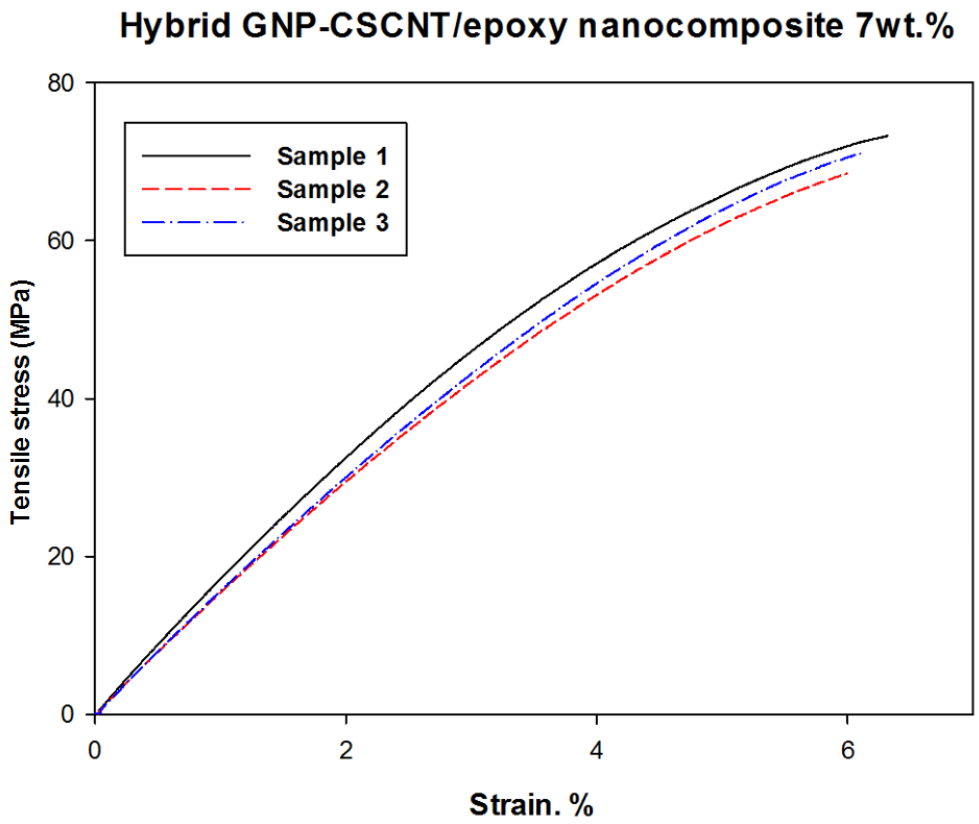

Figure A.3.3. The typical tensile stress-strain curves for the hybrid GNP-CSCNT/epoxy nanocomposites at various weight concentrations.

Table A.3.3. Summary of tensile tests results for the hybrid GNP-CSCNT/epoxy nanocomposites specimens at various weight concentrations in comparison with the pure epoxy composites (base (0)).

Hybrid GNP-CSCNT/ epoxy nanocomposites processed by combined techniques method																		
Specimen Number	Maximum Tensile Strength (MPa)						Tensile Modulus (GPa)						Maximum Strain (%)					
	0 wt. %	***2.5wt.%***	***4wt.%***	***5 wt.%***	***6wt.%***	***7 wt.%***	***0 wt. %***	***2.5 wt.%***	***4wt.%***	***5 wt.%***	***6 wt.%***	***7 wt.%***	***0 wt. %***	***2.5 wt.%***	***4wt.%***	***5 wt.%***	***6 wt.%***	***7 wt.%***
1	67.63	74.90	78.40	74.05	73.50	73.80	1.33	1.47	1.53	1.38	1.51	1.54	8.16	6.90	7.20	7.20	6.36	6.40
2	66.53	75.20	78.10	75.12	73.90	71.20	1.38	1.46	1.61	1.42	1.49	1.47	6.34	6.68	7.01	6.90	6.80	6.01
3	67.60	74.40	77.30	74.15	73.10	72.70	1.30	1.45	1.73	1.40	1.50	1.48	8.16	6.06	6.40	7.40	6.54	6.13
4	68.80	74.82	76.60	72.89	-	-	1.35	1.42	1.65	1.41	-	-	8.18	7.16	7.10	7.90	-	-
Average	67.64	74.83	77.60	74.14	73.50	72.57	1.34	1.45	1.63	1.40	1.50	1.50	7.71	6.70	6.92	7.10	6.56	6.18
S.D	±0.92	±0.33	±0.81	±0.91	±0.40	±1.30	±0.03	±0.02	±0.08	±0.02	±0.01	±0.03	±0.91	±0.47	±0.36	±0.50	±0.22	±0.19
C.V	1.37%	0.44%	1.00%	1.23%	0.54%	1.79%	2.51%	1.48%	5.10%	1.23%	0.66%	2.50%	11.8%	7.00%	5.20%	7.18%	3.30%	3.20%
Incr.%	base(0)	+10.6	+14.7	+9.6	+8.6	+7.3	base(0)	+8.2	+21.6	+4.5	+11.9	+11.9	base(0)	-13.1	-10.2	-7.9	-14.9	-19.8

Appendix B. Flexural Properties

Appendix B.1. Typical flexural stress-strain curves for the pure epoxy composite (base (0)) and three epoxy nanocomposites modified with carbon nanomaterials at various weight concentrations processed by sonication technique.

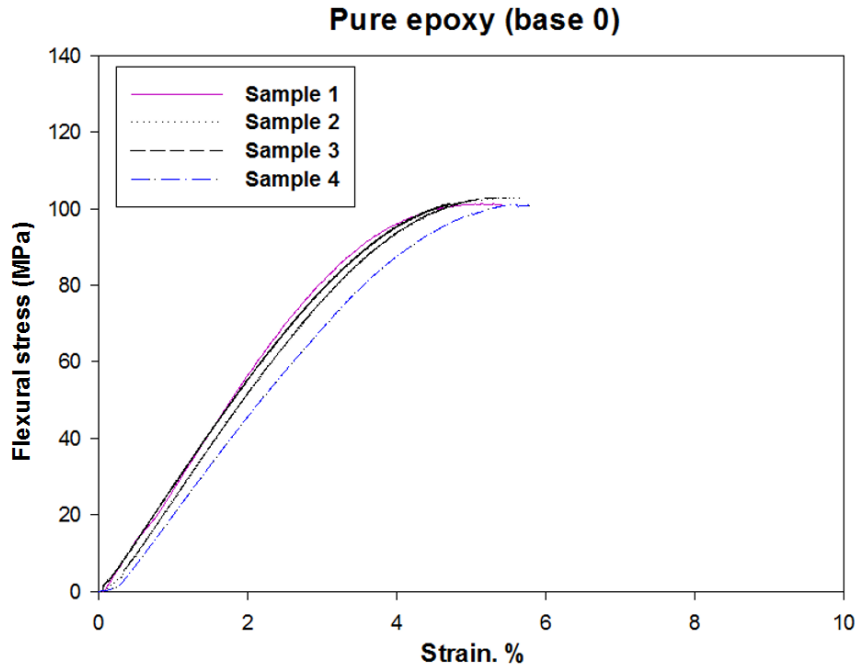

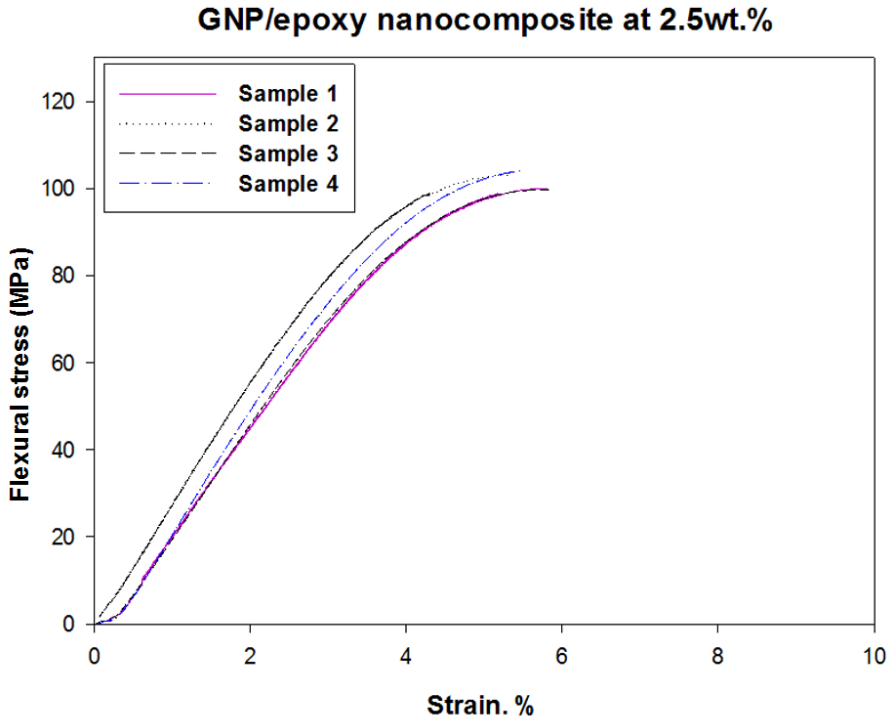

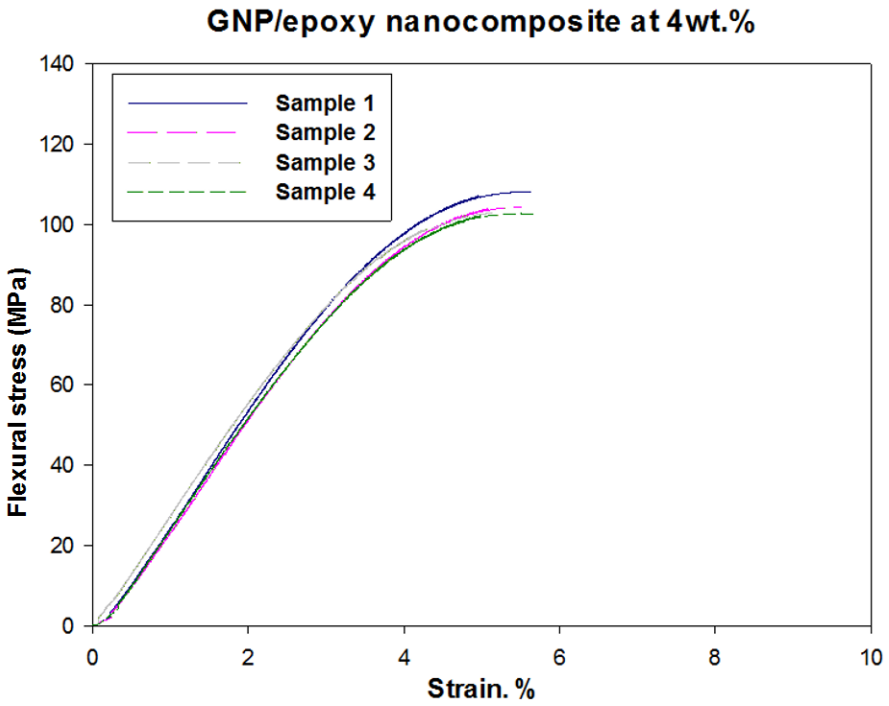
GNP/epoxy nanocomposite at 4wt.%
Sample 1
Sample 2
Sample 3
Sample 4
Flexural stress (MPa)
Strain. %
0
20
40
60
80
100
120
140
0
2
4
6
8
10

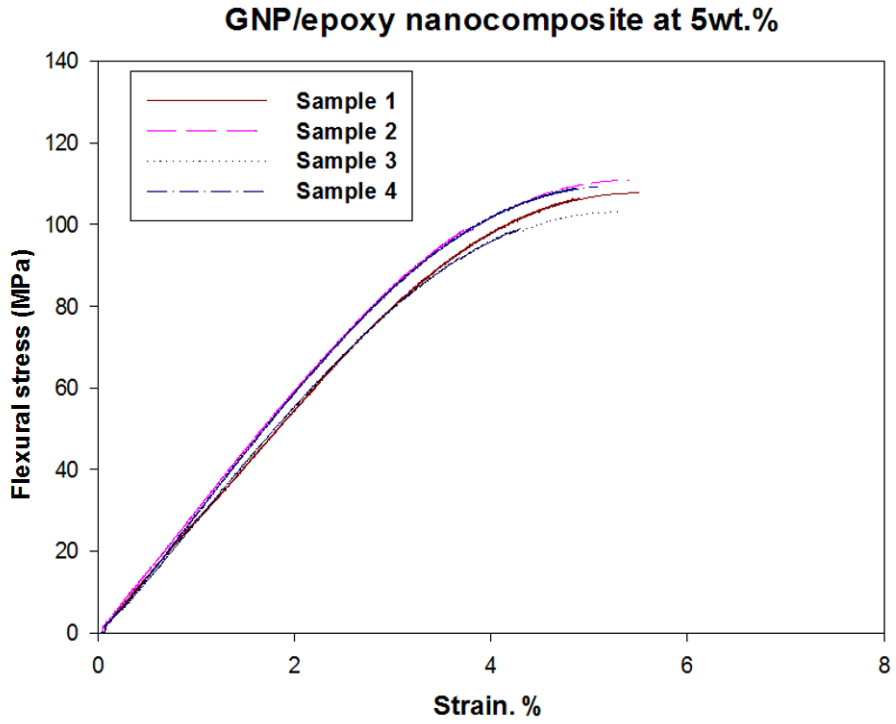
GNP/epoxy nanocomposite at 5wt.%
Sample 1
Sample 2
Sample 3
Sample 4
Flexural stress (MPa)
Strain. %
0
20
40
60
80
100
120
140
0
2
4
6
8

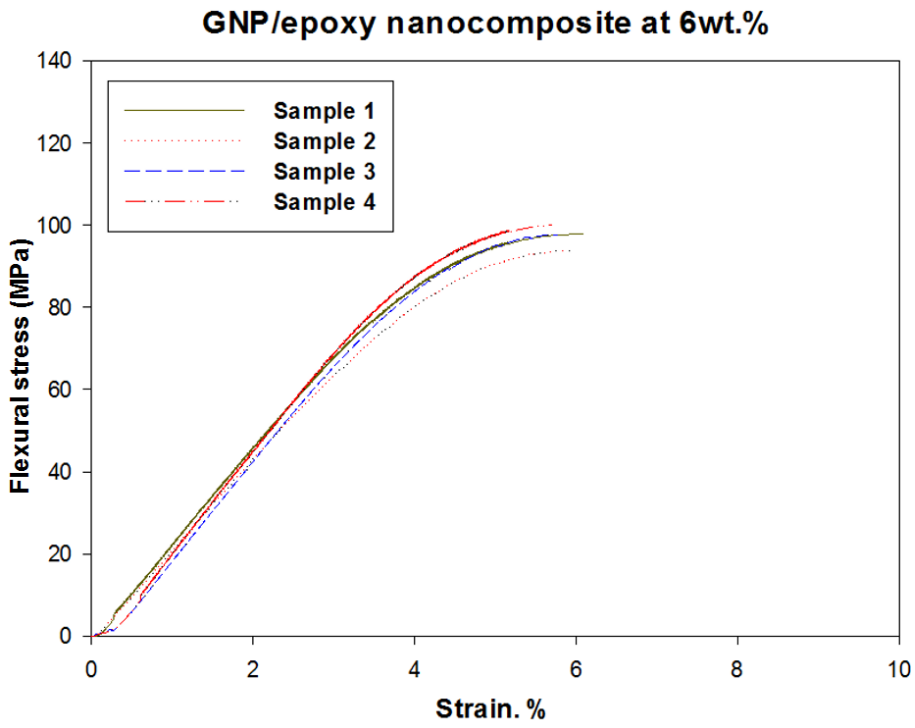

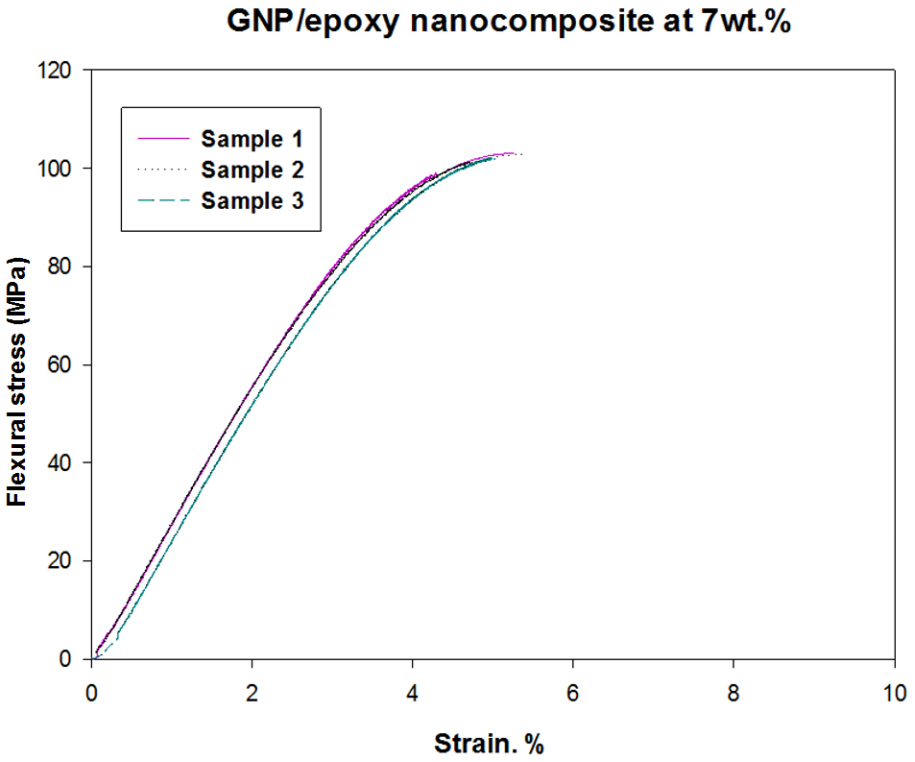

Figure B.1.1. Typical flexural stress-strain curves for the GNP/epoxy nanocomposites at various weight concentrations.

Table B.1.1. Summary of flexural tests results for the GNP/epoxy nanocomposites specimens at various weight concentrations in comparison with the pure epoxy composites (base (0)).

GNP/epoxy nanocomposites processed by sonication method																		
Specimen Number	Maximum Flexural Strength (MPa)						Flexural Modulus (GPa)						Maximum Strain (%)					
	0 wt. %	***2.5wt.%***	***4wt.%***	***5 wt.%***	***6wt.%***	***7 wt.%***	***0 wt. %***	***2.5wt.%***	***4wt.%***	***5 wt.%***	***6 wt.%***	***7 wt.%***	***0 wt. %***	***2.5wt.%***	***4wt.%***	***5 wt.%***	***6wt.%***	***7 wt.%***
1	102.14	102.00	104.40	107.70	97.80	103.30	2.99	2.30	2.55	2.66	2.00	2.66	5.60	5.98	5.80	5.60	6.08	5.40
2	102.48	97.73	108.04	110.80	95.80	103.10	2.75	2.00	2.45	2.67	2.15	2.66	5.72	5.64	5.60	5.52	6.00	5.50
3	101.15	103.01	103.12	103.10	97.70	102.96	2.75	2.01	2.46	2.57	2.10	2.63	5.68	5.20	4.88	5.40	5.78	5.24
4	99.10	97.39	102.15	109.40	100.17	-	2.71	2.10	2.54	2.50	2.22	-	5.88	5.44	5.82	5.10	5.76	-
Average	101.21	100.03	104.43	107.75	97.86	103.12	2.80	2.20	2.50	2.60	2.10	2.65	5.72	5.56	5.52	5.40	5.90	5.38
S.D	±1.52	±1.78	±2.57	±3.34	±1.79	±1.70	±0.13	±0.18	±0.05	±0.08	±0.09	±0.02	±0.11	±0.33	±0.44	±0.21	±0.16	±0.13
C.V	1.50%	2.88%	2.46%	3.10%	1.83%	1.65%	4.56%	1.82%	2.09%	3.09%	4.50%	0.65%	2.05%	5.90%	7.97%	4.00%	2.70%	2.43%
Incr.%	base(0)	-1.2	+3.2	+6.5	-3.3	+1.9	base(0)	-21.4	-10.7	-7.1	-25.0	-5.3	base(0)	-2.8	-3.5	-5.6	+3.1	-5.9

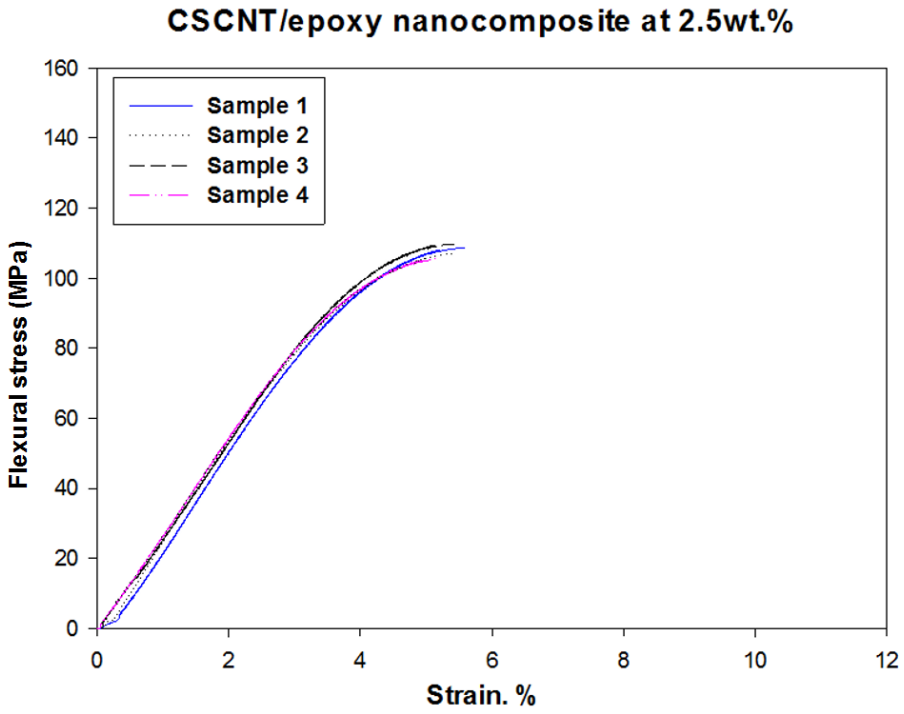
CSCNT/epoxy nanocomposite at 2.5wt.%
Sample 1
Sample 2
Sample 3
Sample 4
Flexural stress (MPa)
Strain. %
0
20
40
60
80
100
120
140
160
0
2
4
6
8
10
12

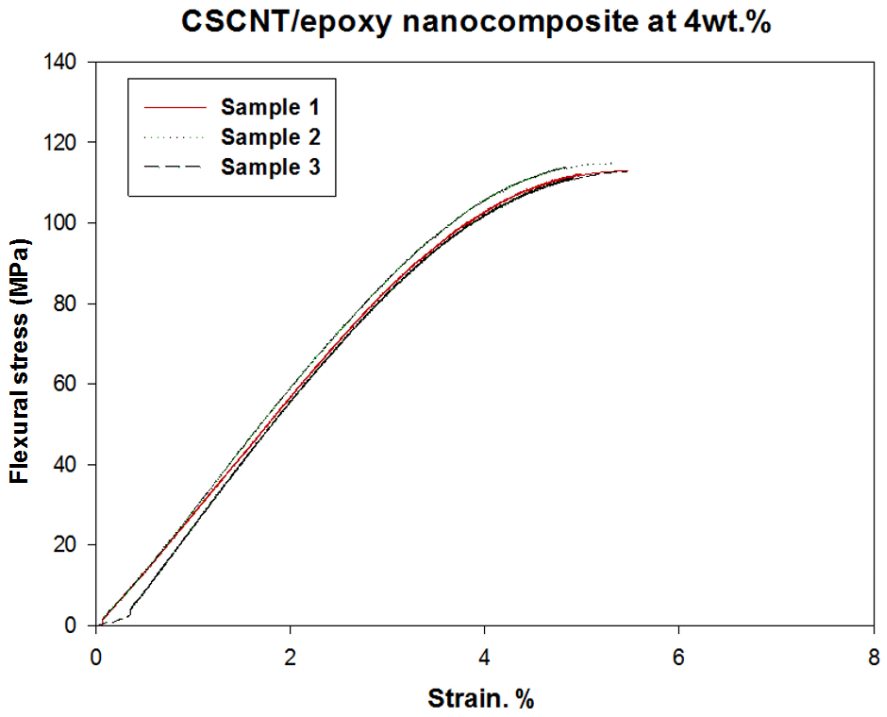
CSCNT/epoxy nanocomposite at 4wt.%
Sample 1
Sample 2
Sample 3
Flexural stress (MPa)
Strain. %
0
20
40
60
80
100
120
140
0
2
4
6
8

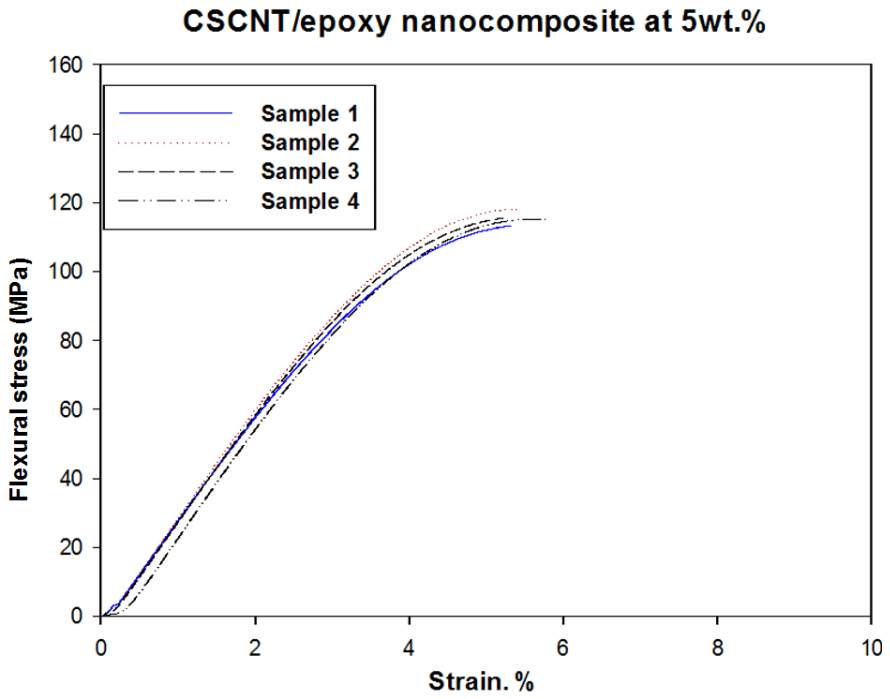
CSCNT/epoxy nanocomposite at 5wt.%
Sample 1
Sample 2
Sample 3
Sample 4
Flexural stress (MPa)
Strain. %
0
20
40
60
80
100
120
140
160
0
2
4
6
8
10

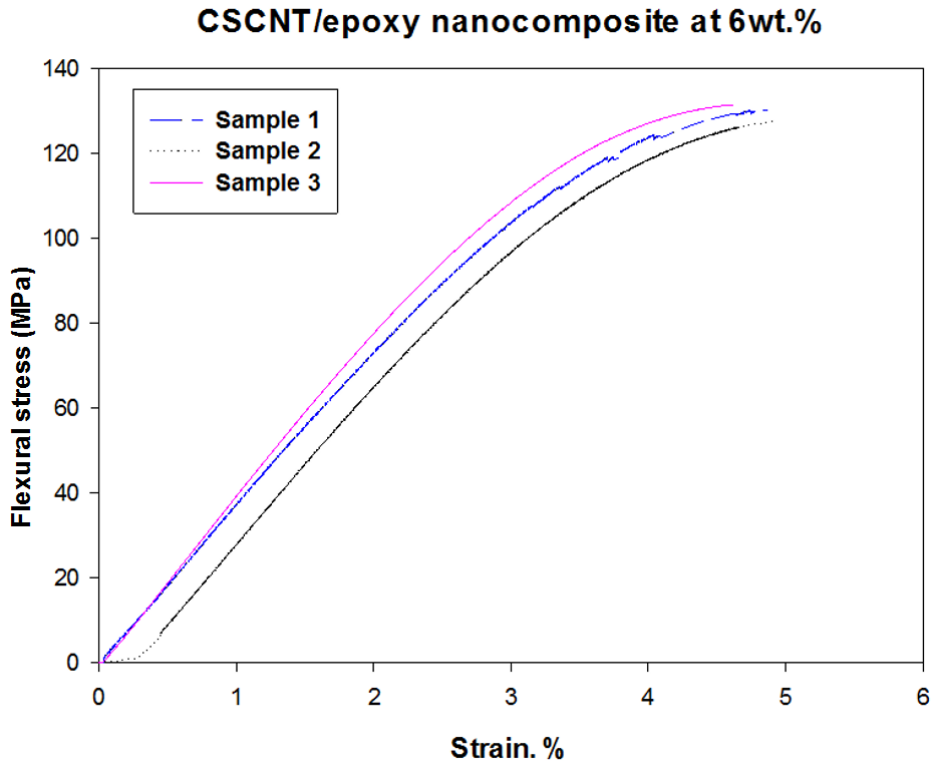
CSCNT/epoxy nanocomposite at 6wt.%
Sample 1
Sample 2
Sample 3
Flexural stress (MPa)
Strain. %
0
20
40
60
80
100
120
140
0
1
2
3
4
5
6

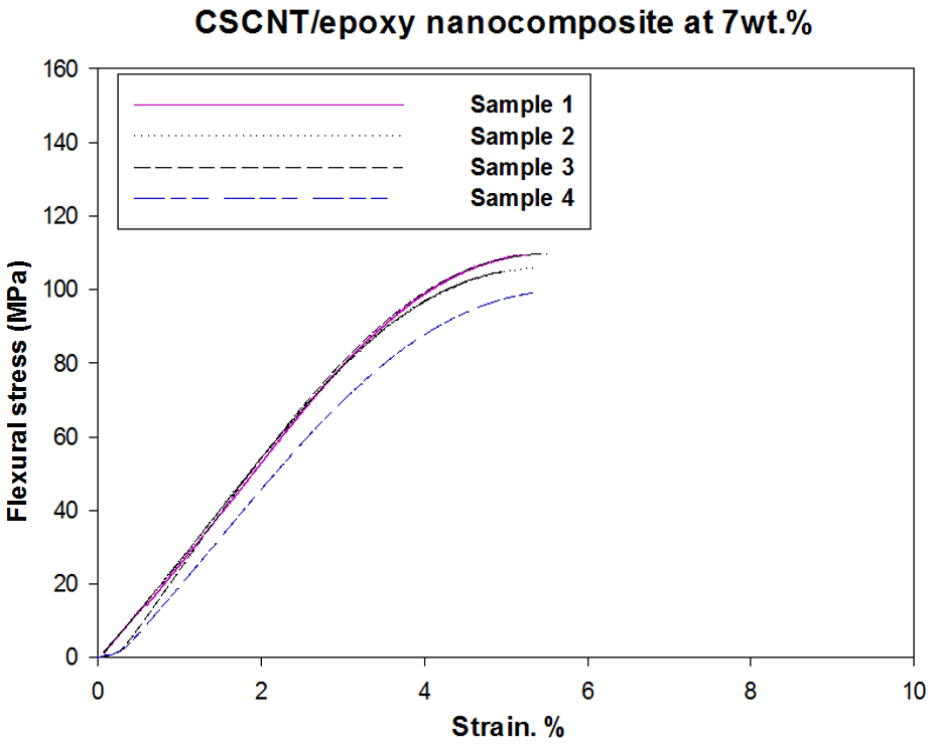

Figure B.1.2. The typical flexural stress-strain curves for the CSCNT/epoxy nanocomposites at various weight concentrations.

Table B.1.2. Summary of flexural tests results for the CSCNT/epoxy nanocomposites specimens at various weight concentrations in comparison to the pure epoxy composites (base (0)).

CSCNT/epoxy nanocomposites processed by sonication method																		
Specimen Number	Maximum Flexural Strength (MPa)						Flexural Modulus (GPa)						Maximum Strain (%)					
	0 wt. %	***2.5 wt.%***	***4 wt.%***	***5 wt.%***	***6wt.%***	***7 wt.%***	***0 wt. %***	***2.5 wt.%***	***4 wt.%***	***5 wt.%***	***6 wt.%***	***7 wt.%***	***0 wt. %***	***2.5 wt.%***	***4 wt.%***	***5 wt.%***	***6wt.%***	***7 wt.%***
1	102.14	107.68	112.70	114.71	130.10	105.91	2.99	2.41	2.83	2.90	3.50	2.80	5.60	5.90	5.44	5.24	4.90	5.10
2	102.48	112.80	112.81	111.79	132.00	109.85	2.75	2.47	2.85	2.90	3.61	2.70	5.72	5.76	5.38	5.38	5.04	5.02
3	101.15	104.90	113.03	113.87	128.20	99.17	2.75	2.36	2.87	2.86	3.39	2.51	5.68	5.82	5.42	5.18	4.40	5.40
4	99.10	110.10	-	118.64	-	108.10	2.71	2.46	-	2.82	-	2.71	5.88	5.62	-	5.80	-	5.01
Average	101.21	108.87	112.84	114.70	130.10	105.96	2.80	2.49	2.85	2.87	3.50	2.68	5.72	5.78	5.41	5.40	4.78	5.13
S.D	±1.52	±3.37	±0.17	±2.86	±1.90	±4.00	±0.13	±0.09	±0.02	±0.04	±0.11	±0.12	±0.11	±0.12	±0.03	±0.28	±0.33	±0.18
C.V	1.50%	3.1%	0.15%	2.49%	1.46%	3.82%	4.56%	3.63%	0.70%	1.33%	4.50%	4.52%	2.05%	2.00%	0.56%	5.10%	6.90%	3.56%
Incr.%	base(0)	+7.5	+11.5	+13.3	+28.5	+4.7	base(0)	-11.1	+1.7	+2.5	+25.0	-4.2	base(0)	+1.0	-5.4	-5.6	-16.4	-10.3

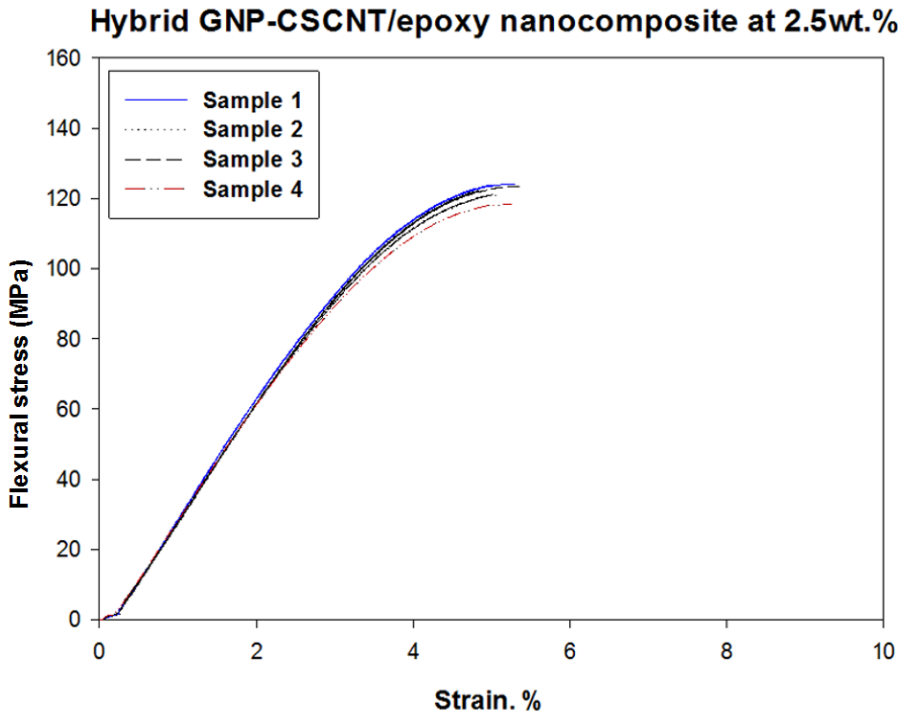
Hybrid GNP-CSCNT/epoxy nanocomposite at 2.5wt.%
Sample 1
Sample 2
Sample 3
Sample 4
Flexural stress (MPa)
Strain. %
0
20
40
60
80
100
120
140
160
0
2
4
6
8
10

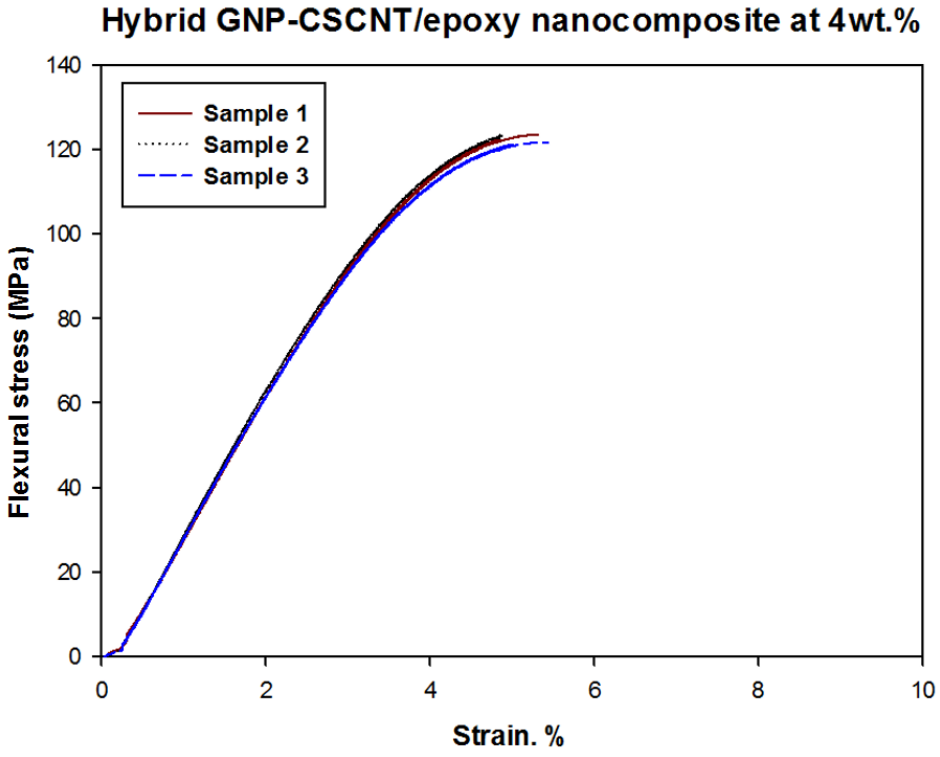
Hybrid GNP-CSCNT/epoxy nanocomposite at 4wt.%
Sample 1
Sample 2
Sample 3
Flexural stress (MPa)
Strain. %
0
20
40
60
80
100
120
140
0
2
4
6
8
10

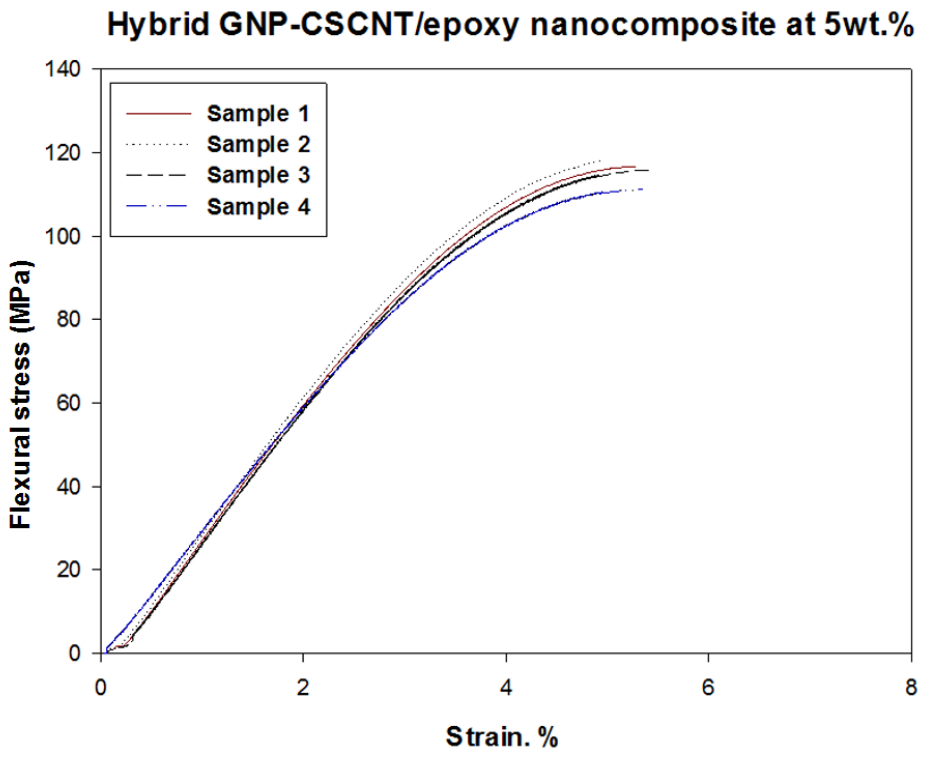
Hybrid GNP-CSCNT/epoxy nanocomposite at 5wt.%
Sample 1
Sample 2
Sample 3
Sample 4
Flexural stress (MPa)
Strain. %
0
20
40
60
80
100
120
140
0
2
4
6
8

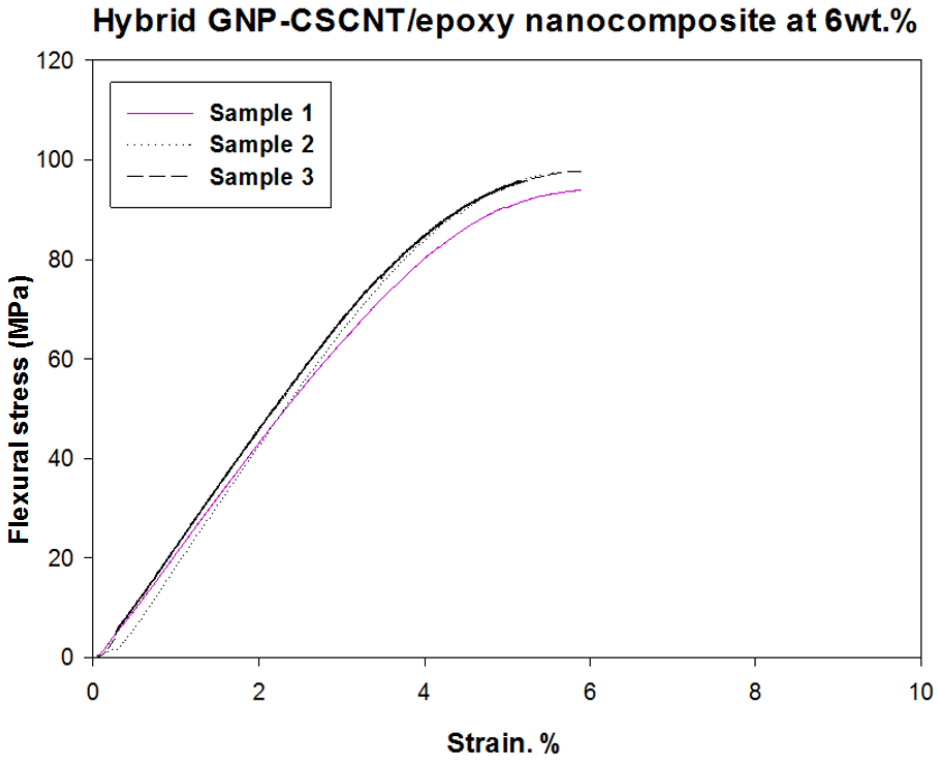
Hybrid GNP-CSCNT/epoxy nanocomposite at 6wt.%
Sample 1
Sample 2
Sample 3
Flexural stress (MPa)
Strain. %
0
20
40
60
80
100
120
0
2
4
6
8
10

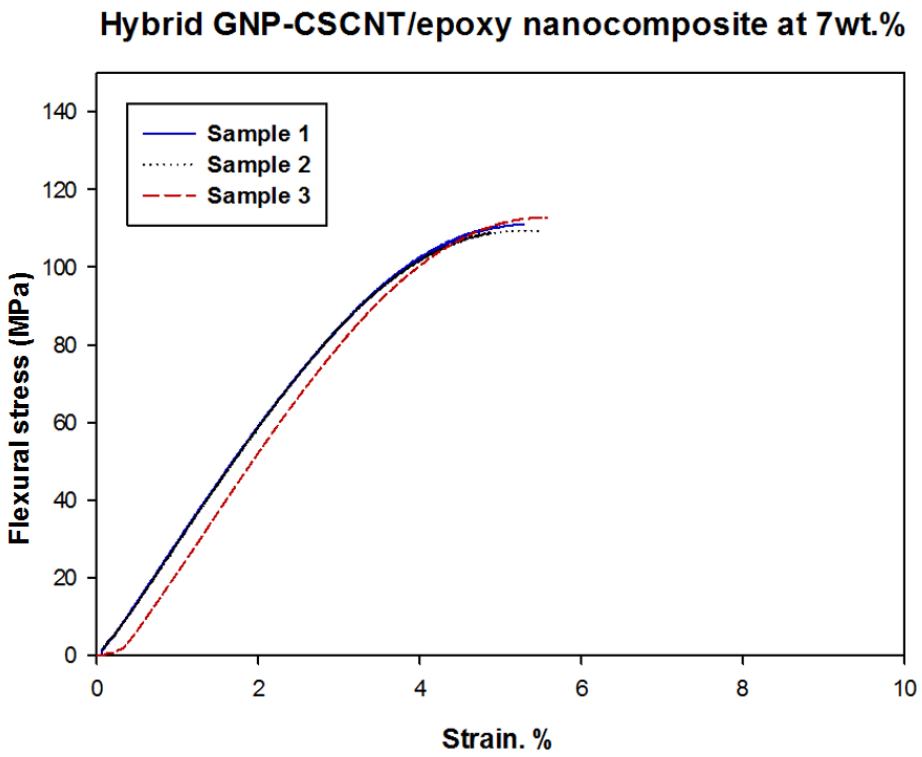

Figure B.1.3. The typical flexural stress-strain curves for the hybrid GNP-CSCNT/epoxy nanocomposites at various weight concentrations.

Table B.1.3. Summary of flexural tests results for the hybrid GNP-CSCNT/epoxy nanocomposites specimens at various weight concentrations in comparison with the pure epoxy composites (base (0)).

Hybrid GNP-CSCNT/epoxy nanocomposites processed by sonication method																		
Specimen Number	Maximum Flexural Strength (MPa)						Flexural Modulus (GPa)						Maximum Strain (%)					
	0 wt. %	***2.5 wt.%***	***4 wt.%***	***5 wt.%***	***6wt.%***	***7 wt.%***	***0 wt. %***	***2.5wt.%***	***4 wt.%***	***5 wt.%***	***6 wt.%***	***7 wt.%***	***0 wt. %***	***2.5 wt.%***	***4 wt.%***	***5 wt.%***	***6 wt.%***	***7 wt.%***
1	102.14	124.10	123.56	116.76	92.84	111.10	2.99	3.23	3.12	3.00	2.10	2.87	5.60	5.40	5.60	5.46	5.82	5.50
2	102.48	121.10	124.20	118.40	94.90	109.53	2.75	3.07	3.20	3.11	2.08	2.78	5.72	5.00	5.04	5.02	5.60	5.62
3	101.15	123.00	121.24	115.90	94.09	112.76	2.75	3.06	3.13	3.10	2.03	2.97	5.68	5.45	5.70	5.50	5.84	5.70
4	99.10	118.10	-	110.00	-	-	2.71	2.94	-	2.89	-	-	5.88	5.28	-	5.48	-	
Average	101.21	121.60	123.00	115.26	93.94	111.13	2.80	3.10	3.15	3.00	2.07	2.87	5.72	5.28	5.44	5.36	5.75	5.60
S.D	±1.52	±2.64	±1.27	±3.66	±1.03	±2.14	±0.13	±0.12	±0.03	±0.10	±0.03	±0.09	±0.11	±0.20	±0.35	±0.23	±0.13	±0.10
C.V	1.50%	2.17%	1.03%	3.17%	1.10%	1.93%	4.56%	3.95%	1.13%	3.56%	1.63%	3.30%	2.05%	3.80%	6.50%	4.30%	2.30%	1.80%
Incr.%	base(0)	+20.1	+21.5	+13.8	-7.2	+9.8	base(0)	+10.7	+12.5	+7.1	-26.0	+2.6	base(0)	-7.7	-4.9	-6.3	+0.5	-2.1

Appendix B.2. Typical flexural stress-strain curves for the pure epoxy composite (base (0)) as well as three epoxy nanocomposites modified with carbon nanomaterials at various weight concentrations processed by ball milling technique.

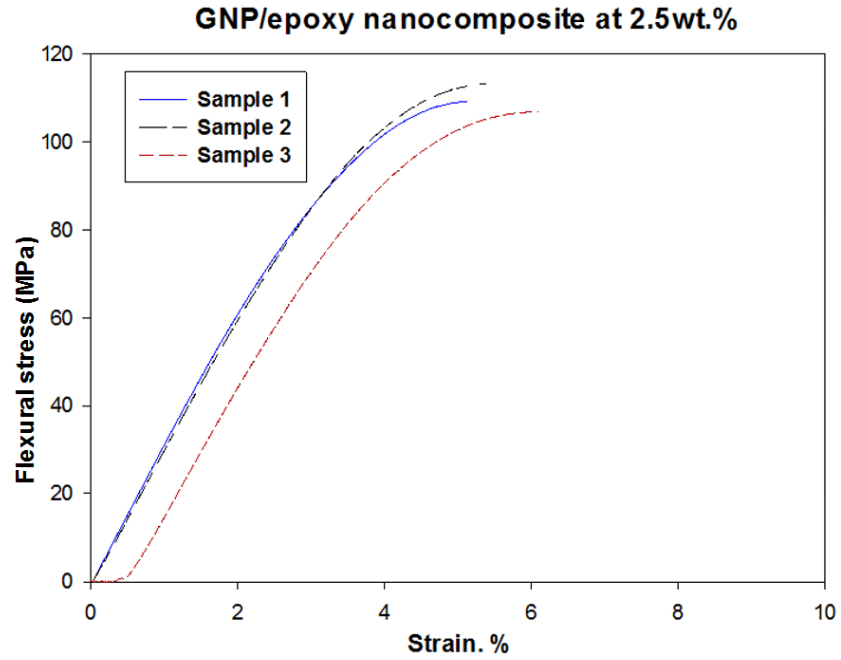

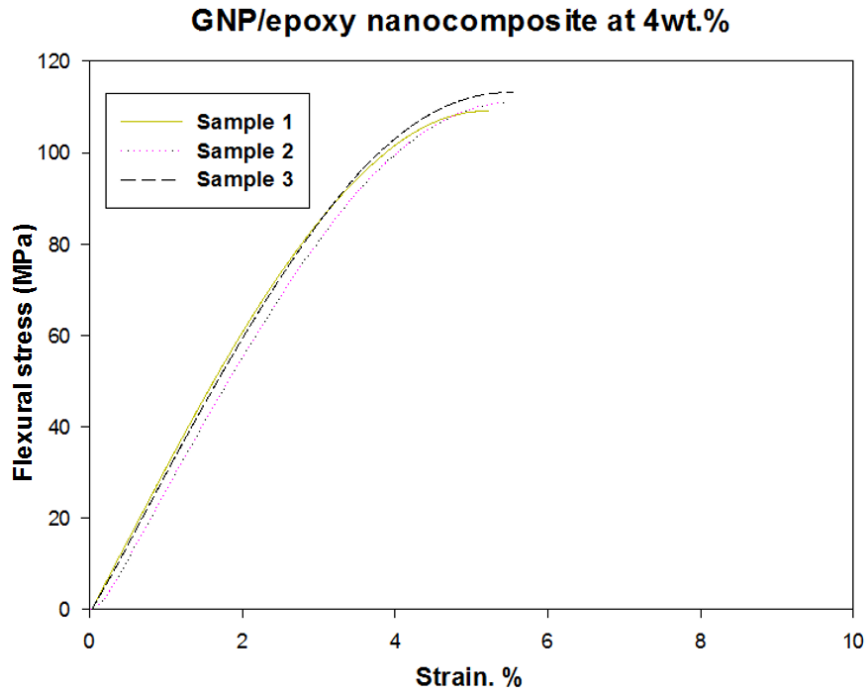

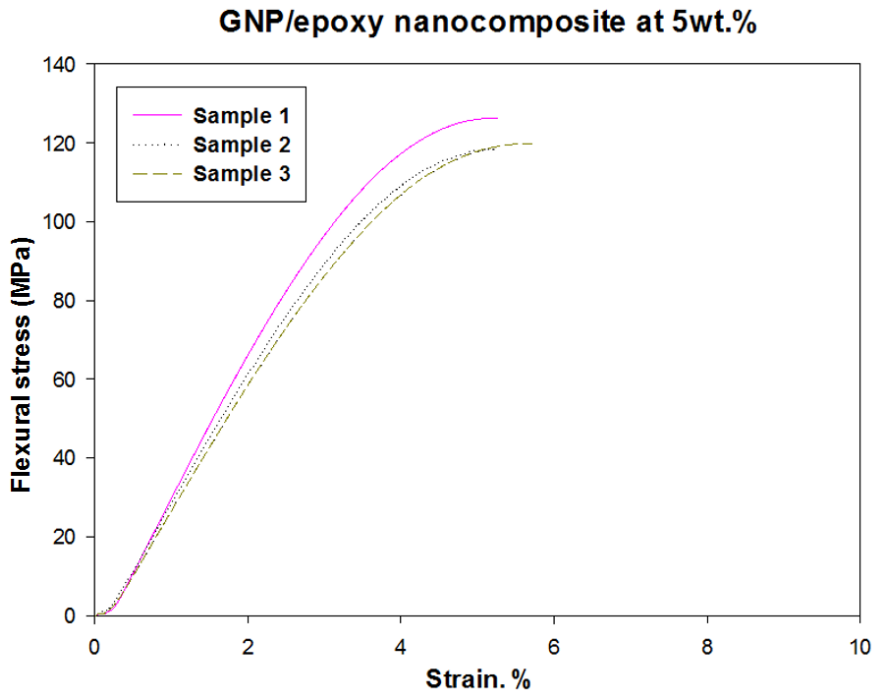
GNP/epoxy nanocomposite at 5wt.%
Sample 1
Sample 2
Sample 3
Flexural stress (MPa)
Strain. %
0
20
40
60
80
100
120
140
0
2
4
6
8
10

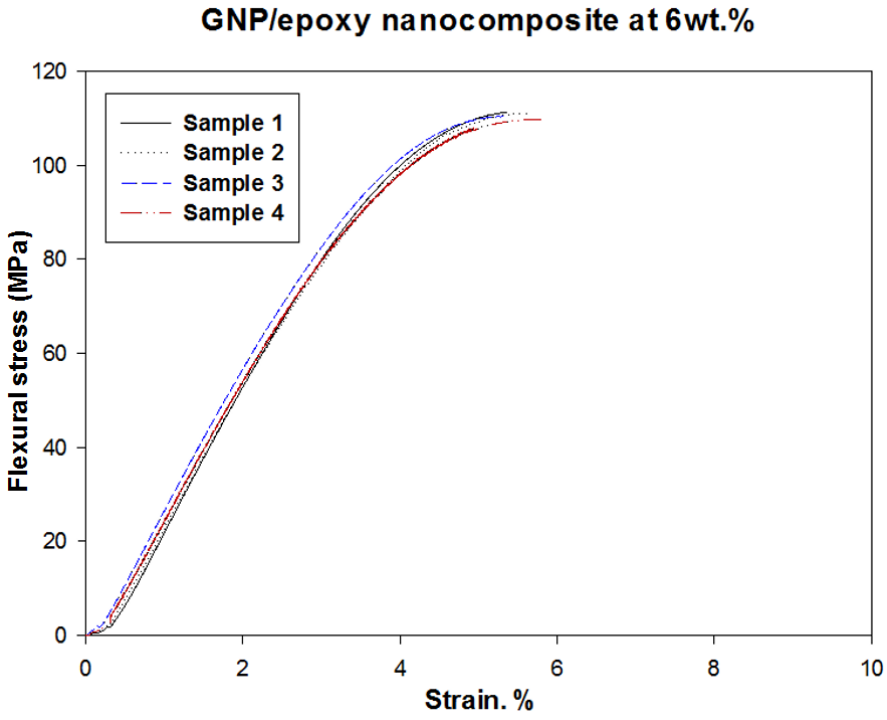
GNP/epoxy nanocomposite at 6wt.%
Sample 1
Sample 2
Sample 3
Sample 4
Flexural stress (MPa)
Strain. %
0
20
40
60
80
100
120
0
2
4
6
8
10

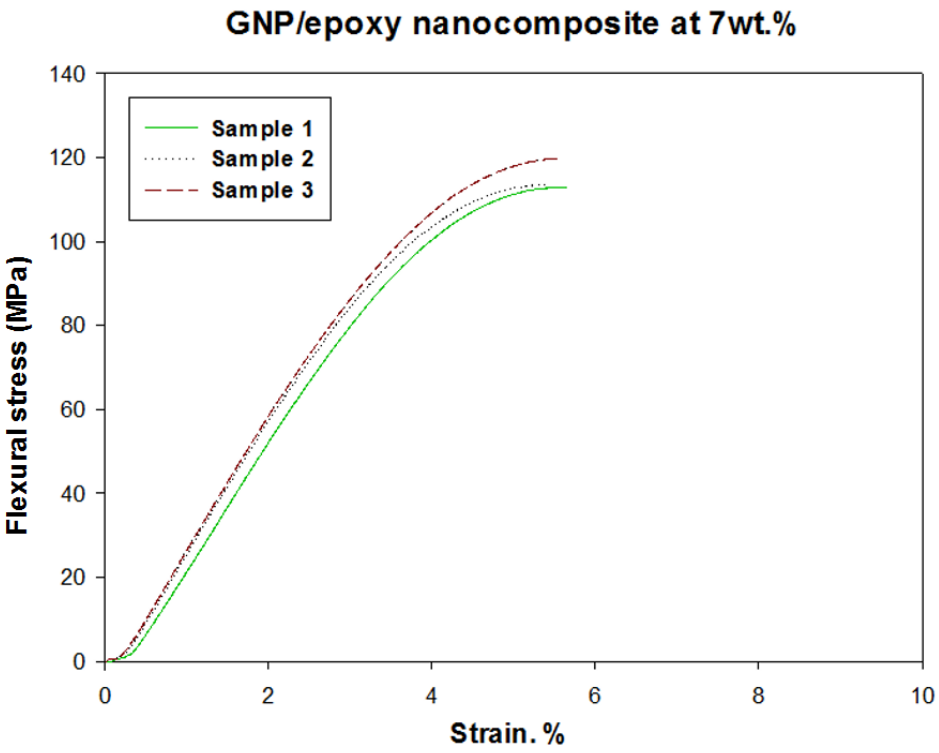

Figure B.2.1. The typical flexural stress-strain curves for the GNP/epoxy nanocomposites at various weight concentrations.

Table B.2.1. Summary of flexural tests results for the GNP/epoxy nanocomposites specimens at various weight concentrations in comparison to the pure epoxy composites (base (0)).

GNP/epoxy nanocomposites processed by ball milling method																		
Specimen Number	Maximum Flexural Strength (MPa)						Flexural Modulus (GPa)						Maximum Strain (%)					
	0 wt. %	***2.5 wt.%***	***4 wt.%***	***5 wt.%***	***6 wt.%***	***7 wt.%***	***0 wt. %***	***2.5 wt.%***	***4 wt.%***	***5 wt.%***	***6 wt.%***	***7 wt.%***	***0 wt. %***	***2.5 wt.%***	***4 wt.%***	***5 wt.%***	***6 wt.%***	***7 wt.%***
1	102.14	108.40	109.80	126.33	110.90	115.20	2.99	2.80	2.90	3.40	2.71	2.76	5.60	5.10	5.48	5.32	5.32	5.72
2	102.48	113.30	111.35	118.60	110.71	111.80	2.75	2.79	2.78	3.00	2.70	2.84	5.72	5.38	5.70	5.30	5.70	5.38
3	101.15	103.10	112.15	124.97	111.10	109.00	2.75	2.75	2.81	3.20	2.80	2.86	5.68	6.10	5.80	5.68	5.30	5.48
4	99.10	-	-	-	112.49	-	2.71	-	-	-	2.83	-	5.88	-	-	-	-	-
Average	101.21	108.30	111.10	123.30	111.30	112.00	2.80	2.78	2.83	3.20	2.76	2.81	5.72	5.52	5.66	5.43	5.44	5.52
S.D C.V	±1.52 1.50%	±5.10 4.71%	±1.19 1.07%	±3.34 3.10%	±0.81 0.72%	±1.50 1.31%	±0.13 4.56%	±0.02 0.80%	±0.061 2.16%	±0.20 6.25%	±0.064 2.35%	±0.05 1.80%	±0.11 2.05%	±0.51 9.30%	±0.16 2.90%	±0.21 3.93%	±0.225 4.10%	±0.17 3.16%
Incr.%	base(0)	+7.0	+9.7	+21.8	+9.9	+10.6	base(0)	-0.7	+1.1	+14.3	-1.4	+0.3	base(0	-3.5	-1.0	-5.0	-4.9	-3.5

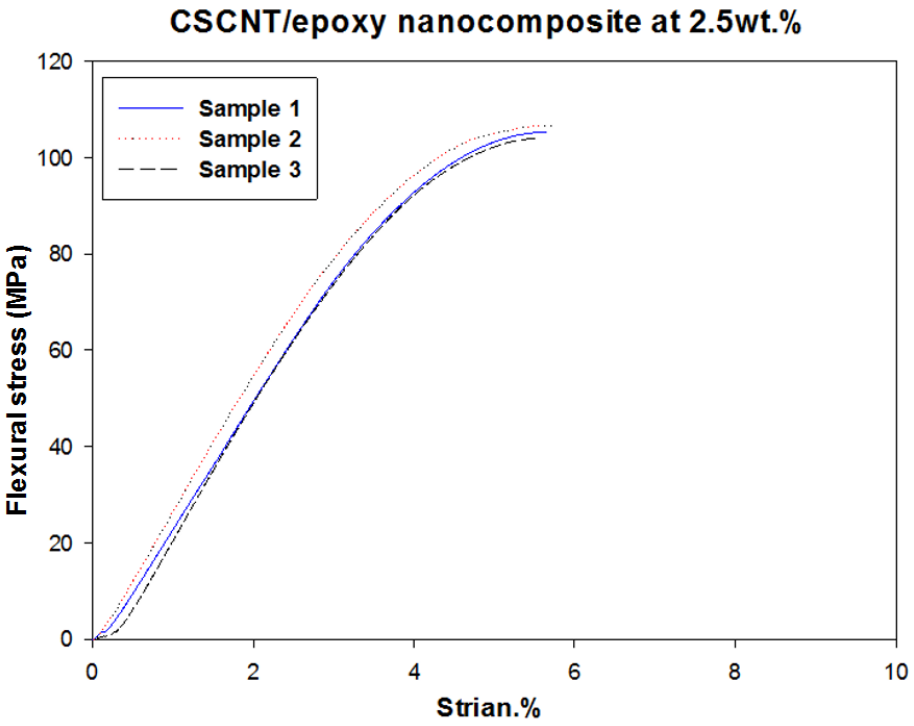
CSCNT/epoxy nanocomposite at 2.5wt.%
Sample 1
Sample 2
Sample 3
Flexural stress (MPa)
Strian.%
0
20
40
60
80
100
120
0
2
4
6
8
10

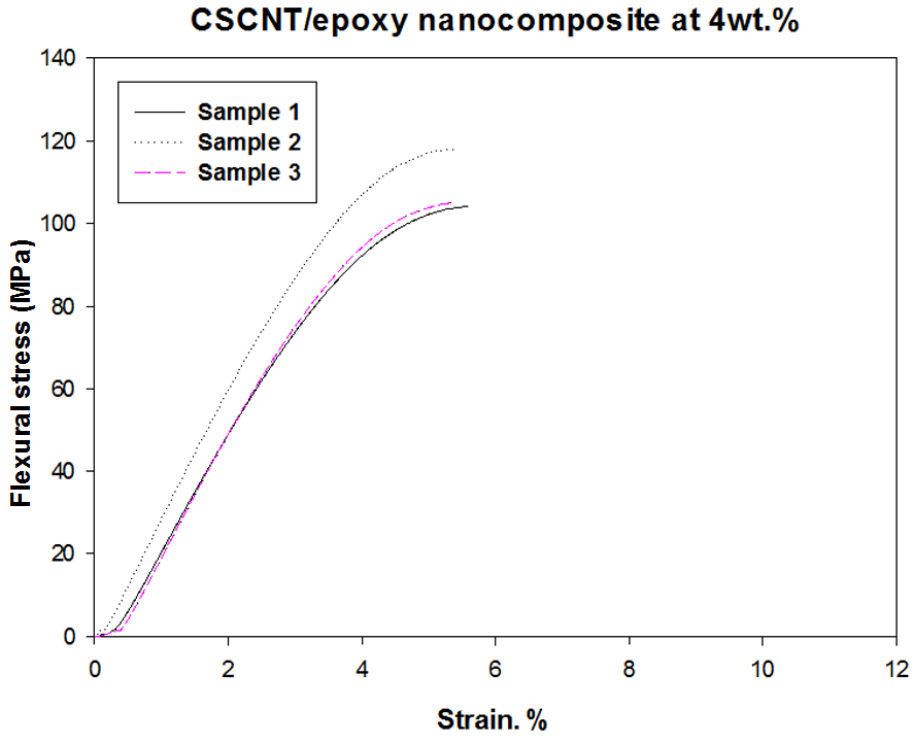
CSCNT/epoxy nanocomposite at 4wt.%
Sample 1
Sample 2
Sample 3
Flexural stress (MPa)
Strain. %
0
20
40
60
80
100
120
140
0
2
4
6
8
10
12

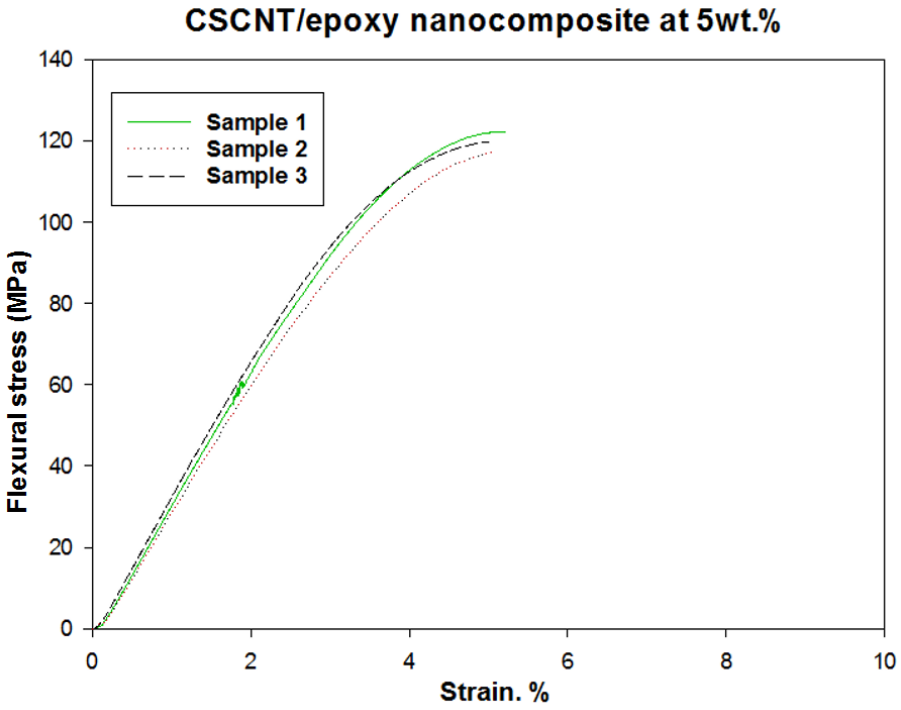
CSCNT/epoxy nanocomposite at 5wt.%
Sample 1
Sample 2
Sample 3
Flexural stress (MPa)
Strain. %
0
20
40
60
80
100
120
140
0
2
4
6
8
10

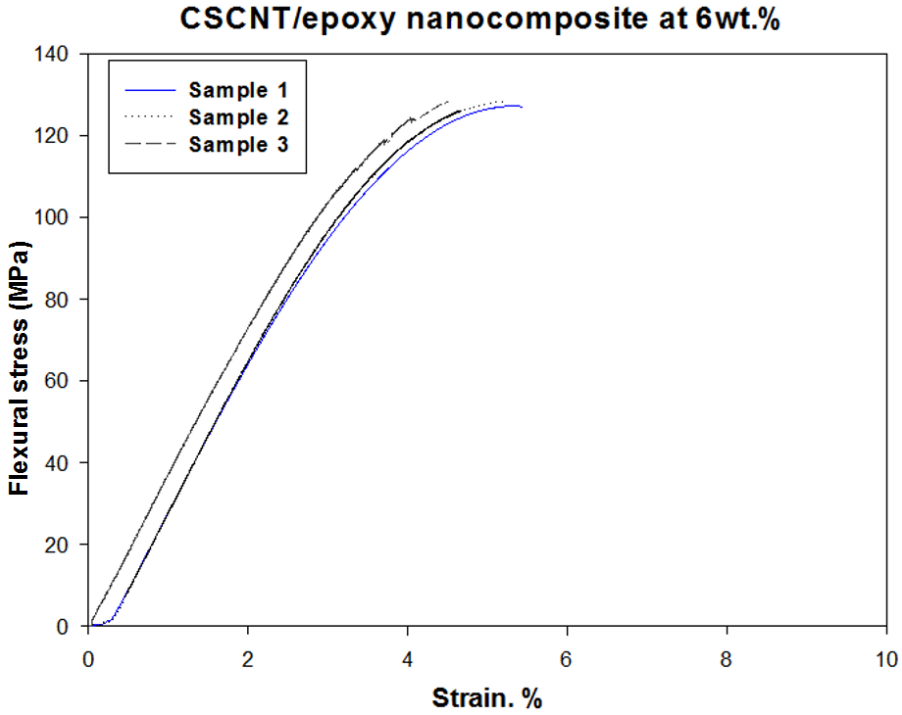
CSCNT/epoxy nanocomposite at 6wt.%
Sample 1
Sample 2
Sample 3
Flexural stress (MPa)
Strain. %
0
20
40
60
80
100
120
140
0
2
4
6
8
10

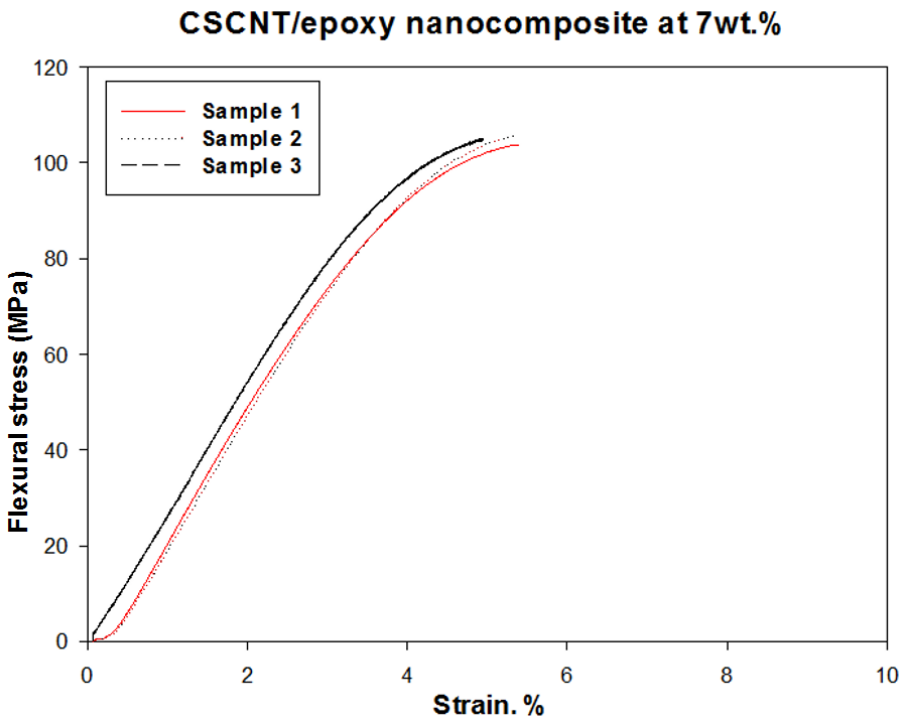

Figure B.2.2. The typical flexural stress-strain curves for the CSCNT/epoxy nanocomposites at various weight concentrations.

Table B.2.2. Summary of flexural tests results for the CSCNT/epoxy nanocomposites specimens at various weight concentrations in comparison with pure epoxy composites (base (0)).

CSCNT/epoxy nanocomposites processed by ball milling method																		
Specimen Number	Maximum Flexural Strength (MPa)						Flexural Modulus (GPa)						Maximum Strain (%)					
	0 wt. %	***2.5 wt.%***	***4 wt.%***	***5 wt.%***	***6 wt.%***	***7 wt.%***	***0 wt. %***	***2.5 wt.%***	***4 wt.%***	***5 wt.%***	***6 wt.%***	***7 wt.%***	***0 wt. %***	***2.5 wt.%***	***4 wt.%***	***5 wt.%***	***6 wt.%***	***7 wt.%***
1	102.14	104.30	107.30	121.40	127.30	104.10	2.99	2.60	2.80	3.46	3.71	2.77	5.60	5.60	5.48	5.40	5.28	5.49
2	102.48	106.95	117.40	115.20	128.30	106.10	2.75	2.80	3.10	3.24	3.73	2.73	5.72	5.68	5.38	5.01	5.06	5.42
3	101.15	103.75	108.00	117.40	129.00	101.80	2.75	2.55	2.80	3.50	3.96	2.72	5.68	5.48	5.32	5.00	4.42	4.98
4	99.10	-	-	-	-	-	2.71	-	-	-	-	-	5.88	-	-	-	-	-
Average	101.21	105.00	110.90	118.00	128.20	104.00	2.80	2.65	2.90	3.40	3.80	2.74	5.72	5.58	5.39	5.13	4.92	5.29
S.D C.V	±1.52 1.50%	±1.71 1.62%	±5.64 5.08%	±3.14 2.66%	±0.85 0.66%	±2.15 2.06%	±0.13 4.56%	±0.13 4.99%	±0.17 5.97%	±0.14 4.12%	±0.14 3.65%	±0.02 0.96%	±0.11 2.05%	±0.10 1.80%	±0.08 1.50%	±0.22 4.40%	±0.44 9.00%	±0.27 5.20%
Incr.%	base(0)	+3.7	+9.5	+16.6	+26.6	+2.7	base(0)	-5.3	+3.5	+21.4	+35.7	-2.1	base(0)	-2.4	-5.7	-10.3	-13.9	-7.5

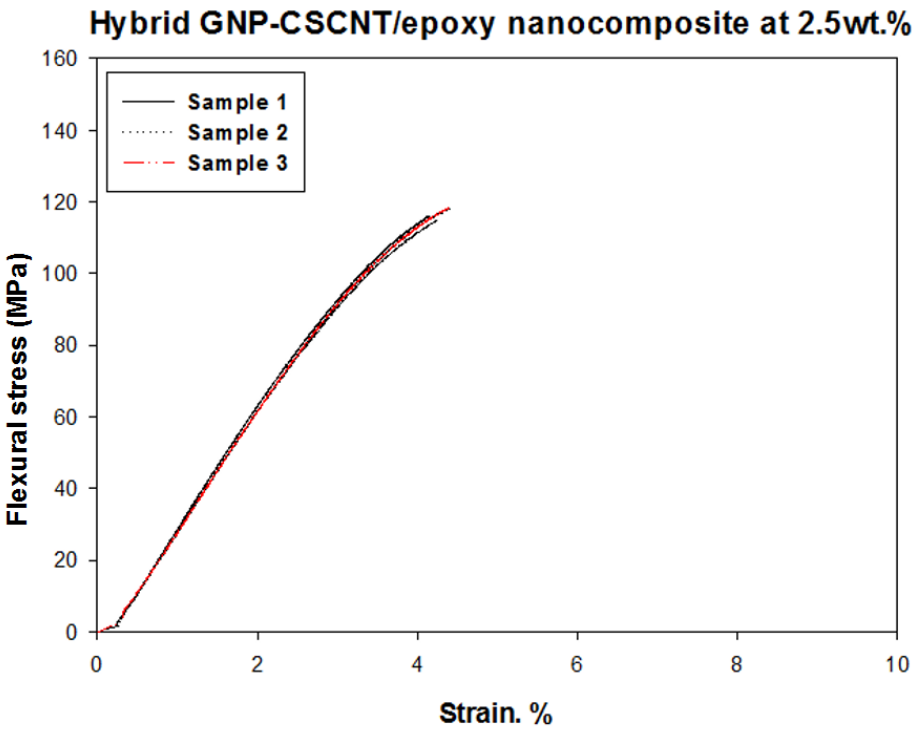
Hybrid GNP-CSCNT/epoxy nanocomposite at 2.5wt.%
Sample 1
Sample 2
Sample 3
Flexural stress (MPa)
Strain. %
0
20
40
60
80
100
120
140
160
0
2
4
6
8
10

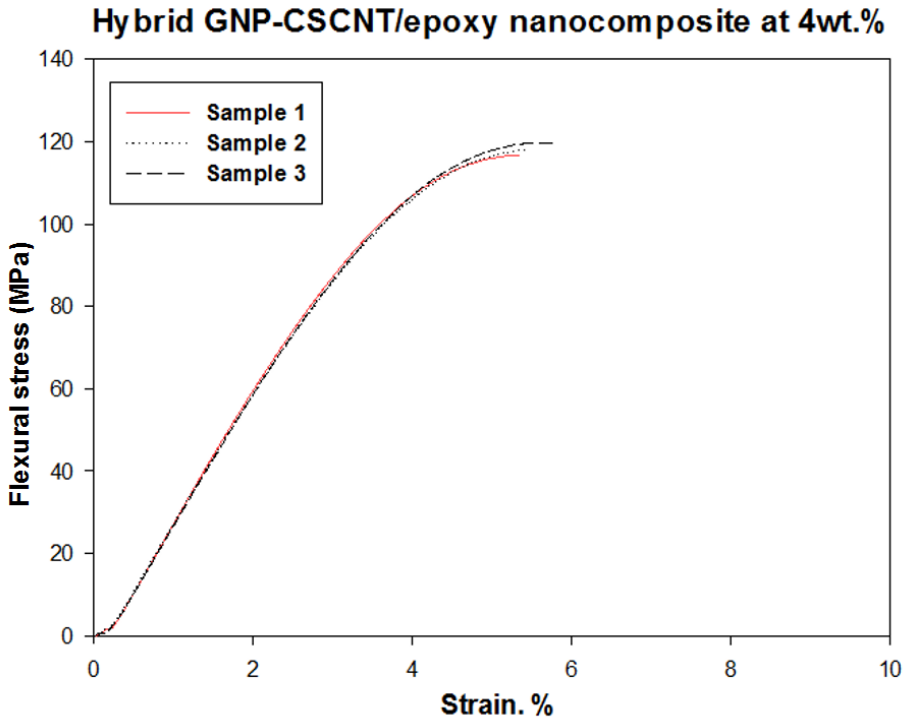
Hybrid GNP-CSCNT/epoxy nanocomposite at 4wt.%
Sample 1
Sample 2
Sample 3
Flexural stress (MPa)
Strain. %
0
20
40
60
80
100
120
140
0
2
4
6
8
10

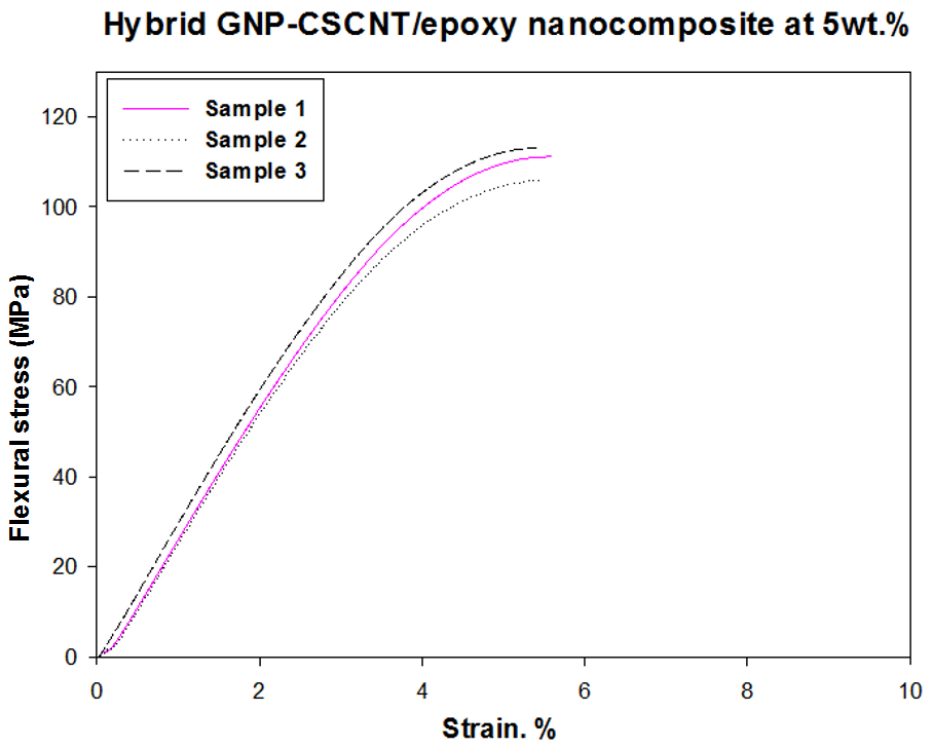
Hybrid GNP-CSCNT/epoxy nanocomposite at 5wt.%
Sample 1
Sample 2
Sample 3
Flexural stress (MPa)
Strain. %
0
20
40
60
80
100
120
0
2
4
6
8
10

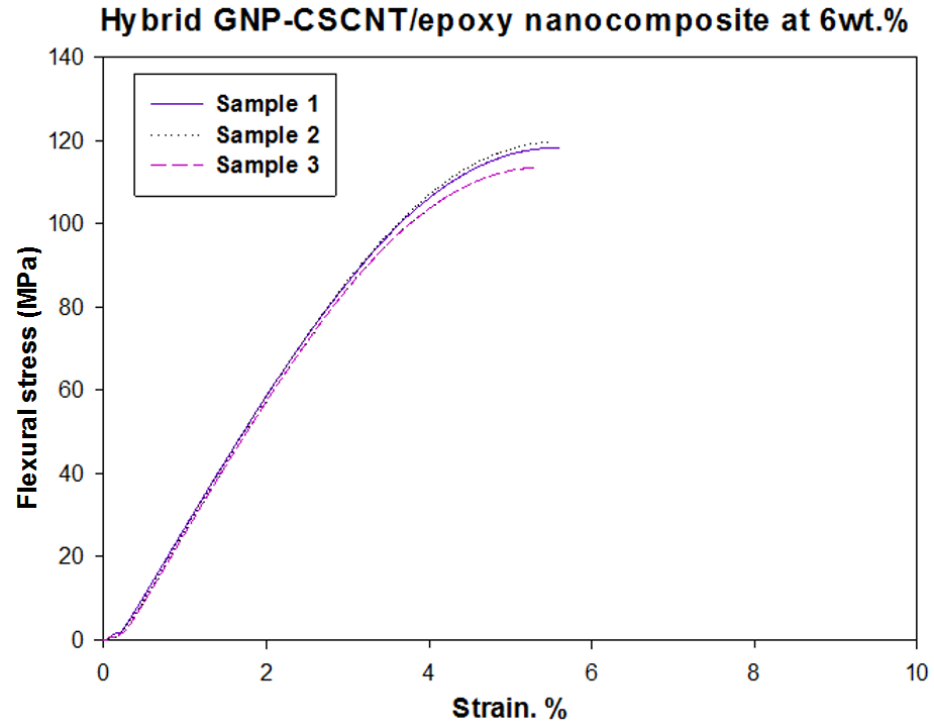
Hybrid GNP-CSCNT/epoxy nanocomposite at 6wt.%
Sample 1
Sample 2
Sample 3
Flexural stress (MPa)
Strain. %
0
20
40
60
80
100
120
140
0
2
4
6
8
10

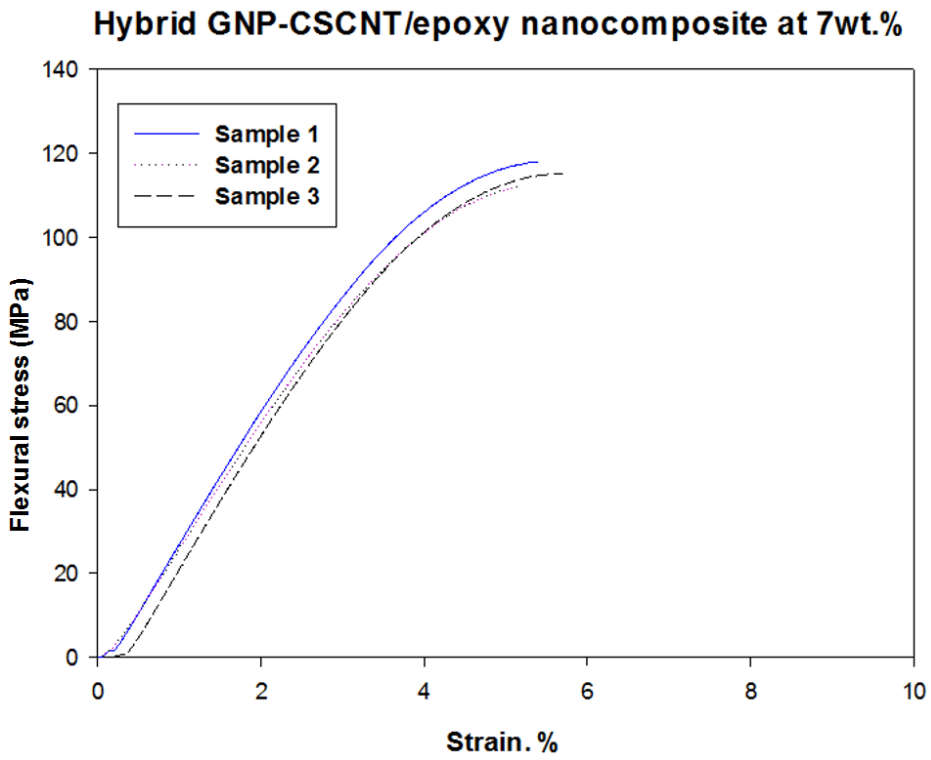

Figure B.2.3. The typical flexural stress-strain curves for the hybrid GNP-CSCNT/epoxy nanocomposites at various weight concentrations.

Table B.2.3. Summary of flexural tests results for the hybrid GNP-CSCNT/epoxy nanocomposites specimens at various weight concentrations in comparison with the pure epoxy composites (base (0)).

Hybrid GNP-CSCNT/ epoxy nanocomposites processed by ball milling method																		
Specimen Number	Maximum Flexural Strength (MPa)						Flexural Modulus (GPa)						Maximum Strain (%)					
	0 wt. %	***2.5 wt.%***	***4 wt.%***	***5 wt.%***	***6 wt.%***	***7 wt.%***	***0 wt. %***	***2.5 wt.%***	***4 wt.%***	***5 wt.%***	***6 wt.%***	***7 wt.%***	***0 wt. %***	***2.5 wt.%***	***4 wt.%***	***5 wt.%***	***6 wt.%***	***7 wt.%***
1	102.14	115.30	116.83	110.40	118.23	116.80	2.99	2.77	3.30	2.84	3.00	2.84	5.60	4.50	5.48	5.80	5.81	5.20
2	102.48	114.30	118.50	106.00	119.80	113.80	2.75	2.93	3.20	2.86	3.10	2.82	5.72	4.58	5.50	5.50	5.72	5.00
3	101.15	115.85	119.57	113.60	113.27	115.00	2.75	3.00	3.10	3.30	2.90	2.80	5.68	4.64	6.08	5.46	5.36	5.78
4	99.10	-	-	-	-	-	2.71	-	-	-	-	-	5.88	-	-	-	-	-
Average	101.21	115.15	118.30	110.00	117.10	115.20	2.80	2.90	3.20	3.00	3.00	2.82	5.72	4.57	5.68	5.58	5.63	5.32
S.D C.V	±1.52 1.50%	±0.78 0.68%	±1.38 1.16%	±3.81 3.46%	±3.40 2.91%	±1.51 1.31%	±0.12 4.56%	±0.12 4.00%	±0.10 3.12%	±0.26 8.66%	±0.10 3.35%	±0.02 0.70%	±0.11 2.05%	±0.07 1.53%	±0.34 6.00%	±0.18 3.30%	±0.23 4.20%	±0.40 7.60%
Incr.%	base(0)	+13.8	+16.9	+8.7	+15.7	+13.8	base(0)	+3.6	+14.3	+7.1	+7.1	+0.7	base 0)	-20.1	-0.7	-2.4	-1.5	-6.9

Appendix B.3. Typical flexural stress-strain curves for the pure epoxy composite (base (0)) as well as three epoxy nanocomposites modified with carbon nanomaterials at various weight concentrations processed by combined techniques.

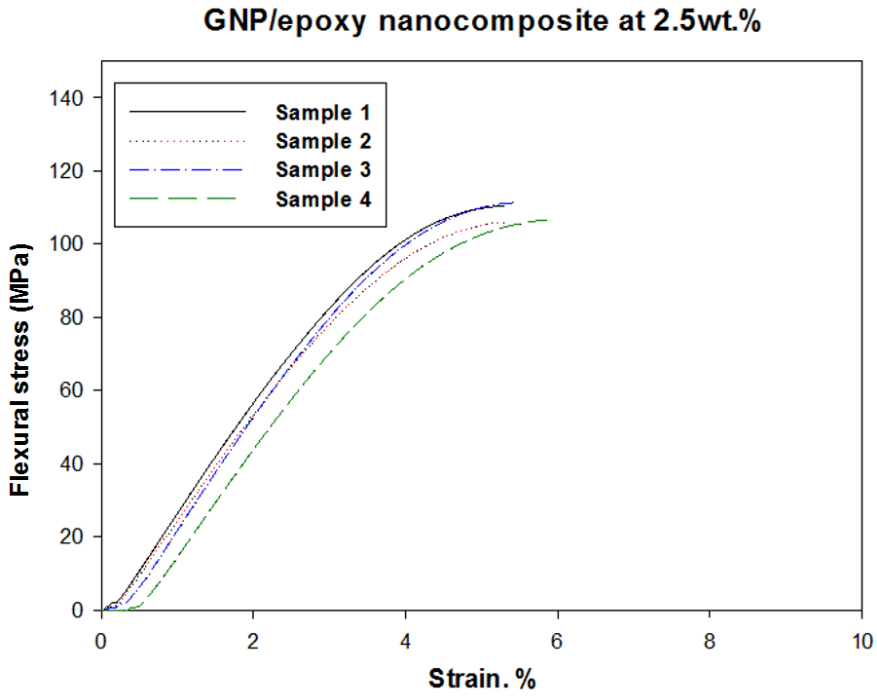

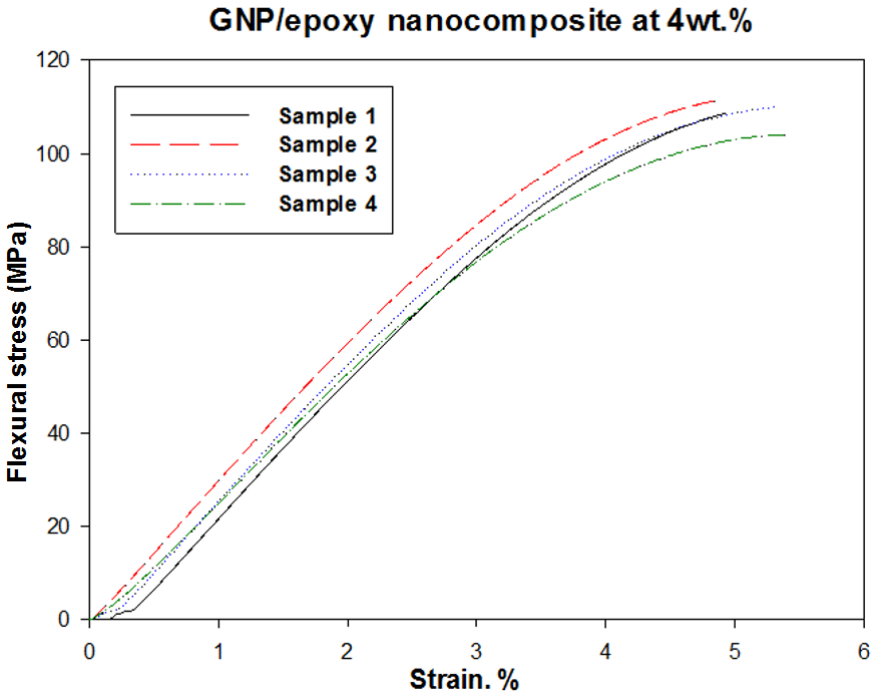

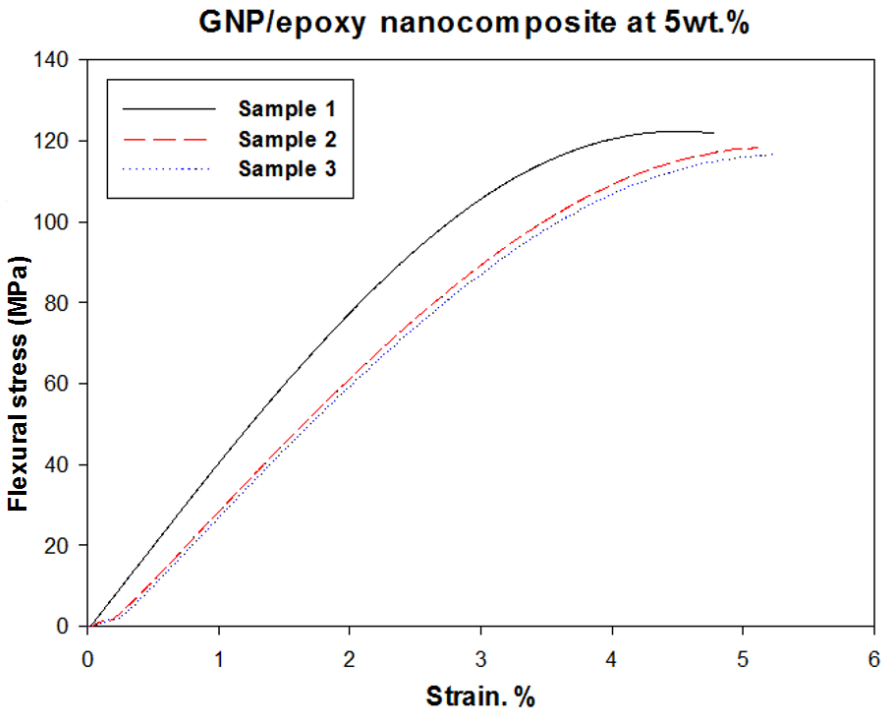
GNP/epoxy nanocomposite at 5wt.%
Sample 1
Sample 2
Sample 3
Flexural stress (MPa)
Strain. %
0
20
40
60
80
100
120
140
0
1
2
3
4
5
6

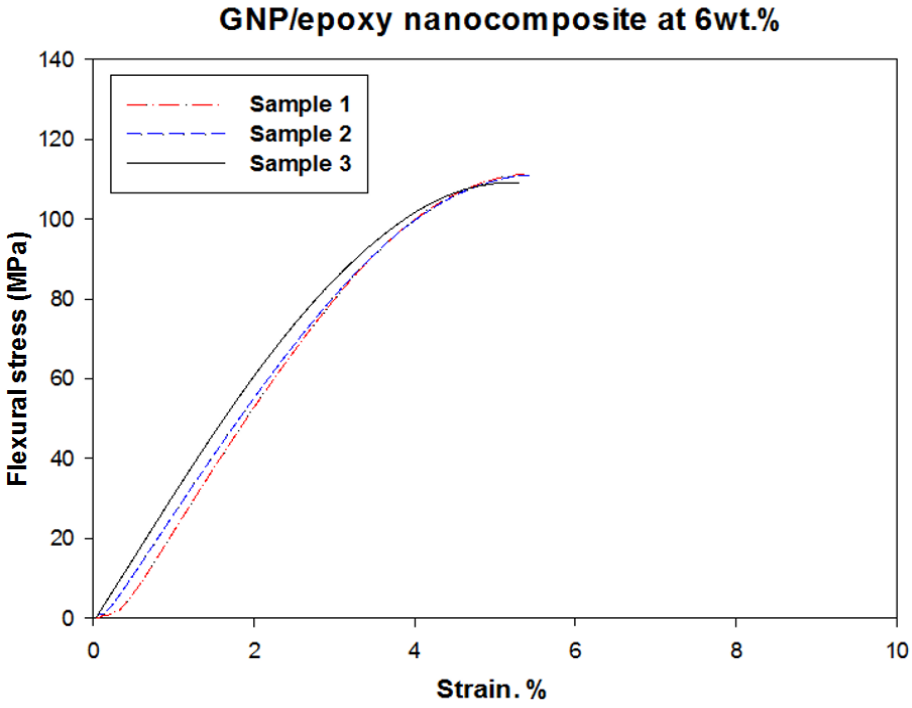
GNP/epoxy nanocomposite at 6wt.%
Sample 1
Sample 2
Sample 3
Flexural stress (MPa)
Strain. %
0
20
40
60
80
100
120
140
0
2
4
6
8
10

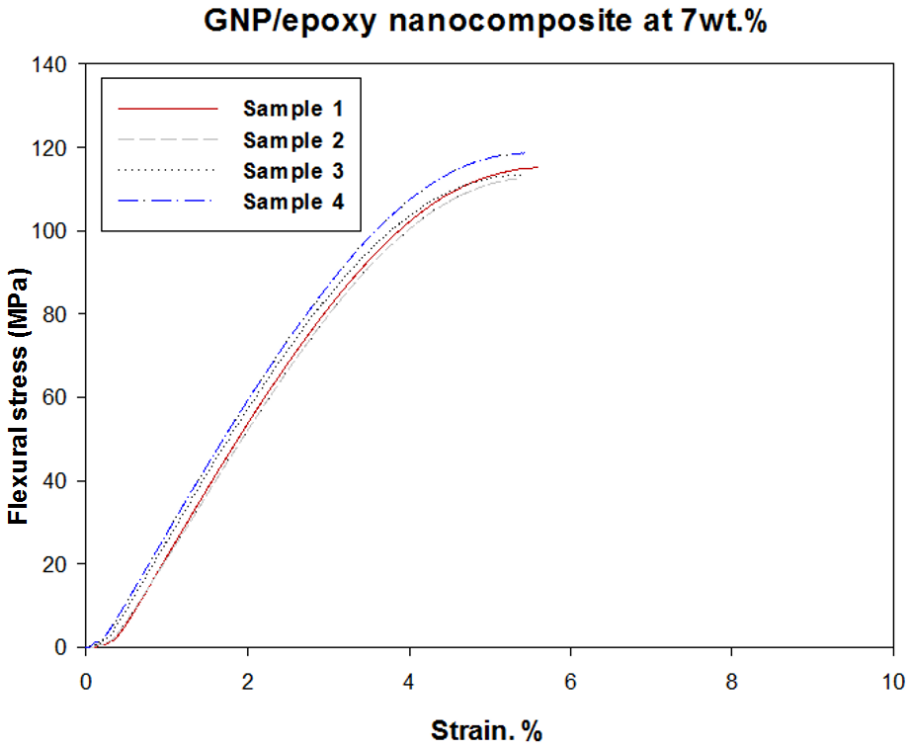

Figure B.3.1. The typical flexural stress-strain curves for the GNP/epoxy nanocomposites at various weight concentrations.

Table B.3.1. Summary of flexural tests results for the GNP/epoxy nanocomposites specimens at various weight concentrations in comparison with the pure epoxy composites (base (0)).

GNP/epoxy nanocomposites processed by combined techniques method																		
Specimen Number	Maximum Flexural Strength (MPa)						Flexural Modulus (GPa)						Maximum Strain (%)					
	0 wt. %	***2.5 wt.%***	***4 wt.%***	***5 wt.%***	***6 wt.%***	***7 wt.%***	***0 wt. %***	***2.5 wt.%***	***4 wt.%***	***5 wt.%***	***6 wt.%***	***7 wt.%***	***0 wt. %***	***2.5 wt.%***	***4 wt.%***	***5 wt.%***	***6 wt.%***	***7 wt.%***
1	102.14	110.10	110.50	122.10	111.40	115.10	2.99	2.95	2.72	3.30	2.85	2.81	5.60	5.40	5.06	4.80	5.41	5.68
2	102.48	105.00	112.30	117.30	111.10	113.56	2.75	2.85	2.90	3.10	2.91	2.80	5.72	5.36	5.00	5.18	5.46	5.41
3	101.15	110.30	111.10	116.40	110.63	114.10	2.75	2.84	2.93	2.90	2.95	2.85	5.68	5.46	5.40	5.24	5.37	5.43
4	99.10	108.20	104.06	-	-	118.20	2.71	2.76	2.97	-	-	2.82	5.88	5.96	5.48	-	-	5.52
Average	101.21	108.40	109.49	118.60	110.98	115.24	2.8	2.85	2.88	3.10	2.90	2.82	5.72	5.54	5.23	5.07	5.41	5.51
S.D C.V	±1.52 1.50%	±2.45 2.26%	±3.69 3.37%	±3.06 2.58%	±0.30 0.27%	±2.68 2.30%	±0.12 4.56%	±0.08 2.73%	±0.11 3.83%	±0.20 6.40%	±0.04 1.41%	±0.02 0.76%	±0.11 2.05%	±0.28 5.00%	±0.24 4.60%	±0.23 4.70%	±0.04 0.84%	±0.12 2.23%
Incr.%	base(0)	+7.1	+8.2	+17.2	+9.6	+13.8	base(0)	+1.8	+2.8	+10.7	+3.6	+0.7	base(0)	-3.1	-8.5	-11.3	-5.4	-3.6

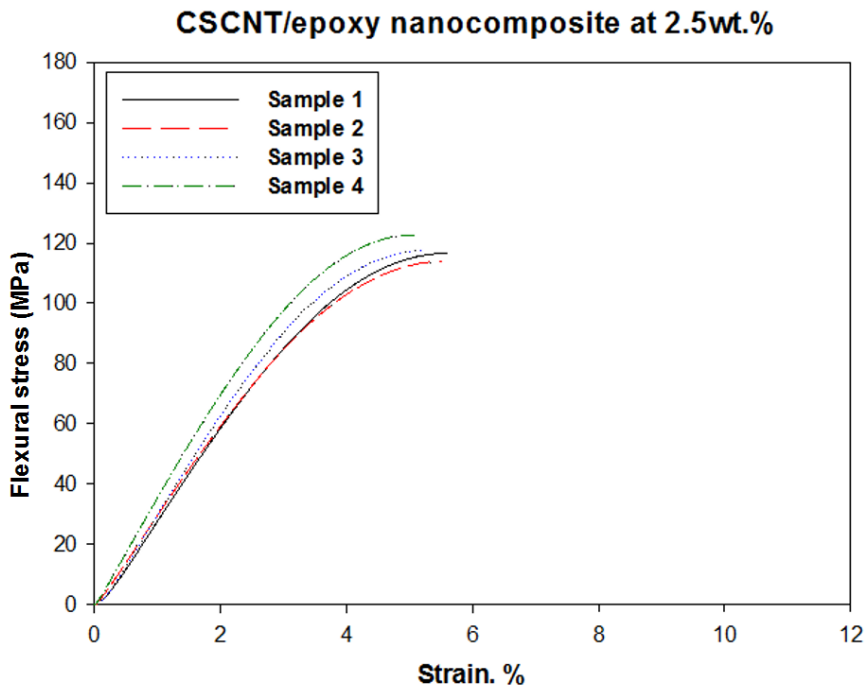
CSCNT/epoxy nanocomposite at 2.5wt.%
Sample 1
Sample 2
Sample 3
Sample 4
Flexural stress (MPa)
Strain. %
0
20
40
60
80
100
120
140
160
180
0
2
4
6
8
10
12

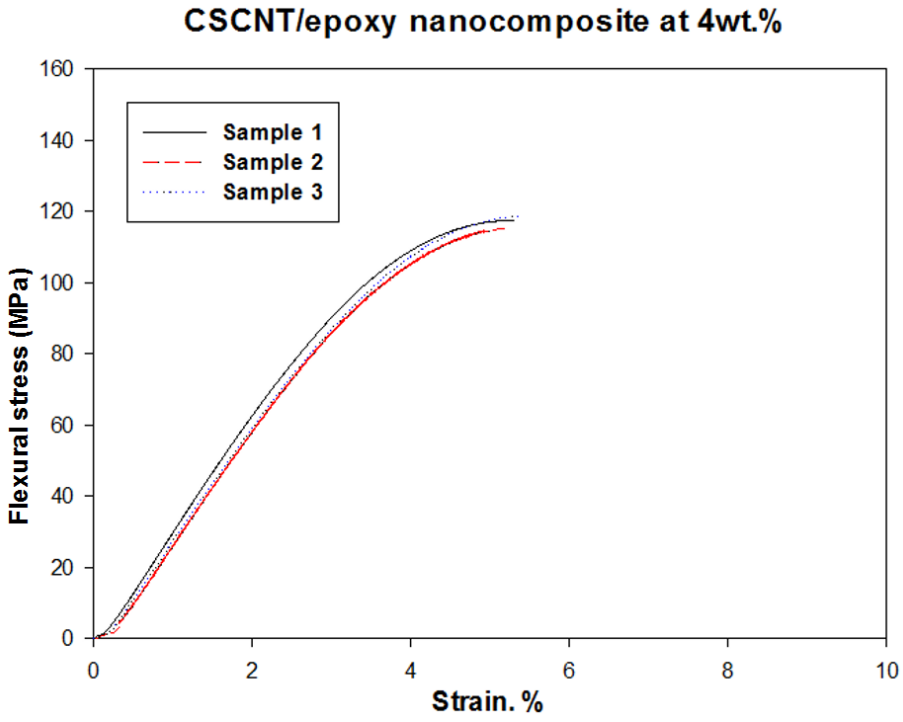
CSCNT/epoxy nanocomposite at 4wt.%
Sample 1
Sample 2
Sample 3
Flexural stress (MPa)
Strain. %
0
20
40
60
80
100
120
140
160
0
2
4
6
8
10

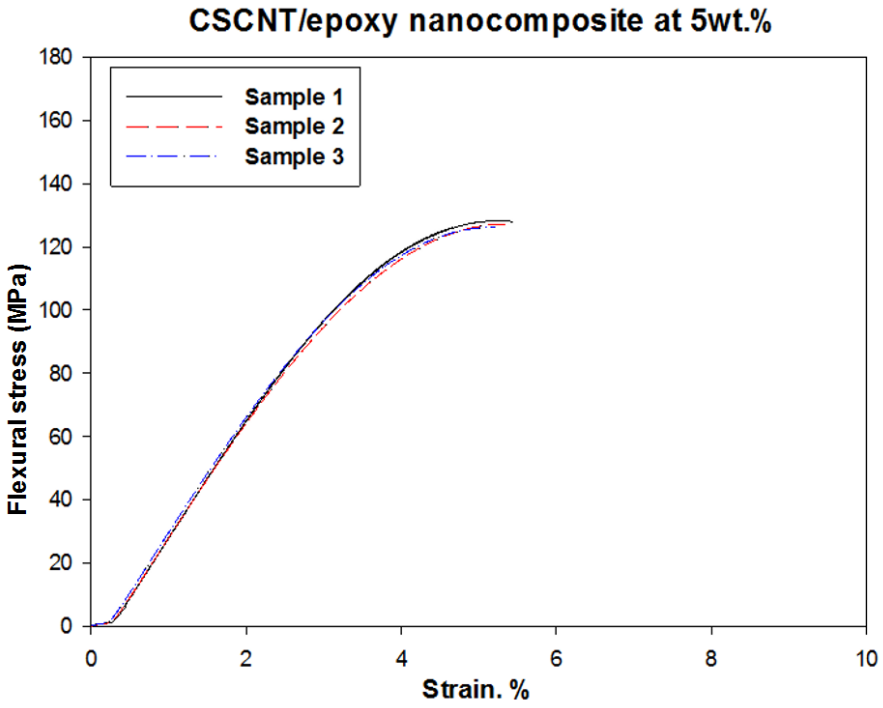
CSCNT/epoxy nanocomposite at 5wt.%
Sample 1
Sample 2
Sample 3
Flexural stress (MPa)
Strain. %
0
20
40
60
80
100
120
140
160
180
0
2
4
6
8
10

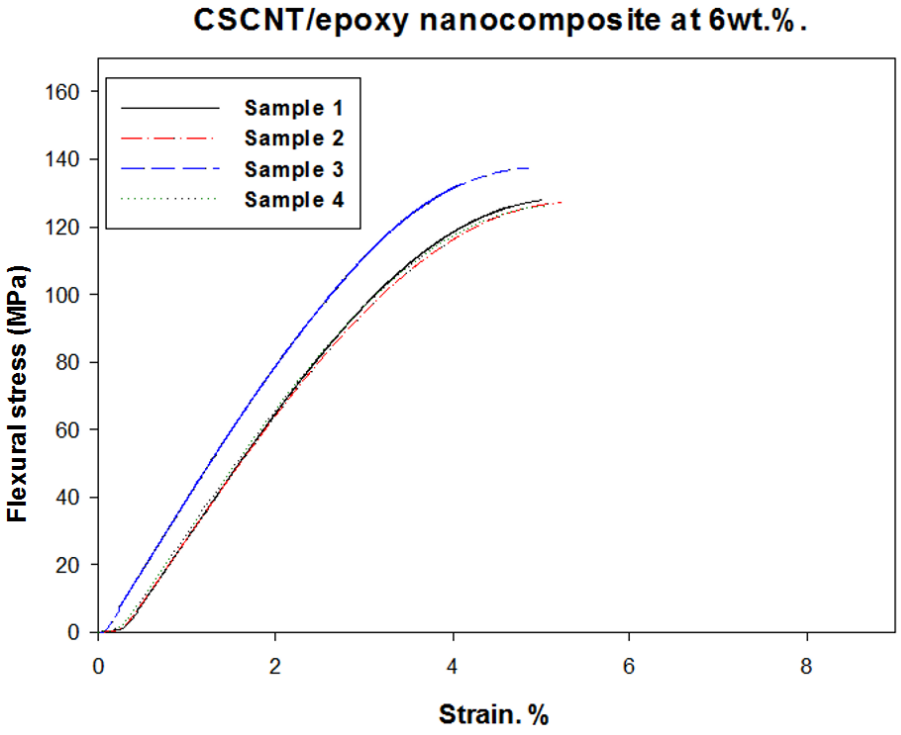
CSCNT/epoxy nanocomposite at 6wt.%.
Sample 1
Sample 2
Sample 3
Sample 4
Flexural stress (MPa)
Strain. %
0
20
40
60
80
100
120
140
160
0
2
4
6
8

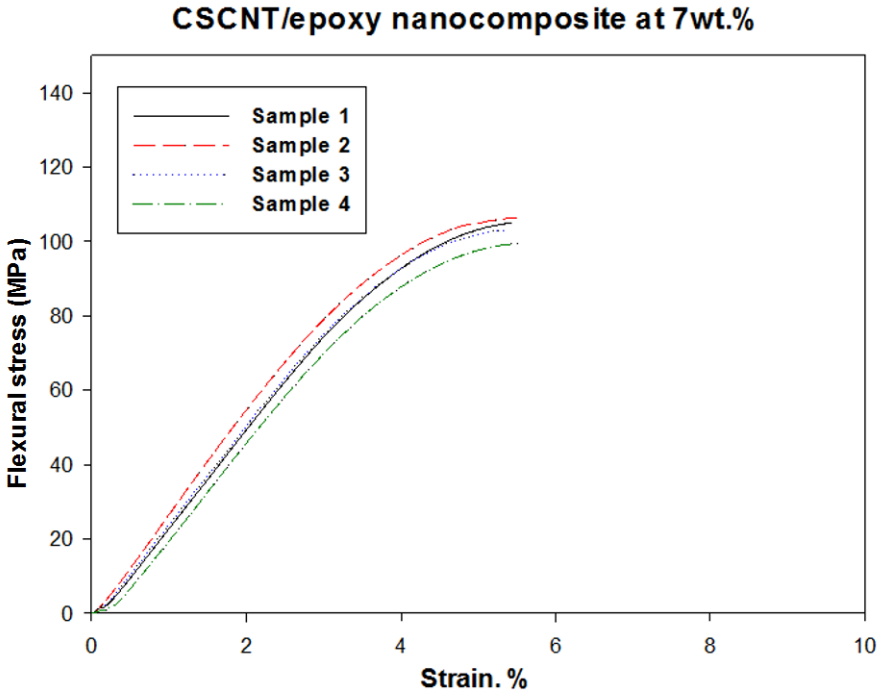

Figure B.3.2. The typical flexural stress-strain curves for the CSCNT/epoxy nanocomposites at various weight concentrations.

Table B.3.2. Summary of flexural tests results for the CSCNT/epoxy nanocomposites specimens at various weight concentrations in comparison with pure epoxy composites (base (0)).

CSCNT/epoxy nanocomposites processed by combined techniques method																		
Specimen Number	Maximum Flexural Strength (MPa)						Flexural Modulus (GPa)						Maximum Strain (%)					
	0 wt. %	***2.5 wt.%***	***4 wt.%***	***5 wt.%***	***6 wt.%***	***7 wt.%***	***0 wt. %***	***2.5 wt.%***	***4 wt.%***	***5 wt.%***	***6 wt.%***	***7 wt.%***	***0 wt. %***	***2.5 wt.%***	***4 wt.%***	***5 wt.%***	***6 wt.%***	***7 wt.%***
1	102.14	115.20	117.00	127.40	128.90	105.10	2.90	2.70	3.40	3.31	3.40	2.81	5.60	5.78	5.56	5.62	4.80	4.60
2	102.48	114.20	117.50	126.10	128.70	106.80	2.75	3.00	3.00	3.38	3.60	2.91	5.72	5.68	5.48	5.20	4.98	4.68
3	101.15	117.20	117.97	128.10	137.40	104.00	2.75	3.00	3.20	3.36	4.10	2.82	5.68	5.30	5.59	5.10	4.64	4.54
4	99.10	120.02	-	-	127.80	100.10	2.71	3.10	-	-	3.70	2.78	5.88	5.22	-	-	4.86	4.58
Average	101.21	116.73	117.49	127.20	130.70	104.00	2.80	2.95	3.20	3.35	3.70	2.83	5.72	5.49	5.54	5.30	4.82	4.60
S.D	±1.52	±2.56	±0.48	±1.01	±4.49	±2.05	±0.13	±0.11	±0.20	±0.08	±0.29	±0.05	±0.11	±0.27	±0.06	±0.27	±0.14	±0.06
C.V	1.50%	2.20%	4.13%	0.80%	3.40%	1.97%	4.56%	3.60%	6.25%	2.35%	7.95%	1.98%	2.05%	5.00%	1.00%	5.20%	2.93%	1.28%
Incr.%	base(0)	+15.3	+16.1	+25.6	+29.1	+2.7	base(0)	+5.3	+14.3	+19.6	+32.1	+1.1	base(0)	-4.0	-3.1	-7.3	-15.7	-19.6

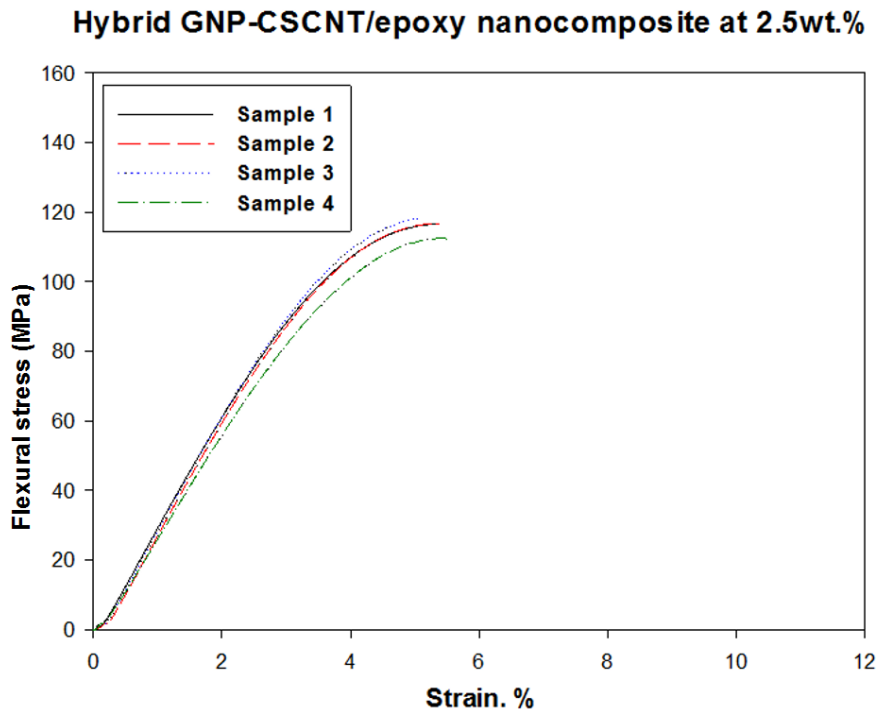
Hybrid GNP-CSCNT/epoxy nanocomposite at 2.5wt.%
Sample 1
Sample 2
Sample 3
Sample 4
Flexural stress (MPa)
Strain. %
0
20
40
60
80
100
120
140
160
0
2
4
6
8
10
12

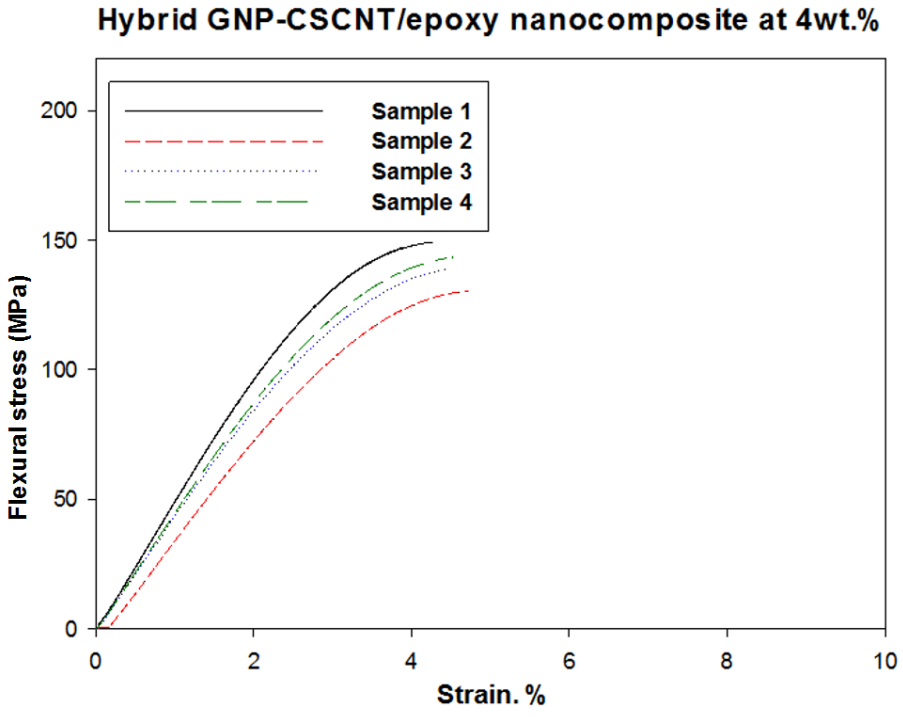
Hybrid GNP-CSCNT/epoxy nanocomposite at 4wt.%
Sample 1
Sample 2
Sample 3
Sample 4
Flexural stress (MPa)
Strain. %
0
50
100
150
200
0
2
4
6
8
10

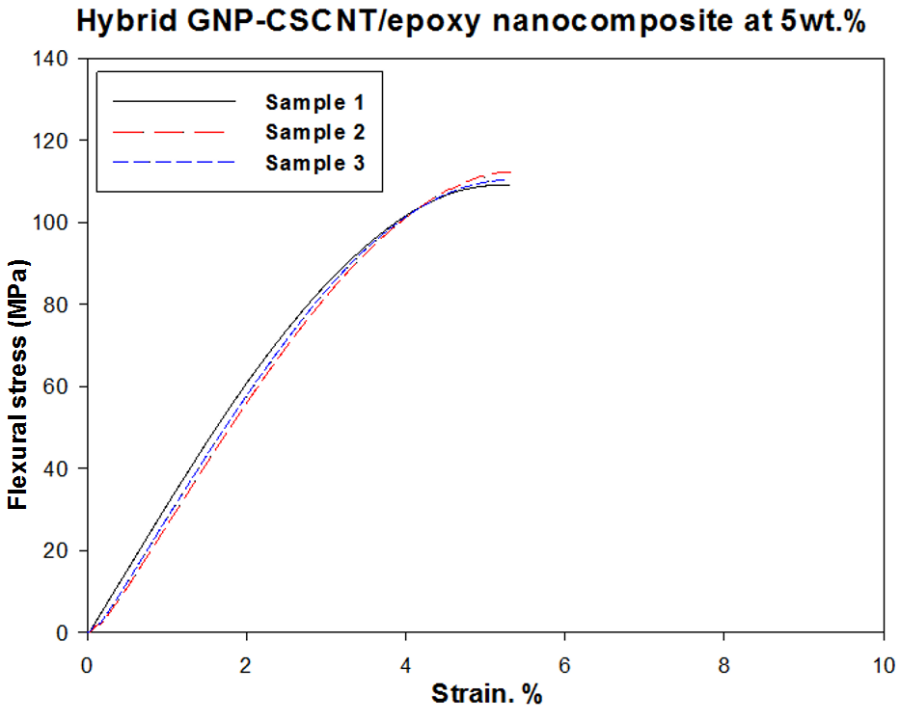
Hybrid GNP-CSCNT/epoxy nanocomposite at 5wt.%
Sample 1
Sample 2
Sample 3
Flexural stress (MPa)
Strain. %
0
20
40
60
80
100
120
140
0
2
4
6
8
10

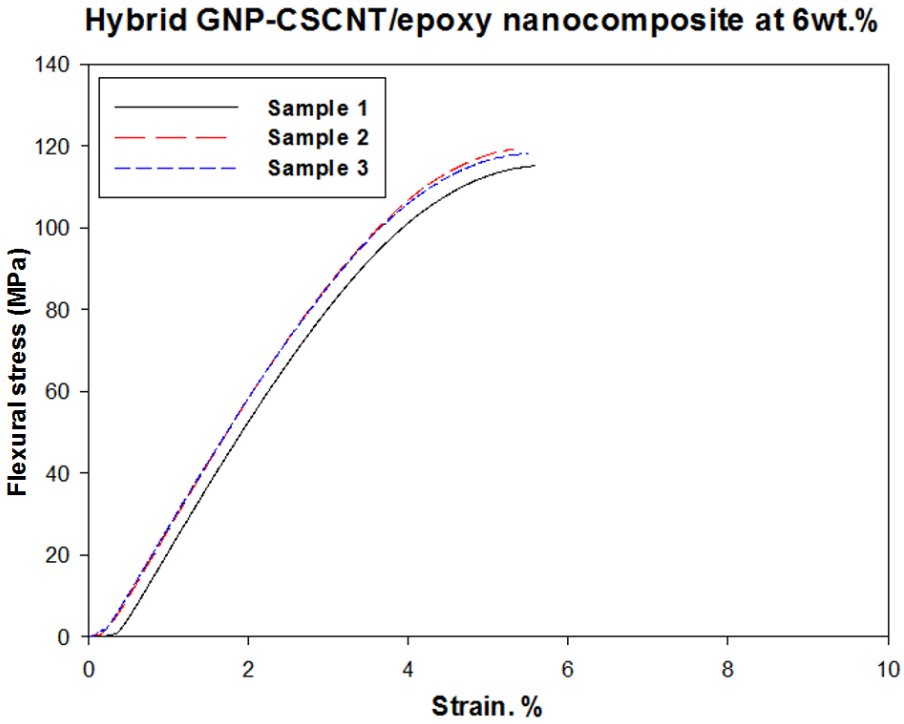
Hybrid GNP-CSCNT/epoxy nanocomposite at 6wt.%
Sample 1
Sample 2
Sample 3
Flexural stress (MPa)
Strain. %
0
20
40
60
80
100
120
140
0
2
4
6
8
10

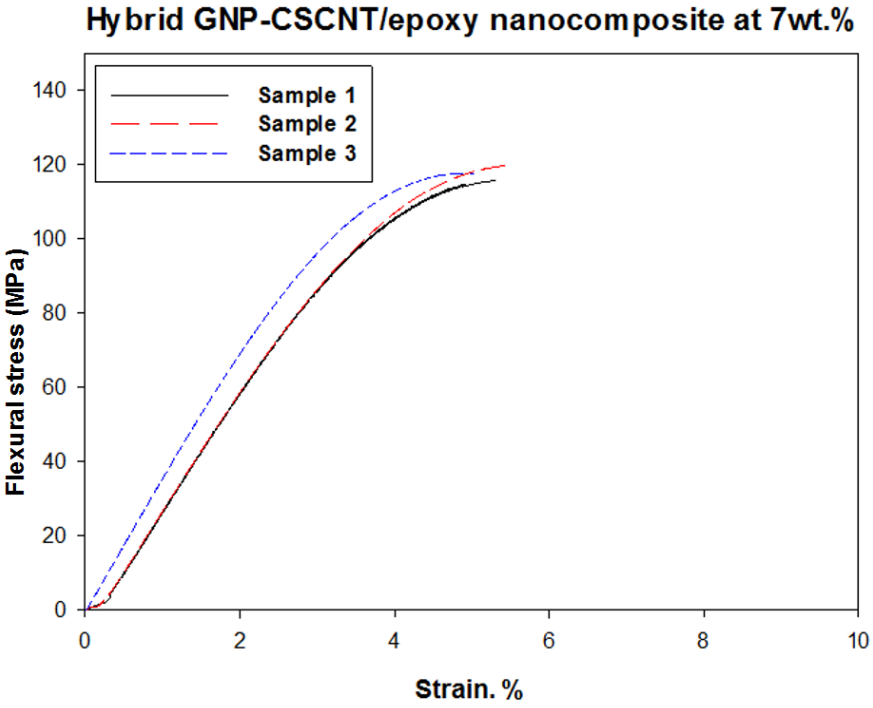

Figure B.3.3. The typical flexural stress-strain curves for the hybrid GNP-CSCNT/epoxy nanocomposites at various weight concentrations.

Table B.3.3. Summary of flexural tests results for the hybrid GNP-CSCNT/epoxy nanocomposites specimens at various weight concentrations in comparison with pure epoxy composites (base (0)).

Hybrid GNP-CSCNT/ epoxy nanocomposites processed by combined techniques method																		
Specimen Number	Maximum Flexural Strength (MPa)						Flexural Modulus (GPa)						Maximum Strain (%)					
	0 wt. %	***2.5 wt.%***	***4 wt.%***	***5 wt.%***	***6 wt.%***	***7 wt.%***	***0 wt. %***	***2.5 wt.%***	***4wt.%***	***5 wt.%***	***6 wt.%***	***7 wt.%***	***0 wt. %***	***2.5 wt.%***	***4 wt.%***	***5 wt.%***	***6 wt.%***	***7 wt.%***
1	102.14	116.82	149.20	110.80	119.10	115.00	2.99	3.32	4.70	3.10	3.31	2.86	5.60	5.41	4.38	5.36	5.8	5.56
2	102.48	116.80	132.83	111.10	119.80	119.10	2.75	3.31	4.27	2.93	3.33	2.88	5.72	5.43	4.48	5.38	4.3	5.49
3	101.15	118.60	140.12	109.48	115.85	117.20	2.75	3.34	4.52	2.97	2.99	2.96	5.68	4.20	4.42	5.32	5.7	5.30
4	99.10	114.02	143.85	-	-	-	2.71	2.95	4.51	-	-	-	5.88	4.47	4.44	-	-	-
Average	101.21	116.56	141.50	110.46	118.25	117.10	2.80	3.23	4.50	3.00	3.21	2.90	5.72	4.87	4.43	5.35	5.26	5.45
S.D	±1.52	±1.89	±6.87	±0.85	±2.10	±2.05	±0.13	±0.19	±0.18	±0.08	±0.12	±0.05	±0.11	±0.63	±0.04	±0.03	±0.83	±0.13
C.V	1.50%	1.62%	4.85%	0.77%	1.78%	1.75%	4.56%	5.79%	3.91%	2.96%	3.73%	1.80%	2.05%	13.00%	0.93%	0.57%	15.90%	2.38%
Incr.%	base(0)	+15.1	+39.1	+9.1	+16.8	+15.7	base(0)	+15.3	+60.7	+7.1	+14.6	+3.6	base(0)	-14.8	-22.5	-6.4	-8.0	-4.7

Appendix C. Fracture Toughness Properties

Appendix C.1. Typical force-deflection curves for the pure epoxy composite (base (0)) as well as three epoxy nanocomposites modified with carbon nanomaterials at optimum weight concentrations.

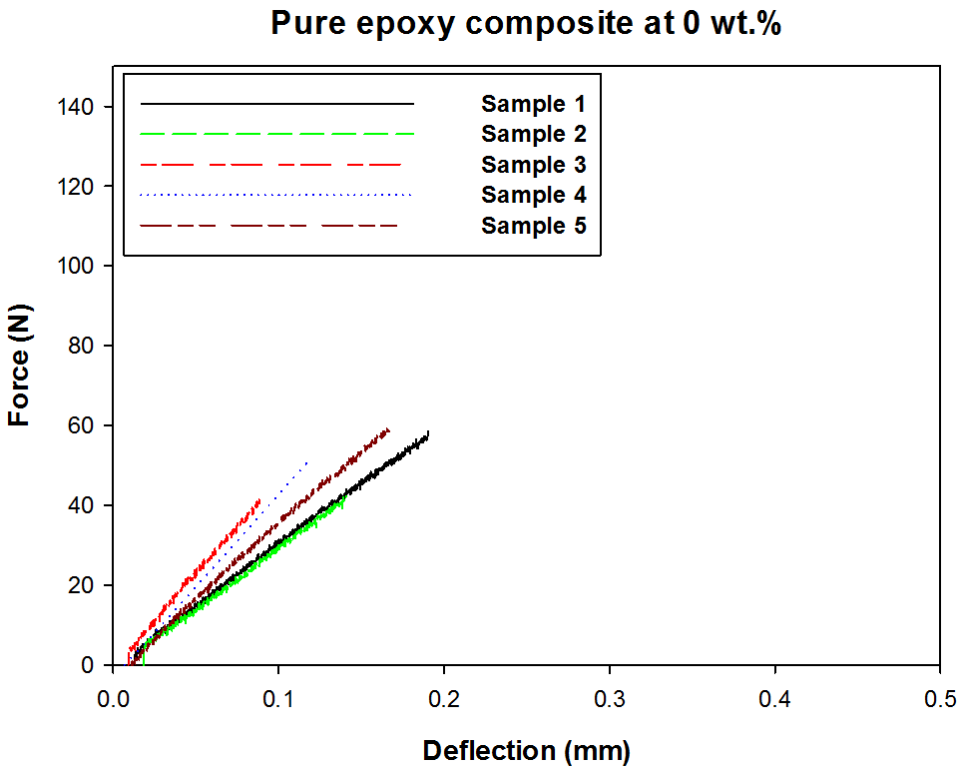

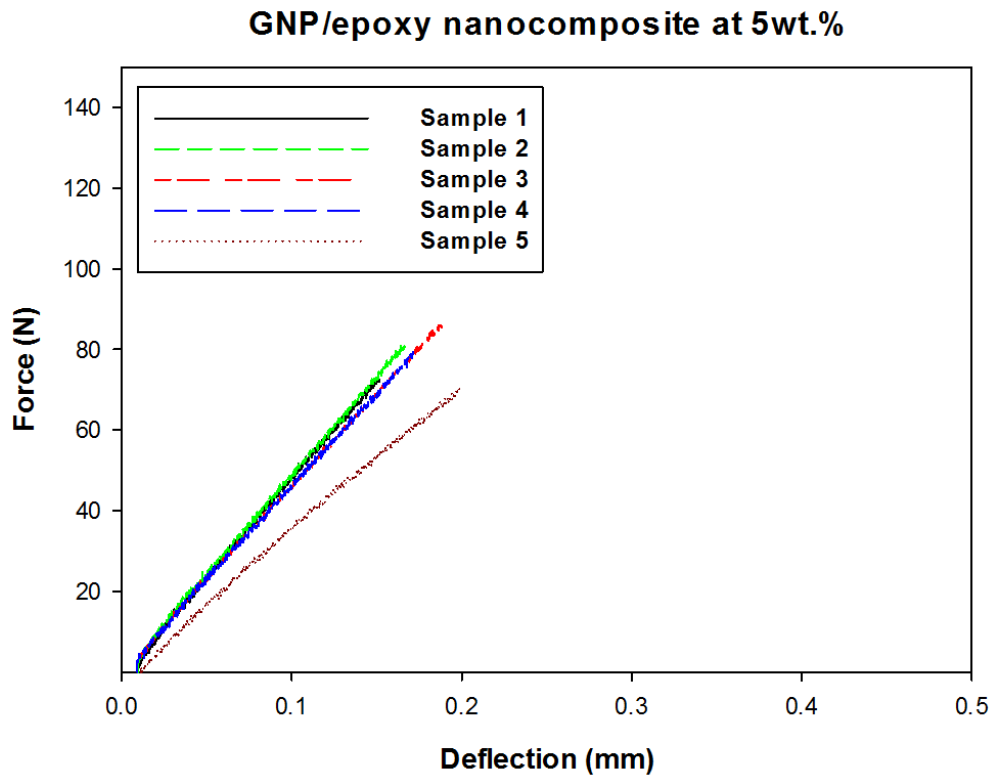
GNP/epoxy nanocomposite at 5wt.%
Sample 1
Sample 2
Sample 3
Sample 4
Sample 5
Force (N)
Deflection (mm)
140
120
100
80
60
40
20
0.0
0.1
0.2
0.3
0.4
0.5

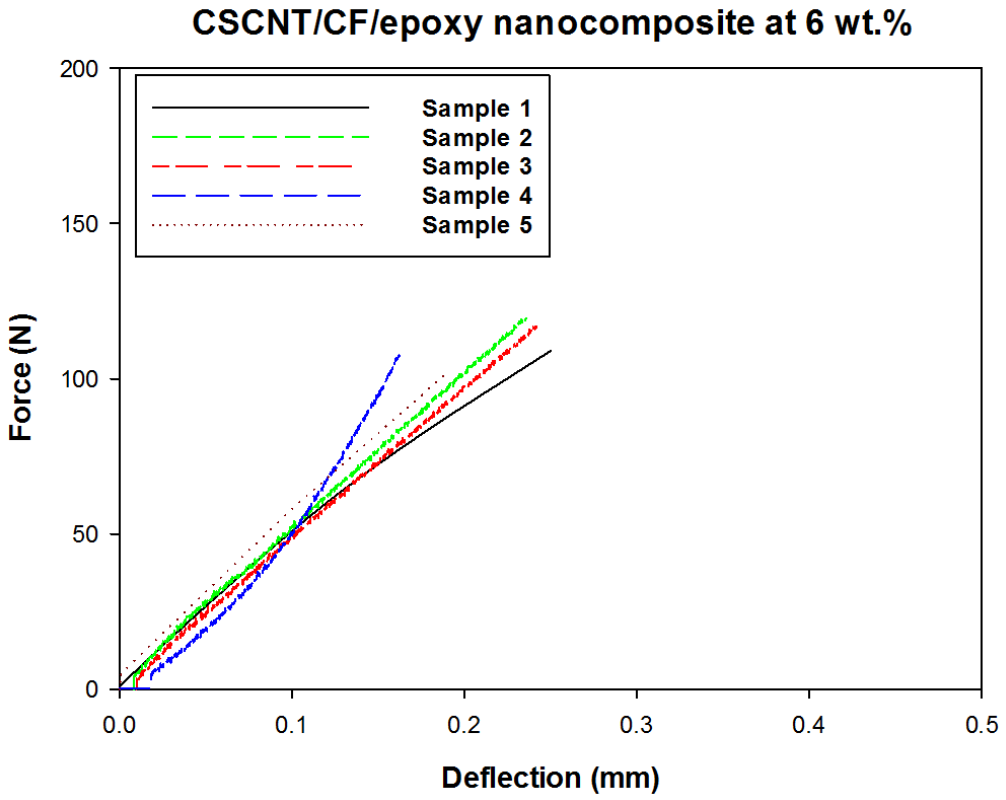
CSCNT/CF/epoxy nanocomposite at 6 wt.%
Sample 1
Sample 2
Sample 3
Sample 4
Sample 5
Force (N)
Deflection (mm)
200
150
100
50
0
0.0
0.1
0.2
0.3
0.4
0.5

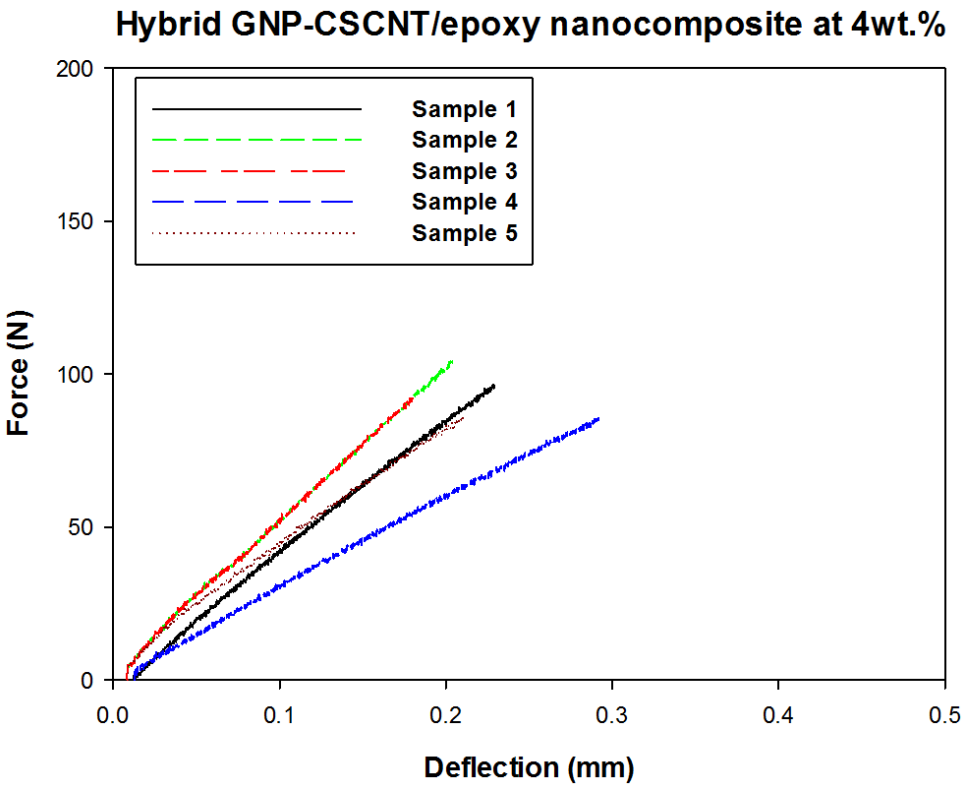

Figure C.1. The typical force deflection curves for the the pure epoxy composites as well as the GNP, CSCNT, and hybrid GNP-CSCNT/epoxy nanocomposites at optimum weight concentration.

Table C.1. Summary of SENB tests results for the three nanocomposites at optimum weight concentration as well as pure epoxy composites (base (0))

Specimen No	**Pure epoxy composites at 0 wt.%**		**GNP/epoxy nanocomposites at 5 wt.%**		**CSCNT/epoxy nanocomposites at 6 wt.%**		**Hybrid GNP-CSCNT/epoxy nanocomposites at 4 wt.%**	
	P_{max} (N)	K_{IC} MPa.m$^{1/2}$	P_{max} (N)	K_{IC} MPa.m$^{1/2}$	P_{max} (N)	K_{IC} MPa.m$^{1/2}$	P_{max} (N)	K_{IC} MPa.m$^{1/2}$
1	57.71	1.10	72.36	1.36	107.19	2.02	96.00	1.80
2	41.11	0.78	80.61	1.52	119.29	2.24	103.00	1.92
3	40.80	0.77	86.35	1.63	116.76	2.20	95.80	1.81
4	53.82	1.02	78.83	1.48	107.68	2.00	92.61	1.74
5	59.10	1.14	70.10	1.32	102.10	1.93	85.70	1.62
Average value	50.50	0.96	77.65	1.46	110.60	2.08	94.60	1.78
S.D	±8.90	±0.17	±6.52	±0.12	±5.70	±0.12	±6.20	±0.10
C.V	17.60%	18.30%	8.39%	8.56%	5.16%	5.95%	6.60%	5.60%
Incr.%	base(0)	base(0)	+53.7	+52.0	+119.0	+116.7	+87.3	+85.4

Appendix D. Interlaminar Shear Strength Properties

Appendix D.1. Typical force-deflection curves of short beam specimens for the CF/epoxy composite unmodified and three types of HCFRP at optimum weight concentrations.

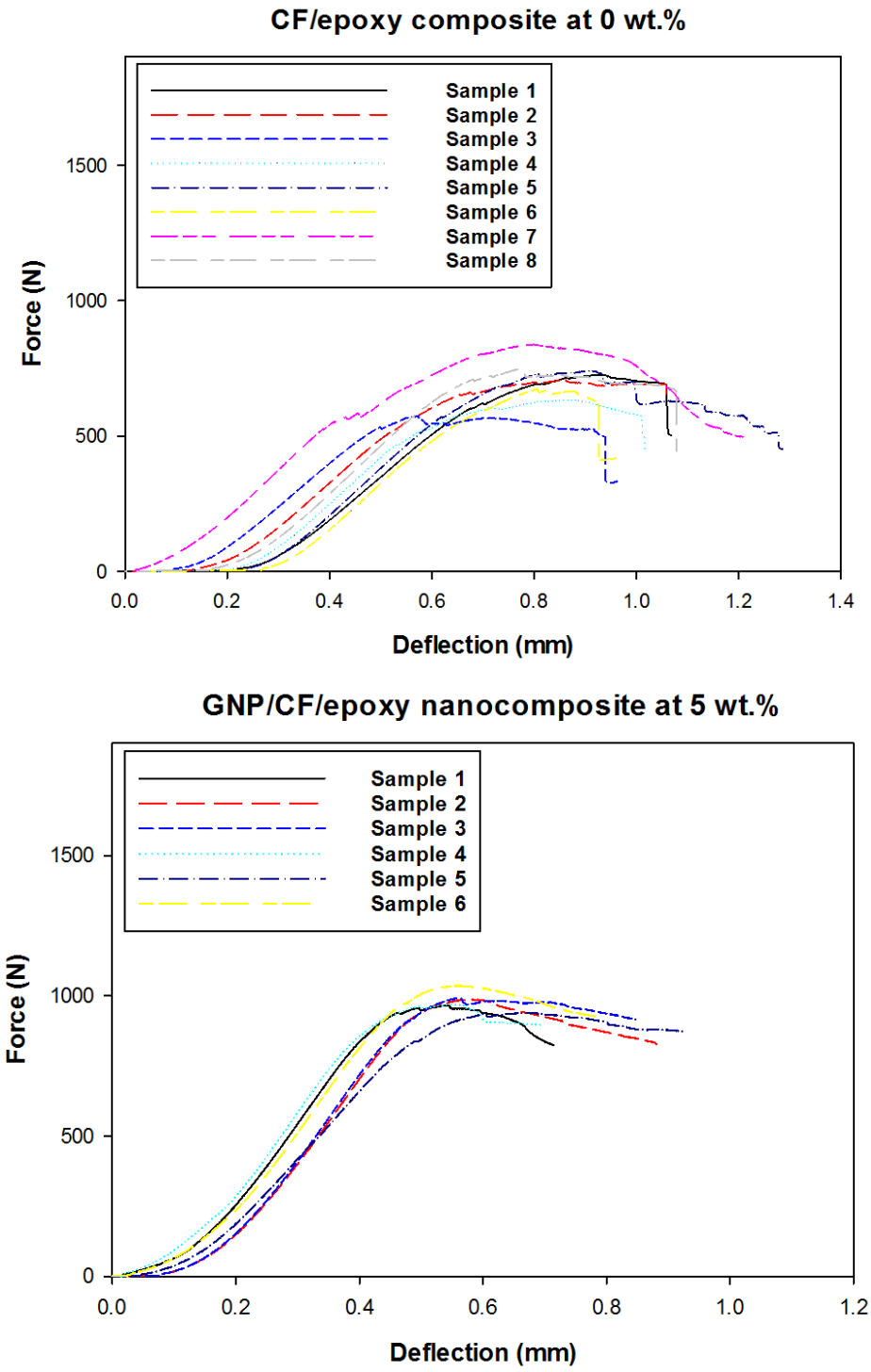

Figure D.1.1. The typical force-deflection curves of short beam specimens for the CF/epoxy composites and GNP/CF/epoxy nanocomposites and CF/epoxy composites unmodified.

Table D.1.1. Summary of SBS tests results for GNP/CF/epoxy nanocomposites specimens compared with CF/epoxy composites unmodified.

GNP/CF/epoxy nanocomposites		
Specimen No	ILSS (MPa)	
	CF/epoxy composite unmodified at 0 wt.%	GNP/CF/epoxy nanocomposite at 5 wt.%
1	26.02	38.34
2	28.95	37.02
3	25.57	37.53
4	26.78	36.96
5	30.75	36.28
6	27.75	38.61
7	31.40	-
8	30.86	-
Average value ILSS	28.50	37.45
S.D C.V	±2.31 8.12%	±0.88 2.36%
Incr.%	base(0)	+31.4

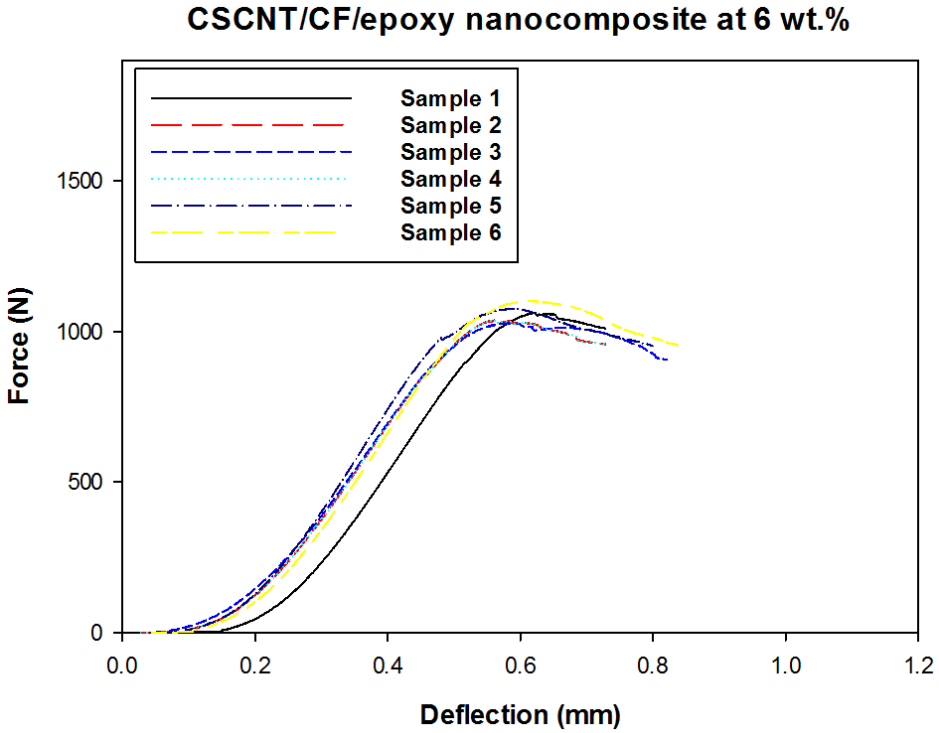

Figure D.1.2. The typical force-deflection curves of short beam specimens for the CSCNT/CF/epoxy nanocomposites.

Table D.1.2. Summary of SBS tests results for the CSCNT/CF/epoxy nanocomposites specimens compared with CF/epoxy composites unmodified.

Specimen No	ILSS (MPa)	
	CF/epoxy composite unmodified at 0 wt.%	**CSCNT/CF/epoxy nanocomposite at 6 wt.%**
1	26.02	39.80
2	28.95	39.21
3	25.57	38.36
4	26.78	38.93
5	30.75	39.00
6	27.75	40.16
7	31.40	-
8	30.86	-
Average value ILSS	28.50	39.24
S.D C.V	±2.31 8.12%	±0.64 1.64%
Incr.%	base(0)	+37.7

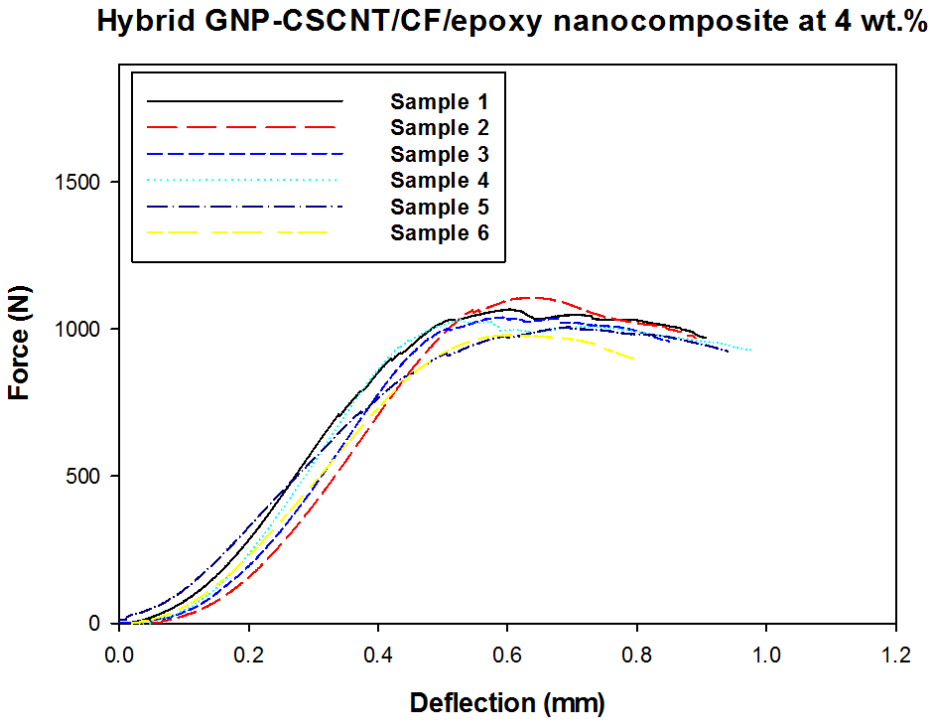

Figure D.1.3. The typical force-deflection curves of short beam specimens for the hybrid GNP-CSCNT/CF/epoxy nanocomposites.

Table D.1.3. Summary of SBS tests results for the hybrid GNP-CSCNT/CF/epoxy nanocomposites specimens compared with CF/epoxy composites unmodified.

Specimen No	**ILSS (MPa)**	
	CF/epoxy composite unmodified at 0 wt.%	**Hybrid GNP-CSCNT/CF/epoxy nanocomposite at 4 wt.%**
1	26.02	40.18
2	28.95	41.51
3	25.57	39.42
4	26.78	38.47
5	30.75	38.09
6	27.75	36.57
7	31.40	-
8	30.86	-
Average value ILSS	28.50	39.04
S.D C.V	±2.31 8.12%	±1.72 4.41%
Incr.%	base(0)	+36.9

Appendix E. Flexural Properties

Appendix E.1. Typical flexural stress-strain curves of the CF/epoxy composite unmodified and three types of HCFRP at optimum weight concentrations.

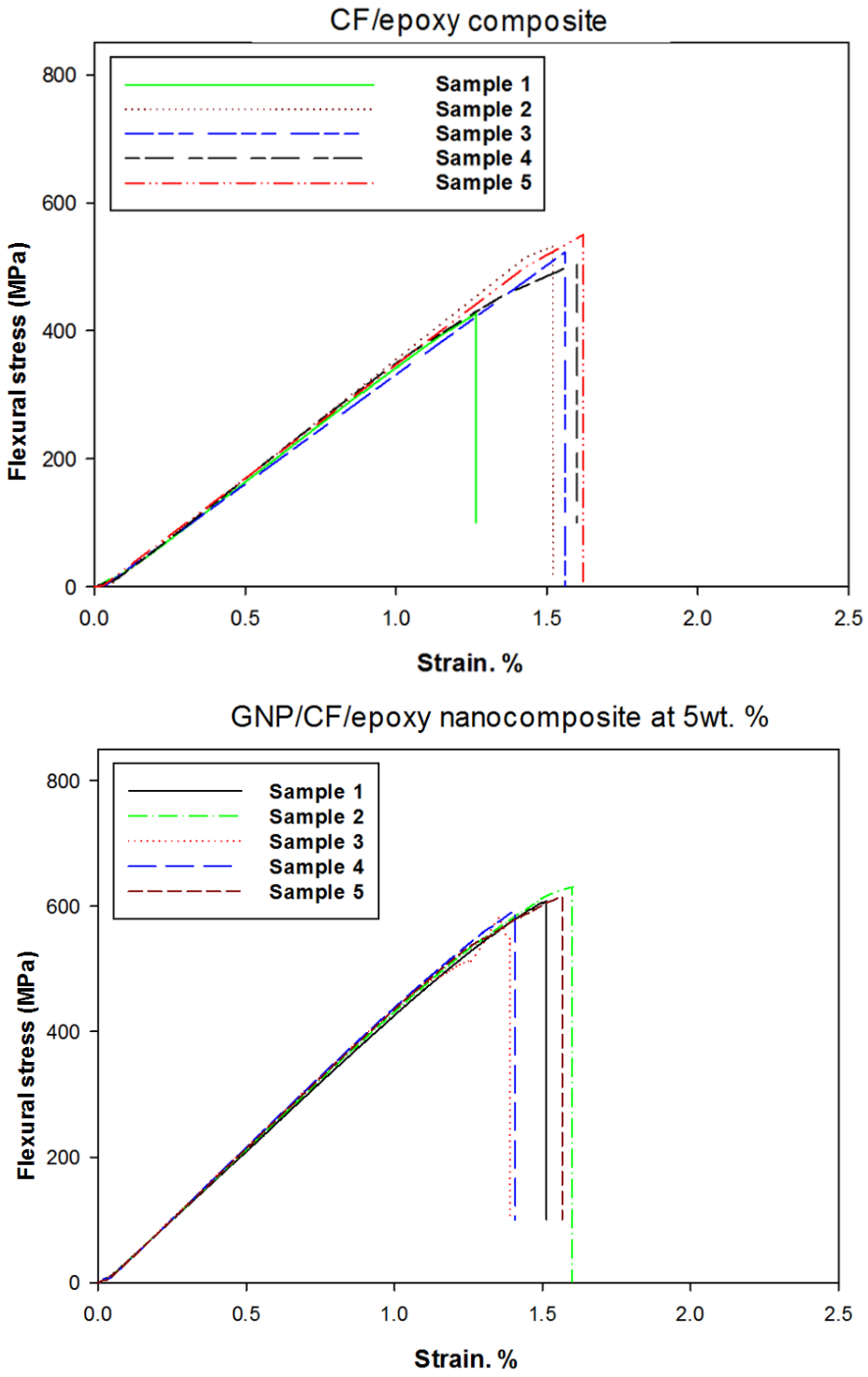

Figure E.1.1. The typical stress-strain curves for GNP/CF/epoxy nanocomposites at optimum weight concentration as well as CF/epoxy composite unmodified.

Table E.1.1. Summary of flexural strength and modulus results for GNP/CF/epoxy nanocomposites at optimum weight concentration in comparison to the CF/epoxy composites unmodified.

GNP/CF/epoxy nanocomposite						
Specimen No	Flexural strength (MPa)		Flexural modulus (GPa)		Elongation at failure (%)	
	0 wt%	5 wt. %	0 wt%	5 wt. %	0 wt%	5 wt. %
1	427.00	617.06	33.30	40.85	1.26	1.51
2	531.45	632.46	34.40	43.70	1.52	1.65
3	523.00	595.16	32.10	43.77	1.56	1.38
4	503.10	599.26	33.70	43.37	1.60	1.40
5	556.95	616.06	34.00	40.80	1.62	1.60
Average	508.30	612.00	33.50	42.50	1.51	1.51
S.D	±49.30	±15.10	±0.88	±1.58	±0.14	±0.12
C.V	9.71%	2.46%	2.62%	3.72%	9.65%	7.87%
Incr.%	base(0)	+20.4	base(0)	+26.8	base(0)	00.0

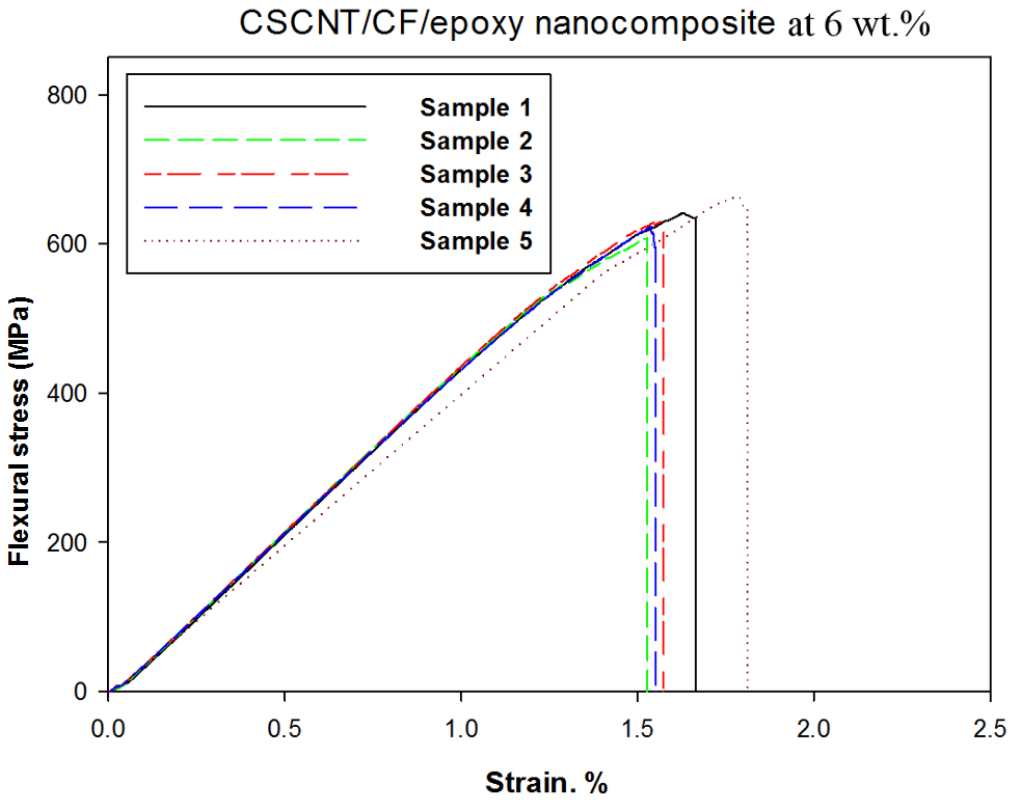

Figure E.1.2. The typical flexural stress-strain curves for the CSCN/CF/epoxy nanocomposites at optimum weight concentration.

Table E.1.2. Summary of flexural strength and modulus results for CSCNT/CF/epoxy nanocomposites at optimum weight concentration in comparison to the CF/epoxy composites unmodified.

CSCNT/CF/epoxy nanocomposite						
Specimen No	Flexural strength (MPa)		Flexural modulus (GPa)		Elongation at failure (%)	
	0 wt%	6 wt. %	0 wt%	6 wt. %	0 wt%	6 wt. %
1	427.00	645.00	33.30	42.10	1.26	1.66
2	531.45	607.50	34.40	41.10	1.52	1.52
3	523.00	641.40	32.10	43.48	1.56	1.57
4	503.10	631.40	33.70	40.50	1.60	1.55
5	556.95	661.73	34.00	39.40	1.62	1.78
Average	508.30	635.50	33.50	41.30	1.51	1.62
S.D	±49.30	±20.49	±0.88	±1.90	±0.14	±0.10
C.V	9.71%	3.22%	2.63%	4.60%	9.65%	6.52%
Incr.%	base(0)	+25.0	base(0)	+23.3	base(0)	+7.3

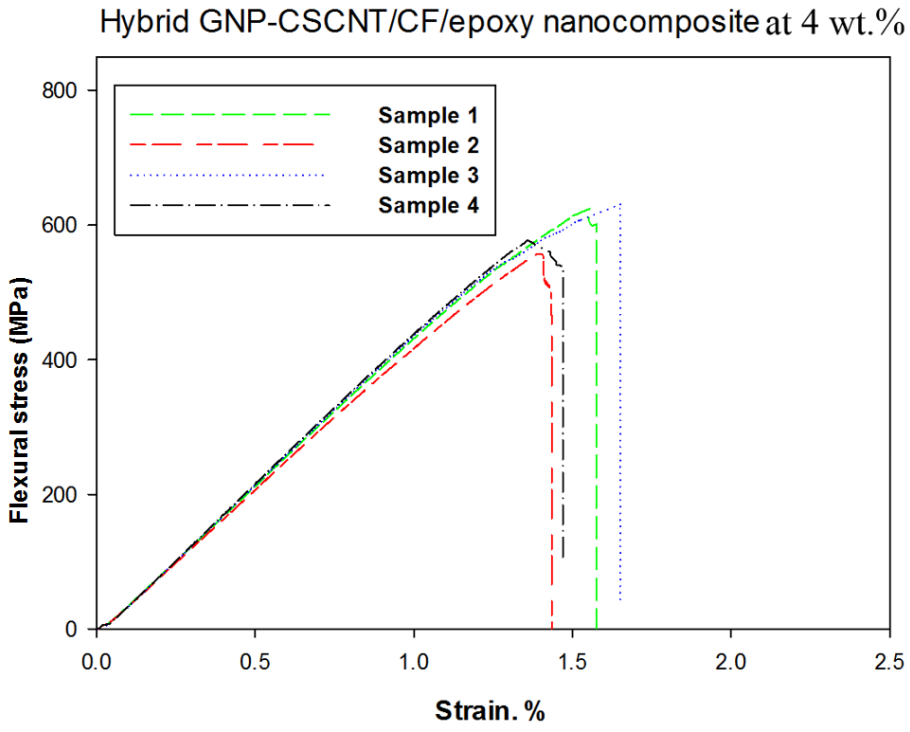

Figure E.1.3.The typical flexural stress-strain curves for the hybrid GNP-CSCN/CF/epoxy nanocomposites at optimum weight concentration.

Table E.1.2. Summary of flexural strength and modulus results for the hybrid GNP-CSCNT/CF/epoxy nanocomposites at optimum weight concentration in comparison to the CF/epoxy composites unmodified.

Hybrid GNP-CSCNT/CF/epoxy nanocomposite						
Specimen No	Flexural strength (MPa)		Flexural modulus (GPa)		Elongation at failure (%)	
	0 wt%	4 wt. %	0 wt%	4 wt. %	0 wt%	4 wt. %
1	427.00	627.70	33.30	42.70	1.26	1.60
2	531.45	557.00	34.40	41.82	1.52	1.39
3	523.00	633.93	32.10	43.30	1.56	1.70
4	503.10	572.97	33.70	43.78	1.60	1.45
5	556.95	-	34.00	-	1.62	-
Average	508.30	597.90	33.50	42.9	1.51	1.54
S.D	±49.30	±53.28	±0.88	±0.844	±0.14	±0.14
C.V	9.71%	8.91%	2.63%	1.96%	9.65%	9.18%
Incr.%	base(0)	+17.6	base(0)	+28.1	base(0)	+1.9

Appendix F. Interlaminar Fracture Toughness (Mode I)

Appendix F.1. Typical force-deflection curves of DCB specimens for the CF/epoxy composite unmodified as well as three types of HCFRP at optimum weight concentrations.

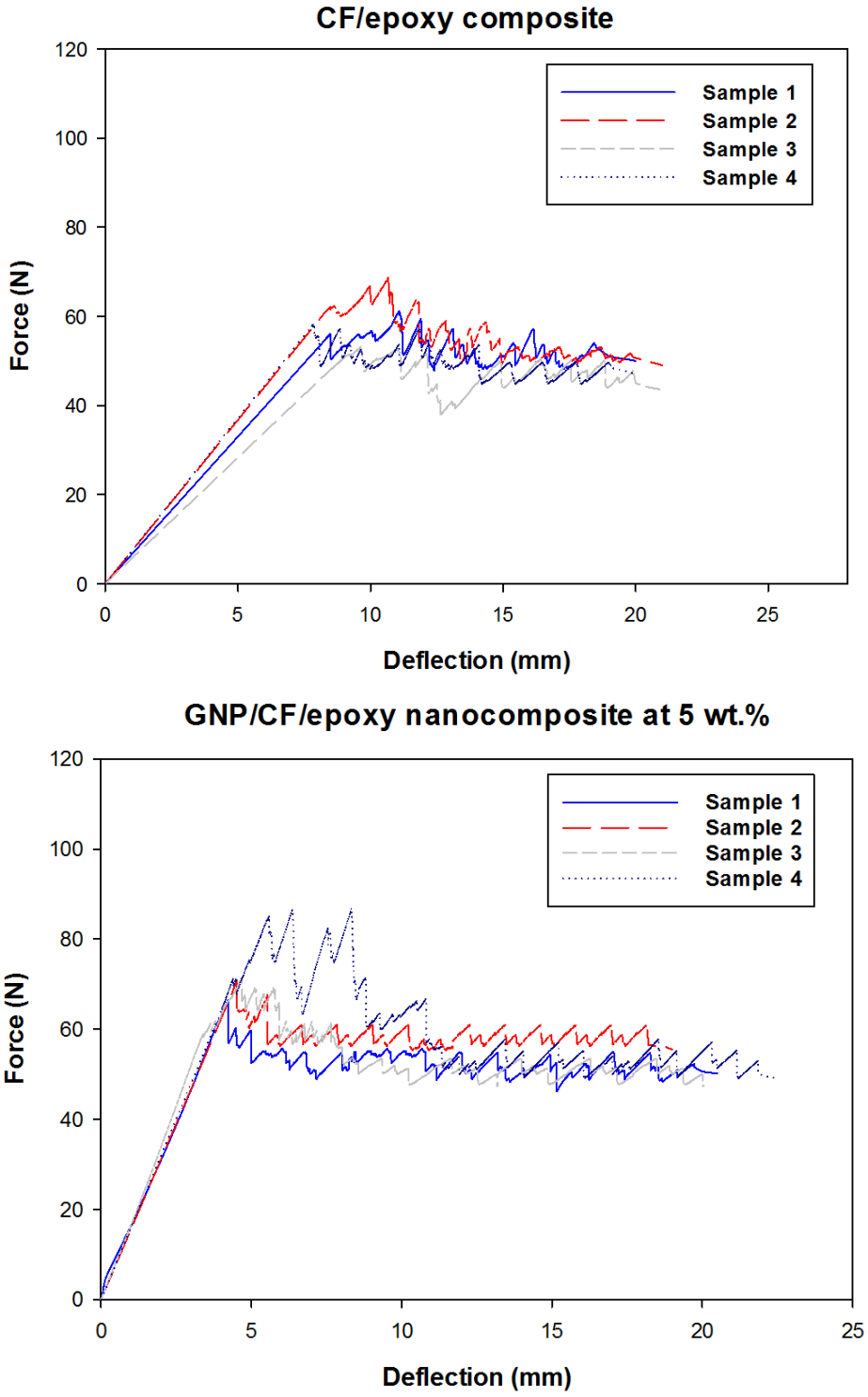

Figure F.1.1. The typical force-deflection curves for the CF/epoxy composites unmodified as well as GNP/CF/epoxy nanocomposites at 5 wt. %.

Table F.1.1. Summary of DCB tests results for GNP/CF/epoxy nanocomposites in comparison with CF/epoxy composites unmodified.

CF/epoxy composites unmodified at 0 wt.%						**GNP/CF/epoxy nanocomposites at 5 wt. %**				
No	Initial propagation toughness ($J.m^{-2}$)			Propagation toughness ($J.m^{-2}$)	Fracture toughness at Max load ($J.m^{-2}$)	Initial propagation toughness($J.m^{-2}$)			Propagation toughness ($J.m^{-2}$)	Fracture toughness at Max load ($J.m^{-2}$)
	Visual onset	Non linear	5% offset			Visual onset	Non linear	5% offset		
1	210.00	303.00	258.00	395.80	437.60	312.40	308.57	328.80	359.60	333.80
2	433.50	432.70	434.70	487.00	455.30	433.20	350.00	410.00	501.22	474.00
3	280.20	220.20	281.40	363.30	403.00	330.90	276.30	362.00	445.10	362.11
4	281.40	301.10	310.80	372.80	423.40	522.00	363.40	249.60	556.20	568.60
Average toughness ($J.m^{-2}$)	301.30	314.25	321.23	405.05	429.82	399.60	324.50	337.60	465.50	435.60
S.D	±9.00	±8.77	±7.80	±5.60	±2.20	±9.00	±3.94	±6.70	±8.38	±10.70
C.V	30.00%	27.94%	24.28%	13.82%	5.13%	23.31%	12.15%	19.98%	18.00%	24.60%
Incr.%	base(0)					+32.6	+3.2	+5.1	+14.9	+1.3

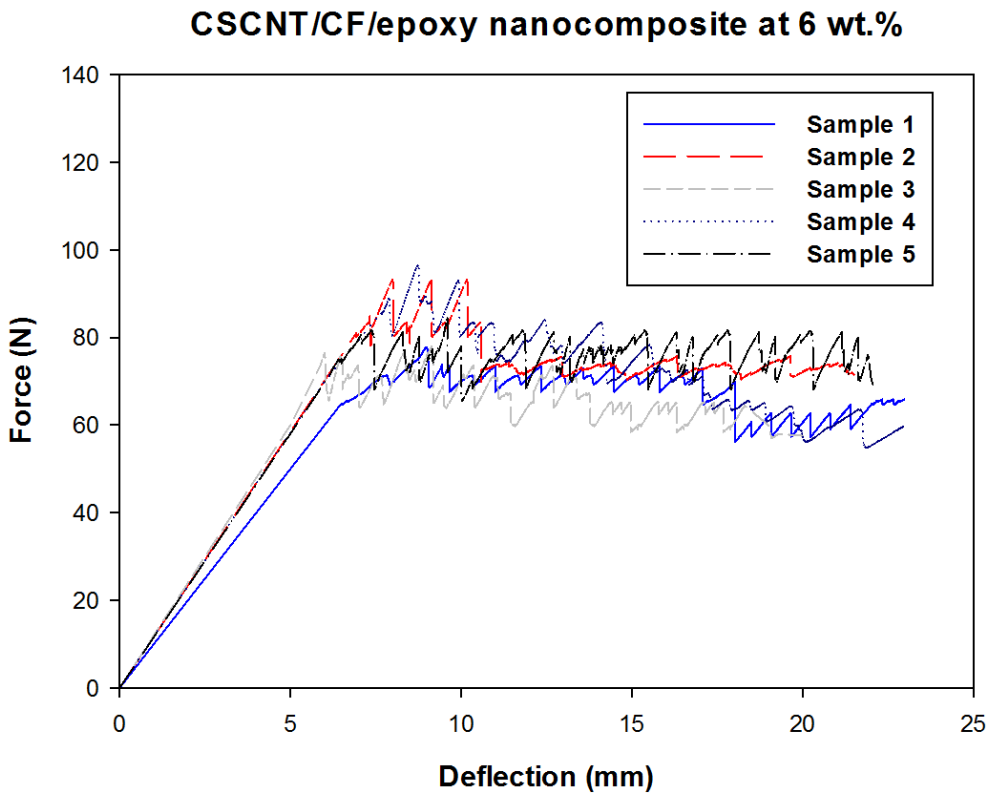

Figure F.1.2. The typical force-deflection curves for the CSCNT/CF/epoxy nanocomposites at 6 wt. %.

Table F.1.2. Summary of DCB tests results for CSCNT/CF/epoxy nanocomposites in comparison with CF/epoxy composites unmodified.

CF/epoxy composites unmodified at 0 wt.%						**CSCNT/CF/epoxy nanocomposites at 6 wt. %**				
No	Initial propagation toughness ($J.m^{-2}$)			Propagation toughness ($J.m^{-2}$)	Fracture toughness at Max load ($J.m^{-2}$)	Initial propagation toughness($J.m^{-2}$)			Propagation toughness ($J.m^{-2}$)	Fracture toughness at Max load ($J.m^{-2}$)
	Visual onset	Non linear	5% offset			Visual onset	Non linear	5% offset		
1	210.00	303.00	258.00	395.80	437.60	540.00	480.00	551.70	663.10	702.00
2	433.50	432.70	434.70	487.00	455.30	610.80	845.00	622.30	980.00	1097.00
3	280.20	220.20	281.40	363.30	403.00	348.00	81.00	376.00	585.00	613.10
4	281.40	301.10	310.80	372.80	423.40	801.60	628.70	806.20	961.30	1160.00
5	-	-	-	-	-	538.10	565.00	599.70	941.90	968.40
Average toughness ($J.m^{-2}$)	301.30	314.25	321.23	405.05	429.82	567.7	579.94	591.18	826.26	908.10
S.D	±9.00	±8.77	±7.80	±5.60	±2.20	±16.3	±17.48	±16.51	±18.27	±24.08
C.V	30.00%	27.94%	24.28%	13.82%	5.13%	28.72%	30.14%	27.92%	22.11%	26.52%
Incr.%	base(0)					+88.4	+84.5	+84.0	+103.9	+111.2

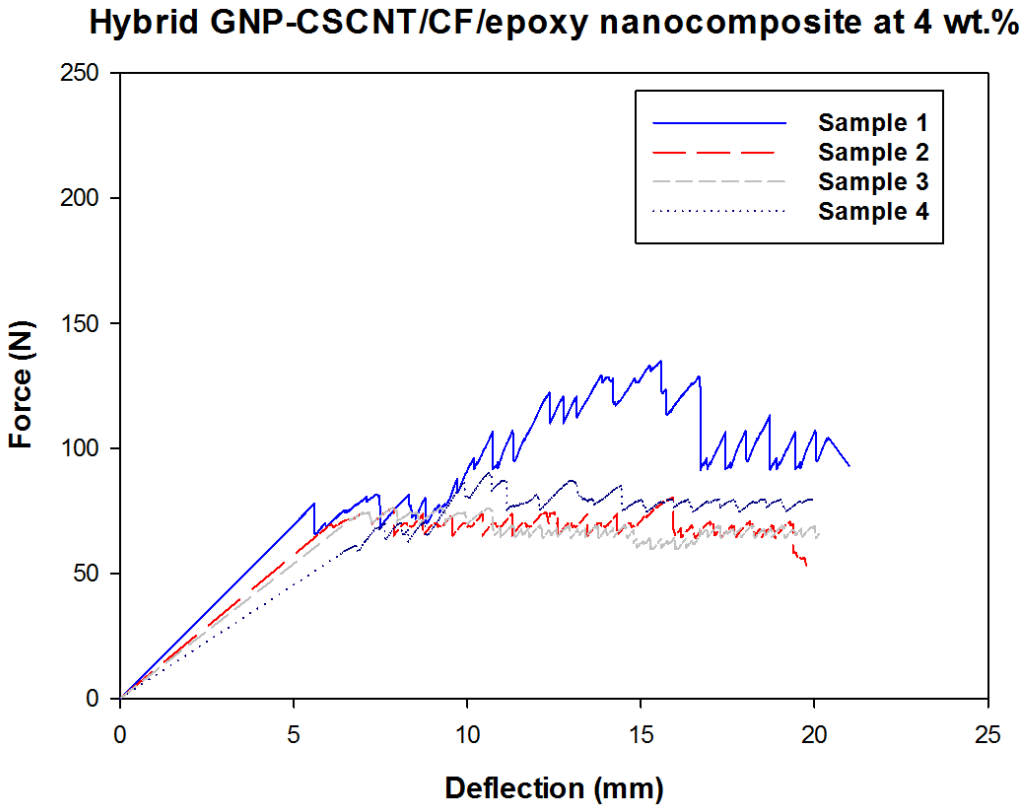

Figure F.1.3. The typical force-deflection curves for the hybrid GNP-CSCNT/CF/epoxy nanocomposites at 4 wt. %.

Table F.1.3. Summary of DCB tests results for hybrid GNP-CSCNT/CF/epoxy nanocomposites in comparison with CF/epoxy composites unmodified.

CF/epoxy composites unmodified at 0 wt.%						**Hybrid GNP-CSCNT/CF/epoxy nanocomposites at 4 wt.%**				
No	Initial propagation toughness ($J.m^{-2}$)			Propagation toughness ($J.m^{-2}$)	Fracture toughness at Max load ($J.m^{-2}$)	Initial propagation toughness($J.m^{-2}$)			Propagation toughness ($J.m^{-2}$)	Fracture toughness at Max load ($J.m^{-2}$)
	Visual onset	Non linear	5% offset			Visual onset	Non linear	5% offset		
1	433.50	432.70	434.70	487.00	455.30	306.70	377.60	434.70	835.90	1335.90
2	280.20	220.20	281.40	363.30	403.00	285.00	358.90	436.40	647.18	714.20
3	281.40	301.10	310.80	372.80	423.40	280.80	280.00	348.20	616.30	608.00
4	433.50	432.70	434.70	487.00	455.30	267.90	240.00	214.00	706.70	960.00
Average toughness ($J.m^{-2}$)	301.30	314.25	321.23	405.05	429.82	285.10	314.10	358.30	700.00	904.50
S.D	±9.00	±8.77	±7.80	±5.60	±2.20	±1.6	±6.5	±10.4	±13.39	±33.03
C.V	30.00%	27.94%	24.28%	13.82%	5.13%	5.60%	20.68%	29.18 %	19.13%	36.50%
Incr.%	base(0)					-5.3	-0.1	+11.5	+72.8	+110.4

Appendix F.2. Typical resistance curves (R-curves) for the CF/epoxy composite unmodified as well as three types of HCFRP at optimum weight concentrations.

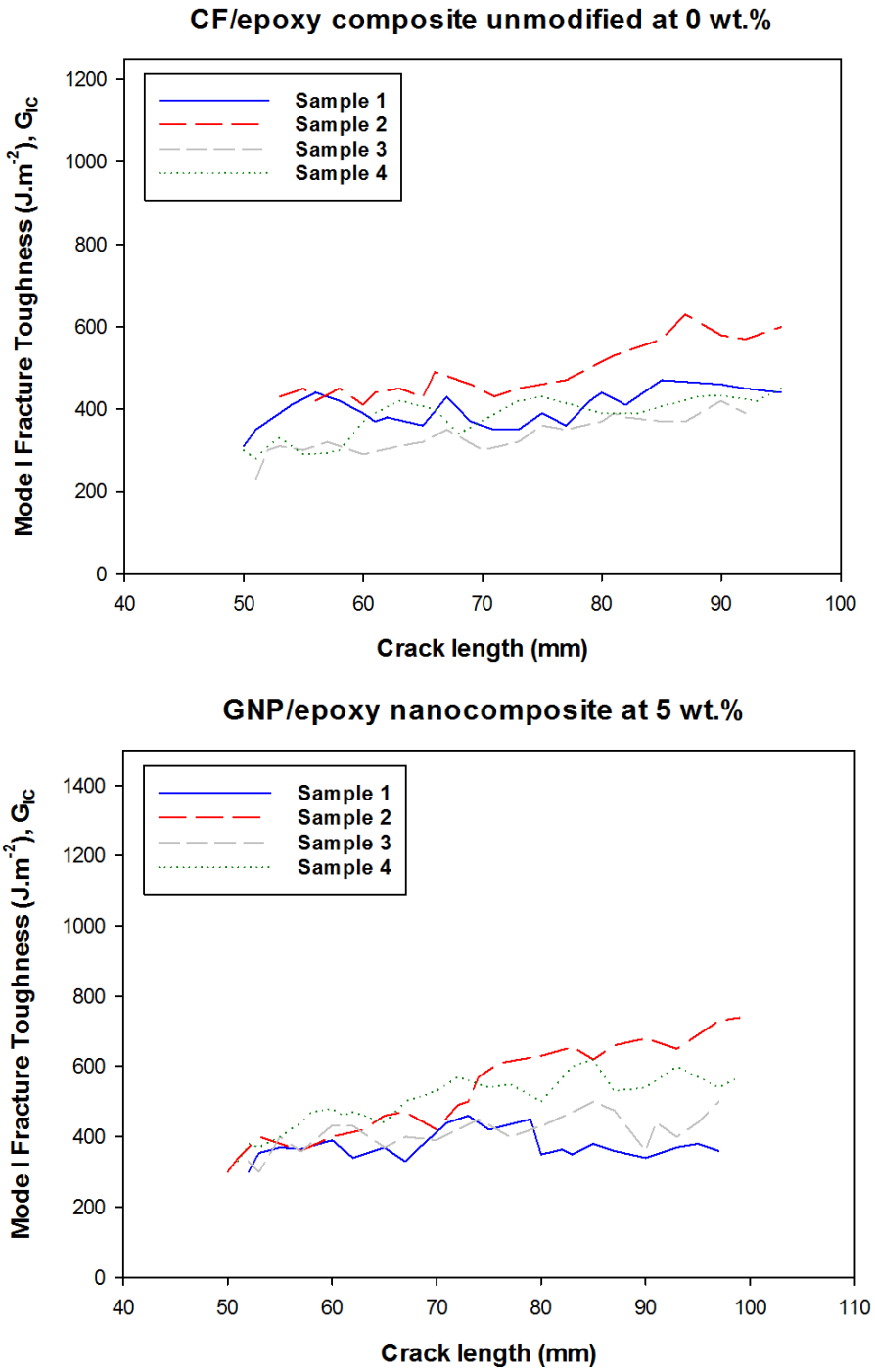

Figure F.2.1. Typical resistance curves (R-curves) for the CF/epoxy composites unmodified as well as GNP/CF/epoxy nanocomposites at 5 wt. %.

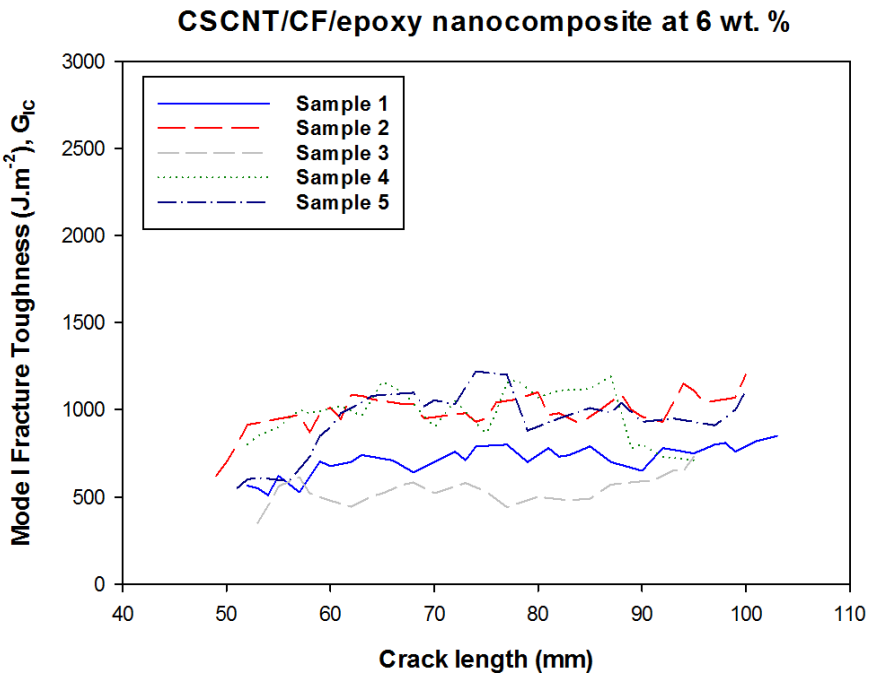

Figure F.2.2. Typical resistance curves (R-curves) for the CF/epoxy composites unmodified as well as CSCNT/CF/epoxy nanocomposites at 6 wt. %.

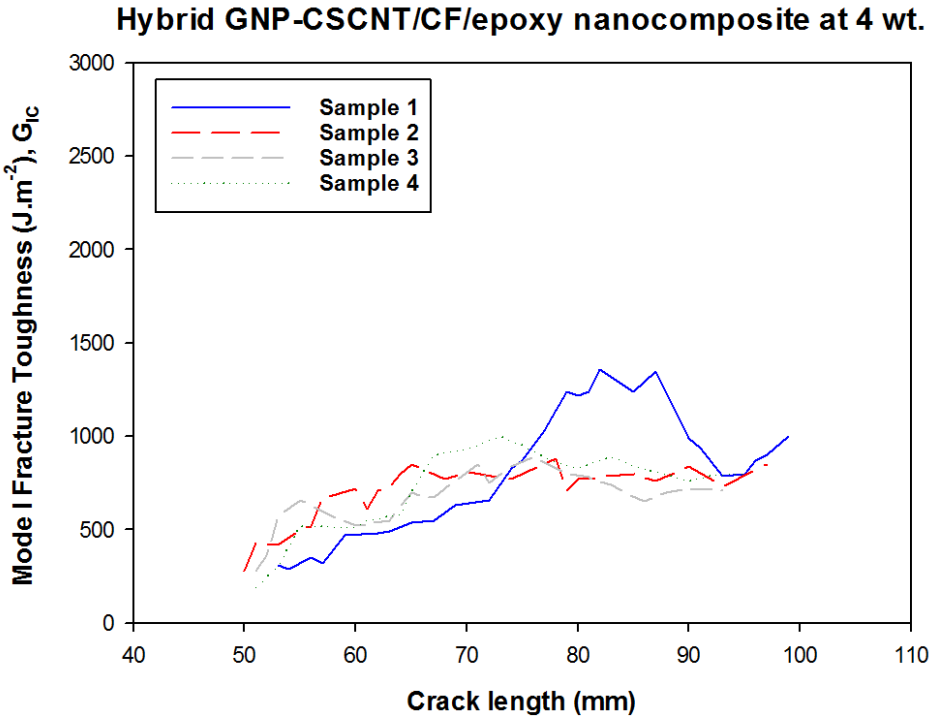

Figure F.2.3. Typical resistance curves (R-curves) for the CF/epoxy composites unmodified as well as hybrid GNP- CSCNT/CF/epoxy nanocomposites at 4 wt. %.

Appendix G. Interlaminar Fracture Toughness (Mode II)

Appendix G.1. Typical force-deflection curves of 3ENF specimens for the CF/epoxy composite unmodified as well as three types of HCFRP at optimum weight concentrations.

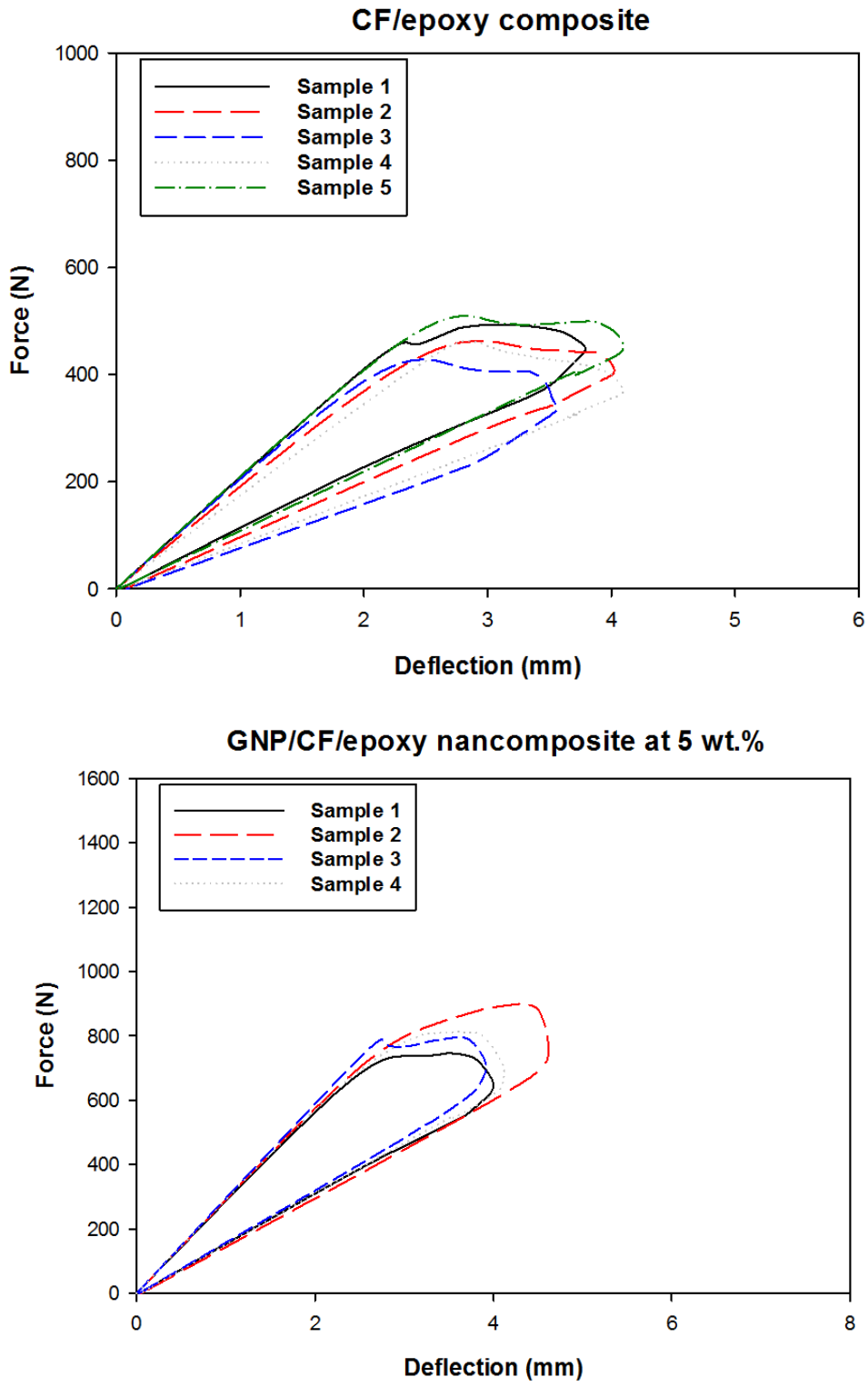

Figure G.1.1. The typical force-deflection curves for the CF/epoxy composites unmodified as well as GNP/CF/epoxy nanocomposites at 5 wt. %.

Table G.1.1. Summary of 3ENF tests results for GNP/CF/epoxy nanocomposites in comparison with CF/epoxy composites unmodified.

CF/epoxy composites unmodified at 0 wt.%						**GNP/CF/epoxy nanocomposites at 5 wt. %**				
No	Initial propagation toughness ($J.m^{-2}$)			Propagation toughness ($J.m^{-2}$)	Fracture toughness at Max load ($J.m^{-2}$)	Initial propagation toughness($J.m^{-2}$)			Propagation toughness ($J.m^{-2}$)	Fracture toughness at Max load ($J.m^{-2}$)
	Visual onset	Non linear	5% offset			Visual onset	Non linear	5% offset		
1	611.00	670.00	723.00	1232.00	1143.20	800.00	1381.00	1402.00	1801.00	1757.80
2	699.10	771.00	810.00	1021.00	938.10	913.00	1598.00	1630.00	2510.00	2695.00
3	665.40	761.20	780.00	1010.50	781.20	910.00	1490.00	1550.00	2071.00	1936.00
4	602.00	681.00	710.00	1180.00	880.00	890.00	1410.00	1511.00	2011.00	2011.90
5	721.00	831.00	861.00	1272.00	1345.50	-	-	-	-	-
Average toughness ($J.m^{-2}$)	659.70	742.80	776.60	1143.10	1017.60	878.20	1469.70	1523.20	2098.00	2100.00
S.D	±5.20	±6.70	±6.20	±12.00	±22.00	±7.00	±9.6	±11.00	±29.00	±41.00
C.V	7.96%	9%	8%	10.77%	22.20%	8.68%	6.60%	7.57%	14.18%	19.50%
Incr.%	base(0)					+33.1	+97.8	+96.1	+83.5	+106.3

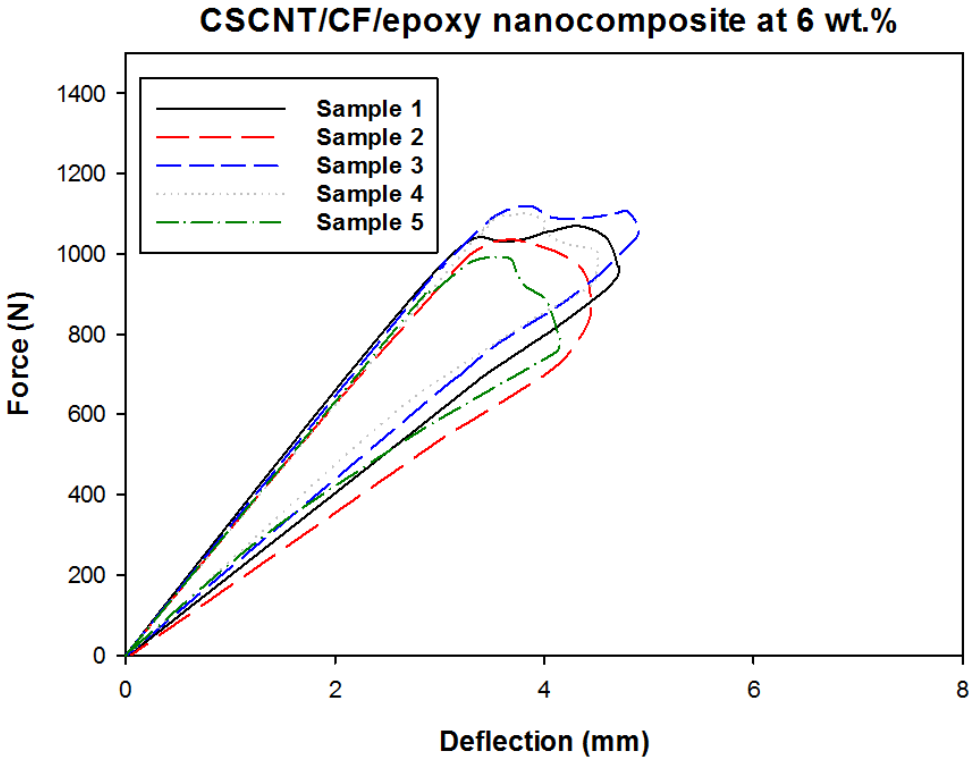

Figure G.1.2. The typical force-deflection curves for CSCNT/CF/epoxy nanocomposites at 6 wt. %.

Table G.1.2. Summary of 3ENF tests results for CSCNT/CF/epoxy nanocomposites in comparison with CF/epoxy composites unmodified.

CF/epoxy composites unmodified at 0 wt.%						**CSCNT/CF/epoxy nanocomposites at 6 wt. %**				
No	Initial propagation toughness ($J.m^{-2}$)			Propagation toughness ($J.m^{-2}$)	Fracture toughness at Max load ($J.m^{-2}$)	Initial propagation toughness($J.m^{-2}$)			Propagation toughness ($J.m^{-2}$)	Fracture toughness at Max load ($J.m^{-2}$)
	Visual onset	Non linear	5% offset			Visual onset	Non linear	5% offset		
1	611.00	670.00	723.00	1232.00	1143.20	1975.00	2162.20	2290.00	2881.00	2980.00
2	699.10	771.00	810.00	1021.00	938.10	1880.00	2166.00	2216.00	2741.00	2730.00
3	665.40	761.20	780.00	1010.50	781.20	2010.00	2700.00	2810.00	3271.00	3720.00
4	602.00	681.00	710.00	1180.00	880.00	1953.00	2230.00	2311.00	2811.00	2700.00
5	721.00	831.00	861.00	1272.00	1345.50	1398.00	1485.00	1510.00	2629.00	2570.00
Average toughness ($J.m^{-2}$)	659.70	742.80	776.60	1143.10	1017.60	1843.20	2148.60	2227.00	2866.60	2940.00
S.D	±5.20	±6.70	±6.20	±12.00	±22.00	±25.00	±43.00	±46.00	±24.00	±46.00
C.V	7.96%	9.00%	8.00%	10.77%	22.20%	13.70%	20.17%	20.80%	8.50%	15.66%
Incr.%	base(0)					+179.4	+189.2	+186.7	+150.7	+188.9

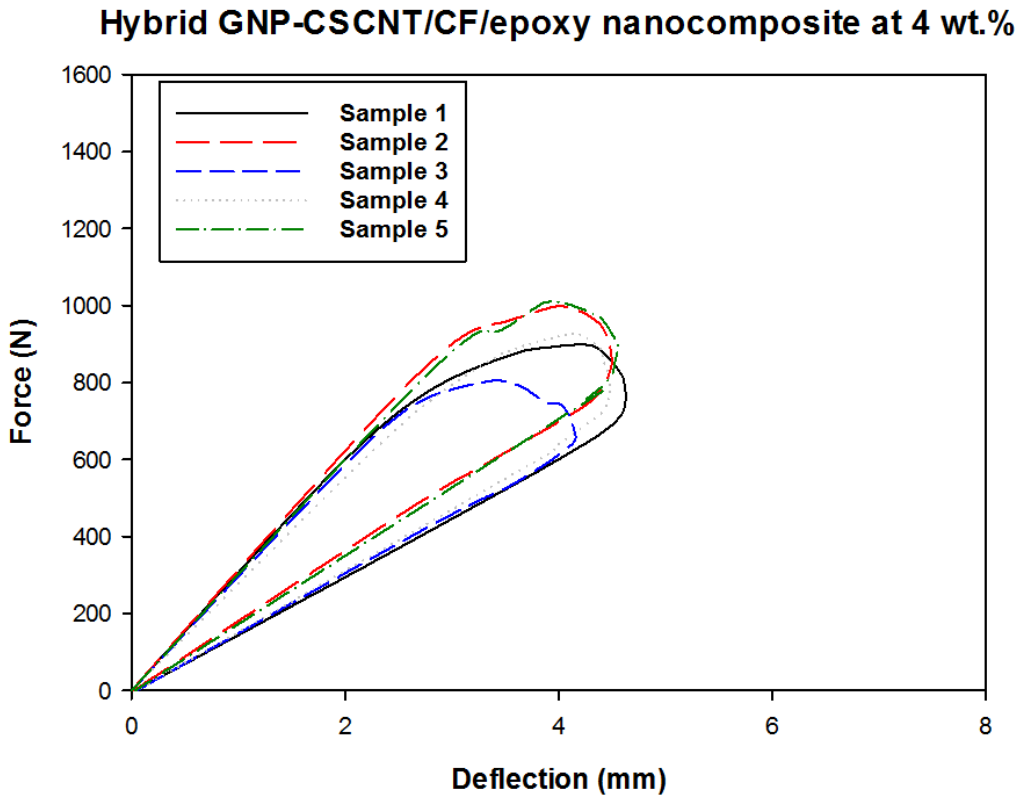

Figure G.1.3. The typical force-deflection curves for hybrid GNP-CSCNT/CF/epoxy nanocomposites at 4 wt. %.

Table G.1.3. Summary of 3ENF tests results for hybrid GNP-CSCNT/CF/epoxy nanocomposites in comparison with CF/epoxy composites unmodified.

CF/epoxy composites unmodified at 0 wt.%						**Hybrid GNP-CSCNT/CF/epoxy nanocomposites at 4 wt. %**				
No	Initial propagation toughness ($J.m^{-2}$)			Propagation toughness ($J.m^{-2}$)	Fracture toughness at Max load ($J.m^{-2}$)	Initial propagation toughness($J.m^{-2}$)			Propagation toughness ($J.m^{-2}$)	Fracture toughness at Max load ($J.m^{-2}$)
	Visual onset	Non linear	5% offset			Visual onset	Non linear	5% offset		
1	611.00	670.00	723.00	1232.00	1143.20	1395.90	1810.00	1860.00	2576.40	2630.00
2	699.10	771.00	810.00	1021.00	938.10	1930.00	2146.00	2200.00	2912.00	2725.00
3	665.40	761.20	780.00	1010.50	781.20	1440.00	1781.00	1811.00	2194.00	1891.00
4	602.00	681.00	710.00	1180.00	880.00	1690.00	2280.00	2381.00	2710.00	2570.00
5	721.00	831.00	861.00	1272.00	1345.50	1964.00	2064.00	2181.00	2884.00	2400.00
Average toughness ($J.m^{-2}$)	659.70	742.80	776.60	1143.10	1017.60	1683.90	2016.20	2086.60	2655.20	2443.20
S.D	±5.20	±6.70	±6.20	±12.00	±22.00	±26.50	±21.50	±24.00	±29.00	±32.00
C.V	7.96%	9.00%	8.00%	10.77%	22.20%	15.76%	10.70%	11.62%	10.97%	13.46%
Incr.%	base(0)					+155.2	+171.4	+168.7	+132.3	+140.1

Appendix G.2. Typical resistance curves (R-curves) for the CF/epoxy composite unmodified as well as three types of HCFRP at optimum weight concentrations.

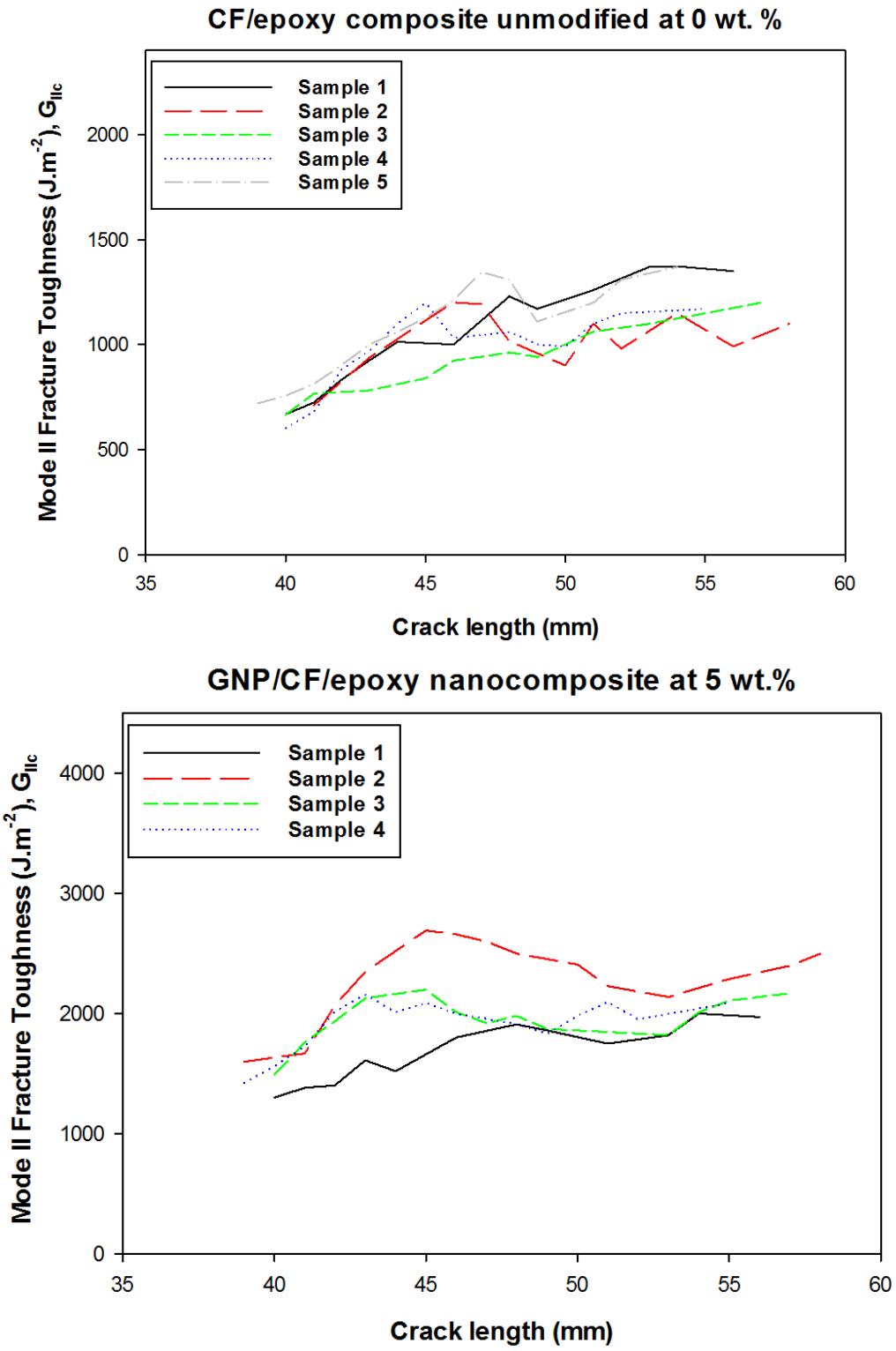

Figure G.2.1. Typical resistance curves (R-curves) for the CF/epoxy composites unmodified as well as GNP/CF/epoxy nanocomposites at 5 wt. %.

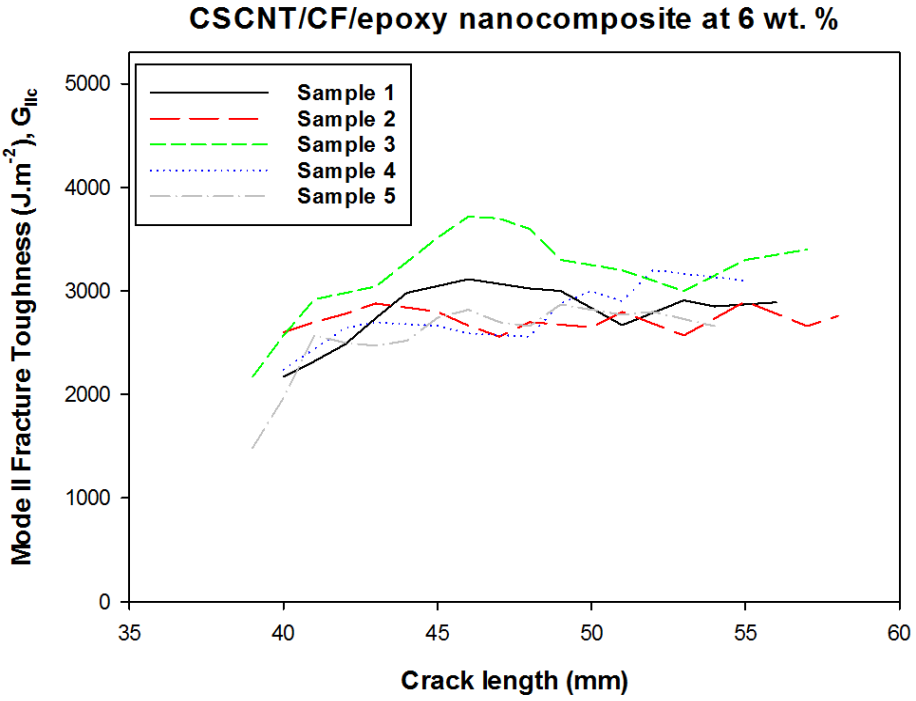

Figure G.2.2. Typical resistance curves (R-curves) for CSCNT/CF/epoxy nanocomposites at 6 wt. %.

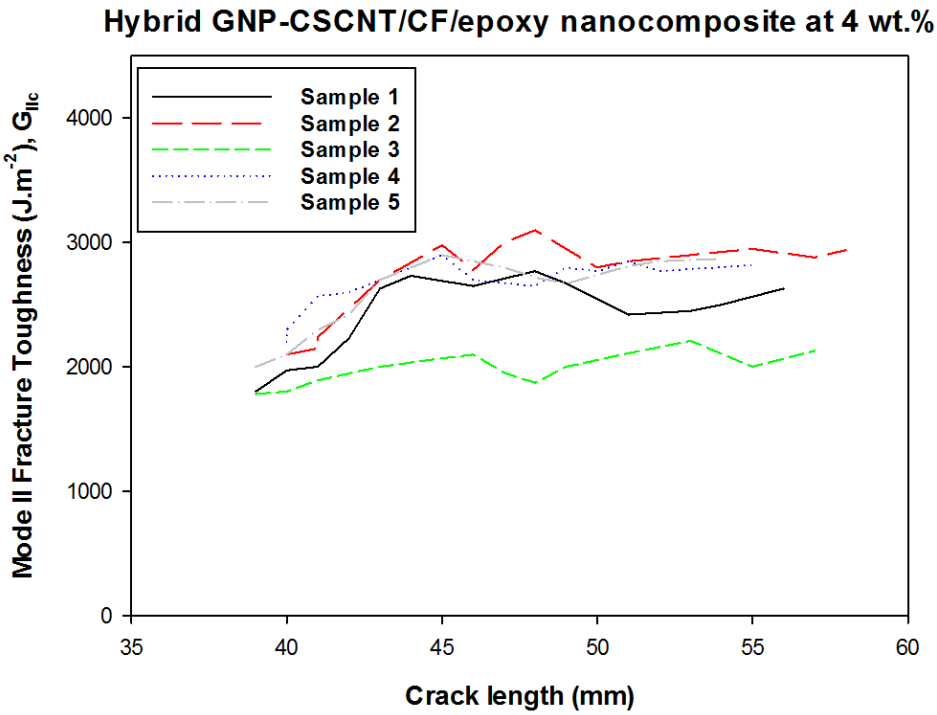

Figure G.2.3. Typical resistance curves (R-curves) for hybrid GNP-CSCNT/CF/epoxy nanocomposites at 4 wt. %.